Remotely Sensing Functional Diversity of Temperate Forest Ecosystems

Dissertation
zur
Erlangung der naturwissenschaftlichen Doktorwürde
(Dr. sc. nat.)
vorgelegt der
Mathematisch-naturwissenschaftlichen Fakultät
der
Universität Zürich

von
Fabian Daniel Schneider
von
Neckertal SG

Promotionskomitee
Prof. Dr. Michael E. Schaepman
(Vorsitz und Leitung der Dissertation)
Dr. Felix Morsdorf
Prof. Dr. Bernhard Schmid
Prof. Dr. Reinhard Furrer

Zürich, 2018

Summary

Biodiversity is a key driver of productivity in a wide range of taxa and ecosystems, with global forests accounting for the majority of terrestrial biomass and gross primary production on Earth. Humans are vastly profiting from forest ecosystem services related to biodiversity, but are at the same time driving biodiversity loss in an unprecedented manner. This might pose a severe threat to human well-being with irreversible consequences for ecosystem functioning and related goods and services. With the recent recognition of the importance of trait based biodiversity assessments, a way to map, monitor and predict changes in plant functional diversity is urgently needed. Therefore, the aim of this thesis is to develop and apply a method to study spatial patterns of forest functional diversity with remote sensing, and its implication on ecosystem functioning.

To achieve this goal, we first developed an integrative framework to optimize, compare and validate airborne laser scanning and imaging spectroscopy data and derived products using a 3D radiative transfer model. On one hand, this allowed to develop and compare two turbid-medium based forest reconstruction approaches. We found that a continuous voxel grid approach was better suited to represent the forest canopy than an individual tree approach. This was an essential finding to further develop a spatially continuous mapping approach. Based on the 3D voxel grid, we could derive morphological forest traits, namely canopy height, layering and density. On the other hand, the modeling framework allowed to validate physiological traits derived from imaging spectroscopy measurements. We were able to map relative leaf chlorophyll, carotenoids and water content without ground based calibration, and validate it with a broad range of leaf-level field and laboratory measurements and database values.

Remotely sensed morphological and physiological trait maps formed the basis for deriving forest functional diversity. To quantitatively map functional diversity at a continuous range of spatial extents, we developed a moving-window based scaling approach to map pixels of a given neighborhood within the functional trait space and subsequently derive functional richness, divergence and evenness. This approach has the advantage to include intra-specific diversity and to be independent of any predefined vegetation units, species or plant functional types. Results show clear spatial patterns of functional diversity following an environmental gradient, consistent between morphological and physiological diversity. Lower diversity on steeper, rockier and more exposed slopes could indicate reduced resource availability and use efficiency leading to lower ecosystem functioning and stability. Besides these patterns of plant adaptability to the environment, we were able to study the scale dependency and functional richness-area relationships of the forest. We found high diversity within species and communities and a lower diversity between communities than expected from established species richness-area relationships. This emphasizes the importance of a continuous mapping approach.

Mapping functional diversity is important since it can reveal information about ecosystem functioning and the susceptibility of a forest to climate change. However, functional diversity maps alone only indicate the potential influence on functioning, without having established a mechanistic link between diversity and productivity. Therefore, we promote the integration of remote sensing data with process-based models, not just for validation purposes but also for the estimation and prediction of energy and carbon fluxes. Preliminary results demonstrate the ability of airborne remote sensing data to inform an Earth system model and improve the prediction of gross primary production over time. However, longer-term simulations of vegetation dynamics reveal that further research is needed to correctly initialize and parametrize models with regard to forest representation in general and simulation of plant-water interactions in particular. We contribute to the development and testing of an Earth system model and its implementation of dynamic plant interactions.

Potential future research directions include upscaling of the diversity mapping from regional to large-scale spaceborne observations and further development of the concept of Essential Biodiversity Variables (EBVs). This may include a scale-dependent analysis to derive a detectability threshold for different ecosystems and a discussion of the necessary relevance and number of functional traits needed for global trait mapping. Future work on the integration of remote sensing data and products with Earth system models will greatly improve our understanding of the relationship and feedback between plant functional traits, trait diversity, their functioning and the environment as a key concept of global change research.

Zusammenfassung

Die Biodiversität ist einer der wichtigsten Faktoren, welche die Produktivität einer Vielzahl von Taxa und Ökosystemen beeinflussen, wobei die globalen Wälder den grössten Teil der terrestrischen Biomasse und der Brutto-Primärproduktion auf der Erde ausmachen. Der Mensch profitiert in hohem Masse von den Leistungen des Ökosystems Wald im Zusammenhang mit der biologischen Vielfalt, fördert aber damit gleichzeitig den Verlust der Biodiversität auf beispiellose Weise. Dies könnte eine ernsthafte Bedrohung für das menschliche Wohlbefinden darstellen, mit irreversiblen Folgen für das Funktionieren von Ökosystemen und damit zusammenhängenden Gütern und Leistungen. Angesichts der jüngsten Anerkennung von merkmalsbasierten Ansätzen zur Untersuchung von Biodiversität ist ein Weg zur Kartierung, Überwachung und Vorhersage von Veränderungen der funktionellen Vielfalt von Pflanzen dringend notwendig. Das Ziel dieser Dissertation ist daher die Entwicklung und Anwendung einer Methode zur Untersuchung von räumlichen Mustern der funktionellen Vielfalt des Waldes mittels Fernerkundung, sowie die Untersuchung ihrer Auswirkungen auf die Funktionsweise von Ökosystemen.

Um dieses Ziel zu erreichen, entwickelten wir zunächst einen integrativen Ansatz zur Optimierung, zum Vergleich und zur Validierung von luftgestützten Laserscanning- und bildgebenden Spektroskopiedaten und daraus abgeleiteten Produkten unter Verwendung eines 3D-Strahlungstransfermodells. Dies ermöglichte zum einen die Entwicklung und den Vergleich von zwei 'Turbid-Medium' basierten Waldrekonstruktionen. Wir konnten zeigen, dass ein kontinuierlicher Voxelgitter-Ansatz besser geeignet ist, den Waldbestand zu repräsentieren, als ein Einzelbaumansatz. Dies war eine wesentliche Erkenntnis, um einen räumlich kontinuierlichen Ansatz zu entwickeln. Basierend auf 3D-Voxelgittern konnten wir die morphologischen Waldeigenschaften, nämlich Kronenhöhe, Schichtung und Dichte, ableiten. Andererseits erlaubte das Modell die Validierung der physiologischen Eigenschaften, die aus bildgebenden Spektroskopiedaten abgeleitet wurden. Wir waren in der Lage, den relativen Chlorophyll-, Carotinoid- und Wassergehalt von Blättern ohne Bodenkalibrierung zu erfassen und mit einer breiten Palette von Feld- und Labormessungen sowie Datenbankwerten zu validieren.

Die mit Hilfe von Fernerkundung gemessenen morphologischen und physiologischen Merkmalskarten bildeten die Grundlage für die Ableitung der Funktionsvielfalt des Waldes. Um die Funktionsvielfalt quantitativ in einem räumlich kontinuierlichen Bereich abzubilden, haben wir einen gleitenden Skalierungsansatz entwickelt, um Bildelemente einer gegebenen Nachbarschaft im funktionalen Merkmalsraum abzubilden und daraus funktionale Reichhaltigkeit, Divergenz und Gleichmässigkeit abzuleiten. Dieser Ansatz hat den Vorteil, dass er Diversität innerhalb einer Art mit einbezieht und unabhängig von vordefinierten Vegetationseinheiten, Arten oder Pflanzenfunktionstypen ist. Die Ergebnisse zeigen eindeutige räumliche Muster der funktionellen Diversität, die einem Umweltgradienten folgen und zwischen morphologischer und physiologischer Diversität konsistent sind. Eine geringere Vielfalt an steileren, felsigeren und exponierteren Hängen könnte auf eine geringere Ressourcenverfügbarkeit und -nutzungseffizienz hindeuten, was zu einer geringeren Funktion und Stabilität des Ökosystems führen würde. Neben diesen Mustern der Anpassbarkeit der Pflanzen an die Umwelt konnten wir auch Skalenabhängigkeit und Zusammenhänge zwischen funktioneller Reichhaltigkeit und Fläche des Waldes untersuchen. Wir fanden eine hohe Diversität innerhalb

einer Art und Gemeinschaft, sowie eine geringere Diversität zwischen den Gemeinschaften als von etablierten Artenreichtum-Flächen-Beziehungen erwartet wurde. Dies unterstreicht die Bedeutung eines kontinuierlichen Kartierungsansatzes.

Die Kartierung der funktionalen Vielfalt ist wichtig, da sie Aufschluss über die Funktionsweise des Ökosystems und die Anfälligkeit eines Waldes für den Klimawandel geben kann. Funktionale Diversitätskarten allein deuten jedoch nur auf den potentiellen Einfluss der Funktionsweise hin, ohne eine zuvor etablierte mechanistische Verbindung zwischen Diversität und Produktivität anzunehmen. Daher fördert diese Arbeit die Integration von Fernerkundungsdaten und prozessbasierten Modellen, nicht nur zur Validierung, sondern auch zur Abschätzung und Vorhersage von Energie- und Kohlenstoffflüssen. Zwischenergebnisse zeigen die Fähigkeit von luftgestützten Fernerkundungsdaten, ein Erdsystemmodell zu informieren und die Vorhersage der Brutto-Primärproduktion in Abhängigkeit der Zeit zu verbessern. Längerfristige Simulationen der Vegetationsdynamik zeigen jedoch, dass weitere Untersuchungen notwendig sind, um das Modell hinsichtlich der Waldrepräsentation und der Simulation von Pflanzen-Wasser-Wechselwirkungen korrekt zu initialisieren und zu parametrisieren. Mit dieser Arbeit tragen wir zur Entwicklung und Erprobung eines Erdsystemmodells und dessen Implementierung dynamischer Pflanzen-Interaktionen bei.

Mögliche zukünftige Forschungsrichtungen sind die Hochskalierung des vorgelegten Ansatzes zur Kartierung von Diversität auf Weltraumbeobachtungen und die Weiterentwicklung wesentlicher Biodiversitätsvariablen. Dies sollte eine Skalenanalyse zur Bestimmung einer Nachweisgrenze für verschiedene Ökosysteme und eine Diskussion über die notwendige Relevanz und Anzahl der benötigten funktionellen Merkmale umfassen. Zukünftige Arbeiten zur Integration von Fernerkundungsdaten und abgeleiteten Produkten für Erdsystemmodelle werden unser Verständnis der Zusammenhänge und Rückkopplungen zwischen pflanzlichen Funktionsmerkmalen, der Merkmalsvielfalt, ihrer Funktionsweise und der Umwelt als Schlüsselkonzept der Erforschung des globalen Wandels grundlegend verbessern.

Table of Contents

List of Abbreviations

1D ..... One-Dimensional
3D ..... Three-Dimensional
a.s.l. ..... Above Sea Level
ALA ..... Average Leaf Angle
ALS ..... Airborne Laser Scanning
ANN ..... Artificial Neural Network
ANOVA ..... Analysis of Variance
AOD ..... Aerosol Optical Depth
APEX ..... Airborne Prism Experiment
CAR ..... Carotenoids
CHL ..... Chlorophyll
CR ..... Continuum Removal
DART ..... Discrete Anisotropic Radiative Transfer
DBH ..... Diameter at Breast Height
DHP ..... Digital Hemispherical Photography
DOY ..... Day of Year
DSM ..... Digital Surface Model
DTM ..... Digital Terrain Model
EBV ..... Essential Biodiversity Variable
ECf ..... Early Conifers
ED ..... Ecosystem Demography
EHw ..... Early Hardwoods
ESA ..... European Space Agency
EWT ..... Equivalent Water Thickness
FDiv ..... Functional Divergence
FEve ..... Functional Evenness
FHD ..... Foliage Height Diversity
FLAIR ..... Four-Scale Linear Model for Anisotropic Reflectance
FLEX ..... Fluorescence Explorer
FLIGHT ..... Forest Light model
FPAR ..... Fraction of Photosenthetically Active Radiation
FRic ..... Functional Richness
FWHM ..... Full Width at Half Maximum
GEDI ..... Global Ecosystem Dynamics Investigation
GEO BON ..... Group on Earth Observation Biodiversity Observation Network
GPP ..... Gross Primary Production
HCRF ..... Hemispherical-Conical Reflectance Factor
IPCC ..... Intergovernmental Panel on Climate Change
ISS ..... International Space Station
LAD ..... Leaf Angle Distribution
LAI ..... Leaf Area Index
LCf ..... Late Conifers
LHw ..... Late Hardwoods

LiDAR ..... Light Detection And Ranging
LOP ..... Leaf Optical Property
LUT ..... Look-Up Table
LWF ..... Long-Term Forest Ecosystem Research Site
MHw ..... Mid Hardwoods
MODIS ..... Moderate-Resolution Imaging Spectrometer
MODTRAN .... Moderate Resolution Atmospheric Transmission
NABEL ..... National Air Pollution Monitoring Network
NASA ..... National Aeronautics and Space Administration
NEP ..... Net Ecosystem Production
NIR ..... Near InfraRed
NOAA ..... National Oceanic and Atmospheric Administration
NPP ..... Net Primary Production
PAC ..... Principal Component Analysis
PAD ..... Plant Area Density
PAI ..... Plant Area Index
PARGE ..... Parametric Geocoding
PAW ..... Precipitable Amount of Water
PFT ..... Plant Functional Type
R ..... Respiration
RAMI ..... Radiative Transfer Model Intercomparison
RT ..... Radiative Transfer
SNR ..... Signal to Noise Ratio
SSI ..... Spectral Sampling Interval
STAR ..... Silhouette to Total Area Ratio
STD ..... Standard Deviation
SWIR ..... ShortWave InfraRed
TLS ..... Terrestrial Laser Scanning
TOA ..... Top Of Atmosphere
TOC ..... Top Of Canopy
UAVLS ..... Unmanned Aerial Vehicle Laser Scanning
URPP GCB ..... University of Zurich Research Priority Program on Global Change and Biodiversity
USGS ..... United States Geological Survey
VALERI ..... Validation of Land European Remote sensing Instruments
VHM ..... Vegetation Height Model
VIS ..... Visible spectral range
WSL ..... Swiss Federal Institute for Forest, Snow and Landscape Research

Chapter

1

Introduction

The integration of remote sensing methods, field-based measurements, and Earth system modeling is a major challenge in biodiversity research, but might ultimately offer the opportunity to study, monitor and predict plant functional traits and trait diversity spatially, from individual plants to global scale, and temporally, from single snapshots, daily observations to decadal predictions. Section 1.1 provides an overview on the relevance of remotely sensing plant functional diversity in a broader context and introduces the main concepts towards such an integrative pathway, but without going into detail on some important aspects. Therefore, more detailed challenges and opportunities related to this thesis' work are presented in Section 1.2. Finally, the thesis aims with the main research questions and hypotheses as well as the structure of the thesis are introduced in Section 1.3.

1.1 Monitoring plant functional diversity from space

Jetz, W., Cavender-Bares, J., Pavlick, R., Schimel, D., Davis, F.W., Asner, G.P., Guralnick, R., Kattge, J., Latimer, A.M., Moorcroft, P., Schaepman, M.E., Schildhauer, M.P., **Schneider, F.D.**, Schrodt, F., Stahl, U., Ustin, S.

This section is based on the peer-reviewed article:
Nature Plants, 2016 (2), 1-5
DOI:10.1038/NPLANTS.2016.24

All authors designed research and wrote the paper, with main contributions of W.J. and J.C.-B.

PUBLISHED: 2 MARCH 2016 | ARTICLE NUMBER: 16024 | DOI: 10.1038/NPLANTS.2016.24

comment

Monitoring plant functional diversity from space

The world's ecosystems are losing biodiversity fast. A satellite mission designed to track changes in plant functional diversity around the globe could deepen our understanding of the pace and consequences of this change, and how to manage it.

Walter Jetz, Jeannine Cavender-Bares, Ryan Pavlick, David Schimel, Frank W. Davis, Gregory P. Asner, Robert Guralnick, Jens Kattge, Andrew M. Latimer, Paul Moorcroft, Michael E. Schaepman, Mark P. Schildhauer, Fabian D. Schneider, Franziska Schrodt, Ulrike Stahl and Susan L. Ustin

The ability to view Earth's vegetation from space is a hallmark of the Space Age. Yet decades of satellite measurements have provided relatively little insight into the immense diversity of form and function in the plant kingdom over space and time. Humans are rapidly impacting biodiversity around the globe[1,2], leading to the loss of ecosystem function[3] as well as the goods and services they provide[4,5]. Recognizing the gravity of this threat, the international community has committed to urgent action to halt biodiversity loss[6–9].

Ecosystem processes[10–12] are often directly linked to the functional biodiversity of plants, that is, to a wide range of plant chemical, physiological and structural properties that are related to the uptake, use and allocation of resources. The functional biodiversity of plants varies in space and time and across scales of biological organization. Capturing and understanding this variation is vitally important for tracking the status and resilience of Earth's ecosystems, and for predicting how our ecological life support systems will function in the future.

We currently lack consistent, repeated, high-resolution global-scale data on the functional biodiversity of the Earth's vegetation[2,10–12]. However, the technological tools, informatics infrastructure, theoretical basis and analytical capability now exist to produce this essential data. Here we suggest that this capability should be used in a satellite mission supporting a 'global biodiversity observatory' that tracks temporal changes in plant functional traits around the globe to fill critical knowledge gaps, aid in the assessment of global environmental change, and improve predictions of future change. The continuous, global coverage in space and time that such a mission would provide has the potential to transform basic and applied science on diversity and function, and to pave the way to a more mechanistically detailed representation of the terrestrial biosphere in Earth system models.

The data and knowledge gap

Plant functional biodiversity encompasses the vast variation in the chemical, physiological and morphological properties of plants, such as the concentration of metabolites and non-structural carbohydrates in leaves and the ratio of leaf mass to leaf area. These attributes are related functionally to the uptake, allocation and use of resources such as carbon and nutrients within the plant, and to the defence against pests and environmental stresses.

Functional properties vary within and among individuals (for instance, as determined by the position of a leaf on a plant, or a tree in a forest), populations, species and communities, and may be measured at any of these levels of biological organization. With increasing spatial scale (and thus decreasing spatial resolution of measurements), the capture of functional

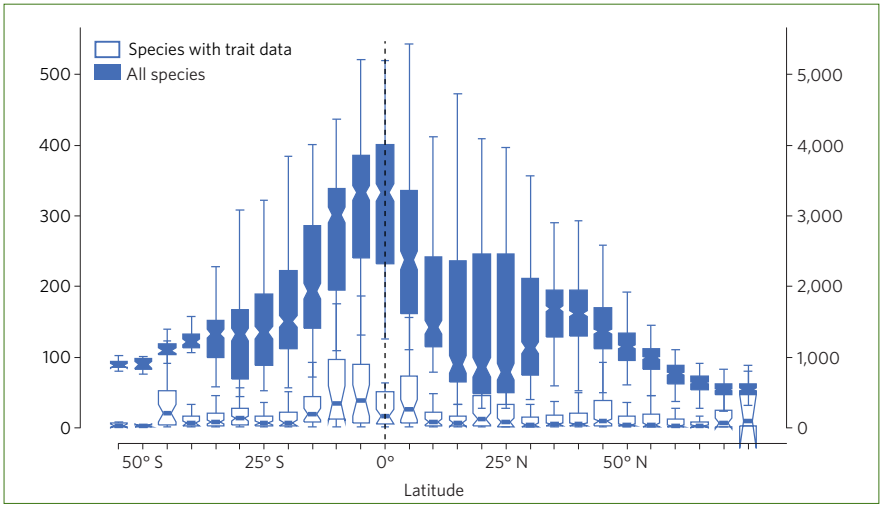

Figure 1 | The data gap in regional species trait measurements. The graph shows the latitudinal variation in the number of vascular plant species for which at least one trait has been measured regionally (open boxes; left axis) in relation to all species expected for that region (filled boxes; right axis). Regions are here defined as 110 × 110 km grid cells (n = 11,626); data on their expected richness is from ref. 25, and region trait data comes from the TRY database (version June 2015)[18]. Regions are analysed at the grid cell level and their variation is summarized in latitudinal bands of 5° width. On average, only about 2% of species have any such regional measurements, and the data gap is largest in the tropics. This limits understanding of both biodiversity and ecosystem function and services.

Table 1 | Key functional plant traits that are remotely observable from space.

Trait	Trait definition	Trait functions	Trait role (refs)	Remote observation (refs)
Leaf mass per area (LMA) ($g\,m^{-2}$)	The dry mass of a leaf divided by its one-sided area measured when fresh. The reciprocal is specific leaf area (SLA).	A primary axis of the global leaf economics spectrum[11].	49,66,67	34,35,68–70
Nitrogen (N) (%)	Concentration of elemental nitrogen in a leaf or canopy.	Important for photosynthesis and other metabolic processes as a constituent of plant enzymes.	67,71,72	34,35,73–75
Non-structural carbohydrates (NSC) (%)	Direct products of photosynthesis (sugars and starches), not yet incorporated into plant structural components and thus readily assimilable.	Indicator of tolerance to environment stress.	76	77
Chlorophyll ($mg\,g^{-1}$)	Green pigments.	Responsible for capturing light in the process of photosynthesis.	78,79	35,80,81
Carotenoids ($mg\,g^{-1}$)	Orange and yellow pigments.	Involved in the xanthophyll cycle for dissipating excess energy and avoiding oxygen radical damage under stress conditions (drought, chilling, low nutrients).	82,83	31,35
Lignin (%)	A complex organic polymer.	Provides mechanical support and a barrier against pests and pathogens; negatively correlated with tree growth rate and microbial decomposition.	84,85	32,35,73,86

See Supplementary Table 1 for more traits.

properties may increasingly represent the aggregate properties of many individuals and species, reflecting the functional biodiversity of whole communities. Aggregate 'functional diversity' metrics that characterize the breadth of functional properties of a group of organisms are known to be strongly associated with taxonomic[13] and phylogenetic[14] measures of biodiversity and their potential decrease under habitat loss[15]. Plant functional biodiversity is also closely linked to ecosystem processes such as carbon, water and energy exchange, which enables a direct integration with Earth system models[16,17]. Global information on the functional composition and diversity of plant communities thus provides a necessary foundation for monitoring, understanding and predicting the productivity of ecosystems, and for relating productivity and carbon uptake to other critical ecosystem services.

Available global data on plant functional biodiversity are grossly incomplete and non-representative taxonomically, geographically, environmentally, temporally and functionally. Although datasets of traits and their connection to function continue to grow[18,19], local observations of plant functional traits are limited along multiple dimensions. On average, only around 2% of currently known vascular plant species have any trait measurements available at the regional scale (here defined as a 110 × 110 km grid cell, $n = 11{,}626$); in the species-rich tropical regions, this figure is even smaller (Fig. 1). Data on other biodiversity attributes such as species occurrence, abundance and biomass hold similar biases[20,21]. These spatial and environmental data gaps and biases are exacerbated by even scarcer information on temporal variation in plant functional biodiversity. Even in areas for which current data are relatively complete, widespread biodiversity change driven by anthropogenic pressures is rapidly outpacing incremental gains in our knowledge of the Earth's biodiversity afforded by *in situ* biodiversity sampling[22]. Furthermore, existing 'global' datasets have not been collected consistently or systematically, but instead compiled post hoc from thousands of disparate research activities, often not designed to address long-term trends or large-scale patterns[23]. These severe sampling inhomogeneities and resulting biases cannot be readily overcome statistically, and continue to impose severe limits on inference and application in global biodiversity science[21,24,25]. An integrated system for rapidly and consistently monitoring plant functional diversity globally is thus urgently needed.

Filling the gap

Remote sensing has already proved to be a pivotal technology for addressing the global biodiversity data gap. Data on plant productivity, phenology, land cover and other environmental parameters from MODIS (moderate resolution imaging spectroradiometer) and Landsat satellites currently serve as reasonably effective covariates for spatiotemporal biodiversity models based on *in situ* data[12,20,26]. However, the coarse spectral resolution of current satellite-borne sensors has prevented a more direct capture of biodiversity, and correlative models are limited by the above-mentioned data gaps.

In contrast, imaging spectroscopy is a well-established, continuously advancing technology capable of monitoring terrestrial plant functional biodiversity in a way that is vastly richer and more sensitive than other remote sensing techniques[22,27,28]. It captures environmental information at extremely fine spectral resolution by simultaneously mapping the reflectance and emission of light from the Earth's surface in hundreds of narrow spectral bands, producing essentially continuous spectra from the visible to infrared wavelengths[29]. Distinctive features are imprinted in these spectra as light interacts with the chemical bonds and structural composition of plants. Spectra are thus an aggregate signal of the chemical and structural composition of vegetation, and can be directly related to a number of leaf biochemical and morphological functional traits (Table 1)[30–32]. Air- or

satellite-borne spectrometers are able to measure the aggregate functional traits of plant communities represented in the top layers of vegetation, and even the attributes of single species directly, depending on community spatial and spectral characteristics[33]. This capability has been successfully demonstrated using airborne spectrometers for many traits at regional scales across multiple biomes[34,35]. There are similar techniques (that are at various stages of development) for characterizing freshwater[36] and tidal ecosystems[37], marine phytoplankton[38,39] and coral reefs[40]. Satellite technology is now poised to provide global coverage at spatial resolutions sufficiently fine (30 to 60 m pixel size) to support biodiversity inference and applications.

Linking data across scales

A global biodiversity observatory would integrate remotely sensed information on functional traits together with other remotely sensed information and *in situ* observations of phylogenetic relationships, functional traits and species distributions (Fig. 2). Developing such an observatory would not be without challenges, however. Cloud cover, especially in the tropics, poses constraints for any optical remote-sensing method aiming to be spatially and temporally representative (but see ref. 41 for some encouraging evidence regarding space-based spectrometry). Further, direct measurements of plant traits by imaging spectroscopy are currently limited to only those traits with a clear spectral signature expressed in the canopy layer (Table 1), rendering root and stem traits hard to capture. Finally, the vast quantity of data generated will constrain the spatial resolution that a global mission can support, at least initially: envisioned spatial grains of around 30 m will limit the direct capture of individuals or stands of single species to only a few select cases.

The convergence of imaging spectroscopy with other remote-sensing advances, together with prominent developments in plant biology and biogeography, can pave the way to a more integrated global assessment of plant functional biodiversity. Specifically, spectroscopic trait measurements combined with LiDAR (light detection and ranging) data on ecosystem vertical structure at similar spatial resolutions may dramatically enhance the ecological interpretation of the spectral imagery and help overcome its current limitation to surface signals only[42,43]. Although significant gaps remain (Fig. 1), select trait data has now been collected *in situ* for more than 100,000 vascular plant species, providing a means to both directly and indirectly connect, through models, spectral observations from the top layer of vegetation to a variety of plant traits[18]. And the global phylogeny ('tree of life') for plants is becoming ever more complete[44], enabling researchers to trace the evolutionary history of plant traits within lineages[45]. Although for some traits and functions convergent evolution has pulled disparate (and often geographically distant) lineages into functional similarity[46–49], traits and associated functions are in many cases conserved to relatively deep phylogenetic levels[50–52]. In combination, this provides several relevant opportunities. For example, advances in macroevolutionary models and data-gap-filling techniques[53–55], when coupled with increasingly complete phylogenies, can allow for the prediction of traits for species lacking observations. Further, the strong phylogenetic signal in the individual traits that make up overall functional biodiversity means that spectral observations of aggregate species may in some cases still be meaningfully connected to specific functional properties or clades, and interpreted or monitored as a unit[56].

The increasing volume of online species occurrence data is a fourth synergistic development that supports the predictive modelling and mapping of species' and plant community distributions[57]. Combined with trait and phylogenetic data, and potentially other ecological information (such as typical stand density), hierarchical statistical models and downscaling techniques[58,59] may, with some uncertainty, allow the pinpointing of particular species and the make-up of communities. We hypothesize that such predictions will generally be much more effective at coarser levels of biological organization, such as higher-level clades

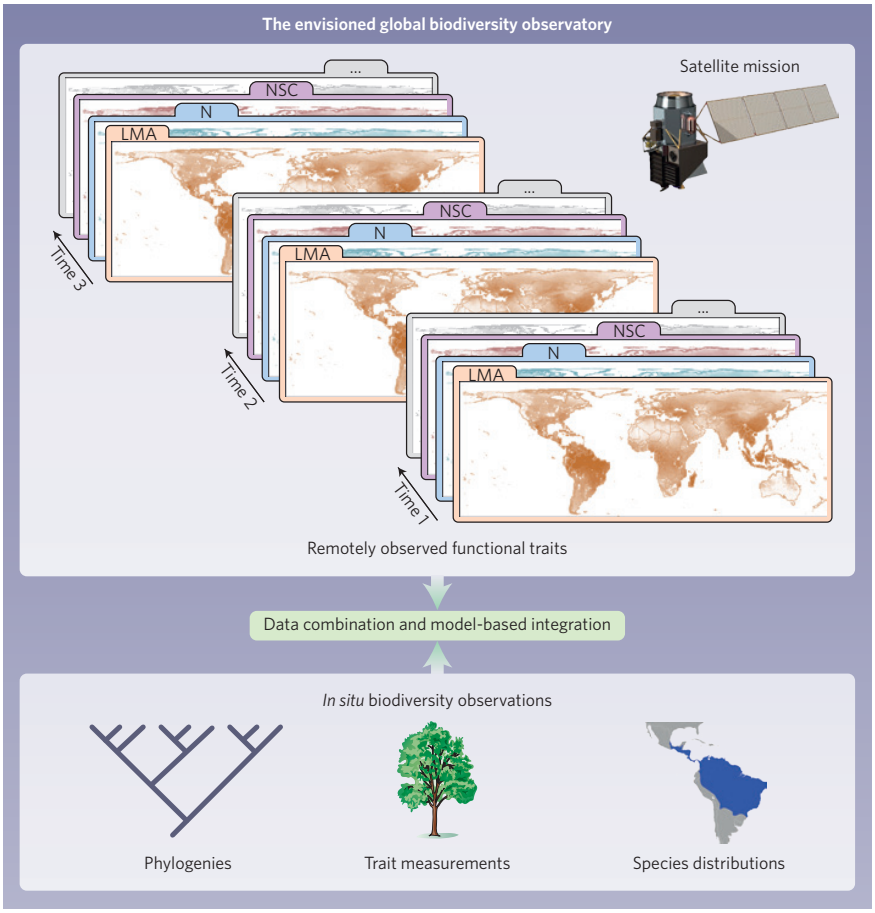

Figure 2 | The envisioned global biodiversity observatory. Top: space-based imaging spectrometer sensors capture global spatial data on key functional attributes in time, including leaf mass per area (LMA), nitrogen concentration (N) and non-structural carbohydrates (NSC), among others (see Table 1). Other sensors (such as LiDAR) may also contribute measurements. An informatics infrastructure and appropriate modelling techniques connect this information with trait, evolutionary and spatial biodiversity information[20] collected worldwide *in situ* at different spatial scales and levels of biological organization (bottom).

or other well-characterized species groups that can be associated with the aggregate functions of the spectral signal of a pixel.

The envisioned imaging spectroscopy mission will naturally provide only some of the data required for global biodiversity monitoring and modelling. Nevertheless, the model-based integration of detailed and global spectral information with other remote sensing data and rapidly growing *in situ* biological information points to an array of transformative new opportunities for monitoring plant functional biodiversity through space and time.

A global biodiversity observatory

Scaling up processes from fine-grained local studies to larger regions (and ultimately the entire globe) is an urgent challenge for all of the Earth sciences. Environmental understanding at larger scales requires observations that capture dimensions of the entire system to place the microscale measurements in context. Plant functional biodiversity observations from space have the potential to provide a global context for biodiversity science, and to link the evolutionary and functional diversity of plants at local scales to ecosystem function around the globe. Such information would link key dimensions of diversity to ecosystem processes including the carbon cycle, the water cycle and the provisioning of ecosystem services. And it would revolutionize large-scale research on the stability and resilience of ecosystems to shocks such as drought, fire and pathogen outbreaks. Several space missions planned for launch within this decade[60] — such as EnMAP (German Spaceborne Imaging Spectrometer Mission)[61] and HISUI (Japan Aerospace Exploration Agency, JAXA)[62] — will have some capability for mapping plant functional diversity over limited geographic areas. However, none of these will provide the spatial coverage, repeat frequency or mission duration needed to monitor ecosystem-relevant changes in global plant functional biodiversity through time. Satellites technology such as that proposed for HyspIRI[63], a mission that was called for in the 2007 National Research Council (NRC) Decadal Survey[64], would be able to serve the initial remote sensing capabilities of the envisioned global biodiversity observatory, but no satellite development process or launch date has yet been determined.

Predicting how ecosystems and the services they provide will respond to accelerating environmental change requires more comprehensive, globally consistent and repeated data on the patterns and dynamics of functional biodiversity. Advanced observing technology (which is available but not yet deployed at scale) integrated with *in situ* measurements[65] could transform this situation. The envisioned global biodiversity observatory offers vastly more biologically relevant and spatially and temporally highly resolved information about vegetation than any existing or otherwise planned global sampling or observation scheme. Rates of change today are so high that the longer a global spectroscopic mission is delayed, the more biological information is irretrievably lost[22]. The earliest possible launch of a mission able to spectroscopically monitor key plant functional traits globally is an urgent priority for understanding and managing our changing biosphere. ❐

Walter Jetz[1], Jeannine Cavender-Bares[2], Ryan Pavlick[3], David Schimel[3], Frank W. Davis[4], Gregory P. Asner[5], Robert Guralnick[6], Jens Kattge[7], Andrew M. Latimer[8], Paul Moorcroft[9], Michael E. Schaepman[10], Mark P. Schildhauer[4], Fabian D. Schneider[10], Franziska Schrodt[11], Ulrike Stahl[7] and Susan L. Ustin[12]

[1]Yale University, 165 Prospect Street, New Haven, Connecticut 06520, USA. [2]Department of Ecology, Evolution and Behavior, University of Minnesota, 1987 Upper Buford Circle, St Paul, Minnesota 55108, USA. [3]Jet Propulsion Laboratory, California Institute of Technology, 4800 Oak Grove Drive, Pasadena, California 91109, USA. [4]National Center for Ecological Analysis and Synthesis, University of California, Santa Barbara, 735 State Street, Suite 300, Santa Barbara, California 93101, USA. [5]Department of Global Ecology, Carnegie Institution of Washington, 260 Panama Street, Stanford, California 94305, USA. [6]Florida Museum of Natural History, University of Florida, Gainesville, Florida 32611, USA. [7]Max Planck Institute for Biogeochemistry, Hans-Knöll-Straße 10, 07745 Jena, Germany. [8]Department of Plant Sciences, University of California, Davis, 139 Veihmeyer Hall, Davis, California 95616, USA. [9]Harvard University, 26 Oxford Street, HMNH, Suite 43, Cambridge, Massachusetts 02138, USA. [10]University of Zurich, Winterthurerstrasse 190, CH-8057 Zurich, Switzerland. [11]School of Geography, University of Brighton, 9 Old Court Close, Brighton BN1 8HF, UK. [12]Center for Spatial Technologies and Remote Sensing, University of California, Davis, 139 Veihmeyer Hall, Davis, California 95616, USA.

e-mail: walter.jetz@yale.edu; cavender@umn.edu

References

1. Pereira, H. M., Navarro, L. M. & Martins, I. S. *Annu. Rev. Environ. Resour.* **37,** 25–50 (2012).
2. Tittensor, D. P. *et al. Science* **346,** 241–244 (2014).
3. Cardinale, B. J. *et al. Nature* **486,** 59–67 (2012).
4. Dobson, A. *et al. Ecology* **87,** 1915–1924 (2006).
5. Quijas, S., Schmid, B. & Balvanera, P. *Basic Appl. Ecol.* **11,** 582–593 (2010).
6. Convention on Biological Diversity *Decision X/2: The Strategic Plan for Biodiversity 2011–2020 and the Aichi Biodiversity Targets* (UNEP, 29 October 2010); https://www.cbd.int/doc/decisions/cop-10/cop-10-dec-02-en.pdf
7. Inouye, D. W. *Front. Ecol. Environ.* **12,** 371 (2014).
8. Cadotte, M. W., Carscadden, K. & Mirotchnick, N. *J. Appl. Ecol.* **48,** 1079–1087 (2011).
9. Díaz, S. *et al. Curr. Opin. Environ. Sustain.* **14,** 1–16 (2015).
10. Pereira, H. M. *et al. Science* **339,** 277–278 (2013).
11. Geijzendorffer, I. R. *et al. J. Appl. Ecol.* http://dx.doi.org/10.1111/1365-2664.12417 (2015).
12. Skidmore, A. K. *et al. Nature* **523,** 403–405 (2015).
13. Petchey, O. L. & Gaston, K. J. *Ecol. Lett.* **5,** 402–411 (2002).
14. Flynn, D. F. B., Mirotchnick, N., Jain, M., Palmer, M. I. & Naeem, S. *Ecology* **92,** 1573–1581 (2011).
15. Keil, P., Storch, D. & Jetz, W. *Nature Commun.* **6,** 8837 (2015).
16. Scheiter, S., Langan, L. & Higgins, S. I. *New Phytol.* **198,** 957–969 (2013).
17. Yang, Y., Zhu, Q., Peng, C., Wang, H. & Chen, H. *Prog. Phys. Geogr.* **39,** 514–535 (2015).
18. Kattge, J. *et al. Glob. Change Biol.* **17,** 2905–2935 (2011).
19. Violle, C., Reich, P. B., Pacala, S. W., Enquist, B. J. & Kattge, J. *Proc. Natl Acad. Sci. USA* **111,** 13690–13696 (2014).
20. Jetz, W., McPherson, J. M. & Guralnick, R. P. *Trends Ecol. Evol.* **27,** 151–159 (2012).
21. Schimel, D. *et al. Glob. Change Biol.* **21,** 1762–1776 (2015).
22. Schimel, D. S., Asner, G. P. & Moorcroft, P. *Front. Ecol. Environ.* **11,** 129–137 (2013).
23. Scholes, R. J. *et al. Science* **321,** 1044–1045 (2008).
24. Sandel, B. *et al. J. Veg. Sci.* **26,** 828–838 (2015).
25. Kreft, H. & Jetz, W. *Proc. Natl Acad. Sci. USA* **104,** 5925–5930 (2007).
26. De Jong, Schaepman, M. E., Furrer, R., Bruin, S. & Verburg, P. H. *Glob. Change Biol.* **19,** 1953–1964 (2013).
27. Homolová, L., Malenovský, Z., Clevers, J. G. P. W., García-Santos, G. & Schaepman, M. E. *Ecol. Complex.* **15,** 1–16 (2013).
28. Schaepman, M. E. *et al. Remote Sens. Environ.* **158,** 207–219 (2015).
29. Schaepman, M. E. *et al. Remote Sens. Environ.* **113,** S123–S137 (2009).
30. Asner, G. P. & Martin, R. E. *Front. Ecol. Environ.* **7,** 269–276 (2009).
31. Ustin, S. L. *et al. Remote Sens. Environ.* **113,** S67–S77 (2009).
32. Serbin, S. P., Singh, A., McNeil, B. E., Kingdon, C. C. & Townsend, P. A. *Ecol. Appl.* **24,** 1651–1669 (2014).
33. Roth, K. L. *et al. Remote Sens. Environ.* **167,** 135–151 (2015).
34. Singh, A., Serbin, S. P., McNeil, B. E., Kingdon, C. C. & Townsend, P. A. *Ecol. Appl.* **25,** 2180–2197 (2015).
35. Asner, G. P., Martin, R. E., Anderson, C. B. & Knapp, D. E. *Remote Sens. Environ.* **158,** 15–27 (2015).
36. Hestir, E. L. *et al. Remote Sens. Environ.* **167,** 181–195 (2015).
37. Turpie, K. R., Klemas, V. V., Byrd, K., Kelly, M. & Jo, Y.-H. *Remote Sens. Environ.* **167,** 206–217 (2015).
38. Palacios, S. L. *et al. Remote Sens. Environ.* **167,** 269–280 (2015).
39. Moisan, T. A. H., Moisan, J. R., Linkswiler, M. A. & Steinhardt, R. A. *Cont. Shelf Res.* **55,** 17–28 (2013).
40. Hochberg, E. J. in *Coral Reefs: An Ecosystem in Transition* (eds Dubinsky, Z. & Stambler, N.) 25–35 (Springer, 2011).
41. Mercury, M. *et al. Remote Sens. Environ.* **126,** 62–71 (2012).
42. Torabzadeh, H., Hossein, T., Felix, M. & Schaepman, M. E. *ISPRS J. Photogramm. Remote Sens.* **97,** 25–35 (2014).
43. Asner, G. P. *et al. Remote Sens. Environ.* **124,** 454–465 (2012).
44. Zanne, A. E. *et al. Nature* **506,** 89–92 (2014).
45. Cornwell, W. K. *et al. J. Ecol.* **102,** 345–356 (2014).
46. Reich, P. B., Walters, M. B. & Ellsworth, D. S. *Proc. Natl Acad. Sci. USA* **94,** 13730–13734 (1997).
47. Meinzer, F. C. *Oecologia* **134,** 1–11 (2003).
48. Reich, P. B. *et al. Int. J. Plant Sci.* **164,** S143–S164 (2003).
49. Wright, I. J. *et al. Nature* **428,** 821–827 (2004).
50. Kerkhoff, A. J., Fagan, W. F., Elser, J. J. & Enquist, B. J. *Am. Nat.* **168,** E103–122 (2006).
51. Edwards, E. J. & Still, C. J. *Ecol. Lett.* **11,** 266–276 (2008).
52. Cavender-Bares, J., Ackerly, D. D. & Kozak, K. H. *Ecology* **93,** S1–S3 (2012).
53. Swenson, N. G. *Ecography* **37,** 105–110 (2014).
54. Jetz, W. & Freckleton, R. P. *Philos. Trans. R. Soc. Lond.* **370,** 20140016 (2015).
55. Schrodt, F. *et al. Glob. Ecol. Biogeogr.* **24,** 1510–1521 (2015).
56. Asner, G. P. *et al. Proc. Natl Acad. Sci. USA* **111,** 5604–5609 (2014).
57. Jetz, W., McPherson, J. M. & Guralnick, R. P. *Trends Ecol. Evol.* **27,** 151–159 (2012).
58. Gelfand, A. E. *et al. J. R. Stat. Soc. Ser. C Appl. Stat.* **54,** 1–20 (2005).
59. Keil, P., Belmaker, J., Wilson, A. M., Unitt, P. & Jetz, W. *Methods Ecol. Evol.* **4,** 82–94 (2013).
60. Staenz, K., Mueller, A. & Heiden, U. in *Geoscience and Remote Sensing Symposium (IGARSS), 2013 IEEE International* 3502–3505 (IEEE, 2013); www.ieeexplore.ieee.org

61. Stuffler, T. *et al. Acta Astronaut.* **61,** 115–120 (2007).
62. Iwasaki, A., Ohgi, N., Tanii, J., Kawashima, T. & Inada, H. in *Geoscience and Remote Sensing Symposium (IGARSS), 2011 IEEE International* 1025–1028 (IEEE, 2011); www.ieeexplore.ieee.org
63. Green, R. O. *et al.* in *Proc. Int. Geoscience and Remote Sensing Symposium (IGARSS '12)* (NASA, 2012); http://ntrs.nasa.gov/archive/nasa/casi.ntrs.nasa.gov/20120014260.pdf
64. Space Studies Board, National Research Council *Earth Science and Applications from Space: National Imperatives for the Next Decade and Beyond* (National Academies, 2007).
65. Turner, W. *Science* **346,** 301–302 (2014).
66. Reich, P. B., Ellsworth, D. S. & Walters, M. B. *Funct. Ecol.* **12,** 948–958 (1998).
67. Walker, A. P. *et al. Ecol. Evol.* **4,** 3218–3235 (2014).
68. Fourty, T. & Baret, F. *Int. J. Remote Sens.* **19,** 1283–1297 (1998).
69. Riaño, D., Vaughan, P., Chuvieco, E., Zarco-Tejada, P. J. & Ustin, S. L. *IEEE Trans. Geosci. Remote Sens.* **43,** 819–826 (2005).
70. Vohland, M., Mader, S. & Dorigo, W. *Int. J. Appl. Earth Obs. Geoinf.* **12,** 71–80 (2010).
71. Evans, J. R. *Oecologia* **78,** 9–19 (1989).
72. Loomis, R. S. *Proc. Natl Acad. Sci. USA* **94,** 13378–13379 (1997).
73. Serrano, L., Peñuelas, J. & Ustin, S. L. *Remote Sens. Environ.* **81,** 355–364 (2002).
74. Martin, M. E., Plourde, L. C., Ollinger, S. V., Smith, M.-L. & McNeil, B. E. *Remote Sens. Environ.* **112,** 3511–3519 (2008).
75. Knyazikhin, Y. *et al. Proc. Natl Acad. Sci. USA* **110,** E185–E192 (2013).
76. O'Brien, M. J., Leuzinger, S., Philipson, C. D., Tay, J. & Hector, A. *Nature Clim. Chang.* **4,** 710–714 (2014).
77. Asner, G. & Martin, R. *Remote Sens.* **7,** 3526–3547 (2015).
78. Govindjee & Rabinowitch, E. *Science* **132,** 355–356 (1960).
79. Grimm, B. *eLS* http://dx.doi.org/10.1038/npg.els.0001310 (Wiley, 2001).
80. Gitelson, A. A. & Merzlyak, M. N. *Int. J. Remote Sens.* **18,** 2691–2697 (1997).
81. Siebke, K. & Ball, M. C. *Funct. Plant Biol.* **36,** 857 (2009).
82. Björkman, O. & Demmig-Adams, B. in *Ecophysiology of Photosynthesis* 17–47 (Springer, 1995).
83. Demmig-Adams, B. & Adams, W. W. 3rd. *New Phytol.* **172,** 11–21 (2006).
84. Melillo, J. M., Aber, J. D. & Muratore, J. F. *Ecology* **63,** 621 (1982).
85. Austin, A. T. & Ballaré, C. L. *Proc. Natl Acad. Sci. USA* **107,** 4618–4622 (2010).
86. Martin, M. E. & Aber, J. D. *Ecol. Appl.* **7,** 431–443 (1997).

Acknowledgments

This study is an output of the 'Biodiversity from Space' Working Group of the National Center for Ecological Analysis and Synthesis (NCEAS) and was produced with support from the National Aeronautics and Space Administration (NASA) grant no. NNX14AN31G to NCEAS, University of California, Santa Barbara. Part of this research was carried out at the Jet Propulsion Laboratory, California Institute of Technology, under a contract with NASA. The work also benefited from National Science Foundation (NSF) grant nos GEO-1408965 (or "Support for the Future Earth Interim Director and Implementation") and DBI-1262600; NASA grant no. NNX11AP72G to W.J. and R.G.; NSF–NASA Dimensions of Biodiversity grant no. DEB-1342872 to J.C.B.; and the University of Zurich Research Priority Program on 'Global Change and Biodiversity' to M.E.S. and F.D.S.

Author contributions

W.J. and J.C.-B. contributed equally to this work.

1.2 Key challenges and opportunities in remote sensing of functional diversity

Light detection and ranging, or short LiDAR, is a remote sensing method to study vegetation structure using laser scanning on terrestrial (TLS, Newnham *et al.*, 2015), unmanned areal vehicle (UAVLS, Morsdorf *et al.*, 2017), airborne (ALS, Morsdorf *et al.*, 2006) and spaceborne platforms (e.g. GEDI, Stavros *et al.*, 2017). It has become the reference for three-dimensional (3D) structure measurements in forestry and 3D forest reconstruction (Wulder *et al.*, 2012). Thanks to the variety of operational laser scanning systems, a range of spatial scales can be covered with grain and extent similar to imaging spectroscopy systems (van Leeuwen & Nieuwenhuis, 2010). Therefore, the integration of laser scanning and imaging spectroscopy can offer a combined view on forest structure and biochemistry through the measurement of morphological and physiological traits, as well as the interaction of radiation with the canopy. For studies on forest traits and forest functional diversity, airborne systems possess the necessary spatial resolution to measure functional traits at individual plant level on a relevant extent of an ecosystem, thus offering the opportunity to study scale-dependencies and test methodologies for larger-scale applications (Schaepman *et al.*, 2009). Very few studies have actually compared remotely sensed morphological and physiological forest traits (Chambers *et al.*, 2007), let alone functional diversity or radiation-canopy interactions at regional scale.

The integration and comparison of ALS and airborne imaging spectroscopy (AIS) data and derived products comes with several challenges. So far, ALS data has mainly been used to improve the geometric accuracy of AIS orthorectification processes or for combined classification purposes (Torabzadeh *et al.*, 2014). In a more advanced way, ALS derived 3D surface models have been used to identify sunlit crown pixels to provide a sampling scheme for spectroscopic measurements (Asner & Martin, 2009; Asner *et al.*, 2017). To actually make use of the full potential of ALS, the challenge is to reduce occlusion and reach the high resolution of AIS data also in the third dimension (Kükenbrink *et al.*, 2017). This would allow a 3D forest reconstruction and the estimation of ecologically relevant morphological forest traits at canopy scale. A comparison with spectroscopy data could then be realized by radiative transfer modeling, allowing to study the interactions of radiation with the canopy at any desired spectral band (Widlowski *et al.*, 2015). Most advanced models are coupled 3D canopy-atmosphere models, incorporating radiative transfer through the atmosphere, interactions with the 3D vegetated Earth surface and the simulation of sensors (Gastellu-Etchegorry *et al.*, 2015). Providing detailed model input and identifying the best way of representing forest in a 3D scene can be challenging, but would not only allow the simulation, testing

and validation of imaging spectroscopy missions but also vastly improve our understanding of forest structure measurements, its 3D representation and influence on canopy reflectance.

Once such a framework is developed and a suitable representation of a forest is identified, spatially continuous and comparable maps of morphological and physiological forest traits could be derived. This forms the basis for further method development to derive functional diversity. Remotely sensed trait maps possess the unique characteristics to be spatially continuous and consistent from individual plants to whole landscapes (Schimel *et al.*, 2013). This allows to derive continuous wall-to-wall measures of functional diversity. However, most existing concepts of functional diversity have never been applied to such data (Petchey & Gaston, 2006). Spatially explicit studies of functional diversity are rare (Biswas *et al.*, 2015), and most functional diversity indexes are still based on fixed units such as plant functional types or species (Mouchet *et al.*, 2010). A measurement of functional diversity independent of predefined vegetation units has not been developed due to the lack of spatially explicit trait data, but might be crucial especially in ecosystems with high intra-specific diversity (Cianciaruso *et al.*, 2009). By averaging trait data across species or plant functional types, much of the relevant information might be lost and a link to ecosystem functioning may no longer be possible. This is different for ecosystems with very high species diversity and potential trait redundancy, where vegetation unit based approaches have already been successfully implemented using airborne remote sensing data (Asner *et al.*, 2017). Since it is largely unknown at which spatial scale forest functional diversity should be measured and how functional diversity changes as a function of scale, a continuous mapping approach across a wide range of scales could reveal important scale-dependencies and to what level functional diversity can be measured from space. The latter might be different for different ecosystems. Therefore, it is crucial to develop test cases and methodologies based on higher resolution data to build on a comprehensive basis testing future space missions.

Functional diversity patterns can reveal important aspects of ecosystem functioning. However, Jetz *et al.* (2016) do not further elaborate on how to link functional diversity with ecosystem functioning, for example in terms of forest productivity (Section 1.1). One way forward, which also offers a pathway to predictive science, is to use Earth system models. Integrating remote sensing data with models can go beyond radiative transfer, and include even more complex dynamic interactions among plants as well as between plants and the environment (Fisher *et al.*, 2017). More advanced Earth system models do not only include energy balance approaches but also water and carbon fluxes, driven by meteorological input variables and a description of the forest and the environment (Medvigy *et al.*, 2009). Thus remote sensing is well suited to inform Earth system models with highly detailed information on forest structure

and composition, as well as topographic variables (Antonarakis *et al.*, 2014). With today's resolution and quality of remote sensing data, the limitation for model initialization in terms of spatial resolution and data quality often does not lie in the forest characterization anymore but rather the meteorological input or the necessary soil data. The advantage of the model environment is that fluxes cannot only be driven by current meteorology, but - once validated with flux measurements - can be used to make predictions based on future climate scenarios (Medvigy *et al.*, 2010). This is essential to study the influence of climate change on forest ecosystems and possible feedbacks, the role of plant functional diversity on long-term productivity or stability of the ecosystem, and to develop climate change mitigation and forest management strategies (Isbell *et al.*, 2015, 2017; Millar & Stephenson, 2015).

1.3 Thesis aims

The aim of this thesis is to develop a method to study spatial patterns of forest functional diversity with remote sensing, and assess its implication on ecosystem functioning. The main challenges related to this overarching research goal lead to three main research questions and corresponding hypotheses.

1.3.1 Research questions and hypotheses

In this thesis, we address the following three research questions:

> *1) How can we integrate airborne laser scanning and imaging spectroscopy data to derive functional traits, and what is the optimal 3D representation of the forest canopy?*

This question is essential to develop a modeling framework for morphological and physiological forest traits. We use two independent remote sensing methods and test which laser scanning based forest representation can best resolve spatial patterns observed by spectrometers. We hypothesize that we can use a 3D radiative transfer model approach to compare and optimize two independent remote sensing datasets. We assess whether an individual tree approach or a continuous voxel grid approach is better suited to represent a forest in 3D, particularly in the context of continuous voxel or raster based trait mapping and modeling. Both concepts have been introduced previously, whereas the individual tree approach was used more frequently. In our second research question, we discuss how this approach can be used to map functional traits and trait diversity, and what spatial patterns we expect to find.

2) How can we map functional diversity from remotely sensed morphological and physiological forest traits, and what spatial patterns can be revealed from those traits?

The main goal is to demonstrate the ability of airborne laser scanning and imaging spectroscopy to map forest functional diversity and prove the consistency of the method by comparing spatial patterns at a range of scales. We hypothesize that morphological and physiological diversity show comparable large-scale patterns, following a broad environmental gradient. We expect functional richness to increase with scale, similarly to the species richness-area relationship. However, little is known about the influence of intra-specific diversity and the scale-dependency of functional traits, as well as trait diversity in a temperate forest ecosystem. We developed our method for a particular test area in Switzerland, covered by a temperate mixed forest. Finally, we try to establish a direct link to forest productivity and predict future changes under changing climatic conditions.

3) What is the relationship between functional diversity and productivity at a temperate mixed forest site, and how does it change under climate change scenarios?

The third research question addresses an important link between forest functional diversity and ecosystem functioning, represented by the productivity of the forest in terms of carbon uptake. We hypothesize that a functionally more diverse forest is more productive and stable over time. Furthermore, we expect diversity to regulate the impact of climate change, mitigating possible negative as well as enhancing positive effects. We aim to establish this link by integrating remote sensing input with an Earth system model. Therefore, a first step is to demonstrate the ability of a remote sensing initialized model to predict gross primary productivity of the forest. We aim to do this for a temperate mixed forest site based on a time series of carbon fluxes and meteorological drivers in Switzerland.

1.3.2 Structure of the thesis

The three research questions resulted in three main chapters of this thesis, namely Chapter 2, 3 and 4. Additionally, we provide an introduction and synthesis in Chapter 1 and 5.

Chapter 1 provides the general context and relevance of the thesis, as published in a peer-reviewed article in Nature Plants (Jetz *et al.*, 2016). Current challenges and opportunities of remotely sensing forest functional diversity are introduced, together with the thesis aim and related research questions.

Chapter 2 addresses the first research question in a collection of four peer-reviewed journal articles and two peer-reviewed conference articles. The main article published by Schneider *et al.* (2014a) in Remote Sensing of Environment introduces a 3D modeling framework to compare ALS derived forest representations to imaging spectrometer measurements by simulating the radiative transfer of the forest. Subsequent articles provide extensions, possible improvements and applications of the modeling framework (Schneider *et al.*, 2014b, 2015; Fawcett *et al.*, 2018; Schaepman *et al.*, 2015; Morsdorf *et al.*, in press).

Chapter 3 addresses the second research question with a peer-reviewed article published in Nature Communications (Schneider *et al.*, 2017). Besides the main article, the chapter includes supplementary information and peer review comments, also openly accessible to all readers. This chapter represents the first contribution in remote sensing to map functional diversity based on spatially continuous forest functional traits, derived from airborne laser scanning and imaging spectroscopy data, as well as a modeling approach presented in Chapter 2. An independent validation of this approach complements this chapter.

Chapter 4 provides an introduction, material and methods to address the third research question (Schneider *et al.*, in preparation). It extends Chapter 2 and 3 to finally establish a link between functional traits, trait diversity and ecosystem functioning by integrating remote sensing with Earth system modeling. The results and discussion provide an overview of the current state of research, with initial comparisons of predicted and measured carbon fluxes at a temperate forest site.

Chapter 5 discusses the main findings of the thesis and general contributions to the research field, and presents an outlook to possible future research.

1.4 References

Antonarakis AS, Munger JW, Moorcroft PR (2014) Imaging spectroscopy- and lidar-derived estimates of canopy composition and structure to improve predictions of forest carbon fluxes and ecosystem dynamics. *Geophysical Research Letters*, **41**, 2535–2542.

Asner GP, Martin RE (2009) Airborne spectranomics: mapping canopy chemical and taxonomic diversity in tropical forests. *Frontiers in Ecology and the Environment*, **7**, 269–276.

Asner GP, Martin RE, Knapp DE, *et al.* (2017) Airborne laser-guided imaging spectroscopy to map forest trait diversity and guide conservation. *Science*, **355**, 385–389.

Biswas SR, Mallik AU, Braithwaite NT, Wagner HH (2015) A conceptual framework for the spatial analysis of functional trait diversity. *Oikos*, **125**, 192–200.

Chambers JQ, Asner GP, Morton DC, *et al.* (2007) Regional ecosystem structure and function: ecological insights from remote sensing of tropical forests. *Trends in Ecology & Evolution*, **22**, 414 – 423.

Cianciaruso MV, Batalha MA, Gaston KJ, Petchey OL (2009) Including intraspecific variability in functional diversity. *Ecology*, **90**, 81–89.

Fawcett D, Verhoef W, Schläpfer D, Schneider F, Schaepman M, Damm A (2018) Advancing retrievals of surface reflectance and vegetation indices over forest ecosystems by combining imaging spectroscopy, digital object models, and 3d canopy modelling. *Remote Sensing of Environment*, **204**, 583 – 595.

Fisher RA, Koven CD, Anderegg WRL, *et al.* (2017) Vegetation demographics in Earth System Models: A review of progress and priorities. *Global Change Biology*, pp. 1–20.

Gastellu-Etchegorry JP, Yin T, Lauret N, *et al.* (2015) Discrete Anisotropic Radiative Transfer (DART 5) for Modeling Airborne and Satellite Spectroradiometer and LIDAR Acquisitions of Natural and Urban Landscapes. *Remote Sensing*, **7**, 1667–1701.

Isbell F, Craven D, Connolly J, *et al.* (2015) Biodiversity increases the resistance of ecosystem productivity to climate extremes. *Nature*, **526**, 574–577.

Isbell F, Gonzalez A, Loreau M, *et al.* (2017) Linking the influence and dependence of people on biodiversity across scales. *Nature*, **546**, 65–72.

Jetz W, Cavender-Bares J, Pavlick R, *et al.* (2016) Monitoring plant functional diversity from space. *Nature Plants*, **2**, 1–5.

Kükenbrink D, Schneider FD, Leiterer R, Schaepman ME, Morsdorf F (2017) Quantification of hidden canopy volume of airborne laser scanning data using a voxel traversal algorithm. *Remote Sensing of Environment*, **194**, 424 – 436.

Medvigy D, Wofsy SC, Munger JW, Hollinger DY, Moorcroft PR (2009) Mechanistic scaling of ecosystem function and dynamics in space and time: Ecosystem Demography model version 2. *Journal of Geophysical Research*, **114**, G01002.

Medvigy D, Wofsy SC, Munger JW, Moorcroft PR (2010) Responses of terrestrial ecosystems and carbon budgets to current and future environmental variability. *Proceedings of the National Academy of Sciences*, **107**, 8275–8280.

Millar CI, Stephenson NL (2015) Temperate forest health in an era of emerging megadisturbance. *Science*, **349**, 823–826.

Morsdorf F, Eck C, Zgraggen C, Imbach B, Schneider FD, Kükenbrink D (2017) Uav-based lidar acquisition for the derivation of high-resolution forest and ground information. **36**, 566–570.

Morsdorf F, Kötz B, Meier E, Itten K, Allgöwer B (2006) Estimation of LAI and fractional cover from small footprint airborne laser scanning data based on gap fraction. *Remote Sensing of Environment*, **104**, 50–61.

Morsdorf F, Kükenbrink D, Schneider FD, Abegg M, Schaepman ME (in press) Close-range laser scanning in forests - towards phphysical-based semantics across scales. *Royal Society Open Science*.

Mouchet MA, Villéger S, Mason NWH, Mouillot D (2010) Functional diversity measures: an overview of their redundancy and their ability to discriminate community assembly rules. *Functional Ecology*, **24**, 867–876.

Newnham GJ, Armston JD, Calders K, *et al.* (2015) Terrestrial laser scanning for plot-scale forest measurement. *Current Forestry Reports*, **1**, 239–251.

Petchey OL, Gaston KJ (2006) Functional diversity: back to basics and looking forward. *Ecology Letters*, **9**, 741–758.

Schaepman ME, Jehle M, Hueni A, *et al.* (2015) Advanced radiometry measurements and earth science applications with the airborne prism experiment (apex). *Remote Sensing of Environment*, **158**, 207–219.

Schaepman ME, Ustin SL, Plaza AJ, Painter TH, Verrelst J, Liang S (2009) Earth system science related imaging spectroscopy - an assessment. *Remote Sensing of Environment*, **113, Supplement 1**, S123–S137.

Schimel DS, Asner GP, Moorcroft P (2013) Observing changing ecological diversity in the anthropocene. *Frontiers in Ecology and the Environment*, **11**, 129–137.

Schneider FD, Leiterer R, Morsdorf F, Gastellu-Etchegorry JP, Lauret N, Pfeifer N, Schaepman ME (2014a) Simulating imaging spectrometer data: 3d forest modeling based on lidar and in situ data. *Remote Sensing of Environment*, **152**, 235–250.

Schneider FD, Leiterer R, Schaepman ME, Morsdorf F (2015) Canopy height and plant area index changes in a temperate forest between 2010-2014 using airborne laser scanning. In: *Proceedings of SilviLaser 2015* (eds. Durrieu S, Véga C), 14th conference on Lidar Applications for Assessing and Managing Forest Ecosystems. La Grande Motte, France.

Schneider FD, Moorcroft P, Paul-Limoges E, Morsdorf F, Guillén Escribà C, Schmid B, Schaepman ME (in preparation) Predicting diversity and productivity under climate change by combining remote sensing and forest modelling. *Global Change Biology*.

Schneider FD, Morsdorf F, Schmid B, Petchey OL, Hueni A, Schimel DS, Schaepman ME (2017) Mapping functional diversity from remotely sensed morphological and physiological forest traits. *Nature Communications*, **8**.

Schneider FD, Yin T, Gastellu-Etchegorry JP, Morsdorf F, Schaepman ME (2014b) At-sensor radiance simulation for airborne imaging spectroscopy. In: *2014 6th Workshop on Hyperspectral Image and Signal Processing: Evolution in Remote Sensing (WHISPERS)*, pp. 1–4.

Stavros N, Schimel D, Pavlick R, *et al.* (2017) Iss observations offer insights into plant function. *Nature Ecology & Evolution*, **1**, 1–4.

Torabzadeh H, Morsdorf F, Schaepman ME (2014) Fusion of imaging spectroscopy and airborne laser scanning data for characterization of forest ecosystems a review. *ISPRS Journal of Photogrammetry and Remote Sensing*, **97**, 25 – 35.

van Leeuwen M, Nieuwenhuis M (2010) Retrieval of forest structural parameters using LiDAR remote sensing. *European Journal of Forest Research*, **129**, 749–770.

Widlowski JL, Mio C, Disney M, *et al.* (2015) The fourth phase of the radiative transfer model intercomparison (RAMI) exercise: Actual canopy scenarios and conformity testing. *Remote Sensing of Environment*, **169**, 418–437.

Wulder Ma, White JC, Nelson RF, *et al.* (2012) Lidar sampling for large-area forest characterization: A review. *Remote Sensing of Environment*, **121**, 196–209.

Chapter

2

An integrative framework to optimize, compare and validate airborne laser scanning and imaging spectroscopy data

In this chapter, we present a 3D radiative transfer modeling approach to optimize, compare and validate airborne laser scanning and imaging spectroscopy data and derived products. The main article published in Schneider *et al.* (2014a) is presented in Section 2.1, introducing the main concept and providing a comparison of airborne laser scanning based forest reconstruction approaches with imaging spectrometer data. Section 2.2 extends the initial approach in order to improve the modeling of airborne data including the correct viewing geometry (Schneider *et al.*, 2014b). A further development of the 3D forest reconstruction is presented in Section 2.3, reducing the effects of laser scanning flight strip overlap and scanning geometry on the retrieval of plant area index (Schneider *et al.*, 2015). Section 2.4 shows an example of the advantage of using a coupled 3D canopy-atmosphere radiative transfer model providing information on direct and diffuse irradiation at the vegetated Earth surface (Fawcett *et al.*, 2018), whereas Section 2.5 discusses a comparison of an improved modeling scheme to measurements by the imaging spectrometer APEX (Schaepman *et al.*, 2015). Finally, the article in Section 2.6 by Morsdorf *et al.* (in press) provides an overview of new advances in close-range laser scanning, which will help to resolve some of the remaining short-comings and uncertainties of the current approach, namely the representation of small-scale structures and clumping with turbid medium voxels as well as the selection of an appropriate voxel size.

2.1 Simulating imaging spectrometer data: 3D forest modeling based on LiDAR and in situ data

Schneider, F.D., Leiterer, R., Morsdorf, F., Gastellu-Etchegorry, J.-P.,
Lauret, N., Pfeifer, N., Schaepman, M.E.

This section is based on the peer-reviewed article:
Remote Sensing of Environment, 2014 (152), 235-249
DOI:10.1016/j.rse.2014.06.015
About 70% of the research has been performed during a specialized Masters in Geography (University of Zurich).

F.D.S., R.L., F.M., and M.E.S. designed research; all authors performed research and wrote the paper,
with main contributions of F.D.S.

Remote Sensing of Environment 152 (2014) 235–250

Contents lists available at ScienceDirect

Remote Sensing of Environment

journal homepage: www.elsevier.com/locate/rse

Simulating imaging spectrometer data: 3D forest modeling based on LiDAR and in situ data

Fabian D. Schneider [a,*], Reik Leiterer [a], Felix Morsdorf [a], Jean-Philippe Gastellu-Etchegorry [b], Nicolas Lauret [b], Norbert Pfeifer [c], Michael E. Schaepman [a]

[a] Remote Sensing Laboratories, Department of Geography, University of Zurich, Winterthurerstrasse 190, CH-8057 Zurich, Switzerland
[b] Centre d'Études Spatiales de la Biosphère, Paul Sabatier University, CNES, CNRS, IRD, 18 Avenue Edouard Belin, BPI 2801, 31401 Toulouse Cedex 9, France
[c] Department of Geodesy and Geoinformation, Vienna University of Technology, Gußhausstrasse 27-29, 1040 Vienna, Austria

ARTICLE INFO

Article history:
Received 2 September 2013
Received in revised form 6 June 2014
Accepted 9 June 2014
Available online 12 July 2014

Keywords:
3D modeling
Radiative transfer
Imaging spectroscopy
At-sensor radiance
Temperate mixed forest
Canopy structure
Airborne laser scanning
Terrestrial laser scanning
Full-waveform

ABSTRACT

Remote sensing offers the potential to study forest ecosystems by providing spatially and temporally distributed information on key biophysical and biochemical variables. The estimation of biochemical constituents of leaves from remotely sensed data is of high interest revealing insight on photosynthetic processes, plant health, plant functional types, and species composition. However, upscaling leaf level observations to canopy level is not a trivial task, in particular due to the inherent structural complexity of forests. A common solution for scaling spectral information is the use of physically-based radiative transfer models. We parameterize the Discrete Anisotropic Radiative Transfer (DART) model based on airborne and in situ measurements. At-sensor radiances were simulated and compared with measurements of the Airborne Prism Experiment (APEX) imaging spectrometer. The study was performed on the Laegern site (47°28′43.0 N, 8°21′53.2 E, Switzerland), a temperate mixed forest characterized by steep slopes, a heterogeneous spectral background, and a high species diversity. Particularly the accurate 3D modeling of the complex canopy architecture is crucial to understand the interaction of photons with the vegetation canopy and its background. Two turbid medium based forest reconstruction approaches were developed and compared; namely based on a voxel grid and based on individual tree detection. Our study shows that the voxel grid based reconstruction yields better results. When using a pixel-wise comparison with the imaging spectrometer data, the voxel grid approach performed better ($R^2 = 0.48$, λ780 nm) than the individual tree approach ($R^2 = 0.34$, λ780 nm). Spatial patterns as compared to APEX data were similar, whereas absolute radiance values differed slightly, depending on wavelength. We provide a successful representation of a 3D radiative regime of a temperate mixed forest, suitable to simulate most spectral and spatial features of imaging spectrometer data. Limitations of the approach include the high spectral variability of leaf optical properties between and within species, which will be further addressed. The results also reveal the need of more accurate parameterizations of small-scale structures, such as needle clumping at shoot level as well as leaf angle.

1. Introduction

Remote sensing offers the potential to provide spatially and temporally distributed information on key biophysical and biochemical variables of forest ecosystems. The estimation of pigment composition (e.g., chlorophyll, carotenoids, anthocyanins) and non-pigment constituents (water, nitrogen, cellulose, lignin) of leaves from remotely sensed data is of high interest revealing insight on photosynthetic processes, plant health, plant functional types, and species composition (Kokaly, Asner, Ollinger, Martin, & Wessman, 2009; Schaepman et al., 2009; Ustin et al., 2009). However, to relate observations at the landscape or stand level to the leaf level remains difficult and requires the inclusion of advanced scaling methods (Malenovský et al., 2007).

Leaf optical properties (LOP) are a function of leaf structure, water content, and biochemical composition and represent only the leaf component contributing to the overall spectral reflectance of a forest canopy. But canopy reflectance is also a function of woody elements, canopy background (understory and soils), canopy structure, illumination conditions, and viewing geometry (Asner, 1998; Goel, 1988; Ollinger, 2011; Verrelst, Schaepman, Malenovský, & Clevers, 2010). Neglecting or simplifying of these components can lead to misinterpretation of the remotely sensed signal (e.g., Knyazikhin et al., 2013; Townsend, Serbin, Kruger, & Gamon, 2013). Hence, there is a need to improve our understanding of the physical processes within the radiative regime of a forest and to identify model and observational

* Corresponding author. Tel.: +41 44 63551 61; fax: +41 44 635 68 46.
E-mail addresses: fabian-daniel.schneider@geo.uzh.ch (F.D. Schneider), reik.leiterer@geo.uzh.ch (R. Leiterer), felix.morsdorf@geo.uzh.ch (F. Morsdorf), jean-philippe.gastellu-etchegorry@cesbio.cnes.fr (J.-P. Gastellu-Etchegorry), nicolas.lauret@cesbio.cnes.fr (N. Lauret), norbert.pfeifer@geo.tuwien.ac.at (N. Pfeifer), michael.schaepman@geo.uzh.ch (M.E. Schaepman).

http://dx.doi.org/10.1016/j.rse.2014.06.015
0034-4257/

limitations. This can be achieved by comparing earth observation data with data, which is simulated using radiative transfer (RT) models in forward simulation mode to scale from leaf to sensor level.

RT models are physical models capable of describing the interaction of photons with the vegetation canopy and its background (Jacquemoud et al., 2009; Niemann, Quinn, Goodenough, Visintini, & Loos, 2012). One-dimensional (1D) models usually describe the canopy as a homogeneous turbid medium of randomly distributed infinitesimally small leaf elements (Monis & Saeki, 1953). These simple models were widely used in homogeneous vegetation stands, coupled with leaf RT models, and extended using multi-layered approaches (Jacquemoud et al., 2009). However, when modeling complex heterogeneous forest canopies with all their radiative processes, including multiple scattering or mutual shading, usually three-dimensional (3D) radiative transfer models are used (Koetz et al., 2004). 3D RT models describe the canopy architecture using individual three-dimensional volume elements (voxels), which are filled with smaller scale vegetation architectural features (such as stems, branches and leaves) and characterized by LOP, leaf area index (LAI), and leaf angle distribution (LAD). Finally, the coupling with an atmospheric model enables the simulation of a variety of illumination and observation angles, as well as different sensor configurations (Gastellu-Etchegorry, Grau, & Lauret, 2012).

A number of 3D radiative transfer models have been developed for this purpose, including FLIGHT (North, 1996), FLAIR (White, Miller, & Chen, 2001), and DART (Gastellu-Etchegorry, Demarez, Pinel, & Zagolski, 1996; Gastellu-Etchegorry et al., 2012). For example, Malenovský et al. (2008) and Verrelst et al. (2010) investigated the influence of woody elements on canopy reflectance using the DART and FLIGHT models, respectively. They used extensive field measurements to parameterize the 3D model environments and compared their results to high resolution imaging spectrometer data. However, both studies focused only on coniferous forest stands. Similar RT-based studies have not been carried out on temperate mixed forests, particularly with a forest architecture derived from airborne laser scanning (ALS) data. The use of ALS data is important, since the 3D heterogeneity of architectural forest properties is usually simplified in models, even though they play a critical role in reflectance simulations (Wang & Li, 2013).

A complete parameterization of the 3D canopy architecture remains challenging, but recent developments in light detection and ranging (LiDAR) offer new possibilities for area-wide retrieval of forest structural variables (van Leeuwen & Nieuwenhuis, 2010; Wulder et al., 2012). Full-waveform scanners allow us to detect multiple echoes from a single laser pulse and describe scattering properties with physical variables such as intensity and echo-width (Wagner, Hollaus, Briese, & Ducic, 2008; Wagner, Ullrich, Ducic, Melzer, & Studnicka, 2006). The resulting 3D point cloud can be used for individual tree detection in forests (Kaartinen et al., 2012; Morsdorf et al., 2004). Besides, attempts are made to estimate LAI from first and last returns based on gap fraction theory (Morsdorf, Kötz, Meier, Itten, & Allgöwer, 2006; Solberg et al., 2009) and more recently from multiple returns (Fleck et al., 2012). Terrestrial laser scanning (TLS) offers higher spatial resolution for retrieving forest structural parameters (Yang et al., 2013) or reconstructing single tree models (Eysn et al., 2013). However, TLS are restricted to field plot acquisitions and cannot cover larger areas, as compared to capabilities of ALS.

1.1. Aim and research objectives

In this paper, we model imaging spectrometer data using a forward simulation based on a 3D RT model with extensive in-situ measurements as well as ALS data and compare the model results with an imaging spectrometer data acquisition. The model is applied to a temperate mixed forest with a complex canopy structure. To model the canopy architecture, two approaches are compared: an individual tree based reconstruction and a voxel grid approach. Both approaches were fully parameterized using ALS data. The study made use of extensive in situ measurements, including TLS, spectral measurements of LOPs and background spectra originating from litter, mosses, and low growing vegetation. The Discrete Anisotropic Radiative Transfer (DART) model was used as 3D RT model (Gastellu-Etchegorry et al., 2012). The spectral bands were simulated and compared with the Airborne Prism Experiment (APEX) imaging spectrometer (Jehle et al., 2010).

The ultimate goal of this study is – once the RT model is fully parameterized – to inversely retrieve a set of variables from observations using look-up tables (LUTs), artificial neural networks (ANNs) (Vohland, Mader, & Dorigo, 2010), or direct radiance based approaches (Laurent, Verhoef, Clevers, & Schaepman, 2011b). However, the usually large number of free model parameters, model uncertainties, as well as instrument performance limitations and cross-correlations between adjacent bands of imaging spectrometer data acquisitions are limiting the applicability of such model inversions (Atzberger & Richter, 2012; Schaepman, 2009). Forward modeling is therefore a key requirement enabling to identify model and observational limitations, to finally better understand underlying physical processes, and provide relevant information for validation and calibration purposes.

2. Materials

2.1. Study area

The study area is a temperate mixed forest located on the south-facing slope of the Laegern mountain northwest of Zurich, Switzerland. It is an old-growth forest, characterized by high species diversity and a complex (i.e., multilayered) canopy structure. Mature beech (*Fagus sylvatica*) and Norway spruce (*Picea abies*) trees are predominant, growing on steep slopes with heterogeneous spectral background. A detailed description of the forest and environmental conditions can be found in Eugster et al. (2007).

The main scene covers an area of 300 × 300 m and is centered at 2 669 810 E, 1 259 060 N (CH1903+ LV95) ranging from 620 to 810 m above sea level (a.s.l.). It comprises a long-term forest ecosystem research site (LWF) of the Swiss Federal Institute for Forest, Snow and Landscape Research (WSL) established in 2012 and a flux tower equipped with measurement units of FLUXNET (Baldocchi et al., 2001), AERONET (Holben et al., 1998), and the Swiss National Air Pollution Monitoring Network (NABEL).

Two subplots labeled S1 and S2 were defined within the main scene as representative sampling units of 40 × 40 m. S1 is located in the eastern part of the scene centered at 2 669 846 E, 1 259 040 N on 672 m a.s.l. It is covered by coniferous trees (*P. abies*, *Abies alba*) and deciduous trees (*Fraxinus excelsior*, *F. sylvatica*) in roughly equal parts. S2 is located in the western part of the scene centered at 2 669 690 E, 1 259 070 N on 701 m a.s.l. It represents a closed deciduous canopy mainly consisting of large beech trees and some smaller maple and ash trees (*Acer pseudoplatanus*, *F. excelsior*).

2.2. Field data

Deciduous leaves were collected at the Laegern site from ten individual trees of five species (*A. pseudoplatanus*, *F. excelsior*, *F. sylvatica*, *Ulmus glabra*, *Tilia platyphyllos*) on June 24th, 2009. To represent the vertical variability of leaf optical properties, leaf samples were taken from the upper, middle, and lower part of the crown representing sunlit, transitional, and shaded light conditions. Hemispherical–conical reflectance (HCRF, terminology following Schaepman-Strub, Schaepman, Painter, Dangel, & Martonchik, 2006) and transmittance were measured in the laboratory at three positions on the abaxial and adaxial side of the leaf. The measurements were performed using an integrating sphere coupled to a field spectroradiometer (ASD FieldSpec 3, Analytical Spectral Devices, USA). Spectral measurements of needle samples were available from an even-aged Norway spruce monoculture in the Šumava National Park, Czech Republic. Shoots of current year and

third year age classes were sampled from sunlit, transitional, and shaded parts of twelve mature trees. Needles were detached in the laboratory and immediately measured following Yáñez-Rausell, Malenovský, Clevers, and Schaepman (2014a), Yáñez-Rausell, Schaepman, Clevers, and Malenovský (2014b) and Rautiainen et al. (2012). The sampled trees were of the same species, growing under comparable environmental conditions, and having similar age and crown dimensions than the Norway spruce trees at the Laegern site.

Dominant ground components (leaf litter, needle litter, bare soil, rock, gravel, moss, understory vegetation up to 50 cm) and bark samples (beech, spruce, pine bark) were measured in the field using a field spectroradiometer (ASD FieldSpec Pro). However, certain background was either located in shaded areas or suffered from substantial adjacency effects due to the proximity of large trees and a generally dense canopy. In such cases, the material was removed and measured under direct solar illumination or in the laboratory. Digital hemispherical photographs (DHPs) were taken under leaf on conditions at the two subplots S1 and S2 following the VALERI sampling scheme (Baret et al., 2003). True and effective plant area index (PAI) and the average leaf angle (ALA) were subsequently derived following (Weiss, Baret, Smith, Jonckheere, & Coppin, 2004). Measurements of aerosol optical depth (AOD) and precipitable amount of water (PAW) were provided by the aerosol robotic network (AERONET) as level 2.0 quality-assured data (Holben et al., 1998).

2.3. LiDAR data

Two independent helicopter-based ALS data acquisition flights were carried out above the Laegern site in 2010. The measurements were performed using an airborne scanner system with a rotating mirror (scan angle ± 15°). The first dataset was acquired on April 10th under leaf-off conditions (RIEGL LMS-Q560, RIEGL Laser Measurement Systems GmbH, Austria), whereas the leaf-on measurements were performed on August 1st (RIEGL LMS-Q680i). Both campaigns were flown with a nominal height of 500 m above ground and a beam divergence of approximately 0.5 mrad resulting in a footprint size of 0.25 m. The wavelength of the laser was 1550 nm. A flight strip overlap of approximately 50% finally leads to a mean point density of 20 m^{-2} in the leaf-off and 40 m^{-2} in the leaf-on dataset. The ALS data was registered to the Swiss national grid CH1903+. The positional accuracy of the ALS data was <0.15 m in vertical and <0.5 m in horizontal direction, as estimated using six terrestrially surveyed rooftops distributed over the entire area.

For each laser pulse, the full waveform was recorded with a sampling interval of 1 ns. Gaussian pulse estimation was used to decompose the waveform in order to obtain range, maximum amplitude, and width of each detected echo, which in turn enabled the computation of physical properties such as the intensity, and by deconvolution, the cross-section (Wagner et al., 2008, 2006). This procedure allowed us to annotate the 3D point cloud with these attributes and subsequently also each scattering object present within the ALS footprint (Mallet & Bretar, 2009).

TLS measurements were performed under nearly windless conditions on the two subplots S1 and S2 using a terrestrial laser scanner (Z + F Imager 5006i, Zoller und Fröhlich GmbH, Germany). The scanner covers almost the whole sphere (320° by 360°) by rotating 320° in zenithal (vertical) and 180° in azimuthal (horizontal) direction. For relative orientation and georeferencing of the 11 scans in S1 and the 13 scans in S2, five planar and 33 spherical targets were placed across the plots. The mean relative deviation between the individual scan positions was below 5 mm, estimated from the overlap between the scans, whereas the absolute positioning according to fixed points of the Swiss national survey was below 15 cm, estimated from total station measurements.

2.4. Imaging spectrometer data

Imaging spectrometer data was acquired on June 16th, 2012 at 10:26 UTC under clear sky conditions using the APEX imaging spectrometer (Jehle et al., 2010). The Laegern site was covered by a single flight line with an off-nadir angle between 3.8° and 9.7°. Illumination and observation geometries at scene center are provided in Table 2. The average flight altitude was 4526 m a.s.l. resulting in a ground pixel size of 2 m. APEX recorded 299 spectral bands ranging from 376 nm to 2502 nm. The spectral sampling interval (SSI) varied between 2.5 nm and 13.9 nm and the full width at half maximum (FWHM) between 3.4 nm and 14.3 nm depending on wavelength.

Data preprocessing included traceable radiometric calibration, including compensation for spatial coregistration effects of the VNIR and SWIR detector, dark current and keystone correction (D'Odorico, Guanter, Schaepman, & Schläpfer, 2011; Hueni, Lenhard, Baumgartner, & Schaepman, 2013). The uncertainty of calibrated radiance values was lying within 0.5% and 3% in the range of 400 to 1900 nm and increasing subsequently up to 10% at 2400 nm. The noise equivalent detection limit of APEX was in the range of 0.5–1.0 mW m^{-2} nm^{-1} sr^{-1} (Schläpfer & Schaepman, 2002). APEX data was georeferenced to the Swiss national grid CH1903+ and orthorectified using the nearest neighbor resampling in PARGE (Schläpfer & Richter, 2002; Schläpfer, Schaepman, & Itten, 1998). The geocorrection was based on the digital terrain model DHM25 of the Swiss Federal Office of Topography (Swisstopo, Switzerland).

3. Methods

3.1. Optical properties

Leaf optical properties were calculated for deciduous and coniferous trees. Since tree specific information about species or needle age classes were not available, a linear spectral forward mixing was applied to calculate the reflectance and transmittance spectra of sunlit, transitional, and shaded leaves and needles. The measured values were lying in the same range as literature based data (Combes et al., 2007; Wang & Li, 2012). Thus, the spectral measurements were used directly instead of using a forward run of the leaf optical properties model PROSPECT (Jacquemoud & Baret, 1990) to reduce the number of model parameters and possible model uncertainties. The broadleaf species composition used for spectral mixing was derived from forest inventory data of 617 trees: 50.8% beech, 19% maple, 10.7% elm, 10.5% linden and 9% ash. The composition of needle age classes was based on Lukeš, Rautiainen, Stenberg, and Malenovský (2011), summarized in Table 1.

The spectra of the four main classes of canopy background were based on the in situ spectrometer measurements. Understory vegetation up to 50 cm was defined being a mixture of 90% grass and shrubs and 10% mosses, unvegetated ground consisted of $\frac{2}{3}$ bare soil and $\frac{1}{3}$ gravel, whereas litter was composed of 85% leaf litter and 15% needle litter. Leaf spectra of the lowest crown layers were assigned to understory vegetation of 0.5 m up to 3 m. The composition of background components was determined from an inventory of forest floor characteristics and compared to a stratified plant sociological classification.

Table 1
Composition of needle age classes per crown layer.

Crown layer	First year needles	Third year needles
Top	41.5%	58.5%
Middle	13.6%	86.4%
Bottom	1.7%	98.3%

3.2. 3D forest reconstruction

3.2.1. Canopy background

The digital terrain model (DTM) was derived from ALS ground returns, which were extracted using an adaptive multi-scale algorithm based on (Evans & Hudak, 2007). An iterative filter process was used to select the ground return echoes and distinguish between height deviations caused by steep terrain and artificial objects or dense vegetation. The remaining points were interpolated to a 1 × 1 m DTM applying ordinary kriging.

Additionally, a classification of the four main classes of canopy background (see Section 3.1) was created from the ALS data. The classification was done on 1 × 1 m grid cells by investigating the point distribution, leaf-on to leaf-off variations, and quantitative statistical measures of the full-waveform variables within the vertical column of each cell (Leiterer, Mücke, Hollaus, Pfeifer, & Schaepman, 2013). Both DTM as well as ground cover classification were finally resampled to 2 × 2 m resolution for radiative transfer modeling. A majority resampling technique was used to remove single, misclassified pixels and match the spatial resolution of APEX.

3.2.2. Individual tree detection

To geometrically reconstruct the forest scene, the ALS point cloud was clustered into groups of ALS echoes presumably being reflected from a single tree. The clustering was based on the method described in Morsdorf et al. (2004) and compared to other methods in Kaartinen et al. (2012). Tree height and crown base height could be directly derived from the ALS returns of each cluster. Additionally, alpha shapes were calculated to derive crown specific metrics such as crown volume, projection area, and diameter in NS and WE direction (Vauhkonen, Tokola, Packalen, & Maltamo, 2009). Together with the tree positions, these crown variables were used to parameterize the geometric primitives (ellipsoids for deciduous trees, truncated cones for coniferous trees) used in radiative transfer modeling.

To distinguish deciduous from coniferous trees, within crown variations of the point distribution between leaf-on and leaf-off acquisitions were assessed. A tree was classified as deciduous, if the percentage of points lying in the uppermost 6 m of the crown was varying more than 5% between leaf-on and leaf-off acquisitions or if it was smaller than 10 m. Otherwise, it was classified as coniferous tree.

Besides the crown geometry, the PAI was determined for each tree. The mean PAI of the in situ measurements was taken as a reference, assuming it to be representative for the whole scene. However, it was not the same PAI assigned to all the trees, because there was a high variability of crown densities within the forest scene. Therefore, a vegetation ratio was calculated for each tree based on Morsdorf et al. (2006) and Lindberg, Olofsson, Holmgren, and Olsson (2012):

$$r_{veg} = \frac{\sum e_{veg}}{\sum e_{total}}, \tag{1}$$

where e_{total} are echoes within the projection area of the tree and $e_{veg} = e_{total} > 3$ m above ground. The vegetation ratio r_{veg} was calculated on the leaf-on dataset to relatively distribute the PAI to the individual trees of the scene. The mean PAI of all trees was kept constant. Each crown was divided into three equally thick vertical layers (Fig. 1). The layering was introduced to assign different optical properties according to the differing light conditions within the crown. Additionally, a weight – calculated based on the vertical distribution of ALS points within the crown – was applied on the tree PAI for each crown layer to account for the vertical heterogeneity in the distribution of plant material.

3.2.3. Voxel grid parameterization

Instead of extracting individual trees, it is possible to directly derive a 3D voxel grid of PAI or plant area density (PAD) values from the ALS point cloud. Especially in a dense mixed forest, it is often difficult to separate individual trees from each other and approximating the crown shapes by ellipsoids or cones may be oversimplifying. Therefore, the voxel grid approach offers a way to model the 3D canopy architecture of a forest independently of pre-defined crown shapes.

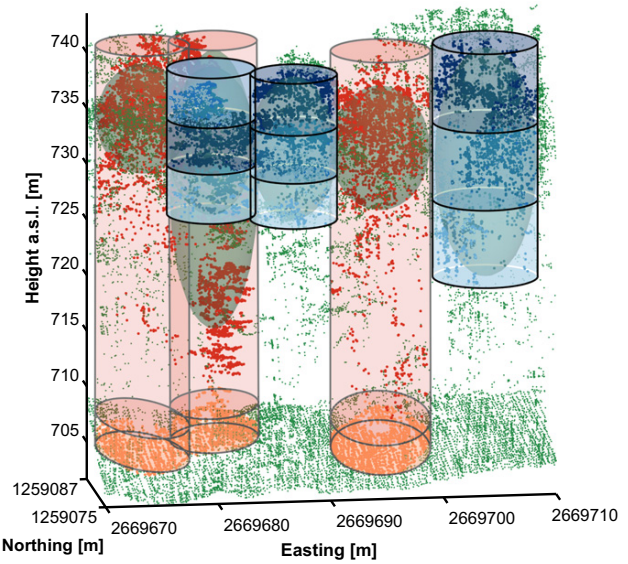

Fig. 1. Visualization of the vegetation ratio and the vertical crown layers, derived from the ALS point cloud. The vegetation ratio was calculated by dividing the number of vegetation points (red) by the total number of points (red + orange). The three vertical crown layers are marked blue, whereas the darker color indicates a higher point density.

The first step to derive the voxel grid was to calculate the PAI over the whole scene on 2 × 2 m grid cells. The PAI was calculated from leaf-on canopy and ground echoes in the vertical column of each cell based on Solberg et al. (2009), modified after Fleck et al. (2012):

$$PAI = c \cdot ln\left(\frac{1 \cdot t_1 + \frac{1}{2} \cdot t_2 + \frac{1}{3} \cdot t_3 + \ldots + \frac{1}{7} \cdot t_7}{1 \cdot g_1 + \frac{1}{2} \cdot g_2 + \frac{1}{3} \cdot g_3 + \ldots + \frac{1}{7} \cdot g_7}\right), \tag{2}$$

where t_1, t_2, t_3, …, t_7 are the total number of echoes within the vertical column of pulses with 1, 2, 3, …, 7 returns and g_1, g_2, g_3, …, g_7 are the number of ground echoes of pulses with 1, 2, 3, …, 7 returns respectively. Ground echoes were defined as echoes below 2 m above ground. The calibration factor c was derived by solving Eq. (2) for c and replacing PAI by PAI_{local}, which is the true PAI measured in situ under leaf-on conditions. Two calibration factors were calculated this way on subplots S1 and S2 and averaged for the use in Eq. (2). In very dense parts of the forest, it can happen that there are no ground echoes at all. In these situations, there will be a saturation of the PAI retrieval. Therefore, the denominator of zero was replaced by the smallest possible value greater than zero (e.g., being $\frac{1}{7}$ with a maximum number of 7 returns per shot).

In a second step, the vertical distribution of plant material had to be determined by the analysis of the ALS point cloud of leaf-on and leaf-off acquisitions. Starting from the lowest point of the scene, each vertical column was divided into 2 × 2 × 2 m sized voxels. The percentage of points in a voxel was calculated with respect to the total amount of points in the vertical column. The PAI of each voxel was then calculated accordingly, assuming that the vertical point distribution represented the canopy architecture.

A discrimination of coniferous and deciduous trees was applied on the 2 × 2 m grid as described in Section 3.2.2. Furthermore, three vertical crown layers were defined according to the vertical plant area distribution in the 3D voxel grid. 50% of plant material was defined to be in the upper most layer of the canopy and 25% in the lower two layers each. Therefore, most of the light is intercepted within the upper most

sunlit layer, whereas the relative light transmission to the transitional and shaded layers can be less than 30% depending on the clumping of leaves or needles (Niinemets, 2009).

3.3. Radiative transfer model parameterization

The radiative transfer model used in this study was the DART model (DART v5.4.3). DART simulates three-dimensional heterogeneous landscapes in three operating modes: flux tracking, LiDAR, and Monte Carlo. Generally, a DART scene is built out of voxels with a predefined size. To simulate vegetation such as grass or tree crowns, voxels can be filled by turbid media parameterized by volume density, angular distribution, and optical properties. Moreover, DART offers the possibility to import detailed 3D models consisting of triangles with individual optical properties. A DART voxel can include vegetation turbid media as well as triangles with an arbitrary size, independent of the voxel size. In ray tracing, two types of radiation interaction are simulated: volume interaction within turbid voxels (Gastellu-Etchegorry, Martin, & Gascon, 2004), and surface interaction on triangles (Gastellu-Etchegorry, 2008). Further details of the DART model and examples of DART simulations can be found in Gastellu-Etchegorry et al. (2012).

Here, flux tracking was used in reflectance mode with the sun and the atmosphere as the only radiation sources. Optical properties described in Section 3.1 and the forest reconstruction described in Section 3.2 were used to parameterize the forest canopy, background, and terrain in DART. The established approach to simulate trees in DART is to use predefined crown shapes (e.g., ellipsoids, cones) filled by turbid media, which are voxelized internally by DART. Whereas most previous studies used generalized tree crowns and positioning of trees (e.g., Barbier, Couteron, Proisy, Malhi, & Gastellu-Etchegorry, 2010; Malenovský et al., 2013, 2008), every single tree was parameterized individually in this study as described in Section 3.2.2. This is called the individual tree approach. Additionally, a new approach was developed to directly parameterize the DART model from a voxel grid. The parameterization of the voxel grid is described in Section 3.2.3 and now referred to as voxel grid approach.

For both the individual tree and voxel grid approach, turbid media were used to model the vegetation volumes. Their leaf angle distribution was assumed to be spherical for coniferous trees, whereas the plagiophile distribution function was better suited to describe the LAD of broadleaved trees (terminology following de Wit, 1965). The decision to choose the plagiophile LAD was based on the average leaf angle of 45° measured at subplot S2 and supported by the findings of Pisek, Sonnentag, Richardson, and Mõttus (2013).

Neither tree trunks nor branches were explicitly included in the model due to the lack of measurements over the whole scene. To study the effect of neglecting woody elements, over 70 geometrical models consisting of cylinders representing the stem and branches were extracted from the TLS point clouds on subplots S1 and S2. The tree skeletons together with the diameter of the stems and branches, thus cylinders, were digitized semi-automatically in the individual scans presented to the operator as range images. While manual interaction is required, the approach is robust in the presence of occlusions, registration errors, and wind (Eysn et al., 2013). After triangulation of the cylinders, the models of stems and branches can be added to the DART scene as 3D triangle meshes. Interactions of rays with woody elements are hence simulated on the basis of individual triangles, which are described by the optical properties of the bark.

To simulate the atmosphere, DART can be used with standard gas and aerosol models as contained in MODTRAN (Berstein & Roberston, 1989). We used the mid-latitude summer gas model and the rural aerosol model with a visibility of 23 km as a reference. The gas and aerosol models were then modified to meet the atmospheric conditions during the APEX overflight. Aerosol optical depth was adjusted based on the local measurement of the AERONET station at seven wavelengths (340, 380, 440, 500, 675, 870, 1020 nm). Besides the water vapor data provided by AERONET, the measurements of Rayleigh scattering were used to finalize the atmosphere parameterization. Sensor height, solar and viewing geometry were set according to the sun–earth-sensor geometries of the date and time of the APEX acquisition. The main model parameters of the 300 × 300 m scene are summarized in Table 2.

3.4. DART simulations

DART simulates images of radiance or reflectance at the top of canopy (TOC), top of atmosphere (TOA), and sensor altitude. For best comparability, the at-sensor radiance orthoimage was used as the main output. An orthoimage is the 2D distribution of radiance values for each pixel (x,y) and a given view direction (θ_v, ϕ_v). In order to create orthoimages, DART stores each radiative flux $\Phi_v(x, y, z, \theta_v, \phi_v)$ that exits the vertical column (x,y) reaching the top of canopy level. Radiance of the orthoimage at pixel x,y for any view direction (θ_v, ϕ_v) is (terminology following Schaepman-Strub et al., 2006):

$$L(x,y) = \frac{\sum_i \Phi_v(x,y,z_i,\theta_v,\phi_v)}{A_{xy} \cdot \cos\theta_v \cdot \omega_v}, \quad (3)$$

where $\sum_i \Phi_v(x, y, z_i, \theta_v, \phi_v)$ is the sum of all DART fluxes leaving the column (x,y) reaching the TOC level, A_{xy} is the area of pixel (x,y) and ω_v is the solid angle associated to direction (θ_v, ϕ_v). The angles θ_v, ϕ_v and ω_v depend on the horizontal location (x,y) and also on the vertical location z_i associated to each flux that leaves the column (x,y) towards the sensor. Both the geometric representation in DART as well as the projection of the APEX data were based on the Swiss national grid CH1903+. The pixel size of 2 × 2 m was chosen to exactly match the spatial resolution of the projected APEX data.

Table 2
Main model parameters of the 300 × 300 m scene with individual trees.

Scene parameters			
Scene dimension in x,y	[m]		300 × 300
Voxel size in x,y,z	[m]		2 × 2 × 2
Altitude at scene center	[m]		680.4
Solar geometry (at scene center)			
Zenith angle θ_s	[°]		27.1
Azimuth angle ϕ_s	[°]		147.4[a]
Viewing geometry (at scene center)			
Zenith angle θ_v	[°]		6.76
Azimuth angle ϕ_v	[°]		331.8[a]
Individual trees		Deciduous	Coniferous
Number of trees	[]	1526	312
PAI range	[m^2/m^2]	2.1–5.5	3.2–5.5
LAD		Plagiophile	Spherical
Tree height range	[m]	7.2–48.9	11.4–47.8
Atmosphere parameters			
Sensor altitude	[m a.s.l.]		4526
Aerosol optical depth	[]	λ500 nm	0.15495[b]
Rayleigh optical depth	[]	λ500 nm	0.14321[b]
Precipitable water	[cm]		2.37849[b]
DART specific parameters			
Number of directions[c]	[]		100
Number of cell subcenters	[]		400
Propagation threshold	[W m^{-2} sr^{-1}]		0.0001

[a] From north clockwise.
[b] At sea level.
[c] Yin, Gastellu-Etchegorry, Lauret, Grau, and Rubio (2013).

Simulations were carried out for 281 bands on the two subplots S1 and S2 to cover the full spectral range of 400 to 2400 nm, whereas the whole 300 × 300 m scene was simulated with four selected wavelengths (533, 570, 680, 780 nm), allowing a distinct set of vegetation indices (PRI, NDVI) to be calculated. The simulations on the large scene and the two subscenes were once performed using the voxel grid approach and once using the individual tree approach. The other parameters were kept constant. The DART simulations are summarized in Table 3. Simulation time for 281 bands at subplot level (S1, S2) was 20 h, whereas the simulation of a single band at the scene level (300 × 300 m) took 21 h on a fast computer (6-core processor, 32 GB RAM). In the future, this constraint will be reduced by a multi-threading approach being implemented in the upcoming DART version (v5.4.7).

To be able to interpret the results, additional simulations were carried out on the two subplots S1 and S2 (see Table 3). For this, the parameterized DART scene based on the voxel grid was used as reference. To study the effect of neglecting woody elements, simulations with detailed 3D models of trunks and branches were carried out on S1 and S2. The 3D models were added to the subplots without adapting the PAI of voxels already filled by turbid media, leading to an overestimation of the scene PAI of 6.5% and 7.6% for S1 and S2 respectively. The influence of the background on the radiative regime was examined by replacing the background classification and the corresponding spectral properties by a black 100% absorbing background, since using a black background is a common simplification in radiative transfer modeling of forests (e.g., Knyazikhin et al., 2013). Additionally, the influence of the parameters used to describe the vegetation turbid media was studied by simulating the two subplots with the minimal and maximal canopy spectra and changing PAI and LAD values.

4. Results

4.1. Optical properties

The results of the linear spectral forward mixing of the optical properties of individual species are the mean reflectance and transmittance spectra of deciduous and coniferous trees, for both adaxial and abaxial sides of sunlit, transitional, and shaded leaves and needles, respectively. The mean adaxial spectra and the minimum and maximum values, measured among individual tree species and among different measurement positions on the leaf, are presented in Fig. 2. The optical properties of background components and barks are presented in Fig. 3.

4.2. 3D forest reconstruction

4.2.1. Canopy background

The canopy background, consisting of the DTM and the background cover classification, is shown in Fig. 4. Verification of the DTM, based on absolute DTM values derived from the TLS measurements at subplots S1 and S2, shows a mean vertical deviation of ± 10 cm. The positional accuracy of the TLS derived DTM was evaluated based on 53 surveying points linked to accurately fixed control points of the Swiss national land survey. For the ground cover classification, a reference dataset derived from TLS data, field measurements, and a plant sociological classification were used to calculate accuracy measures based on Liu, Frazier, and Kumar (2007). An overall accuracy of ≈64% for all classes and a detection rate of understory vegetation of ≈89% are achieved (see Leiterer et al., 2013 for more details).

Table 3
DART simulations carried out on the whole scene (300 × 300 m) and subplots S1 and S2 (40 × 40 m).

Scene size	Canopy	Background	Woody elements	Comments
300 × 300 m			–	4 spectral bands: 533.6 nm ± 3.9 nm 569.6 nm ± 3.0 nm 678.8 nm ± 2.2 nm 780.7 nm ± 3.2 nm
			–	
40 × 40 m			–	281 spectral bands: WVL: 400–2400 nm SSI: 2.5–13.9 nm FWHM: 3.4–14.3 nm
			–[a] 	[a]Additional simulations with a mean PAI of 3 and 7, an erectophile and planophile LAD, and minimal and maximal reflectance and transmittance of leaves and needles
		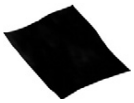		

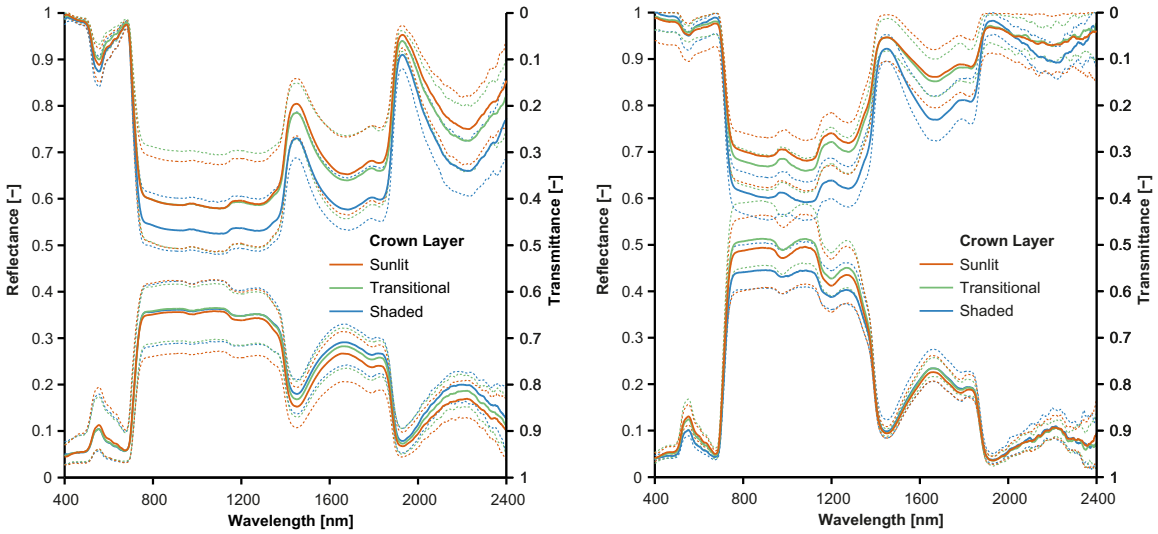

Fig. 2. Leaf optical properties of broadleaves (left) and needles (right): mean adaxial reflectance and transmittance (—) with minimum and maximum values (— —).

4.2.2. Individual tree and voxel grid parameterization

The mean PAI derived from in situ measurements at S1 and S2 is 5.05 ± 0.52 m^2 m^{-2}. This value was used as reference in the 3D forest reconstruction. The result of the individual tree approach is a 3D representation of the forest scene composed of 1526 deciduous and 312 coniferous trees. The individual trees and the PAI voxel grid of the 300 × 300 m scene are illustrated in Fig. 5. The two raster maps show the PAI values in 2D, whereas the values for the individual tree approach were derived after internal voxelization in DART.

The tree detection accuracy and the delineation of tree crown variables were assessed based on a stratified random sampling approach using TLS, orthoimages, and field-map system data. The commission and omission errors for the tree detection are 5.2% and 13.1% respectively, whereas deciduous trees are discriminated from coniferous trees with an overall accuracy of 89.7% and a Kappa coefficient of 0.74 (terminology following Liu et al., 2007). Because of sloped terrain, positional uncertainty using ALS results in a vertical tree height variation of ±1 m, as determined from the DTM and tree positions. Remaining uncertainties stemming from other error sources (e.g., underestimation of tree height as described in Morsdorf et al., 2004; Heurich, 2008) likely result in a total uncertainty up to 4 m. Crown dimensions show a high consistency using a cross-comparison with TLS measurements and orthoimages, but could not be verified quantitatively due to the complexity of the dense forest canopy.

4.3. Simulation results

4.3.1. Forest spectra

Spectrally contiguous radiance spectra (400–2400 nm) were simulated for two representative subplots S1 and S2 using the voxel grid approach. The inner 10 × 10 pixels of each plot were averaged, whereas a buffer of five pixels was disregarded due to possible boundary effects when using DART. The results of modeled mean at-sensor radiance ±

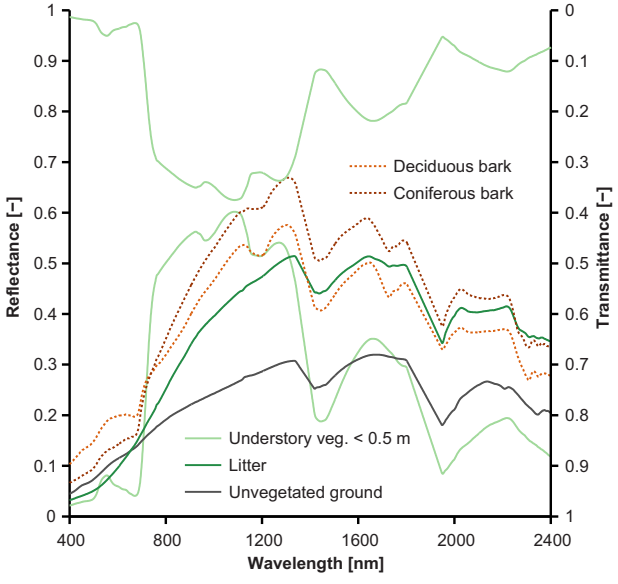

Fig. 3. Optical properties of understory vegetation up to 50 cm, litter, unvegetated ground (—) as well as deciduous and coniferous bark (— —).

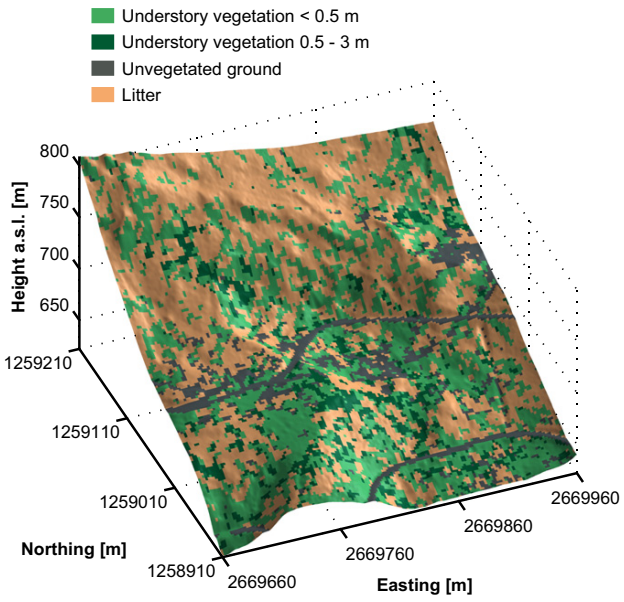

Fig. 4. Four main classes of canopy background visualized on the digital terrain model.

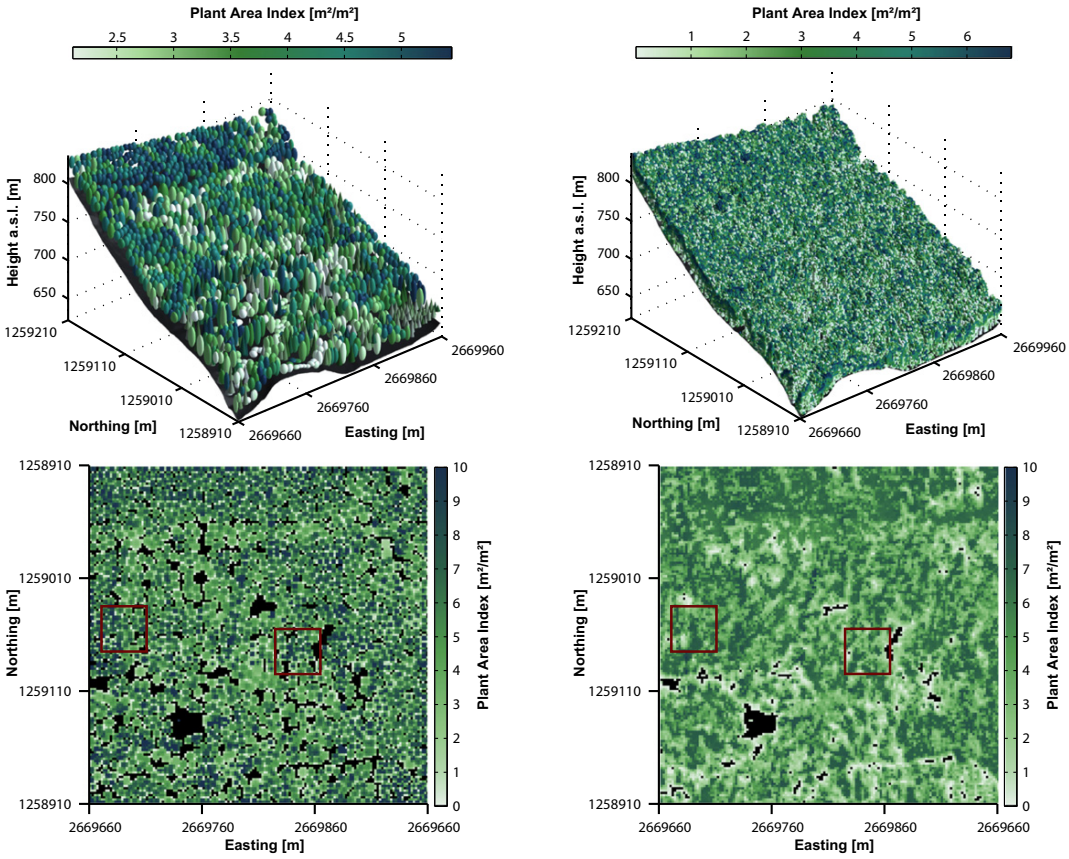

Fig. 5. Reconstruction of the forest canopy by the individual tree (left) and the voxel grid approach (right) in 3D (above) and 2D (below). The 2D raster map shows the individual tree shapes after voxelization by DART. Rectangles indicate the locations of subplots S1 and S2.

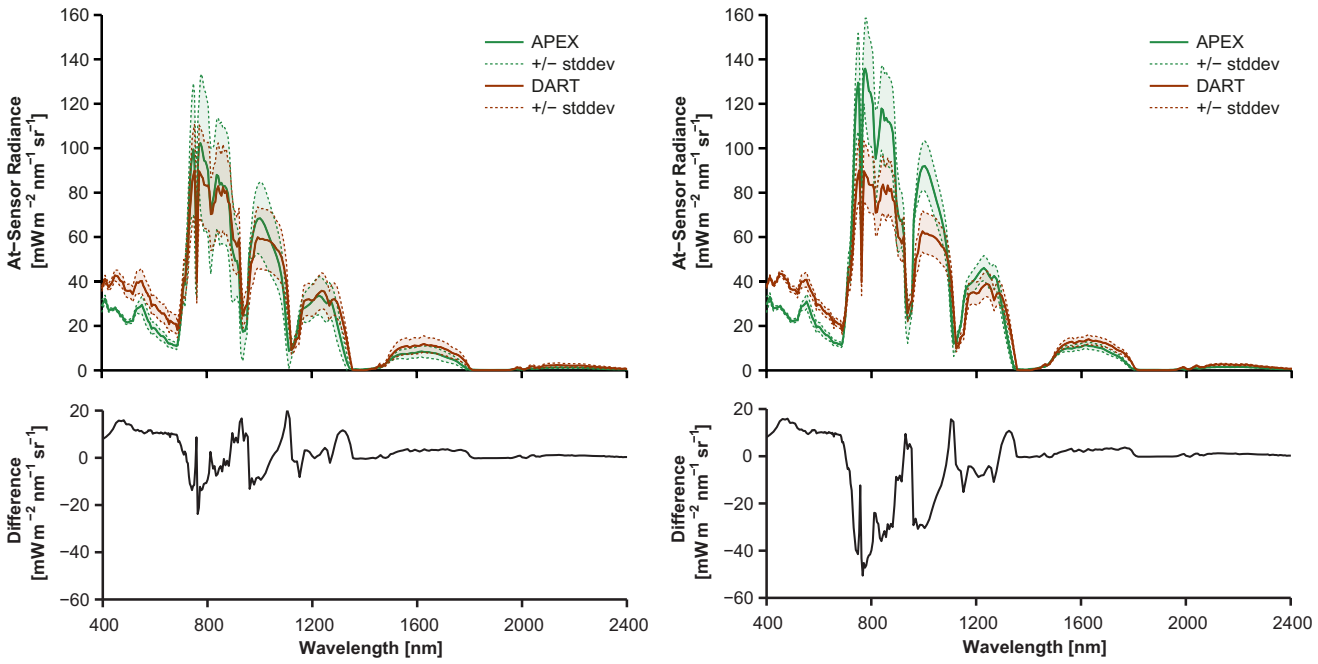

Fig. 6. Mean at-sensor radiance ± standard deviations of APEX compared to the modeled output of DART on the two subplots S1 (left) and S2 (right). Plots of 40 × 40 m were simulated using the voxel grid approach, whereas the inner 20 × 20 m was used for this comparison to avoid border effects in RT modeling. Differences are calculated by subtracting the APEX from the DART signal.

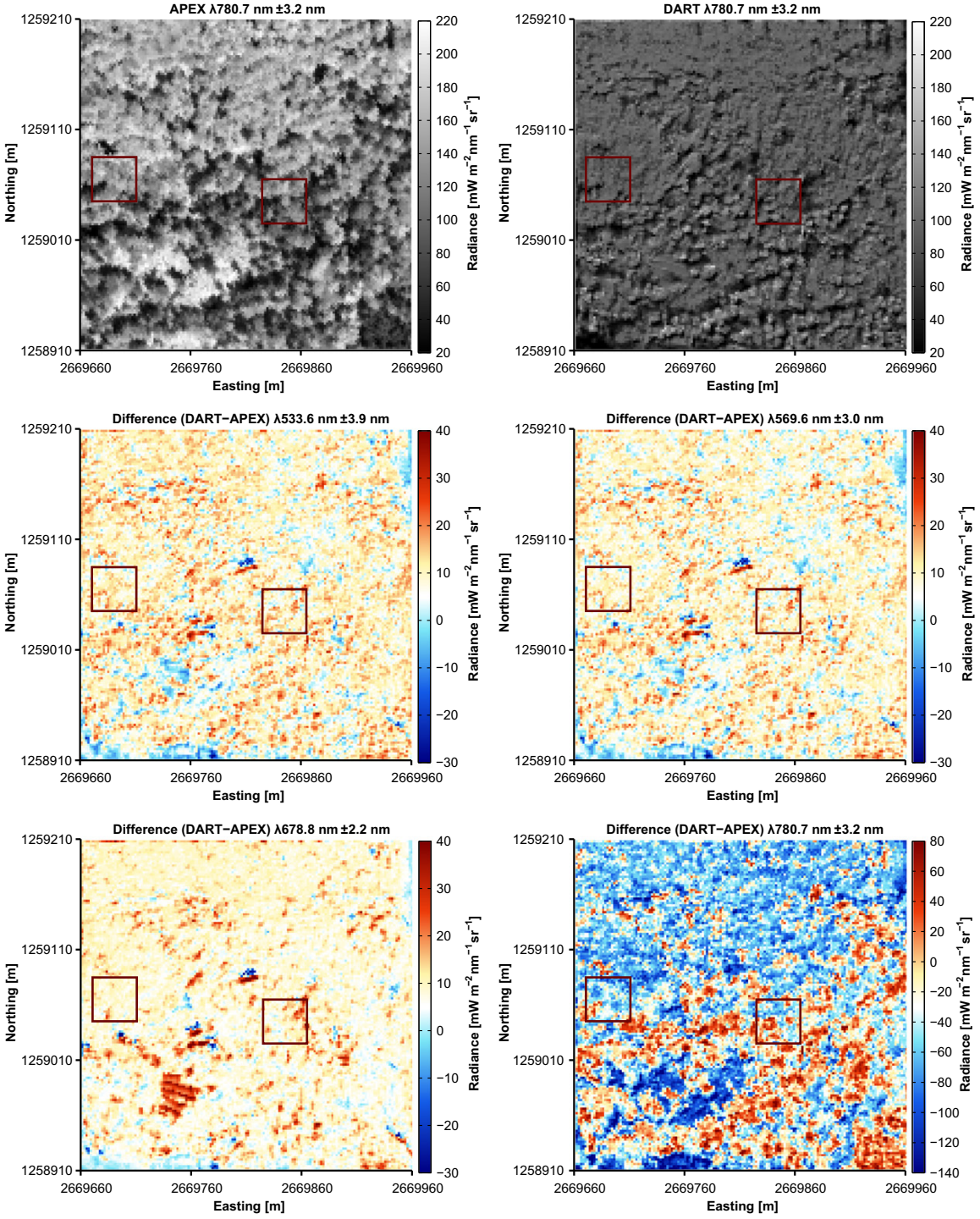

Fig. 7. Measured (APEX) and simulated (DART) remote sensing images at 780 nm and difference images at 533, 570, 680, and 780 nm. Simulations are conducted using the voxel grid approach, differences are calculated by the subtraction of the APEX from the DART image. Rectangles indicate the locations of subplots S1 and S2.

standard deviations are presented in Fig. 6. When comparing the modeled spectra to at-sensor radiances measured by APEX, we detect general overestimation in the visible spectral range (VIS, 400–700 nm) and underestimation in the near infrared (NIR, 700–1100 nm). On subplot S1, mean at-sensor radiance simulated by DART differs by 4.98 mW m^{-2} nm^{-1} sr^{-1} from APEX on average. The mean relative difference is 37.3% in the VIS, 14.6% in the NIR range, and 37.6% in the shortwave infrared (SWIR, 1100–2400 nm). On subplot S2, the differences are larger, being 8.82 mW m^{-2} nm^{-1} sr^{v1} on average due to a strong difference in the NIR range. The relative difference is 35.4% in the VIS, 35.5% in the NIR, and 34.4% in the SWIR range.

4.3.2. Airborne remote sensing images

The simulated and measured airborne remote sensing images at 780 nm and the corresponding difference images at 533, 570, 680, and 780 nm are shown in Fig. 7 using the voxel grid approach and in Fig. 8

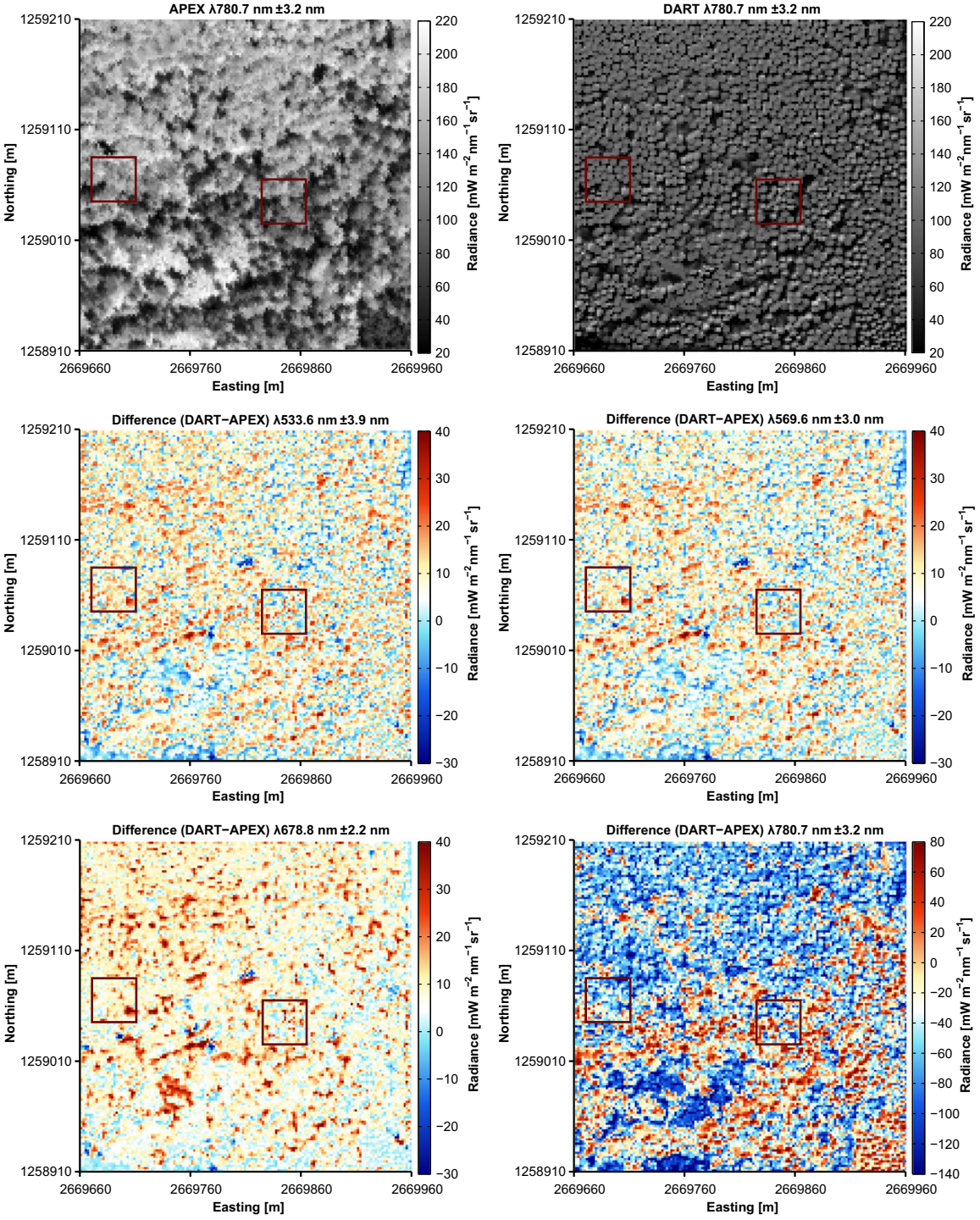

Fig. 8. Measured (APEX) and simulated (DART) remote sensing images at 780 nm and difference images at 533, 570, 680, and 780 nm. Simulations are conducted using the individual tree approach, differences are calculated by the subtraction of the APEX from the DART image. Rectangles indicate the locations of subplots S1 and S2.

using the individual tree approach. Averaging the inner 120 × 120 pixels of the difference images results in 9.41, 8.85, 9.50, and 36.65 mW m^{-2} nm^{-1} sr^{-1} mean difference at 533, 570, 680, and 780 nm respectively. A linear regression between the 120 ×120 APEX and DART pixels resulted in a coefficient of determination (R^2) of 0.55, 0.56, 0.39, and 0.48 using the voxel grid approach and 0.41, 0.41, 0.29, and 0.34 using the individual tree approach at 533, 570,680, and 780 nm.

4.3.3. Influence of scattering elements and turbid medium parameterization

The radiance spectra simulated using the individual tree approach, including woody elements, and a black background (see Table 3) were compared to the reference simulation, which itself is based on the voxel grid approach (Fig. 9). Using individual trees instead of the voxel grid approach leads to slightly smaller values in most bands. On S1, values are on average 4.6% and 6.3% smaller in the VIS and NIR

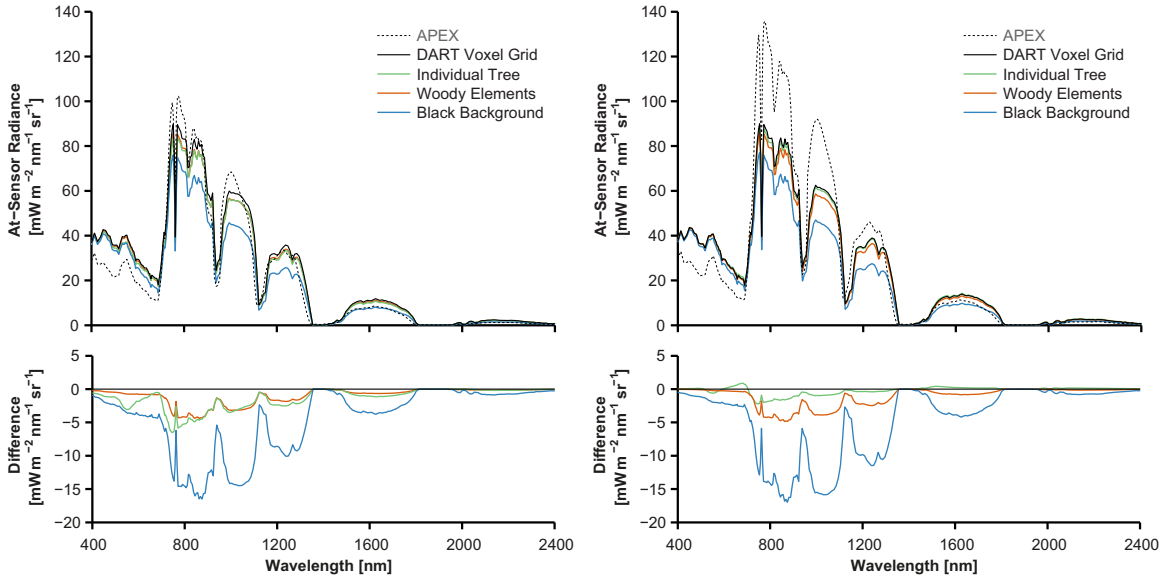

Fig. 9. Influence of the forest reconstruction approach, woody elements, and the canopy background on mean at-sensor radiance on subplots S1 (left) and S2 (right).

range. Minor differences can be observed on the structurally more homogeneous subplot S2 with differences of 1.6% and 1.9% in the VIS and NIR range. Adding woody elements to the subplots has most influence in the NIR and SWIR range with a mean difference of 4.9% and 5.7% on S1, and 5.2% and 5.3% on S2. Using a black background has a relatively strong influence in all spectral bands. The radiance is on average 13.1%, 19.9%, and 30.4% smaller in the VIS, NIR, and SWIR range on S1, whereas it is 7.6%, 19.7%, and 27.0% smaller on S2 respectively.

Turbid media scatterers as used in DART are parameterized by using PAI, LAD, and LOP. Changing the values of these parameters strongly influences the simulated at-sensor radiances as a whole as well as in each individual spectral band. The result of simulations using a mean PAI of 3.0 and 7.0, with erectophile and planophile LAD functions, and using the minimum and maximum reflectance and transmittance spectra (see Fig. 2) is shown in Fig. 10. The strongest influence is caused by a change of leaf optical properties. The maximal reflectance and transmittance values are about 60%, 20%, and 25% higher in the VIS, NIR, and SWIR range than the input values used in the voxel grid reference simulation, resulting in an average increase of at-sensor radiances of 23.9%, 46.1%, and 29% on S1 and 30.3%, 47.9%, and 33.7% on S2. Minimal reflectance and transmittance values are about 50%, 20%, and 25% smaller in the VIS, NIR, and SWIR range, resulting in an average decrease of at-sensor radiances of 13.7%, 30.6%, and 22.5% on S1 and 17.5%, 34.4%, and 26.1% on S2. The influence of LAD on at-sensor radiance is strongest in the NIR spectral range, where a planophile function leads to an increase of 13.4% on S1 and 11.8% on S1 and an erectophile function leads to a decrease of 11.3% on S1 and 11.9% on S2. The influence of PAI is relatively small. A 40% higher PAI leads to a mean difference to

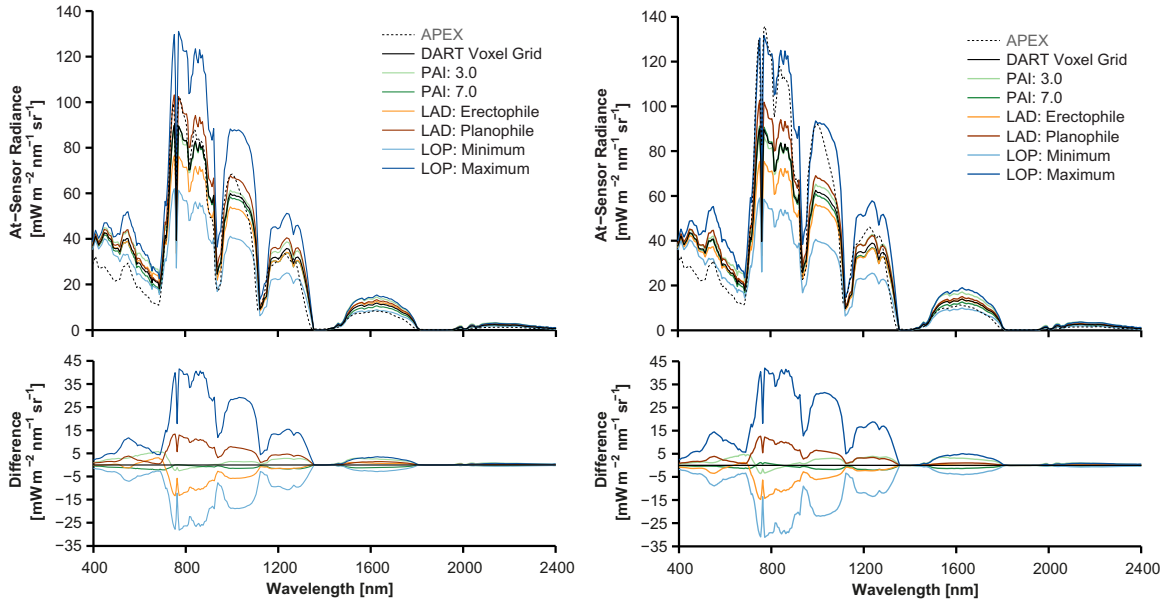

Fig. 10. Influence of the parameterization of turbid media by PAI, LAD, and LOP on mean at-sensor radiance on subplots S1 (left) and S2 (right).

the voxel grid reference of 8% on S1 and 7% on S2 over the whole spectral range, whereas a 40% lower PAI leads to a mean difference to the reference of 19.2% on S1 and 19.1% on S2 over the whole spectral range.

5. Discussion

5.1. Leaf optical properties

Leaf optical properties are varying considerably among individual measurements, as indicated in Fig. 2 by the minimum and maximum values. These variations are primarily related to differences in leaf surface properties, internal leaf structure, biochemical constituents, and the LOP measurement process itself (Yáñez-Rausell et al., 2014a, 2004b). Leaf pigments mainly determine the optical properties in the VIS, being the important spectral range for plant photosynthesis (Asner, 1998). Scattering in the NIR range is primarily a function of the leaf structure (arrangement of cells, thickness of cell walls, etc.) and the dry matter content (Knyazikhin et al., 2013), whereas the SWIR range is mainly influenced by water, lignin, and cellulose (Kokaly et al., 2009).

In contrast, leaf surface reflectance is not restricted to certain wavelengths being a constant additive effect to scattering processes within the leaf (Niinemets, 2010). Interestingly enough, the strongest variation is present between measurements at different positions on the leaf (data not shown). Whether this is due to changing leaf interior or surface characteristics, or a combination of both, cannot be determined from the measurements. Dealing with the large variability of leaf optical properties and the disentanglement of signals from leaf surface and interior are current challenges in RT modeling, which are not met yet. Furthermore, there is a need for a more coherent approach to LOP measurements, since comparisons among studies are currently hampered due to the fact that varying measurement techniques and units are used throughout the literature.

What is particularly addressed in this study are variations of optical properties along a vertical light extinction gradient within the canopy. These originate from the adaptation of the leaves' efficiency of light interception to the light availability (Niinemets, 2010). Higher transmittance and lower reflectance in shaded compared to sunlit parts of the crown are the consequence, also observed by (Lukeš, Stenberg, Rautiainen, Mõttus, & Vanhatalo, 2013) for boreal tree species. However, the change of LOPs along the light gradient is relatively small, since light harvesting is regulated not only by leaf-level traits but also by leaf area, leaf angle, and clumping within the canopy (Niinemets, 2010).

5.2. 3D forest reconstruction

3D canopy structure and background determine how radiation interacts with leaves, woody elements, and background components, affecting the sensitivity of canopy reflectance to leaf optical properties (Knyazikhin et al., 2013). The DTM, the canopy background (Fig. 4), and the canopy architecture (Fig. 5) are solely derived from ALS leaf-on and leaf-off data. This allows automating the forest reconstruction and applying it on various forest ecosystems ranging from plot to landscape level, given the availability of suitable ALS data.

The DTM shows a high level of detail, especially considering the density of the forest. Understory vegetation is mainly present in sparsely forest covered areas or forest glades and classified with high accuracy. Some occurrences can be observed in areas dominated by coniferous trees due to the higher canopy gap fraction. We observe a typical distribution of understory vegetation as described by Eriksson, Eklundh, Kuusk, and Nilson (2006). Main uncertainties in the classification of canopy background are stemming from the delineation of litter and unvegetated ground, mainly due to the similarity of the optical properties of organic material rich bare soil and litter.

The individual tree detection method applied in this study was reviewed and compared to other methods in Kaartinen et al. (2012). Even though we used a point cloud derived from full-waveform ALS data with a much higher point density, the resulting errors are comparable to the ones found by Kaartinen et al. (2012). The reason may lie in the complexity of the forest being characterized by a large number of understory, clustered, and multistemmed trees, which are difficult to detect. Thus there is a need for high-resolution, multitemporal ALS data in such complex forests, although some errors will remain saturating at high point densities.

Comparing the 2D PAI map of the individual tree to the one of the voxel grid approach shows the limitations of the former (Fig. 5). The general pattern is comparable, but the individual tree approach is not capable of describing the mostly closed canopy layer in a realistic way. The gap fraction is generally too high, whereas the plant material is clustered into small patches. The application of the voxel grid approach leads to a more realistic and coherent horizontal distribution of plant material. Moreover, the 3D canopy architecture derived using the voxel grid approach does better represent the underlying ALS point cloud, since tree crowns in a closed forest canopy can generally not be described sufficiently by using simple ellipsoidal or conical shapes.

Nevertheless, some limitations exist in the derivation of the vertical PAI distribution from ALS data. The vertical distribution of ALS points is influenced by the penetration rate of the laser beam through the forest canopy, which is dependent not only on the density of the canopy but also on the sensor and scanning characteristics (Côté et al., 2012; Næsset, 2009). A low flight altitude and overlapping flight strips result in high point densities and a variation of scan angles per unit area, reducing the effects of occlusion in dense parts of the forest. The combination of leaf-on with the leaf-off data further improves the ability to detect plant material in the lower parts of deciduous canopies, although limited to woody or evergreen elements. However, effects of occlusion – mainly expressed by reduced point densities in lower canopy parts – are still present and difficult to quantify. For the voxel grid approach, the logarithmic transformation in Eq. (2) is in accordance with Beer's law and should yield a linear, non-intercept relation to effective PAI (Solberg et al., 2009). To be able to explicitly correct the laser light extinction through the canopy, further studies are needed to better model effects of occlusion by using physical models and assessing them in a quantitative fashion (e.g., Morsdorf, Nichol, Malthus, & Woodhouse, 2009).

5.3. Simulation results

Both DART and APEX at-sensor radiance spectra show typical atmospheric absorption features as expected (see Fig. 6). Atmospheric path radiance is strongest in the VIS part of the spectrum, adding to the reflected radiance from the forest canopy and background. The high atmospheric visibility during the APEX overflight was measured and confirmed by the AERONET station on the flux tower. However, the actual atmospheric absorption could still not be fully matched by basing our parameterization on MODTRAN's standard atmospheres due to a skewed mix of absorbing and reflecting aerosol concentrations and the unknown distribution of aerosols in the vertical path. Hence, we observe a systematic shift of about 8–12 mW m^{-2} nm^{-1} sr^{-1} in the VIS due to enhanced atmospheric path radiance in the DART simulation.

The systematic shift of radiance values in the VIS is present in the difference images, however the spatial pattern remains consistent across space (Fig. 7). The results of Section 4.3.2 confirm our conclusion that the voxel grid approach is better suited to describe the complex 3D canopy architecture, even though there is a potential scale issue linked to clumping and voxel size (Béland et al., 2014). The difference images in Fig. 8 indicate strong local deviations from the APEX images due to the differing shape and arrangement of the individual trees. The concentration of plant material paired with the large gap fraction results in too many shaded canopy parts and partially enhanced radiance values in sunlit parts. Additionally, the influence of the canopy background is enhanced, especially in the red region where vegetation is mostly

absorbing. This is also reflected in the radiance spectrum as displayed in Fig. 9.

In general, the influence of canopy background is higher than expected, even though considered negligible in other studies (c.f., Knyazikhin et al., 2013). Modeling a black background has a much higher impact on the simulated radiance spectra than adding woody elements or using the individual tree compared to the voxel grid approach (see Section 4.3.3). This stresses the importance of an area-wide canopy background classification being necessary for a solid modeling approach at regional scale, where heterogeneous clumping occurs. The influence of woody elements was assessed before by others such as Malenovský et al. (2008). However, this was limited to using TOC reflectances in a different type of forest (less heterogeneity of the gap fraction), and using a different modeling approach. Nonetheless, our results are in agreement with the findings of Malenovský et al. (2008). Adding woody elements results in slightly lower radiance values at all wavelengths due to increased multiple scattering similar to the photon-trapping within a coniferous shoot (Rautiainen & Stenberg, 2005).

5.3.1. Voxel grid approach

Looking at the difference images in Fig. 7, the two bands at 533 and 570 nm show a similar homogeneous spatial difference pattern. This is important since these two wavelengths are used to describe the photosynthetic efficiency of plants (Garbulsky, Peñuelas, Gamon, Inoue, & Filella, 2011). Stronger differences can be observed locally, where the canopy has small gaps or glades. On one hand, these local differences can be explained by uncertainties in the spatial registration of the APEX data. At the border of sunlit and shaded crown parts, a shift of one pixel can already lead to strong differences when performing a pixel-wise comparison. On the other hand, there is a temporal difference between the ALS and the APEX acquisition of about two years, which can easily cause small differences in canopy structure.

Some differences in the scattering of understory exist at 680 nm, where the chlorophyll absorption of the vegetation is strongest. DART simulates higher radiance values on the forest glade located in the southwestern part of the scene, indicating that there was more absorbing vegetation present during the APEX overflight than modeled. If a small understory vegetation layer is modeled, the signal is sensitive to the reflectance of the underlying soil being higher than that of vegetation in the red region. Additionally, the corresponding APEX band shows a low signal to noise ratio (SNR) due to the low radiant flux (see Schaepman, Schlaepfer, & Mueller, 2002), leading to the weakest coefficient of determination of all four selected bands.

The most conspicuous spatial pattern is present at the 780 nm difference image. The distinct pattern of over- and underestimation of APEX values corresponds with the distribution of coniferous and deciduous trees. This also explains the intensity differences between subplots S1 and S2 in the NIR range, since over- and underestimation even out on S1 (Fig. 6). There are several possible reasons why the radiance of deciduous trees is simulated too low, whereas the signal of coniferous trees is too strong.

First, the rather strong absorption present in the NIR range of the deciduous leaf optical properties could explain the low radiance values in the simulation output (see Fig. 2). Secondly, the selection of leaf and needle samples is limited and does not represent the high spectral variability of the different tree species. Using only one mean spectrum per vertical crown layer for deciduous and one for coniferous tree species may be too generalizing, since the strong variations on the single leaf level scale up to the canopy level (Fig. 10). For example, the APEX image shows above-average radiance values in the southwestern part of the scene, where young beech trees are growing in a dense vegetation layer. This distinct type of vegetation is not modeled appropriately in the DART image, because specific LOPs of young trees are not considered in the model. In ongoing field work, the location, species, and diameter at breast height (DBH) of all trees are being determined to model individual tree species. Paired with more detailed LOP measurements (including measurements of biochemistry), we will be better able to understand how spectral differences among species and species' development stages are influencing the model output.

Besides the optical properties, structural characteristics are known to have a strong influence in the NIR spectral range. Generally, the 3D architecture of the canopy is well modeled using the voxel grid approach, but our approach has its limits in the description of small-scale structures on the branch or shoot level. The clumping of needles into shoots is strongly influencing the scattering behavior of coniferous trees. Multiple scattering within shoots is considered to be the most important structural effect responsible for the low NIR reflectance of coniferous trees (Rautiainen & Stenberg, 2005). Therefore, the scattering and absorption of radiation are determined not only by the arrangement of shoots within crowns but also by the arrangement of needles within shoots, but neither the resulting absorption of radiation nor the shoot scattering phase function can be directly modeled by the turbid medium approach used in this study (Mõttus et al., 2012; Rautiainen et al., 2012; Stenberg, Mõttus, & Rautiainen, 2008).

A way to alternatively approximate the shoot-level clumping would be to reduce the voxel size by one order of magnitude (e.g., Malenovský et al., 2013, 2008) or to use shoots as basic scattering elements (e.g., van Leeuwen et al., 2013). To model the coniferous trees in a physically more consistent fashion, 3D models would need to be able resolving single needles (e.g., Côté et al., 2011, 2012). Theoretically, all of these approaches can be put into practice using DART, but are usually limited to smaller plots due to the high computational costs. Moreover, the parameterization is mainly based on TLS measurements and thus limited to plots accessible by foot. Our forest reconstruction approaches though are automated and applicable on the landscape level, wherever multi-temporal ALS data is available. A much simpler and therefore promising approach is the upscaling of coniferous needle spectra to shoot spectral albedo based on the spherically averaged silhouette to total area ratio (STAR), which could be included in future RT models (Mõttus et al., 2012; Rautiainen et al., 2012).

Moreover, the LAD and PAI are the structural parameters used to parameterize the voxels filled by turbid media. It is not surprising that PAI variations have a comparably low impact on the modeled spectrum (Fig. 9), since they are known to be saturating in dense, closed canopies having a PAI ≥ 3 (Baret & Guyot, 1991; Gitelson, 2004). Our results of Section 4.3.3 support previous findings about the LAD having a much stronger impact on canopy reflectance and at-sensor radiance (e.g., Ollinger, 2011; Laurent, Verhoef, Clevers, & Schaepman, 2011a). Applying a universal distribution function for deciduous and coniferous trees based on literature and ALA measurements is considered a good approximation, but still fails to account for the wide range of leaf angles observed within a tree (Falster & Westoby, 2003; Pisek et al., 2013).

Especially in closed canopies, the leaf angle distribution is assumed to be varying along the vertical canopy profile. Optimally, steeper leaf angles would prevail in the upper sunlit canopy parts, whereas flat leaves would be predominant in shaded understory layers (Niinemets, 1998, 2010). However, there are very few studies supporting these assumptions due to the difficulty and costs of measuring the large number of leaf angles needed to describe the variations among vertical crown layers and species (Pisek et al., 2013). Nonetheless, we recommend parameterizing LAD on different vertical canopy layers in future studies, since it would improve our model approaches for remotely sensed data and increase the ability of RT models to be inverted.

6. Conclusion and outlook

In this study we have reconstructed a temperate mixed forest using a high resolution canopy–atmosphere 3D RT model and compared it to imaging spectrometer data. To address the complex 3D canopy architecture, we developed and compared two forest reconstruction approaches: an individual tree based approach and a voxel grid approach. Our results show that the voxel grid approach performs

better than a parameterization based on individual trees. In a pixel-wise comparison with the imaging spectrometer data, the voxel grid approach better represented hotspots and shadows, leading to a slightly higher predictive power ($R^2 = 0.48$, λ780 nm) as when using the individual tree approach ($R^2 = 0.34$, λ780 nm). The images simulated using the voxel grid approach exhibit similar spatial patterns than the APEX images, whereas absolute radiance values are partially differing depending on particular wavelengths.

The work emphasized on two important constraining factors of the 3D RT model parameterization. Firstly, the high spectral variability of leaf optical properties needs to be considered not only along a vertical light extinction gradient within the canopy but also between individual species and leaves. For a specific leaf level simulation allowing to better understand spectral variations, an improved sampling of leaves and needles including validation will be needed. Secondly, the accurate parameterization of small-scale structures, such as the clumping of needles into shoots or the distribution of leaf angles is still a key challenge, even when using combined ALS and TLS approaches. Both have a particularly strong influence on the model output and therefore are critical for RT modeling of forests. Future model improvements might include a scaling approach. This would imply that voxels with high canopy clumping but little filling are modeled using a shoot scaling approach, since the turbid medium assumption might be violated (e.g., Rautiainen et al., 2012).

We conclude that our proposed method provides an advanced representation of the 3D radiative regime within a temperate mixed forest. This reconstruction is well capable of simulating most spectral and spatial features of imaging spectrometer data. The results indicate the potential to simulate future Earth observation missions, such as ESAs optical Sentinels (Malenovský et al., 2012). Limitations were discussed in detail and have to be considered for future research. Beyond this, our approach offers a wider range of possibilities for further investigations, namely the simulation of virtually any range of band combinations, permutations of parameter combinations, to even testing the effect of changing object composition of the scene (e.g., needle thinning effects and pigment shifts). Simulating a multitude of parameter combinations would support local and global sensitivity analysis and help to define priorities when running DART in an inverse mode. For more specific testing of the impact of structural effects, the model can be applied to mono-species stands, allowing to reduce uncertainties in the LOPs.

Acknowledgments

This study has been supported by the European Space Agency (ESA) Support to Science Element (STSE) ESRIN contract No. AO/1-6529/10/I-NB, '3D Vegetation Laboratory'. Contributions of MS and FM were funded by the University of Zurich Research Priority Program on 'Global Change and Biodiversity' (URPP GCB). Needle optical properties data was provided by the Global Change Research Centre (Academy of Sciences of the Czech Republic) and Laboratory of Geo-information Science and Remote Sensing (Wageningen University). We thank Z. Malenovský for providing the leaf scale sampling and measurements, L. Yáñez for processing the needle optical properties, J. Weyermann for processing APEX data, T. Yin for assisting with DART, A. Hauser for maintaining the Laegern AERONET site, and A. Damm for providing a tool for spectral filtering. We thank Paul Sabatier University and the French Space Center (CNES) for supporting the DART development (TOSCA project STEM-LEAF). We thank Phil Lewis for the comprehensive comments on an earlier version as well as the anonymous reviewers' comments helping to improve the manuscript.

References

Asner, G. P. (1998). Biophysical and biochemical sources of variability in canopy reflectance. *Remote Sensing of Environment*, *234–253*.

Atzberger, C., & Richter, K. (2012). Spatially constrained inversion of radiative transfer models for improved LAI mapping from future sentinel-2 imagery. *Remote Sensing of Environment*, *208–218*.

Baldocchi, D., Falge, E., Gu, L., Olson, R., Hollinger, D., Running, S., et al. (2001). FLUXNET: A new tool to study the temporal and spatial variability of ecosystem-scale carbon dioxide, water vapor, and energy flux densities. *Bulletin of the American Meteorological Society*, *82*, 2415–2434.

Barbier, N., Couteron, P., Proisy, C., Malhi, Y., & Gastellu-Etchegorry, J. -P. (2010). The variation of apparent crown size and canopy heterogeneity across lowland amazonian forests. *Global Ecology and Biogeography*, *72–84*.

Baret, F., & Guyot, G. (1991). Potentials and limits of vegetation indices for LAI and APAR assessment. *Remote Sensing of Environment*, *161–173*.

Baret, F., Weiss, M., Allard, D., Garrigue, S., Leroy, M., Jeanjean, H., et al. (2003). *Valeri: A network of sites and a methodology for the validation of medium spatial resolution land satellite products.* (Available online at http://w3.avignon.inra.fr/valeri/, Accessed June 10, 2013).

Béland, M., Baldocchi, D. D., Widlowski, J. -L., Fournier, R. A., & Verstraete, M. M. (2014). On seeing the wood from the leaves and the role of voxel size in determining leaf area distribution of forests with terrestrial LiDAR. *Agricultural and Forest Meteorology*, *82–97*.

Berstein, L., & Roberston, D. (1989). *MODTRAN: A moderate resolution model for LOWTRAN 7. Technical Report GL-TR-89-0122 GeophysMA*: Lab Bedford.

Combes, D., Bousquet, L., Jacquemoud, S., Sinoquet, H., Varlet-Grancher, C., & Moya, I. (2007). A new spectrogoniophotometer to measure leaf spectral and directional optical properties. *Remote Sensing of Environment*, *107–117*.

Côté, J. -F., Fournier, R. A., & Egli, R. (2011). An architectural model of trees to estimate forest structural attributes using terrestrial lidar. *Environmental Modelling & Software*, *761–777*.

Côté, J. -F., Fournier, R. A., Frazer, G. W., & Niemann, K. O. (2012). A fine-scale architectural model of trees to enhance LiDAR-derived measurements of forest canopy structure. *Agricultural and Forest Meteorology*, *−167*, 72–85.

D'Odorico, P., Guanter, L., Schaepman, M. E., & Schläpfer, D. (2011). Performance assessment of onboard and scene-based methods for Airborne Prism Experiment spectral characterization. *Applied Optics*, *4755–4764*.

de Wit, C. (1965). Photosynthesis of leaf canopies. *Agricultural Research Report no. 663*. Wageningen.

Eriksson, H. M., Eklundh, L., Kuusk, A., & Nilson, T. (2006). Impact of understory vegetation on forest canopy reflectance and remotely sensed LAI estimates. *Remote Sensing of Environment*, *408–418*.

Eugster, W., Zeyer, K., Zeeman, M., Michna, P., Zingg, A., Buchmann, N., et al. (2007). Methodical study of nitrous oxide eddy covariance measurements using quantum cascade laser spectrometry over a Swiss forest. *Biogeosciences*, *927–939*.

Evans, J., & Hudak, A. (2007). A multiscale curvature algorithm for classifying discrete return LiDAR in forested environments. *IEEE Transactions on Geoscience and Remote Sensing*, *45*, 1029–1038.

Eysn, L., Pfeifer, N., Ressl, C., Hollaus, M., Grafl, A., & Morsdorf, F. (2013). A practical approach for extracting tree models in forest environments based on equirectangular projections of terrestrial laser scans. *Remote Sensing*, *5424–5448*.

Falster, D. S., & Westoby, M. (2003). Leaf size and angle vary widely across species: What consequences for light interception? *New Phytologist*, *509–525*.

Fleck, S., Raspe, S., Cater, M., Schleppi, P., Ukonmaanaho, L., Greve, M., et al. (2012). *Leaf area measurements. In Manual on methods and criteria for harmonized sampling, assessment, monitoring and analysis of the effects of air pollution on forests.* Hamburg: UNECE ICP Forests Programme Co-ordinating Centre (Available online at http://www.icp-forests.org/Manual.htm, Accessed June 10, 2013).

Garbulsky, M. F., Peñuelas, J., Gamon, J., Inoue, Y., & Filella, I. (2011). The photochemical reflectance index (PRI) and the remote sensing of leaf, canopy and ecosystem radiation use efficiencies: A review and meta-analysis. *Remote Sensing of Environment*, *281–297*.

Gastellu-Etchegorry, J. P. (2008). 3D modeling of satellite spectral images, radiation budget and energy budget of urban landscapes. *Meteorology and Atmospheric Physics*, *187–207*.

Gastellu-Etchegorry, J., Demarez, V., Pinel, V., & Zagolski, F. (1996). Modeling radiative transfer in heterogeneous 3-D vegetation canopies. *Remote Sensing of Environment*, *131–156*.

Gastellu-Etchegorry, J., Grau, E., & Lauret, N. (2012). DART: A 3D model for remote sensing images and radiative budget of earth surfaces. In C. Alexandru (Ed.), *Modeling and simulation in engineering chapter 2*.

Gastellu-Etchegorry, J., Martin, E., & Gascon, F. (2004). DART: A 3-D model for simulating satellite images and surface radiation budget. *International Journal of Remote Sensing*, *25*, 75–96.

Gitelson, A. A. (2004). Wide dynamic range vegetation index for remote quantification of biophysical characteristics of vegetation. *Journal of Plant Physiology*, *165–173*.

Goel, N. S. (1988). Models of vegetation canopy reflectance and their use in estimation of biophysical parameters from reflectance data. *Remote Sensing Reviews*, *1–212*.

Heurich, M. (2008). Automatic recognition and measurement of single trees based on data from airborne laser scanning over the richly structured natural forests of the Bavarian forest national park. *Forest Ecology and Management*, *2416–2433*.

Holben, B., Eck, T., Slutsker, I., Tanré, D., Buis, J., Setzer, A., et al. (1998). AERONET — A federated instrument network and data archive for aerosol characterization. *Remote Sensing of Environment*, *1–16*.

Hueni, A., Lenhard, K., Baumgartner, A., & Schaepman, M. (2013). Airborne prism experiment calibration information system. *IEEE Transactions on Geoscience and Remote Sensing*, 1-1.

Jacquemoud, S., & Baret, F. (1990). PROSPECT: A model of leaf optical properties spectra. *Remote Sensing of Environment*, *75–91*.

Jacquemoud, S., Verhoef, W., Baret, F., Bacour, C., Zarco-Tejada, P. J., Asner, G. P., et al. (2009). PROSPECT + SAIL models: A review of use for vegetation characterization. *Remote Sensing of Environment*(Supplement 1), S56–S66.

Jehle, M., Hueni, A., Damm, A., D'Odorico, P., Weyermann, J., Kneubühler, M., et al. (2010). APEX — Current status, performance and validation concept. *Sensors*. (pp. 533–537) IEEE (2010).

Kaartinen, H., Hyyppä, J., Yu, X., Vastaranta, M., Hyyppä, H., Kukko, A., et al. (2012). An international comparison of individual tree detection and extraction using airborne laser scanning. *Remote Sensing*, 950–974.

Knyazikhin, Y., Schull, M. A., Stenberg, P., Mõttus, M., Rautiainen, M., Yang, Y., et al. (2013). Hyperspectral remote sensing of foliar nitrogen content. *Proceedings of the National Academy of Sciences*, *110*, E185–E192.

Koetz, B., Schaepman, M., Morsdorf, F., Bowyer, P., Itten, K., & Allgöwer, B. (2004). Radiative transfer modeling within a heterogeneous canopy for estimation of forest fire fuel properties. *Remote Sensing of Environment*, *332–344*.

Kokaly, R. F., Asner, G. P., Ollinger, S. V., Martin, M. E., & Wessman, C. A. (2009). Characterizing canopy biochemistry from imaging spectroscopy and its application to ecosystem studies. *Remote Sensing of Environment*(Supplement 1), S78–S91.

Laurent, V. C., Verhoef, W., Clevers, J. G., & Schaepman, M. E. (2011a). Estimating forest variables from top-of-atmosphere radiance satellite measurements using coupled radiative transfer models. *Remote Sensing of Environment*, *1043–1052*.

Laurent, V. C., Verhoef, W., Clevers, J. G., & Schaepman, M. E. (2011b). Inversion of a coupled canopy–atmosphere model using multi-angular top-of-atmosphere radiance data: A forest case study. *Remote Sensing of Environment*, *2603–2612*.

Leiterer, R., Mücke, W., Hollaus, M., Pfeifer, N., & Schaepman, M. E. (2013). Operational forest structure monitoring using airborne laser scanning. *Photogrammetrie — Fernerkundung — Geoinformation*, *2013*, 173–184.

Lindberg, E., Olofsson, K., Holmgren, J., & Olsson, H. (2012). Estimation of 3D vegetation structure from waveform and discrete return airborne laser scanning data. *Remote Sensing of Environment*, *151–161*.

Liu, C., Frazier, P., & Kumar, L. (2007). Comparative assessment of the measures of thematic classification accuracy. *Remote Sensing of Environment*, *606–616*.

Lukeš, P., Rautiainen, M., Stenberg, P., & Malenovský, Z. (2011). Empirical test of the spectral invariants theory using imaging spectroscopy data from a coniferous forest. *International Journal of Applied Earth Observation and Geoinformation*, *13*, 668–675.

Lukeš, P., Stenberg, P., Rautiainen, M., Mõttus, M., & Vanhatalo, K. M. (2013). Optical properties of leaves and needles for boreal tree species in Europe. *Remote Sensing Letters*, *667–676*.

Malenovský, Z., Bartholomeus, H. M., Acerbi-Junior, F. W., Schopfer, J. T., Painter, T. H., Epema, G. F., et al. (2007). Scaling dimensions in spectroscopy of soil and vegetation. *International Journal of Applied Earth Observation and Geoinformation*, *9*, 137–164.

Malenovský, Z., Homolová, L., Zurita-Milla, R., Lukeš, P., Kaplan, V., Hanuš, J., et al. (2013). Retrieval of spruce leaf chlorophyll content from airborne image data using continuum removal and radiative transfer. *Remote Sensing of Environment*, *85–102*.

Malenovský, Z., Martin, E., Homolová, L., Gastellu-Etchegorry, J. -P., Zurita-Milla, R., Schaepman, M. E., et al. (2008). Influence of woody elements of a Norway spruce canopy on nadir reflectance simulated by the DART model at very high spatial resolution. *Remote Sensing of Environment*, *1–18*.

Malenovský, Z., Rott, H., Cihlar, J., Schaepman, M. E., García-Santos, G., Fernandes, R., et al. (2012). Sentinels for science: Potential of Sentinel-1, -2, and -3 missions for scientific observations of ocean, cryosphere, and land. *Remote Sensing of Environment*, *91–101*.

Mallet, C., & Bretar, F. (2009). Full-waveform topographic lidar: State-of-the-art. *ISPRS Journal of Photogrammetry and Remote Sensing*, *64*, 1–16.

Monis, M., & Saeki, T. (1953). Über den Lichtfaktor in den Pflanzengesellschaften und seine Bedeutung für die Stoffproduktion. *Japanese Journal of Botany*, *22–52*.

Morsdorf, F., Kötz, B., Meier, E., Itten, K., & Allgöwer, B. (2006). Estimation of LAI and fractional cover from small footprint airborne laser scanning data based on gap fraction. *Remote Sensing of Environment*, *50–61*.

Morsdorf, F., Meier, E., Kötz, B., Itten, K. I., Dobbertin, M., & Allgöwer, B. (2004). LiDAR-based geometric reconstruction of boreal type forest stands at single tree level for forest and wildland fire management. *Remote Sensing of Environment*, *353–362*.

Morsdorf, F., Nichol, C., Malthus, T., & Woodhouse, I. H. (2009). Assessing forest structural and physiological information content of multi-spectral LiDAR waveforms by radiative transfer modelling. *Remote Sensing of Environment*, *2152–2163*.

Mõttus, M., Rautiainen, M., & Schaepman, M. E. (2012). Shoot scattering phase function for Scots pine and its effect on canopy reflectance. *Agricultural and Forest Meteorology*, *-155*, 67–74.

Næsset, E. (2009). Effects of different sensors, flying altitudes, and pulse repetition frequencies on forest canopy metrics and biophysical stand properties derived from small-footprint airborne laser data. *Remote Sensing of Environment*, *148–159*.

Niemann, K., Quinn, G., Goodenough, D., Visintini, F., & Loos, R. (2012). Addressing the effects of canopy structure on the remote sensing of foliar chemistry of a 3-dimensional, radiometrically porous surface. *IEEE Journal of Selected Topics in Applied Earth Observations and Remote Sensing*, *5*, 584–593.

Niinemets, Ü. (1998). Adjustment of foliage structure and function to a canopy light gradient in two co-existing deciduous trees. Variability in leaf inclination angles in relation to petiole morphology. *Trees*, *12*, 446–451.

Niinemets, Ü. (2009). Packing the photosynthetic machinery: From leaf to canopy. In A. Laisk, L. Nedbal, & Govindjee (Eds.), Springer Science+Business Media B.V

Niinemets, Ü. (2010). A review of light interception in plant stands from leaf to canopy in different plant functional types and in species with varying shade tolerance. *Ecological Research*, *693–714*.

North, P. (1996). Three-dimensional forest light interaction model using a Monte Carlo method. *IEEE Transactions on Geoscience and Remote Sensing*, *34*, 946–956.

Ollinger, S. V. (2011). Sources of variability in canopy reflectance and the convergent properties of plants. *New Phytologist*, *375–394*.

Pisek, J., Sonnentag, O., Richardson, A. D., & Mõttus, M. (2013). Is the spherical leaf inclination angle distribution a valid assumption for temperate and boreal broadleaf tree species? *Agricultural and Forest Meteorology*, *186–194*.

Rautiainen, M., Mõttus, M., Yáñez-Rausell, L., Homolová, L., Malenovský, Z., & Schaepman, M. E. (2012). A note on upscaling coniferous needle spectra to shoot spectral albedo. *Remote Sensing of Environment*, *469–474*.

Rautiainen, M., & Stenberg, P. (2005). Application of photon recollision probability in coniferous canopy reflectance simulations. *Remote Sensing of Environment*, *98–107*.

Schaepman, M. E. (2009). Imaging spectrometers. In T. A. Warner, M. D. Nellis, & G. M. Foody (Eds.), *The SAGE handbook of remote sensing* (pp. 166–178). SAGE Publications Ltd (chapter 12).

Schaepman, M. E., Schlaepfer, D., & Mueller, A. A. (2002). Performance requirements for airborne imaging spectrometers. In M. Descour, & S. Shen (Eds.), *Imaging spectrometry VII. San Diego: Proceedings of SPIE, Vol. 4480*. (pp. 23–31).

Schaepman, M. E., Ustin, S. L., Plaza, A. J., Painter, T. H., Verrelst, J., & Liang, S. (2009). Earth system science related imaging spectroscopy — An assessment. *Remote Sensing of Environment*(Supplement 1), S123–S137.

Schaepman-Strub, G., Schaepman, M., Painter, T., Dangel, S., & Martonchik, J. (2006). Reflectance quantities in optical remote sensing — Definitions and case studies. *Remote Sensing of Environment*, *27–42*.

Schläpfer, D., & Richter, R. (2002). Geo-atmospheric processing of airborne imaging spectrometry data. Part 1: Parametric orthorectification. *International Journal of Remote Sensing*, *23*, 2609–2630.

Schläpfer, D., & Schaepman, M. E. (2002). Modeling the noise equivalent radiance requirements of imaging spectrometers based on scientific applications. *Applied Optics*, *5691–5701*.

Schläpfer, D., Schaepman, M. E., & Itten, K. I. (1998). PARGE: Parametric geocoding based on GCP-calibrated auxiliary data. *Imaging Spectrometry IV*, *Vol. 3438*. (pp. 334–344). The International Society for Optical Engineering.

Solberg, S., Brunner, A., Hanssen, K. H., Lange, H., Næsset, E., Rautiainen, M., et al. (2009). Mapping LAI in a Norway spruce forest using airborne laser scanning. *Remote Sensing of Environment*, *2317–2327*.

Stenberg, P., Mõttus, M., & Rautiainen, M. (2008). Modeling the spectral signature of forests: Application of remote sensing models to coniferous canopies. In S. Liang (Ed.), *Advances in land remote sensing: System, modeling, inversion and application* (pp. 147–171). Springer-Verlag.

Townsend, P. A., Serbin, S. P., Kruger, E. L., & Gamon, J. A. (2013). Disentangling the contribution of biological and physical properties of leaves and canopies in imaging spectroscopy data. *Proceedings of the National Academy of Sciences*, *110*, E1074.

Ustin, S. L., Gitelson, A., Jacquemoud, S., Schaepman, M. E., Asner, G. P., Gamon, J. A., et al. (2009). Retrieval of foliar information about plant pigment systems from high resolution spectroscopy. *Remote Sensing of Environment*(Supplement 1), S67–S77.

van Leeuwen, M., Coops, N. C., Hilker, T., Wulder, M. A., Newnham, G. J., & Culvenor, D. S. (2013). Automated reconstruction of tree and canopy structure for modeling the internal canopy radiation regime. *Remote Sensing of Environment*, *286–300*.

van Leeuwen, M., & Nieuwenhuis, M. (2010). Retrieval of forest structural parameters using LiDAR remote sensing. *European Journal of Forest Research*, *749–770*.

Vauhkonen, J., Tokola, T., Packalen, P., & Maltamo, M. (2009). Identification of Scandinavian commercial species of individual trees from airborne laser scanning data using alpha shape metrics. *Forest Science*, *37–47*.

Verrelst, J., Schaepman, M. E., Malenovský, Z., & Clevers, J. G. (2010). Effects of woody elements on simulated canopy reflectance: Implications for forest chlorophyll content retrieval. *Remote Sensing of Environment*, *647–656*.

Vohland, M., Mader, S., & Dorigo, W. (2010). Applying different inversion techniques to retrieve stand variables of summer barley with PROSPECT + SAIL. *International Journal of Applied Earth Observation and Geoinformation*, *12*, 71–80.

Wagner, W., Hollaus, M., Briese, C., & Ducic, V. (2008). 3D vegetation mapping using small-footprint full-waveform airborne laser scanners. *International Journal of Remote Sensing*, *29*, 1433–1452.

Wagner, W., Ullrich, A., Ducic, V., Melzer, T., & Studnicka, N. (2006). Gaussian decomposition and calibration of a novel small-footprint full-waveform digitising airborne laser scanner. *ISPRS Journal of Photogrammetry and Remote Sensing*, *60*, 100–112.

Wang, Q., & Li, P. (2012). Hyperspectral indices for estimating leaf biochemical properties in temperate deciduous forests: Comparison of simulated and measured reflectance data sets. *Ecological Indicators*, *56–65*.

Wang, Q., & Li, P. (2013). Canopy vertical heterogeneity plays a critical role in reflectance simulation. *Agricultural and Forest Meteorology*, *111–121*.

Weiss, M., Baret, F., Smith, G., Jonckheere, I., & Coppin, P. (2004). Review of methods for in situ leaf area index (LAI) determination: Part II. Estimation of LAI, errors and sampling. *Agricultural and Forest Meteorology*, 37–53.

White, H., Miller, J., & Chen, J. (2001). Four-scale linear model for anisotropic reflectance (FLAIR) for plant canopies. I. Model description and partial validation. *IEEE Transactions on Geoscience and Remote Sensing*, *39*, 1072–1083.

Wulder, M. A., White, J. C., Nelson, R. F., Næsset, E., Ørka, H. O., Coops, N. C., et al. (2012). Lidar sampling for large-area forest characterization: A review. *Remote Sensing of Environment*, *196–209*.

Yáñez-Rausell, L., Malenovský, Z., Clevers, J. G. P. W., & Schaepman, M. E. (2014a). Minimizing measurement uncertainties of coniferous needle-leaf optical properties. Part II: Experimental setup and error analysis. *IEEE Journal of Selected Topics in Applied Earth Observations and Remote Sensing*, *7*, 406–420.

Yáñez-Rausell, L., Schaepman, M., Clevers, J., & Malenovský, Z. (2014b). Minimizing measurement uncertainties of coniferous needle-leaf optical properties. Part I: Methodological review. *IEEE Journal of Selected Topics in Applied Earth Observations and Remote Sensing, 7*, 399–405.

Yang, X., Strahler, A. H., Schaaf, C. B., Jupp, D. L., Yao, T., Zhao, F., et al. (2013). Three-dimensional forest reconstruction and structural parameter retrievals using a terrestrial full-waveform lidar instrument (Echidna ®). *Remote Sensing of Environment, 36–51*.

Yin, T., Gastellu-Etchegorry, J. -P., Lauret, N., Grau, E., & Rubio, J. (2013). A new approach of direction discretization and oversampling for 3D anisotropic radiative transfer modeling. *Remote Sensing of Environment, 213–223*.

2.2 At-sensor radiance simulation for airborne imaging spectroscopy

Schneider, F.D., Yin, T., Gastellu-Etchegorry, J.-P., Morsdorf, F., Schaepman, M.E.

This section is based on the peer-reviewed conference article:
IEEE Whispers, 2014, June 24-27, Lausanne, Switzerland
DOI: 10.1109/WHISPERS.2014.8077586

All authors designed and performed research, F.D.S. wrote the paper.

AT-SENSOR RADIANCE SIMULATION FOR AIRBORNE IMAGING SPECTROSCOPY

F.D. Schneider[1], *T. Yin*[2], *J.-P. Gastellu-Etchegorry*[2], *F. Morsdorf*[1], *M.E. Schaepman*[1]

[1] Remote Sensing Laboratories, University of Zurich, Winterthurerstrasse 190, 8057 Zurich, Switzerland, Email: fabian-daniel.schneider, felix.morsdorf, michael.schaepman@geo.uzh.ch
[2] Centre d'Études Spatiales de la Biosphère, Paul Sabatier University - CNES - CNRS - IRD, 18 Avenue Edouard Belin, BPI 2801, 31401 Toulouse, Cedex 9, France, Email: yint, jean-philippe.gastellu-etchegorry@cesbio.cnes.fr

ABSTRACT

Physically-based radiative transfer modeling is the key to remote sensing of forest ecosystems. To scale spectral information from the leaf to the sensor level, the canopy architecture of a forest, illumination conditions and the viewing geometry have to be taken into account. Therefore, a new airborne image simulation approach is being developed for the 3D radiative transfer model DART to model individual viewing angles for each pixel of a scene. A first comparison to actual imaging spectrometer data showed promising results, mainly because the atmosphere simulation could be improved compared to previous versions of the DART model.

***Index Terms*—** Radiative transfer modeling, Airborne image simulation, Airborne imaging spectroscopy

1. INTRODUCTION

Scaling spectral information from the leaf to the sensor level is one of the main challenges in the remote sensing of forest ecosystems. The estimation of biochemical constituents of leaves or needles from remotely sensed data is of high interest, but not trivial due to atmospheric influences and the structural complexity of natural forests [1, 2]. The reflectance of a forest canopy is not only determined by the leaf optical properties but also by factors like canopy structure, illumination conditions and viewing geometry [3, 4, 5]. Their influence is especially large for natural forests growing on steep slopes. Thus, a sophisticated radiative transfer model is needed to scale leaf or needle optical properties to at-sensor radiance.

The DART model (Discrete Anisotropic Radiative Transfer [6]) is one of the most complete coupled canopy-atmosphere 3D radiative transfer models. It was initially designed to simulate spaceborne remote sensing images of natural landscapes [7]. The physically based 3D model allows to simulate virtually any illumination or viewing angle, but was limited to parallel incoming and outgoing rays. This simplification was acceptable for simulating spaceborne sensors, but not made for airborne sun-earth-sensor constellations having a much larger angular variation within a scene. Since DART is predestined to simulate high-dimensional airborne imaging spectrometer data, a new module is being implemented to simulate airborne pushbroom scanners and frame cameras. We present here first results of the new airborne imaging simulation in comparison to previous modeling results and real measurements of the state-of-the-art airborne imaging spectrometer APEX (Airborne Prism EXperiment [8]).

2. STUDY AREA AND DATA

The study area covers 300 m x 300 m and is located at the Laegern, a temperate mixed forest in Switzerland. It is a highly diverse forest dominated by beech and Norway spruce trees, which is characterized by steep, rugged terrain, a heterogeneous spectral background and a complex canopy architecture. Airborne and terrestrial laser scanning as well as leaf optical properties measurements were combined with in situ data of plant area index and leaf angle distribution to fully describe the test site (see [9] for more details).

Imaging spectrometer data was acquired on June 16th, 2012 at 10:26 UTC at a solar illumination angle of 27.1° in zenith and 147.4° in azimuth (defined from north clockwise). The study area was measured under clear sky conditions and covered by a single flight line. The average flight altitude was 4526 m above sea level resulting in a ground pixel size of 2 m. The airborne imaging spectrometer APEX was used being a state-of-the-art pushbroom scanner system with a spectral sampling interval varying between 2.5 nm and 13.9 nm and a full width at half maximum between 3.4 nm and 14.3 nm, depending on wavelength. The viewing angle at scene center was 6.76° in zenith and 331.8° in azimuth. The exact viewing angles of each pixel are shown in Figure 1.

Traceable radiometric calibration of the APEX data included compensation for spatial coregistration effects of the VNIR and SWIR detector, dark current and keystone correction. The uncertainty of calibrated radiance values was lying within 0.5% and 3% in the range of 400 to 1900 nm, as estimated by a calibration model. APEX data was georefer-

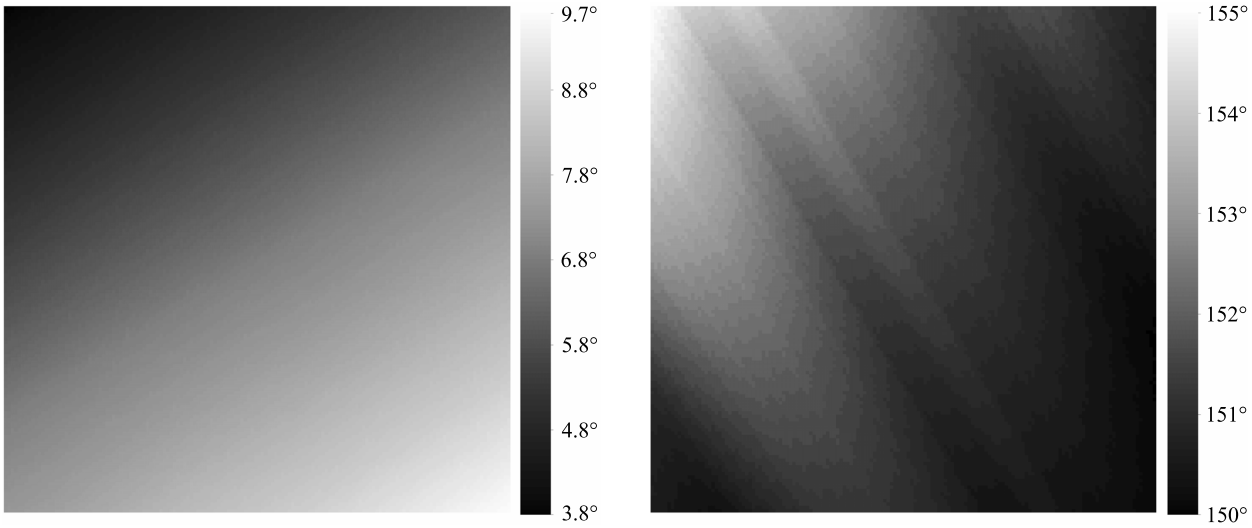

(a) Zenith angle (b) Azimuth angle

Fig. 1. Specific viewing angle of each pixel, as derived from the APEX acquisition of the scene.

enced to the Swiss national grid CH1903+ and orthorectified using nearest neighbor resampling in PARGE [10]. The geocorrection was based on the digital terrain model DHM25 of the Swiss Federal Office of Topography (Swisstopo, Switzerland).

3. METHODS

A forest scene of 300 m x 300 m was parameterized in DART following a voxel-based forest reconstruction approach described in [9]. In the DART model, a vegetation volume is modeled as a turbid medium parameterized by leaf optical properties, leaf angle distribution, and a plant area index. The final DART scene, which was used for the radiative transfer simulations, consisted of the canopy background (terrain model, background optical properties) and a 3D voxel grid, which was filled by turbid media according to airborne laser scanning and in situ measurements. The voxel size was 2 m x 2 m x 2 m, matching the resolution of the APEX data.

The DART atmosphere was parameterized based on standard gas and aerosol models of MODTRAN and in situ measurements of AERONET [11, 12]. The main principle of atmosphere radiative transfer modeling in DART is described in [13]. It is based on voxels of the bottom, mid, and high atmosphere, being filled by gases and aerosols. To model the interactions of radiation (scattering, absorption) with the gases and aerosols, specific phase functions are modeled in DART. Recently, the vertical distribution of gases and aerosols as well as the Henyey-Greenstein coefficients that define the aerosol phase function were improved according to the MODTRAN atmosphere model, which can be seen as a standard for radiative transfer modeling within the atmosphere. Compared to results simulated with previous DART versions (v5.4.3 and earlier), an improved accuracy of the atmosphere simulation is expected.

Furthermore, a new module is under development to simulate radiance and reflectance values as measured by passive optical airborne imaging systems. However, the so called airborne image simulation is not limited to sensors mounted on an airplane. It refers to any situation, where the distance between the sensor and the measured target is not large enough to neglect angular variations in viewing geometry by assuming parallel outgoing rays along a single viewing direction.

Instead of one universal viewing direction, a specific azimuth and zenith angle can be defined for each pixel (x,y) of the scene. The ray tracing is then calculated along specific virtual directions, whose vector can change according to the position of the scattering element and the sensor. The concept of virtual directions as additional outputs to discretized directions over the 2-π upper hemisphere was introduced in [14]. It is an efficient way to track rays along arbitrary directions without further contributing to the ray tracing along the fixed, discretized paths.

For a first evaluation of the newly implemented DART functionalities, airborne image simulations were carried out at four selected bands (533, 570, 680, 780 nm) and compared to APEX data and simulations of DART version 5.4.3 along a single view direction. The images were simulated according to the APEX acquisition of the scene and orthorectified for best comparability. The viewing angles were defined according to the azimuth and zenith angles shown in Figure 1.

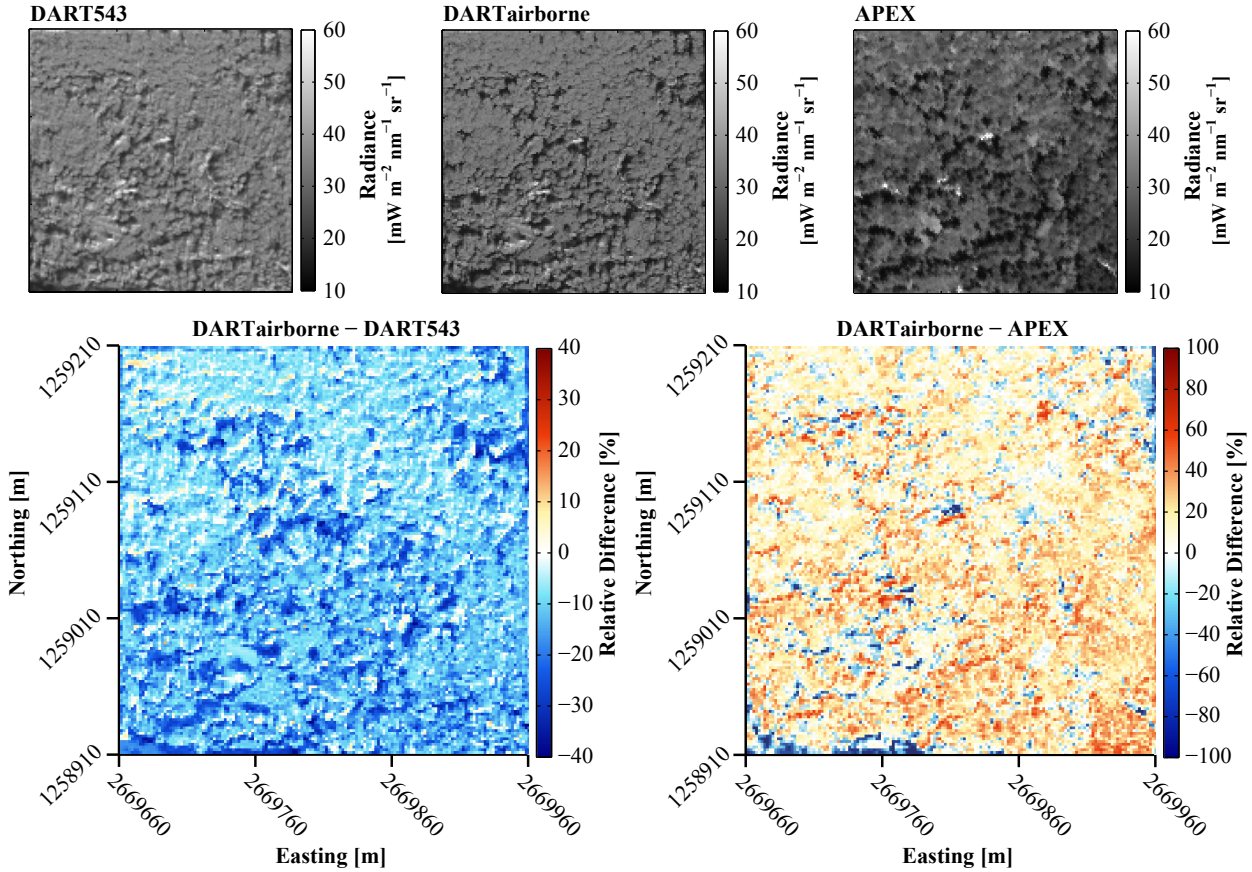

Fig. 2. Images of at-sensor radiance and corresponding relative differences at 570 nm, as simulated by DART version 5.4.3 (DART543), the new airborne image simulation (DARTairborne), and measured by APEX (APEX).

4. RESULTS AND DISCUSSION

We present here the first results of the new airborne image simulation. The simulated and measured at-sensor radiance images at 570 nm and the relative difference images are shown in Figure 2. The new simulation leads to lower radiance values over the whole scene, but especially in shadowed areas. The values can be up to 40% lower and are therefore closer to the values measured by APEX. Generally, the dynamic range is slightly lower in the newly simulated image, because a simplified orthorectification algorithm was used. To calculate an orthorectified image for the airborne image simulation is much more difficult than for a simple directional image, which is why a more sophisticated algorithm is still under development.

Lower radiance values can be observed in all bands of the visible, whereas higher values can be observed in the near infrared. This can be explained by an improved atmosphere modeling using the new airborne image simulation. On one hand, the aerosol phase functions and vertical distribution of gases and aerosols were improved. On the other hand, the atmosphere flux tracking is more accurate if the correct viewing angles are simulated. This effect is especially strong, when at-sensor radiance is simulated.

Since vegetation is absorbing most of the radiation in the visible range, a lower atmospheric path radiance leads to lower at-sensor radiance. The opposite can be observed in the near infrared, because vegetation is strongly scattering. Even though the atmosphere simulation was improved, atmospheric effects are still slightly smaller in the APEX data. The average difference to the APEX image is 4.27, 4.37, 2.08, -25.73 mW m^{-2} nm^{-1} sr^{-1} at 533, 570, 680, 780 nm respectively, whereas it was 9.26, 8.59, 9.14, -37.12 mW m^{-2} nm^{-1} sr^{-1} with DART version 5.4.3.

A pixel-wise comparison with the APEX data shows that there are still major differences at all simulated bands. In the visible, some of the larger differences occur due to local shifts between the images. This is because the projection of modeled (DART) and measured (APEX) data is not exactly the same. More distinct patterns of under- and overestimation

can be observed in the near infrared, which are mainly due to small-scale structural effects. These effects were discussed in detail in [9].

5. CONCLUSION AND OUTLOOK

We presented here first results of a new airborne image simulation within the 3D radiative transfer model DART. The new module allows to define specific viewing angles for each pixel (x,y), instead of assuming parallel outgoing rays along a single viewing direction. A temperate mixed forest scene was simulated according to the measurement of the airborne imaging spectrometer APEX. Compared to the APEX data and simulations of the previous DART release, modeling results could be improved by introducing the airborne image simulation as well as new phase functions and vertical distributions of aerosols and gases. Both, the DART as well as the APEX orthorectification should be improved for future comparisons. Finally, a larger scene has to be modeled to further study the influence of angular variations from near to far range.

6. ACKNOWLEDGEMENTS

This study has been supported by European Space Agency (ESA) Support to Science Element (STSE) ESRIN contract No. AO/1-6529/10/I-NB, '3D Vegetation Laboratory'. Contributions of FS, FM and MS were funded by the University of Zurich Research Priority Program on 'Global Change and Biodiversity'. We thank Paul Sabatier University and French Space Center (CNES) for supporting DART development (TOSCA project STEM-LEAF).

7. REFERENCES

[1] Z. Malenovský, H.M. Bartholomeus, F.W. Acerbi-Junior, J.T. Schopfer, T.H. Painter, G.F. Epema, and A.K. Bregt, "Scaling dimensions in spectroscopy of soil and vegetation," *International Journal of Applied Earth Observation and Geoinformation*, vol. 9, no. 2, pp. 137 – 164, 2007.

[2] M.E. Schaepman, S.L. Ustin, A.J. Plaza, T.H. Painter, J. Verrelst, and S. Liang, "Earth system science related imaging spectroscopy - an assessment," *Remote Sensing of Environment*, vol. 113, Supplement 1, no. 0, pp. S123 – S137, 2009.

[3] N.S. Goel, "Models of vegetation canopy reflectance and their use in estimation of biophysical parameters from reflectance data," *Remote Sensing Reviews*, vol. 4, no. 1, pp. 1–212, 1988.

[4] G.P. Asner, "Biophysical and biochemical sources of variability in canopy reflectance," *Remote Sensing of Environment*, vol. 64, no. 3, pp. 234 – 253, 1998.

[5] J. Verrelst, M.E. Schaepman, Z. Malenovský, and J.G.P.W. Clevers, "Effects of woody elements on simulated canopy reflectance: Implications for forest chlorophyll content retrieval," *Remote Sensing of Environment*, vol. 114, no. 3, pp. 647 – 656, 2010.

[6] J.P. Gastellu-Etchegorry, E. Grau, and N. Lauret, "DART: A 3D model for remote sensing images and radiative budget of earth surfaces," in *Modeling and Simulation in Engineering*, Catalin Alexandru, Ed., chapter 2. 2012.

[7] J.P. Gastellu-Etchegorry, V. Demarez, V. Pinel, and F. Zagolski, "Modeling radiative transfer in heterogeneous 3-D vegetation canopies," *Remote Sensing of Environment*, vol. 58, no. 2, pp. 131 – 156, 1996.

[8] M. Jehle, A. Hueni, A. Damm, P. D'Odorico, J. Weyermann, M. Kneubühler, D. Schläpfer, M.E. Schaepman, and K. Meuleman, "APEX - current status, performance and validation concept," in *Sensors, 2010 IEEE*, 2010, pp. 533–537.

[9] F.D. Schneider, R. Leiterer, F. Morsdorf, J.-P. Gastellu-Etchegorry, N. Lauret, N. Pfeifer, and M.E. Schaepman, "Simulating imaging spectrometer data: 3D forest modeling based on LiDAR and in situ data," *Remote Sensing of the Environment*, 2014, in revision.

[10] D. Schläpfer, M.E. Schaepman, and K.I. Itten, "PARGE: parametric geocoding based on gcp-calibrated auxiliary data," in *Imaging Spectrometry IV*. The International Society for Optical Engineering, 1998, vol. 3438, pp. 334–344.

[11] L.S. Berstein and D.C. Roberston, "MODTRAN: a moderate resolution model for LOWTRAN 7," Tech. Rep. GL-TR-89-0122, Geophys. Lab, Bedford, MA, 1989.

[12] B.N. Holben, T.F. Eck, I. Slutsker, D. Tanré, J.P. Buis, A. Setzer, E. Vermote, J.A. Reagan, Y.J. Kaufman, T. Nakajima, F. Lavenu, I. Jankowiak, and A. Smirnov, "AERONET - a federated instrument network and data archive for aerosol characterization," *Remote Sensing of Environment*, vol. 66, no. 1, pp. 1–16, 1998.

[13] E. Grau and J.-P. Gastellu-Etchegorry, "Radiative transfer modeling in the earth-atmosphere system with DART model," *Remote Sensing of Environment*, vol. 139, no. 0, pp. 149 – 170, 2013.

[14] T. Yin, J.-P. Gastellu-Etchegorry, N. Lauret, E. Grau, and J. Rubio, "A new approach of direction discretization and oversampling for 3d anisotropic radiative transfer modeling," *Remote Sensing of Environment*, vol. 135, no. 0, pp. 213 – 223, 2013.

2.3 Canopy height and plant area index changes in a temperate forest between 2010-2014 using airborne laser scanning

Schneider, F.D., Leiterer, R., Schaepman, M.E., Morsdorf, F.

This section is based on the peer-reviewed conference article:
Proceedings of SilviLaser, 2015, September 28-30, La Grande Motte, France
DOI: 10.5167/uzh-116915

F.D.S., M.E.S., and F.M. designed research; F.D.S., R.L., and F.M. performed research and F.D.S. wrote the paper.

Canopy height and plant area index changes in a temperate forest between 2010–2014 using airborne laser scanning

Fabian D Schneider, Reik Leiterer, Michael E Schaepman, Felix Morsdorf

Remote Sensing Laboratories, University of Zurich, Winterthurerstrasse 190, 8057 Zurich, Switzerland.

Highlights: Changes in canopy height and plant area index (PAI) in a temperate mixed forest were assessed between 2010 and 2014 using airborne laser scanning. Patterns of canopy height change could be identified and related to forest management and tree growth. PAI changes followed no clear patterns and need further investigation.

Key words: *airborne laser scanning, forest change, canopy height, LAI, PAI, full-waveform.*

Introduction

Airborne laser scanning (ALS) is increasingly being used for forestry applications as well as ecosystem monitoring [1]. Its ability to cover large areas in a spatially continuous way offers unique possibilities to characterize canopy architecture. The fast acquisition and repeatability over time allow for monitoring changes in forested ecosystems, for instance due to forest management, forest degradation, logging, or natural changes like tree growth and tree mortality. Two of the most widely used variables to describe canopy architecture of forests are canopy height and leaf- or plant area index (PAI) [2]. Both are essential variables linked to biomass, ecosystem productivity and biodiversity. In particular, the change in canopy height can be assigned to tree growth, a major ecosystem function and important measure for timber production and increase in biomass. [3]

In this study, we assess changes in canopy height over four years in a temperate mixed forest and compared them to changes in plant area index derived from full-waveform airborne laser scanning data. We expect to detect patterns of forest management (selective logging, clear cutting) and change due to tree growth. However, it was not possible to fully link the canopy height change to PAI change (describing the density of leaves and wood). PAI values might be more heavily affected by varying acquisition geometry and point cloud processing, therefore falsely indicating change patterns due to technology and not ecology. The goal of this paper is to assess the change patterns and to attribute potential change sources: forest management, natural change, data acquisition and quality.

Study area & Data

The study area is a temperate mixed forest at Laegern, Switzerland, covering an area of roughly 2 x 2 km. The site is centered at 8.36° lon, 47.48° lat at an altitude of 680 m a.s.l. Deciduous trees are predominant (mainly *Fagus sylvatica, Fraxinus excelsior, Acer pseudoplatanus*) with patches of needle trees (mainly *Picea abies, Abies alba*). The terrain is characterized by a ridge, spanning from east to west, and a gradient of steep (>45°) to less pronounced (0-10°) slopes north and south of the ridge. The forest is semi-natural, since it is partly managed by selective cutting and natural regeneration [4].

Airborne laser scanning data were acquired on August 1, 2010 using a Riegl LMS-Q680i sensor. Data was recorded at a nominal height of 500 m above ground, resulting in a footprint size of approximately 0.25 m. In 2014, Laegern data was acquired between June 19 and July 25 as part of a larger flight campaign. The same sensor was flown (LMS-Q680i) at a nominal height of 700 m above ground, resulting in a footprint size of approximately 35 cm.

Methods

The processing of the canopy height model (CHM) and PAI values was done for both 2010 and 2014 ALS full-waveform data using the same methodology, described in detail below. Local spatial averaging was applied to reduce the influence of representation errors using a circular averaging filter with a radius of 2 pixels. Differences were subsequently calculated by subtracting the 2010 CHM and PAI values from the 2014 values respectively.

The digital terrain model (DTM) was derived from ALS ground returns, which were extracted using an adaptive multi-scale algorithm, filtered and interpolated to a 1x1 m DTM applying ordinary kriging as described in [5]. For each 1x1 m grid cell, the highest point above DTM was used to calculate the CHM.

The PAI was calculated for 2x2 m grid cells following [5]:

$$PAI = c \cdot ln\left(\frac{1 \cdot t_1 + \frac{1}{2} \cdot t_2 + \ldots + \frac{1}{n} \cdot t_n}{1 \cdot g_1 + \frac{1}{2} \cdot g_2 + \ldots + \frac{1}{n} \cdot g_n}\right)$$

where c is a calibration factor determined from in-situ PAI measurements, t_1, t_2,…, t_n are the total number of echoes for each echo type weighted by the total number of returns (*1, 2, …, n* returns) and g_1, g_2,…, g_n are the corresponding number of ground echoes respectively. The echoes for each grid cell were determined by selecting the canopy echoes first, which lie within the 2x2 m grid and more than 4 m above ground. The pulses of the canopy echoes were then tracked to the ground to find the corresponding ground echoes below 4 m above ground, no matter if they lie inside or outside the current grid cell. This leads to a reduced impact of scan angle and scan geometry compared to [5], where total number of echoes and ground echoes were selected strictly within the vertical column of each 2x2 m grid cell. Moreover, the point cloud was restricted to a maximum of 100 pulses per 2x2 m grid cell to reduce bias from extremely high pulse densities in densely vegetated areas.

Results & Discussion

Figure 1 shows the difference images of 2014 CHM and PAI minus 2010 CHM and PAI respectively. The CHM difference map shows clear patterns. The larger dark blue patches show areas of clear cutting, often connected to forest roads. There are also many areas of selective cutting, where single trees were taken out. In total, roughly 48’000 m^2 of forested area was clear-cut in the time between 2010 and 2014. Besides these clear negative change values, there are many patches showing strong increase in canopy height. Especially in the center region, many areas with more than 2 m increase in canopy height due to tree growth were identified. These areas can be assigned to fast growing rejuvenating forest. In 2010, the mean canopy height of these patches was 10.6 m ± 5.8 m.

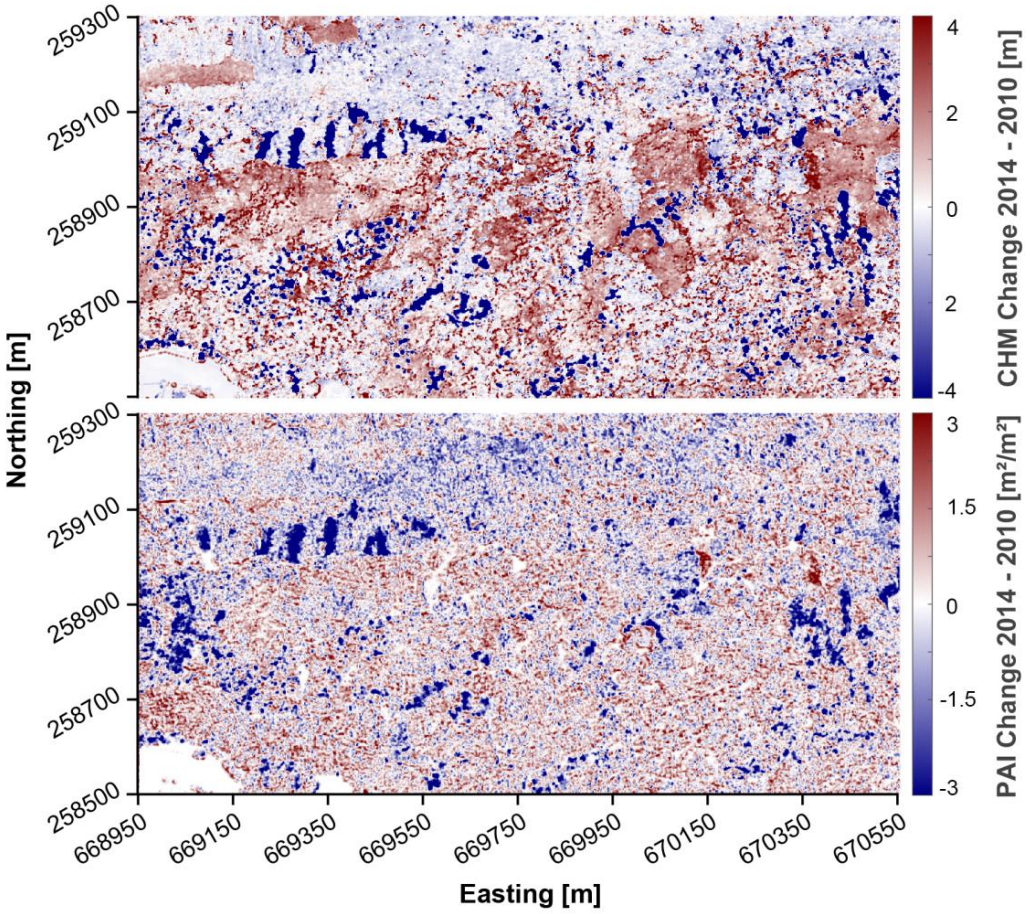

Figure 1: Changes in CHM and PAI between 2010 and 2014 of a 1600 x 800 m subset of the study area (Swiss coordinates CH1903 LV95).

There might be minor local CHM change due to small differences in geo-location of the ALS data. Both datasets have a positional accuracy of < 0.15 m in vertical and < 0.5 m in horizontal direction, as estimated from terrestrially surveyed rooftops. There was no additional co-registration performed between the two datasets. Another reason for the local CHM differences might be representation errors, where the same 3D objects are scanned from two different angles. This can cause CHM differences, which are not linked with the positional accuracy of the datasets. Local spatial averaging helped to reduce these effects, which resulted in a clearer change pattern (Figure 1).

There is a slight underestimation of canopy height in the 2014 dataset compared to 2010. In 2014, the canopy top was probably not captured as reliably as in 2010 due to lower pulse density and higher flight altitude. As reported in [6], an increase in tree height underestimation with increasing flight altitude can be caused by missing the tree tops due to lower pulse density or lower energy being reflected from the canopy surface. Differences in the DTM can represent another source of error, especially in areas of dense understory vegetation. Within the Laegern study area, the mean difference between the DTM of 2010 and 2014 is 0.3 m ± 0.2 m.

The PAI difference map in Figure 1 is more difficult to interpret. The areas of clear cutting and selective cutting can be seen as well. However, all other parts are rather noisy. Some patches with an increase in canopy height also show an increase in PAI, but not all patterns of CHM and PAI change are consistent. In some parts, PAI might already be saturated and not showing an increase in PAI where there is still an increase in CHM observed. When comparing PAI values derived from different acquisitions, representation errors might have a stronger influence than for CHM comparisons. The two datasets were acquired with a different scan geometry: One was flown in east-west direction, whereas the other was flown in north-south direction. So depending on the local observation angle, different parts of the crowns and the ground were observed.

There is no obvious pattern related to pulse density variation, but the pulse density can influence the PAI retrieval in very densely forested areas with few or no ground returns.

Conclusion

We applied CHM and PAI retrieval algorithms on ALS full-waveform data of 2010 and 2014 to compare changes in canopy height and density. Possible sources of the main canopy height changes are forest management (clear cutting, selective cutting) and tree growth (young fast growing trees). Representation errors, differences in data acquisition and geo-correction may lead to a slightly noisy pattern and potential underestimation of canopy height in 2014 compared to 2010. Except for the selective cutting, there are no clear trends in plant area index change. The PAI change patterns are noisier and partly inconsistent with CHM change. Further studies are needed to investigate the influence of pulse density and flight geometry on the PAI retrieval.

Acknowledgements

This study has been supported by the University of Zurich Research Priority Program on ‘Global Change and Biodiversity’ (URPP GCB).

References

[1] Maltamo, M., Næsset, E., & Vaukhonen, J. (2014). Forestry Applications of Airborne Laser Scanning: Concepts and Case Studies. (Managing Forest Ecosystems, 27). Dordrecht: Springer.
[2] van Leeuwen, M., & Nieuwenhuis, M. (2010). Retrieval of forest structural parameters using LiDAR remote sensing. European Journal of Forest Research, 129, 749-770.
[3] Ishii, H.T., Tanabe, S.I., & Hiura, T. (2004). Exploring the relationships among canopy structure, stand productivity, and biodiversity of temperate forest ecosystems. Forest Science, 50, 342-355.
[4] Eugster, W., Zeyer, K., Zeeman, M., Michna, P., Zingg, A., Buchmann, N., & Emmenegger, L. (2007). Methodological study of nitrous oxide eddy covariance measurements using quantum cascade laser spectrometery over a Swiss forest. Biogeosciences, 4, 927-939.
[5] Schneider, F.D., Leiterer, R., Morsdorf, F., Gastellu-Etchegorry, J.-P., Lauret, N., Pfeifer, N., & Schaepman, M.E. (2014). Simulating imaging spectrometer data: 3D forest modeling based on LiDAR and in situ data. Remote Sensing of Environment, 152, 235-250.
[6] Morsdorf, F., Frey, O., Meier, E., Itten, K.I., & Allgöwer, B. (2008). Assessment of the influence of flying altitude and scan angle on biophysical vegetation products derived from airborne laser scanning. International Journal of Remote Sensing, 29, 1387-1406.

2.4 Advancing retrievals of surface reflectance and vegetation indices over forest ecosystems by combining imaging spectroscopy, digital object models, and 3D canopy modelling

Fawcett, D., Verhoef, W., Schläpfer, D., **Schneider, F.D.**, Schaepman, M.E., Damm, A.

This section is based on the peer-reviewed article:
Remote Sensing of Environment, 2018 (204), 583-595
DOI:10.1016/j.rse.2017.09.040

D.F., M.E.S., and A.D. designed research; all authors performed research and wrote the paper, with main contributions of D.F.

Remote Sensing of Environment 204 (2018) 583–595

Contents lists available at ScienceDirect

Remote Sensing of Environment

journal homepage: www.elsevier.com/locate/rse

Advancing retrievals of surface reflectance and vegetation indices over forest ecosystems by combining imaging spectroscopy, digital object models, and 3D canopy modelling

D. Fawcett[a,b,*], W. Verhoef[c], D. Schläpfer[d], F.D. Schneider[a], M.E. Schaepman[a], A. Damm[a,e]

[a] Remote Sensing Laboratories, University of Zurich, Winterthurerstrasse 190, 8057 Zurich, Switzerland
[b] Environment and Sustainability Institute, University of Exeter, Penryn, Cornwall TR10 9DF, United Kingdom
[c] University of Twente, Faculty of Geo-Information Science and Earth Observation (ITC), P.O. Box 217, Enschede 7500 AE, The Netherlands
[d] ReSe Applications Schläpfer, Langeggweg 3, Wil 9500, Switzerland
[e] Department of Surface Waters – Research and Management, Eawag, Swiss Federal Institute of Aquatic Science and Technology, 8600 Dübendorf, Switzerland

ARTICLE INFO

Keywords:
Imaging spectroscopy
Remote sensing
Atmospheric correction
Shadow
APEX
Diffuse and direct irradiance
DOM
DART
NDVI
PRI
Chlorophyll
Carotenoids

ABSTRACT

Imaging spectroscopy based methods offer unique capabilities for retrieving narrow-band vegetation indices which can be empirically related to functional traits of plants. However, in areas with complex topography, illumination effects affect the retrieval of such indices from high spatial resolution airborne or satellite data. Irradiance components at the pixel level are determined by atmospheric composition, as well as instantaneous illumination-surface-sensor geometries. An accurate pixel-wise description of direct and diffuse irradiance components is necessary to perform atmospheric corrections, finally resulting in improved surface reflectances and hence products. We assess three atmospheric correction strategies, differing in their approaches to simulate instantaneous as well as pixel-wise abundances of diffuse and direct irradiance. We use physically-based approaches in combination with either digital elevation models (DEM), fine resolution digital object models (DOM), or 3D modelling output from the Discrete Anisotropic Radiative Transfer (DART) model. The such obtained top-of-canopy reflectances at the Laegern test-site in Switzerland, are used to assess retrieval improvement for a set of indices (Normalized Difference Vegetation Index (NDVI), Photochemical Reflectance Index (PRI), as well as chlorophyll and carotenoid indices). We demonstrate that both, the DOM and the DART based approach, improve the retrievals for flat cast-shadows by ≤71% compared to using a DEM. In dense forest areas, improvements are less significant. Remaining key issues are related to overestimating surface reflectance under extreme illumination conditions.

1. Introduction

Imaging spectroscopy is often employed to infer physiological, biochemical, and structural vegetation traits that eventually allow assessing and monitoring spatio-temporal variations in vegetation functioning, health and status. A wide range of different analytical methods (e.g. vegetation indices, model inversion techniques) are available to retrieve such quantitative information from measured radiometric signals (Kokaly et al., 2009; Schaepman et al., 2009; Ustin et al., 2009). Increasing spectral resolution of optical sensors offers new opportunities in vegetation monitoring, which were not possible before. Besides biochemical vegetation information (e.g. leaf chlorophyll content and leaf water content), functional information such as the de-epoxidation state of xanthophylls (Gamon et al., 1990) and sun-induced chlorophyll fluorescence (Damm et al., 2015a; Rascher et al., 2015) can be retrieved nowadays. The retrieval of such vegetation information is achieved by either measuring subtle changes of leaf reflectance using reflectance based approaches or exploiting narrow atmospheric absorption features using radiance based approaches. Advancements in sensor technology allow combining high spectral with high spatial resolution (Wulder et al., 2004). This information is complex in its nature, in particular due to the increasing shadow fraction for each pixel, in particular in highly vertically structured vegetation. In particular, measurements of individual species, such as trees, are always composed of a mixture of sunlit and shaded parts, complicating retrievals of surface reflectance values as well as functional traits (Gastellu-Etchegorry et al., 1999). Further, highly accurate estimates of surface irradiance are of increasing interest for specialised applications (e.g. Damm et al., 2014). Irradiance varies in intensity and spectral composition, depending on atmospheric composition (Seidel et al., 2012). Direct irradiance at

* Corresponding author.
E-mail address: fawcettdominic@gmail.com (D. Fawcett).

http://dx.doi.org/10.1016/j.rse.2017.09.040
Received 27 January 2017; Received in revised form 24 September 2017; Accepted 30 September 2017
Available online 16 October 2017

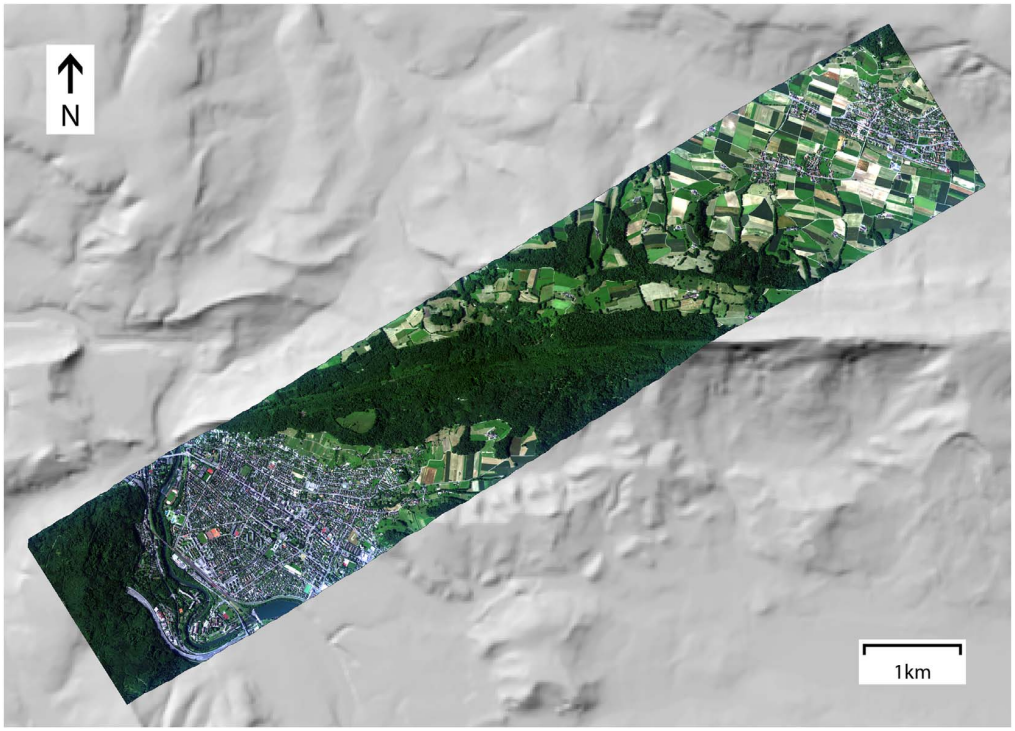

Fig. 1. APEX flight line (at-sensor radiance, RGB colour composite) of the Laegern study site (June 26, 2010, 15:30 UTC). The background is a hillshaded DEM illustrating scene topography (DHM25 from Swisstopo, Switzerland). (For interpretation of the references to colour in this figure legend, the reader is referred to the web version of this article.)

surface level represents radiation which remains un-scattered while diffuse irradiance contains radiation which was previously scattered by gases or aerosols in the atmosphere and by the surroundings of the target surface. Multiple scattering within the atmosphere leads to a wavelength dependent increase of the atmospheric pathway and thus an increase of atmospheric molecular absorption compared to the direct path. It has been demonstrated that these wavelength dependent differences between direct and diffuse irradiance lead to considerable errors in retrieved surface reflectance and subsequently derived vegetation information if pixel-wise estimates of direct and diffuse irradiance are uncertain (Damm et al., 2015b). Accurate and instantaneous atmospheric corrections of high spectral and spatial resolution data are challenging (Matthew et al., 2002; Seidel et al., 2010). The state of the atmosphere at acquisition time plays a vital role because local and temporal variations in water vapour and aerosol loadings impact spectral irradiance estimates (Cho et al., 2003). To overcome this limitation, a precise parameterization of the atmosphere for radiative transfer codes is required (Key and Schweiger, 1998). In order to properly describe these complex irradiance fields, one can no longer assume uniformly flat Earth surfaces or use coarse digital elevation models (DEM) which do not resolve small scale height differences for correction (Richter, 1990, 1998). Several approaches have been discussed to minimize those uncertainties. Minimizing varying illumination effects can be achieved by only considering sunlit pixels (Asner et al., 2015; Malenovský et al., 2013). Other methods include the use of matched filtering of reflectance data to detect and correct shadows (Adler-Golden et al., 2002). More sophisticated approaches make intensive use of auxiliary data. Digital object models (DOM) derived from LiDAR data are used to better represent the surface (Friman et al., 2011). Other approaches involving ray tracing through LiDAR based voxel grids have been proposed (Schläpfer et al., 2003; Kükenbrink et al., 2016). In this study, we hypothesize that (1) more accurate irradiance fields can be modelled by using auxiliary, scene specific data and that (2) these irradiance fields can be integrated in the atmospheric correction process to minimize product sensitivity to illumination effects. This will finally lead to (3) retrievals of vegetation indices showing a substantially reduced sensitivity to surface illumination. We evaluate three approaches for atmospheric correction that are all using four-stream theory (Verhoef and Bach, 2003) and account for direct and diffuse irradiance variations by employing different auxiliary data. All approaches are applied to data acquired with the Airborne Prism Experiment (APEX) imaging spectrometer (Schaepman et al., 2015), allowing an evaluation based on commonly encountered illumination situations. We derive vegetation indices (Normalized Difference Vegetation Index (NDVI), Photochemical Reflectance Index (PRI) and two pigment indices for chlorophyll (CHL) and carotenoids (CAR)) to demonstrate the impact of the correction methods on remote sensing products.

2. Study site and data

2.1. Study site

The Laegern study site is a limestone hill northwest of Zurich, Switzerland (47° 28′ 54.75″ N 8° 23′ 37.82″ E, 866 m a.s.l.), stretching West to East. The site is mainly covered by a temperate mixed forest with a high diversity of tree species (dominated by beech, ash, sycamore and spruce) of different ages and sizes (Eugster et al., 2007). The Laegern is a well-studied site and contains a flux tower which is part of the AERONET (Holben et al., 1998) and FLUXNET (Baldocchi et al., 2001) measurement networks. The extent of the study site used here contains the Laegern forest as well as surrounding agricultural areas.

2.2. Imaging spectrometer data

The main data sets used are two flight lines covering the study site (Fig. 1). They were acquired by APEX on the 26th of June 2010 at 15:30 UTC and on the 29th of June 2010 at 10:00 UTC. The solar zenith and azimuth angles at acquisition time are listed in Table 1. APEX is an airborne pushbroom imaging spectrometer covering the 372 nm to

Table 1
Solar zenith and azimuth angles at acquisition time for the two acquisitions.

Day	Time	Solar zenith	Solar azimuth
June 26	15:30 UTC	48.1	259.0
June 29	10:00 UTC	29.3	138.5

2500 nm region in 312 contiguous spectral bands. In this study, a spectral subset of the available bands is used, ranging from 399 nm to 914 nm, as these bands contain the necessary information to derive the desired vegetation indices and processing time is reduced. In this wavelength range, APEX shows a spectral sampling interval of 0.45–7.5 nm and a spectral resolution of 0.86–15 nm (Schaepman et al., 2015). The data was pre-processed and provided as radiometrically, spectrally and geometrically calibrated radiances (level 1) (Hueni et al., 2009). The two data sets were then georectified using the PARGE software (Schläpfer and Richter, 2002). The resulting pixel size was 2.0 m and based on 18 ground control points, a root mean square error (RMSE) of 2.05 m ± 1.1 m was calculated. Most of the analysis is constrained to a spatial subset covering around 3.5 km^2 with a maximum width of 3.6 km and maximum length of 2.4 km due to the smaller spatial extent of the auxiliary data used. The data set acquired on the 26th acts as primary data set since it shows more extreme illumination conditions at acquisition time. The data set of the 29th is used for cross-validation purposes.

2.3. Elevation models and derived data sets

Two data sources were used to calculate elevation data for further analysis, 1) the swissALTI3D data product (Swisstopo, Switzerland), resolving terrain elevation in 2 m spatial resolution, and 2) airborne laser scanning (ALS) based surface height measurements with a 1 m foot print size (cf. Schneider et al., 2014). The ALS data set was integrated in the swissALTI3D elevation model to increase precision of available height and crown topography information. The spatial resolution of this combined data set was resampled to 2 m to fit the APEX resolution. Two elevation models are derived from this elevation data set for further analysis, a DOM and a DEM. The DOM features the surface height information of 2 m spatial resolution. For the DEM, elevation information was smoothed using a large window low-pass filter. This preserves overall canopy height over forested areas but single trees are not resolved due to the smoothing. From both elevation models, data sets of slope, aspect and illumination were derived using the PARGE software, neglecting reflected terrain irradiance from adjacent pixels. The illumination value is represented by the cosine of the local illumination angle ($cos\theta_{il}$). For the DOM, a binary cast-shadow mask was calculated using PARGE. The cast shadow calculation is based on a ray tracing algorithm which requires the solar azimuth and elevation angles as well as the DOM as input. Obscured pixels are flagged as cast shadows. These are pixels which cannot be reached by rays originating from the sun direction, due to topographic occlusion. The mask is applied to the illumination data so that the illumination equals zero in cast shadows.

3. Methods

3.1. Atmospheric correction approaches

According to Verhoef and Bach (2003), the radiative transfer in the atmosphere-surface system can be sufficiently approximated with the so-called four-stream theory comprising four spectral flux types. The fluxes considered are the downward solar flux, the diffuse downward flux, the diffuse upward flux and the upward spectral radiance in the direction of the observer. This study focuses exclusively on radiative transfer modelling approaches based on this theory to determine top-of-canopy (TOC) hemispherical-directional reflectance factors (HDRF). To elaborate, irradiance is considered hemispherically while reflected radiances are measured by a sensor with a very small but non-zero IFOV (i.e., APEX IFOV is 0.025°). In theory, this results in hemispherical-conical reflectance factors (HCRF). In practice, however, reflectances from such small IFOV measurements are generally referred to as HDRF to differentiate them from wide IFOV instrument results (cf. Schaepman-Strub et al., 2006 for details on terminology). Calibrated radiance data is processed to HDRF data using a simplified atmospheric correction approach compared to the state of the art atmospheric correction software ATCOR-4 (Richter and Schläpfer, 2002, 2016). The simplified approach includes the complete four-stream radiative transfer calculations but excludes atmospheric parameter retrieval, spectral polishing, and radiometric fine tuning steps as implemented in ATCOR-4. We decided on a simplified atmospheric correction approach to ease evaluations and adjustments of atmospheric correction strategies. We also applied ATCOR-4 and used obtained HDRF as a reference to evaluate reliability of results stemming from the simplified atmospheric correction approach. In general, the atmospheric correction process can be divided into the following four steps: i) the simulation and storage of atmospheric transfer functions in look-up tables (LUT), ii) the estimation of spectral shifts and band broadening, iii) the convolution of the atmospheric functions considering the actual spectral sensor configuration, and iv) the calculation of HDRF values by combining measured at-sensor radiances and simulated LUT entries. The simulation of atmospheric functions is performed for five different ground heights using MODTRAN5 (Berk et al., 2006) and the MODTRAN interrogation technique as introduced by Verhoef and Bach (2003). Atmospheric variables water vapour and aerosol optical thickness (AOT), required to parameterize MODTRAN5, were chosen based on sun-photometer measurements from a close by AERONET station (Holben et al., 1998) and ATCOR-4 image-based retrievals. The simulation of combined atmospheric functions (e.g., combined downward and upward transmittances) was performed in this step to avoid violation of the Beer-Lambert law in subsequent calculations with convolved functions (Verhoef et al., 2014). The estimation of potential spectral misregistrations, also known as spectral smile, common to pushbroom spectrometers, and band broadening of APEX was performed with a method included in ATCOR-4 (Richter et al., 2011). Obtained spectral characteristics of APEX are used to generate spectral response functions to eventually convolve simulated atmospheric functions. The atmospheric correction approaches used in this study are listed in Table 2. The method of simulating irradiance is varied in three steps of theoretically increasing accuracy. Each method requires a different set of auxiliary data as input. The first approach approximates irradiance variations using a coarse DEM and serves as a reference (DEMAC). The second approach follows the same procedure but uses a DOM to determine irradiance (DOMAC). Finally, the third approach utilizes irradiance scaling factors derived from TOC irradiances simulated by the 3D Discrete Anisotropic Radiative Transfer (DART) model

Table 2
Reference for the atmospheric correction approaches used, their acronyms and auxiliary data inputs from which irradiance is derived.

Acronym	Input	Description
ATCOR	DEM	Atmospheric correction performed with the ATCOR-4 software
DEMAC	DEM	Simplified atmospheric correction procedure based on four-stream theory
DOMAC	DOM	Identical to DEMAC but using a DOM as input
DARTAC	Parameterized voxel grid	Identical to DEMAC but utilizing DART derived irradiance fraction maps as scaling factors

(Gastellu-Etchegorry et al., 2015) (DARTAC). The three methods are elaborated in the following sections.

3.1.1. DEMAC: simple atmospheric correction using a smoothed digital elevation model

Verhoef et al. (2014) have used the four-stream theory to simulate top-of-atmosphere (TOA) radiances using combined models (e.g., SCOPE (Van der Tol et al., 2009), and MODTRAN4). According to them, the radiative transfer through the atmosphere yielding TOA radiance for a target (L_{TOA}) can be described as (Eq. (1)):

$$L_{TOA} = \rho_{so}\frac{E_s^o \cos\theta_s}{\pi} + \left[\frac{\tau_{ss} r_{so} E_s^o \cos\theta_s}{\pi} + \frac{(\tau_{sd}+\tau_{ss}\overline{r_{sd}}\rho_{dd})E_s^o \cos\theta_s/\pi}{1-\overline{r_{dd}}\rho_{dd}} r_{do}\right]\tau_{oo} + \left[\frac{(\tau_{sd}\overline{r_{dd}}+\tau_{ss}\overline{r_{sd}})E_s^o \cos\theta_s/\pi}{1-\overline{r_{dd}}\rho_{dd}}\right]\tau_{do}. \quad (1)$$

Eq. (1) is formed by three additive terms including the atmospheric path radiance, the target's surface radiance, and the adjacency effect. The surface reflectance can be described by four terms: r_{so} is the bi-directional reflectance factor of the target (BRF), r_{do} the hemispheric-directional reflectance factor of the target (HDRF), $\overline{r_{sd}}$ is the smoothed directional-hemispherical reflectance factor (DHRF) of the surroundings and $\overline{r_{dd}}$ is the smoothed bi-hemispherical reflectance factor (BHRF) of the surroundings. ρ_{so} is the atmospheric bi-directional reflectance and ρ_{dd} is the spherical albedo at the bottom of the atmosphere. τ_{ss} represents the direct atmospheric transmittance in sun-direction, τ_{oo} the direct atmospheric transmittance in view-direction, τ_{sd} the diffuse atmospheric transmittance for the solar incidence, and τ_{do} the directional atmospheric transmittance for diffuse incidence. E_s^o is the extra-terrestrial solar spectral irradiance on a plane perpendicular to the sun-rays. θ_s is the local solar zenith angle (Cogliati et al., 2015). Eq. (1) can be written following the T-18 system as introduced by Verhoef et al. (2014). When adding viewing factors for direct and diffuse irradiance (V_{sun}, V_{sky}) (Verhoef and Bach, 2012), L_{TOA} of a non-Lambertian, non-uniform and tilted surface can be expressed as (Eq. (2)):

$$L_{TOA} \approx T_1 T_2 + \frac{T_1(T_8 r_{so} V_{sun} + T_9 r_{do} V_{sky} + T_{10}\overline{r_{sd}} + T_{11}\overline{r_{dd}})}{1-\overline{r_{dd}}T_3}. \quad (2)$$

While T_n represent atmospheric transfer functions (Table 3), $\bar{r}$ indicate smoothed averaged reflectances and V_{sun}, V_{sky} can be expressed as (Eqs. (3) and (4)):

$$V_{sun} = \cos\theta_t + \tan\theta_s \sin\theta_t \cos(\varphi_s - \varphi_t) \quad (3)$$

$$V_{sky} = \frac{1+\cos\theta_t}{2}. \quad (4)$$

V_{sun} and V_{sky} are scaling factors that express in a simple way how the direct irradiance of the sun and the diffuse irradiance of the sky are changed by the local topography. θ_t is the terrain slope inclination, φ_t the terrain slope azimuth, and φ_s the solar azimuth angle.

Table 3
Atmospheric functions and their abbreviations. Angled brackets represent convolved quantities.

Atmospheric function	Name
$\langle E_s^o\rangle \cos\theta_s/\pi$	T_1
$\langle\rho_{so}\rangle$	T_2
$\langle\rho_{dd}\rangle$	T_3
$\langle\tau_{ss}\rangle$	T_4
$\langle\tau_{sd}\rangle$	T_5
$\langle\tau_{oo}\rangle$	T_6
$\langle\tau_{do}\rangle$	T_7
$\langle\tau_{ss}\tau_{oo}\rangle$	T_8
$\langle\tau_{sd}\tau_{oo}\rangle$	T_9
$\langle\tau_{ss}\tau_{do}\rangle$	T_{10}
$\langle\tau_{sd}\tau_{do}\rangle$	T_{11}

Assuming a Lambertian Earth surface, reflectance quantities can be assumed similar (i.e., TOC reflectance (r) = $r_{so} = r_{do}$ and TOC adjacent reflectance ($\bar{r}$) = $\overline{r_{sd}} = \overline{r_{dd}}$) so that one can rewrite Eq. (2) to yield r from the measured at-sensor radiance. However, since $\bar{r}$ is still unknown it must be estimated in two steps using a simplified version of Eq. (2) where we assume a non-tilted, uniform Lambertian Earth surface and use filtered radiances ($\overline{L_{TOA}}$) (Eq. (5)). The employed kernel is sharply peaked towards the centre and was derived from the results of a Monte Carlo simulation of photon scattering, which allows a description of the adjacency effect by considering the contribution of photons from ring-shaped intervals of increasing distance to the target. Commonly, adjacency is estimated using only smoothed reflectance values (e.g. Richter, 1998).

$$\bar{r} = \frac{\overline{L_{TOA}} - T_1 T_2}{T_1(T_8+T_9+T_{10}+T_{11}) + (\overline{L_{TOA}} - T_1 T_2)T_3}. \quad (5)$$

This finally allows a retrieval of r as follows (Eq. (6)):

$$r = \frac{(L_{TOA} - T_1 T_2)(1-\bar{r}T_3) - \bar{r}T_1(T_{10}+T_{11})}{T_1(T_8 V_{sun} + T_9 V_{sky})}. \quad (6)$$

This reflectance retrieval method is applied in combination with the smoothed DEM and further referred to as DEMAC.

3.1.2. DOMAC: simple atmospheric correction using a digital object model

The smoothed DEM used in the DEMAC approach does not resolve single canopies and therefore can't be employed to describe the strongly varying irradiance at canopy scale. In order to do this, we use a LiDAR based DOM instead. This effectively influences only the scaling factors V_{sun} and V_{sky} while the processing steps remain identical to DEMAC, reflectance being retrieved with Eq. (6). The geometric surface description with a DOM has some limitations as it will yield V_{sun} values of 0 for strongly inclined tree canopies with slopes facing away from the sun as well as for cast-shadows. While a complete lack of direct irradiance is unlikely in these situations, the assumption was deemed adequate for this experiment and resulting overestimates of HDRF taken into account. This reflectance retrieval approach is referred to further as DOMAC.

3.1.3. DARTAC: DART radiance output approach

The DART model (Gastellu-Etchegorry et al., 2015) is increasingly applied in vegetation analysis, for example as a tool to simulate at-sensor radiance data by parameterizing the model using LiDAR data (Schneider et al., 2014). The potential of such 3D radiative transfer modelling frameworks to derive accurate irradiance estimates has been suggested in previous work (Schläpfer et al., 2003). For our study site, LiDAR point cloud measurements were acquired by an ALS system close to the acquisition of APEX data. The point cloud was converted into a voxel grid and associated with different properties. A tree canopy voxel, for example, was assumed as turbid medium with certain leaf optical properties, plant area index (PAI) and a specific angular distribution of leaves (Gastellu-Etchegorry et al., 2015). For a detailed description of the parameterization of the 3D voxel grid, we refer to Schneider et al. (2014) and Schneider et al. (2015), while details on the DART simulation process can be found in Gastellu-Etchegorry et al. (2015). Due to computational constraints, only 24 scattering directions were used and a maximum of 3 iterations were performed. Direct and diffuse irradiances at TOC were derived from DART simulation outputs as 2D grids of irradiance in W/m^2 for four wavelengths representing blue, green, red and NIR. The irradiance fractions per pixel (henceforth K_{dir} and K_{dif}) were derived relative to the maximum direct or diffuse irradiance, excluding outliers resulting from processing artefacts, and linearly interpolated for the wavelengths not simulated. For direct irradiance, the scaling factors remain constant over all wavelengths, while for diffuse

irradiance there are wavelength dependent differences. As the wavelengths used for further analysis lie close to the simulated wavelengths, this approximation is deemed sufficient. The fractions can be applied directly as scaling factors for the direct and diffuse fluxes to retrieve r (Eq. (7)):

$$r = \frac{(L_{TOA} - T_1 T_2)(1 - \bar{r} T_3) - \bar{r} T_1 (T_{10} + T_{11})}{T_1 (T_8 K_{dir} + T_9 K_{dif})}. \quad (7)$$

This approach is further referred to as DARTAC.

3.2. Field spectrometer measurements

Two ASD field spectroradiometer (ASD FieldSpec, Analytical Spectral Devices, USA) measurements acquired during the 2010 APEX validation campaign in Wettingen, Switzerland were used as ground-truth data for this study. The measured spectra allow an evaluation of the atmospheric correction method's performance. The reference surfaces were selected based on uniformity of the target, lack of inclination and are pseudo-invariant features. The surfaces are yellow tartan of the Wettingen sports-ground (47° 28′ 02.30″ N 8° 18′ 33.90″ E) and a black roof of the swimming baths (47° 27′ 58.84″ N 8° 18′ 38.86″ E) which showed near uniform reflectance over all wavelengths. The measurements were conducted close to acquisition time for both dates and perpendicular to the surfaces.

3.3. Deriving vegetation indices

A number of vegetation indices were derived from TOC reflectance data to evaluate the impact of irradiance effects and their compensation using the three approaches under evaluation. The use of vegetation indices is an empirical approach to relate light measurements to vegetation information. Even if properly calibrated for a specific site, vegetation type and phenological period, wrong estimates of surface irradiance pose an additional sensitivity to these indices and complicate their interpretation. We focus our choice on indices that incorporate spectral information from the VIS/NIR wavelength regions since they are more strongly affected by illumination effects and estimated errors can serve as worst case scenarios. Calculated indices include the NDVI, commonly used as a proxy for canopy chlorophyll content and fAPAR (Tucker, 1979) (Eq. (8)) and the PRI, indicative of the de-epoxidation state of xanthophylls and often applied as proxy for light use efficiency (LUE) (Gamon et al., 1992, 1997) (Eq. (9)). Further, we applied two indices sensitive to the relative content of chlorophyll and carotenoids as proposed by (Gitelson et al., 2006) (Eqs. (10) and (11)).

$$NDVI = \frac{r_{800} - r_{640}}{r_{800} + r_{640}} \quad (8)$$

$$PRI = \frac{r_{531} - r_{570}}{r_{531} + r_{570}} \quad (9)$$

$$CHL \propto [r_{540-560}^{-1} - r_{790}^{-1}] \times r_{790} \quad (10)$$

$$CAR \propto [r_{510-520}^{-1} - r_{560-570}^{-1}] \times r_{790}. \quad (11)$$

Subscripts in Eqs. (10) and (11) indicate wavelength ranges in nanometers used for the calculation of both indices. Gitelson et al. (2006) provide two models each for CHL and CAR, one incorporating green wavelengths and the other the red edge. We use the mean values over the proposed green wavelength ranges here as they should be more susceptible to differences in irradiance composition.

3.4. Assessment of irradiance effects on vegetation indices

The performance of the DEMAC, DOMAC and DARTAC approaches for the removal of illumination effects in vegetation products is evaluated by comparing obtained index values with reference values representing fully illuminated cases. We set up two tests, the first evaluating the performance of the three approaches in cast-shadows, the second focussing on a forest subset. For the cast-shadow test, a number of areas were chosen and divided into sparsely and densely vegetated surfaces. “Sparsely” vegetated surfaces are surfaces with very low vegetation fraction (e.g. below 10%), close to bare-soil. “Densely” vegetated surfaces have a vegetation cover of 100%. It must be noted that slight changes in the species composition are possible for sparsely vegetated surfaces. We assume, however, that these changes are negligible and do not impact our results. The reference value is extracted over horizontal, fully illuminated areas of the same surface type in the DEMAC result. For the forest test, reference values represent the mean of horizontally oriented and fully illuminated areas (tops of tree canopies) extracted from the DEMAC result. For both tests, mean values of pixel-wise absolute differences between the index and the reference mean value are calculated. The pixel-wise differences are used in order to reflect heterogeneity in the result. Pixel values outside of physically feasible ranges are omitted. Finally, the improvement of the DOMAC and DARTAC approaches over the DEMAC approach is expressed as percentage by which the difference of the index to the reference value for the DEMAC approach could be reduced with either the DOMAC or DARTAC approach. The significance of this difference is assessed using a paired t-test with 95% significance level ($p \ll 0.05$).

4. Results

4.1. DEMAC in comparison with ATCOR

An evaluation of DEMAC with ATCOR-4 was performed to confirm its suitability for further analysis. We particularly compared derived HDRF obtained from both approaches for two acquisition dates of pseudo-invariant features and related them to surface HCRF measurements obtained with a field spectroradiometer (ASD FieldSpec, Analytical Spectral Devices, USA). The results for one such surface are displayed in Fig. 2. For both the 26th and the 29th of June 2010, the mean difference in percent over all bands between DEMAC and ATCOR-4 is around 16% on average. Considering ASD measured HCRF, the DEMAC approach differs by 8.7% for the 26th of June and 23.2% for the 29th of June. ATCOR-4 HDRF values differ from ASD measurements by 9.2% for the 26th and 5.0% for the 29th. Comparisons of HCRF with HDRF should be made with caution as they represent different physical quantities. Furthermore, the deviations between solar zenith angles during APEX and ASD acquisitions are up to 20°. The mean difference in percent between ATCOR-4 based HDRF for the two days is 14.5% while this difference is 13% for DEMAC. It is possible that this variation can be partly explained by the difference in solar zenith angle in combination with reflectance anisotropy effects. Absolute deviations of obtained HDRF values between DEMAC and ATCOR-4 are not detrimental for subsequent analysis. However, some differences appear to be wavelength dependent. ATCOR-4 results appear more robust over wavelengths, while the DEMAC results fit better with each other and to the ASD spectrum in the 500–600 nm range but deviate more in the NIR. The precise reason, especially for the deviation in the NIR, could not be identified, but there are two differences between the DEMAC approach and ATCOR-4 that likely explains observed differences: i) ATCOR-4 uses the horizon algorithm providing a more accurate value for V_{sky} than the slope based calculation used in DEMAC. ii) In the chosen ATCOR-4 configuration, atmospheric conditions are specified with a constant AOT across the scene but varying water vapour over the image, and viewing angle dependent scattering functions for the correction of aerosol effects were used. In DEMAC, atmospheric parameters were obtained from AERONET and ATCOR-4 and only distributed considering ground and sensor height. The compensation of adjacency effects was evaluated by observing the averaged HDRF of a black rooftop (height 5 m) (Fig. 3). ASD measurements suggest a spectrally featureless reflectance behaviour with average values of 5%. The rooftop is located in a valley situation and is surrounded by vegetation (trees and

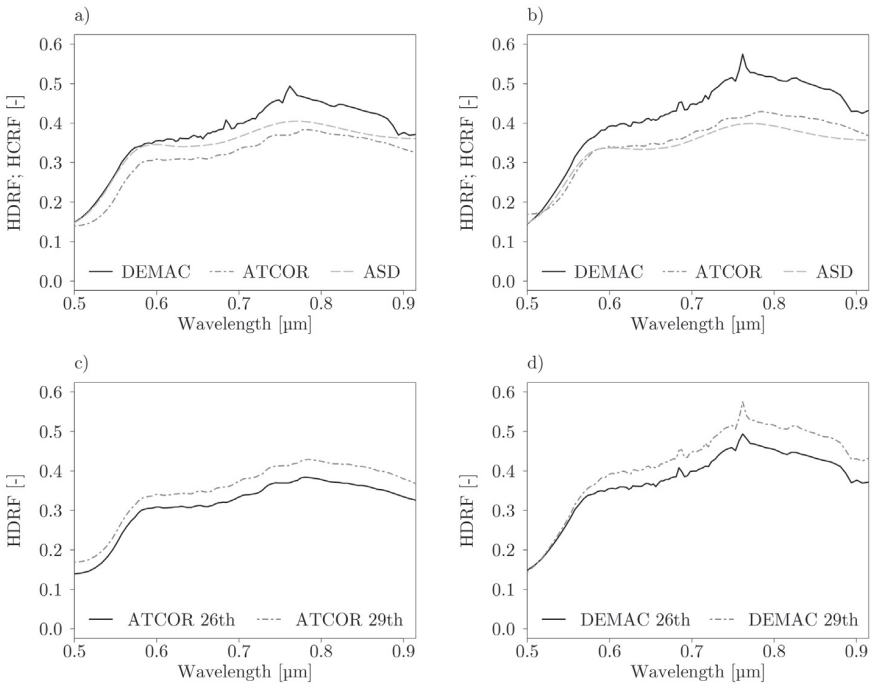

Fig. 2. Comparison of reflectance spectra of a yellow tartan sports-surface, resulting from ASD measurements (HCRF), the DEMAC approach (HDRF), and the ATCOR-4 processing (HDRF). a) 26.06.2010 data set. b) 29.06.2010 data set. c) ATCOR-4 result comparison between the two dates. d) DEMAC comparison between the two dates. It must be noted that results for the DEMAC and DOMAC approach are identical for flat surfaces such as the investigated tartan. (For interpretation of the references to colour in this figure legend, the reader is referred to the web version of this article.)

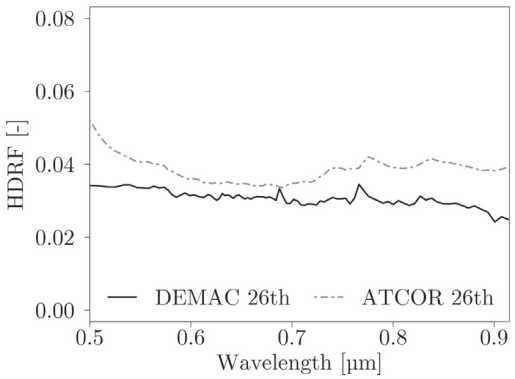

Fig. 3. Comparison of HDRF spectra averaged over a dark, spectrally uniform reflecting roof for the DEMAC approach and the ATCOR-4 processing, both for the 26.06.2010 data set.

vegetated mountains). Scattering of adjacent vegetation surfaces would add a signal to the almost non-reflective rooftop contribution if not adequately corrected. There are no remnants of any vegetation signals visible in obtained HDRF spectra and barring a very slight slope towards NIR wavelengths, the adjacency effect compensation appears to be sufficient. It must be noted that HDRF values resulting from DEMAC were not smoothed or interpolated as is done in ATCOR-4, resulting in the visible spikes in the spectrum; differences attributed to this were deemed negligible. The spikes originate from residual errors in estimated spectral shift and band broadening. If such spectral information is used to convolve atmospheric functions to match the in-flight spectral setting of the sensor, spikes typically occur across strong atmospheric or solar absorption lines. Despite certain deviations between HDRFs obtained from ATCOR-4 and our implementation, for the evaluated situations the DEMAC procedure was deemed to perform within sufficient accuracy which is comparable to a more complex correction scheme in common use.

4.2. *Improvement of reflectance retrieval with digital object models*

The evaluated DOMAC approach incorporating a DOM to improve irradiance estimates by considering crown geometry yields diverse results. Shaded canopy areas show overestimates of obtained HDRF values (above 100% reflectance) (Fig. 4). This is mainly since V_{sun}

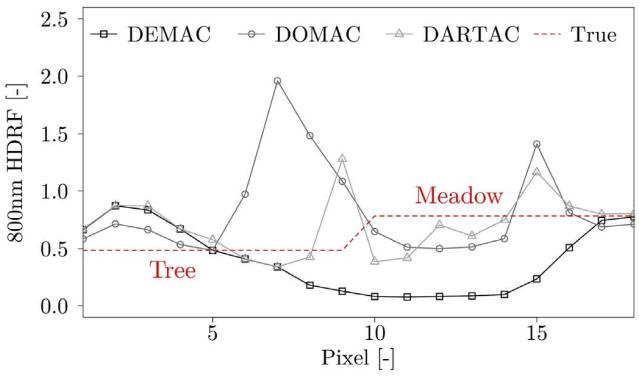

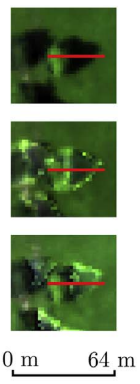

Fig. 4. Left: HDRF at 800 nm along a tree-crown to meadow cast-shadow transect (left to right) resulting from DEMAC, DOMAC and DARTAC. The red dashed line indicates the expected true HDRF along the transect for the tree and meadow surfaces. Right: Illustration of the transect for the DEMAC, DOMAC and DARTAC based results as true colour RGB images (top to bottom). The red line indicates the transect as shown in the left figure. (For interpretation of the references to colour in this figure legend, the reader is referred to the web version of this article.)

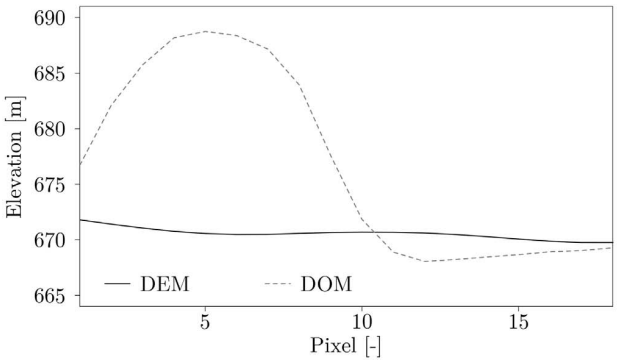

Fig. 5. Left: Surface elevation along a tree-crown to meadow cast-shadow transect for the smoothed digital elevation model (DEM) and the digital object model (DOM). Right: Image representation of the smoothed DEM (top) and DOM (bottom). The red line indicates the transect as shown in the left figure. (For interpretation of the references to colour in this figure legend, the reader is referred to the web version of this article.)

approaches 0 and due to the large slope angle ($\cos\theta_t$) for such canopy areas, the diffuse component is also heavily reduced through V_{sky}. For sunlit canopy areas, HDRF differences are reduced. This observation could be confirmed also for a large forest canopy subset, where small slope angles yielded improved corrections and steep angles led to overcorrections.

While an offset remains, areas affected by cast-shadows experience an improved correction of illumination effects when compared to fully illuminated regions, as also visible in the transect of Fig. 4 and the region of interest (ROI) comparison of Fig. 6. Exceptions are transition zones from fully illuminated to fully shaded areas, visible as spikes in the transect (Fig. 4). The observed effect is caused by a complex interplay of different factors, including residual geometric co-registration errors between the DOM and the spectroscopy data, the simplified radiative transfer scheme applied that neglects vertical radiation entering the surface, as well as canopy transparency at the outer crown leading to a very uneven illumination pattern in the transition zone of cast shadow and full illumination i.e. mixture of sun flecks and shade. The percentage deviation of retrieved HDRF in cast-shadows from illuminated areas was calculated. The DEMAC-illuminated pixels with little to no slope are considered as reference under the assumption that these are closest to the sought surface reflectance under illuminated conditions, as the surface covered by these pixels receives full direct and diffuse illumination. DEMAC-shade and DOMAC-shade belong to pixels of shaded vegetated surfaces. Since the DEM approach does not resolve canopy topography (see Fig. 5), the approach assumes full illumination for these cast-shadow pixels although they predominantly receive diffuse irradiance. This yields an underestimation of retrieved reflectance because irradiance is overestimated (L/E). Conversely, the use of a DOM provides an improved estimate of E, thus retrieved reflectance is closer to the reflectance of the fully illuminated surface. The deviation of HDRF between illuminated and shaded ROIs decreased on average over all bands from 86.4% for DEMAC to 37.5% for the DOMAC approach. There are still deviations between calculated means of up to 56.55%, mainly around 700 nm. Finally, the spatial difference between illuminated reference and shaded ROIs guarantee variance but this was considered during selection and kept as small as possible.

4.3. Improvement of reflectance retrieval with simulated irradiance fractions

Using scaling factors derived from DART simulations to adjust estimates of diffuse and direct irradiance components in atmospheric correction approaches should in theory provide benefits over the DOMAC approach: They are ray-tracing based which allows accounting for multiple scattering within the canopy. Indeed, we observe fewer

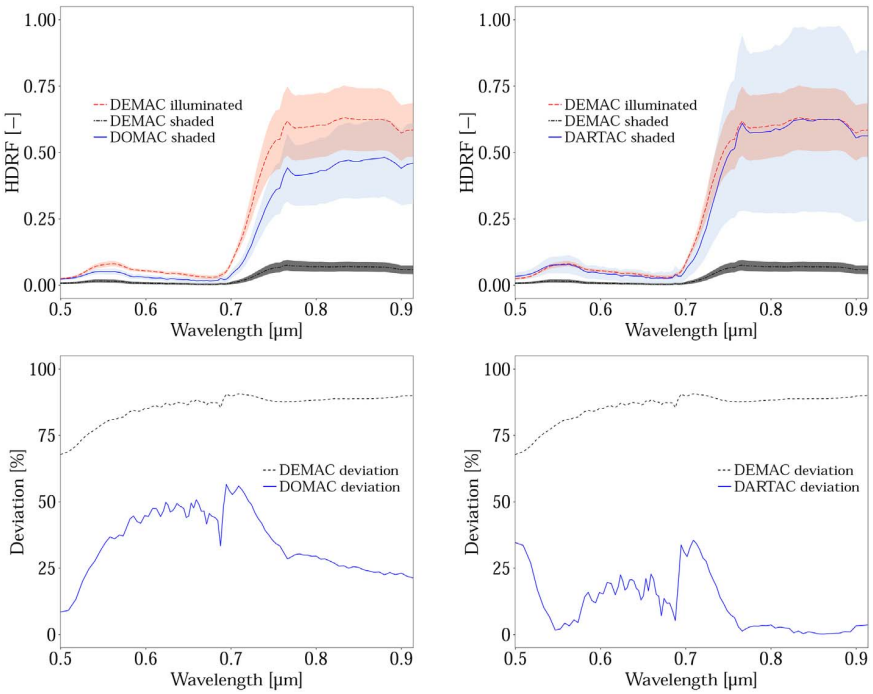

Fig. 6. Top: HDRF of shaded surfaces before and after correction. Left: HDRF from the DEMAC approach averaged over fully illuminated regions of interest (ROIs) on highly vegetated surfaces (illuminated), HDRF obtained from the DEMAC approach over cast-shadow ROIs on highly vegetated surfaces (shaded), corrected HDRF from the DOMAC approach averaged over the same cast-shadow ROIs (shaded), and the ribbons representing mean ± one standard deviation for each spectrum. Right: the same as left but with the correction from the DARTAC approach. Bottom: Deviation in percent of the cast-shadow reflectances in respect to the fully illuminated case. Left: Deviation of the DEMAC HDRF and the DOMAC HDRF. Right: the same as left but for DARTAC.

Table 4
Impact of illumination effects on NDVI, PRI, chlorophyll and carotenoid index retrievals for densely vegetated surfaces. Index values in cast-shadow and fully illuminated areas were compared. The compensation of illumination effects using three atmospheric correction strategies (DEMAC, DOMAC and DARTAC approaches) was evaluated. Calculated statistics include mean, standard deviation, mean pixel-wise absolute difference to the illuminated reference value and percent reduction of this difference in respect to the DEMAC case.

		Mean	StDev	Abs Diff	% Diff reduced
NDVI	Reference	0.863	0.039	–	–
	DEMAC	0.860	0.057	0.046	–
	DOMAC	0.900	0.042	0.046	−0.2
	DARTAC	0.890	0.044	0.042	8.6
PRI	Reference	−0.012	0.014	–	–
	DEMAC	0.109	0.024	0.121	–
	DOMAC	0.061	0.024	0.074	39.4
	DARTAC	0.053	0.030	0.067	44.9
CHL	Reference	6.536	1.219	–	–
	DEMAC	3.678	1.202	2.912	–
	DOMAC	7.300	2.208	1.778	38.9
	DARTAC	6.448	1.837	1.504	48.3
CAR	Reference	7.435	2.137	–	–
	DEMAC	1.541	0.575	5.893	–
	DOMAC	4.222	1.357	3.249	44.9
	DARTAC	4.045	1.445	3.393	42.4

overestimates of HDRF values over tree canopies in DARTAC results, but reflectance gradients seem to have been conserved for the most part (Fig. 4). Evaluating corrected HDRF values at 800 nm over a forest subset, there appear to be generally lower reflectances compared to the DEMAC with a number of single pixels showing seemingly arbitrary high reflectance. These over estimated HDRF values are associated with gaps between trees where both direct and diffuse irradiance drop to near zero. We did not find a significant correction of shadowing effects across the tree canopies. Overestimated HDRF values are mainly visible in transition zones from shade to full illumination, where we observe a spatial mismatch between simulated and actual cast-shadows in the order of up to two pixels (4 m) in the most extreme cases, as well as for aforementioned small gaps between trees in the forest. The cast-shadow transect (Fig. 4) reveals a spike where the simulated shadow extends further than the actual shadow but the difference between shaded and illuminated pixels is clearly reduced. In the ROI comparison, we found a far larger heterogeneity with small scale over and under corrections of HDRF values. When averaged, their reflectance is comparable to fully illuminated counterparts (Fig. 6). Averaged over all bands, the deviation in percentage from illuminated areas to corrected shaded counterparts has decreased to 9.6% when using DARTAC. The highest deviation between the averages is 35.5% and is observable at the red-edge.

4.4. Vegetation indices

Results for the evaluation of correction approaches for all vegetation products are presented in Tables 4 and 5 for the cast-shadow test and for the forest test in Table 6. Differences between index and reference values larger than for the DEMAC case result in negative percentages for “Diff reduced” while an equal difference corresponds to 0% and a full reduction of differences and therefore a perfect match of index with reference values corresponds to 100%. A paired *t*-test with 95% significance level indicates that mean values of all DOMAC and DARTAC results are significantly different from the DEMAC result. Fig. 7 illustrates results for a subset of the scene containing a heterogeneous vegetation cover and illumination conditions, while Fig. 8 depicts the spatial differences from the DEMAC results as well as images of the direct illumination and DOM for reference.

Table 5
Impact of illumination effects on NDVI, PRI, chlorophyll and carotenoid index retrievals for sparsely vegetated surfaces. Index values in cast-shadow and fully illuminated areas were compared. Statistics are described in Table 4.

		Mean	StDev	Abs Diff	% Diff reduced
NDVI	Reference	0.489	0.032	–	–
	DEMAC	0.450	0.069	0.063	–
	DOMAC	0.579	0.058	0.093	−47.9
	DARTAC	0.572	0.070	0.088	−39.6
PRI	Reference	−0.063	0.009	–	–
	DEMAC	0.039	0.024	0.103	–
	DOMAC	−0.006	0.022	0.058	43.8
	DARTAC	−0.030	0.023	0.035	65.7
CHL	Reference	2.226	0.232	–	–
	DEMAC	0.815	0.294	1.411	–
	DOMAC	2.127	0.498	0.409	71.0
	DARTAC	2.279	0.777	0.563	60.1
CAR	Reference	1.071	0.207	–	–
	DEMAC	0.101	0.104	0.970	–
	DOMAC	0.592	0.194	0.491	49.3
	DARTAC	0.979	0.561	0.464	52.2

Table 6
Impact of illumination effects on NDVI, PRI, chlorophyll and carotenoid index retrievals for a forest canopy. Index values in inclined and flat, fully illuminated areas were compared. Statistics are described in Table 4.

		Mean	StDev	Abs Diff	% Diff reduced
NDVI	Reference	0.904	0.020	0.000	0.0
	DEMAC	0.902	0.026	0.015	0.0
	DOMAC	0.910	0.024	0.018	−14.9
	DARTAC	0.900	0.026	0.016	−1.8
PRI	Reference	−0.013	0.016	0.000	0.0
	DEMAC	−0.002	0.031	0.021	0.0
	DOMAC	−0.014	0.026	0.019	13.0
	DARTAC	0.000	0.028	0.021	3.5
CHL	Reference	9.146	1.654	–	–
	DEMAC	8.981	1.657	1.297	–
	DOMAC	10.645	3.058	2.393	−84.5
	DARTAC	8.738	1.801	1.401	−8.0
CAR	Reference	9.253	1.674	–	–
	DEMAC	8.107	2.593	2.109	–
	DOMAC	9.805	2.958	2.171	−3.0
	DARTAC	7.696	2.377	2.148	−1.9

4.4.1. NDVI

The difference in NDVI between shaded and fully illuminated areas is very small for both dense and sparse vegetation cover. Applying both, the DOMAC and the DARTAC approach yields overestimated NDVI values in cast-shadow. For densely vegetated surfaces this is a slight overestimation, leading to a reduction of the difference by 8.6% for DARTAC and next to no change for DOMAC. For sparse vegetation the overestimation is more extreme, leading to values deviating more from the illuminated reference (47.9% and 39.6% increase). For the forest subset, both approaches do not yield any improvement and DOMAC results show a 14.9% increased difference.

4.4.2. PRI

For the PRI, differences between shaded and fully illuminated areas are large for dense and sparse vegetation cover. Applying both, the DOMAC and the DARTAC approach yields slightly overestimated PRI values in cast-shadow. The reduction of illumination effects is considerable: for sparse vegetation the improvement is between 43.8% for the DOMAC approach and 65.7% for the DARTAC approach. A similar picture can be observed for dense vegetation. For the forest subset, the DOMAC approach slightly reduces uncertainties while the DARTAC approach yields results close to the DEM result.

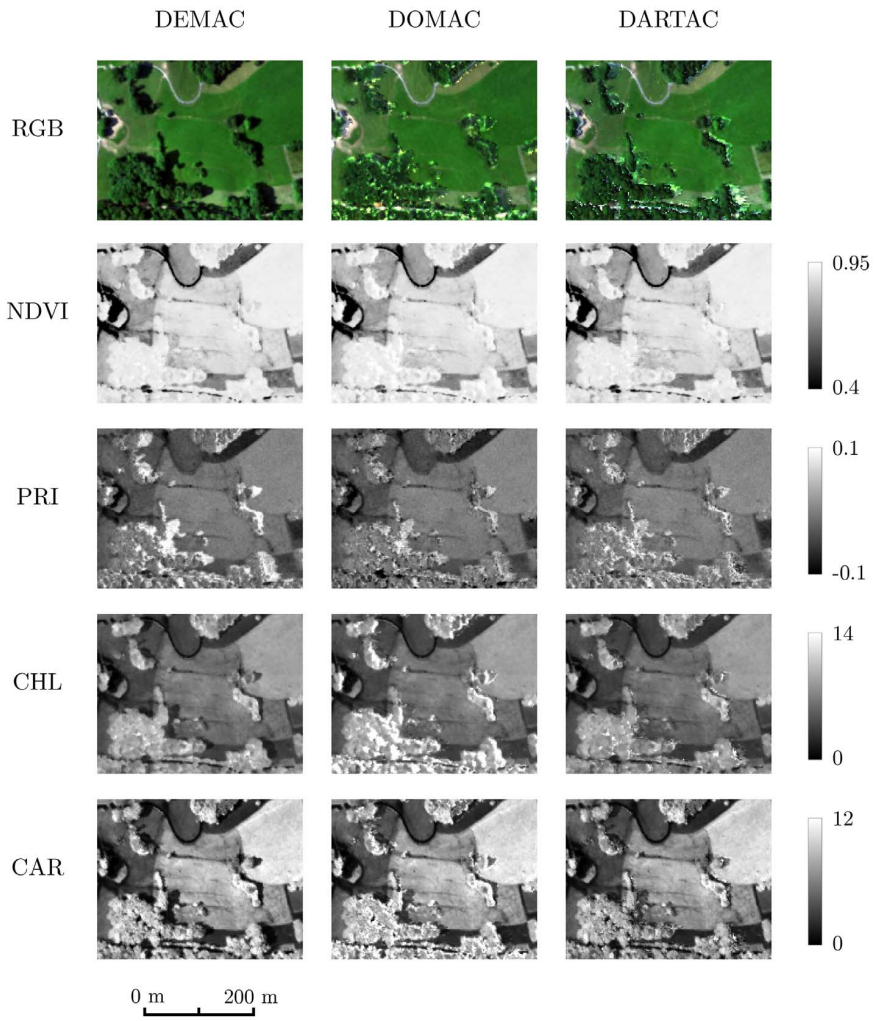

Fig. 7. Impact of illumination effects on HDRF data and subsequently calculated vegetation indices. Results indicate the impact and compensation considering three different atmospheric correction approaches. Displayed are the true colour RGB representations and vegetation products (NDVI, PRI, chlorophyll and carotenoid indices) for a subset of the scene including fields, trees and cast-shadows. Shadows are visible as dark patches in the DEMAC RGB depiction. (For interpretation of the references to colour in this figure legend, the reader is referred to the web version of this article.)

4.4.3. Chlorophyll index

Both, the DOMAC and the DARTAC approach yield consistent improvements of CHL estimates compared to the DEMAC approach of 38.9 to 71.0% for cast-shadows in sparse and dense vegetation. Of note is however that the DARTAC approach increases the standard deviation considerably. The DOMAC approach shows higher consistency across surface types. The improvements for cast-shadows are clearly visible in Fig. 7, however, trees display an overestimation of retrieved chlorophyll content in the DOMAC result (difference to reference is increased by 84.5%). For the DARTAC approach, chlorophyll is slightly underestimated.

4.4.4. Carotenoid index

Retrieved carotenoid contents in cast-shadow show significant improvements for both approaches. Improvements are consistently above 40% with DARTAC performing the best for sparsely vegetated areas with 52.2%. Here mean values are much closer to the reference but the standard deviation is clearly increased, accounting for the medium reduction overall. For the forest subset there is no notable change regarding the pixel-wise differences from the reference value.

5. Discussion

5.1. Capability to advance estimates of direct and diffuse irradiance

Simple atmospheric correction approaches typically assume flat Earth surfaces or coarsely approximate topography with smoothed DEMs and need minimal inputs to calculate reflectance (e.g. Ouaidrari and Vermote, 1999; Richter, 1990). These approaches are not suitable for high resolution imagery and complex terrain. In early approaches seeking to compensate terrain influences, the cosine correction based on $\cos\theta_{il}$ is applied (often directly to TOA radiances), using a DEM (Teillet et al., 1982). However, it was observed to be unsuitable for terrain containing steep inclines where the solar incident angle approaches 90° or above (Itten and Meyer, 1993; Teillet et al., 1982). Results of our DEMAC approach show no extreme underestimation of surface irradiance due to the use of a smoothed DEM. This strategy eliminates abrupt changes in geometry and diffuse irradiance estimates in relation to $\cos\theta_t$. However, since the DEM does not include single canopy geometries, correct irradiance values for tree crowns and cast-shadows cannot be estimated. Small-scale illumination based HDRF variations persist. The use of DOM's theoretically provides more accurate irradiance estimates since complex canopy geometry can be considered. In our experimental analysis, we however faced several difficulties and less consistent results than expected. HDRF in shaded parts of tree canopies was strongly overestimated due to an underestimation of irradiance, rendering an inherent problem in the DOM's 2.5-dimensional smooth description of canopy surfaces (Schläpfer et al., 2003). In regions with steep slopes, direct irradiance tends towards zero while diffuse irradiance is also reduced due to the slope. Overestimates of HDRF due to geometric effects have been observed in other studies and put down to inadequate spatial resolution of the DEM used (Sandmeier

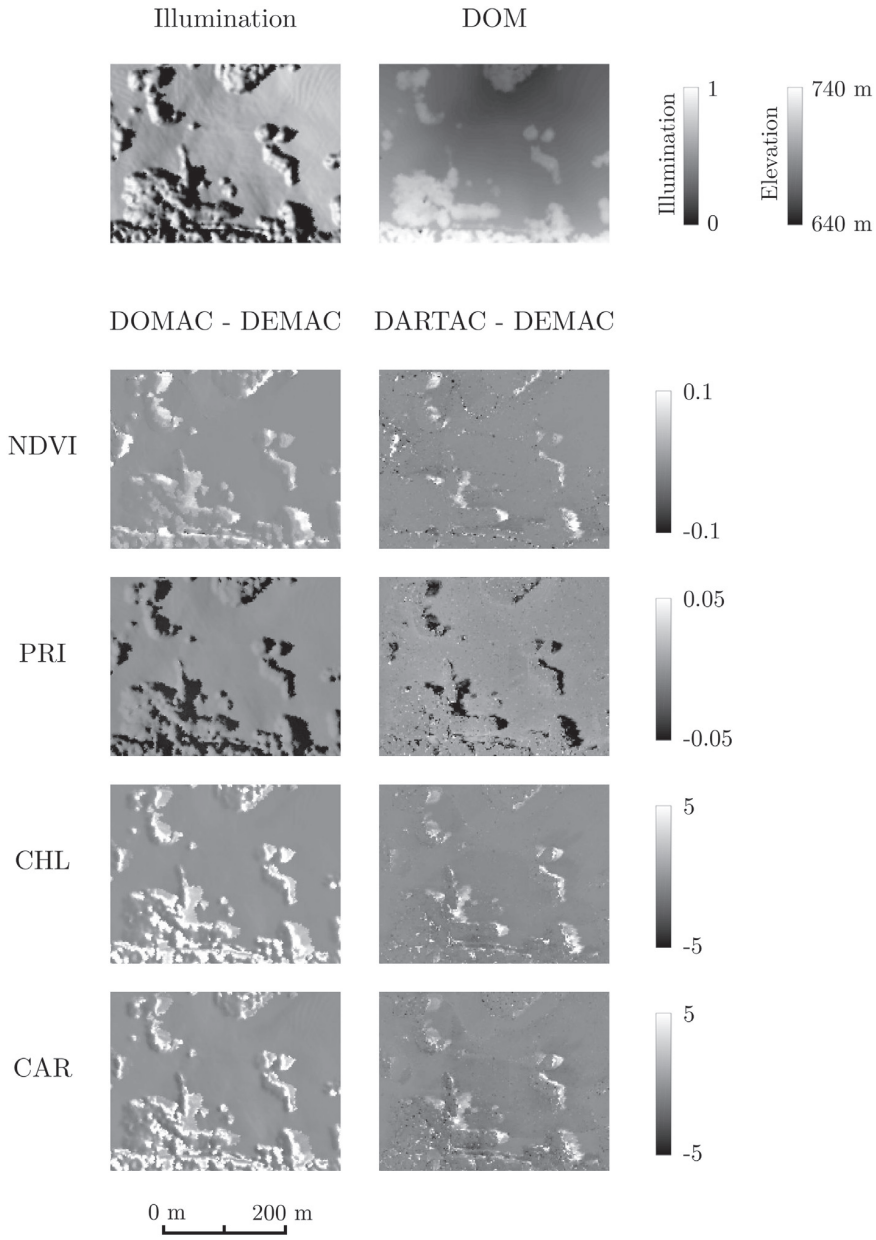

Fig. 8. Top: Illumination map (relative direct illumination, with cast-shadow pixels in black) and digital object model (DOM) of the test scene. Bottom: Difference maps of vegetation indices derived from the DOMAC and DEMAC (left) and DARTAC and DEMAC approach (right).

and Itten, 1997). It is possible that the effect could be partly counteracted in our case by a DOM resolution which is slightly higher (1 m) compared to the pixel size of the image data (2 m). We expect that remaining effects are mainly caused by the fact that the canopies' 3-dimensional structure (e.g., leaf orientation) is insufficiently represented. The binary nature of the applied cast-shadow mask causes an under estimation of the direct irradiance. Despite this, we still observe an underestimation of reflectance in the result for most cast-shadows. This can be explained by the fact that flat surfaces receive an overestimated amount of diffuse irradiance due to the slope-based calculation. The whole hemisphere is considered when in fact a large part of it is obscured by the trees casting the shadow. Simply omitting all diffuse irradiances from these directions would however in turn ignore multiple scattering effects from neighbouring canopies. It is likely that the combination of these effects cause the observed deviations between the corrected and illuminated reference regions. Moreover, direct and diffuse irradiance gradients in tree-canopy cast-shadows are not well understood and warrant further study. Irradiance estimates using 3D radiative transfer models such as DART was judged to be the most adequate strategy to account for the complex 3D architecture of forest canopies. Surprisingly, illumination patterns in DARTAC HDRF data persisted and strong over and underestimates of irradiance partially occurred. The insufficient correction of irradiance effects can be mainly attributed to the voxel size being too large to accurately approximate the canopy shape, especially as there is no slope information to scale irradiance in this approach. The voxel size of $2 \times 2 \times 2$ m corresponds to the image pixel size of 2×2 m but ideally the resolution used for the radiative transfer simulation would be higher and up-scaled to sensor resolution (Malenovský et al., 2007). Concerning the large uncertainties when finally deriving HDRF products, primarily the irradiance scaling factors as obtained from DART are the underlying cause: DART simulations were limited in their complexity due to computation time constraints. The spatial distribution of resulting diffuse scaling factors display a considerable deviation from the expected spatial distribution

as obtained for direct irradiance. This kind of spatial mismatch is caused by an insufficient number of possible scattering directions during the simulation. A full convergence of diffuse and direct cast-shadows requires several hundreds to thousands of scattering directions in 4π space (as opposed to the 24 used in this study), requiring considerable processing power and time. Studies using DART to simulate RS data of smaller scenes use 100+ angles (Gastellu-Etchegorry et al., 1996; Schneider et al., 2014). An efficient method to improve the simulation of canopy multiple scattering is an oversampling of certain angular regions, for example of the hot-spot configuration (Yin et al., 2013).

5.2. Reducing irradiance-based variation in vegetation indices using advanced atmospheric correction

Spectral vegetation indices derived over complex structured forest ecosystems can be subject to substantial illumination effects. The evaluated DOMAC and DARTAC approaches yield in general more reliable HDRF and index information but results are diverse. This diversity is mainly associated with the difficulty to accurately estimate shadow fractions and the wavelength dependency of illumination effects. For cast shadow where the actual fraction of direct irradiance can be reliably constrained, the DOMAC approach leads to most vegetation index products being significantly less sensitive to the illumination differences in cast-shadow, by roughly 50%. An exception is the NDVI, which involves signals in the NIR that were affected by uncertainties in the estimation of direct irradiance. The main conceptual difference in forest canopies is that surfaces receiving purely diffuse irradiance are rare and, at the 2 m spatial scale investigated, varying amounts of direct and diffuse irradiance are actually present. Consequently, the overall differences between the reference case and DEMAC values at varying illuminations are much smaller. The correction results appear to be more diverse, which can be explained by the increasing uncertainty in actual irradiance estimates in combination with a wavelength dependency of this uncertainty. While no correction effect was found for the CAR index, the evaluated DOMAC approach shows spatially more consistent vegetation index values across canopies for PRI but slightly worse results for NDVI and substantially worse for CHL. The calculation of PRI incorporates wavelength regions in the visible strongly affected by fractional changes of direct and diffuse irradiance. The applied corrections seem overall to slightly improve HDRF retrievals at these wavelengths, possibly stemming from the DOMAC inclined surfaces leading to a better representation of the actual diffuse irradiance field. The calculation of NDVI and CHL incorporates reflectance values in the NIR that are exaggerated if modelled direct irradiance is too small. Wavelength dependent improvements of the applied DOMAC approach appear to mainly affect the visible and less the NIR for inclined surfaces. This might explain the increasing sensitivity of both indices for illumination effects when using DOMAC. Across dense forest, there seems to be no advantage in using irradiance estimates obtained from DART simulations; results are overall very similar to the DEMAC case or slightly worse. The lacking variability in modelled direct irradiance is the primary cause for this. It is likely that the smoothed DEM still provides a better approximation of canopy surfaces than the surface described by the voxel grid. A final issue of note is that we evaluated the improvement of vegetation index retrievals by comparing values of partly shaded canopy areas to those of illuminated canopy areas. This strategy assumes that reflectances and thus indices are identical across illumination conditions if fully corrected. This is an imprecise assumption as the difference is not entirely due to wrong irradiance estimates but also surface properties and plant physiological responses. The PRI, for example, has been shown to vary throughout the day in response to a physiological reaction (de-epoxidation state of xanthophylls) to changing illumination conditions, being enhanced in low-light conditions (Gamon and Bond, 2013; Hall et al., 2008), while the discussed uncertainty on directional PRI caused by illumination effects is deemed to be of the same magnitude as the physiological response (Mõttus et al., 2015). Separating the three influences on derived vegetation indices represents a challenge and would require extensive field physiological sampling.

5.3. Towards a reliable retrieval of vegetation information in heterogeneous canopies

The methods presented here are able to describe the geometrical optical scattering, which dominates at high resolutions, to a certain degree and can partially compensate it, as was demonstrated. However, they cannot sufficiently describe volumetric scattering, as occurs within tree canopies. In order to incorporate these kinds of effects, so-called image-based methods are regarded as promising, which are methods that have an increased focus on retrieving unknown parameters in the model based on information contained in the image. There are multiple different implementations of image based methods. Novel approaches seek to describe the radiative transfer in the coupled atmospheric canopy system and move the retrieval problem to the at-sensor radiance level (Laurent et al., 2013). The strength of these TOA approaches is that they avoid error propagation common in other methods due to i) the sequential processing (e.g., posterior anisotropy correction), ii) the retrieval of plant traits via indices and empirical models, and iii) the comparison of different physical quantities (i.e., BRF from canopy radiative transfer models versus HDRF derived from measurements (Laurent et al., 2011). Further methods which are currently being developed are based on empirical cast-shadow detection (Schläpfer et al., 2013) and use a comparison between cast-shadows and illuminated surfaces to derive accurate values for atmospheric visibility. Based on this, the irradiance description for the entire scene can be improved, in turn leading to advanced vegetation information retrieval.

6. Conclusions

We provide further experimental evidence that scene reflectance and derived vegetation information is considerably uncertain if the relative contribution of direct and diffuse irradiance to total irradiance is not estimated accurately. We conclude that improvements in the retrieval of surface reflectance and spectral indices by ingesting further auxiliary data to account for varying irradiance fractions in atmospheric correction approaches are limited. Using a DOM or DART simulated irradiance fractions to estimate irradiance leads to some improvements over a simplified approach using spatially coarse resolution DEMs. However, a number of issues and requirements were identified limiting the applicability of the two proposed approaches. This includes the resolution of the DOM and the DART voxel grid that should ideally be an order of magnitude larger than the image data. Further, applied approaches are limited in their physical representation of the complex radiative transfer in heterogeneous canopies. DOM based approaches being 2.5 dimensional represents an oversimplification while DART based approaches would require a very large number of scattering angles and iterations to accurately simulate irradiance. As currently the computational requirements for this are still prohibitive, we propose further investigating other options which are promising as operational solutions. Going forward, we emphasize the potential of image-based approaches to derive accurate irradiance fields and vegetation variables. Such approaches include the use of combined atmosphere-surface models with inversion schemes applied on at-sensor radiance data or more sophisticated empirical strategies to quantitatively describe the shadow fraction.

Acknowledgments

The contribution of A. Damm was supported by a grant of the Swiss University Conference and ETH-Board in frame of the KIP-5 project Swiss Earth Observatory Network (SEON) and the contribution of M. E.

Schaepman was supported by the University of Zurich Research Priority Program on Global Change and Biodiversity. We thank the DART team for making their model freely available to scientists. The authors' sequence is listed following the FLAE approach (doi: 10.1371/journal.pbio.0050018). We thank the two anonymous reviewers for their helpful comments.

References

Adler-Golden, S.M., Matthew, M.W., Anderson, G.P., Felde, G.W., Gardner, J.A., 2002. Algorithm for de-shadowing spectral imagery. In: Shen, S.S. (Ed.), Imaging Spectrometry. VIII, pp. 203–210. http://dx.doi.org/10.1117/12.451691.

Asner, G.P., Martin, R.E., Anderson, C.B., Knapp, D.E., 2015. Quantifying forest canopy traits: imaging spectroscopy versus field survey. Remote Sens. Environ. 158, 15–27. http://dx.doi.org/10.1016/j.rse.2014.11.011.

Baldocchi, D., Falge, E., Gu, L.H., Olson, R., Hollinger, D., Running, S., Anthoni, P., Bernhofer, C., Davis, K., Evans, R., Fuentes, J., Goldstein, A., Katul, G., Law, B., Lee, X.H., Malhi, Y., Meyers, T., Munger, W., Oechel, W., Paw, K.T., Pilegaard, K., Schmid, H.P., Valentini, R., Verma, S., Vesala, T., Wilson, K., Wofsy, S., 2001. FLUXNET: a new tool to study the temporal and spatial variability of ecosystem-scale carbon dioxide, water vapor, and energy flux densities. Bull. Am. Meteorol. Soc. 82, 2415–2434. http://dx.doi.org/10.1175/1520-0477(2001)082<2415:FANTTS>2.3.CO;2.

Berk, A., Anderson, G.P., Acharya, P.K., Bernstein, L.S., Muratov, L., Lee, J., Fox, M., Adler-Golden, S.M., Chetwynd Jr., J.H., Hoke, M.L., Lockwood, R.B., Gardner, J.A., Cooley, T.W., Borel, C.C., Lewis, P.E., Shettle, E.P., 2006. MODTRAN5: 2006 update. In: Proceedings of SPIE - The International Society for Optical Engineering. 6233 IIhttp://dx.doi.org/10.1117/12.665077.

Cho, H.K., Jeong, M.J., Kim, J., Kim, Y.J., 2003. Dependence of diffuse photosynthetically active solar irradiance on total optical depth. J. Geophys. Res.: Atmos. 108, 4267. http://dx.doi.org/10.1029/2002JD002175.

Cogliati, S., Verhoef, W., Kraft, S., Sabater, N., Alonso, L., Vicent, J., Moreno, J., Drusch, M., Colombo, R., 2015. Retrieval of sun-induced fluorescence using advanced spectral fitting methods. Remote Sens. Environ. 169, 344–357. http://dx.doi.org/10.1016/j.rse.2015.08.022.

Damm, A., Guanter, L., Laurent, V.C.E., Schaepman, M.E., Schickling, A., Rascher, U., 2014. FLD-based retrieval of sun-induced chlorophyll fluorescence from medium spectral resolution airborne spectroscopy data. Remote Sens. Environ. 147, 256–266. http://dx.doi.org/10.1016/j.rse.2014.03.009.

Damm, A., Guanter, L., Paul-Limoges, E., Van der Tol, C., Hueni, A., Buchmann, N., Eugster, W., Ammann, C., Schaepman, M.E., 2015a. Far-red sun-induced chlorophyll fluorescence shows ecosystem-specific relationships to gross primary production: an assessment based on observational and modeling approaches. Remote Sens. Environ. 166, 91–105. http://dx.doi.org/10.1016/j.rse.2015.06.004.

Damm, A., Guanter, L., Verhoef, W., Schläpfer, D., Garbari, S., Schaepman, M., 2015b. Impact of varying irradiance on vegetation indices and chlorophyll fluorescence derived from spectroscopy data. Remote Sens. Environ. 156, 202–215. http://dx.doi.org/10.1016/j.rse.2014.09.031.

Eugster, W., Zeyer, K., Zeeman, M., Michna, P., Zingg, A., Buchmann, N., Emmenegger, L., 2007. Methodical study of nitrous oxide eddy covariance measurements using quantum cascade laser spectrometry over a Swiss forest. Biogeosciences 4, 927–939. http://dx.doi.org/10.5194/bg-4-927-2007.

Friman, O., Tolt, G., Ahlberg, J., 2011. Illumination and shadow compensation of hyperspectral images using a digital surface model and non-linear least squares estimation. In: Proceedings of SPIE — The International Society for Optical Engineering. 8180http://dx.doi.org/10.1117/12.898084.

Gamon, J.A., Bond, B., 2013. Effects of irradiance and photosynthetic downregulation on the photochemical reflectance index in Douglas-fir and ponderosa pine. Remote Sens. Environ. 135, 141–149. http://dx.doi.org/10.1016/j.rse.2013.03.032.

Gamon, J.A., Field, C.B., Bilger, W., Björkman, O., Fredeen, A.L., Peñuelas, J., 1990. Remote sensing of the xanthophyll cycle and chlorophyll fluorescence in sunflower leaves and canopies. Oecologia 85 (1), 1–7. http://dx.doi.org/10.1007/BF00317336.

Gamon, J.A., Peñuelas, J., Field, C., 1992. A narrow-waveband spectral index that tracks diurnal changes in photosynthetic efficiency. Remote Sens. Environ. 41, 35–44. http://dx.doi.org/10.1016/0034-4257(92)90059-S.

Gamon, J.A., Serrano, L., Surfus, J.S., 1997. The photochemical reflectance index: an optical indicator of photosynthetic radiation use efficiency across species, functional types, and nutrient levels. Oecologia 112, 492–501. http://dx.doi.org/10.1007/s004420050337.

Gastellu-Etchegorry, J.-P., Demarez, V., Pinel, V., Zagolski, F., 1996. Modeling radiative transfer in heterogeneous 3-D vegetation canopies. Remote Sens. Environ. 58, 131–156. http://dx.doi.org/10.1016/0034-4257(95)00253-7.

Gastellu-Etchegorry, J.-P., Guillevic, P., Zagolski, F., Demarez, V., Trichon, V., Deering, D., Leroy, M., 1999. Modeling BRF and radiation regime of boreal and tropical forests. Remote Sens. Environ. 68, 281–316. http://dx.doi.org/10.1016/S0034-4257(98)00119-9.

Gastellu-Etchegorry, J.-P., Yin, T., Lauret, N., Cajgfinger, T., Gregoire, T., Grau, E., Feret, J.-b., Guilleux, J., Cook, B.D., Morton, D., Rubio, J., Durrieu, S., Cazanave, G., Martin, E., Ristorcelli, T., Thenkabail, P.S., 2015. Discrete anisotropic radiative transfer (DART 5) for modelling airborne and satellite spectroradiometer and LIDAR acquisitions of natural and urban landscapes. Remote Sens. 7, 1667–1701. http://dx.doi.org/10.3390/rs70201667.

Gitelson, A.A., Keydan, G.P., Merzlyak, M.N., 2006. Three-band model for noninvasive estimation of chlorophyll, carotenoids, and anthocyanin contents in higher plant leaves. Geophys. Res. Lett. 33, L11402. http://dx.doi.org/10.1029/2006GL026457.

Hall, F.G., Hilker, T., Coops, N.C., Lyapustin, A., Huemmrich, K.F., Middleton, E., Margolis, H., Drolet, G., Black, T.A., 2008. Multi-angle remote sensing of forest light use efficiency by observing PRI variation with canopy shadow fraction. Remote Sens. Environ. 112, 3201–3211. http://dx.doi.org/10.1016/j.rse.2008.03.015.

Holben, B.N., Eck, T.F., Slutsker, I., Tanré, D., Buis, J.P., Setzer, A., Vermote, E., Reagan, J.A., Kaufman, Y.J., Nakajima, T., Lavenu, F., Jankowiak, I., Smirnov, A., 1998. AERONET — a federated instrument network and data archive for aerosol characterization. Remote Sens. Environ. 66, 1–16. http://dx.doi.org/10.1016/S0034-4257(98)00031-5.

Hueni, A., Biesemans, J., Meuleman, K., Dell'Endice, F., Schläpfer, D., Odermatt, D., Kneubühler, M., Adriaensen, S., Kempenaers, S., Nieke, J., Itten, K.I., 2009. Structure, components, and interfaces of the airborne prism experiment (APEX) processing and archiving facility. IEEE Trans. Geosci. Remote Sens. 47, 29–43. http://dx.doi.org/10.1109/TGRS.2008.2005828.

Itten, K.I., Meyer, P., 1993. Geometric and radiometric correction of TM data of mountainous forested areas. IEEE Trans. Geosci. Remote Sens. 31, 764–770. http://dx.doi.org/10.1109/36.239898.

Key, J.R., Schweiger, A.J., 1998. Tools for atmospheric radiative transfer: STREAMER and FLUXNET. Comput. Geosci. 24, 443–451. http://dx.doi.org/10.1016/S0098-3004(97)00130-1.

Kokaly, R.F., Asner, G.P., Ollinger, S.V., Martin, M.E., Wessman, C.A., 2009. Characterizing canopy biochemistry from imaging spectroscopy and its application to ecosystem studies. Remote Sens. Environ. 113, S78–S91. http://dx.doi.org/10.1016/j.rse.2008.10.018.

Kükenbrink, D., Leiterer, R., Schneider, F.D., Schaepman, M.E., Morsdorf, F., 2016. Quantification of hidden canopy volume of airborne laser scanning data using a voxel traversal algorithm. Remote Sens. Environ. http://dx.doi.org/10.1016/j.rse.2016.10.023. In Press.

Laurent, V.C., Verhoef, W., Clevers, J.G., Schaepman, M.E., 2011. Estimating forest variables from top-of-atmosphere radiance satellite measurements using coupled radiative transfer models. Remote Sens. Environ. 115, 1043–1052. http://dx.doi.org/10.1016/j.rse.2010.12.009.

Laurent, V.C., Verhoef, W., Damm, A., Schaepman, M.E., Clevers, J.G.P.W., 2013. A Bayesian object-based approach for estimating vegetation biophysical and biochemical variables from APEX at-sensor radiance data. Remote Sens. Environ. 139, 6–17. http://dx.doi.org/10.1016/j.rse.2013.07.032.

Malenovský, Z., Bartholomeus, H.M., Acerbi-Junior, F.W., Schopfer, J.T., Painter, T.H., Epema, G.F., Bregt, A.K., 2007. Scaling dimensions in spectroscopy of soil and vegetation. Int. J. Appl. Earth Obs. Geoinf. 9, 137–164. http://dx.doi.org/10.1016/j.jag.2006.08.003.

Malenovský, Z., Homolová, L., Zurita-Milla, R., Lukeš, P., Kaplan, V., Hanuš, J., Gastellu-Etchegorry, J.P., Schaepman, M.E., 2013. Retrieval of spruce leaf chlorophyll content from airborne image data using continuum removal and radiative transfer. Remote Sens. Environ. 131, 85–102. http://dx.doi.org/10.1016/j.rse.2012.12.015.

Matthew, M.W., Adler-Golden, S.M., Berk, A., Felde, G., Anderson, G.P., Gorodetzky, D., Paswaters, S., Shippert, M., 2002. Atmospheric correction of spectral imagery: evaluation of the FLAASH algorithm with AVIRIS data. In: Proceedings of the 31st Applied Imagery Pattern Recognition Workshop, pp. 157–163. http://dx.doi.org/10.1109/AIPR.2002.1182270. Washington, DC.

Mõttus, M., Takala, T.L., Stenberg, P., Knyazikhin, Y., Yang, B., Nilson, T., 2015. Diffuse sky radiation influences the relationship between canopy PRI and shadow fraction. ISPRS J. Photogramm. Remote Sens. 105, 54–60. http://dx.doi.org/10.1016/j.isprsjprs.2015.03.012.

Ouaidrari, H., Vermote, E.F., 1999. Operational atmospheric correction of Landsat™ data. Remote Sens. Environ. 70, 4–15. http://dx.doi.org/10.1016/S0034-4257(99)00054-1.

Rascher, U., Alonso, L., Burkart, A., Cilia, C., Cogliati, S., Colombo, R., Damm, A., Drusch, M., Guanter, L., Hanus, J., Hyvärinen, T., Julitta, T., Jussila, J., Kataja, K., Kokkalis, P., Kraft, S., Kraska, T., Matveeva, M., Moreno, J., Muller, O., Panigada, C., Pikl, M., Pinto, F., Prey, L., Pude, R., Rossini, M., Schickling, A., Schurr, U., Schüttemeyer, D., Verrelst, J., Zemek, F., 2015. Sun-induced fluorescence — a new probe of photosynthesis: first maps from the imaging spectrometer HyPlant. Glob. Chang. Biol. 21, 4673–4684. http://dx.doi.org/10.1111/gcb.13017.

Richter, R., 1990. A fast atmospheric correction algorithm applied to Landsat™ images. Int. J. Remote Sens. 11, 159–166. http://dx.doi.org/10.1080/01431169008955008.

Richter, R., 1998. Correction of satellite imagery over mountainous terrain. Appl. Opt. 37, 4004–4015. http://dx.doi.org/10.1364/AO.37.004004.

Richter, R., Schläpfer, D., 2002. Geo-atmospheric processing of airborne imaging spectrometry data. Part 2: atmospheric/topographic correction. Int. J. Remote Sens. 23, 2631–2649. http://dx.doi.org/10.1080/01431160110115834.

Richter, R., Schläpfer, D., 2016. Atmospheric/Topographic Correction for Airborne Imagery (ATCOR-4 User Guide), 7th. DLR, Wessling, Germany, pp. 260.

Richter, R., Schläpfer, D., Müller, A., 2011. Operational atmospheric correction for imaging spectrometers accounting for the smile effect. IEEE Trans. Geosci. Remote Sens. 49, 1772–1780. http://dx.doi.org/10.1109/TGRS.2010.2089799.

Sandmeier, S., Itten, K.I., 1997. A physically-based model to correct atmospheric and illumination effects in optical satellite data of rugged terrain. IEEE Trans. Geosci. Remote Sens. 35, 708–717. http://dx.doi.org/10.1109/36.581991.

Schaepman, M.E., Jehle, M., Hueni, A., D'Odorico, P., Damm, A., Weyermann, J., Schneider, F.D., Laurent, V., Popp, C., Seidel, F.C., Lenhard, K., Gege, P., Küchler, C., Brazile, J., Kohler, P., De Vos, L., Meuleman, K., Meynart, R., Schläpfer, D., Kneubühler, M., Itten, K.I., 2015. Advanced radiometry measurements and Earth science applications with the Airborne Prism Experiment (APEX). Remote Sens. Environ. 158, 207–219. http://dx.doi.org/10.1016/j.rse.2014.11.014.

Schaepman, M.E., Ustin, S.L., Plaza, A.J., Painter, T.H., Verrelst, J., Liang, S., 2009. Earth system science related imaging spectroscopy — an assessment. Remote Sens. Environ. 113, S123–S137. http://dx.doi.org/10.1016/j.rse.2009.03.001.

Schaepman-Strub, G., Schaepman, M.E., Painter, T.H., Dangel, S., Martonchik, J.V., 2006. Reflectance quantities in optical remote sensing — definitions and case studies. Remote Sens. Environ. 103, 27–42. http://dx.doi.org/10.1016/j.rse.2006.03.002.

Schläpfer, D., Koetz, B., Gruber, S., Morsdorf, F., 2003. The influence of DEM characteristics on preprocessing of DAIS/ROSIS data in high altitude alpine terrain. In: 3rd EARSeL Workshop on Imaging Spectroscopy, pp. 13–16 Herrsching, Germany.

Schläpfer, D., Richter, R., 2002. Geo-atmospheric processing of airborne imaging spectrometry data. Part 1: parametric orthorectification. Int. J. Remote Sens. 23, 2609–2630. http://dx.doi.org/10.1080/01431160110115825.

Schläpfer, D., Richter, R., Damm, A., 2013. Correction of shadowing in imaging spectroscopy data by quantification of the proportion of diffuse illumination. In: 8th EARSeL Workshop on Imaging Spectroscopy, Nantes, France.

Schneider, F.D., Leiterer, R., Morsdorf, F., Gastellu-Etchegorry, J.P., Lauret, N., Pfeifer, N., Schaepman, M.E., 2014. Simulating imaging spectrometer data: 3D forest modeling based on LiDAR and in situ data. Remote Sens. Environ. 152, 235–250. http://dx.doi.org/10.1016/j.rse.2014.06.015.

Schneider, F.D., Leiterer, R., Schaepman, M.E., Morsdorf, F., 2015. Canopy height and plant area index changes in a temperate forest between 2010–2014 using airborne laser scanning. In: Durrieu, S., Véga, C. (Eds.), Proceedings of SilviLaser 2015, 14th conference on Lidar Applications for Assessing and Managing Forest Ecosystems, http://dx.doi.org/10.5167/uzh-116915. La Grande Motte, France.

Seidel, F.C., Kokhanovsky, A.A., Schaepman, M.E., 2010. Fast and simple model for atmospheric radiative transfer. Atmos. Meas. Tech. 3, 1129–1141. http://dx.doi.org/10.5194/amt-3-1129-2010.

Seidel, F.C., Kokhanovsky, A.A., Schaepman, M.E., 2012. Fast retrieval of aerosol optical depth and its sensitivity to surface albedo using remote sensing data. Atmos. Res. 116, 22–32. http://dx.doi.org/10.1016/j.atmosres.2011.03.006.

Teillet, P.M., Guindon, B., Goodenough, D.G., 1982. On the slope-aspect correction of multispectral scanner data. Can. J. Remote. Sens. 8 (2), 84–106. http://dx.doi.org/10.1080/07038992.1982.10855028.

Tucker, C.J., 1979. Red and photographic infrared linear combinations for monitoring vegetation. Remote Sens. Environ. 8, 127–150. http://dx.doi.org/10.1016/0034-4257(79)90013-0.

Ustin, S.L., Gitelson, A.A., Jacquemoud, S., Schaepman, M.E., Asner, G.P., Gamon, J.A., Zarco-Tejada, P., 2009. Retrieval of foliar information about plant pigment systems from high resolution spectroscopy. Remote Sens. Environ. 113, S67–S77. http://dx.doi.org/10.1016/j.rse.2008.10.019.

Van der Tol, C., Verhoef, W., Timmermans, J., Verhoef, A., Su, Z., 2009. An integrated model of soil-canopy spectral radiances, photosynthesis, fluorescence, temperature and energy balance. Biogeosciences 6, 3109–3129. http://dx.doi.org/10.5194/bg-6-3109-2009.

Verhoef, W., Bach, H., 2003. Simulation of hyperspectral and directional radiance images using coupled biophysical and atmospheric radiative transfer models. Remote Sens. Environ. 87, 23–41. http://dx.doi.org/10.1016/S0034-4257(03)00143-3.

Verhoef, W., Bach, H., 2012. Simulation of Sentinel-3 images by four-stream surface-atmosphere radiative transfer modeling in the optical and thermal domains. Remote Sens. Environ. 120, 197–207. http://dx.doi.org/10.1016/j.rse.2011.10.034.

Verhoef, W., Van der Tol, C., Middleton, E.M., 2014. Vegetation canopy fluorescence and reflectance retrieval by model inversion using optimization. In: 5th International Workshop on Remote Sensing of Vegetation Fluorescence, pp. 759–770 Paris, France.

Wulder, M.A., Hall, R.J., Coops, N.C., Franklin, S.E., 2004. High spatial resolution remotely sensed data for ecosystem characterization. BioScience 54, 511–521. http://dx.doi.org/10.1641/0006-3568(2004)054[0511:HSRRSD]2.0.CO;2.

Yin, T., Gastellu-Etchegorry, J.P., Lauret, N., Grau, E., Rubio, J., 2013. A new approach of direction discretization and oversampling for 3D anisotropic radiative transfer modeling. Remote Sens. Environ. 135, 213–223. http://dx.doi.org/10.1016/j.rse.2013.03.030.

2.5 Advanced radiometry measurements and Earth science applications with the Airborne Prism Experiment (APEX)

Schaepman, M.E., Jehle, M., Hueni, A., D'Odorico, P., Damm, A., Weyermann, J.,
Schneider, F.D., Laurent, V., Popp, C., Seidel, F.C., Lenhard, K., Gege, P.,
Küchler, C., Brazile, J., Kohler, P., De Vos, L., Meuleman, K.,
Meynart, R., Schläpfer, D., Kneubühler, M., Itten, K.I.

This section is based on the peer-reviewed article:
Remote Sensing of Environment, 2015 (158), 207-219
DOI:10.1016/j.rse.2014.11.014

M.E.S. and K.I.I. designed research; all authors performed research and wrote the paper, with main contributions of M.E.S.

Remote Sensing of Environment 158 (2015) 207–219

Contents lists available at ScienceDirect

Remote Sensing of Environment

journal homepage: www.elsevier.com/locate/rse

Advanced radiometry measurements and Earth science applications with the Airborne Prism Experiment (APEX)

Michael E. Schaepman [a,*], Michael Jehle [a], Andreas Hueni [a], Petra D'Odorico [a,1], Alexander Damm [a], Jürg Weyermann [a], Fabian D. Schneider [a], Valérie Laurent [a,2], Christoph Popp [b], Felix C. Seidel [c], Karim Lenhard [d], Peter Gege [d], Christoph Küchler [e], Jason Brazile [f], Peter Kohler [f], Lieve De Vos [g], Koen Meuleman [h], Roland Meynart [i], Daniel Schläpfer [j], Mathias Kneubühler [a], Klaus I. Itten [a,3]

[a] Remote Sensing Laboratories, University of Zurich, Winterthurerstrasse 190, CH-8057 Zurich, Switzerland
[b] NMNH, Smithsonian Institution, Washington, DC 20013-7012, USA
[c] Jet Propulsion Laboratory, California Institute of Technology, 4800 Oak Grove Drive, Pasadena, CA 91109, USA
[d] Earth Observation Center, German Aerospace Center, Oberpfaffenhofen, 82234 Wessling, Germany
[e] RUAG Schweiz AG, RUAG Aviation, Seetalstrasse 175, 6032 Emmen, CH, Switzerland
[f] Netcetera AG, Zypressenstrasse 71, 8004 Zurich, CH, Switzerland
[g] OIP Sensor Systems, Westerring 21, 9700 Oudenaarde, Belgium
[h] VITO, Boeretang 200, 2400 Mol, Belgium
[i] ESA-ESTEC, Keperlaan 1, 2201 AZ Noordwijk, Netherlands
[j] ReSe Applications Schläpfer, Langeggweg 3, 9500 Wil, CH, Switzerland

ARTICLE INFO

Article history:
Received 17 April 2014
Received in revised form 15 September 2014
Accepted 9 November 2014
Available online 5 December 2014

Keywords:
Imaging spectroscopy
Earth observation
APEX
Calibration
Processing
Validation
Earth science applications

ABSTRACT

We present the Airborne Prism Experiment (APEX), its calibration and subsequent radiometric measurements as well as Earth science applications derived from this data. APEX is a dispersive pushbroom imaging spectrometer covering the solar reflected wavelength range between 372 and 2540 nm with nominal 312 (max. 532) spectral bands. APEX is calibrated using a combination of laboratory, in-flight and vicarious calibration approaches. These are complemented by using a forward and inverse radiative transfer modeling approach, suitable to further validate APEX data. We establish traceability of APEX radiances to a primary calibration standard, including uncertainty analysis. We also discuss the instrument simulation process ranging from initial specifications to performance validation. In a second part, we present Earth science applications using APEX. They include geometric and atmospheric compensated as well as reflectance anisotropy minimized Level 2 data. Further, we discuss retrieval of aerosol optical depth as well as vertical column density of NOx, a radiance data-based coupled canopy–atmosphere model, and finally measuring sun-induced chlorophyll fluorescence (Fs) and infer plant pigment content. The results report on all APEX specifications including validation. APEX radiances are traceable to a primary standard with <4% uncertainty and with an average SNR of >625 for all spectral bands. Radiance based vicarious calibration is traceable to a secondary standard with ≤6.5% uncertainty. Except for inferring plant pigment content, all applications are validated using in-situ measurement approaches and modeling. Even relatively broad APEX bands (FWHM of 6 nm at 760 nm) can assess Fs with modeling agreements as high as $R^2 = 0.87$ (relative RMSE = 27.76%). We conclude on the use of high resolution imaging spectrometers and suggest further development of imaging spectrometers supporting science grade spectroscopy measurements.

1. Introduction

Imaging spectroscopy has emerged as an extremely efficient observational approach for mapping the Earth system (Schaepman et al., 2009a). The efficiency gain has its foundation in technical progress made on one hand, and on the improved understanding and modeling of the molecular scattering and absorption mechanisms, on the other. Imaging spectrometers—particularly airborne instruments—are frequently available nowadays, either targeting specific applications, or

* Corresponding author. Tel.: +41 44 635 51 60.
E-mail address: michael.schaepman@geo.uzh.ch (M.E. Schaepman).
[1] Present address: Institute of Agricultural Sciences, Swiss Federal Institute of Technology, Universitätsstrasse 2, 8092 Zurich, CH, Switzerland.
[2] Present address: Irstea—UMR Tetis, Maison de la Télédétection, 500 rue J.F. Breton, 34093 Montpellier, France.
[3] Permanent address: Hintere Rietstrasse 9, 8103 Unterengstringen, CH, Switzerland.

http://dx.doi.org/10.1016/j.rse.2014.11.014
0034-4257/

serving as 'general purpose' instruments, covering a wide range of applications (for a detailed review see Schaepman, 2009).

While the general procedure of constructing and operating airborne imaging spectrometers has reached a high level of maturity, requirements on specific instrument aspects might challenge any component of the full data acquisition chain, ranging from sensor modeling to calibration to product delivery. In particular, spectral fidelity (stability, Signal-to-Noise Ratio (SNR), etc.) was very early on identified as a key performance requirement for successful spectroscopy applications (Green et al., 1998).

Emerging satellite concepts utilizing principles of spectroscopy as their prime observational approach led to the idea to build a next generation airborne imaging spectrometer in Switzerland during the early 1990s. In fact, the idea emerged following a successful joint NASA/ESA Multisensor Airborne Campaign (MAC-Europe) in July 1991 in Europe (Itten, Meyer, Staenz, Kellenberger, & Schaepman, 1992). The funding source identified for such an endeavor was the European Space Agency's PRODEX (PROgramme de Développement d'Expériences scientifiques) program, allowing small ESA member states to develop their own instruments. A joint Swiss–Belgian team proposed to build an airborne imaging spectrometer termed 'Airborne Prism Experiment' (APEX), under the scientific lead of Klaus Itten at the University of Zurich. He served as APEX principal investigator from 1995 to 2009 and Michael Schaepman from 2009 onwards. A potential APEX system was for the first time presented to a wider public in 1997 (Itten et al., 1997).

The scientific, industrial and operational consortium of APEX was subsequently established as follows. The science lead is with the University of Zurich, tasked to perform model simulations, establish system specifications and validate instrument performance, develop a science grade processing facility, and perform the project management. The institutional partner and co-investigator VITO is responsible for the operational implementation of the APEX processor, APEX operations and data distribution. The industrial consortium is composed of RUAG Aerospace, Switzerland (integration, mechanical and electrical subsystems, navigation and control), OIP Sensor Systems, Belgium (optical subsystem), and Netcetera AG, Switzerland (readout electronics, software). In addition, ESA as overall project responsible established two further contracts, one with Sofradir, France (short-wave infrared (SWIR) detector) and the German Aerospace Center (DLR), Germany (calibration home base). APEX went into operations in 2009 and acquires science grade spectroscopy data since 2010. APEX is on lease by ESA to the University of Zurich and VITO until 2015 and thereafter under ownership of the latter two institutions.

In this contribution, we discuss the evolution of the APEX instrument starting with simulating its key performance indicators, and definition of specifications, its optical, electronic and mechanical design. We then elaborate on the calibration procedure and finally demonstrate new Earth science applications allowing monitoring the Earth surface and atmosphere with unprecedented accuracy. We finally conclude by discussing emerging instrument capabilities and applications being of relevance for future, upcoming imaging spectrometers.

2. APEX advanced radiometry measurements

2.1. APEX specifications and performance modeling

The APEX system was specified to allow simulating spaceborne imaging spectrometers, supporting mission calibration and validation efforts. The following specifications are outlined as *boundary conditions* (Schaepman, De Vos, & Itten, 1998):

- Pushbroom imaging with ≤1000 imaging pixels across track, covering a swath width of 2.5–5 km, depending on flight altitude,
- Spectral wavelength range covering 450–2500 nm,
- At least 200 programmable or 300 predefined spectral bands, adaptable to specific application requirements,
- Spectral sampling interval <15 nm and a spectral sampling width of <1.5 the sampling interval, and
- Ability to provide calibrated data and products to geocoded and calibrated data.

Further on, the dispersive system of APEX had to be based on prisms, given a requirement from European Space Agency. The initial idea was do demonstrate that the ENVISAT/MERIS design can be used in APEX as a demonstrator for a full spectral coverage mission (400–2500 nm) as well as precursor mission of a planned imaging spectrometer in space (Menenti et al., 2002).

Using the above specifications, a performance modeling approach could be initiated. First, a forward model simulating 1D generic imaging spectrometers is implemented (Schaepman, Schläpfer, & Müller, 2002). Key science requirements from various applications are compiled as a list of 55 variables used to forward model the instrument performance. Application requirements are forward simulated using a reflectance model and then converted to at-sensor radiances using a radiance model and finally convolved using a sensor specific model. This leads to the possibility to model (still noise free and in 1D space) pixel-wise requirements for a given instrument. Subsequently, certain noise components are added (Schläpfer & Schaepman, 2002) as well as a spatial component allowing to assess spatial noise as well (Börner et al., 2001). These activities finally lead to a set of performance requirements for APEX which are used as engineering specifications (Schaepman, Schläpfer, & Itten, 2000) (Table 1, Section 4.1). However, not all specifications can be simulated using the above approach, such as stability requirements over time. These specifications are either taken over from existing publications (Green, 1998; Mouroulis, Green, & Chrien, 2000) or from engineering knowledge available through the support of ESA's engineers.

2.2. APEX instrument description

APEX is composed of an optical system including two detector channels (Fig. 1), a mechanical subsystem, an electrical subsystem, and an in-flight calibration assembly. External to the core APEX imager is a control and storage unit (CSU), as well as a processing and archiving facility (PAF) and a calibration home base (CHB).

The optical system is a dual prism dispersion pushbroom imaging spectrometer using a path-folding mirror followed by a ground imager with a slit in its image plane (Schaepman et al., 2003). The spectrometer consists of a collimator that directs the light transmitted by the slit towards the prisms, where a dichroic coating applied to the first prism separates the two spectrometer channels into a VNIR and SWIR channel (Visible/Near Infrared 372–1015 nm; Shortwave Infrared 904–2508 nm). The dispersed light is imaged on the detectors of these two channels. A commercial-off-the-shelf VNIR detector (CCD 55-30, E2V Technologies) and a custom made SWIR detector (Nowicki-Bringuier & Chorier, 2009) are implemented. The SWIR focal plane array is a HgCdTe detecting module hybridized on a CMOS multiplexer. It has 1000 × 256 pixels with a 30 μm pitch. Integration time is variable, but limited by the detector frame rate (34.5 ms). Standard integration time is set to 29 ms [22 … 34.5 ms], resulting in almost square pixels using the default aircraft (DO-228). Its spatial direction (1000 pixels) is parallel to the detector rows and its spectral direction (256 pixels) parallel to the detector columns, which is also the readout direction on the focal plane. The detector is implemented in a dewar with a sapphire window coated with anti-reflection material (transmission >0.96). A Stirling cycle cooler allows operating the SWIR detector with low dark current at 130 K detector temperature. The mount of the spectrometer is liquid cooled using a transfer line and cold finger (Ulbrich et al., 2004). The 1000 across-track spatial pixels are recorded for both channels simultaneously. Both detectors are not fully illuminated in spectral direction, allowing non-illuminated lines to be used as dark current reference. The VNIR and SWIR detectors are externally

Table 1
APEX specifications and corresponding validated performances for each key instrument parameter.

Parameter	Specification	Performance	Ref.
Field of view (FOV)	±14 … ±20° ±244.35 … ±349.07 mrad	28.10° (±14.05°) 490.44 mrad (±245.22 mrad)	Versluys, Van Vooren and De Vos (2008)
Instantaneous Field of View (IFOV)	0.0275 … 0.0401° 0.48 … 0.70 mrad	0.028° 0.489 mrad	Versluys et al. (2008)
Flight altitude	4000–10,000 m a.s.l.	Onboard DO-228-101: 60–7620 m a.s.l.	EUFAR (2014)
Spectral channels	VNIR: approx. 140 SWIR: approx. 145 Total: approx. 285	VNIR: max. 334; nominal 114 SWIR: nominal 198 Total: max. 532; nominal 312	Jehle et al., in review (2010)
Spectral range	400–2500 nm	372–2540 nm VNIR: 372–1015 nm SWIR: 940–2540 nm (SWIR cutoff at 50% of the max. response)	Chorier and Martino (2004), Jehle et al. 2015 (in press)
Spectral sampling interval	400–1050 nm: <5 nm, 1050–2500 nm: <10 nm	0.45–7.5 nm 5–10 nm	Jehle et al. 2015 (in press)
Spectral sampling width	<1.5 ∗ Spectral sampling interval	VNIR: 0.86–15 nm SWIR: 7.4–12.3 nm	Dell'Endice and Alberti (2009)
Center wavelength accuracy	<0.2 nm	After laboratory calibration: <0.1 nm For a single flight line knowledge is ≤0.2 nm	Dell'Endice and Alberti (2009), Jehle et al. 2015 (in press)
Signal to noise (SNR)	None specified	625 (average of a 50% reflecting target, sun zenith at 24.4°)	Hueni, Schlaepfer, Jehle and Schaepman (2014), Hueni, Wooliams and Schaepman (2014)
Noise Equivalent Delta Radiance (NeDL)	None specified	0.1 mW/m^2/sr/nm	Hueni, Schlaepfer, Jehle and Schaepman (2014), Hueni, Wooliams and Schaepman (2014)
PSF (Point Spread Function)	≤1.75 ∗ Sampling interval	<1.5 ∗ Sampling interval	Dell'Endice et al. (2009)
Smile	<0.2 pixel	<0.16 pixel for 90% of all pixels <0.35 pixel for 10% of all pixels	Dell'Endice and Alberti (2009)
Frown (Keystone)	<0.16 pixel	<0.16 pixel for 80% of all pixels <0.35 pixel for 20% of all pixels	Dell'Endice and Alberti (2009)
Co-registration	<0.16 pixel	Average <0.55 pixel	Dell'Endice and Alberti (2009)
Bad pixels	VNIR: clusters of bad pixels <3 SWIR: not specified	VNIR: no bad pixels SWIR: <0.64%	Dell'Endice and Alberti (2009)
Scanning mechanism	Pushbroom	Pushbroom	Jehle et al. (2010)
Absolute radiometric calibration uncertainty	≤2%	VNIR: 372–1015 nm: 4.2% SWIR: 940–2540 nm: 6.6% (with uncalibrated sphere-filter reflections still to be removed)	Hueni, Schlaepfer, Jehle and Schaepman (2014), Hueni, Wooliams and Schaepman (2014)
Storage capacity on board (online/offline)	>60 GB/>150 GB	500 GB on SSD	Jehle et al. (2010)
Dynamic Range	12 … 16 bit	VNIR: 14 bit SWIR 13 bit	Jehle et al. (2010)
Positional knowledge	20% of the ground sampling distance	50% of ground sampling distance	Jehle et al. (2010)
Attitude knowledge	20% of IFOV	After boresight calibration: better than 5 pixels (≪1% of FOV)	Jehle et al. (2010)
Navigation system, flight line repeatability	±5% of FOV	After 3 years of operation: less than 50 pixels (<±2.5% of FOV)	Jehle et al. (2010)
Positional and attitude data	Recording of data onto a housekeeping channel	Fully implemented and operational	Jehle et al. (2010)

synchronized (uncertainty ±0.5 ms) allowing us to acquire images simultaneously, even under varying integration time settings. Users receive a maximum of 334 (VNIR) + 198 (SWIR) = 532 spectral bands, which can be programmed to fit a variable band setting depending on their requirements (Dell'Endice, Nieke, Koetz, Schaepman, & Itten, 2009).

Key to the mechanical subsystem is the optical compartment, including the optical base plate, on which all optical components are mounted. The optical base plate is isolated from the instrument housing and equipped with a separate, closed-loop cooling system. The temperature of the base plate is kept constant at 19 °C ± 1 °C, minimizing noise sources and temperature gradients. Most of the electronic boards and power supplies are mounted on a remote position in the baffle compartment, situated below the optical base plate, optimizing the thermal isolation. The optical compartment is sealed and the instrument is operated in a dry Nitrogen atmosphere with partial differential pressure control during data acquisition (ΔP < 250 mbar). The APEX instrument is mounted on a stabilizing platform (Leica PAV-30) providing the link between aircraft and instrument and enclosed in an environmental control box to minimize temperature fluctuations and gradients as much as possible.

The electrical subsystem of APEX is composed of the frontend electronics, supporting frame rates of up to 43.3 Hz. Following an analog–digital conversion and multiplexing the two detector channels, data are processed in a Field Programmable Gate Array (FPGA) to stream 16 bit words in a serialized fashion through an optical high-speed link at 700 Mbit/s to the control rack. Ancillary information is transmitted in parallel over a serial RS422 link to the control and storage rack.

The final APEX instrument component contains a built-in in-flight calibration facility (IFC). Before and after ground data acquisition, a mirror mechanism allows imaging an internal stabilized Quartz Tungsten Halogen lamp. The lamp is located near the baffle of the instrument, therefore it's light is transmitted through a fiber-bundle and a diffusor, followed by a set of spectral calibration filters fully illuminating diffusely the ground imager in the optical path of APEX (Schläpfer, Schaepman, Bojinski, & Börner, 2000). A moveable and calibrated ground mirror is the only optical element not seen by APEX during in-flight calibration. A filter wheel with six filter positions in this path holds four spectral

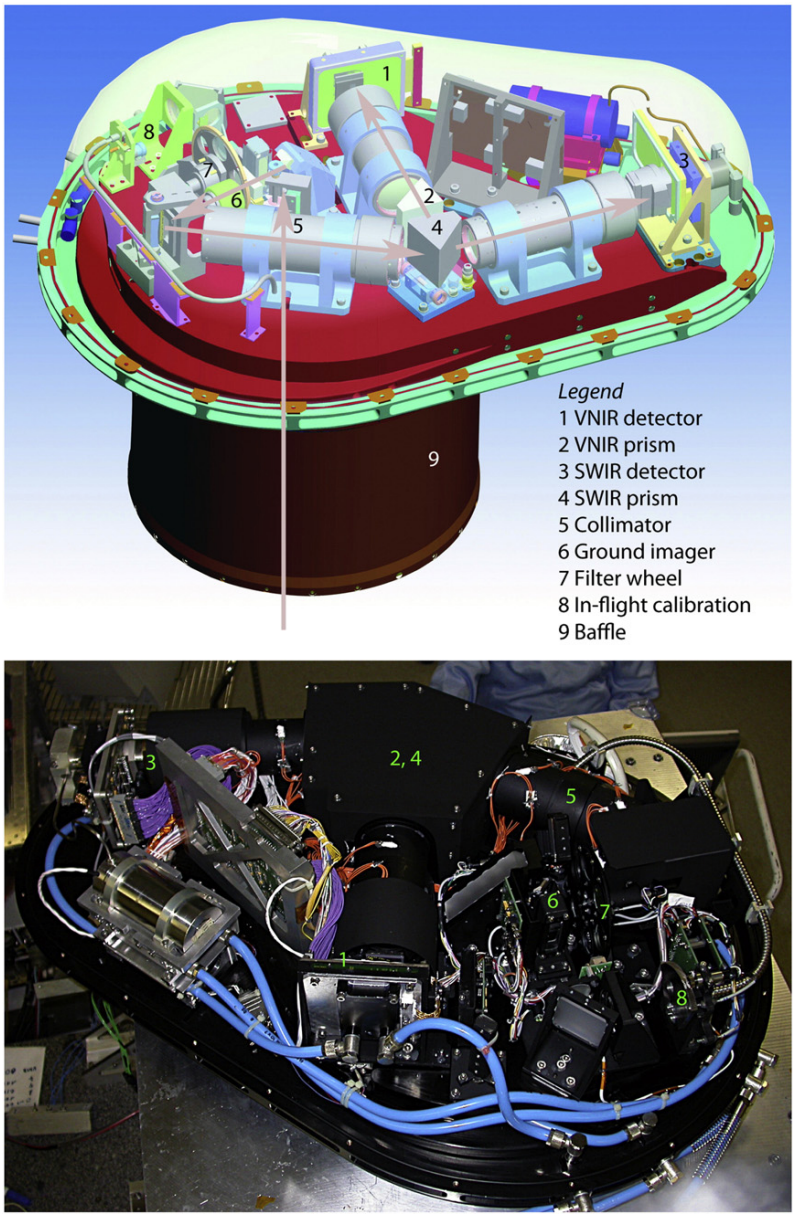

Fig. 1. Top: APEX optical system including two detector channels. Bottom: APEX optical system in production without cover. CAD drawing and photo: L. De Vos

filters used for instrument spectral stability monitoring. The filters are bandpass filters (Spectrogon) with transmission features at 700, 1000 and 2218 nm, and a Standard Reference Material (SRM) filter from the National Institute for Standards and Technology (NIST) with many distinct absorption features throughout the VNIR and SWIR spectral range. A fifth slot holds a neutral density glass filter (Schott NG4) and is used to avoid saturation in the VNIR channel at (very rare) expected maximum radiance levels (e.g., above snow). The sixth slot is left empty for standard Earth surface data acquisition. The APEX in-flight calibration capabilities are primarily used to assess spectral performance changes during in-flight and serve as comparison baseline between laboratory and in-flight conditions (D'Odorico, Alberti, & Schaepman, 2010). Simultaneous measurements of temperature and pressure ensure monitoring of environmental conditions in the lab, during in-flight calibration and data acquisition. This information is used for stability modeling and monitoring (Jehle, Hueni, Baumgartner, Lenhard & Schaepman, in press). IFC data analysis relies on the use of a feature-fitting algorithm comparing laboratory and in-flight shifts of particular filter absorption lines. In addition, the same method is used on atmospheric absorption lines during normal imaging, allowing monitoring the instrument's spectral stability (D'Odorico, Guanter, Schaepman, & Schläpfer, 2011). Remaining spectral and radiometric variations are mostly due to changing pressure/humidity/temperature affecting the prisms refraction properties, and can be estimated using ancillary data recorded by the APEX instrument (Jehle et al., in press).

2.3. Control and storage unit

The control and storage unit (CSU) hosts instrumentation to operate APEX (Fig. 2). This includes the Inertial Navigation System (INS) with dGPS data processing capabilities (Applanix POS/AV 410 IMU/GPS). APEX optical and positional data are linked using GPS based timestamps

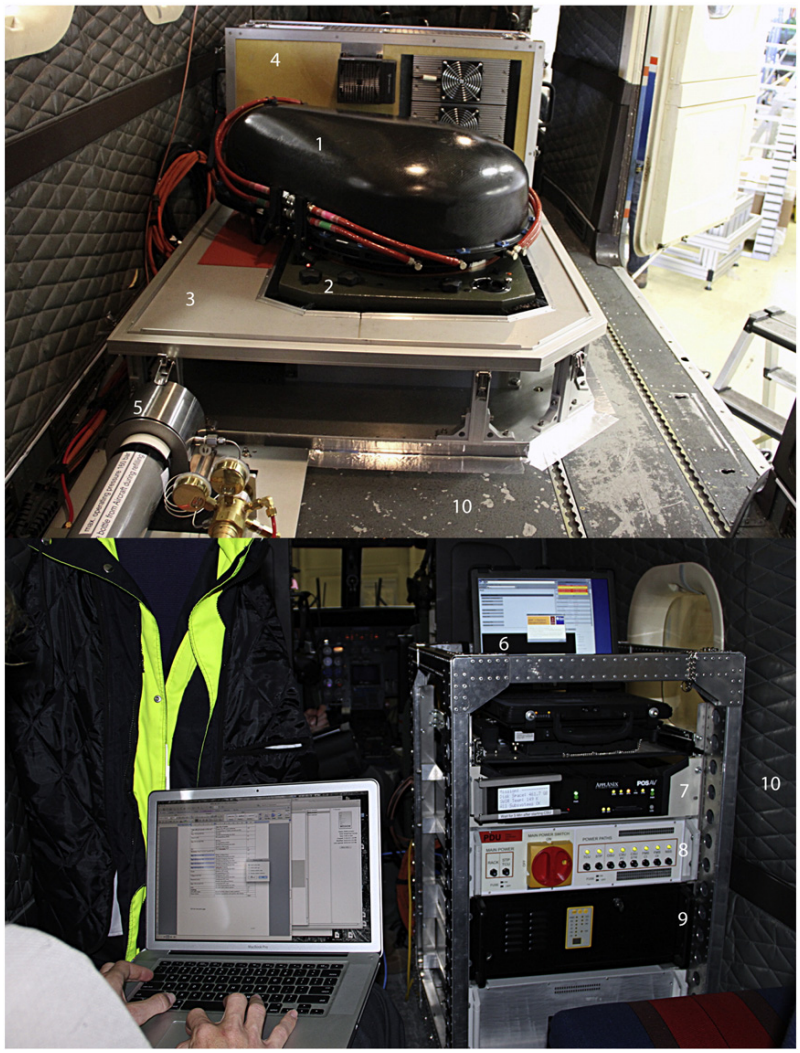

Fig. 2. Top: APEX instrument as mounted in Dornier DO-228 aircraft with N2 pressure system (bottom left), APEX on stabilizing platform (middle) and climate control (top); bottom: operator rack (right) and upload of configuration and flight data (left). Legend: 1 APEX instrument, 2 stabilizing platform, 3 interface plate, 4 thermal control unit, 5 nitrogen supply, 6 flight management computer, 7 inertial navigation system and GPS, 8 power distribution, 9 central storage unit, 10 aircraft bay.
Photo: M. Jehle

during processing by forming a smoothed, best-estimate trajectory for each acquired imaging frame. Further components are the flight management system with interfaces to the operator and pilot (TRACK'AIR XTrack), the APEX computer with its storage unit (Solid State Disks) and the power supply units. While largely everything in the CSU is available as commercial-off-the-shelf, only a custom-made PCI card is needed to be developed in order to connect the optical link from the instrument to the host system. Data originating from the PCI card use a multi-threaded shared memory architecture to ensure sufficient data throughput to the solid-state-memory disks. All of the CSU is driven by a tiered software approach. Low-level interfaces control disk read/write operations, while a middle tier level handles all logging and alerting. High-level software controls and enables configuring the system, its status and displays a waterfall image in real-time on screen for the operator. Finally, the power distribution unit connects the aircraft power supply with all APEX instruments requiring power.

2.4. Calibration and validation approach

APEX calibration and validation invokes a full set of integrated activities with the aim to producing high quality, reproducible radiometric measurements for each pixel–spectral band combination (Fox et al., 2003; Nieke et al., 2004). Unique to the APEX overall calibration approach is the use of a combination of laboratory, in-flight, and vicarious calibration activities (Schläpfer et al., 2000) based on methods using combined in-flight, scene-based and atmospheric approaches (Brazile et al., 2006; D'Odorico et al., 2011). Vicarious calibration is methodologically based on Kneubühler, Schaepman, Thome, and Schläpfer (2003), while in situ measurements (spectral radiance and reflectance using field spectrometers) are performed on standard targets (artificial sportgrounds, concrete) (Jehle et al., 2010), covering a limited range of radiances measured at sensor (Hueni et al., 2009a). The initial design foresees to assimilate calibration measurements into a coherent set of radiance measurements (Kaiser et al., 2004). This results in the development of both, a calibration and validation approach and software supporting in-situ measurements of field spectroradiometer measurements (Bojinski, Schaepman, Schläpfer, & Itten, 2002; Hueni et al., 2009a; Schaepman & Dangel, 2000) as well as handling calibration data (Hueni, Malthus, Kneubuehler, & Schaepman, 2011; Hueni et al., 2009a; Hueni, Lenhard, Baumgartner and Schaepman, 2013).

The laboratory calibration approach is based on a calibration home base (CHB, located at the German Aerospace Center (DLR)), which is

particularly designed to calibrate APEX and other airborne imaging spectrometers with similar properties, as well as the spectrometers used for on-ground reference measurements (Gege et al., 2009). This has been demonstrated with a number of airborne and field spectrometers calibrated in the CHB (Lenhard, Baumgartner, & Schwarzmaier, 2014 (in revision)). This traceable calibration approach facilitates the intercomparison of calibration data, and close cooperation with the German national metrology institute PTB (Physikalisch-Technische Bundesanstalt) assures state-of-the-art accuracy and traceability. By providing light sources with fully characterized properties (Taubert et al., 2013), the CHB allows to determine the functional relationship between at-sensor radiances and the signal measured by APEX (Nieke et al., 2008). The measurements can be classified in three categories: a) radiometric, allowing to convert raw sensor signals to physical units of radiance traceable to the système international (SI) (Taubert et al., 2013); b) spectral, allowing to assign center wavelength and spectral resolution for each detector element; and c) geometric, allowing to determine the view angles and angular resolution of each detector element. The latter two include the characterization of the optical distortions typical for pushbroom sensors known as smile and keystone. In addition, the CHB supports a multitude of auxiliary measurements required to fully characterize an imaging spectrometer such as detector linearity, sensitivity to linearly polarized light, radiometric noise or pixel response non-uniformity.

Finally, vicarious calibration efforts are performed in every flight season using selected reference targets on ground while the APEX instrument is acquiring data. The approach used follows guidelines as developed for other imaging spectrometer vicarious calibration (Kneubühler et al., 2003; Milton et al., 2009).

2.5. Processing and archiving facility

APEX data processing and archiving is split into the development of a science grade APEX processor, designed to produce calibrated radiances in a coherent observation geometry (i.e., Level 1), and an operational grade APEX processor and archiving facility, facilitating reproducible data processing and distribution (Hueni et al., 2009a). All processing beyond Level 1 (e.g., orthorectification, atmospheric compensation, and higher level products) are discussed in the application development section.

The science grade APEX processor is designed to process large quantities of imaging spectrometer data, including calibration and housekeeping data (Schaepman, Schläpfer, Brazile, & Bojinski, 2002). Its design is based on an iterative prototyping approach and from beginning on includes considerations to build look-up tables for atmospheric compensation (Brazile et al., 2004), as well as optimized processing speed requirements (Brazile, Richter, Schläpfer, Schaepman, & Itten, 2008; Brazile et al., 2005).

The science grade APEX processor is developed to integrate calibration data with actual measurements, allowing to reconstruct each geometrical position and each radiance of any given detector element (Fig. 4). Processing data from raw to Level 1 is a two-stage process. Raw data generated by the APEX CSU computer are first segregated into imaging, in-flight calibration and dark current data blocks basing on a finite-state machine (FSM) fed with sensor parameters. Level 1 data processing is frame based, applying a sequence of algorithms comprising true dark current correction based on a shutter mechanism in front of the ground imager, de-smearing of the VNIR channel, compensations of radiometric effects due to spectral shifts (Hueni et al., 2014), radiometric calibration by applying gains and offsets, bad pixel replacement by spatial interpolation and optional spectral/spatial resampling to register the data within the nominal geometric and spectral coordinate space, thereby compensating for spectral and spatial misregistration. All calibration data is contained in the 'Calibration Parameters Cube' (cf. Fig. 4) and available upon request. The raw to Level 1 processor as well as the APEX Calibration Information System are continuously improved to refine the sensor model (Hueni, Sterckx, & Jehle, 2013) and data calibration. (See Fig. 3.)

3. APEX Earth science applications

3.1. Introduction

Increasingly, imaging spectrometer data are delivered as calibrated radiance data (Level 1) as well as science products (Levels 2 & 3). Reasons to deliver a multitude of processing levels are based on modeling requirements using radiance based approaches (Laurent, Verhoef, Clevers, & Schaepman, 2011a; Laurent, Verhoef, Clevers, & Schaepman, 2011b; Laurent et al., 2010), or applications of narrow- and broadband indices at surface reflectance or radiance levels (Verrelst, Schaepman, Kötz, & Kneubühler, 2008). Imaging spectrometer data are used for many purposes nowadays and comprehensive overviews are found in the scientific literature (cf., Ben-Dor et al., 2009; Dozier, Green, Nolin, & Painter, 2009; Gao, Montes, Davis, & Goetz, 2009; Jacquemoud et al., 2009; Kokaly, Asner, Ollinger, Martin, & Wessman, 2009; Milton et al., 2009; Plaza et al., 2009; Schaepman et al., 2009b; Ustin et al., 2009). We concentrate here on describing a few key applications, which are either unique to APEX or significantly advance the use of APEX-like data. APEX data itself are available as a general purpose APEX data set, which can be downloaded (http://www.apex-esa.org) (Hueni et al., 2012). On the same site, APEX quick-looks are also listed. Many of those datasets can be obtained free of charge for scientific use by contacting the responsible person.

Although representative at regional scale, advanced APEX products have also implications for environmental research at larger scales. Process models, for example dynamic global vegetation models (LPG-GUESS (Smith et al., 2001)), are unique tools to quantify the impact of environmental change on ecosystem functioning. Their reliability is however limited due to static parameterization or model assumptions (Friedlingstein et al., 2006). APEX like EO-data at local and regional scale face increasing attention to improve models (Plummer, 2000; Poulter et al., 2011). Long term environmental monitoring programs are usually based on modeling approaches and continuous satellite data series (Scholes et al., 2009). Providing continuous series of satellite data is non-trivial, especially in case of instrument replacement or sensor degradation, and can only be guaranteed by applying data harmonization strategies (Teillet et al., 1997). APEX data are suited to simulate data and products of current and future space missions (e.g., Sentinel-2; D'Odorico, Gonsamo, Damm, & Schaepman, 2013). Such simulations provide the base to define technical specifications of upcoming instruments or for identifying data harmonization needs and strategies (Steven et al., 2003). The traceability of EO data quality is of outstanding importance if data are intended to be assimilated in process models (Fox et al., 2003). The rigorous implementation of physical based algorithms for the APEX product retrieval (e.g., Bayesian optimization algorithm in combination with coupled atmosphere–canopy models; Laurent et al., 2011b), and the comprehensive data quality assessment of APEX (i.e., calibration in CHB, IFC monitoring) enables to trace uncertainties throughout the entire processing chain. Products following the above reasoning are discussed in the following section.

3.2. Operational and science grade processing

APEX operational grade data processing is performed within the Central Data Processing Centre (CDPC) at VITO. First, spectral misregistration is performed using a spectrum-matching technique (Gao, Montes, & Davis, 2004). Geometric processing is performed using direct georeferencing, including the use of standard or user-provided Digital Elevation Models (DEM). Subsequently, a smile-aware atmospheric correction is performed to retrieve hemispherical–conical reflectance factors (HCRF) in combination with MODTRAN5. Finally coordinate

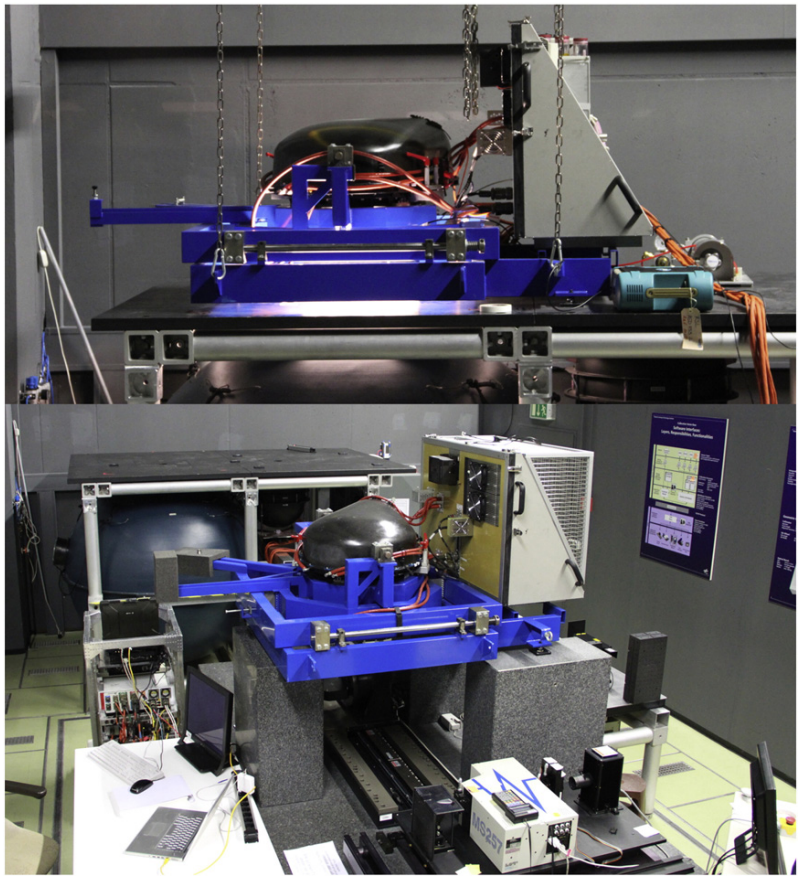

Fig. 3. Laboratory calibration of APEX. Top: APEX mounted on integrating sphere for radiance calibration. Bottom: APEX mounted on optical bench for spectral/geometric calibration. Photo: M. Jehle, Calibration Home Base at DLR, Oberpfaffenhofen (GER)

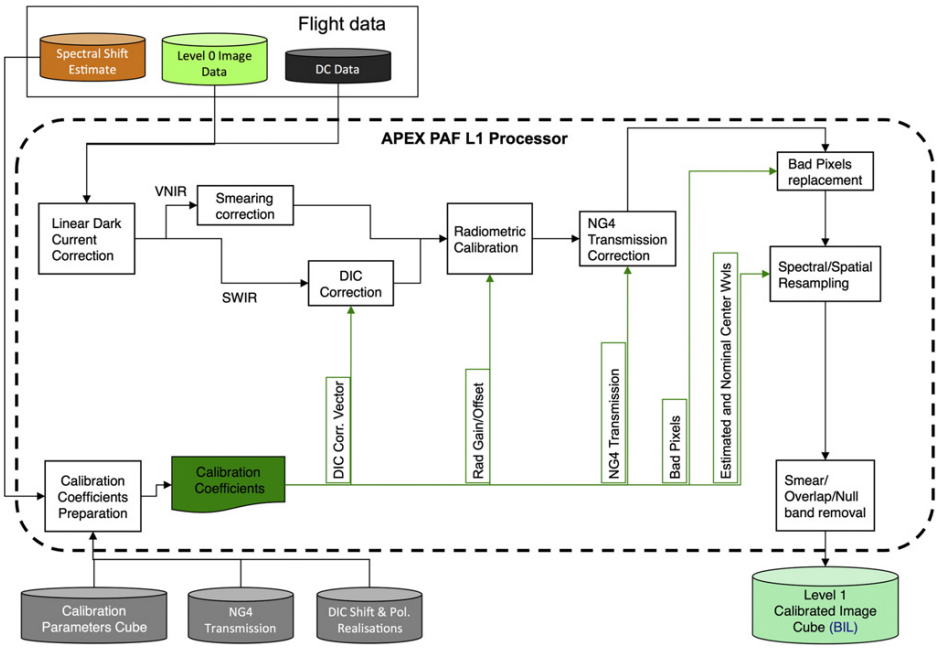

Fig. 4. High level processing scheme of the APEX processor. DIC = Dichroic Filter Correction (Hueni, Schlaepfer, Jehle, & Schaepman, 2014; Hueni, Wooliams, & Schaepman, 2014), NG4 = Neutral density glass filter (Schott NG4), L1 = Level 1 Processor, BIL = Band Interleaved by Line format, Pol. = Polarization, VNIR = Visible/Near Infrared, SWIR = Shortwave Infrared.

projection is performed using the General Cartographic Transformation Package (GCTP) (USGS, 1998). For all reprojections, a seven parameter Helmert transformation is used. In a final step, HCRF data are resampled to the central wavelengths as calibrated in the CHB for the actual acquisition (Biesemans et al., 2007).

APEX science grade data processing is corrected to minimize the impact of atmospheric and topographic effects (Richter & Schläpfer, 2002; Schläpfer & Richter, 2002). The subsequent automated atmospheric compensation process accounts for irradiance properties in complex terrain, atmospheric scattering and absorbers, as well as instrument smile effects (Richter, Schlapfer, & Muller, 2011). This combined geo-atmospheric processing is used for all situations, where users wish to obtain uniform geo-locatable bottom of atmosphere reflectance values. In addition, APEX data can be normalized to contain nadir-viewing geometries by applying a Li-Ross BRDF correction based on a continuous land cover classification (Weyermann, Damm, Kneubuhler, & Schaepman, 2014). Using a spectral unmixing based approach, land cover types with substantial BRDFs are extracted from the APEX scene and expressed as linear combinations of three kernels (isotropic, geometric (Li-kernel), volumetric (Ross-kernel)). This approach allows seamless mosaicking of several APEX flight lines, while minimizing angular effects dominating flight patterns that are chosen to comply with minimal operational constraints and not optimized for minimal directional illumination influences (Laurent, Schaepman, Verhoef, Weyermann, & Chavez, 2014).

While operational APEX data processing is available to everyone browsing data in the CDPC archive of VITO, science grade data processing is highly experimental and only applied on request. However, the APEX PAF is upgraded to include always latest developments of the science grade processing.

3.3. AOD and critical surface albedo

If able to directly retrieve aerosol optical depth (AOD) from APEX data, it is possible to improve the atmospheric compensation procedure by generating a priori probability distribution functions. We suggest a forward model approach, identifying a SNR of $\geq$100 at 550 nm being sufficient for AOD retrieval on surfaces with 10% reflectance or less (Seidel, Schläpfer, Nieke, & Itten, 2008). However, even if reflectance spectroscopy data are combined with dedicated aerosol remote sensing instruments measuring at multiple angles including polarization sensitivity (Diner et al., 2013), aerosol optical and especially micro-physical property retrieval remain challenging. Computationally extensive algorithms limit the AOD retrieval to far real-time data processing. We suggest a simple model for atmospheric radiative transfer (SMART), critically balancing computational speed and retrieval accuracy to the benefit of AOD retrievals (Seidel, Kokhanovsky, & Schaepman, 2010) as well as simulations of Hemispherical–Conical Reflectance Factors (HCRF, following (Schaepman-Strub, Schaepman, Painter, Dangel, & Martonchik, 2006)) for space- and airborne sensors. SMART is used in a fast optimization scheme for the retrieval of AOD using APEX data (Seidel, Kokhanovsky, & Schaepman, 2012) avoiding the critical surface albedo regions (Seidel & Popp, 2012) to maximize the AOD retrieval sensitivity on radiance data at sensor level.

3.4. NO_2 vertical column densities

Atmospheric trace gas retrievals using Earth looking airborne imaging spectrometers are of increasing interest and with increased instrument performance and spectral resolution become more feasible (Marion, Michel, & Faye, 2004; Thorpe, Frankenberg, & Roberts, 2014). Nitrogen dioxide (NO_2) is a reactive trace gas in the troposphere, which acts as an ozone and aerosol precursor and can negatively affect human health and ecosystem functions. Anthropogenic emissions are a major source of atmospheric NO_2 and NO_2 thresholds are still regularly exceeded in many European countries. We take advantage of the APEX band binning/unbinning capability (Dell'Endice et al., 2009) to derive vertical column densities (VCD) of NO_2 from APEX. A two-step approach (Popp et al., 2012) based on differential optical absorption spectroscopy (DOAS) is applied to unbinned APEX measurements whose higher spectral sampling enables good coverage of the narrow absorption lines of atmospheric gases. First, the number of NO_2 molecules along the average photon path through the atmosphere to the sensor (slant column densities (SCD)) are computed by fitting absorption cross sections of NO_2 and other interfering gases (i.e., H_2O, O_2–O_2, or O_3) in the 470–510 nm spectral region to the differential optical depth calculated from image-based reference spectra. Second, the resulting NO_2-SCD is normalized to NO_2-VCD with a so-called air mass factor (AMF). The AMF is computed by radiative transfer calculations including forward model parameters such as surface reflectance retrieved from the APEX data, a digital elevation model, a-priori model NO_2 profiles, and an aerosol extinction profile (Popp et al., 2012). The resulting two-dimensional NO_2-VCD maps now allow the quantification of the spatio-temporal highly variable NO_2 field as well as the detection of major NO_2 sources at an unparalleled local scale and synoptic view.

3.5. Coupled canopy–atmosphere modeling

Imaging spectrometers are used to map dedicated absorption features present in Earth surface materials or in the atmosphere. This requires that spectral bands should be positioned at (or sufficiently close to) the absorption features. Spectral instabilities will lead to detection of unrelated phenomena and even render retrieval algorithms (such as vegetation indices) instrument specific and/or dependent. In addition, data are usually converted to surface reflectance. For this conversion to be successful, we must assume certain parameters at the interface between canopy and atmosphere (i.e., topography, surface anisotropy, adjacency effects, location of top-of-canopy). We therefore suggest the use of a coupled canopy–atmosphere RT model combined with a Bayesian optimization algorithm for vegetation (Laurent, Verhoef, Damm, Schaepman, & Clevers, 2013). This approach does not invoke atmospheric compensation before applying the inverse model and is largely independent of the number of bands used (limitations are related to larger uncertainties when using fewer bands). Using the hybrid canopy RT model Soil–Leaf–Canopy (SLC) (Verhoef & Bach, 2007) and the atmosphere RT model MODTRAN5 (Berk et al., 2004), the canopy–atmosphere coupling is based on the 4-stream theory (Laurent et al., 2011b), making full use of the directional information contained in the four canopy reflectance components as modeled by SLC. Variable estimation is then performed using Bayesian optimization of the coupled model (Tarantola, 2005).

3.6. Sun-induced chlorophyll fluorescence (Fs) retrieval

From the early APEX instrument development phase on, the pushbroom design allowed only one given wavelength to be chosen for the adjustment between dispersing elements and detector(s). Once this wavelength is chosen, all the others are defined by geometric constraints. This wavelength was set to be the 760 nm O_2-A absorption line in the VNIR detector since it has the advantage of being useful for in-flight calibration purposes. With the advent of having this line well calibrated, it became evident that APEX can be used for the retrieval of sun-induced chlorophyll fluorescence (Fs) (Damm et al., 2011). In the near infrared, emitted Fs contributes to about 2–5% to the reflected radiance flux of a vegetation canopy (R). Both fluxes have to be decoupled to quantify the Fs emission signal. For medium resolution instruments, the Fraunhofer Line Depth (FLD) approach introduced by Plascyk (1975) serves as de-facto standard for Fs retrieval using medium resolution instruments (Meroni et al., 2009). The Fs retrieval algorithm implemented for APEX data follows the approach proposed by Guanter et al. (2010) and is based on a constrained FLD approach exploiting the broader O_2-A absorption feature. Reference surfaces with known Fs

emission (e.g., bare soil) are used to constrain the Fs retrieval (Damm et al., 2014; Guanter et al., 2010).

3.7. Pigment retrieval

Retrieval of plant pigments and pigment systems has seen substantial progress paralleled with increased performance of imaging spectrometers (Kokaly et al., 2009; Ustin et al., 2009). Pigments are not only relevant to determine leaf functioning (Carvalho, Takaki, & Azevedo, 2011), but are used as proxies for light use efficiency in models of net primary productivity (Coops, Hilker, Hall, Nichol, & Drolet, 2010) or assessing functional traits (Homolova, Malenovsky, Clevers, Garcia-Santos, & Schaepman, 2013). However, high accurate retrieval of functional traits is highly dependent on narrow and stable bands in a spectrometer system. Finally, as photoacclimation and time kinetics (Hallik, Niinemets, & Kull, 2012) become more feasible to be measured, accurate pigment estimates will steadily gain in importance. We use index based approaches for combined retrieval of chlorophyll, carotenoids and anthocyanins from APEX data (Gitelson, Keydan, & Merzlyak, 2006). The original band positions are adapted to match specific APEX bands, which are smaller in bandwidth than the sensor used for the original development of the retrievals.

4. Results

4.1. APEX advanced radiometry measurements

Following acceptance testing in 2009, APEX was transferred to the University of Zurich and VITO in spring 2010 for regular operations. Since summer 2010, APEX is producing science grade spectrometry measurements and has acquired >3 Terabytes of data corresponding to >3 Mio. scan-lines (approx. 30,000 km^2) and several factors more in calibration and product data until the end of 2013. APEX has received airworthiness certification for two of DLR's research aircraft (Dornier DO-228-101 (D-CODE), Dornier DO-228-212 (D-CFFU)) with VITO and the University of Zurich providing instrument operators for data flights. In parallel, updates to the instrument, CHB, and PAF have been made to further improve the instruments measurements. We present the following table (Table 1) summarizing the initial specifications used to design the instrument and list validated performances for all specifications as well as other relevant instrument parameters including associated references following upgrades and calibration efforts.

APEX radiometric performance is validated using a four-fold approach. Following calibration in the CHB, APEX is calibrated traceable to a primary calibration standard with less than 4% uncertainty (Fig. 5A). Second, APEX is calibrated using radiance based vicarious calibration approaches with in-situ measurements performed using a field spectroradiometer (ASD FieldSpec Pro FR) and a sunphotometer (CIMEL) (Fig. 5B). Uncertainties are in the range of $\leq$6.5%, but lower spectral resolution of the field spectroradiometer as compared to APEX are limiting the calibration effort. Also with a spatial resolution of 1–2 m, identifying homogeneous areas on ground is very challenging. At this spatial scale, sports fields, concrete or other artificial targets are usually not homogeneous enough to serve as calibration surfaces. Therefore, validation efforts are also put in place using spatially distributed data and inverse (Fig. 5C) as well as forward (Fig. 5D) modeling approaches. The latter two still show deviations from the APEX measurements, largely due to simplified model approaches.

In-flight calibration information is used in combination with atmospheric measurements allowing to monitor (D'Odorico et al., 2011) and model instrument stability (Jehle et al., in press) and can therefore not be used in addition as independent calibration source.

4.2. APEX Earth science applications development

APEX Earth science applications span a wide range of products. While calibrated radiances are a standard product for many science grade instruments, we have developed individual and joint approaches for atmospheric correction and allowing minimizing the impact of surface anisotropy effects. These products are of high operational use,

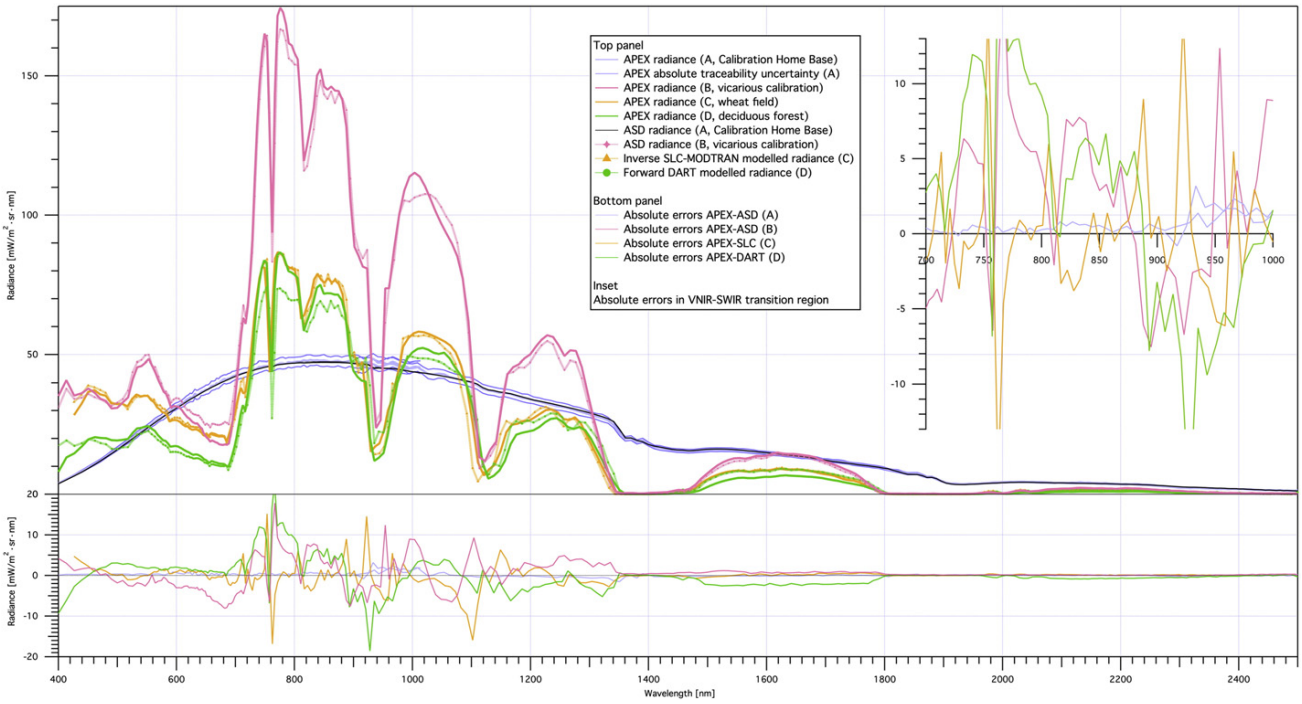

Fig. 5. Comparison of four APEX validation approaches. A) traceable, calibrated laboratory measurements (Hueni, Schlaepfer, Jehle, & Schaepman, 2014; Hueni, Wooliams, & Schaepman, 2014); B) radiance based vicarious calibration effort using in-situ spectroradiometric measurements (Damm, pers. comm.); C) radiance level based comparison from Bayesian optimization (Laurent et al., 2013); and D) forward simulated at-sensor-radiances using 3D modeling (Schneider et al., 2014 (in revision)).

since increasingly well corrected surface reflectance data are required form a more operational or stakeholder oriented user community. However, a complete physically based surface anisotropy correction remains challenging. Instruments like APEX are limited in angular data acquisition as well as by having a relatively small FOV. Additional efforts are needed to constrain the BRDF correction, likely with the support of a priori information.

We report on a second class of Earth science applications, namely retrieving information from the atmosphere (VCD of NO_2 as well as AOD), and deriving the concept of critical surface albedo, allowing to decouple atmospheric and land surface based products, further increasing the retrieval quality of the atmospheric products. Columnar retrievals of NO_2 using airborne instruments cannot be compared with in-situ point measuring networks. However, current existing in situ measurements can be complemented by columnar NO_2 information, allowing policy validation with a higher level of process understanding in the coupled surface–atmosphere system (Popp et al., 2012). Finally AOD retrievals are optimized using simplified approaches, carefully balancing retrieval accuracy and computational requirements. The AOD information can be later used as prior information in an atmospheric compensation procedure in an iterative fashion.

Many of the current retrieval schemes used in spectroscopy rely on retrieving surface reflectance and subsequently infer biochemical or biophysical information. We demonstrate with APEX a new retrieval scheme by coupling a canopy–atmosphere model and invert the coupled model. This allows us to avoid two separate steps of atmospheric correction and invoking an inverse canopy model in a second step. The coupled model approach clearly shows advantages by minimizing interfacing complexity between these two models at the cost of increased inversion complexity. The particular model combination (SLC and MODTRAN) shows excellent performance in vegetation corresponding closest turbid media scattering, which is the physical foundation of the SLC model. Validation of this process is performed using a radiance based vicarious calibration procedure, ensuring consistency when comparing in-situ and airborne measurements (see Fig. 4B).

We finally apply simultaneous fluorescence line depth (FLD) and pigment retrieval approaches to APEX data (Fig. 6). Vegetation fluorescence (Fs) is derived using the constrained 3FLD approach (Damm et al., 2014). Because of a very low Fs signal, residual along-track striping is still visible in the APEX data. Fs values range between 0 … 10 mW m^{-2} nm^{-1} sr^{-1}. Simultaneous field validation using a field spectroradiometer (ASD FieldSpec FR Pro) is carried out. We use a spectral deconvolution approach to minimize Fs retrieval differences between APEX and the field spectroradiometer measurements (Zhao, Jia, & Li, 2010). In situ data were collected using a stratified random sampling approach while measuring reflected and emitted radiances at each calibration point ($n = 16$), resulting in a good agreement between airborne and in situ Fs ($R^2 = 0.87$, relative RMSE = 27.76%). Spatial distribution of Fs, such as measured with APEX, can serve as proxy for instantaneous plant photosynthesis. Pigments are derived in relative units and visual validation suggests feasibility of the method. Measurements of pigments in leaves are well understood (Gitelson, Chivkunova, & Merzlyak, 2009), however their validation using leaf pigment concentrations is ongoing, and leaf models including separate representation of these pigments and plant structure are sparse (Townsend, Serbin, Kruger, & Gamon, 2013) and not applied in an inverse fashion to remotely sensed data as of yet. Relative pigment abundances will support improved plant functioning and estimates of light use efficiency. Also they represent an important functional trait per se.

5. Conclusions and outlook

We report on the latest status of APEX with focus on advanced radiometry measurements and Earth science applications. APEX has undergone a complete development cycle, ranging from modeling system specifications to analyzing APEX data in a coherent fashion. Following the start of the operational activities of APEX in 2010, small improvements were made to the hardware (more reliable electronics boards, update of storage capacity, etc.), and major improvements to sensor modeling, refinement of the PAF and development of science grade retrieval algorithms. APEX has very high compliance with its initial specifications (though not in all parts), and currently allows operational data acquisition of traceable radiometric measurements and production of Earth science applications.

The APEX instrument has demonstrated to deliver traceable spectroradiometric measurements. The PAF processes data using the latest calibration information, individually optimized for each single scene. This results in scene-specific band positions. While this is no threat to individually analyzing scenes, most of the commercially available software does not support convolution techniques 'on-the-fly', putting a de-convolution/convolution effort on those users using multiple scenes for their analysis. Controversial discussions are ongoing, if

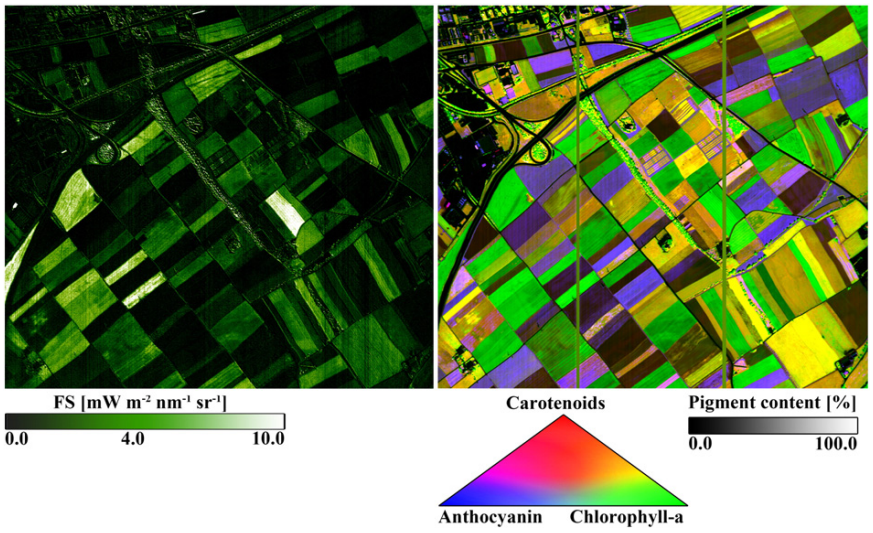

Fig. 6. Left: Fs retrieval following Damm et al. (2014) in absolute units [0–10 mW m^{-2} nm^{-1} sr^{-1}, black–white]. Right: Pigment content retrieval following Gitelson et al. (2006) in relative units [0–100%]. Pigment abundances are red: carotenoids, green: chlorophyll-a and blue: anthocyanin (APEX data June 16, 2012; 10:48 UTC; Oensingen, Fluxnet site 314; 47.2863°N, 7.7343°E, Switzerland).

APEX band settings should be resampled to a 'common band set', or leaving the original measurements unaltered. Currently, the latter is the case.

APEX was designed using a robust approach to sensor modeling. Even though the instrument model was updated on a regular basis, a key challenge remains to develop a sensor independent model, allowing for forward and inverse modeling approaches. Currently, the APEX PAF contains substantial APEX specific correction algorithms, being inherent to the functioning and performance of this specific instrument (Hueni et al., 2009). A more generic and generally applicable instrument and application model would serve all of the spectroscopy community much better, allowing for instrument and product cross-comparison in a much more coherent fashion.

While APEX, with its very high spectral resolution, is capable of simulating existing and future missions at very high accuracy, it can also be used to ensure consistency of indices-based approaches. Many of the existing narrow- (and broad-) band indices are developed using a specific instrument. High spectral resolution instruments can easily be convolved to fit original band settings, but can in addition be used as a model intermediate to ensure continuity and uncertainty estimates of different instruments (D'Odorico et al., 2013) in combination with in situ measurements. Availability of spatial and temporal discontinuous data of high spectral resolution is of key importance to fulfilling this goal.

APEX product development has shown key important development of band-specific products for advanced indices and combined indices for simultaneous retrieval of regional scale pigments and chlorophyll fluorescence. Equally, it was shown that inversion of coupled models substantially profit from high dimensional spectral data. Other, emerging applications using APEX will further demonstrate the usefulness of high dimensional data for applications (cf., Demarchi, Canters, Cariou, Licciardi, & Chan, 2014; Kneubühler et al., 2014; Schepers et al., 2014; Schweiger et al., 2014). Key to all approaches is a continuing requirement for higher spectral resolution instruments with higher SNR and therefore higher dimensionality. This will further foster the development of new models or retrieval algorithms—both empirical and physical—allowing a new generation of spectroscopy instruments and science professionals to be trained and developing new ideas.

With APEX we still explore only a tiny fraction of what could actually be explored with Earth related imaging spectroscopy. Key to the successful application of spectroscopy is still acquisition of a coherent set of independent and simultaneous retrievals of the Earth system spheres. We encourage everyone to make the best use of these data to further tackle these plentiful opportunities much better in the near future!

Acknowledgments

We thank the University of Zurich for continued funding and support to APEX. APEX is further supported through ESA, ESA PRODEX (16298/02/NL/US and 15449/01/NL/Sfe), the Swiss National Science Foundation (SNSF), the Belgian Science Policy Office (BELSPO), the Swiss University Conference (SUK, KIP-SEON), the University of Zurich Research Priority Program on 'Global Change and Biodiversity' (URPP GCB), the Swiss Space Office (SSO), the European Metrology Research Programme (EMRP, which is jointly funded by the EMRP participating countries within EURAMET and the European Union), and the German Aerospace Center (DLR). We thank former UZH APEX project managers Jens Nieke and Edoardo Alberti and former ESA APEX project managers Gerd Ulbrich, Jose Gaviras, and Hilde Schroeven-Deceuninck for their support. We thank the reviewers for helpful comments, allowing us to improve the manuscript.

References

Ben-Dor, E., Chabrillat, S., Demattê, J.A.M., Taylor, G.R., Hill, J., Whiting, M.L., et al. (2009). Using imaging spectroscopy to study soil properties. *Remote Sensing of Environment*, *113*(Suppl. 1), S38–S55.

Berk, A., Anderson, G. P., Acharya, P. K., Bernstein, L. S., Muratov, L., Lee, J., Fox, M., Adler-Golden, S. M., Chetwynd, J. H., Hoke, M. L., Lockwood, R. B., Gardner, J. A., Cooley, T. W. , & Lewis, P. E. (2004). MODTRAN5: A reformulated atmospheric band model with auxiliary species and practical multiple scattering options. *Proceedings of SPIE - The International Society for Optical Engineering*, *5425*, 341–347.

Biesemans, J., Sterckx, S., Knaeps, E., Vreys, K., Adriaensen, S., Hooyberghs, J., et al. (2007). Image processing workflows for airborne remote sensing. *5th EARSeL workshop on imaging spectroscopy*. Bruges, B: EARSeL.

Bojinski, S., Schaepman, M.E., Schläpfer, D., & Itten, K. (2002). SPECCHIO: A web-accessible database for the administration and storage of heterogeneous spectral data. *ISPRS Journal of Photogrammetry and Remote Sensing*, *57*, 204–211.

Börner, A., Wiest, L., Keller, P., Reulke, R., Richter, R., Schaepman, M.E., et al. (2001). SENSOR: A tool for the simulation of hyperspectral remote sensing systems. *ISPRS Journal of Photogrammetry and Remote Sensing*, *55*, 299–312.

Brazile, J., Kaiser, J.W., Schläpfer, D., Nieke, J., Schaepman, M.E., & Itten, K.I. (2005). Parallelization of APEX airborne imaging spectrometer product generation. In B. Zagajewski, & M. Sobczak (Eds.), *Imaging spectroscopy — New quality in environmental studies* (pp. 109–117). Warsaw (Pl): EARSeL.

Brazile, J., Neville, R.A., Staenz, K., Schlapfer, D., Lixin, S., & Itten, K.I. (2006). Scene-based spectral response function shape discernibility for the APEX imaging spectrometer. *IEEE Geoscience and Remote Sensing Letters*, *3*, 414–418.

Brazile, J., Richter, R., Schläpfer, D., Schaepman, M.E., & Itten, K.I. (2008). Cluster versus grid for operational generation of ATCOR's MODTRAN-based look up tables. *Parallel Computing*, *34*, 32–46.

Brazile, J., Schaepman, M.E., Schläpfer, D., Kaiser, J.W., Nieke, J., & Itten, K.I. (2004). Cluster versus grid for large-volume hyperspectral image preprocessing. In H.A. Huang, & H.J. Bloom (Eds.), *Proceedings of SPIE Vol. 5548, Atmospheric and environmental remote sensing data processing and utilization: An end-to-end system perspective* (pp. 48–58).

Carvalho, R.F., Takaki, M., & Azevedo, R.A. (2011). Plant pigments: The many faces of light perception. *Acta Physiologiae Plantarum*, *33*, 241–248.

Chorier, P., & Martino, F. (2004). APEX detector IDM08102 acceptance test. In A.A. Test (Ed.), Grenoble, F: Sofradir.

Coops, N.C., Hilker, T., Hall, F.G., Nichol, C.J., & Drolet, G.G. (2010). Estimation of light-use efficiency of terrestrial ecosystems from space: A status report. *BioScience*, *60*, 788–797.

D'Odorico, P., Guanter, L., Schaepman, M.E., & Schläpfer, D. (2011). Performance assessment of onboard and scene-based methods for Airborne Prism Experiment spectral characterization. *Applied Optics*, *50*, 4755–4764.

Damm, A., Erler, A., Hillen, W., Meroni, M., Schaepman, M.E., Verhoef, W., et al. (2011). Modeling the impact of spectral sensor configurations on the FLD retrieval accuracy of sun-induced chlorophyll fluorescence. *Remote Sensing of Environment*, *115*, 1882–1892.

Damm, A., Guanter, L., Laurent, V.C.E., Schaepman, M.E., Schickling, A., & Rascher, U. (2014). FLD-based retrieval of sun-induced chlorophyll fluorescence from medium spectral resolution airborne spectroscopy data. *Remote Sensing of Environment*, *147*, 256–266.

Dell'Endice, F., & Alberti, E. (2009). In M.E. Schaepman (Ed.), *APEX characterisation at CHB: Campaign report* (pp. 65). Zurich, CH: University of Zurich.

Dell'Endice, F., Nieke, J., Koetz, B., Schaepman, M.E., & Itten, K. (2009). Improving radiometry of imaging spectrometers by using programmable spectral regions of interest. *ISPRS Journal of Photogrammetry and Remote Sensing*, *64*, 632–639.

Demarchi, L., Canters, F., Cariou, C., Licciardi, G., & Chan, J.C.W. (2014). Assessing the performance of two unsupervised dimensionality reduction techniques on hyperspectral APEX data for high resolution urban land-cover mapping. *ISPRS Journal of Photogrammetry and Remote Sensing*, *87*, 166–179.

Diner, D.J., Xu, F., Garay, M.J., Martonchik, J.V., Rheingans, B.E., Geier, S., et al. (2013). The Airborne Multiangle SpectroPolarimetric Imager (AirMSPI): A new tool for aerosol and cloud remote sensing. *Atmospheric Measurement Techniques*, *6*, 2007–2025.

D'Odorico, P., Alberti, E., & Schaepman, M.E. (2010). In-flight spectral performance monitoring of the Airborne Prism Experiment. *Applied Optics*, *49*, 3082–3091.

D'Odorico, P., Gonsamo, A., Damm, A., & Schaepman, M.E. (2013). Experimental evaluation of Sentinel-2 spectral response functions for NDVI time-series continuity. *IEEE Transactions on Geoscience and Remote Sensing*, *51*, 1336–1348.

Dozier, J., Green, R.O., Nolin, A.W., & Painter, T.H. (2009). Interpretation of snow properties from imaging spectrometry. *Remote Sensing of Environment*, *113*(Suppl. 1), S25–S37.

EUFAR (2014). DO228/D-CODE — DLRIn http://www.eufar.net/experiment/aircraft/specaircraft2.php?num=73 (Ed.), .

Fox, N., Aiken, J., Barnett, J.J., Briottet, X., Carvell, R., Frohlich, C., et al. (2003). Traceable radiometry underpinning terrestrial- and helio-studies (TRUTHS). *Advances in Space Research*, *32*, 2253–2261.

Friedlingstein, P., Cox, P., Betts, R., Bopp, L., von Bloh, W., Brovkin, V., Cadule, P., Doney, S., Eby, M., Fung, I., Bala, G., John, J., Jones, C., Joos, F., Kato, T., Kawamiya, M., Knorr, W., Lindsay, K., Matthews, H. D., Raddatz, T., Rayner, P., Reick, C., Roeckner, E., Schnitzler, K. -G., Schnur, R., Strassmann, K., Weaver, A. J., Yoshikawa, C., & Zeng, N. (2006). Climate-carbon cycle feedback analysis: Results from the C4MIP model intercomparison. *Journal of Climate*, *19*(14), 3337–3353.

Gao, B.C., Montes, M.J., & Davis, C.O. (2004). Refinement of wavelength calibrations of hyperspectral imaging data using a spectrum-matching technique. *Remote Sensing of Environment*, *90*, 424–433.

Gao, B. -C., Montes, M.J., Davis, C.O., & Goetz, A.F.H. (2009). Atmospheric correction algorithms for hyperspectral remote sensing data of land and ocean. *Remote Sensing of Environment*, *113*(Suppl. 1), S17–S24.

Gege, P., Fries, J., Haschberger, P., Schötz, P., Schwarzer, H., Strobl, P., et al. (2009). Calibration facility for airborne imaging spectrometers. *ISPRS Journal of Photogrammetry and Remote Sensing*, *64*, 387–397.

Gitelson, A.A., Chivkunova, O.B., & Merzlyak, M.N. (2009). Nondestructive estimation of anthocyanins and chlorophylls in anthocyanic leaves. *American Journal of Botany*, *96*, 1861–1868.

Gitelson, A.A., Keydan, G.P., & Merzlyak, M.N. (2006). Three-band model for noninvasive estimation of chlorophyll, carotenoids, and anthocyanin contents in higher plant leaves. *Geophysical Research Letters*, *33*.

Guanter, L., Alonso, L., Gómez-Chova, L., Meroni, M., Preusker, R., Fischer, J., & Moreno, J. (2010). Developments for vegetation fluorescence retrieval from spaceborne high-resolution spectrometry in the O2-A and O2-B absorption bands. *Journal of Geophysical Research: Atmospheres*, *115*(19) art. no. D19303.

Green, R.O. (1998). Spectral calibration requirement for Earth-looking imaging spectrometers in the solar-reflected spectrum. *Applied Optics*, *37*, 683–690.

Green, R.O., Eastwood, M.L., Sarture, C.M., Chrien, T.G., Aronsson, M., Chippendale, B.J., et al. (1998). Imaging spectroscopy and the Airborne Visible/Infrared Imaging Spectrometer (AVIRIS). *Remote Sensing of Environment*, *65*, 227–248.

Hallik, L., Niinemets, U., & Kull, O. (2012). Photosynthetic acclimation to light in woody and herbaceous species: A comparison of leaf structure, pigment content and chlorophyll fluorescence characteristics measured in the field. *Plant Biology*, *14*, 88–99.

Homolova, L., Malenovsky, Z., Clevers, J.G.P.W., Garcia-Santos, G., & Schaepman, M.E. (2013). Review of optical-based remote sensing for plant trait mapping. *Ecological Complexity*, *15*, 1–16.

Hueni, A., Biesemans, J., Dell'Endice, F., Alberti, E., Meuleman, K., & Schaepman, M.E. (2009a). The structure of the APEX (Airborne Prism Experiment) processing and archiving facility. In J. Chanussot (Ed.), *WHISPERS — First workshop on hyperspectral image and signal processing: Evolution in remote sensing* (pp. 4). Grenoble (F): IEEE.

Hueni, A., Biesemans, J., Meuleman, K., Dell'Endice, F., Schlapfer, D., Odermatt, D., et al. (2009b). Structure, components, and interfaces of the airborne prism experiment (APEX) processing and archiving facility. *IEEE Transactions on Geoscience and Remote Sensing*, *47*, 29–43.

Hueni, A., Lenhard, K., Baumgartner, A., & Schaepman, M.E. (2013). Airborne prism experiment calibration information system. *IEEE Transactions on Geoscience and Remote Sensing*, *51*, 5169–5180.

Hueni, A., Malthus, T., Kneubuehler, M., & Schaepman, M.E. (2011). Data exchange between distributed spectral databases. *Computers & Geosciences*, *37*, 861–873.

Hueni, A., Nieke, J., Schopfer, J., Kneubühler, M., & Itten, K.I. (2009). The spectral database SPECCHIO for improved long-term usability and data sharing. *Computers and Geosciences*, *35*, 557–565.

Hueni, A., Schlaepfer, D., Jehle, M., & Schaepman, M. (2014). Impacts of dichroic prism coatings on radiometry of the airborne imaging spectrometer APEX. *Applied Optics*, *53*, 5344–5352.

Hueni, A., Sterckx, S., & Jehle, M. (2013). Operational calibration of APEX. *Geoscience and remote sensing symposium (IGARSS), 2013 IEEE International* (pp. 4423–4426).

Hueni, A., Sterckx, S., Jehle, M., D'Odorico, P., Vreys, K., Bomans, B., et al. (2012). Operational status of APEX and characteristics of the APEX open science data set. *Geoscience and remote sensing symposium (IGARSS), 2012 IEEE International* (pp. 5009–5012).

Hueni, A., Wooliams, E., & Schaepman, M.E. (2014). APEX radiometric uncertainty. *European metrology research programme/EURAMET* (pp. 48). Zurich, CH: University of Zurich.

Itten, K.I., Meyer, P., Staenz, K., Kellenberger, T., & Schaepman, M.E. (1992). Evaluation of the AVIRISwiss '91 campaign data. In R. Green (Ed.), *Summaries of the third annual JPL airborne geoscience workshop* (pp. 108–110). Pasadena, CA: NASA.

Itten, K.I., Schaepman, M.E., De Vos, L., Hermans, L., Schlaepfer, H., & Droz, F. (1997). APEX — Airborne PRISM Experiment: A new concept for an airborne imaging spectrometer. *Third international airborne remote sensing conference and exhibition* (pp. 181–188). Copenhagen: ERIM.

Jacquemoud, S., Verhoef, W., Baret, F., Bacour, C., Zarco-Tejada, P.J., Asner, G.P., et al. (2009). PROSPECT & SAIL models: A review of use for vegetation characterization. *Remote Sensing of Environment*, *113*(Suppl. 1), S56–S66.

Jehle, M., Hueni, A., Baumgartner, A., Lenhard, K., & Schaepman, M.E. (2015). Detection and correction of radiance variations during spectral calibration of APEX. *IEEE Geoscience and Remote Sensing Letters* (in press).

Jehle, M., Schaepman, M., Hueni, A., Damm, A., D'Odorico, P., Weyermann, J., et al. (2010). APEX — current status, performance and validation concept. *Sensors, 2010 IEEE* (pp. 533–537). Waikoloa, HI, USA: IEEE Sensors.

Kaiser, J.W., Schläpfer, D., Brazile, J., Strobl, P., Schaepman, M.E., & Itten, K.I. (2004). Assimilation of heterogeneous calibration measurements for the APEX spectrometer. In R. Meynart (Ed.), *Proceedings of SPIE: Sensors, systems, and next-generation satellites VII* (pp. 211–220).

Kneubühler, M., Damm, A., Schweiger, A.K., Risch, A.C., Schütz, M., & Schaepman, M.E. (2014). Continuous fields from imaging spectrometer data for ecosystem parameter mapping and their potential for animal habitat assessment in alpine regions. *IEEE Journal of Selected Topics in Applied Earth Observations and Remote Sensing*, *7*, 2600–2610.

Kneubühler, M., Schaepman, M.E., Thome, K.J., & Schläpfer, D.R. (2003). MERIS/ENVISAT vicarious calibration over land. In R. Meynart, S.P. Neeck, H. Shimoda, J.B. Lurie, & M.L. Aten (Eds.), *Sensors, systems, and next-generation satellites VII* (pp. 614–623). Barcelona: SPIE.

Kokaly, R.F., Asner, G.P., Ollinger, S.V., Martin, M.E., & Wessman, C.A. (2009). Characterizing canopy biochemistry from imaging spectroscopy and its application to ecosystem studies. *Remote Sensing of Environment*, *113*(Suppl. 1), S78–S91.

Laurent, V.C.E., Schaepman, M.E., Verhoef, W., Weyermann, J., & Chavez, R.O. (2014). Bayesian object-based estimation of LAI and chlorophyll from a simulated Sentinel-2 top-of-atmosphere radiance image. *Remote Sensing of Environment*, *140*, 318–329.

Laurent, V., Verhoef, W., Clevers, J.G.P.W., & Schaepman, M.E. (2010). Estimating forest parameters from top-of-atmosphere radiance measurements using coupled radiative transfer models. In H. Lacoste-Francis (Ed.), *Proceedings of the hyperspectral workshop 2010* (pp. 1–8). Frascati (It): ESA.

Laurent, V.C.E., Verhoef, W., Clevers, J.G.P.W., & Schaepman, M.E. (2011a). Inversion of a coupled canopy–atmosphere model using multi-angular top-of-atmosphere radiance data: A forest case study. *Remote Sensing of Environment*, *115*, 2603–2612.

Laurent, V.C.E., Verhoef, W., Clevers, J.G.P.W., & Schaepman, M.E. (2011b). Estimating forest variables from top-of-atmosphere radiance satellite measurements using coupled radiative transfer models. *Remote Sensing of Environment*, *115*, 1043–1052.

Laurent, V.C.E., Verhoef, W., Damm, A., Schaepman, M.E., & Clevers, J.G.P.W. (2013). A Bayesian object-based approach for estimating vegetation biophysical and biochemical variables from APEX at-sensor radiance data. *Remote Sensing of Environment*, *139*, 6–17.

Lenhard, K., Baumgartner, A., & Schwarzmaier, T. (2014). Independent laboratory characterization of NEO HySpex imaging spectrometers VNIR-1600 and SWIR-320M-E. *IEEE Transactions on Geoscience and Remote Sensing*, http://dx.doi.org/10.1109/TGRS.2014.2349737 (in revision).

Marion, R., Michel, R., & Faye, C. (2004). Measuring trace gases in plumes from hyperspectral remotely sensed data. *IEEE Transactions on Geoscience and Remote Sensing*, *42*, 854–864.

Menenti, M., Rast, M., Baret, F., Mauser, W., Miller, J., Schaepman, M., et al. (2002). Understanding vegetation response to climate variability from space: the scientific objectives, the approach and the concept of the SPECTRA mission. *IGARSS 2002: IEEE International geoscience and remote sensing symposium and 24th Canadian symposium on remote sensing, Vols I–VI, proceedings* (pp. 964–966).

Meroni, M., Rossini, M., Guanter, L., Alonso, L., Rascher, U., Colombo, R., & Moreno, J. (2009). Remote sensing of solar-induced chlorophyll fluorescence: Review of methods and applications. *Remote Sensing of Environment*, *113*(10), 2037–2051.

Milton, E.J., Schaepman, M.E., Anderson, K., Kneubühler, M., & Fox, N. (2009). Progress in field spectroscopy. *Remote Sensing of Environment*, *113*(Suppl. 1), S92–S109.

Mouroulis, P., Green, R.O., & Chrien, T.G. (2000). Design of pushbroom imaging spectrometers for optimum recovery of spectroscopic and spatial information. *Applied Optics*, *39*, 2210–2220.

Nieke, J., Itten, K.I., Meuleman, K., Gege, P., Dell'Endice, F., Hueni, A., et al. (2008). *Supporting facilities of the airborne imaging spectrometer APEX, V502–V505.*

Nieke, J., Kaiser, J., Schläpfer, D., Brazile, J., Itten, K., Strobl, P., et al. (2004). Calibration methodology for the airborne dispersive pushbroom imaging spectrometer (APEX). In R. Meynart, S.P. Neeck, & H. Shimoda (Eds.), *Sensors, systems, and next-generation satellites VIII* (pp. 445–452). Maspalomas: SPIE.

Nowicki-Bringuier, Y.R., & Chorier, P. (2009). Sofradir SWIR hyperspectral detectors for space applications. *Sensors, systems, and next-generation satellites XIII* (pp. 12). Berlin: SPIE.

Plascyk, James A. (1975). MK II Fraunhofer Line Discriminator (FLD-II) for Airborne and Orbital Remote Sensing of Solar-Stimulated Luminescence. *Optical Engineering*, *14*(4), 339–346.

Plaza, A., Benediktsson, J.A., Boardman, J.W., Brazile, J., Bruzzone, L., Camps-Valls, G., et al. (2009). Recent advances in techniques for hyperspectral image processing. *Remote Sensing of Environment*, *113*(Suppl. 1), S110–S122.

Plummer, S. E. (2000). Perspectives on combining ecological process models and remotely sensed data. *Ecological Modelling*, *129*(2–3), 169–186.

Poulter, B., Frank, D. C., Hodson, E. L., & Zimmermann, N. E. (2011). Impacts of land cover and climate data selection on understanding terrestrial carbon dynamics and the CO 2 airborne fraction. *Biogeosciences*, *8*(8), 2027–2036.

Popp, C., Brunner, D., Damm, A., Van Roozendael, M., Fayt, C., & Buchmann, B. (2012). High-resolution NO_2 remote sensing from the Airborne Prism EXperiment (APEX) imaging spectrometer. *Atmospheric Measurement Techniques*, *5*, 2211–2225.

Richter, R., & Schläpfer, D. (2002). Geo-atmospheric processing of airborne imaging spectrometry data. Part 2: Atmospheric/topographic correction. *International Journal of Remote Sensing*, *23*, 2631–2649.

Richter, R., Schlapfer, D., & Muller, A. (2011). Operational atmospheric correction for imaging spectrometers accounting for the smile effect. *IEEE Transactions on Geoscience and Remote Sensing*, *49*, 1772–1780.

Schaepman, M.E. (2009). Imaging spectrometers. In T.A. Warner, M. Duane Nellis, & G. Foody (Eds.), *The SAGE handbook of remote sensing* (pp. 166–178). London (UK): SAGE.

Schaepman, M.E., & Dangel, S. (2000). Solid laboratory calibration of a nonimaging spectroradiometer. *Applied Optics*, *39*, 3754–3764.

Schaepman, M.E., De Vos, L., & Itten, K.I. (1998). APEX — Airborne PRISM Experiment: Hyperspectral radiometric performance analysis for the simulation of the future ESA land surface processes earth explorer mission. In M.R. Descour, & S.S. Shen (Eds.), *Imaging spectrometry IV* (pp. 253–262). San Diego: SPIE.

Schaepman, M.E., Itten, K.I., Schläpfer, D., Kaiser, J.W., Brazile, J., Debruyn, W., et al. (2003). Status of the airborne dispersive pushbroom imaging spectrometer APEX (Airborne Prism Experiment). *International geoscience and remote sensing symposium (IGARSS)* (pp. 4304–4306). Toulouse: IEEE.

Schaepman, M.E., Schläpfer, D., Brazile, J., & Bojinski, S. (2002). Processing of large-volume airborne imaging spectrometer data: The APEX approach. In S.S. Shen (Ed.), *Imaging spectrometry VIII* (pp. 72–79). Seattle: SPIE.

Schaepman, M.E., Schläpfer, D., & Itten, K.I. (2000). APEX — A new pushbroom imaging spectrometer for imaging spectroscopy applications: Current design and status. *International geoscience and remote sensing symposium (IGARSS)* (pp. 828–830). Hawaii: IEEE.

Schaepman, M.E., Schläpfer, D., & Müller, A. (2002). Performance requirements for airborne imaging spectrometers. In M.R. Descour, & S.S. Shen (Eds.), *Imaging spectrometry VII* (pp. 23–31). San Diego: SPIE.

Schaepman, M.E., Ustin, S.L., Plaza, A.J., Painter, T.H., Verrelst, J., & Liang, S. (2009a). Earth system science related imaging spectroscopy—An assessment. *Remote Sensing of Environment*, *113*, S123–S137.

Schaepman, M.E., Ustin, S.L., Plaza, A.J., Painter, T.H., Verrelst, J., & Liang, S. (2009b). Earth system science related imaging spectroscopy—An assessment. *Remote Sensing of Environment*, *113*(Suppl. 1), S123–S137.

Schaepman-Strub, G., Schaepman, M.E., Painter, T.H., Dangel, S., & Martonchik, J.V. (2006). Reflectance quantities in optical remote sensing — Definitions and case studies. *Remote Sensing of Environment*, *103*, 27–42.

Schepers, L., Haest, B., Veraverbeke, S., Spanhove, T., Vanden Borre, J., & Goossens, R. (2014). Burned area detection and burn severity assessment of a heathland fire in Belgium using Airborne Imaging Spectroscopy (APEX). *Remote Sensing*, *6*, 1803–1826.

Schläpfer, D., & Richter, R. (2002). Geo-atmospheric processing of airborne imaging spectrometry data. Part 1: Parametric orthorectification. *International Journal of Remote Sensing*, *23*, 2609–2630.

Schläpfer, D., & Schaepman, M.E. (2002). Modeling the noise equivalent radiance requirements of imaging spectrometers based on scientific applications. *Applied Optics*, *41*, 5691–5701.

Schläpfer, D., Schaepman, M.E., Bojinski, S., & Börner, A. (2000). Calibration and validation concept for the airborne PRISM experiment (APEX). *Canadian Journal of Remote Sensing*, *26*, 455–465.

Schneider, F.D., Leiterer, R., Morsdorf, F., Gastellu-Etchegorry, J. -P., Lauret, N., Pfeifer, N., et al. (2014). Simulating imaging spectrometer data: 3D forest modeling based on LiDAR and in situ data. *Remote Sensing of Environment*, *152*, 235–250.

Scholes, R. J., Monteiro, P. M. S., Sabine, C. L., & Canadell, J. G. (2009). Systematic long-term observations of the global carbon cycle. *Trends in Ecology and Evolution*, *24*(8), 427–430.

Schweiger, A.K., Risch, A.C., Damm, A., Kneubühler, M., Haller, R., Schaepman, M.E., et al. (2014). Using imaging spectroscopy to predict above-ground plant biomass in alpine grasslands grazed by large ungulates. *Journal of Vegetation Science* (n/a-n/a) http://onlinelibrary.wiley.com/doi/10.1111/jvs.12214/abstract.

Seidel, F.C., Kokhanovsky, A.A., & Schaepman, M.E. (2010). Fast and simple model for atmospheric radiative transfer. *Atmospheric Measurement Techniques*, *3*, 1129–1141.

Seidel, F.C., Kokhanovsky, A.A., & Schaepman, M.E. (2012). Fast retrieval of aerosol optical depth and its sensitivity to surface albedo using remote sensing data. *Atmospheric Research*, *116*, 22–32.

Seidel, F.C., & Popp, C. (2012). Critical surface albedo and its implications to aerosol remote sensing. *Atmospheric Measurement Techniques*, *5*, 1653–1665.

Seidel, F., Schläpfer, D., Nieke, J., & Itten, K.I. (2008). Sensor performance requirements for the retrieval of atmospheric aerosols by airborne optical remote sensing. *Sensors*, *8*, 1901–1914.

Steven, M. D., Malthus, T. J., Baret, F., Xu, H., & Chopping, M. J. (2003). Intercalibration of vegetation indices from different sensor systems. *Remote Sensing of Environment*, *88*(4), 412–422.

Smith, B., Prentice, I. C., & Sykes, M. T. (2001). Representation of vegetation dynamics in the modelling of terrestrial ecosystems: Comparing two contrasting approaches within European climate space. *Global Ecology and Biogeography*, *10*(6), 621–637.

Tarantola, A. (2005). *Inverse problem theory and methods for model parameter estimation.* SIAM.

Taubert, D.R., Hollandt, J., Sperfeld, P., Pape, S., Höpe, A., Hauer, K.O., et al. (2013). Providing radiometric traceability for the calibration home base of DLR by PTB. *AIP Conference Proceedings* (pp. 376–379).

Teillet, P. M., Horler, D. N. H., & O'Neill, N. T. (1997). Calibration, validation, and quality assurance in remote sensing: A new paradigm. *Canadian Journal of Remote Sensing*, *23*(4), 401–414.

Thorpe, A.K., Frankenberg, C., & Roberts, D.A. (2014). Retrieval techniques for airborne imaging of methane concentrations using high spatial and moderate spectral resolution: Application to AVIRIS. *Atmospheric Measurement Techniques*, *7*, 491–506.

Townsend, P.A., Serbin, S.P., Kruger, E.L., & Gamon, J.A. (2013). Disentangling the contribution of biological and physical properties of leaves and canopies in imaging spectroscopy data. *Proceedings of the National Academy of Sciences of the United States of America*, *110*.

Ulbrich, G.J., Meynart, R., Nieke, J., Itten, K.I., Kaiser, J.W., Schläpfer, D., et al. (2004). APEX — Airborne Prism Experiment: The realization phase of an airborne imaging spectrometer. *Proc. SPIE Vol. 5570, sensors, systems, and next-generation satellites VIII* (pp. 453–459).

USGS (1998). *General cartographic transformation package (GCTP).* (p. ftp://edcftp.cr.usgs.gov/software/gctpc/).

Ustin, S.L., Gitelson, A.A., Jacquemoud, S., Schaepman, M., Asner, G.P., Gamon, J.A., et al. (2009). Retrieval of foliar information about plant pigment systems from high resolution spectroscopy. *Remote Sensing of Environment*, *113*(Suppl. 1), S67–S77.

Verhoef, W., & Bach, H. (2007). Coupled soil–leaf–canopy and atmosphere radiative transfer modeling to simulate hyperspectral multi-angular surface reflectance and TOA radiance data. *Remote Sensing of Environment*, *109*, 166–182.

Verrelst, J., Schaepman, M.E., Kötz, B., & Kneubühler, M. (2008). Angular sensitivity of vegetation indices derived from CHRIS/PROBA data. *Remote Sensing of Environment*, *112*, 2341–2353.

Versluys, J., Van Vooren, N., & De Vos, L. (2008). APEX optical test report. *APEX acceptance reporting* (pp. 39). Oudenaarde, BE: OIP Sensor Systems.

Weyermann, J., Damm, A., Kneubuhler, M., & Schaepman, M.E. (2014). Correction of reflectance anisotropy effects of vegetation on airborne spectroscopy data and derived products. *IEEE Transactions on Geoscience and Remote Sensing*, *52*, 616–627.

Zhao, H.J., Jia, G.R., & Li, N. (2010). Transformation from hyperspectral radiance data to data of other sensors based on spectral superresolution. *IEEE Transactions on Geoscience and Remote Sensing*, *48*, 3903–3912.

2.6 Close-range laser scanning in forests - towards physically-based semantics across scales

Morsdorf, F., Kükenbrink, D., **Schneider, F.D.**, Abegg, M., Schaepman, M.E.

This section is based on the peer-reviewed article:
Royal Society Open Science,
in press

All authors designed research, performed research and wrote the paper, with main contributions of F.M.

ROYAL SOCIETY OPEN SCIENCE

rsos.royalsocietypublishing.org

Research

Article submitted to journal

Subject Areas:
biogeography, computer vision, ecology, environmental science, plant science

Keywords:
laser scanning, UAV, forests, light regime, radiative transfer modelling, ray-tracing, LAI, canopy cover, laser intensity

Author for correspondence:
Felix Morsdorf
e-mail: felix.morsdorf@geo.uzh.ch

Close-range laser scanning in forests - towards physically-based semantics across scales

F. Morsdorf[1,3], D. Kükenbrink[1], F.D. Schneider[1,3], M. Abegg[1,2] and M.E. Schaepman[1,3]

[1]Remote Sensing Laboratories, Department of Geography, University of Zürich, Winterthurerstr. 190, 8057 Zürich, Switzerland, [2]Forest Resources and Management, WSL Swiss Federal Institute for Forest, Snow and Landscape Research WSL, Zürcherstrasse 111, 8903 Birmensdorf, Switzerland, [3]URPP Global Change and Biodiversity, University of Zürich, Winterthurerstrasse 190, 8057 Zürich, Switzerland

Laser scanning with its unique measurement concept holds the potential to revolutionize the way we assess and quantify 3d vegetation structure. Modern laser systems used at close-range, be it on terrestrial, mobile or unmanned aerial platforms, provide dense and accurate 3D data whose information *just* waits to be harvested. However, the transformation of such data to information is not as straightforward as for airborne and space-borne approaches, where typically empirical models are built using ground-truth of target variables. Simpler variables, such as diameter at breast height, can be readily derived and validated. More complex variables, e.g. leaf area index (LAI), need a thorough understanding and consideration of the physical particularities of the measurement process and semantic labeling of the point cloud. Quantified structural models provide a framework for such labelling by deriving stem and branch architecture, a basis for many of the more complex structural variables. The physical information of the laser scanning process is still under-used and we show how it could play a vital role in conjunction with 3D radiative transfer models to shape the information retrieval methods of the future. Using such a combined forward and physically-based approach will make methods robust and transferable. In addition, it avoids replacing observer bias from field inventories with instrument bias from different laser instruments. Still, an intensive dialogue with the users of the derived information is mandatory to potentially re-design structural concepts and variables so that they profit most of the rich data that close-range laser scanning provides.

THE ROYAL SOCIETY PUBLISHING

1. Introduction

Within forests, the horizontal and vertical arrangement of plants has a large impact on ecological processes, such as competition, carbon balance and nutrient and water cycling. This large role of forest structure for ecosystem functioning establishes a link between structure and diversity [MacArthur and Horn, 1969; McElhinny et al., 2005], making forests of special relevance for biodiversity [Barlow et al., 2007]. For instance, light scattering within the forest is strongly influenced by vegetation structure and can itself feedback to structure, as light availability is an important aspect of plant establishment and survival. Thus, forest ecologists have long sought to describe the structure of forests, e.g. by measuring foliage profiles [MacArthur and Horn, 1969] or by establishing semantics and topology of tree architecture, such as Halle [1986]. Looking back, the used tools may appear to be simple, MacArthur and Horn [1969] used adapted photographic cameras to estimate height and abundance of leaves in the canopy, while Halle [1986] used observations and drawings to derive modular structural concepts of tropical trees.

However, the variables of interest are still very relevant today. MacArthur and Horn [1969] provided a method to derive a biophysical parameter (the foliage profile) devoid of architectural semantics or topology. Halle [1986]'s aim was to represent the complex tree architecture in forms of smaller, repeating patterns, effectively capturing the tree structure *and* semantically labeling the constituent objects (e.g. shoots, leaves and branches).

Nowadays, laser scanning is a unique and established technology, offering a convenient way to assess 3d vegetation structure. Laser scanning can be applied on different scales, from airborne systems to very high resolution ground based sensors. Such systems provide extremely dense and illustrative data sets, named "point-clouds". Opposed to traditional airborne laser scanners, close-range laser systems provide point clouds where stem, branches and even single leaves are resolved and easily identified by the human observer (see Figure 1). The point-cloud itself is, however, devoid of any semantic information or topology. As the datasets are typically very large and unorganized, the meaningful derivation of information is a major challenge and remains an obstacle in the way of widespread application of this technology in ecology.

Traditionally (i.e. for airborne laser scanning, ALS), many forest variables were derived in an empirical fashion by correlating field inventoried parameters (biomass, stem volume, basal area) with a set of ALS derived predictor variables [Næsset, 1997, 2002]. Such approaches are infeasible with close-range laser scanning, as it is very time consuming and in most cases impossible to provide ground truth at the relevant scales (branches, leaves). Hence, for close-range laser scanning, a different, forward approach is needed to convert data to information, without the need for prior information. This manifests the particular relevance of semantic labeling and physically-based approaches for close-range laser scanning.

In this paper, we will highlight the physical basics of laser scanning, provide some relevant technical information on current implementations in instruments (Section 2) and introduce a selection of methods that convert data to information (Section 3), devided into physical approaches and semantic labeling. In addition, we will discuss and illustrate the problematic validation of close-range laserscanning derived variables and a possible solution by radiative transfer modeling of the measurement process (Section 4). Furthermore, we will show that different types of instruments provide valuable information across scales (Section 5). Concluding, we discuss what will be needed to make the most of this recent technology for forest structure assessments.

2. Laser scanning - principles and implementations

Although the terms LiDAR and laser scanning are often used synonymously, strictly speaking, a LiDAR (Light Detection and Ranging) is only one part of an laser scanning system. With LiDARs, a laser pulse is used to measure distances between the instrument and reflecting objects (e.g. leaves, branches or stems). The distance can either be computed using the time-of-flight of a

Figure 1. Laser scanning point cloud as obtained by multi-view terrestrial laser scanning in a mature temperate beech forest in leaf-off conditions. Each dot has an exact 3d coordinate and the brightness of the points is depicting the strength of the backscattered signal.

laser pulse or the phase difference of an amplitude-modulated signal. Using the instrument's location and orientation, this distance measurement can then be converted to a 3d coordinate. In terrestrial laser scanning systems, high precision measurements of the instruments rotational angles (azimuth and elevation) provide data in a local, polar coordinate system, i.e. the scanning is performed by rotating the instrument in two dimensions, while the instrument itself is stationary.

On the other hand, differential GPS and inertial navigation systems are used along side a physical scanning mechanism to transform a LiDAR into a laser scanner in airborne systems. In these systems, only one dimension is covered by the scanner, generally with a narrow field of view, while the second dimension to get 2d coverage is covered by the platform movement itself. These distinct scanning approaches lead to large within point-cloud differences in point spacing, footprint size and occlusion, which need to be considered when deriving physically-based information such as plant area index (PAI).

Since the scanning frequencies of modern systems have moved beyond the mega-Hertz mark (i.e. more than 100.000 distance measurements per second), very dense point clouds of the 3d coordinate triplets can be obtained. Most modern laser scanning systems are inherently full-waveform (FW), recording the backscattered energy over time (and range) and using processing such a Gaussian decomposition to detect the range distances of reflecting objects. FW systems provide as well the backscattered energy (opposed to just amplitude) [Wagner, 2010] and allow for the derivation of higher order moments potentially useful for discrimination of vegetation traits [Bruggisser et al., 2017]. Using the intensity as an additional source of information, detailed and to the human eye informative visualizations of the point clouds can be made. These have ever since led to high expectations as to what information could be derived from such datasets (Figure 1).

Opposed to passive optical imaging, laser intensity is not ridden by the problem of shadows, since the mono-static LiDAR setup always measures in the "hot-spot", i.e. the angle of maximum reflectance [Maignan et al., 2004]. Thus, LiDAR intensity should be very well suited to capture the reflectance of objects at the particular laser wavelength and with a properly chosen wavelength, e.g. 1064 nm, it should be possible to differ between "green" and "brown" biomass. However, one problem of laser intensity in forests (which is valid for all scales, from space-borne to ground-based) are effects of partially hit leaves leading to mixed pixels. As the laser footprint, i.e. the area that is illuminated by the laser, has a certain extent, some laser shots may only partially hit

leaves or branches. Consequently, the measured intensity is not only a function of leaf reflectance at the laser wavelength (and leaf inclination angle in case of non-Lambertian behaving leaves), but as well of the illuminated area, which can be more or less randomly distributed. For time-of-flight systems, only the intensity is affected by this, but for phase measurements even the range measurement is impaired, leading to ghost points in-between two partially illuminated reflecting objects, often termed mixed-pixels in literature. If it was not for this setback, phase-based terrestrial laser scanners (TLS) were actually better suited for forest applications, since they are scanning much faster than time-of-flight system and are often implemented as panorama scanners, being able to cover the whole hemisphere with one scan.

Time-of-flight systems are often camera or hybrid scanners, where a second scan using a tilt mount is needed to capture the canopy directly above the scanner. Typical examples for hybrid, time-of-flight scanners is the Riegl VZ-XXXX range, while FARO and Zoller and Fröhlich a mostly using the phase measurement concept and a full-hemispherical design. A blend of airborne laser scanning and TLS are mobile laser scanning (MLS) systems and laser scanners mounted on ultra-light aerial vehicles (UAVs or drones). MLS systems are typically using cars as the measurement platform, which limits the application in forests somewhat. These systems generally have as well a close-range to the objects of interest, so that branches and potentially leaves can be resolved, but use the advantage of the moving platform to cover more area. Depending on the choice of platform, the distribution of echoes and the perspective of the point cloud can be very different, making cross-comparisons between MLS, TLS and UAVLS difficult (Section (b)). For a technical reference, please see Vosselman and Maas [2010] and for an overview of forest applications see Maltamo et al. [2014]. The latter provides as well very relevant theoretical considerations for LiDAR systems in forested environments (Chapters 2 and 3).

3. The point cloud - from data to information

As discussed above, modern laser scanning systems can produce a wealth of data, quickly reaching several gigabytes of points per plot unit or even within a single scan. In contrast to image data, where pixels in a grid establish spatial reference and neighborhoods and enable efficient compression, this data is unorganized and much more difficult to store, access and process. Thankfully, with the advance of the LAS format[1] and the open-source compressor LASZip[2], the former two are less of problem nowadays; the times where point-clouds would mostly come in the flavor of ill-suited ASCII files are thankfully over. However, information derivation from the point-cloud is still a challenge and we will provide some more details on typical variables and approaches, split into two parts along the lines of the works of MacArthur and Horn [1969] (physical parameters, Section (a)) and Halle [1986] (semantic labeling, Section (b)).

(a) Physical parameters and approaches

Ever since the ground-breaking work of MacArthur and Horn [1969], ecologists have used sunlight and its interception to derive quantitative biophysical parameters such as LAI or canopy cover.

The current state of the art in that respect is digital hemispherical photography (DHP), where below canopy photographs are brightness thresholded and the number of vegetation and sky pixel are computed for a range of azimuth and elevation angles. [Jonckheere et al., 2004; Weiss et al., 2004]. When the ground-based laser systems became available, first studies showed that the gap fraction information derived by TLS and DHP are very comparable [Danson et al., 2007]. However, only with TLS it is possible to measure gap sizes, as in DHPs large distant gaps and close small gaps may have the same gap fraction value. TLS produced hemispherical images add a range distance to each pixel, which helps to discern gaps of different sizes at different distances

[1]www.lasformat.org
[2]www.laszip.org

from the instrument. It has been shown that this additional information is very helpful for LAI computation [Woodgate et al., 2015] and snow interception modeling [Moeser et al., 2015, 2014].

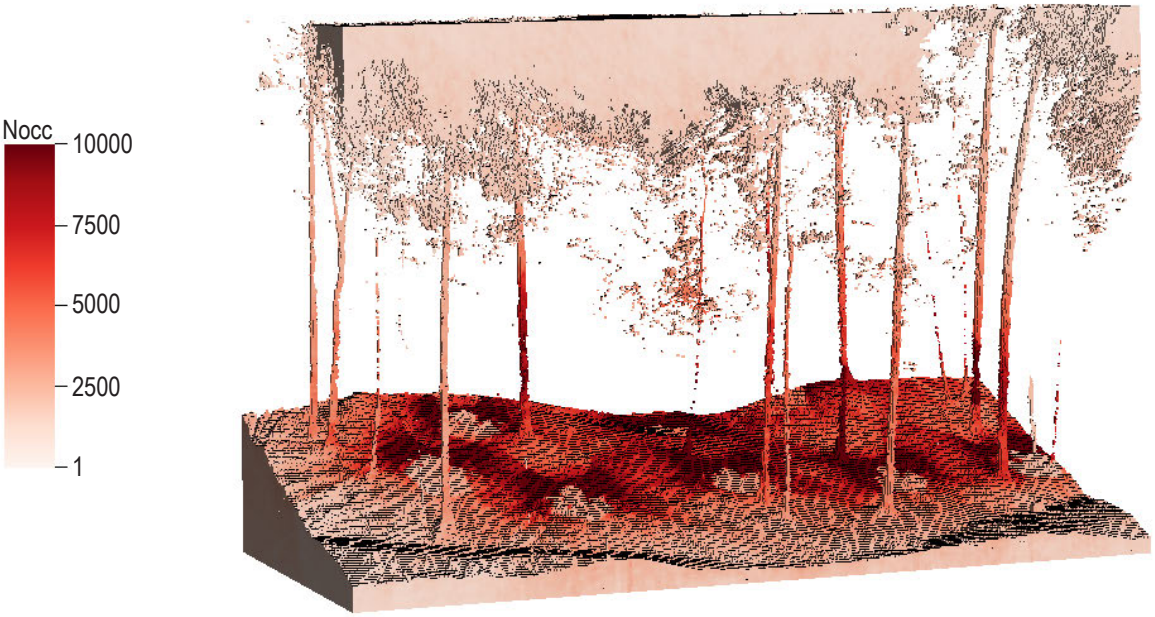

Figure 2. Number of occluded laser shots per voxel as derived by ray-tracing each laser shot. Voxel size is 10 cm. Tree trunks occlude a high number (all) of the incoming shots. This physically derived information could be used to aid semantic labeling of the point cloud. For details of the methodology, see Kükenbrink et al. [2017].

One problem with estimating gap-fraction or LAI from laser scanning systems is that many approaches are very sensitive to changes in sensor and survey configuration. For instance, the echo ratios used a predictor variable can depend on laser wavelength and echo detection method implemented in a particular system. Although developed for ALS, approaches such as the one of Armston et al. [2013] could as well contribute to making close-range laser scanning based biophysical parameters transferable across sites and sensors. Armston et al. [2013] basically established a vicarious (i.e. in-situ) calibration of their laser-based gap fraction estimate under the assumption of a constant reflectance ratio between canopy and ground. This worked well in the Savannah-type ecosystem used in their study, but its performance in more complex forests and with the different constraints of close-range laser scanning still needs to be tested.

TLS focused studies have exploited laser intensity as well, for instance to derive leaf chlorophyll content [Eitel et al., 2010] or wheat nitrogen content [Eitel et al., 2011]. However, as laser intensity can suffer from edge effects making the retrieval of leaf reflectance ill-posed (Section 2), such approaches are better suited in canopies with large leaves (such as in Eitel et al. [2010]) or extensive filtering of the point cloud is needed to retain only returns from extended targets, where the laser footprint is fully contained within the reflecting object [Eitel et al., 2011].

While the information content of the point-cloud depicted in Figure 1 may already seem overwhelming, the measurement process of laser scanning actually provides much more data. For instance, for each laser shot, we know the origin and the pointing direction, together with detected returns along the one-dimensional range spanned by the LiDAR distance measurement. Thus, we can setup a voxel grid, and trace each shot and populate the voxel with information on how many shots went through, were intersected (i.e. produced returns) or were occluded from a particular voxel. The power of this approach has been introduced to TLS by Bienert et al. [2010] and applied and extended to ALS by Kükenbrink et al. [2017] and a similar approach is used in Grau et al. [2017]. These approaches provide additional information useful for a better derivation of PAI and help to reduce the data to facilitate segmentation of single trees [Bienert et al., 2010].

Using the approach from Kükenbrink et al. [2017], Figure 2 shows the occluded voxel in multi-station TLS dataset from a winterly (leaf-off) beech forest (Lägeren, Switzerland). Interestingly, besides below ground and upper canopy (or above the canopy) showing up as occluded, the inside of the stems are occluded as well. Thus, the quite simple physics of wood (i.e. that it is not transparent) in conjunction with a ray-tracing approach help us to bring some semantics into the data, in the form of stem candidate voxel.

An additional feature, that can be derived from full-waveform laser scanning, is the skewness of the echo. It was shown that multiple scattering could lead to asymmetrical return waveforms for large footprint airborne laser scanners [Hancock et al., 2011, 2012] and such effects might be visible in smaller footprint laser scanning data as well. For instance, Bruggisser et al. [2017] were able to show that the skewness of the echo had some explanatory power in discriminating tree species.

Most laser scanning based derivations of leaf area index have effectively computed plant area index, since it was not possible to differentiate echoes from leafy and woody canopy components. Hence, the problem of computing true LAI based on laser scanning returns is one of semantic labeling of the point cloud into leaf and wood returns. Here several approaches seem feasible, e.g. by using a genuine multi-spectral LiDAR [Woodhouse et al., 2011] or by applying approaches such as the one presented in Section (b) to label stems and branches and then remove those points from the subsequent LAI computation.

(b) Geometric reconstruction and semantic labeling

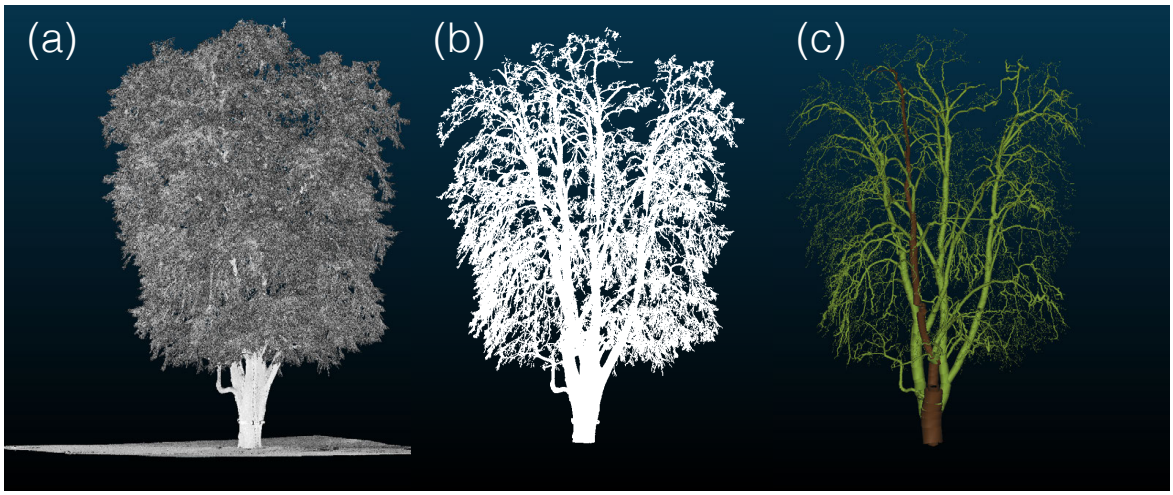

Figure 3. QSM processing of an urban tree in the context of deriving better biomass allometries for carbon accounting. The original point cloud [a], the segmented and filtered point cloud [b] and the resulting cylindrical model [c] are shown.

For trees growing in forests, extensive biomass reference data including allometries is already available [Chave et al., 2014]. For urban trees however, such reference data is currently mostly unavailable and this research gap recently received some attention [McPherson et al., 2016]. The Swiss research project REFETREE appointed by the Swiss Federal Office for the Environment (FOEN) seeks to build a reference database of 52 trees distributed over five major cities and 29 species naturally found in the Swiss mid-lands. The trees were measured with conventional field measurement protocols according to the national forest inventory (NFI) and the following variables were derived: tree height, diameter at breast height (DBH), crown diameter and crown base height. Later, the trees were cut down and weighted using a lorry scale. Additionally, multi-station TLS acquisitions of the trees were performed using a Riegl VZ-1000 at a resolution of 0.02°. For each tree, 3-4 scan locations have been used, each resulting in a point cloud of up to 45

million points. From the co-registered point cloud a 3D cylindrical representation of the tree was extracted by using a quantitative structural model (QSM) [Raumonen et al., 2013] implemented in the SimpleTree plug-in for the CompuTree toolbox [Hackenberg et al., 2015].

The QSM fits cylindrical elements into the point cloud from which essential tree parameters such as the wood volume can be extracted. However, for the QSM to work properly, heavy filtering of the original point cloud is required to exclude noise from foliar material, moving branches due to wind or scanning artifacts (Figure 3). With the extensive reference values acquired, these tree parameters extracted from TLS measurements can now be validated and biomass allometries can be established for urban trees. One of the aims of the project was to derive coarse wood volume, i.e. the volume of all stem and branch parts being larger than 7 cm in diameter. Given the urban multi-station scan setting, occlusion was minimized and it was possible to estimate coarse wood volume. From the reconstructed cylinders and their topology (connections), further information can be derived, for instance branching structures and angles and the tapering of branch diameter and branch lengths. Such variables form a valuable set of morphological traits, which can be used in species classification [Åkerblom et al., 2017].

4. Abstracting reality - sensors in the virtual domain

Ever since the early days, forestry applications of TLS faced a validation problem. DBH is quickly validated in the field using a tape measure, but it is a less sophisticated variable in respect to the general ability of TLS and the associated surveying and processing costs. When it comes to more complex variables, such as canopy cover and LAI for instance, validation is either very complex, costly, time consuming or all of those. For LAI, the most accurate approach would be destructive sampling and leaf counting and sizing, but this is impractical for larger areas or impossible for natural conservation sites. Consequently, indirect methods [Weiss et al., 2004] are most often used for validation, but such attempts are merely a cross-validation. In Danson et al. [2007], the TLS obtained angular gap fraction was compared to DHP based estimates, and while showing high correlation, the experimental design was not suited to prove the hypothesis of a better performance of the TLS, especially so considering effects such as sun flare and bright spots negatively affecting DHPs.

Hence, taking the TLS and the forest stand into the virtual domain using radiative transfer models and a detailed 3d representation of the vegetation canopy (e.g. as in Widlowski et al. [2015] or Schneider et al. [2014]) is a possible solution. Almost everything (e.g. LAI, biomass, wood volume) can be measured for 3d models of trees and their assemblages into virtual forest stands as in Figure 4. The modeling of TLS systems and their use in different stands and survey configurations enables the testing of various environmental constraints on the measurement and to test the accuracy of different retrieval methods for a set of target variables (e.g. coarse wood volume).

The Swiss NFI is currently considering to use TLS to provide additional information for their several thousand sampling plots all over Switzerland. To apply TLS at such a large scale, the cost-benefit ratio of the technology needs to be positively evaluated. Using a too high scan resolution or inappropriate scanner locations can result in tremendous costs. Consequently, Abegg et al. [2017] used a virtual modeling setup within the *Blender* software to test different scanner location patterns and scanning resolution settings in more than 2000 simulated stands. They were able to show that the scanner locations in a multi-scan design need to be evenly distributed within a plot, and not placed at the plot edges. Such simulations complement real-world experiments like the one from Wilkes et al. [2017].

On the other hand, TLS derived information like tree models [Eysn et al., 2013] and PAI can be used to parameterize 3d radiative transfer models to facilitate simulation of other earth observation data. Schneider et al. [2014] used ALS and TLS derived voxel grids of PAI to simulate spectra of the airborne imaging spectrometer APEX [Schaepman et al., 2015] and were able to show good agreement between real-world measured spectra and simulated ones. Such approaches can be further extended to provide detailed simulations of the light regime within

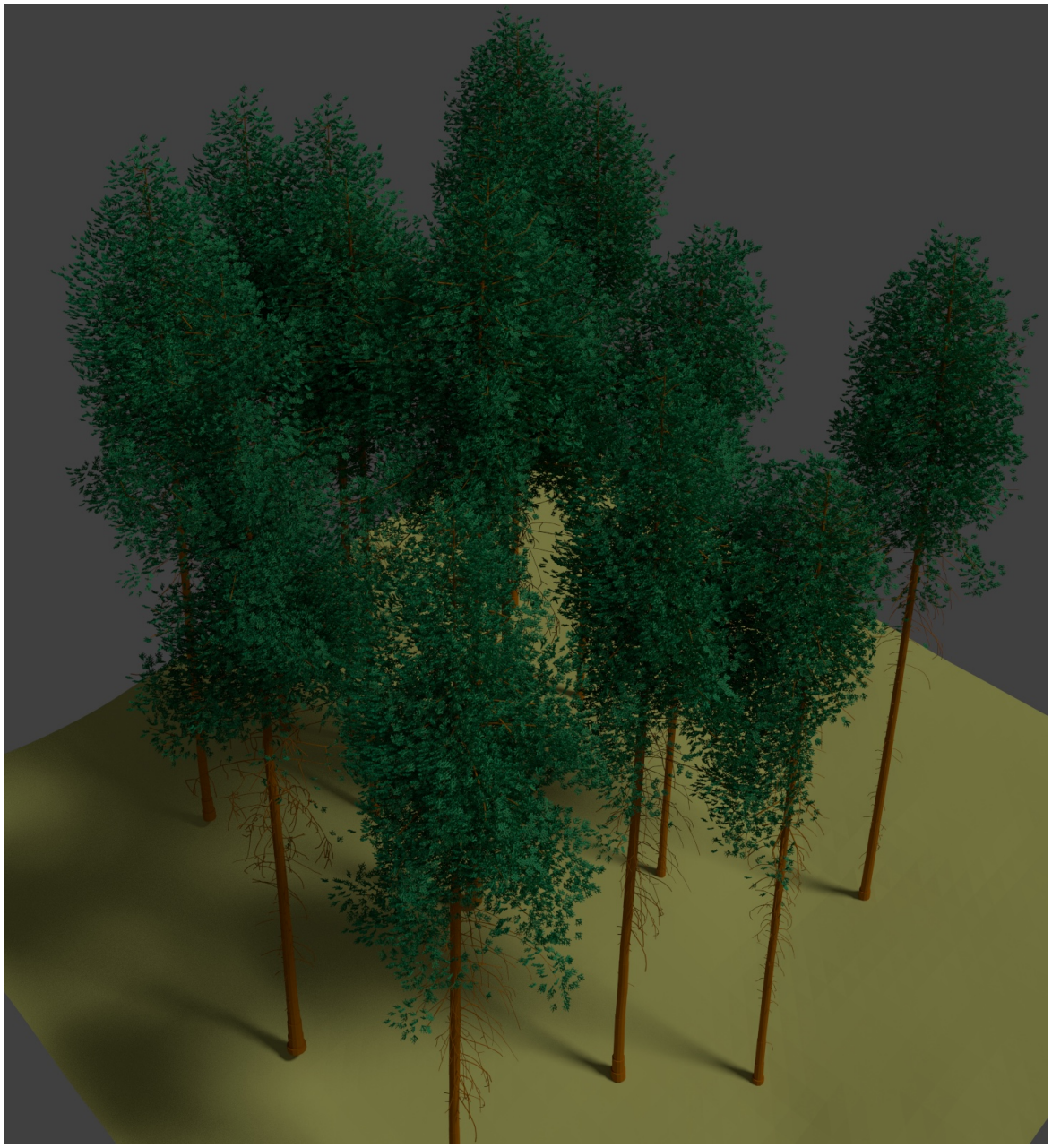

Figure 4. Virtual pine tree stand as established in the European Space Agency "3D Vegetation Laboratory" project. Stems and branches were geometrically reconstructed using the approach of Eysn et al. [2013] and a lab-derived shoot model was cloned into the tree models to match the distribution of canopy material derived by TLS and ALS point clouds. The ALS point clouds were needed to mitigate the occlusion-caused lack of TLS points towards the crown tops.

a canopy, which is highly relevant for a number of ecological processes and will increase our understanding of such.

5. Scales and perspectives

(a) A change of perspective - TLS from a crane

When measuring a forest plot with TLS, the quality and completeness of the data is mainly determined by the applied measurement scheme. The main goal is to reduce occlusion and reach a complete coverage among all vertical layers of the canopy. Occlusion has been identified as a major source of uncertainty in forest reconstruction [Béland et al., 2014], but very few studies have

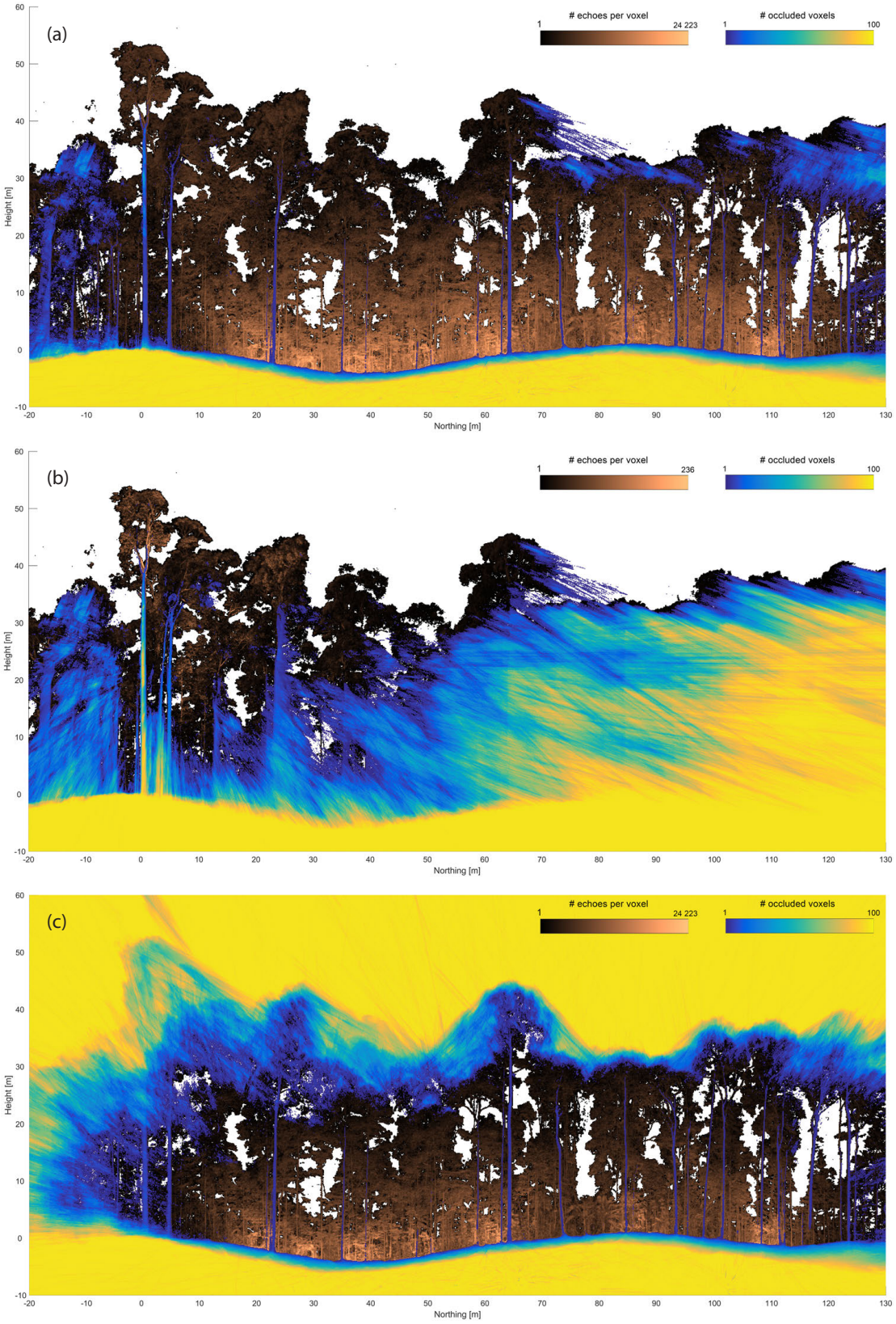

Figure 5. Occlusion mapping in a 10 x 150 m transect of tropical rain-forest based on (a) TLS scans from the canopy crane and the ground, (b) scans from the crane only, and (c) scans from the ground only. Black to orange colors indicate the number of echoes per voxel with a side length of 10 cm. Blue to yellow colors show the number of occluded voxel across the 10 m depth of the transect, whereas 100% occlusion corresponds to 100 occluded voxel.

specifically investigated occlusion in TLS data, likely since occlusion is hard to map in real-world data.

In this experiment, we applied a ray tracing based algorithm developed by Kükenbrink et al. [2017] to map occlusion in a 1 ha forest plot. We scanned 1 ha of tropical rain-forest in the Lambir Hills National Park (Sarawak, Malaysia) from 93 positions on the ground. Additionally, we performed 32 TLS scans from four platforms of a canopy crane at 24, 39, 59 and 76 m above ground. The profile in Figure 5 shows parts of the canopy close to the crane (crane is at 0 m in distance, but outside image plane) with a 10 m deep transect through the surrounding trees.

Our results show that it is crucial to have many different scan positions to maximize tree coverage in a tropical forest. Furthermore, Figure 5 (c) shows that parts of the upper canopy are occluded when scanning from the ground only. This suggests that the scans from the canopy crane mainly contribute to the coverage and quality of the data in the uppermost canopy layers. The occlusion in the top-most layers may not be too large of a problem for biomass estimation, as stems generally taper off towards the top.

However, if the data is planned to be used to derive general 3d structure information, e.g. to be used in radiative-transfer modeling approaches Schneider et al. [2014]; Widlowski et al. [2015], missing top-of-canopy information will severely impact the comparability with other remote sensing data acquired from above the canopy. Missing out on the top-of-canopy information in ground-based laser scanning is not only a function of occlusion by canopy material within the canopy, but as well a function of distance from the scanner.

As Abegg et al. [2017] showed in their simulation study, the point density above TLS scanners is the lowest when compared with all considered elevation angles and decreases with distance from the scanner. Thus, this under-sampling of the upper canopy is partly system imminent and can only be mitigated by very dense placement of scanner locations, i.e. as if the TLS was used as a vertical profiler.

(b) UAVs to bridge the scale gap between ground-based and airborne laser scanning

A recent development in laser scanning is the deployment of lightweight laser scanners such as the Riegl VUX-1 on unmanned aerial vehicles (UAV) platforms [Lin et al., 2011; Mandlburger et al., 2015; Wallace et al., 2012]. These systems fall in-between TLS and ALS, being close to TLS in terms of resolution (i.e. point density), but closer to ALS in terms of perspective (top-down) and sampling distribution. Using Aeroscout's gas powered helicopter as UAV platform, 12 ha of the Laegeren forest research site were surveyed on a wind-still day in March 2017, with the trees still in leaf-off condition. During the same day of the UAV laser acquisition, a ground-based TLS survey was carried out, using a Riegl VZ1000 instrument. A total of 40 scans on 20 scan locations in a area of roughly 60 m by 60 m in size were taken. About 50 reflective targets were placed within the scene, to be later used for co-registration of the scans. The single-scans were co-registered using RiScan Pro and the UAV data was subsequently globally adjusted to the unified TLS point cloud. The absolute lack of wind on that day greatly facilitated matching of finer features, such as small branches.

Table 1 presents the most relevant survey settings; for more details on the UAV acquisition and processing see Morsdorf et al. [2017]. Figure 6 illustrates the complementarity of TLS and UAV laser scanning, with UAV not providing as many stem returns, and TLS providing less information on the upper parts of the canopy.

Flying an UAV with a large field of view low above the canopy should yield minimal occlusion, as many different viewing angles into the canopy are sampled. As Figure 7 shows, this is the case. Compared to TLS, which suffers again from some occlusion towards the top of the canopy, UAV laser scanning is able to penetrate the canopy in leaf-off conditions fully, with only very little occlusion. The leaf-on data shows some more occlusion of lower canopy layers (Figure 7c), but the flying altitude was higher and the flight line spacing was lower for the summer UAV data. The

Nominal flying height above ground	80 m
Nominal flying height above tree canopy	50 m
Spacing between flight lines	20 m
Scanned area	12 ha
Scanning rate	550 kHz
Field of view	240 deg
Nominal shot density	230 points/m^2
Nominal shot spacing	0.06 m
Actual point density returns	3200 points/m^2

Table 1. Settings of UAV laser scanning acquisition. Please note that nominal values are per flight strip and actual point density is computed using all returns, including strip overlap and multiple returns.

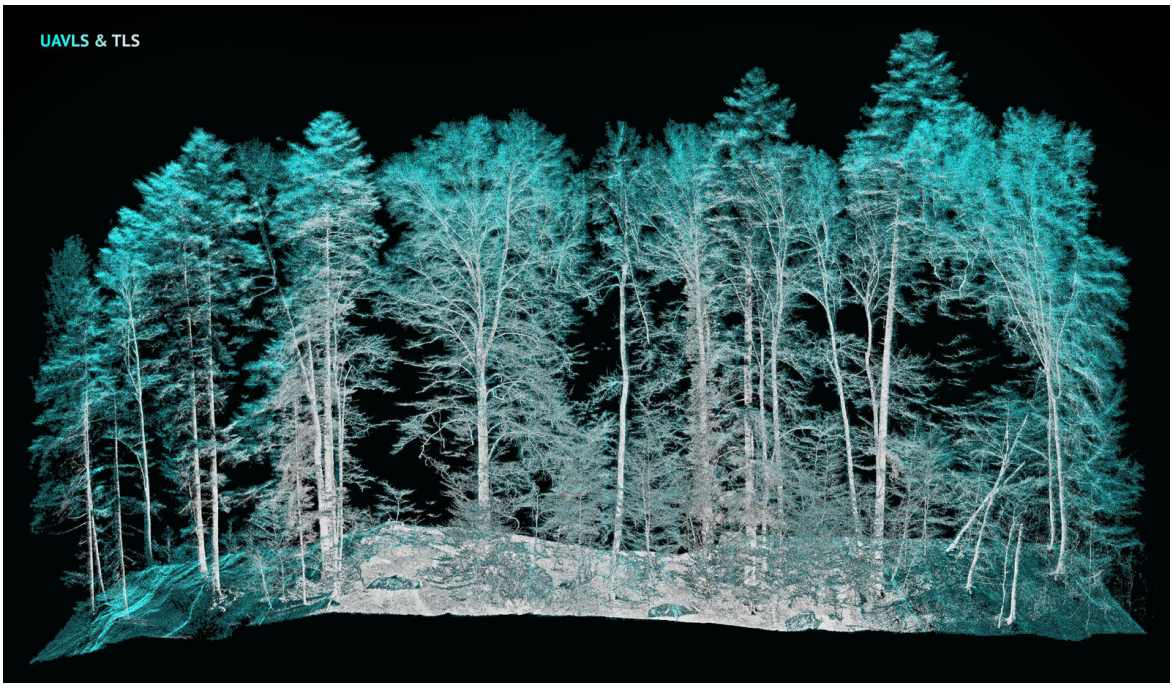

Figure 6. Combination of TLS (grey-scale) and UAVLS (cyan) point-clouds acquired on the same day at Laegeren Forest, Switzerland. Foliage condition was leaf-off.

findings of this experiment in a temperate mixed forest agree very well with both the simulation experiment from Abegg et al. [2017], who was able to show that TLS suffers from lower sampling density towards the top-of-canopy, which only can be mitigated by a large increase of the number of scans, which might come at prohibitively high costs.

On the other hand, having more points does not always mean getting more information. Comparing plot-level canopy profiles of the UAV and traditional airborne laser scanning data, very high correlations were observed, despite the large difference in point density of about 15/m^2 for ALS and 3200/m^2 for UAV laser scanning [Morsdorf et al., 2017]. This corresponds well to the ALS based findings of Leiterer et al. [2015], who observed a saturation of information towards higher point densities and underlines the issue of dedicated experiments to test cost-benefit relationship before large-scale application of TLS technology, as e.g. in NFIs.

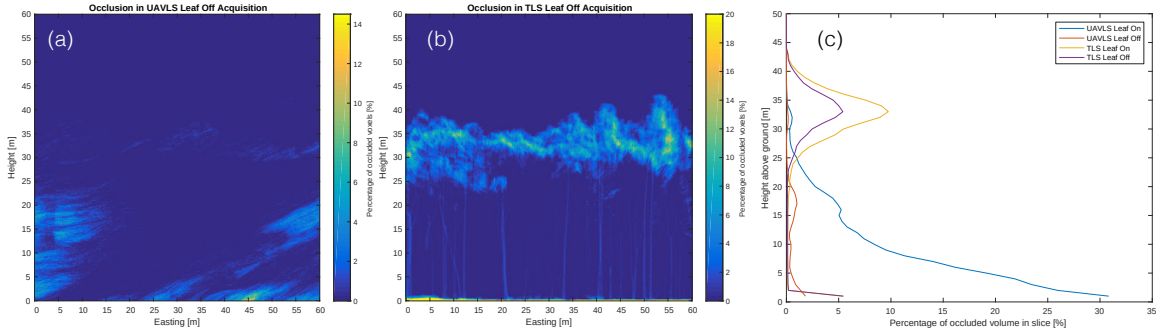

Figure 7. Occlusion mapping using the approach of Kükenbrink et al. [2017] for the UAV data (a) and the TLS data (b) acquired over the same area and the same day in leaf-off conditions. Aggregated profiles for occlusion over transect shown in (a) and (b) are shown in (c), both for leaf-on and -off cases. Voxel size was 0.1 m and the percentage denotes the amount of voxel occluded related to all voxel in the 60 m deep transect. The profiles in (c) are based on the full 60 m by 60 m dataset.

6. Summary and Conclusion

TLS and the upcoming UAV-based laser scanners provide data which has the potential to revolutionize the way the assess and quantify 3D vegetation structure. However, the transformation of data to information is not always straightforward and empirical approaches known from ALS will not work as well in close-range laserscanning.

Consequently, better use of the extensive physical information provided by the instruments is key to advance information retrieval, e.g. the voxel-based occlusion mapping can be used to aid the filtering and semantic labeling of the point clouds. However, the particular implementations in instruments need to be considered as well, otherwise we might just replace the well-known observer bias of traditional field inventories with an instrument bias.

QSMs are a promising way of abstracting the point cloud and are able to derive topological information, but the pre-processing (e.g. filtering) needed still hinders a wide-spread operational application of this method. But the semantic labeling done in QSMs is mandatory to derive variables such as stem and branch volume.

The validation problem for variables which are too cumbersome or costly to measure in the field (almost all except for DBH) can be overcome by 3d modeling of virtual forest stands. This will help us to learn about instrument biases and to test and implement the methods needed to make this technology a valuable asset in the toolboxes of foresters and ecologists alike.

Technology is evolving quickly and the costs, both in terms of labor and hardware, of laser scanner use in forests is decreasing. There are certain limitations regarding further miniaturization of UAV laser scanners in their current form, i.e. the dependence on highly accurate inertial navigation systems. However, new technologies such as focal plane arrays, driven by the demand for self-driving cars, will become mass market products and will fuse the power of range imaging with computer vision and photogrammetric approaches, ultimately making small, self-navigating laser drones possible. Once these devices will become available, the methods need to be ready to automatically convert the huge data-streams into meaningful information, otherwise such drones will remain not much more than toys.

While the data collected by TLS and UAV laser scanning is impressive, it can only be complementary to a full NFI approach, as many relevant variables, e.g. the management history of a site or the occurrence of pests can only be determined through manual interpretation on the respective sites.

But when applied properly, laser scanning can provide objective and accurate structural measurements of semantic objects constituting the forest canopies across scales (i.e. trees, stems, branches, leaves). This will leave more time for the humans in the plot to assess the biotic variables

of the forest ecosystem invisible to the laser. Hence, we see close-range laser scanning as valuable complement to NFI approaches, but not as a replacement.

Acknowledgments

The contributions of Felix Morsdorf, Fabian D. Schneider, and Michael E. Schaepman are supported by the University of Zurich Research Priority Program on *Global Change and Biodiversity* and the contribution of Daniel Kükenbrink was with support from the European Union's 7th Framework Programme (FP7/2014-2018) under EUFAR2 contract no. 312609.

References

Abegg, M., Kükenbrink, D., Zell, J., Schaepman, M. E., Morsdorf, F., 2017. Terrestrial laser scanning for forest inventories—tree diameter distribution and scanner location impact on occlusion. Forests 8 (6), 184.

Åkerblom, M., Raumonen, P., Mäkipää, R., Kaasalainen, M., 2017. Automatic tree species recognition with quantitative structure models. Remote Sensing of Environment 191, 1 – 12.

Armston, J., Disney, M., Lewis, P., Scarth, P., Phinn, S., Lucas, R., Bunting, P., Goodwin, N., 2013. Direct retrieval of canopy gap probability using airborne waveform lidar. Remote Sensing of Environment 134 (0), 24 – 38.

Barlow, J., Gardner, T. A., Araujo, I. S., Ávila-Pires, T. C., Bonaldo, A. B., Costa, J. E., Esposito, M. C., Ferreira, L. V., Hawes, J., Hernandez, M. I. M., Hoogmoed, M. S., Leite, R. N., Lo-Man-Hung, N. F., Malcolm, J. R., Martins, M. B., Mestre, L. A. M., Miranda-Santos, R., Nunes-Gutjahr, A. L., Overal, W. L., Parry, L., Peters, S. L., Ribeiro-Junior, M. A., da Silva, M. N. F., da Silva Motta, C., Peres, C. A., 2007. Quantifying the biodiversity value of tropical primary, secondary, and plantation forests. Proceedings of the National Academy of Sciences 104 (47), 18555–18560.

Béland, M., Baldocchi, D. D., Widlowski, J.-L., Fournier, R. A., Verstraete, M. M., 2014. On seeing the wood from the leaves and the role of voxel size in determining leaf area distribution of forests with terrestrial lidar. Agricultural and Forest Meteorology 184 (0), 82 – 97.

Bienert, A., Queck, R., Schmidt, A., Bernhofer, C., Maas, H.-G., 2010. Voxel space analysis of terrestrial laser scans in forests for wind field modeling. In: International Archives of Photogrammetry, Remote Sensing and Spatial Information Sciences, Vol. XXXVIII, Part 5 Commission V Symposium, Newcastle upon Tyne, UK.

Bruggisser, M., Roncat, A., Schaepman, M. E., Morsdorf, F., 2017. Retrieval of higher order statistical moments from full-waveform lidar data for tree species classification. Remote Sensing of Environment 196, 28 – 41.

Chave, J., Réjou-Méchain, M., Búrquez, A., Chidumayo, E., Colgan, M. S., Delitti, W. B., Duque, A., Eid, T., Fearnside, P. M., Goodman, R. C., Henry, M., Martínez-Yrízar, A., Mugasha, W. A., Muller-Landau, H. C., Mencuccini, M., Nelson, B. W., Ngomanda, A., Nogueira, E. M., Ortiz-Malavassi, E., Pélissier, R., Ploton, P., Ryan, C. M., Saldarriaga, J. G., Vieilledent, G., 2014. Improved allometric models to estimate the aboveground biomass of tropical trees. Global Change Biology 20 (10), 3177–3190.

Danson, F. M., Hetherington, D., Morsdorf, F., Koetz, B., Allgöwer, B., 2007. Forest canopy gap fraction from terrestrial laser scanning. IEEE Geoscience and Remote Sensing Letters 4 (1), 157–160.

Eitel, J. U., Vierling, L. A., Long, D. S., 2010. Simultaneous measurements of plant structure and chlorophyll content in broadleaf saplings with a terrestrial laser scanner. Remote Sensing of Environment 114 (10), 2229 – 2237.

Eitel, J. U., Vierling, L. A., Long, D. S., Hunt, E. R., 2011. Early season remote sensing of wheat nitrogen status using a green scanning laser. Agricultural and Forest Meteorology 151 (10), 1338 – 1345.

Eysn, L., Pfeifer, N., Ressl, C., Hollaus, M., Grafl, A., Morsdorf, F., 2013. A practical approach for extracting tree models in forest environments based on equirectangular projections of terrestrial laser scans. Remote Sensing 5 (11), 5424–5448.

Grau, E., Durrieu, S., Fournier, R., Gastellu-Etchegorry, J.-P., Yin, T., 2017. Estimation of 3d vegetation density with terrestrial laser scanning data using voxels. a sensitivity analysis of influencing parameters. Remote Sensing of Environment 191, 373 – 388.

Hackenberg, J., Spiecker, H., Calders, K., Disney, M., Raumonen, P., 2015. Simpletree —an efficient open source tool to build tree models from tls clouds. Forests 6 (11), 4245–4294.

Halle, F., 1986. Modular growth in seed plants. Philosophical Transactions of the Royal Society B: Biological Sciences 313 (1159), 77–87.

Hancock, S., Disney, M., Muller, J.-P., Lewis, P., Foster, M., 2011. A threshold insensitive method for locating the forest canopy top with waveform lidar. Remote Sensing of Environment 115 (12), 3286 – 3297.

Hancock, S., Lewis, P., Foster, M., Disney, M., Muller, J.-P., 2012. Measuring forests with dual wavelength lidar: A simulation study over topography. Agricultural and Forest Meteorology 161 (0), 123 – 133.

Jonckheere, I., Fleck, S., Nackaerts, K., Muys, B., Coppin, P., Weiss, M., Baret, F., 2004. Review of methods for in situ leaf area index determination: Part i. theories, sensors and hemispherical photography. Agricultural and Forest Meteorology 121 (1-2), 19–35.

Kükenbrink, D., Schneider, F. D., Leiterer, R., Schaepman, M. E., Morsdorf, F., 2017. Quantification of hidden canopy volume of airborne laser scanning data using a voxel traversal algorithm. Remote Sensing of Environment 194, 424 – 436.

Leiterer, R., Furrer, R., Schaepman, M. E., Morsdorf, F., 2015. Forest canopy-structure characterization: A data-driven approach. Forest Ecology and Management 358, 48 – 61.

Lin, Y., Hyyppä, J., Jaakkola, A., 2011. Mini-uav-borne lidar for fine-scale mapping. IEEE Geoscience and Remote Sensing Letters 8 (3), 426–430.

MacArthur, R. H., Horn, H. S., 1969. Foliage profile by vertical measurements. Ecology 50, 802–804.

Maignan, F., Bréon, F.-M., Lacaze, R., 2004. Bidirectional reflectance of earth targets: evaluation of analytical models using a large set of spaceborne measurements with emphasis on the hot spot. Remote Sensing of Environment 90 (2), 210 – 220.

Maltamo, M., Naesset, E., Vauhkonen, J. (Eds.), 2014. Forestry Applications of Airborne Laser Scanning. Springer Netherlands.

Mandlburger, G., Pfennigbauer, M., Riegl, U., Haring, A., Wieser, M., Glira, P., Winiwarter, L., 2015. Complementing airborne laser bathymetry with uav-based lidar for capturing alluvial landscapes. Vol. 9637.

McElhinny, C., Gibbons, P., Brack, C., Bauhus, J., 2005. Forest and woodland stand structural complexity: Its definition and measurement. Forest Ecology and Management 218 (1/3), 1 – 24.

McPherson, E. G., van Doorn, N. S., Peper, P. J., 86 p. 2016. Urban tree database and allometric equations. Tech. Rep. Gen. Tech. Rep. PSW-GTR-253. Albany, CA, U.S. Department of Agriculture, Forest Service, Pacific Southwest Research Station.

Moeser, D., Morsdorf, F., Jonas, T., Aug 2015. Novel forest structure metrics from airborne lidar data for improved snow interception estimation. Agricultural and Forest Meteorology 208, 40–49.

Moeser, D., Roubinek, J., Schleppi, P., Morsdorf, F., Jonas, T., 2014. Canopy closure, {LAI} and radiation transfer from airborne lidar synthetic images. Agricultural and Forest Meteorology 197, 158 – 168.

Morsdorf, F., Eck, C., Zgraggen, C., Imbach, B., Schneider, F., Kükenbrink, D., 2017. UAV-based LiDAR acquisition for the derivation of high-resolution forest and ground information. Leading Edge 36 (7), 566–570.

Næsset, E., 1997. Estimating timber volume of forest stands using airborne laser scanner data. Remote Sensing of Environment 61 (2), 246 – 253.

Næsset, E., 2002. Predicting forest stand characteristics with airborne scanning laser using a practical two-stage procedure and field data. Remote Sensing of Environment 80 (1), 88 – 99.

Raumonen, P., Kaasalainen, M., Åkerblom, M., Kaasalainen, S., Kaartinen, H., Vastaranta, M., Holopainen, M., Disney, M., Lewis, P., 2013. Fast automatic precision tree models from terrestrial laser scanner data. Remote Sensing 5 (2), 491.

Schaepman, M. E., Jehle, M., Hueni, A., D'Odorico, P., Damm, A., Weyermann, J., Schneider, F. D., Laurent, V., Popp, C., Seidel, F. C., Lenhard, K., Gege, P., Küchler, C., Brazile, J., Kohler, P., Vos, L. D., Meuleman, K., Meynart, R., Schläpfer, D., Kneubühler, M., Itten, K. I., 2015. Advanced radiometry measurements and earth science applications with the airborne prism experiment (apex). Remote Sensing of Environment 158 (0), 207 – 219.

Schneider, F. D., Leiterer, R., Morsdorf, F., Gastellu-Etchegorry, J.-P., Lauret, N., Pfeifer, N., Schaepman, M. E., 2014. Simulating imaging spectrometer data: 3d forest modeling based on lidar and in situ data. Remote Sensing of Environment 152, 235–250.

Vosselman, G., Maas, H.-G., 2010. Airborne and Terrestrial Laser Scanning. Whittles Publishing, ISBN 1439827982.

Wagner, W., 2010. Radiometric calibration of small-footprint full-waveform airborne laser scanner measurements: Basic physical concepts. ISPRS Journal of Photogrammetry and Remote Sensing 65 (6), 505 – 513, iSPRS Centenary Celebration Issue.

Wallace, L., Lucieer, A., Watson, C., Turner, D., 2012. Development of a uav-lidar system with application to forest inventory. Remote Sensing 4 (6), 1519–1543.

Weiss, M., Baret, F., Smith, G. J., Jonckheere, I., Coppin, P., 2004. Review of methods for in situ leaf area index (LAI) determination: Part II. Estimation of LAI, errors and sampling. Agricultural and Forest Meteorology 121 (1-2), 37–53.

Widlowski, J.-L., Mio, C., Disney, M., Adams, J., Andredakis, I., Atzberger, C., Brennan, J., Busetto, L., Chelle, M., Ceccherini, G., Colombo, R., Côté, J.-F., Eenmäe, A., Essery, R., Gastellu-Etchegorry, J.-P., Gobron, N., Grau, E., Haverd, V., Homolová, L., Huang, H., Hunt, L., Kobayashi, H., Koetz, B., Kuusk, A., Kuusk, J., Lang, M., Lewis, P. E., Lovell, J. L., Malenovský, Z., Meroni, M., Morsdorf, F., Mõttus, M., Ni-Meister, W., Pinty, B., Rautiainen, M., Schlerf, M., Somers, B., Stuckens, J., Verstraete, M. M., Yang, W., Zhao, F., Zenone, T., 2015. The fourth phase of the radiative transfer model intercomparison (rami) exercise: Actual canopy scenarios and conformity testing. Remote Sensing of Environment 169, 418 – 437.

Wilkes, P., Lau, A., Disney, M., Calders, K., Burt, A., de Tanago, J. G., Bartholomeus, H., Brede, B., Herold, M., 2017. Data acquisition considerations for terrestrial laser scanning of forest plots. Remote Sensing of Environment 196, 140 – 153.

Woodgate, W., Jones, S. D., Suarez, L., Hill, M. J., Armston, J. D., Wilkes, P., Soto-Berelov, M., Haywood, A., Mellor, A., 2015. Understanding the variability in ground-based methods for retrieving canopy openness, gap fraction, and leaf area index in diverse forest systems. Agricultural and Forest Meteorology 205, 83 – 95.

Woodhouse, I., Nichol, C., Sinclair, P., Jack, J., Morsdorf, F., Malthus, T., Patenaude, G., 2011. A multispectral canopy lidar demonstrator project. Geoscience and Remote Sensing Letters, IEEE 8 (5), 839 –843.

Chapter

3

Mapping functional diversity of forests with remote sensing

This chapter consists of a peer-reviewed journal article, corresponding supplementary information, and peer review comments, which the authors opted to make publicly accessible within the journals publishing system.

3.1 Mapping functional diversity from remotely sensed morphological and physiological forest traits

Schneider, F.D., Morsdorf, F., Schmid, B., Petchey, O.L.,
Hueni, A., Schimel, D.S., Schaepman, M.E.

This section is based on the peer-reviewed article:
Nature Communications, 2017 (8), 1-12
DOI:10.1038/s41467-017-01530-3

F.D.S., F.M., B.S., O.L.P., and M.E.S. designed research; F.D.S., B.S., and M.E.S. performed research; F.D.S., F.M., A.H., and M.E.S. analyzed data; and all authors wrote the paper, with main contributions of F.D.S.

nature COMMUNICATIONS

ARTICLE

DOI: 10.1038/s41467-017-01530-3 OPEN

Mapping functional diversity from remotely sensed morphological and physiological forest traits

Fabian D. Schneider [1], Felix Morsdorf [1], Bernhard Schmid [2], Owen L. Petchey [2], Andreas Hueni [1], David S. Schimel [3] & Michael E. Schaepman [1]

Assessing functional diversity from space can help predict productivity and stability of forest ecosystems at global scale using biodiversity–ecosystem functioning relationships. We present a new spatially continuous method to map regional patterns of tree functional diversity using combined laser scanning and imaging spectroscopy. The method does not require prior taxonomic information and integrates variation in plant functional traits between and within plant species. We compare our method with leaf-level field measurements and species-level plot inventory data and find reasonable agreement. Morphological and physiological diversity show consistent change with topography and soil, with low functional richness at a mountain ridge under specific environmental conditions. Overall, functional richness follows a logarithmic increase with area, whereas divergence and evenness are scale invariant. By mapping diversity at scales of individual trees to whole communities we demonstrate the potential of assessing functional diversity from space, providing a pathway only limited by technological advances and not by methodology.

[1] Remote Sensing Laboratories, Department of Geography, University of Zurich, Winterthurerstrasse 190, CH-8057 Zurich, Switzerland. [2] Department of Evolutionary Biology and Environmental Studies, University of Zurich, Winterthurerstrasse 190, CH-8057 Zurich, Switzerland. [3] Jet Propulsion Laboratory, California Institute of Technology, 4800 Oak Grove Drive, Pasadena, CA 91011, USA. Correspondence and requests for materials should be addressed to F.D.S. (email: fabian-daniel.schneider@geo.uzh.ch)

Understanding community structure and the impact of changing biodiversity on ecosystem functioning are key tasks in ecology. Progress has been made on a wide variety of taxa, including plants[1], fish[2], birds[3] and insects[4], amongst others. In plant ecology, biodiversity research has focused on the distribution of species based on taxonomic identity[5]. More recently, with the emergence of functional biogeography[6], tree species or individuals of a community are described in relation to their functional identity and distribution in space. Functional traits are of particular interest due to their response to environmental conditions and direct link to growth, reproduction and survival[7, 8]. Trait-based approaches are emerging rapidly in plant ecology, underpinning community assembly and structure, species interactions and interlinkages between vegetation and biogeochemical cycles[9].

The assessment of plant functional traits and plant functional diversity is of particular relevance when predicting ecosystem productivity and stability. A multitude of experimental studies demonstrated positive relationships between plant diversity and ecosystem functioning[10–12] and increasingly such positive relationships are also found in comparative observational studies[13, 14]. A positive relationship over extended time scales is mainly driven by functional diversity due to an increased resource use efficiency and utilization as well as sampling effects in a changing environment, allowing plant communities to sustain high productivity over time[15–17]. Besides productivity, higher functional diversity has been linked to enhanced tree growth and ecosystem stability due to complementarity effects, better adaptability to changing environmental conditions and lower vulnerability to diseases, insect attacks, fire and storms[18–20]. However, to make use of the increasing knowledge about biodiversity–ecosystem functioning relationships in forest ecosystems, it would be necessary to develop methods to assess plant functional diversity efficiently over large continuous areas. Our first aim is therefore to develop such a method for a regional test area, see Fig. 1, as a base for larger scale biodiversity scoping studies.

Spatial variation in plant functional traits and diversity depend on community structure[21] and thus represent a potential signal of community assembly processes. However, plant traits and functional diversity do not only depend on community structure represented by particular species abundance distributions within a specific geographical unit, but may vary as much within species as they do between species[22]. Different species can also be redundant in terms of their functional traits, and thus not contribute to functional diversity[16, 23]. Therefore, functional diversity is best derived from a given set of traits including their intraspecific variability[24, 25]. By incorporating individual-level functional traits, functional diversity may better predict ecosystem functioning than species-level means[16].

A multitude of forest monitoring networks exist[26] as well as trait-based studies in forested ecosystems[27], fostered by standardized measurement procedures[28] and global trait databases[29]. However, these procedures usually require taxonomic information about tree individuals and indirectly assess trait variation and functional diversity combining information about species abundances and mean traits, thus ignoring variation in tree functional traits within species, which can be large even within individuals[30]. In addition, there is a global bias in the distribution of forest plots, leading to large data gaps particularly in remote areas[31]. Furthermore, trait measurements in forests are typically limited in extent and magnitude due to the complexity of destructive crown-level measurements, as well as associated georeferencing challenges and plot representativeness[32]. Consequently, continuous spatial data of traits and especially on trait diversity are still very sparse. Recent advances in remote sensing provide the opportunity to map traits and trait diversity, thus filling the existing data gaps[33–35]. Here, we use three morphological and three physiological functional traits that we assess directly, i.e. without reference to taxonomic information, to provide a spatially continuous description of functional diversity in a forest at local scale (≈925 ha), with the potential to scale up to regional and to the global level.

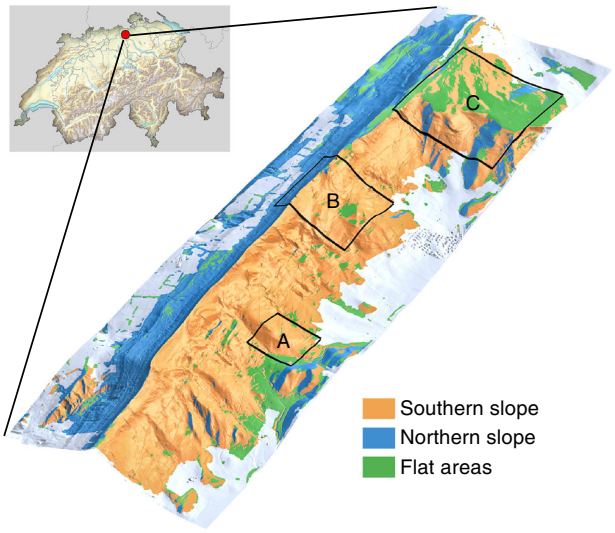

Fig. 1 Laegern mountain temperate mixed forest site in Switzerland. The test site is located near Zurich and covers about 2 × 6 km. The mountain range is divided by a ridge running from east to west, separating the forested area in north facing (blue) and south facing (orange) slopes. Flat areas are defined with a slope <10° (green). Areas not covered by forest (agriculture, grassland, urban areas) are shown in grey

The selected morphological and physiological traits can be assessed with high-resolution airborne remote sensing methods[33, 36] and are relevant for plant and ecosystem function. Three morphological traits, namely canopy height (CH, vertical distance between canopy top and ground), plant area index (PAI, projected plant area per horizontal ground area) and foliage height diversity (FHD, measure of variation and number of canopy layers), are essential to describe canopy architecture, encompassing the horizontal and vertical structure of forests and influencing light availability, thus affecting competitive and complementary light use and ecosystem productivity[18, 37]. Three physiological traits, namely leaf chlorophyll (CHL, relative content of chlorophyll a+b per unit leaf area), leaf carotenoids (CAR, relative content of carotenoids per unit leaf area) and equivalent water thickness (EWT, leaf water content per unit leaf area), do not modify light availability but rather describe light use at the level of single leaves. The chlorophylls are functionally important pigments, since they control the amount of photosynthetically active radiation absorbed for photosynthesis[38]. Carotenoids are contributing to the chlorophylls by absorbing additional radiation for photosynthesis and protecting leaves from over-exposition to high amounts of incoming solar radiation by releasing excess energy[38]. The third, EWT, is important for plant responses to drought, which could reduce the physiological performance through decreased photosynthetic carbon assimilation and electron transport rate[39].

We use the above traits to derive measures of functional diversity separately for the morphological and leaf physiological traits. Our functional diversity measures are combining multiple traits, as is typically done for such measures[23]. We calculate three measures, related to different aspects of functional diversity—functional richness, divergence and evenness[40, 41]. Functional

NATURE COMMUNICATIONS | DOI: 10.1038/s41467-017-01530-3 ARTICLE

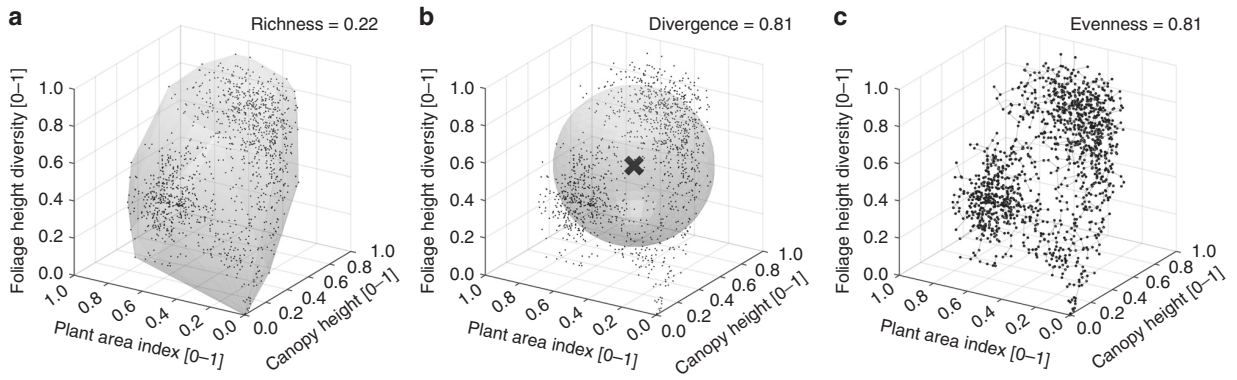

Fig. 2 Three aspects of functional diversity based on morphological forest traits of a circular area with a radius of 120 m. The three traits are foliage height diversity, plant area index and canopy height in relative units from 0 to 1. **a** The shaded volume is functional richness, **b** the distance from the surface of the shaded sphere is functional divergence and **c** the variation of segment length in the minimum spanning tree is functional evenness

richness is calculated as the convex hull volume of the community niche[42], as illustrated in Fig. 2a for an assemblage of pixels mapped in the morphological trait space. It corresponds to the niche extent and defines the outer boundary of the occupied functional space. A disadvantage of this measure may be a strong influence by extreme values. In contrast, functional divergence and evenness describe how sample points are distributed within the community niche (Fig. 2b, c). Functional divergence is a measure of how sample points are spread with regard to the mean distance to the centre of gravity, whereas functional evenness indicates how evenly traits are distributed with regard to spacing among similar sample points in functional space. These three indices have mainly been applied to functional diversity of plants[43], where sample points represent species, with an increasing number of studies on forest ecosystems[44]. However, this concept has not yet been applied to continuously measured trait data independent of taxonomy, vegetation units or even plant individuals. Remote sensing methods offer to measure functional traits continuously and directly across large spatial extents. This has a twofold advantage: (1) there is no need to identify species, vegetation units or individuals and (2) prediction of ecosystem functions using independently established functional diversity–ecosystem functioning relationships are consistent across large scales. In contrast, recent efforts to map forest biodiversity have used forest functional classes as remotely sensed vegetation units with constant trait values assigned to these units[35].

Our second aim is to test the consistency of our method. For this, we compare the results obtained with the two independent sets of traits. Morphological diversity was found to be the main driver of forest productivity in poly- and monocultures of mature forests[45–47], whereas physiological diversity reflects different resource allocation strategies to maximize light capture and protective mechanisms and is more closely linked to species diversity[48, 49]. Since most functional traits show consistent variation along broad environmental gradients, we expect both morphological and physiological diversity to show similar patterns at larger scales. For the leaf physiological traits, we also compare the remotely sensed trait values with those directly obtained from spectroscopic measurements on single leaves. This should indicate how well the retrieval method can be scaled from the leaf to the canopy level. Furthermore, we test the general agreement of trends in trait relationships between community weighted means of the functional trait database TRY and the retrieved traits for communities composed of the 13 tree species present in our test area.

Finally, we examine scale dependency of different functional diversity measures. We demonstrate that functional diversity measures can be quantified at any desired unit area within the sampled region, limited only by the spatial resolution of the trait maps. This will allow—in future efforts—for direct and continuous mapping of functional diversity from space. Functional diversity, due to redundancy and trait plasticity, may not show the same increase with area as is typically found for species richness. Nevertheless, scale dependency of functional diversity could still lead to scale-dependent functional diversity–ecosystem functioning relationships. Such effects would be expected if ecosystem functions are not scale-dependent above a certain minimum area, which is likely the case, such as for example for productivity per area. Studies on spatial patterns and scale dependency of functional diversity are still sparse[50]. We expect functional richness to increase with scale. A strong increase at small scales would indicate high diversity within communities, which can mean higher resilience to disturbance[51], while an increase at larger scales would indicate high diversity between communities. The exact slope and shape of the relationship, however, cannot be predicted by known species–area relationships, since functional richness is influenced by trait correlations, redundancies among species and intra-specific trait variation. Even less is known about other components of functional diversity. A study based on four plant communities on the Santorini Archipelago found no relationship with area for functional divergence and evenness[52].

Results

Functional traits. Figure 3 shows the spatial distribution of morphological and physiological traits, as derived from airborne laser scanning and airborne imaging spectroscopy, respectively. Blue areas in the morphological trait map are characterized by high canopy density, low canopy height and little canopy layering. When comparing with independent community data, around 83% of these areas are classified as juvenile forest with tree height below 21 m and diameter at breast height below 30 cm (Supplementary Fig. 1). The largest such area is marked as subregion A, covering ~1.4 ha, and is likely affected by disturbance caused by a winter storm. Physiologically, these patches are characterized by very high chlorophyll concentration as compared to an undisturbed, mature forest canopy.

Larger patches with a dense and closed canopy as well as high relative chlorophyll and carotenoids content are represented by pink and orange areas in the morphological and physiological

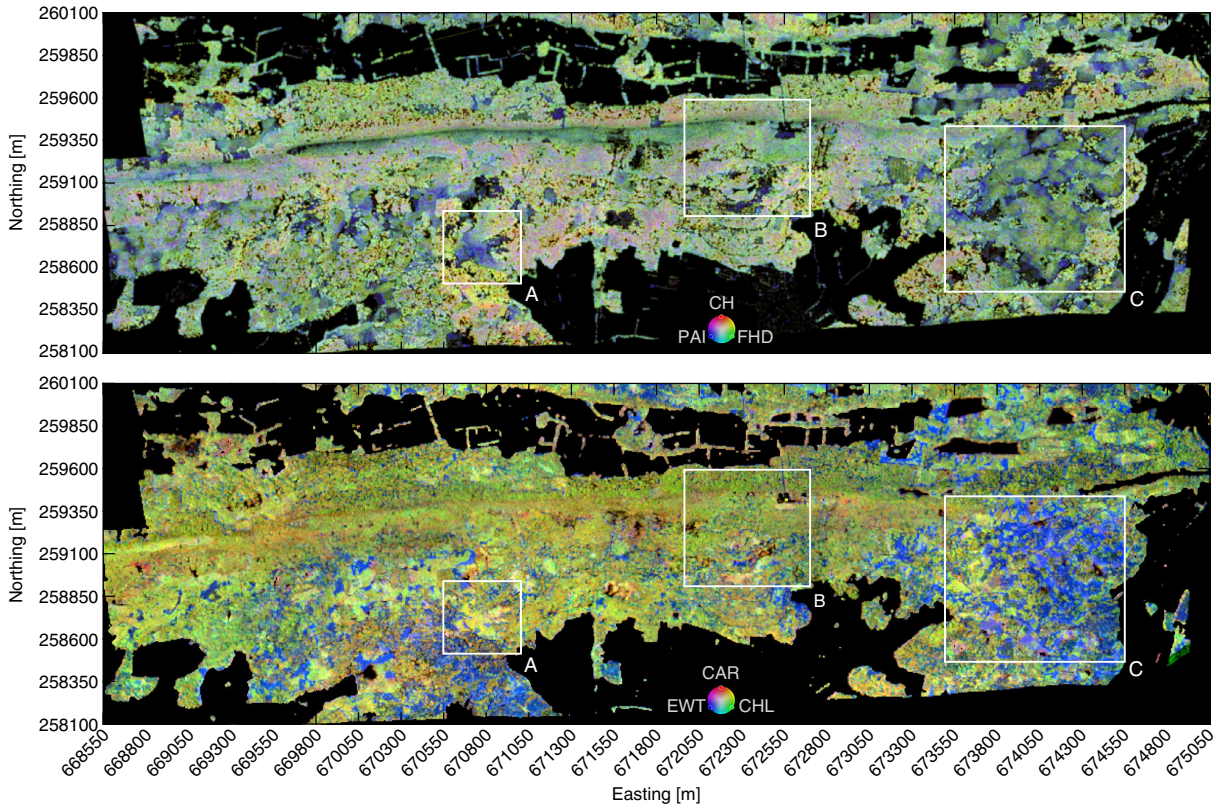

Fig. 3 Spatial composition of morphological and physiological forest traits. RGB colour composites of morphological traits (upper panel) plotted as abundance-scaled plant area index (PAI, blue), canopy height (CH, red) and foliage height diversity (FHD, green), and physiological traits (lower panel) plotted as abundance-scaled equivalent water thickness (EWT, blue), carotenoids (CAR, red) and chlorophyll (CHL, green)

trait maps (Fig. 3). According to community data, these areas are dominated by beech trees (>50% *Fagus sylvatica*, see Supplementary Fig. 1). They appear mainly in submontane locations with shallow, but fertile alkaline soils (e.g. *Rendzina*), as well as in lower altitudes on southern slopes with deeper neutral to acidic *Podsol* and *Cambisol* soils. On the physiological trait map, blue areas with a high relative water content and low relative chlorophyll and carotenoids content are dominated by evergreen coniferous needle trees. They are more abundant in flatter areas and on southern slopes with deeper, acidic soils. These areas can further be characterized by morphological traits. A managed plantation, marked as subregion C, with 20 m tall conifers (green areas covering about 25%) can be distinguished from up to 55 m high and complexly structured canopies (yellow areas covering around 3%). The Laegern mountain is forested up to the top of the ridge, but tree height decreases to a shrub type forest with a layered but low and sparse canopy covering about 25% of the forested area. On dry and rocky habitats, sessile oak (*Quercus petraea*) and beech (*Fagus sylvatica*) are the dominating tree species.

PAI, CH and FHD have a mean and standard deviation of 0.46 ±0.21, 0.49±0.17 and 0.59±0.20, respectively, when normalized between 0 and 1 (Supplementary Fig. 2a). CH and FHD are correlated with $r^2 = 0.70$, CH and PAI with $r^2 = 0.31$, and FHD and PAI with $r^2 = 0.35$ (Supplementary Fig. 3). Figure 4 shows median and standard deviation of the functional traits along altitudinal belts. 5.5%, 10.5% and 5.6% of the variance in CH, PAI and FHD can be explained by soil and topography (Supplementary Fig. 4). Soil variables alone explain 1.4%, 8.2% and 4.1% of the variance, respectively. CHL, CAR and EWT have a mean and standard deviation of 0.58±0.18, 0.50±0.21 and 0.39±0.18, respectively, when normalized between 0 and 1 (Supplementary Fig. 2b). CHL and CAR are correlated with $r^2 = 0.57$, CHL and EWT with $r^2 = 0.004$, and CAR and EWT with $r^2 = 0.08$ (Supplementary Fig. 3). 11.9%, 20.3% and 34.8% of the variance in CHL, CAR and EWT can be explained by soil and topography. Soil variables alone explain 9.9%, 14.1% and 27.5% of the variance. Radiation is correlated with soil and topography ($r^2 =$ 0.56) and therefore only explains an additional 0.1–0.5% of variance of the functional traits (Supplementary Figs. 4 and 5).

Estimated physiological trait ranges based on imaging spectroscopy correspond with modelled ranges based on leaf optical properties measured in the field (Supplementary Fig. 6). General trends of community-weighted mean trait values agree with the functional trait database TRY (Supplementary Fig. 7). Although TRY is not suitable for assessing intra-specific trait variation or trait plasticity, we find a positive relationship to remotely sensed trait estimates of chlorophyll ($r^2 = 0.36$) and EWT ($r^2 = 0.48$). Simulations using lab measurements of traits and leaf optical properties in a 3D forest model show that spectral indices can be applied at the canopy level, if high quality imaging spectroscopy data with little influence of shadows are available (Supplementary Figs. 8 and 9). Canopy reflectance-based estimates of chlorophyll and carotenoids (<15 µg/cm^2) correlate with traits measured in the laboratory ($r^2 = 0.86$, $r^2 = 0.74$). The weakest correlation between lab measured traits and estimates from canopy spectra could be observed for EWT ($r^2 = 0.51$, Supplementary Fig. 9), since water absorption was measured in the near infrared where

NATURE COMMUNICATIONS | DOI: 10.1038/s41467-017-01530-3 ARTICLE

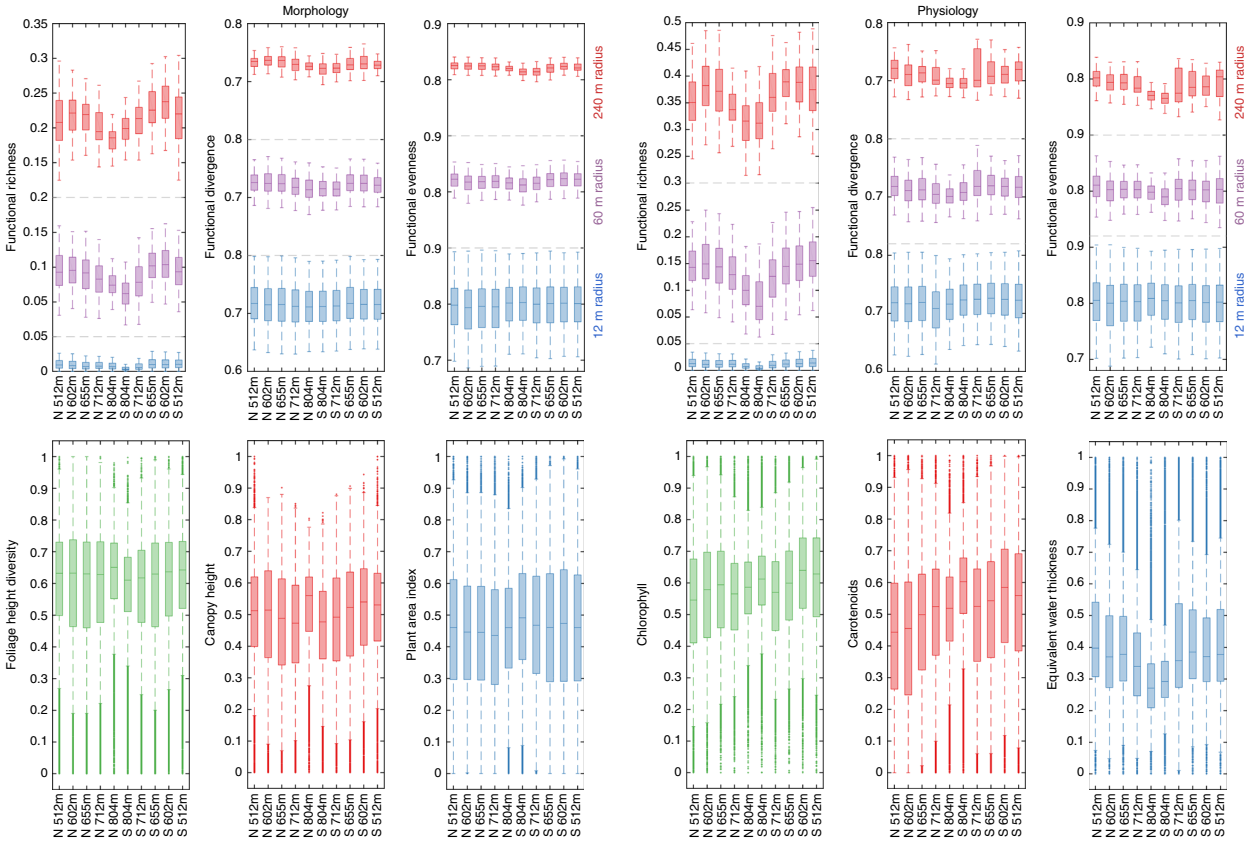

Fig. 4 Boxplots of functional diversity indices and traits grouped by altitudinal belts. Functional richness, divergence and evenness (top panel) are shown for three spatial scales at 12 m (blue), 60 m (purple) and 240 m (red) radius. Underlying functional trait values are displayed below, with morphological traits on the left and physiological traits on the right side. Boxes show the median and ±1 standard deviation and whiskers mark ±2 standard deviations. Altitude values on the *x*-axis of the boxplots indicate the middle of the altitudinal belt for the north (N) and the south (S) side of the mountain ridge

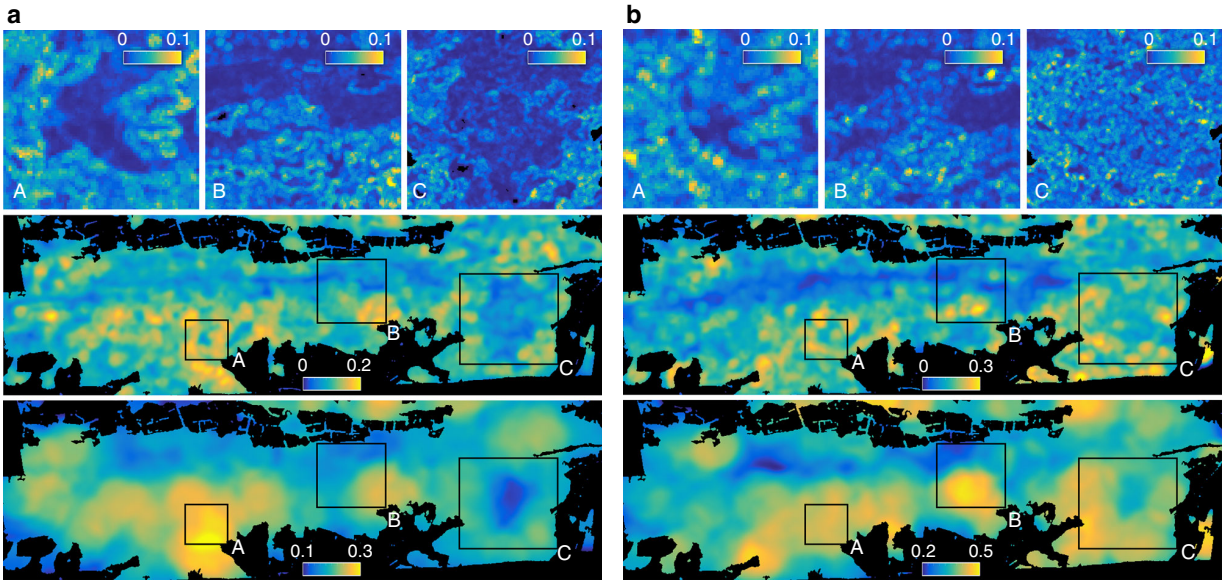

Fig. 5 Spatial patterns of morphological and physiological richness at three different scales. Functional richness was computed at 12 m (top), 60 m (middle) and 240 m (bottom) radius based on **a** morphological traits and **b** physiological traits. At 12 m radius (top panels), subregions A, B and C are plotted only. The colour is scaled from the lowest (dark blue) to the highest (yellow) richness value with a maximum possible range from 0 to 1

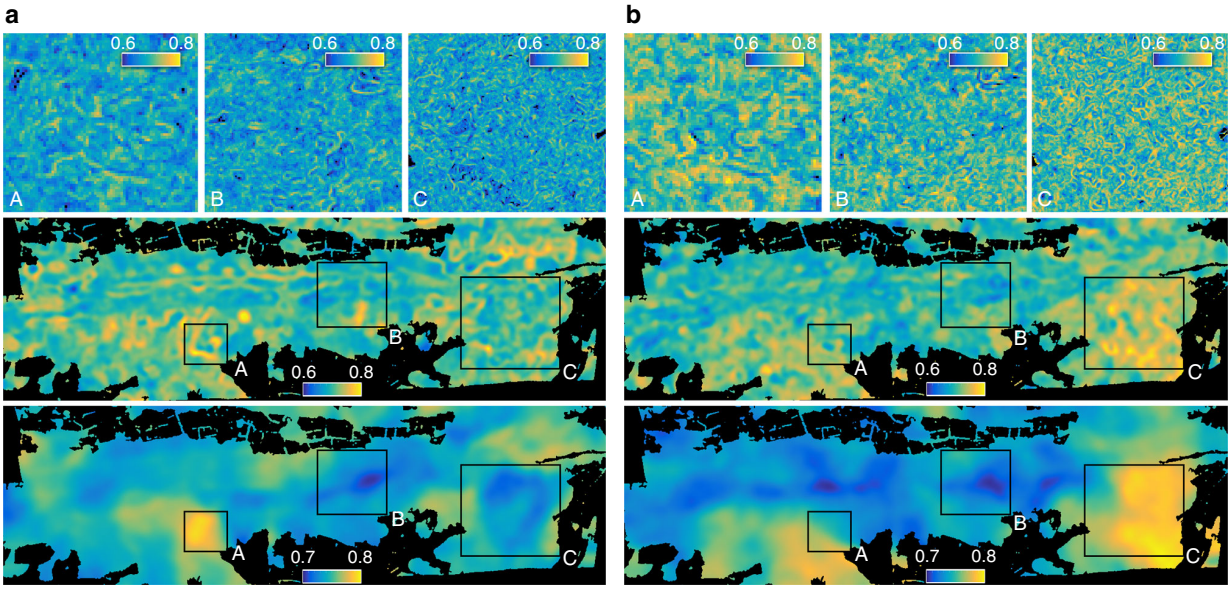

Fig. 6 Spatial patterns of morphological and physiological divergence at three different scales. Functional divergence was computed at 12 m (top), 60 m (middle) and 240 m (bottom) radius based on **a** morphological traits and **b** physiological traits. At 12 m radius (top panels), subregions A, B and C are plotted only. The colour is scaled from the lowest (dark blue) to the highest (yellow) divergence value with a maximum possible range from 0 to 1

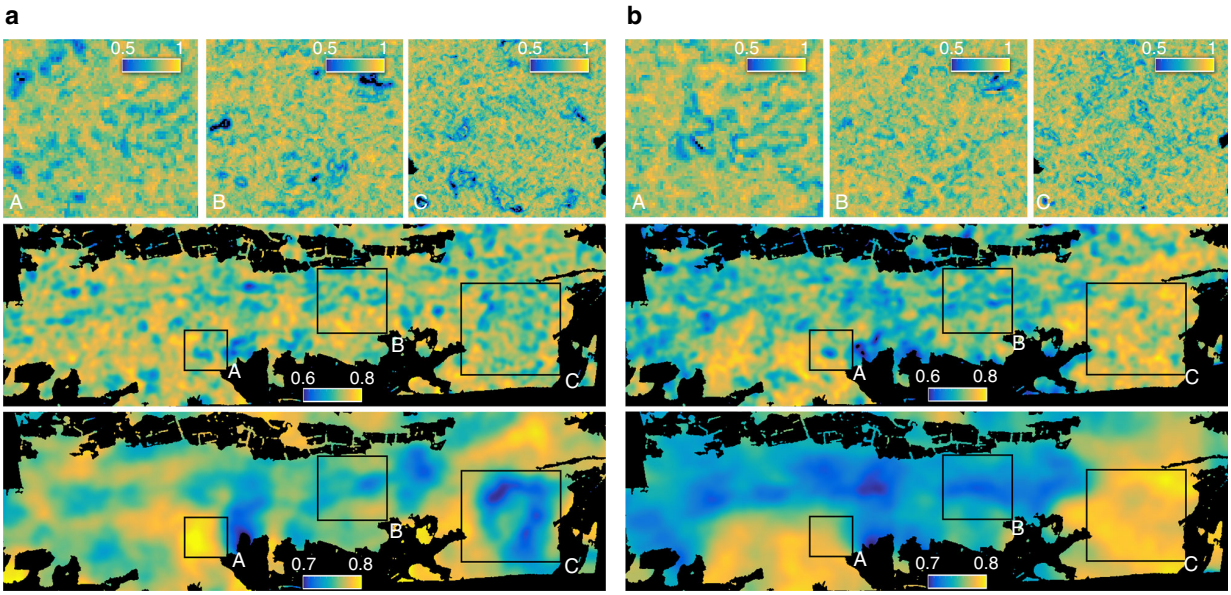

Fig. 7 Spatial patterns of morphological and physiological evenness at three different scales. Functional evenness was computed at 12 m (top), 60 m (middle) and 240 m (bottom) radius based on **a** morphological traits and **b** physiological traits. At 12 m radius (top panels), subregions A, B and C are plotted only. The colour is scaled from the lowest (dark blue) to the highest (yellow) evenness value with a maximum possible range from 0 to 1

scaling from leaf to canopy level is hampered by multiple scattering effects.

Functional diversity. Maps of functional richness, divergence and evenness are shown in Figs. 5–7. Patterns of morphological and physiological richness exhibit strongest correlation at medium scale between 60 and 240 m radius. The correlation coefficient (r) is 0.37, 0.44 and 0.40 at 12, 60 and 240 m radius, respectively. Differences among northern, southern and flat areas are significant for both morphological (DF = 2, $F = 5.8$, $p < 0.01$) and physiological richness (DF = 2, $F = 9.1$, $p < 0.01$) based on a generalized linear model and an ANOVA test. Figure 4 shows a consistent decrease of functional richness towards the mountain ridge for morphological and physiological richness. Soil and topography together explain 24.2% and 40.1% of variance in morphological and physiological richness, whereas 19.6% and 34.6% of variance is explained by soil alone and 15.3% and 37.9% by topography alone (Supplementary Fig. 4). For morphological richness, altitude (DF = 1, $F = 48.4$, $p < 0.001$) and curvature (DF

NATURE COMMUNICATIONS | DOI: 10.1038/s41467-017-01530-3 ARTICLE

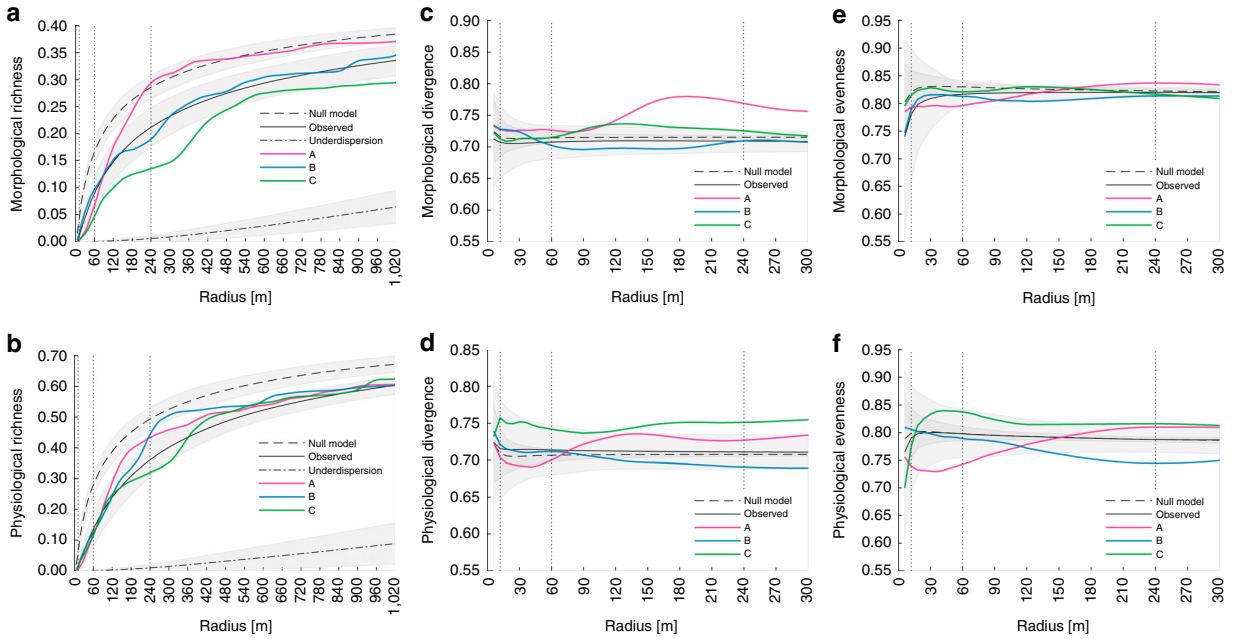

Fig. 8 Scale dependency of the three functional diversity measures for morphological and physiological traits. Functional **a**, **b** richness, **c**, **d** divergence and **e**, **f** evenness are displayed as a function of radius (diversity-area) for **a**, **c**, **e** morphological and **b**, **d**, **f** physiological traits. Null model corresponds to randomly distributed traits as dashed line. Observed corresponds to remotely sensed data as solid line. Underdispersion assuming direct neighbours corresponds to dashed-dotted line. Curves A, B C are stemming from a single pixel in the centre of subregions as in Fig. 5. Vertical dotted lines correspond to radii as in Fig. 5

= 2, $F = 3.8$, $p < 0.05$) explain most of the variance. Physiological richness is more strongly linked to slope (DF = 1, $F = 121.5$, $p < 0.001$), being steepest on the south side of the ridge and indirectly linked to radiation, followed by altitude (DF = 1, $F = 20.5$, $p < 0.001$). With slope explaining most of the variance, aspect is not significant any more (Supplementary Table 1).

The correlation (r) between patterns of morphological and physiological divergence is 0.36, 0.13 and 0.21 at 12, 60 and 240 m radius, respectively. Divergence remains in a relatively small range, leading to small relative differences between high and low diversity areas. Only altitude is significantly related to morphological divergence (DF = 1, $F = 8.4$, $p < 0.01$) based on a generalized linear model and an ANOVA test, whereas variance in physiological divergence is mainly explained by slope (DF = 1, $F = 23.4$, $p < 0.001$). Soil and topography together explain only 7.7% and 17.4% of total variance, with soil being the more important factor. Functional evenness patterns of morphological and physiological traits strongly correlate at small scales, for example with a correlation coefficient (r) of 0.54 at 12 m radius. The correlation decreases towards 0.19 and 0.23 at 60 and 240 m radius, respectively. Evenness is slightly higher on southern than on northern slopes and flat areas, but the deviation from the average is below 2% for morphological and below 3% for physiological traits. Morphological and physiological evenness vary mainly with altitude (DF = 1, $F = 14.0$, $p < 0.001$) and slope (DF = 1, $F = 14.8$, $p < 0.001$) respectively. Similar to divergence, soil and topography explain 10.7% and 12.1% of variance, respectively.

Figure 8 shows how functional richness of morphological and physiological traits change as a function of spatial scale (see Supplementary Fig. 10 for mean and standard deviations of all pixels in the subregions). Fitting a power-law function to the observed mean functional richness–area relationship results in a slope of 0.195 and 0.213 for morphological and physiological richness, respectively (Supplementary Fig. 11). This is close to previously reported slopes for species richness–area relationships of 0.161 and 0.177 for the biome 'temperate broadleaf and mixed forest' and the land-cover class 'temperate mixed forest'[53]. The increase of functional richness with the logarithm of the area is linear for areas above 1 ha. Therefore, a logarithmic function fits the mean observed values better than the power-law, although both r^2-values are very high ($r^2 > 0.9$). In contrast, mean functional divergence and evenness are scale invariant. They remain stable with changing extent (<1.3% change between radius 60 and 240 m) and do not vary between different trait values and distributions (Fig. 8c–f). The main difference between observed and random spatial distribution of traits is the magnitude of the variance.

A modelled random spatial distribution of functional traits (Fig. 8, null model), preserving the relationship among the three traits of a pixel, leads to a relatively high functional richness. Especially at smallest scales below 50 m radius, richness following a random distribution is one to five times higher than based on the observed distribution of traits. Null model richness is 35% and 37% higher at 240 m radius, decreasing to 15% and 11% at the largest scales for morphological and physiological traits respectively. A simulated distribution of traits following the assumption of under-dispersion, where trees being close in functional space are assumed to be close in geographic space, leads to a very low functional richness at all scales (<19% (a) and <15% (b) of observed values).

Discussion

Various measures of functional diversity, with different advantages and disadvantages[54, 55], have the common aim to map species in functional trait space using mean trait values and weighted species abundances[40, 41]. With our new method we create continuous maps of functional diversity without a need to identify species or individuals, since inter- as well as intra-specific

variability is inherent to remotely sensed functional traits. Especially in relatively species-poor temperate forests, such as the one studied here, functional diversity might be strongly underestimated when ignoring intra-specific variability[16, 56]. Our method avoids this pitfall, because it is fully continuous in space and only depends on resolution, it can thus even be applied below the individual level. Within-individual variation, for example in leaf traits, is common in plants and can reflect different light competition or leaf ages[30]. With evolving sensor technologies and miniaturization, higher spectral and spatial resolution of remotely sensed data will allow to study within-individual tree functional diversity.

The resulting spatial distribution of morphological and physiological diversity generally agree with regard to the spatial patterns, especially for functional richness. This is related to the environmental gradient on the mountain in the observed test area and the coinciding reduced trait variability towards the ridge (Fig. 4). The mountain ridge is the most prominent landscape feature of our study area with shallow and rocky soil, steep slopes and high incoming radiation on the south side of the ridge (Supplementary Fig. 5). We can therefore show that both morphological and physiological diversity change consistently with topography and soil. In this case, the abiotic conditions at the ridge might act as an environmental filter, only allowing trees with particular functional traits to exist. This is important because functional richness represents the total extent of the community niche. The lower functional richness at higher elevation with dry, rocky and shallow soil suggests a smaller range of resource availability. Thus smaller biotope space constrained the community niche in this area, which as a consequence may reduce the performance of the present plant community[57] and its adaptability to changing environmental conditions[40]. Therefore, we would expect the forest communities on the ridge to have lower ecosystem functioning and stability.

Besides similarities in the spatial distribution of functional diversity following broad environmental gradients, there are also expected differences between morphological and physiological diversity. These differences are more pronounced for functional divergence and evenness than for functional richness. On the one hand, physiological divergence is mainly driven by differences between tree functional groups (needle, broadleaf), because they have different leaf structure and composition of pigments and compounds related to different resource allocation strategies and are therefore clearly divergent in their biochemical characteristics. In areas with mixtures of broadleaf and needle trees, as for example in subregion C or generally in lower altitudes, productivity might be increased because the resource use is partitioned among the different functional groups leading to lower resource competition[40]. At the same time, functional evenness is higher too, indicating that the niche is filled evenly and available resources can potentially be fully exploited. In higher altitudes where the trait range is reduced, lower divergence and evenness could mean that there is a stronger competition for resources (nutrients, water) and that some of the resources might be unused, leading to lower productivity and stability of the community.

Morphological diversity, on the other hand, is more strongly linked to the different stages of forest development (e.g. due to disturbance) and management. For example, subregion A shows high morphological diversity at larger scales because there is a juvenile forest patch in the centre surrounded by structurally different mature trees. In contrast, morphological richness, divergence and evenness are low in the managed forest in subregion C due to equal canopy height and structure. This may result in lower productivity due to a lower efficiency in light capture, although higher physiological diversity could indicate better resource use partitioning among functional groups. The strong link to the development stage is clearly reflected in the morphological traits themselves. Differences in functional traits between juvenile and mature forest communities can be explained by changing physiology and morphology with tree age, ranging from densely and fast growing highly productive juvenile to mature trees, being characterized by lower growth rate, similar height, smaller leaves and greater leaf thickness and longevity[58]. Since the occurrence of patches of juvenile forest is mainly driven by disturbance and forest management, there is no clear altitudinal gradient in functional traits.

In contrast, physiological traits are linked more closely to topographic and soil variables. Equivalent water thickness in particular shows the strongest altitudinal gradient, because there is a gradient in soils and steepness leading to lower potential water availability towards the top of the ridge. Furthermore, needle trees mainly occurring in lower altitudes show higher EWT and lower relative chlorophyll and carotenoids content compared to broadleaf trees. This is in accordance with values from the TRY database (Supplementary Fig. 7) and a study conducted at three sites in Switzerland, reporting higher water and lower nitrogen content, being closely linked to chlorophyll content[59]. In general, our remotely sensed functional traits are consistent with independent in situ knowledge of the forests in the study region. We could show that functional traits are mapped in the correct range and that our measurement values are compatible with values derived from optical and functional trait databases. To map functional diversity, relative trait values can be used but they need to be measured consistently over space. The proposed remote sensing method has the advantage that it is based on continuous and consistent large-scale measurements without bias due to subjective interpretation or differences in measurement techniques or protocols, which can occur when traits are measured over large areas in the field.

Given the continuous nature of the remotely sensed functional trait maps, we were able to study functional diversity at multiple scales and to develop a highly resolved scaling relationship. The relationship of functional richness and area should be related to the species–area relationship, which is one of the most studied ecological patterns due to its relevance for predicting biodiversity patterns and species extinction rates[53]. Typically, the power-law is used to model species–area relationships resulting in a linear relationship on the log–log scale. Our results are generally consistent between morphological and physiological richness. Furthermore, the slope of the relationship on the log–log scale is very similar to large-scale species models for temperate mixed forests[53]. However, we also found deviations of the relationship from the power-law, as was also reported by Pereira and colleagues for smaller spatial scales[60]. Increased within-community diversity when considering intra-specific variability might explain the steeper slope at small scales, whereas species might be redundant with regard to their functional traits at large scales, leading to a flattening of the log–log relationship. Therefore, we found that a logarithmic function could better predict functional richness than did the power-law.

Deviations from the average can be observed locally, when looking at particular subregions within the test area. Exemplary for a steep transition from low to high functional richness with increasing area is subregion A. Juvenile trees that grow in a disturbed area result in low within and high between community diversity. In this case, underdispersion at local scale might not only be driven by abiotic conditions (e.g. environmental filtering) or anthropogenic influence but also by competitive exclusion[61]. Beech trees might have been planted in disturbed areas or favoured by environmental conditions, or both, but at the same time only the fastest growing beech trees with similar functional traits might have survived and occupied the new space. When

NATURE COMMUNICATIONS | DOI: 10.1038/s41467-017-01530-3 ARTICLE

competing for light, a competitive ability difference leads to the elimination of individuals that grow slowly and are therefore too short to gather enough light[61]. According to Siefert[62], local under-dispersion leads to locally decreased functional divergence and increased divergence between environmental patches. This is in agreement with what we observed in subregion A (Fig. 8).

By comparing functional richness–area relationships of observed with randomly distributed traits, we found trait convergence to be predominant in our forest. However, a general link between community structure and underlying assembly processes can not easily be established, because many processes can lead to trait divergence or convergence, including anthropogenic factors due to certain management strategies. Opposing processes can balance each other and not be disentangled any more[44, 63, 64]. The latter might be the case when looking at the average signal of functional divergence and evenness, which is scale invariant and almost similar to the null model. This, however, does not mean that there is no spatial variation of these two aspects of diversity at all. To study the scale dependency of biodiversity, it is therefore crucial to not only focus on general relationships but also on spatially continuous diversity patterns at different scales.

In conclusion, combined airborne imaging spectroscopy and laser scanning allow for mapping functional diversity continuously across large areas of forest using a trait-based, pixel-level approach. We evaluated the diversity of six key traits at a variety of spatial scales and were able to validate these measurements against in situ data, as well as to assess community structure across an entire landscape. By concentrating on functional traits at a continuous spatial resolution without reference to species identities or individuals, we were able to include intraspecific variability, which is crucial to assess functional diversity of temperate forests and often neglected when functional diversity is indirectly calculated from taxonomic data. Future studies can advance the integration of remotely sensed functional data with databases of plant functional traits, environmental and ecosystem data, and dynamic vegetation models to increase our understanding of the mechanistic linkages between functional diversity and ecosystem function.

To map functional diversity from space and predict global patterns of ecosystem functioning, our method could also be applied to satellite measurements, even though at lower spatial resolution. To test the scalability of our approach we suggest looking at changing extent and grain in a combined fashion. Supplementary Figure 12 indicates how well richness patterns correlate at a given neighbourhood radius when changing grain as pixel size. For example, satellite data at 30 m spatial resolution might be able to capture richness patterns at 200 m radius with a correlation coefficient of 0.7–0.8. This paves the way for possible large-scale applications, but further research is needed to quantify how much small-scale variability would be lost when pixel size is increased, and how this would affect diversity–productivity relationships.

Methods

Study area. The study area is a temperate mixed forest at the Laegern mountain in Switzerland (47° 28′43.0 N, 8° 21′53.2 E). The Laegern is characterized by a mountain ridge spanning in east–west direction with an altitudinal gradient of 450–860 m above sea level (Fig. 1). The extent of the study area is ~2 km × 6 km. In December 1999, the Laegern mountain was affected by a winter storm. The western part of the temperate forest was severely hit, resulting in disturbance areas filling in with beech trees as new stands are initiated. Since forest clear cuts are limited to a maximum area of 0.5 ha, larger patches of juvenile trees likely exist due to the storm. In 2010, the juvenile trees were 10–15 m high and growing in dense patches with a growth rate of around one metre per year[65]. The mainly closed canopy consists of a total of 13 species and seven canopy structure types, from single- to multi-layered canopies[66]. Roughly 70% of the total forested area is covered by deciduous broadleaf trees, whereas the remaining 30% of the area is covered by evergreen coniferous trees (forest inventory data). The dominating deciduous species are common beech (*Fagus sylvatica*), European ash (*Fraxinus excelsior*) and sycamore maple (*Acer pseudoplatanus*). The dominating coniferous species are Norway spruce (*Picea abies*) and silver fir (*Abies alba*). Most of the conifers at Laegern were introduced anthropogenically. Naturally, the whole Laegern forest would be dominated by different hilly to submontane beech communities with few scattered coniferous needle trees. There are mature trees up to 165 years of age, 150 cm of diameter and canopies up to 55 m of height. The study area comprises a reference site for forest ecosystem research with an extensive set of ground measurements[36, 66].

Airborne remote sensing data. The data of the Laegern study area was acquired in 2010 using airborne laser scanning based on the principle of light detection and ranging (LiDAR) and airborne imaging spectroscopy. The LiDAR acquisition was flown on 1 August 2010 using a helicopter-based scanner system with a rotating mirror (RIEGL LMS-Q680i, scan angle ±15°). The campaign was flown under leaf-on conditions with a nominal height of 500 m above ground, resulting in a footprint size of 0.25 m and an average point density of 40 pts/m^2. The 3D point cloud was extracted from the full waveforms of individual laser pulses using Gaussian decomposition. The LiDAR data was registered to the Swiss national grid CH1903+ with a positional accuracy of <0.15 m in vertical and <0.5 m in horizontal direction.

Imaging spectroscopy acquisitions were flown on 26 June and 29 June 2010 under clear sky conditions using the APEX imaging spectrometer[34]. The study area was covered with three flight lines on each of the acquisition dates. The average flight altitude was 4,500 m a.s.l. resulting in an average ground pixel size of 2 m. APEX measured at-sensor radiances in 316 spectral bands ranging from 372 nm to 2,540 nm. APEX data were processed to hemispherical-conical reflectance factors in the APEX Processing and Archiving Facility[67]. Processing started with the raw instrument data, which was split into image, dark current and housekeeping data, thus forming level 0. Level 1 (L1) calibrated radiances were obtained by inverting the instrument model, applying coefficients established during calibration and characterization at the APEX Calibration Home Base[68]. The position and orientation of each pixel in 3D space was based on automatic geocoding in PARGE v3.2[69], using the swissALTI3D digital terrain model. L1 data were then converted to HCRF by employing ATCOR4 v7.0 in the smile aware mode. This essentially accounts for the spectral response function of each individual pixels of the spectrometer to reduce biases due to spectral shifts[34].

Environmental data. Stand polygons of Kanton Aargau and Zurich include forest stand information on development stage, the percentage coverage of the six most dominant species, and the percentage coverage of deciduous broadleaf and coniferous needle trees. The data from Kanton Aargau was provided by Aargauisches Geografisches Informationssystem (AGIS), Departement Bau, Verkehr und Umwelt, Abteilung Wald (last updated on 27 February 2015). The data from Kanton Zurich was provided by Geographisches Informationssystem (GIS-ZH), Amt für Landschaft und Natur, Abteilung Wald (last updated on 16 September 2015). Soil data corresponds to Bodenkarte Baden (Landeskarte der Schweiz 1:25′000, Blatt 1070), provided by Eidgenössische Forschungsanstalt für Agrarökologie und Landbau (FAL).

Topographic variables (altitude, slope, aspect, curvature) were calculated based on the digital terrain model derived from a LiDAR acquisition on 10 April under leaf-off conditions. The campaign was flown with a nominal height of 500 m above ground, resulting in a footprint size of 0.25 m and an average point density of 20 pts/m^2. Radiation was simulated as incoming photosynthetically active radiation at the top of canopy (see Supplementary Note 1 for details). Supplementary Fig. 13 shows a comparison between simulated and measured radiation at the fluxtower in the Laegern forest.

Field data. At the Laegern reference site, field survey was conducted on an area of ~5.5 ha to map the exact ground location and taxonomic identity of all dominant and co-dominant trees (1,307 trees with dbh >20 cm). The positions measured on the ground were linked to a detailed crown map derived from high-resolution drone images. Leaf optical properties of sunlit leaves were measured for ten *Acer pseudoplatanus*, *Fraxinus excelsior*, *Fagus sylvatica*, *Ulmus glabra* and *Tilia platyphyllos* trees in June 2009 and for 50 *Fagus sylvatica* trees in July 2016. For the 50 trees, SPAD measurements were taken of the same leaves. Leaf optical properties and lab measured traits (chlorophyll, carotenoids, EWT) of 168 *Acer pseudoplatanus* trees were used from the ANGERS spectral database.

Functional traits. Functional traits were measured and mapped using state-of-the-art airborne remote sensing methods. A set of three morphological and three physiological traits was selected and mapped based on airborne laser scanning and imaging spectroscopy data respectively. The whole work-flow from remote sensing data to functional diversity measures is illustrated in Supplementary Fig. 14.

We selected CH, PAI and FHD as the three main morphological traits, being of high ecological relevance and measurable using airborne laser scanning methods. CH was measured as the distance between the highest laser return from the canopy and the corresponding ground point following Schneider et al.[36]. PAI was retrieved as the projected surface area of plant material per unit ground area. This includes

woody as well as foliar material, since laser returns from twigs or leaves can not be distinguished. PAI was derived from the LiDAR point cloud data on a 2 × 2 m grid[36, 65]. FHD is a measure of canopy layering and has been recognized as a major functional trait for characterizing biodiversity of a variety of species and habitats[70]. FHD was calculated by applying the Shannon–Wiener diversity index on vertical PAI profiles as described by MacArthur and MacArthur[71]:

$$\mathrm{FHD} = -\sum_i p_i \cdot \log_e p_i, \quad (1)$$

where p_i is the proportion of the total foliage which lies in the ith canopy layer. FHD is a combined measure of how different the layers are with respect to layer density (PAI) and how many layers there are in total. Therefore, a certain correlation to CH can be expected, since the maximum possible number of layers is given by the canopy depth in conjunction with the vertical resolution of the laser system. The three morphological traits were normalized to values between 0 and 1 and resampled to 6 × 6 m spatial resolution using bilinear interpolation, approximating the average basal crown area of the Laegern forest.

Gitelson et al.[72] developed a band specific model to derive CHL and CAR from imaging spectroscopy data in relative units. It has been applied to a wide range of ecosystems, from crops to grasslands and forests[38, 73]. To derive CHL and CAR using the three-band model[72], the following band combinations were used:

$$\mathrm{CHL} = \left(\frac{1}{R_{540-560}} - \frac{1}{R_{760-800}}\right) \cdot R_{760-800}, \quad (2)$$

$$\mathrm{CAR} = \left(\frac{1}{R_{510-520}} - \frac{1}{R_{690-710}}\right) \cdot R_{760-800}, \quad (3)$$

where R_{i-j} is the mean reflectance in the spectral range of i to j nanometre. The model includes anthocyanins as a third pigment[72]. We decided not to include it in our study, since anthocyanins can mainly be observed during leaf development or leaf senescence[38]. Concentrations are generally low during the summer months and are difficult to detect, since the absorption features are strongly overlapping with chlorophyll and carotenoids absorption.

As a third physiological trait, we included EWT. We estimated relative EWT with a simple ratio water content index based on Underwood *et al.*[74]:

$$\mathrm{EWT} = 1 - \frac{R_{1,193}}{R_{1,126}}, \quad (4)$$

where R_i is the reflectance at i nanometre.

To reduce the effects of shadows in the traits retrieval, we combined two airborne imaging spectroscopy acquisitions flown at different times of the day and aggregated 3 × 3 pixels to 6 × 6 m resolution trait data by averaging the three brightest pixels. To fuse the flight lines, we performed an additional geometrical co-registration using scale-invariant feature transform and random sample consensus algorithms of the VLFeat package (VLFeat, sift_mosaic, Matlab). Finally, we normalized to values between 0 and 1.

Estimating physiological forest traits from airborne observations is a challenging task due to the difficulty of linking leaf and canopy level biochemistry. Airborne imaging spectroscopy measures a spatially integrated signal of the sunlit upper canopy of the forest. The mapping of functional diversity relies on relative trait values being derived from these consistent radiometric measurements. The relationship of relative trait values and their physical counterparts can be demonstrated by parametrizing the radiometric simulation of selected species with field data and generic data from two functional trait databases. The ranges of physiological traits were compared with modelled trait ranges based on the leaf optical properties measured in the field in July 2009 (Supplementary Fig. 6). The same modelling framework as in ref. [36] was used to simulate canopy reflectance spectra and subsequently derive physiological traits. Constant optical properties for broadleaf and needle trees were expected to result in a narrower trait range due to the lack of intra- and inter-specific trait variability within functional groups. For further details on the modelling approach, see Supplementary Note 2.

Field data of the 5.5 ha area at Laegern was used to calculate community-weighted mean chlorophyll and EWT. Species abundances and mean traits were calculated per 30 × 30 m plot. Remotely sensed mean trait values were then compared to community-weighted means of the functional trait database TRY[29], based on the plot-level species abundances and species-level trait values from TRY (Supplementary Fig. 7). There were not enough measurements in the TRY database to calculate community-weighted means of carotenoids.

To illustrate the scalability of the spectral indices from the leaf to the canopy level, we used the field data to simulate canopy reflectances for the 518 *Fagus sylvatica* and the 168 *Acer pseudoplatanus* trees on the 5.5 ha area. We used the leaf optical properties of 50 *Fagus sylvatica* trees measured in July 2016, and randomly distributed them over the 518 *Fagus sylvatica* trees according to field survey. Chlorophyll values were then derived from the reflectance spectra at leaf and canopy level, to be compared to the SPAD measurements of the same leaves (Supplementary Fig. 8). Additionally, we simulated canopy spectra for the 168 *Acer pseudoplatanus* trees with leaf optical properties of the ANGERS database. Lab measurements of chlorophyll, carotenoids and EWT from the database were then compared to traits estimated using spectral indices at leaf and canopy level (Supplementary Fig. 9). Since we did not expect very high carotenoids concentrations at Laegern in summer, we fitted a second linear regression in Supplementary Fig. 9c, d for values below 15 µg/m^2. For further details on the modelling approach, see Supplementary Note 2.

For mapping in Fig. 3, we used red, green and blue (RGB) colour composites of the three normalized morphological and physiological traits respectively. We define blue areas in the morphological trait map as values of CH<0.5, FHD<0.5 and PAI>0.5, pink areas as CH>0.5, FHD>0.5 and PAI>0.5, and green areas as CH<0.5, FHD>0.3, PAI<0.5. A small area appearing yellow is defined by CH>0.7, FHD>0.7 and PAI<0.6. In the physiological trait map, we define blue areas as values of CHL<0.5, CAR<0.5 and EWT>0.5, bright green areas as CHL>0.8, CAR>0.5 and EWT<0.5, and green areas as CHL>0.5, CAR<0.5 and EWT<0.5. Orange areas are characterized by CHL<0.7, CAR>0.7 and EWT<0.5.

The forested area was determined based on CH. To derive the forest mask, we first applied a threshold of 10 m CH to select the mature forest pixels and remove possible agricultural fields. We then filled the gaps within the forest to include juvenile forest patches again. Finally, a threshold of 4 m CH was applied to remove gaps and understorey vegetation. We defined a tree to be four or more metres high, as was done in Schneider et al.[36] to separate understorey and the canopy.

Functional diversity. Having tens to hundreds of thousands of pixels to map is computationally demanding, guiding our choice of index. As a consequence, we selected functional richness, divergence and evenness being computationally manageable and relatively easy to interpret, since different aspects of functional diversity are covered by separate indices. The indices for functional richness, divergence and evenness were calculated based on the remote sensing derived physiological and morphological traits. We mapped pixels within a certain radial neighbourhood in the functional trait space, using a moving window approach with varying neighbourhoods to cover the whole study area. Figure 2 shows an example of functional richness, evenness and divergence calculated based on pixels in a radius of 120 m mapped in trait space. Abundance weighting is not needed since every pixel represents a set of trait measurements, not averaged by communities or species. With continuous area-based data, however, a single pixel does not necessarily cover an individual crown. Contributions of more than one individual or species to the functional traits of a singular pixel is possible and therefore represents no direct link to species. Detailed information on the three indices and pixel based application is given in the following paragraphs.

Functional richness is a measure of niche extent, where niche is the functional space occupied by a species, community or assemblage of trees. It was calculated by mapping pixels of a certain neighbourhood in functional space, whose axes are defined by the functional traits. Richness was then calculated as the convex hull volume of the mapped pixels (convhull, Matlab). Supplementary Figure 15 illustrates an artificial example of an increasing functional richness from 0.17 to 0.31.

Since we assign equal weighting to all pixels (no abundances), we calculated divergence (FDiv) based on Villéger et al.[41] as follows:

$$\Delta|d| = \sum_{i=1}^{S} \frac{1}{S} \cdot |dG_i - \overline{dG}|, \quad (5)$$

$$\mathrm{FDiv} = \frac{\overline{dG}}{\Delta|d| + \overline{dG}}, \quad (6)$$

where S is the number of pixels mapped in the functional space, dG_i is the Euclidean distance between the ith pixel and the centre of gravity and $\overline{dG}$ is the mean distance of all pixels to the centre of gravity. In this specific case, a functional divergence of 1 would mean that all pixels lie on a sphere with equal distance to the centre of gravity (Supplementary Fig. 15).

The functional evenness index (FEve) was calculated based on the minimum spanning tree (Fig. 2). A distance matrix with Euclidean distances between all the points in the functional space was the basis for deriving the minimum spanning tree using the algorithm of Prim[75] (graphminspantree, Matlab). Finally, evenness was calculated following Villéger et al.[41]:

$$\mathrm{PEW}_l = \frac{\mathrm{EW}_l}{\sum_{l=1}^{S-1} \mathrm{EW}_l}, \quad (7)$$

$$\mathrm{FEve} = \frac{\sum_{l=1}^{S-1} \min\left(\mathrm{PEW}_l, \frac{1}{S-1}\right) - \frac{1}{S-1}}{1 - \frac{1}{S-1}}, \quad (8)$$

where EW_l is the Euclidean distance of branch l in the minimum spanning tree, PEW is the partial weighted evenness and S is the number of pixels mapped in the functional space. Thus S–1 corresponds to the number of branches in the minimum spanning tree. A weighting by species abundance is not necessary when mapping pixels, since abundance is inherent in the data (Supplementary Fig. 15).

NATURE COMMUNICATIONS | DOI: 10.1038/s41467-017-01530-3 ARTICLE

Scaling. To calculate the functional diversity indices for the whole forest, we used a moving window approach (Supplementary Fig. 16). This means that the index values were calculated for each pixel by iterating through all pixels of the functional trait maps. Since diversity is always measured within a certain geographical unit, we used a radial neighbourhood of pixels to calculate the indices. Therefore, the initial pixel size of 6 × 6 m of the functional trait maps corresponds to the grain, whereas the neighbourhood of pixels corresponds to the extent (Supplementary Fig. 16). We calculated the diversity indices for an increasing neighbourhood of 6–1,020 m radius with steps of 6 m, resulting in an extent ranging from 113 to 3.27×10^6 m^2. To derive diversity–area curves, we averaged the index values of all forested pixels for each of the 170 extents. For display in Figs. 5–7 and visual assessment, we applied a circular averaging filter (fspecial, disk, Matlab).

Null models. We created a null model of randomly distributed trees, or here pixels, to test if the functional traits distribution follows a random distribution, over- or under-dispersion. For each tree or pixel, we kept the traits relationship among the three morphological and physiological traits constant. We then reshuffled the pixels to create random distribution in geographic space (rand, Matlab). Opposed to randomly distribute each trait individually, the trait relationships still hold in the null model. However, there is no spatial autocorrelation any more.

A second null model is used to simulate maximal under-dispersion, which could be resulting from maximal environmental filtering. In this case, we assume that neighbouring pixels in geographic space are also neighbours in functional trait space. For each pixel, it is not the neighbouring pixels in a certain radius which are used to calculate the diversity indices. Instead, the same number of neighbouring pixels are selected from the trait space according to minimal Euclidean distance. This results in a purely theoretical null model, where closest neighbours in geographic space would be closest neighbours in trait space.

Statistical analysis. We tested whether patterns of functional traits and trait diversity can be explained by abiotic factors related to topography, soil and radiation (see Supplementary Fig. 4 and Supplementary Table 1). To account for spatial autocorrelation, we used a spatially simultaneous autoregressive error model estimation based on first order neighbours (R package spdep, errorsarlm[76]) to fit a generalized linear model.

Subsequent analysis of variance (ANOVA) with type-I sum of squares was performed at 60 m radius scale. The forest was sampled using 467 pixels projected on a regular grid such that their circular neighbourhood areas did not overlap and remained fully within forest boundaries. Continuous explanatory variables were averaged within 60 m radius, whereas simple majority was used for categorical variables. Continuous explanatory variables were altitude, slope, soil depth and amount of rocky materials. The categorical variable aspect was subdivided in three categories, namely north, south and flat slopes. Curvature was grouped in categories valley, ridge and flat areas. Soil type consisted of eight soil classes (*Dystric Cambisols*, *Luvisols*, *Endogleyic Cambisols*, *Stagnic Cambisols*, *Cambisols*, *Calcic Cambisols*, *Leptosols* and *Regosols*, see Supplementary Fig. 5). Supplementary Figure 4 shows the variance explained based on type-I sum of squares of soil (top panels) and topography (bottom panels), as well as additionally explained factors when adding topography or soil, and radiation to the model. Within groups, the order of the explanatory variables was kept constant. For Supplementary Table 1, the order of the explanatory variables related to topography were determined by the significance when tested individually, with the most significant used first in the combined model.

Data availability. The data that support the findings of this study are available from the corresponding author upon reasonable request. An example of the airborne laser scanning and imaging spectroscopy data is available at http://www.geo.uzh.ch/microsite/3dveglab/eod/ for a subset of 300 × 300 m. Community and soil data has to be requested directly from the Swiss cantons Zurich or Aargau.

Received: 30 September 2016 Accepted: 25 September 2017
Published online: 13 November 2017

References

1. Roscher, C. et al. A functional trait-based approach to understand community assembly and diversity-productivity relationships over 7 years in experimental grasslands. *Perspect. Plant Ecol., Evol. Syst.* **15**, 139–149 (2013).
2. Mouillot, D., Graham, N. A., Villéger, S., Mason, N. W. & Bellwood, D. R. A functional approach reveals community responses to disturbances. *Trends Ecol. Evol.* **28**, 167–177 (2013).
3. Calba, S., Maris, V. & Devictor, V. Measuring and explaining large-scale distribution of functional and phylogenetic diversity in birds: separating ecological drivers from methodological choices. *Glob. Ecol. Biogeogr.* **23**, 669–678 (2014).
4. Fründ, J., Dormann, C. F., Holzschuh, A. & Tscharntke, T. Bee diversity effects on pollination depend on functional complementarity and niche shifts. *Ecology* **94**, 2042–2054 (2013).
5. Gotelli, N. J. & Colwell, R. K. Quantifying biodiversity: procedures and pitfalls in the measurement and comparison of species richness. *Ecol. Lett.* **4**, 379–391 (2001).
6. Violle, C., Reich, P. B., Pacala, S. W., Enquist, B. J. & Kattge, J. The emergence and promise of functional biogeography. *Proc. Natl Acad. Sci. USA* **111**, 13690–13696 (2014).
7. Violle, C. et al. Let the concept of trait be functional! *Oikos* **116**, 882–892 (2007).
8. Liu, X. et al. Linking individual-level functional traits to tree growth in a subtropical forest. *Ecology* **97**, 2396–2405 (2016).
9. Sakschewski, B. et al. Resilience of amazon forests emerges from plant trait diversity. *Nat. Clim. Change* **6**, 1032–1036 (2016).
10. Hooper, D. U. et al. Effects of biodiversity on ecosystem functioning: a consensus of current knowledge. *Ecol. Monogr.* **75**, 3–35 (2005).
11. Balvanera, P. et al. Quantifying the evidence for biodiversity effects on ecosystem functioning and services. *Ecol. Lett.* **9**, 1146–1156 (2006).
12. Cardinale, B. J. et al. The functional role of producer diversity in ecosystems. *Am. J. Bot.* **98**, 572–592 (2011).
13. Barrufol, M. et al. Biodiversity promotes tree growth during succession in subtropical forest. *PLoS ONE* **8**, e81246 (2013).
14. Liang, J. et al. Positive biodiversity-productivity relationship predominant in global forests. *Science* **354**, aaf8957 1–12 (2016).
15. Hillebrand, H., Bennett, D. M. & Cadotte, M. W. Consequences of dominance: a review of evenness effects on local and regional ecosystem processes. *Ecology* **89**, 1510–1520 (2008).
16. Cadotte, M. W., Carscadden, K. & Mirotchnick, N. Beyond species: functional diversity and the maintenance of ecological processes and services. *J. Appl. Ecol.* **48**, 1079–1087 (2011).
17. Zhang, Y., Chen, H. Y. H. & Reich, P. B. Forest productivity increases with evenness, species richness and trait variation: a global meta-analysis. *J. Ecol.* **100**, 742–749 (2012).
18. Williams, L. J., Paquette, A., Cavender-Bares, J., Messier, C. & Reich, P. B. Spatial complementarity in tree crowns explains overyielding in species mixtures. *Nat. Ecol. Evol.* **1**, 63 (2017).
19. Chamagne, J. et al. Forest diversity promotes individual tree growth in central european forest stands. *J. Appl. Ecol.* **54**, 71–79 (2017).
20. Ruiz-Benito, P. et al. Functional diversity underlies demographic responses to environmental variation in european forests. *Glob. Ecol. Biogeogr.* **26**, 128–141 (2017).
21. McGill, B. J., Enquist, B. J., Weiher, E. & Westoby, M. Rebuilding community ecology from functional traits. *Trends Ecol. Evol.* **21**, 178–185 (2006).
22. Cianciaruso, M. V., Batalha, M. A., Gaston, K. J. & Petchey, O. L. Including intraspecific variability in functional diversity. *Ecology* **90**, 81–89 (2009).
23. Petchey, O. L. & Gaston, K. J. Functional diversity (fd), species richness and community composition. *Ecol. Lett.* **5**, 402–411 (2002).
24. Laughlin, D. C., Joshi, C., van Bodegom, P. M., Bastow, Z. A. & Fulé, P. Z. A predictive model of community assembly that incorporates intraspecific trait variation. *Ecol. Lett.* **15**, 1291–1299 (2012).
25. Luo, Y.-H. et al. Trait-based community assembly along an elevational gradient in subalpine forests: quantifying the roles of environmental factors in inter- and intraspecific variability. *PLoS ONE* **11**, 1–20 (2016).
26. Ferretti, M. & Fischer, R. *Forest Monitoring: Methods for Terrestrial Investigations in Europe with an Overview of North America and Asia*, *vol. 12 of Developments in Environmental Science* (UK, Elsevier Science, 2013).
27. Bussotti, F., Pollastrini, M., Holland, V. & Brüggemann, W. Functional traits and adaptive capacity of European forests to climate change. *Environ. Exp. Bot.* **111**, 91–113 (2015).
28. Pérez-Harguindeguy, N. et al. New handbook for standardised measurement of plant functional traits worldwide. *Aust. J. Bot.* **61**, 167–234 (2013).
29. Kattge, J. et al. TRY-a global database of plant traits. *Glob. Change Biol.* **17**, 2905–2935 (2011).
30. Li, X., Pei, K., Kéry, M., Niklaus, P. A. & Schmid, B. Decomposing functional trait associations in a chinese subtropical forest. *PLoS ONE* **12**, e0175727 (2017).
31. Jetz, W. et al. Monitoring plant functional diversity from space. *Nat. Plants* **2**, 1–5 (2016).
32. Gray, A. Monitoring stand structure in mature coastal douglas-fir forests: effect of plot size. *For. Ecol. Manag.* **175**, 1–16 (2003).
33. Homolová, L., Malenovský, Z., Clevers, J. G., García-Santos, G. & Schaepman, M. E. Review of optical-based remote sensing for plant trait mapping. *Ecol. Complex.* **15**, 1–16 (2013).
34. Schaepman, M. E. et al. Advanced radiometry measurements and earth science applications with the airborne prism experiment (apex). *Remote Sens. Environ.* **158**, 207–219 (2015).
35. Asner, G. P. et al. Airborne laser-guided imaging spectroscopy to map forest trait diversity and guide conservation. *Science* **355**, 385–389 (2017).
36. Schneider, F. D. et al. Simulating imaging spectrometer data: 3d forest modeling based on lidar and in situ data. *Remote Sens. Environ.* **152**, 235–250 (2014).

37. Ishii, H. T., Tanabe, S.-i & Hiura, T. Exploring the relationships among canopy structure, stand productivity, and biodiversity of temperate forest ecosystems. *For. Sci.* **50**, 342–355 (2004).
38. Ustin, S. L. et al. Retrieval of foliar information about plant pigment systems from high resolution spectroscopy. *Remote Sens. Environ.* **113**, S67–S77 (2009).
39. Lawlor, D. W. & Cornic, G. Photosynthetic carbon assimilation and associated metabolism in relation to water deficits in higher plants. *Plant Cell Environ.* **25**, 275–294 (2002).
40. Mason, N. W. H., Mouillot, D., Lee, W. G. & Wilson, J. B. Functional richness, functional evenness and functional divergence: the primary components of functional diversity. *Oikos* **111**, 112–118 (2005).
41. Villéger, S., Mason, N. W. H. & Mouillot, D. New multidimensional functional diversity indices for a multifaceted framework in functional ecology. *Ecology* **89**, 2290–2301 (2008).
42. Salles, J. F., Poly, F., Schmid, B. & Roux, X. L. Community niche predicts the functioning of denitrifying bacterial assemblages. *Ecology* **90**, 3324–3332 (2009).
43. Letts, B., Lamb, E. G., Mischkolz, J. M. & Romo, J. T. Litter accumulation drives grassland plant community composition and functional diversity via leaf traits. *Plant Ecol.* **216**, 357–370 (2015).
44. van der Plas, F. et al. A new modeling approach estimates the relative importance of different community assembly processes. *Ecology* **96**, 1502–1515 (2015).
45. Silva Pedro, M., Rammer, W. & Seidl, R. Disentangling the effects of compositional and structural diversity on forest productivity. *J. Veg. Sci.* **28**, 649–658 (2017).
46. Bohn, F. J. & Huth, A. The importance of forest structure to biodiversity-productivity relationships. *R. Soc. Open Sci.* **4**, 160521 (2017).
47. Forrester, D. I. & Bauhus, J. A review of processes behind diversity-productivity relationships in forests. *Curr. For. Rep.* **2**, 45–61 (2016).
48. Asner, G. P. et al. Amazonian functional diversity from forest canopy chemical assembly. *Proc. Natl Acad. Sci. USA* **111**, 5604–5609 (2014).
49. Martin, R. E., Asner, G. P. & Sack, L. Genetic variation in leaf pigment, optical and photosynthetic function among diverse phenotypes of Metrosideros polymorpha grown in a common garden. *Oecologia* **151**, 387–400 (2007).
50. Biswas, S. R., Mallik, A. U., Braithwaite, N. T. & Wagner, H. H. A conceptual framework for the spatial analysis of functional trait diversity. *Oikos* **125**, 192–200 (2015).
51. Mori, A. S., Furukawa, T. & Sasaki, T. Response diversity determines the resilience of ecosystems to environmental change. *Biol. Rev.* **88**, 349–364 (2013).
52. Karadimou, E. K., Kallimanis, A. S., Tsiripidis, I. & Dimopoulos, P. Functional diversity exhibits a diverse relationship with area, even a decreasing one. *Sci. Rep.* **6**, 35420 (2016).
53. Gerstner, K., Dormann, C. F., Václavík, T., Kreft, H. & Seppelt, R. Accounting for geographical variation in species-area relationships improves the prediction of plant species richness at the global scale. *J. Biogeogr.* **41**, 261–273 (2014).
54. Petchey, O. L. & Gaston, K. J. Functional diversity: back to basics and looking forward. *Ecol. Lett.* **9**, 741–758 (2006).
55. Mouchet, M. A., Villéger, S., Mason, N. W. H. & Mouillot, D. Functional diversity measures: an overview of their redundancy and their ability to discriminate community assembly rules. *Funct. Ecol.* **24**, 867–876 (2010).
56. Albert, C. H. et al. A multi-trait approach reveals the structure and the relative importance of intra- vs. interspecific variability in plant traits. *Funct. Ecol.* **24**, 1192–1201 (2010).
57. Dimitrakopoulos, P. G. & Schmid, B. Biodiversity effects increase linearly with biotope space. *Ecol. Lett.* **7**, 574–583 (2004).
58. Bond, B. J. Age-related changes in photosynthesis of woody plants. *Trends Plant Sci.* **5**, 349–353 (2000).
59. Huber, S., Kneubühler, M., Psomas, A., Itten, K. & Zimmermann, N. E. Estimating foliar biochemistry from hyperspectral data in mixed forest canopy. *For. Ecol. Manag.* **256**, 491–501 (2008).
60. Pereira, H. M., Borda-de Água, L. & Martins, I. S. Geometry and scale in species-area relationships. *Nature* **482**, E3–E4 (2012).
61. Mayfield, M. M. & Levine, J. M. Opposing effects of competitive exclusion on the phylogenetic structure of communities. *Ecol. Lett.* **13**, 1085–1093 (2010).
62. Siefert, A. Spatial patterns of functional divergence in old-field plant communities. *Oikos* **121**, 907–914 (2012).
63. Botta-Dukát, Z. & Czúcz, B. Testing the ability of functional diversity indices to detect trait convergence and divergence using individual-based simulation. *Methods Ecol. Evol.* **7**, 114–126 (2016).
64. Chacón-Labella, J., de la Cruz, M., Pescador, D. S. & Escudero, A. Individual species affect plant traits structure in their surroundings: evidence of functional mechanisms of assembly. *Oecologia* **180**, 975–987 (2016).
65. Schneider, F. D., et al. in *Proc. SilviLaser 2015*, 14th *Conference on Lidar Applications for Assessing and Managing Forest Ecosystems* (eds Durrieu, S. & Véga, C.) (La Grande Motte, France, 2015).
66. Leiterer, R., Furrer, R., Schaepman, M. E. & Morsdorf, F. Forest canopy-structure characterization: a data-driven approach. *For. Ecol. Manag.* **358**, 48–61 (2015).
67. Hueni, A. et al. Structure, components, and interfaces of the airborne prism experiment (apex) processing and archiving facility. *IEEE Trans. Geosci. Remote Sens.* **47**, 29–43 (2009).
68. Hueni, A., Lenhard, K., Baumgartner, A. & Schaepman, M. E. Airborne prism experiment calibration information system. *IEEE Trans. Geosci. Remote Sens.* **51**, 5169–5180 (2013).
69. Schläpfer, D. & Richter, R. Geo-atmospheric processing of airborne imaging spectrometry data. Part 1: parametric orthorectification. *Int. J. Remote Sens.* **23**, 2609–2630 (2002).
70. August, P. V. The role of habitat complexity and heterogeneity in structuring tropical mammal communities. *Ecology* **64**, 1495–1507 (1983).
71. MacArthur, R. & MacArthur, J. On bird species diversity. *Ecology* **42**, 595–599 (1961).
72. Gitelson, A. A., Keydan, G. P. & Merzlyak, M. N. Three-band model for noninvasive estimation of chlorophyll, carotenoids, and anthocyanin contents in higher plant leaves. *Geophys. Res. Lett.* **33**, 1–5 (2006).
73. Viña, A. Evaluating vegetation indices for assessing productivity along a tropical rain forest chronosequence in western amazonia. *Israel J. Plant Sci.* **60**, 123–133 (2012).
74. Underwood, E., Ustin, S. & DiPietro, D. Mapping nonnative plants using hyperspectral imagery. *Remote Sens. Environ.* **86**, 150–161 (2003).
75. Prim, R. C. Shortest connection networks and some generalizations. *Bell Syst. Tech. J.* **36**, 1389–1401 (1957).
76. Bivand, R. & Piras, G. Comparing implementations of estimation methods for spatial econometrics. *J. Stat. Softw.* **63**, 1–36 (2015).

Acknowledgements

This study has been supported by the University of Zurich Research Priority Program on Global Change and Biodiversity (URPP GCB). The research carried out at the Jet Propulsion Lab, California Institute of Technology, was under a contract with the NationalAeronautics and Space Administration. Government sponsorship is acknowledged. Part of the work is based on output from the working group of the National Center for Ecological Analysis and Synthesis on 'Prospects and priorities for satellite monitoring of global terrestrial biodiversity'. Data processing was supported by S3IT (University of Zurich), with assistance of Riccardo Murri and Sergio Maffioletti. We thank Carla Guillén Escribà, Irene Garonna, Walter Jetz, Reinhard Furrer, Meinrad Abegg and Daniel Kükenbrink for fruitful discussions on aspects of the manuscript.

Author contributions

F.D.S., F.M., B.S., O.L.P., and M.E.S. designed research; F.D.S., B.S., and M.E.S. performed research; F.D.S., F.M., A.H., and M.E.S. analysed data; and F.D.S., F.M., B.S., O.L. P., A.H., D.S.S. and M.E.S. wrote the paper.

Additional information

Supplementary Information accompanies this paper at doi:10.1038/s41467-017-01530-3.

Competing interests: The authors declare no competing financial interests.

Reprints and permission information is available online at http://npg.nature.com/reprintsandpermissions/

Publisher's note: Springer Nature remains neutral with regard to jurisdictional claims in published maps and institutional affiliations.

3.2 Supplementary Information

3.2.1 Supplementary Note 1. Simulating the radiative budget using the 3D radiative transfer model DART

Radiation was simulated as incoming photosynthetically active radiation (PAR) in the range of 400 - 700 nm at top of canopy. The simulation was performed using the 3D coupled canopy-atmosphere radiative transfer model DART (Gastellu-Etchegorry *et al.*, 2015) according to clear sky atmospheric conditions for a rural aerosol model with a visibility of 23 km. The whole Laegern forest was represented as 3D voxel grid with 2 m voxel side length in DART following the parametrisation of Schneider *et al.* (2014). Mean daily incoming radiation of 2010 was approximated by deriving the total amount of incoming radiation for 8 days during the year, of which each day was simulated with nine sun angles and a 4th order polynomial to integrate the radiation over the whole day. A comparison to the fluxtower based on global radiation on 26 June 2010 shows a good agreement between simulated and measured values (Supplementary Fig. 13).

3.2.2 Supplementary Note 2. Simulating canopy spectra using the 3D radiative transfer model DART

To assess the applicability of spectral indices from the leaf to the canopy level, we modelled canopy spectra with the 3D radiative transfer model DART (Gastellu-Etchegorry *et al.*, 2015). The DART model was parametrised following Schneider *et al.* (2014) with a 3D description of the forest canopy at Laegern based on airborne laser scanning data. A scene of 400 x 400 m was simulated to cover the 5.5 ha Laegern core site and a buffer area to avoid any border effects at the edges of the site. The simulations were performed with 2 m spatial resolution based on the spectral band definitions, illumination and viewing geometry of the two imaging spectrometer acquisitions on 26 and 29 June 2010. The simulated ortho-images of canopy reflectance were combined and aggregated to 6 m spatial resolution to reduce shadow effects, following the same approach as applied to the imaging spectrometer data (see Methods of main manuscript).

References

Gastellu-Etchegorry JP, Yin T, Lauret N, *et al.* (2015) Discrete Anisotropic Radiative Transfer (DART 5) for Modeling Airborne and Satellite Spectroradiometer and LIDAR Acquisitions of Natural and Urban Landscapes. *Remote Sensing*, **7**, 1667–1701.

Schneider FD, Leiterer R, Morsdorf F, Gastellu-Etchegorry JP, Lauret N, Pfeifer N, Schaepman ME (2014) Simulating imaging spectrometer data: 3d forest modeling based on lidar and in situ data. *Remote Sensing of Environment*, **152**, 235–250.

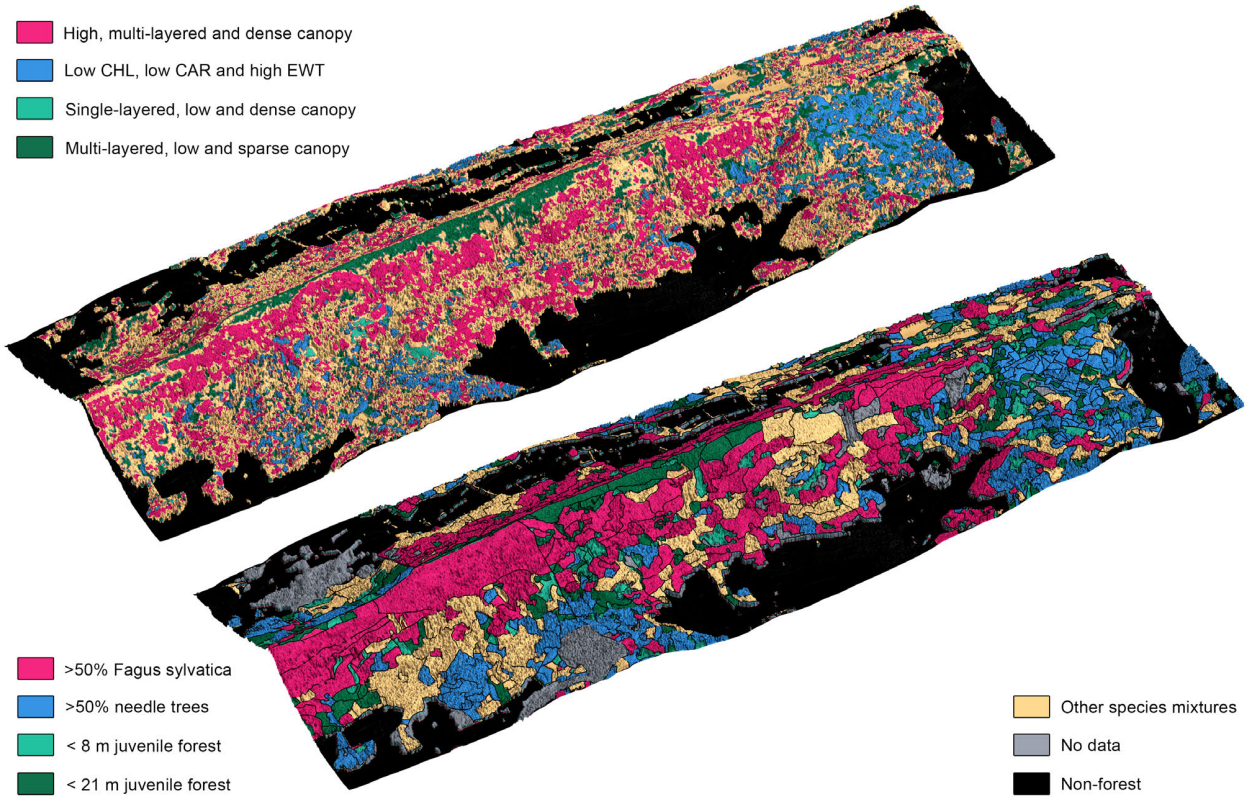

Supplementary Figure 1: Maps showing trait classes based on remotely sensed morphological and physiological traits and stand polygons of the state government (Kt. AG + ZH). The trait classes shown here in pink, turquoise and green are based on canopy height (CH), layering (FHD) and density (PAI), whereas the class shown in blue is based on chlorophyll (CHL), carotenoids (CAR) and equivalent water thickness (EWT).

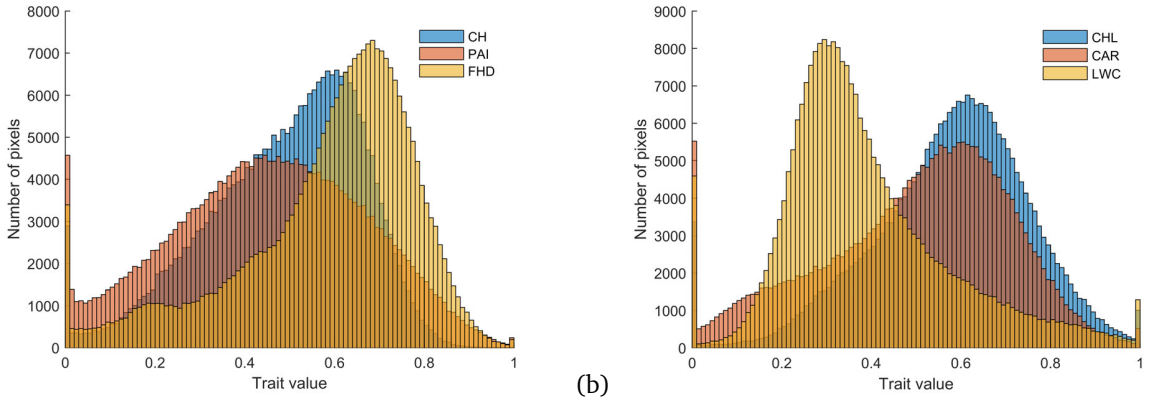

(a) (b)

Supplementary Figure 2: Frequency distributions of (a) morphological traits canopy height (CH), plant area index (PAI), and foliage height diversity (FHD) and (b) physiological traits chlorophyll (CHL), carotenoids (CAR), and equivalent water thickness (EWT).

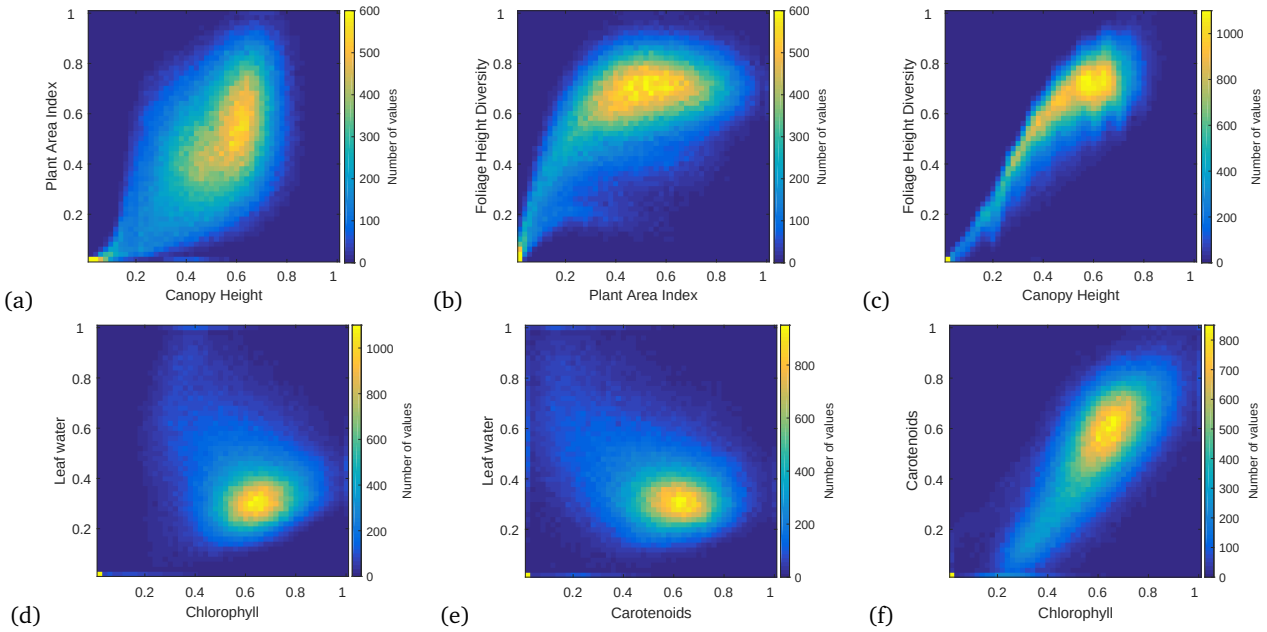

Supplementary Figure 3: Trait correlations among the morphological traits plant area index, canopy height and foliage height diversity (a-e) and among the physiological traits leaf water, chlorophyll and carotenoids (d-f).

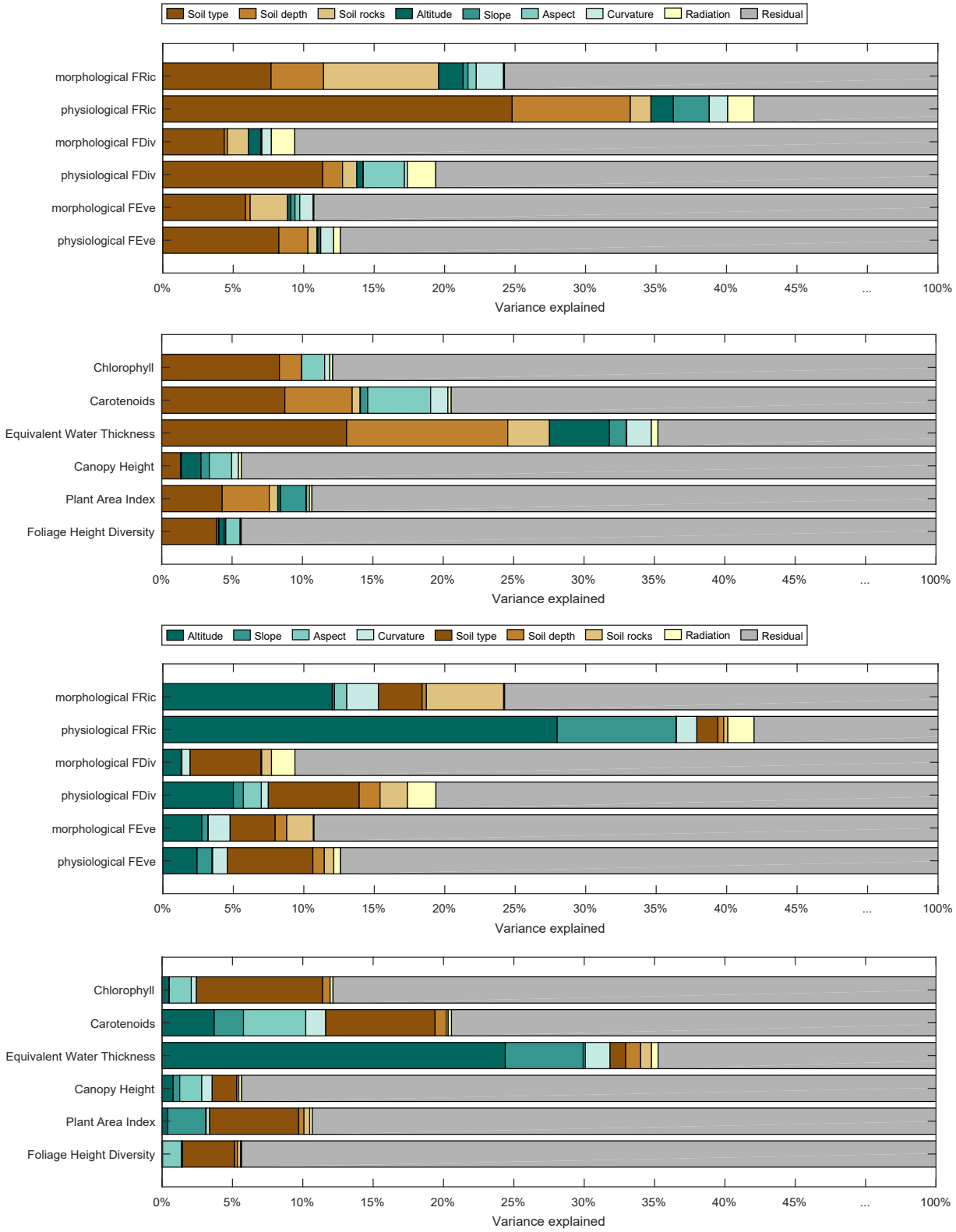

Supplementary Figure 4: Amount of variance in functional diversity and functional traits explained by soil (soil type, soil depth, amount of rocky material), topography (altitude, slope, aspect, curvature) and radiation (mean daily photosynthetically active radiation). The order of the legend corresponds to the order in the ANOVA type I, with soil variables first (upper panel) and topographic variables first (lower panel). The independent variables used in the ANOVA are shown in Supplementary Fig. 5

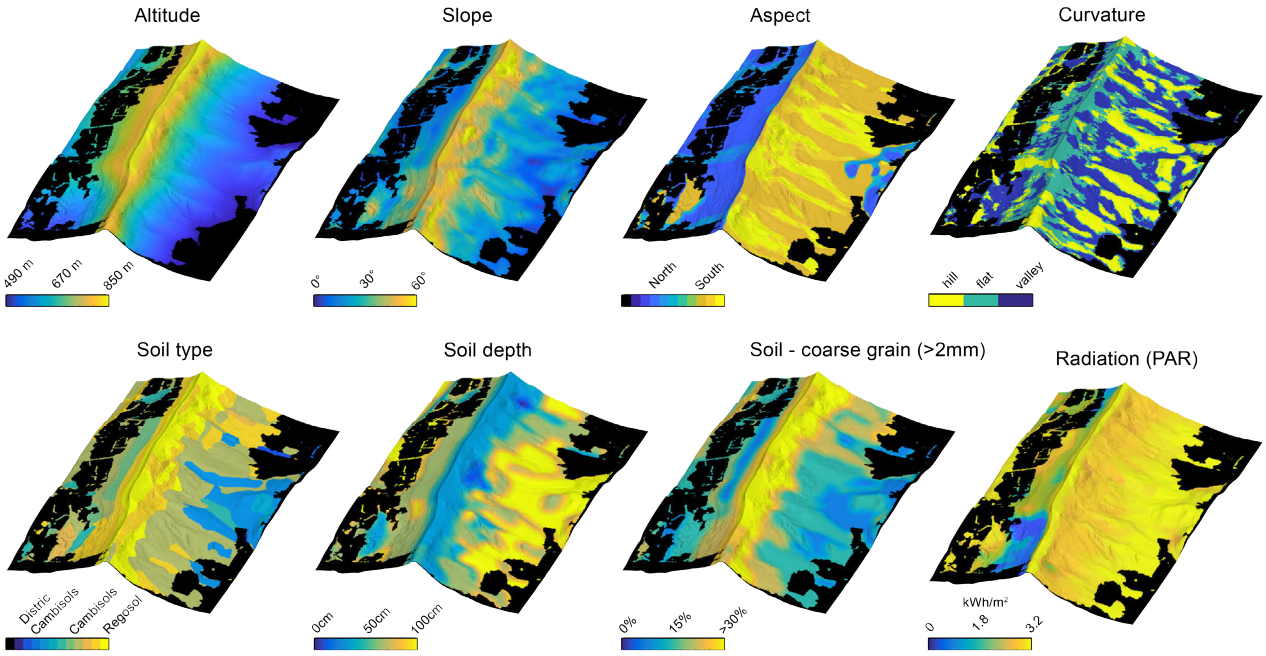

Supplementary Figure 5: Environmental variables covering the western part of the study area. Altitude, slope, soil depth, amount of coarse grain material in the soil and radiation (mean daily PAR, see Supplementary Note 1) are continuous variables, averaged at 60 m radius for use in an ANOVA (see Statistical analysis in Methods of main manuscript). Aspect, curvature and soil type are categorical variables. Soil type consists of 8 classes, whereas Distric Cambisols (blue), Cambisols (olive) and Regosol (yellow) are among the most abundant soils.

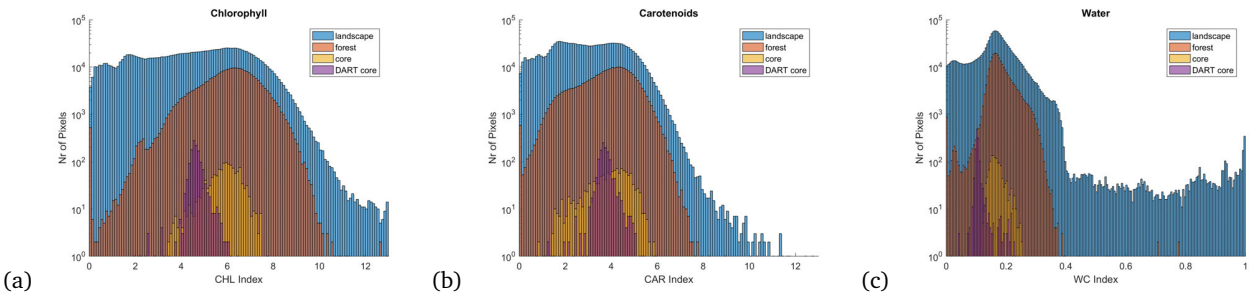

Supplementary Figure 6: Observed trait ranges derived from imaging spectroscopy at landscape level (including agricultural fields), at forest level (whole Laegern), and at a core site of 1307 trees on 5.5 ha for (a) chlorophyll, (b) carotenoids, and (c) equivalent water thickness. The figures show a comparison to modelled trait ranges at the core site using the 3D radiative transfer model DART. The modelled ranges are narrower since constant leaf optical properties were used for broadleaf and needle trees.

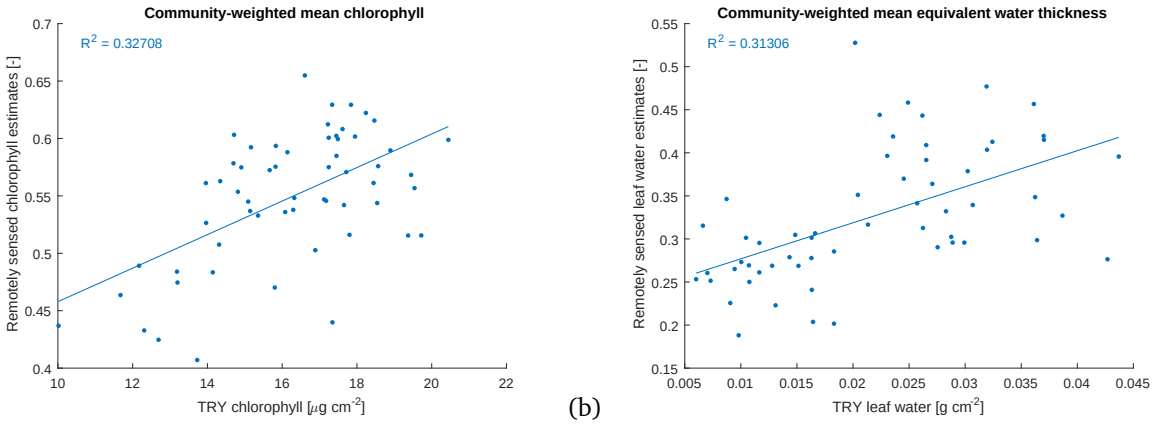

(a) (b)

Supplementary Figure 7: Community-weighted mean (a) chlorophyll and (b) equivalent water thickness of 13 deciduous broadleaf and evergreen coniferous tree species at the 5.5 ha core site compared to trait values calculated based on the functional trait database TRY.

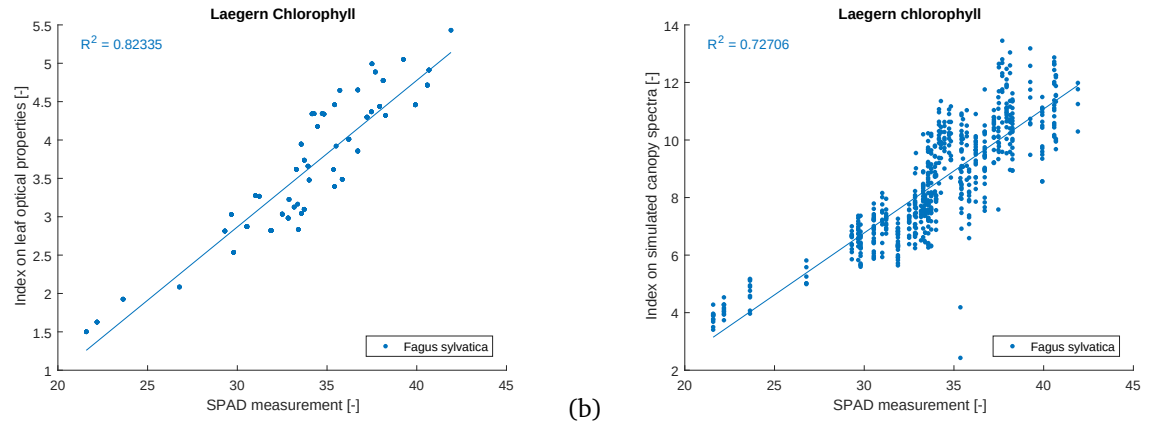

(a) (b)

Supplementary Figure 8: SPAD measurements of 50 *Fagus sylvatica* trees at the 5.5 ha core site compared to corresponding chlorophyll estimates as derived applying a spectral index on (a) leaf optical properties and (b) modelled canopy spectra.

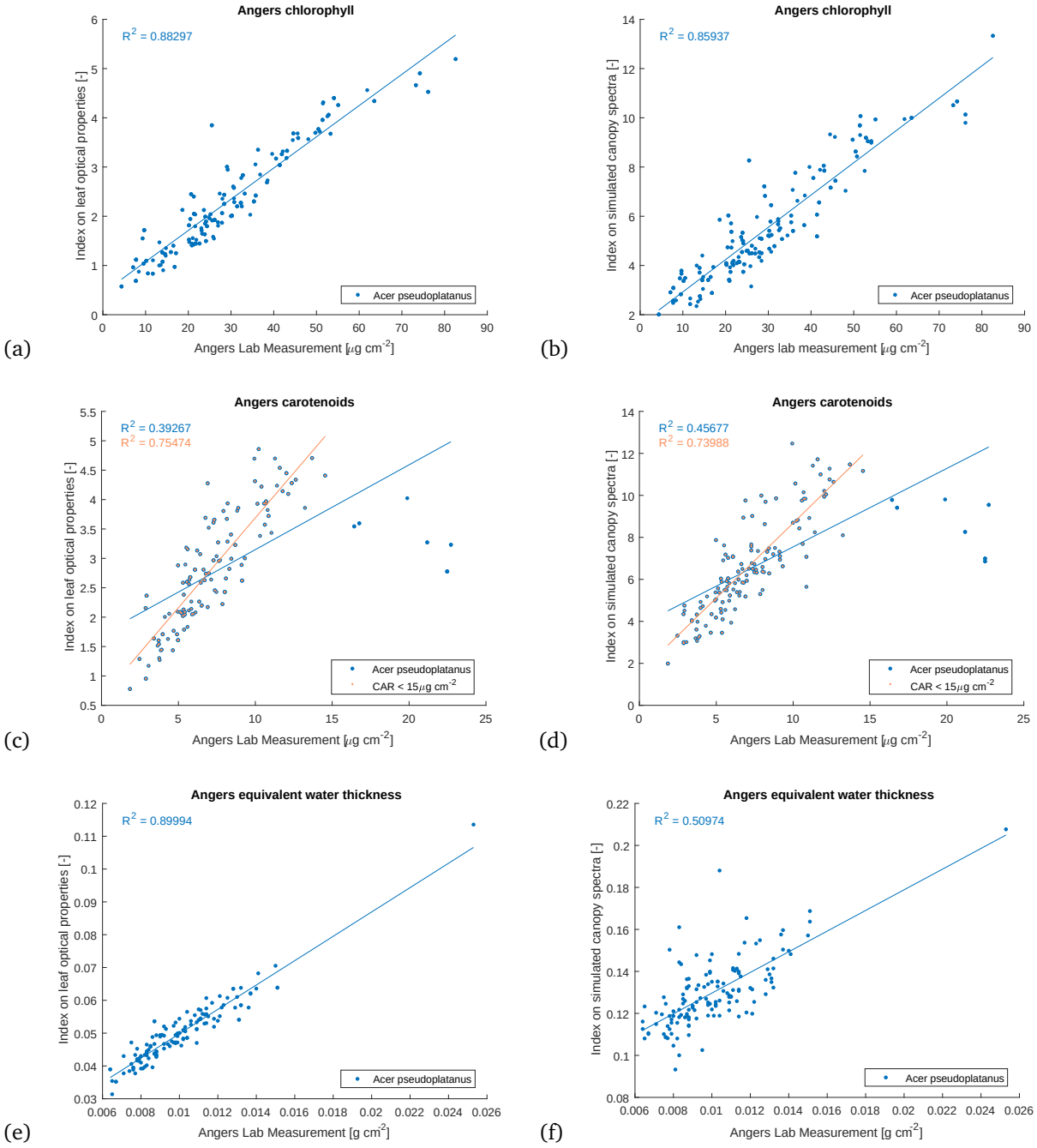

Supplementary Figure 9: Lab measurements of 168 *Acer pseudoplatanus* trees from the ANGERS database of (a-b) chlorophyll, (c-d) carotenoids, and (e-f) equivalent water thickness compared to corresponding trait estimates as derived applying spectral indices on (a,c,e) leaf optical properties and (b,d,f) modelled canopy spectra. Since very high carotenoids values are unlikely to appear at the Laegern forest in summer, a second linear regression was fitted for values below 15 $\mu g\ cm^{-2}$ (orange line, c-d).

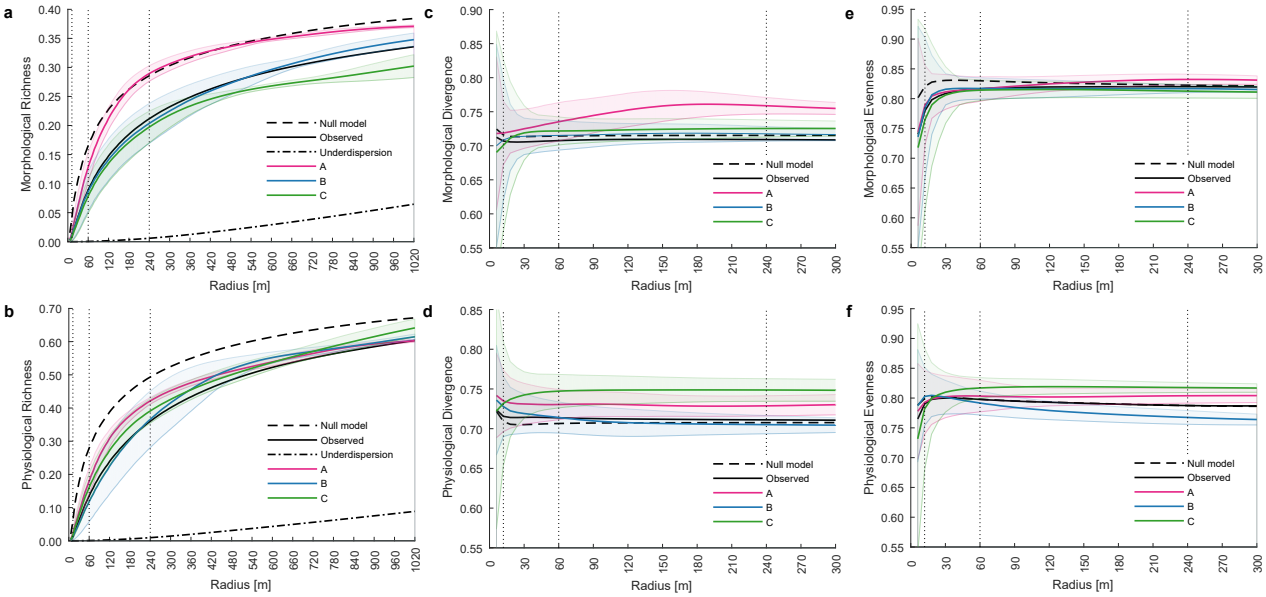

Supplementary Figure 10: Scale dependency of the three functional diversity measures for morphological and physiological traits. Functional (a,b) richness, (c,d) divergence, and (e,f) evenness as a function of radius (diversity-area) for (a,c,e) morphological and (b,d,f) physiological traits. Coloured solid lines A, B, C and coloured areas correspond to mean and standard deviation of subregions A, B, C. Vertical dotted lines correspond to radii as in Fig. 8 (main manuscript).

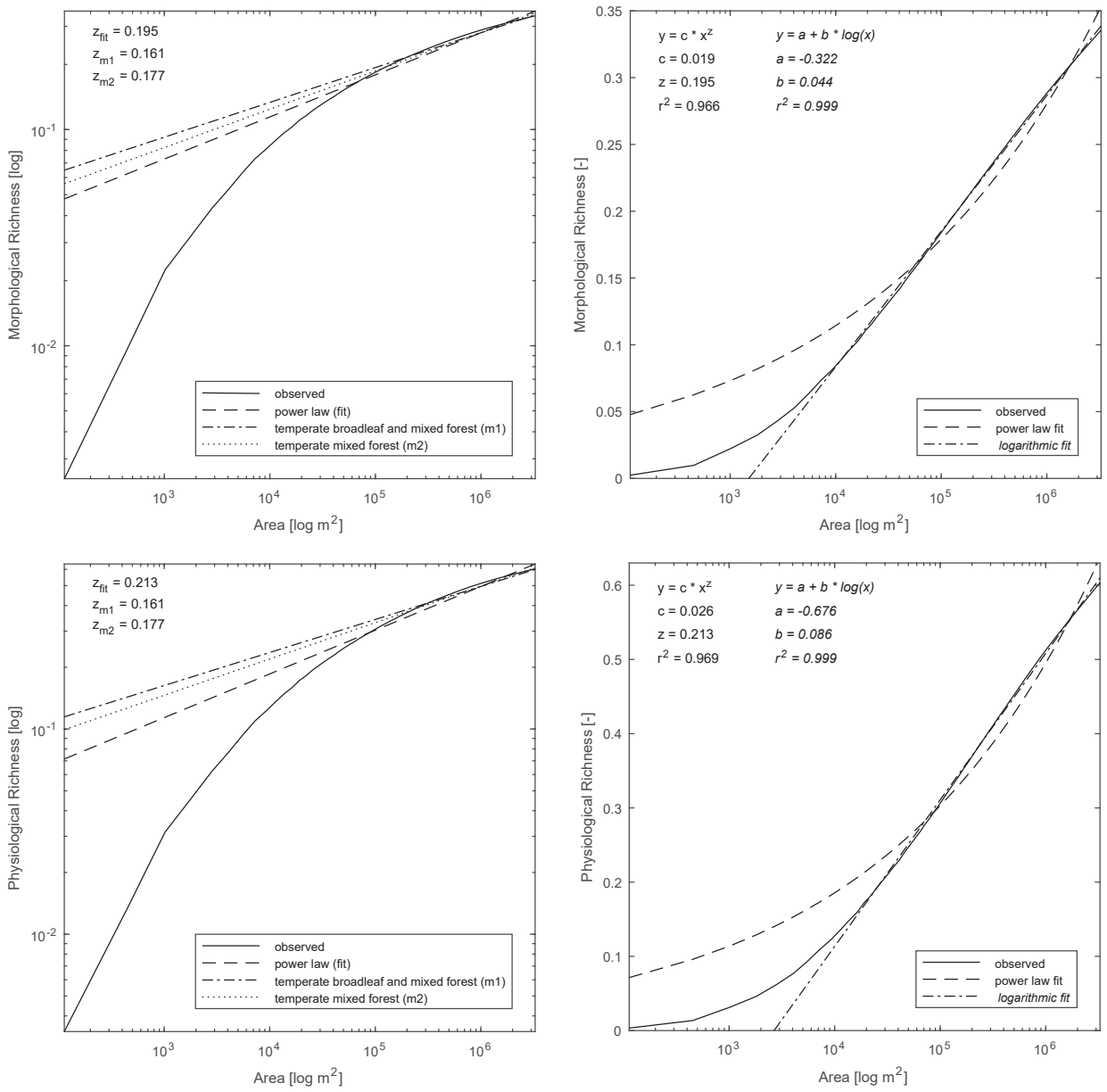

Supplementary Figure 11: Morphological (upper panels) and physiological (lower panels) functional richness-area relationships. Left panels are in log-log scale and show the fit of a power law function (dashed line) to the observed relationship based on the ecosystem mean (solid line) in comparison to two large scale species richness-area relationships based on global models of Gerstner et al. 2014. Right panels show the fit of a power law (dashed line) and a logarithmic (dash-dotted line) function in log-area scale. The logarithmic function has been fitted to areas above 10^4 m^2, where the observed mean values are linear in log-area scale.

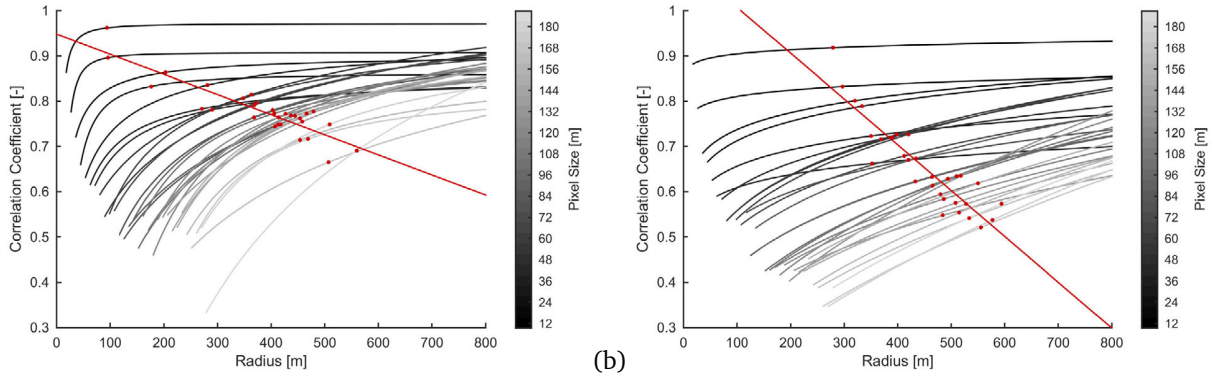

Supplementary Figure 12: Correlation between functional richness patterns of high spatial resolution (6 m pixel size) and increasing pixel size at a given neighbourhood radius for (a) morphological and (b) physiological traits. The red line indicates a linear fit to the knees (red dots) of the curves.

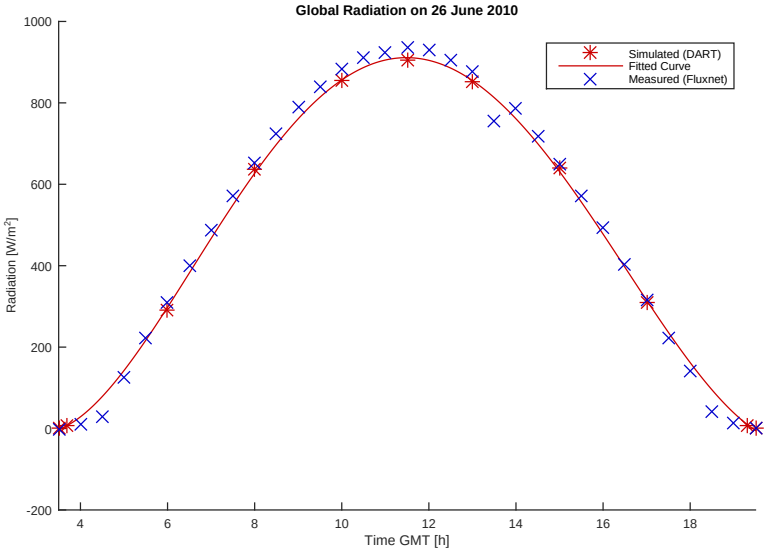

Supplementary Figure 13: Diurnal global radiation as simulated using the DART model and measured on a fluxtower of FLUXNET (CH-Lae).

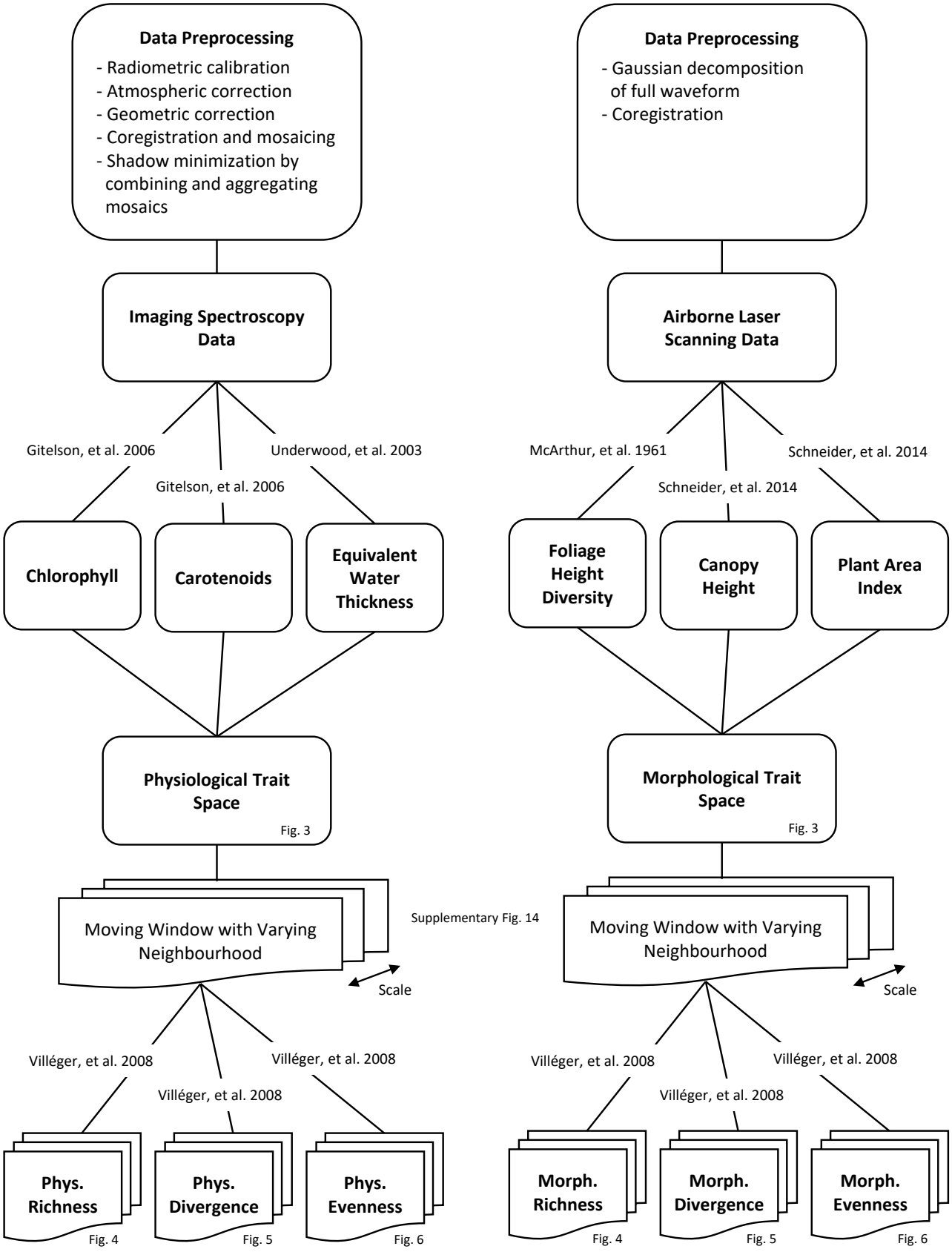

Supplementary Figure 14: Flowchart visualising the work-flow from remote sensing data to physiological (left) and morphological (right) diversity measures. The functional traits are combined to a three-dimensional trait space. By iterating through the pixels using a moving window approach and changing the extent of the neighbourhood, functional diversity measures can be calculated for many scales.

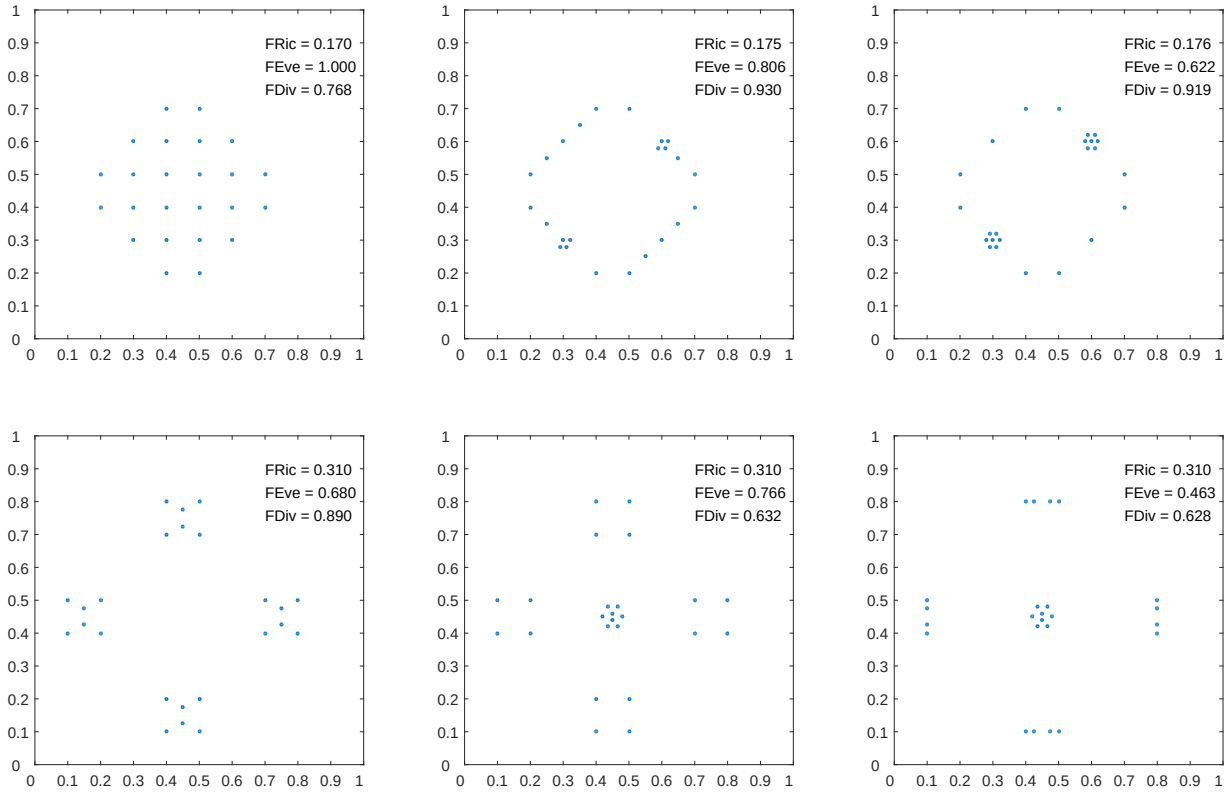

Supplementary Figure 15: Visualization of the three functional diversity indices functional richness, functional evenness and functional divergence.

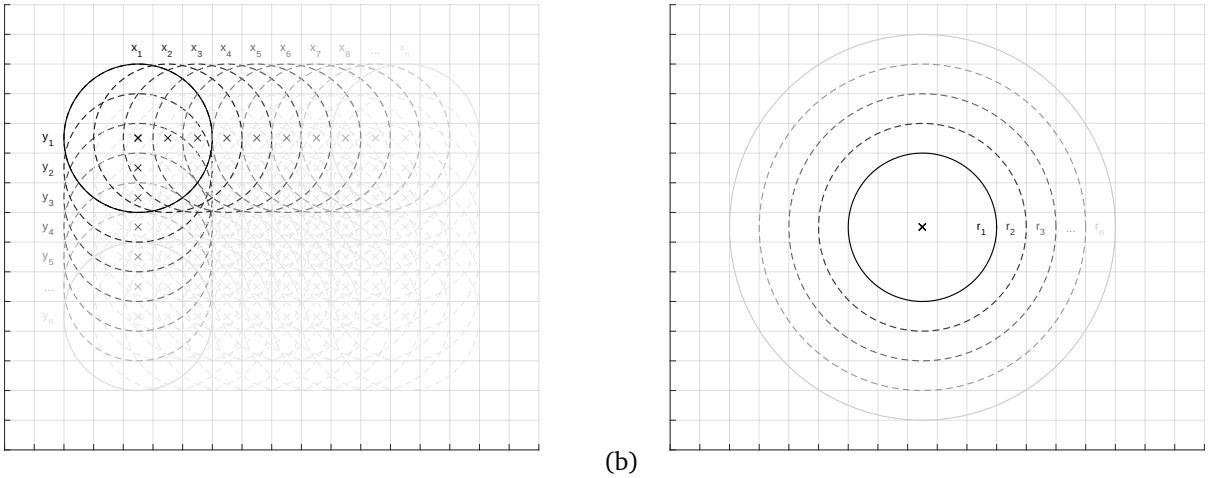

(a) (b)

Supplementary Figure 16: Schematic illustration of (a) the moving window approach and (b) increasing extent. Every pixel $p_{x_{1..n},y_{1..n}}$ is assigned the diversity value calculated based on the radial neighbourhood area with radius $r_{1..n}$.

Supplementary Table 1: ANOVA type I results for functional richness (FRic), divergence (FDiv) and evenness (FEve) explained by topographic variables. The order of the independent variables has been determined by the significance of the variables when tested individually, whereas the most significant are used first in the combined model. The variable 'Aspect' includes the three factors north, south, and flat slopes, whereas 'Curvature' is grouped in valley, ridge, and straight areas. 'Altitude' and 'Slope' are continuous variables. Stars indicate significance levels ***0.001, **0.01 and *0.05.

Dependent Variable	Variable	SumSq	DF	MeanSq	F	pValue	r^2
Morphological FRic	Altitude	0.024352	1	0.024352	48.3763	***1.214e-11	0.246
	Curvature	0.003841	2	0.0019205	3.8152	*0.02273	
	Slope	0.000113	1	0.000113	0.2251	0.63543	
	Aspect	0.001981	2	0.0009905	1.9676	0.14097	
	Error	0.231557	460	0.0005034			
Physiological FRic	Slope	0.16622	1	0.16622	121.4982	*** $<$ 2.2e-16	0.71395
	Altitude	0.02802	1	0.02802	20.4843	***7.665e-06	
	Aspect	0.00260	2	0.001299	0.9495	0.3877	
	Curvature	0.01070	2	0.005350	3.9104	*0.0207	
	Error	0.62931	460	0.001368			
Morphological FDiv	Altitude	0.004961	1	0.004961	8.4499	**0.003827	0.034
	Curvature	0.000625	2	0.0003125	0.5322	0.587650	
	Aspect	0.001408	2	0.0007040	1.1991	0.302397	
	Slope	0.000060	1	0.000060	0.1021	0.749410	
	Error	0.270054	460	0.0005871			
Physiological FDiv	Slope	0.010496	1	0.010496	23.4252	***1.776e-06	0.169
	Aspect	0.001859	2	0.0009294	2.0743	0.1268	
	Altitude	0.000019	1	0.000019	0.0415	0.8386	
	Curvature	0.000509	2	0.0002545	0.5680	0.5671	
	Error	0.206111	460	0.0004481			
Morphological FEve	Altitude	0.004251	1	0.004251	13.9823	***0.0002078	0.054
	Curvature	0.002039	2	0.0010196	3.3537	*0.0358118	
	Aspect	0.000703	2	0.0003515	1.1563	0.3155759	
	Slope	0.000194	1	0.000194	0.6396	0.4242760	
	Error	0.139854	460	0.0003040			
Physiological FEve	Slope	0.005621	1	0.005621	14.8399	***0.0001336	0.130
	Aspect	0.000844	2	0.0004218	1.1136	0.3292436	
	Altitude	0.000249	1	0.000249	0.6580	0.4177012	
	Curvature	0.001997	2	0.0009987	2.6364	0.0726994	
	Error	0.174246	460	0.0003788			

3.3 Peer Review Comments

3.3.1 NComms-16-23291A

Reviewer #1 (Remarks to the Author):

Overall this manuscript is a well written and interesting effort at combining imaging spectroscopy and lidar to look at physiological and morphological traits across a site in Switzerland. I agree with the general conclusions and the sentiment of the paper that these emerging remote sensing tools can tell us volumes about biodiversity. The main conclusion, however, as described in the abstract - that diversity was driven by disturbance and harsh environmental conditions, is qualitative at best, given the approaches used in the paper. I describe this concern in more detail below. I think this paper would be much stronger if it included some field validation of the spectral indices, and/or a more compelling suite of indices, and more quantification of the landscape in question.

We appreciate the reviewers interest in our approach to map functional diversity from remotely sensed forest traits. We are thankful for the recommendations to include both, a more quantitative approach as well as additional field-based information and data on environmental conditions of the study site. We have included those suggestions and refer to additional results in the main text and back them up using additional supplementary figures and tables, as described in detail in the remarks below.

My main concern with this manuscript is the total absence of field validation of either the spectral indices or the 'conclusions' about specific parts of the landscape and drivers. Regarding the spectral indices, quite a bit of progress has been made in this field since the methods papers referenced in this ms (Gitelson et al 2006 for CHL and CAR and Underwood et al 2003 for LWC), and, importantly, the Gitelson paper's indices were developed based on leaf spectra (not airborne), and the Underwood index for LWC is based on 'image inspection' of an AVIRIS collection in California with very different vegetation than is found in Switzerland. These spectral indices are no more or less robust than the many other hyperspectral indices available, but that doesn't mean much.

We appreciate this comment and clarify our approach by including three-fold validation approaches. We agree with the general fact, that indices must be treated with care. Indices, applied independently, may risk high collinearity. PLSR may risk infeasible physical solutions, and MCMC approaches may risk too high costs of informative priors needed. Progress has been made on all three aspects. We here use indices with demonstrated applicability in our temperate forest example. We validate leaf-level spectral signatures of 50 beech trees located within the study site (per tree, nine sunlit leaves of three branches at the top of the tree canopy were sampled) using a field measured trait (SPAD meter for Chl). Jointly with data extracted from the ANGERS database (http://opticleaf.ipgp.fr/index.php?page=database, lab measured traits and leaf optical properties), we demonstrate the applicability of spectral indices at leaf level. We also simulated canopy spectra using the 3D radiative transfer model DART (Schneider, et al. 2014) for the exact illumination/observation angles during airborne data acquisitions, by using the above leaf optical properties (in-situ measurements and ANGERS database). We then derived chlorophyll, carotenoids and equivalent water thickness for the simulated canopy spectra using the same approach as for the remotely sensed canopy spectra at various illumination angles. Finally, we compared all validation approaches and conclude that frequency distribution, magnitude, and trait correlations of measured and simulated spectra correspond well (r2 $>$ 0.5) with our airborne data. We added a paragraph in the manuscript on lines 115-124 as well as in the supplementary information on lines 10-31 and additional figures (Supp. Figs 7-8).

They also are not particularly compelling as a suite of traits for 'assessing functional diversity' - given the abundance of work on trait axes, focusing on foliar nitrogen and leaf mass per area would make much more sense (e.g. Daz et al 2016) and are readily mappable with imaging spectroscopy (e.g. Lepine et al 2016, Serbin et al 2014 and Singh et al 2015).

We fully concur with this comment we do not claim general applicability of those 6 traits beyond the study site. Currently, there is little convergence (in the remote sensing community) on the optimal choice of traits derived from remote sensing and their ability to map functional diversity. We focus on traits that are directly observable using imaging spectrometer reflectance data. The important works of Lepine, Serbin, Singh (and also Asner) use either proxies of proxies (for LMA and N) or in-situ data based calibration methods. We explain our selection of traits and their ecological relevance in more detail in the introduction (lines 55-63). Though very important, the Díaz et al. 2016 study is focusing on trait variation worldwide. Our method will be extended to using more traits in the future. Currently, our 6 traits feed three diversity measures, resulting in an over-determined system. The inverse (how well these 6 traits actually describe functional diversity at larger scales (and across biomes)) has not been assessed here and is subject to future work.

Using partial least squares regression (PLSR; as these papers do) to map traits would require field work, but would lead to a more robust statement about actual trait variation. I have very little faith that the three spectral indices used here have substantial correlations to the same measurements from the field at this site, though it's impossible to assess in this paper -

one piece of evidence, though, is that there are many zero values in Figs S1 and S2, which suggests either the indices aren't great or the image wasn't properly masked to screen out non-veg pixels (which could seriously impact your conclusions about functional richness - see below).

Scaling traits between leaf and canopy level is a main challenge (especially for traits related to leaf water or nitrogen). We refer to the discussions by Knyazikhin, et al. 2012 and subsequent replies, stating the limitations of PLSR. In our approach, we combined data acquisitions at different illumination/observation angles and used spatial aggregation leading to a reduction of shadow and illumination/structure effects, which is crucial to be able to apply spectral indices at canopy level (statement added on lines 118-120). Regarding zero values, we used confusing terminology. In fact, zero values reflect scaling by which minimum values of vegetated pixels were converted to zero. We are thankful for this comment and include a more comprehensive description of how forested pixels were defined (lines 413-417).

At minimum, if you have plot data with composition information you could use area weighted means of published trait values for the species from something like the TRY database (Kattge et al 2011) to at least know if your indices and therefore trait patterns are in the ballpark of the real values, or if someone else has done a field to index comparison for these indices in or near this site, that would help too.

Thank you for this suggestion. Indeed, we have a core study site at the Laegern forest of approximately 5.5 ha, where we measured location and taxonomic identity of all trees with a DBH above 20 cm (resulting in 1307 trees of 13 different species). We used these plot data to calculate community-weighted means using the plot-level species abundances and species-level trait values from the TRY database. Although TRY is not suitable for assessing intra-specific trait variation and is ignoring trait plasticity, we find a positive relationship to index values for chlorophyll and equivalent water thickness (lines 116-118). Unfortunately, there are not enough values in TRY for carotenoids, making it impossible to apply gap-filling and compare to the remotely sensed trait values. In addition, we added Supplementary Figure 5 (on trait ranges) and Figure 6 (remote sensing vs. TRY) based on this suggestion.

My own experience with hyperspectral vegetation indices applied outside of where they were developed is that they are typically weakly correlated with the actual field measures, but sometimes not correlated at all or even negatively correlated, hence the widespread focus on techniques like PLSR.

Additionally to the above-mentioned points, we also include a comparison of trait ranges from the remotely sensed trait maps to trait ranges simulated based on Schneider, et al. 2014 with independently measured leaf optical properties (LOP). The model was used with the same in-situ LOPs, averaged for deciduous broadleaf and coniferous needle trees, respectively, and parameters as described in Schneider, et al. 2014. The traits occur in a similar part of the whole trait range of the forest (see lines 115-116 and Suppl. Fig. 5). The variation in remotely sensed traits is caused by the actual physiological trait variation between individuals within and among species. PLSR methods may be superior to index-based approaches, in particular where models used reflect well the canopy architecture. We used inversion schemes with SLC (Hapke soil model, PROSPECT, 4SAIL2) based on PLSR and Bayesian approaches (Laurent et al. 2013, 2014) and found trait retrievals to be worse in forests than in optimal turbid medium scatterer (such as agricultural canopies). We therefore used the forward model approach based on DART, allowing to independently validate trait retrievals in sub-optimal turbid medium architectures, such as this temperate forest.

Similarly, much of the Discussion is focused on qualitative assessments of the correspondence between the morphological and physiological traits and the landscape being studied. Statements like lines 121-122 saying blue areas of the morphological trait map are due to disturbance and lines 129-131 saying the pink and orange areas of the physiological trait map are beech read as speculation given that there's no information about what's actually in the field. If there were (again) some plot data for the site this could be resolved and these differences could be quantified, but as the paper is written currently we are left to simply trust that the authors know the site well enough to make these blanket statements. They very well may, but I found myself asking a lot of questions - are ALL the blue areas on the morphological map due to the 1999 storm? etc. Even a land cover map, if one exists for the area, could be used to ask these questions in a more quantifiable way, as was done by Dahlin et al 2013.

We agree that plot data or a landcover map as well as additional environmental variables would help to support the qualitative assessment and make the manuscript stronger. Therefore, we add forest stand polygon data from the Cantons of Aargau and Zurich with information on the most dominant species and juvenile forest patches (c.f., Suppl. Fig. 2) and for quantitative statements (lines 95-99, 106-110, 242-245). We reformulate the first paragraph of the discussion (lines 181-186) to be more precise about disturbance areas. For an additional quantification of the landscape, we include the topographic variables altitude, slope, aspect and curvature and provide additional ANOVA tests (lines 131-144, 147-149, 153-156, Suppl. Tab. 1). Finally, we add figures on topography, radiation and soil variables (Suppl. Fig. 10) and demonstrate a significant difference between the ridge and lower altitudes (Fig. 7, lines 231-238, Suppl. Tab. 2). See also comments of reviewer 3.

Below are some additional specific comments and places illustrating the broader points above.
line 7: "informing on" -> "informing"

Corrected on line 27.

lines 13-15: "On the one hand" and "on the other hand" or similar are used 4 times in this paper - too many in my opinion.

Thank you for the comment, we removed or replaced the phrase except for lines 33-36.

line 18: what does 'and their gaps' refer to?

It should refer to the data gaps in in-situ data. We clarified the sentence on line 38.

line 22: 'environmental filtering, limiting similarity, or neutral theory' - it would be nice to cite the originators of these ideas, not just a review.

We removed this sentence (due to another reviewer comment) and added the respective references later in the text on lines 225-228.

lines 44-45: worth mentioning that convex hull volume is a range measure - depends on outermost values - so if you have outliers/nonveg pixels (as you appear to from Figs S1 and S2) that could dramatically alter your CHV and therefore functional richness.

Indeed, that is right. We now mention this on line 68.

lines 59-60: 'Are forest communities structured by ...?" do they have to be mutually exclusive?

We agree that they are not exclusive. We rephrase the question on lines 89-90.
line 62 - Fig 3. What are all the masked areas? I'm guessing agriculture, but this isn't described anywhere. How did you mask non-veg pixels?

We add a paragraph in the Methods on lines 413-417, describing how we derived the forest mask.
lines 62-66: relying on visual interpretation of an RGB image like this is a difficult way of presenting these results. They're described as though you've classified the images but in reality in an RGB it's tough to see these colors clearly.

We prefer to show the trait maps using continuous (RGB) color-scales, since it corresponds to the 3D trait space definition and how the traits are used to calculate the FD indices. However, we agree that our classification for interpretation purposes is not optimal (definition given in methods lines 406-412). We updated the graph by adding Supplementary Figure 2, where the main classes are shown and compared to plot data.

lines 78-79: why correlate the morpho and physio richness? (and other measures)? what does that tell us? is that related to your overall questions? also describing a correlation plot that isn't shown - could these go in SI?

Following other reviewer's comments (see below) we added a statement in the introduction (lines 83-87) and the conclusions (lines 307-311) why the comparison between patterns of morphological and physiological is relevant.

lines 81 - end of methods: Any stats for any of these differences? a lot of these differences are very small (2.7-5.7% for example in line 82) - are they statistically significant? I think an ANOVA or a t-test could be used to check these things.

We added results of an ANOVA test in the manuscript (lines 131-144,147-149,153-156) and the full ANOVA table in Supplementary Table 1.

line 101 - Fig 7: I realize it would make a messy graph, but error bars on the A, B, & C lines in this plot would help clarify whether these results are really outside of the noise.

The A, B, C lines are from a single pixel in the center of the subregions. We apologize for the misunderstanding and clarify on lines 161-163 and in the caption of Fig. 8. We agree that error bars for the whole subregions would be helpful but a bit messy, why we add it to Supplementary Figure 9.

line 103: 'Black lines' -> 'Solid black lines'

Changed on line 163.

line 111-112: these are the correlations between the actual line and a true log curve?

We clarified that it is with regard to the richness-area relationship with area on the x-axis (lines 171-173). The function used to fit is: $y = a*log(x) + b$

lines 120-128: a lot of this description should go in the site description, not the discussion.

We provide description only relevant for the discussion of the functional traits and trait diversity maps. We prefer to leave this section unchanged, otherwise the context of our discussion might be lost.

lines 129-135: any references for these site characteristics?

Additional data is described in a new paragraph Environmental data in Materials and Methods (lines 353-364), added to Results as well as Supplementary Figures 2 and 10.

lines 131-132: 'on one hand'/'on the other hand'

Changed on lines 195/197.

line 143: 'On the other hand'

Changed on line 208.

lines 156-170: These paragraphs seems like they should be in the methods or intro.

We move the first paragraph to Methods (lines 419-425) and rephrase the second paragraph (lines 222-230).

lines 187-188: 'On one side'/'On the other side'

Changed on lines 254-255.

line 212: I'm curious how much the 'null model' line would drop if you removed all the pixels with zero values for the six traits from this analysis (as shown in Fig S1). If you trust your metrics, anything with zeros for any of these metrics/indices shouldn't be a plant, so it shouldn't be going in to your diversity metrics. And the abundance of these zeroes means they could really be inflating your null diversity models.

We agree that an absolute value of 0 in any of the traits would not be a plant (or an infeasible retrieval). However, zero values result from scaling index values from 0 to 1, which do not include absolute 0 values. Therefore, our scaling index values do influence absolute values (maximum richness), but do not show an influence on patterns and shapes of the curves.

lines 218-219: 'Our results show that...' - this sentence isn't particularly illuminating.

We rephrase the paragraph on lines 293-297 by adding an example of the scalability of the method to coarser spatial resolutions.

lines 225-226: 'were able to validate these measurements against in-situ community data' - where?

lines 228-229: 'High functional diversity...' again - this reads as speculation given the lack of in-situ data presented.

lines 224-231: While I agree with the sentiments of the conclusion, overall it is lacking in strong conclusions from this actual paper, just speculation about what could be done with more data.

We hope to have resolved these three issues by adding additional plot data, extending the results and supplementary information as well as rephrasing the conclusions (lines 301-320), see main comments above.

Dahlin, K. M. et al. 2013. Environmental and community controls on plant canopy chemistry in a Mediterranean-type ecosystem. - Proc. Natl. Acad. Sci. U. S. A. 110: 6895900.

Daz, S. et al. 2016. The global spectrum of plant form and function. - Nature 529: 167171.

Kattge, J. et al. 2011. TRY - a global database of plant traits. - Glob. Chang. Biol. 17: 29052935.

Lepine, L. C. et al. 2016. Examining spectral reflectance features related to foliar nitrogen in forests: Implications for broad-scale nitrogen mapping. - Remote Sens. Environ. 173: 174186.

Serbin, S. P. et al. 2014. Spectroscopic determination of leaf morphological and biochemical traits for northern temperate and boreal tree species. - Ecol. Appl. 24: 16511669.

Singh, A. et al. 2015. Imaging spectroscopy algorithms for mapping canopy foliar chemical and morphological traits and their uncertainties. - Ecol. Appl. 25: 21802197.

Knyazikhin, Y. et al. 2013. Hyperspectral remote sensing of foliar nitrogen content. PNAS 110(3): E185-E192.

Laurent, V.C.E., et al. 2014. Bayesian object-based estimation of LAI and chlorophyll from a simulated Sentinel-2 top-of-atmosphere radiance image. Remote Sens. Environ. 140: 318-329.

Laurent, V.C.E., et al. 2013. A Bayesian object-based approach for estimating vegetation biophysical and biochemical variables from APEX at-sensor radiance data. Remote Sens. Environ. 139: 6-17.

Schneider, F.D. et al. 2014. Simulating imaging spectrometer data: 3D forest modeling based on LiDAR and in situ data. Remote Sens. Environ. 152: 235-250.

Reviewer #2 (Remarks to the Author):

This manuscript is overall clear and weel written; the focus on functional diversity is up to date and challenging. The paper, as it stands, is still difficult to be followed in detail and the following major points should be considered:

-ACRONYMS: The use of acronyms to indicate functional variables renders the paper difficult to read in some parts.

We substantially reduced the use of acronyms and hope to have increased the readability of the manuscript overall.

-BACKGROUND THEORY: Major explanations are also needed in some of the figures to be fully understood. As an example, Figure 1 shows graphs which are not rooted in the text and the data being used are not described in detail. In this view, this figure is very difficult to read.

We extended the explanation and embedded Fig. 1 in the manuscript on lines 68-76 and 428-430.

-DIVERGENCE VS. EVENNESS: Functional divergence versus functional evenness are not described in detail apart for some sentences. This renders the whole paper a bit technical and it might better focus on such concepts overall from a theoretical

point of view.

We add some more theoretical background on the concept of functional divergence and evenness on lines 68-76. Although important to include, we found functional divergence and evenness to be less relevant to assess scale-dependent functional diversity than functional richness. We clarify this in the Discussion (lines 280-283) and the Conclusions (lines 311-313).

-CASE STUDY PRESENTED: The case study might be cool. However, as a reader, I feel that the part describing it is too long with several figures which hamper to catch the real take home message. moreover, again, the theoretical background must be also stengthened.

Based on this recommendation, we have reshaped the description as well as the figures to improve readability and not dilute the main message. With all changes proposed by the other reviewers and in particular rewriting the introduction and conclusions (lines 301-320), we feel the take home message to be much clearer now.

-TAXONOMIC DIVERSITY - IMPORTANT. A number of papers have dealt with the relationship between functional and taxonomic diversity. Moreover, a number of papers attempted to estimate taxonomic diversity from remote sensing considering both alpha and beta diversity (and also richness versus evenness). This paper does not take into account such approaches. As an example, a good conclusion of the ms might be based on an explicit statement about the power of functional versuss mere taxonomic diversity and what is its hadded values, together with a critique on the use of RS in this framework. At the time being the final take home message is still a bit unclear and technical.

We explain more clearly in the Introduction the interest why we measure functional diversity independently of taxonomic diversity. We also add additional references on the importance of considering variation within species and possible redundancy of different species with regard to functional diversity (lines 44-47). The focus of this paper is clearly on mapping functional diversity. As mentioned above, we have rewritten the conclusions to sharpen the main message of the paper.

-THEORY BEYOND THE PRESENTED CURVES: No asymptote is reached in Figure 7. Does this mean that total diversity has not been finally catched despite the radius being considered, or, theoretically, in this case the asymptote has no ecological meaning like in rarefaction curves (see Gotelli and Colwell)?

Indeed, the total diversity has not been caught by the largest radius applied. The curve is supposed to reach the asymptote as soon as the maximum range of traits in the ecosystem is captured by a certain neighborhood area. If we were to extend the radius further, we must include landscape level diversity effects (agriculture, urban, permanent grasslands, etc.) and may be able to validate or invalidate if the asymptote has ecological meaning. In our case, the limited site extend will not allow us to do so, but it remains an important and interesting question!

-FLOW: I feel that this paper might benefit from a flowchart addressing the whole analysis, variables, concepts.

We have added a flowchart to the supplementary information illustrating the workflow from the remote sensing measurement to the final diversity maps (line 368-369, Suppl. Fig. 12).

-A CRITIQUE TO SHANNON WEAVER THEORY APPLIED TO BIOLOGICAL DIVERSITY: one of the main problems of using Shannon-Weaver theory is that fhd might be high from RS data despite the real values of the RS images. As an example imagine a vector of values [1,2,3,4,5,6,7,8,9] and another one like [1,150,70,25,250,255,44,200,100]. The two vectors will attain exactly the same fhd. This is an important issue. Moreover, fhd might represents both richness and relative abundance with no chance to distinguish them from the final metric. This might be a problem too, but it is not addressed explicitly in the ms.

Maybe there is a misunderstanding on how we applied the index. We do not calculate relative abundance how it is done for species (Shannon-Index), but we use the proportion of foliage in a respective canopy layer instead (see lines 378-380). So for example the vector p [18%, 19%, 20%, 21%, 22%] with 18% of foliage in the first layer, 19% in the second, and so on, does not have the same FHD value as the vector p [5%, 15% 20%, 25%, 35%]. We agree on the second part of the comment, saying that FHD is not just a measure of how different the layers are but also how many layers there are. We add a comment on this and possible correlation with canopy height in the manuscript on lines 380-382.

Reviewer #3 (Remarks to the Author):

The manuscript from Schneider et al uses metrics of functional trait diversity, based on six remotely sensed functional traits, detected at very high spatial resolution, to reveal ecological insights in a Swiss forest system. Using hyperspectral remote sensing at high spatial resolution and at multiple scales to understand plant function and plant functional diversity is a critical advance in ecology. This is the first study to develop an approach to measure remotely sensed plant functional diversity and apply it empirically. The methods developed here are very compelling and relevant to continuous monitoring of ecological changes with global climate change. Both the quality of the data and the analyses are quite high. In short, both the novelty of the work and the quality of it merit publication in a high impact journal like Nature Communications.

We are happy to see that the reviewer appreciates the novelty and significance of our work, combining remote sensing

and ecological methodologies to map and understand patterns of functional diversity. We appreciate the detailed comments and recommendations, and answer point by point as follows.

However, the paper falls short in developing a believable framework for linking functional trait diversity to community assembly processes. The introduction is very light on explaining how these metrics can be related to community assembly processes, citing good papers, but not actually using the methods proposed in those papers. Much has been written in the community ecology literature about the difficulties of discerning processes from pattern, and these issues require attention. Some convincing efforts have been made in the literature to build a logical hypothesis testing framework for making the leap from pattern to process, and a logical hypothesis testing framework would help this paper. E.g., "If we find pattern x, we can infer process y (and not z) because..."

We agree that our interpretation of the described patterns in terms of potential processes underpinning them is too generalizing and partly even speculative. It was actually not intended to be the main message of the paper, neither did we mean that this interpretation should serve as the hypothesis framework. Therefore, we realized that we need to step back from the strong interpretation about processes responsible for patterns and focus more on revealing the patterns (e.g. with regards to trait convergence and divergence). We changed the wording throughout the manuscript and clarified the focus, being more precise about possible reasons causing the observed patterns and relations to environmental factors.

The best that I can make out is an attempt to do this using the null models, which can sometimes be designed to tease apart, or rule out, alternative interpretations of pattern. Here they are used to identify under- or overdispersion patterns in functional diversity. Those patterns are then interpreted in an oversimplified manner, equating functional similarity with environmental filtering and functional overdispersion with competition. There are many, many processes that can give rise to the same patterns, and so I dont feel the paper is as thoughtful as it needs to be in making inferences about community assembly or other ecological processes. A classical functional trait paper would not be able to draw sweeping conclusions about the respective roles of environmental filtering and limiting similarity based solely on patterns of over and underdispersion functional diversity. Here we have a novel measurement approach, but the same issues are relevant. I believe the authors have a framework in mind that needs to be better articulated. For example, what are the inferences that are believed to be possible when diversity patterns and richness-area relationships are similar for morphological and physiological traits? Lay this out in the introduction so it is clear why the comparison is important.

Indeed, the hypothesis to be tested in the context of functional diversity patterns was the one of over- and underdispersion or trait divergence and convergence, respectively. We adapted the research question on lines 89-90 and the discussion on lines 225-230. As mentioned above in comments to reviewer 1, we now better justify our selection of functional traits and our interest in comparing the two groups of traits. The study of Daz et al. 2016, among many others, has shown strong correlations among traits. By demonstrating their similar patterns we therefore provide justification that these are mapped correctly and are representative for functional traits in general. We add this to the Introduction (lines 55-63, 83-87) and the Conclusions (lines 307-316).

I will give a specific example from the manuscript about concerning the difficulty of inferring community assembly processes from pattern. Line 212 states environmental filtering is the predominant assembly process, since it is consistently below the null model of randomly distributed traits at all radii. However, line 177 clarifies that FRic for the physiological traits is mainly driven by the difference between conifers and broadleaved trees. And in line 136, we learn that conifers were largely planted by humans. So the low FRic relative to a null model may indicate the presence of only conifers or only angiosperms, which may be an anthropogenic phenomenon, influenced by decisions humans made about where they thought conifers would best be planted.

Thank you for the clarification. We agree that we are observing trait convergence, but cannot make the direct link to environmental filtering especially due to anthropogenic influence in parts of the forest. We changed the manuscript text accordingly and add a statement specifically on lines 225-230, 253-256.

The term environmental filtering itself is very vague and much more meaningful when we have a sense of what the environmental factor is that is driving the vegetation pattern. Can the authors marshall more evidence as to which factors in the environment are causing filtering of the vegetation and how the filtering process might operate?

We realize that a more detailed description of the environment at the studied forest is needed (see also comments above to reviewer 1). By including topographic variables (altitude, slope, aspect, curvature) as well as data on radiation and soil (type, depth, coarse material), we are able to better describe the environmental conditions possibly leading to environmental filtering. Especially at the mountain ridge we can observe trait convergence and reduced diversity, which coincides with significantly different conditions regarding soil (shallower, rockier), radiation (higher) and topography (steeper) than in all other areas. We add this to the discussion on lines 231-238, 242-245 and add Fig. 7, Suppl. Fig. 10, and Suppl. Tab. 1 & 2.

The null models themselves are difficult to follow because their description is so brief. The supplement did not offer further explanation. These should be explained carefully so that the reader can decipher how the null models are being used to discern non-random patterns that reveal something about process.

Since we are stepping back from strongly inferring processes from patterns, we do not include any new null models. The current null models are mainly used to show over- or underdispersion or a random distribution of traits. We

apologize for not being clear enough and therefore extend the description of the null models on lines 466-476.

On line 166-168, the authors state that FRic can indicate that trees are assembled following the principle of limiting similarity, which leads to overdispersion due to direct competition between trees. Again, there are many different processes beyond competition that can lead to overdispersion, and some important studies have shown that competition can actually lead to clumping patterns and underdispersion. Empirically, there is not a clear link. In this study, certainly dispersal processes and phenotypic variation that accompanies ontogenetic changes can contribute to the overidispersion found in the gaps. The authors in fact conclude in line 228, that high functional diversity was related to the occurrence of disturbance areas and patches with mixtures of evergreen coniferous and deciduous broadleaf trees. So in the end, they do not equate overdispersion with competition. At times, the authors apply frameworks from other studies to make ecological inferences, and at other times, they disregard these frameworks and make inferences based on their understanding of a well-studied system. So there seems to be awareness of the issue.

We agree that these interpretations were not made clearly enough. As mentioned in previous comments, we have adapted the argumentation throughout the manuscript.

I suggest the authors rewrite to 1) set up a hypothesis testing framework so we can see how inferences are being made, 2) be very careful about the problem of making inferences about process from pattern, and 3) tone down the definitive conclusions drawn about environmental filtering and explain what information would be required to show this. For example, more convincing arguments for environmental filtering would include the relationship between trait values and the environment surely the data is all there already to do this; linking physiology to performance (as in [19]), if performance measures can be derived from some of the morphological traits at multiple time intervals; looking at changes in physiology and function over time with changes in environment. The study could also link functional diversity to ecosystem processes. This would be quite exciting.

As mentioned in previous comments, we are stepping back from making strong inferences from patterns about processes. We have added environmental variables and regressions of functional diversity on these variables but prefer not to extend this to regressions of individual traits because we think this is outside the scope of this paper. The focus should lie on revealing and interpreting the functional diversity patterns. We do hope to link functional diversity and ecosystem functioning in future work, by combining remotely sensed traits and forest composition with remotely-sensed ecosystem-function variables. However, this will require a whole new study and manuscript and we feel that including more aspects like productivity measures would make the present paper losing focus.

The scale dependence of diversity is quite interesting in this paper and more could be done with that.

We are very interested in working on the scale dependence of diversity, but we believe that it would exceed the scope and make the manuscript difficult to follow. Future work on this aspect is planned for new submissions. We now do, however, mention the potential to upscale our approach for monitoring diversity from space, in a paragraph at the end of the Discussion (lines 293-297) and a figure in supplementary information (Supp. Fig. 11).

A few smaller points:

Line 108: A simulated distribution of traits following the assumption of underdispersion where trees being close in functional space are assumed to be close in geographic space, leads to a very low functional richness at all scales. Please clarify exactly how this was done, somewhere.

We extended the description of the null models in the Methods section on lines 466-476.

Line 301-317: In contrast, I am not sure the equations for all the functional diversity metrics need to be included in the methods (can go in the supplement), since they are the same as in the original publication [34]. Note some authors argue there are better metrics of functional diversity (see Scheiner et al). However, I think these are fine.

We included the diversity metrics (formulas) in the main manuscript, because they are crucial to understand the resulting index values and they are not exactly the same due to the lack of abundance weighting (although the formula behind is the same). Thank you for this comment. We are aware of the many diversity metrics, each with advantages and disadvantages. However, since there are already many studies on this topic, we did not want this study to be focused on the selection of index.

Line 306: Without defining the particular niche concept applied, calling FRic a measure of niche extent is not clear.

We extend the description to be clear what we mean by niche (lines 433-434).

Line 241: Trees of 165 years or greater are not necessarily old-growth trees. They are mature trees that are old. Unless this is a forest not used by humans (or barely used) for millennia, they would not, strictly, be called old growth.

Changed on line 330.

Line 263: Give definition of plant area index somewhere.

The definition is given on lines 374-375.

Lines 229-232: Extending the scale of investigation to individual trees and globally will help to improve our understanding of the interactions of species and traits including genetic, phylogenetic and functional diversity, ultimately allowing to monitor functional diversity from space. The idea of extending the scale globally is excellent. Throwing in the genetic and

phylogenetic diversity is gratuitous; it is not clear what is meant or how it would be done based what is in the manuscript. It seems more important to focus on how ecological inferences would be made globally, based on functional diversity patterns. Surely, emphasizing a temporal component that would allow observation of changes over time, and pairing functional data with environmental data, are critical. It would be nice if this paper could make that case.
Thank you for this suggestion. We agree that it is of high importance to head towards a global system for assessing functional diversity as well as including the temporal component. We try to make that case at the end of the Conclusions on lines 317-320.

3.3.2 NComms-16-23291B

Editor's Comment To address the central remaining points raised by Reviewers 1 and 2, we request that you revise the paper to better integrate the field data validations (Supplementary Figures 7-8) with the main text. If you do not think that putting the results/figures themselves in the main text would be possible, please at least add detail on the justification, methods and analyses to the main text. In general, we encourage all methods to be in the main text, to aid the reader.

We appreciate the recommendations and are glad that our additional work has been recognized as an essential improvement of the manuscript. To better integrate the field data validation, we applied three major changes. First, we added a paragraph to the introduction defining the testing of the consistency of our method and the field data validations as one of the main goals of the study. Second, we added more detailed results and discussed them in the sections Results as well as Discussion, but we decided to keep the figures in the supplementary material. Third, we added a detailed description of the field data and methods to the main text. We include a PDF-Version of the manuscript, where related text passages are highlighted in orange. Similarly, we highlighted text in green, yellow and blue, respectively, for the three main points among reviewer 3s comments.

Reviewer #1 (Remarks to the Author):

Overall I think that this manuscript shows much improvement over the previous version and I appreciate the additional work that the authors have put in to it. However, it seems as though much of the additional work has been added to the supplement and (some) mentioned in the results section but has not been described in the methods (e.g. comparisons between field & TRY traits and RS, ANOVA approach) making it difficult to evaluate these additions - there are some descriptions of these new methods in the rebuttal, but they should be in the actual manuscript.

We added the subsections Field data and Field validation of physiological traits to the main manuscript on line 391 and 440, describing additional data and methods in more detail.

A few examples of now unanswered questions:

How were the categorical variables handled in the ANOVA?

We added an additional section on Statistical analysis in the Methods section on line 541, explaining the ANOVA approach and a detailed description of the independent categorical variables. With regard to Supplementary Tab. 2, we realized that ANOVA is not the suitable statistical analysis when both dependent and independent variables are categorical. We replaced this table by Supplementary Fig. 9, showing the results of a variance partitioning based on soil, topography and radiation.

What do the yellow lines in Sup Fig 8 c and d represent?

We added clarification to the caption of the Figure. The proposed spectral index to derive carotenoids seems not to be suitable for very high carotenoids values. Since we do not find very high carotenoids values at our study site, we applied a second linear regression on carotenoids values below 15 $\mu g/cm^2$.

What's the rationale for supplementary table 2?

We replaced Supplementary Tab. 2 by Supplementary Fig. 9, showing a variance partitioning based on soil variables, topographic variables and radiation for all functional diversity indices and functional traits. This new figure shows the relationship of spatial patterns in functional traits, and especially functional richness, and the environmental gradients of soil and topography more convincingly.

I think this manuscript is moving in the right direction, but much of the continuity has been lost as more analyses have been done but the text has not been appropriately or comprehensively updated.

We revised the text to ensure consistency and continuity throughout the manuscript. By defining three main goals of the study, we better outline the main aspects, relevance and novelty of the study.

Reviewer #2 (Remarks to the Author):

I am feeling that the authors did a great job to reply to my comments together with those of the other reviewers. I am also feeling that some of the comments from Reviewer #1 should still be considered in full detail. E.g. the need of field data to

calibrate hyperspectral traits and indices. A more convincing statement should be put in the main text.

We appreciate this suggestion and added a separate subsection Field validation of physiological traits and a specific statement on lines 101-106 and 441-446.

Another minor point concerns the Supplementary material. I am feeling that the frequency distribution of FHD is a key concept in this manuscript which might deserve space in the main ms instead of being basically hidden in the Supplementary material. This is also true for trait correlations. However, this is not only an authors' decision but overall an editorial one. This said, the paper is robust enough to deserve publication. Duccio Rocchini

We appreciate the valuation of our work and we are happy that our article is recommended for publication. Since trait correlations are presented in the results section and we would like to emphasize the functional diversity approach in a spatial context, we decided to keep the figures in the supplementary material.

Among Reviewer 3's comments, please focus on the following points:

Editor's Comment We request that you provide better context in the Introduction and Discussion regarding the importance of understanding functional trait diversity patterns (e.g. the implications for ecosystem function).

Thank you for this suggestion. We agree that the relevance of studying functional diversity patterns has to be pointed out specifically in the manuscript. We do so now by including an additional paragraph in the introduction citing recent literature on diversity-productivity relationships and the impact of diversity on ecosystem stability. We also discuss potential implications for ecosystem functioning based on the observed diversity patterns. However, to establish a link between functional diversity and ecosystem functioning at our site would exceed the scope of this study.

Editor's Comment Please consider addressing Reviewer 3s point about correlating forest traits with a detailed soil map, perhaps by making use of the data in Supplementary Figure 10.

We agree that soil variables are important to explain and potentially predict functional diversity patterns. Therefore, we perform a variance partitioning based on soil variables (soil type, soil depth, amount of coarse grains), topographic variables (altitude, slope, aspect, curvature) and radiation (mean daily photosynthetically active radiation). We add Supplementary Fig. 9, the results on lines 148, 152, 175, 187 and discuss it on lines 228-239, 264-270. We can show that the environmental gradient of changing soil and topography towards the top of the mountain consistently links to the functional richness patterns of morphological and physiological traits.

Editor's Comment Please establish predictions regarding how functional trait diversity should change with scale (in the context of existing literature on diversity-area relationships).

We introduce our hypothesis on changing functional trait diversity with increasing area in the introduction. We expect functional richness to increase with scale similarly to species-area relationships. However, the exact shape of the curve cannot be predicted due to intra-specific trait variability, trait plasticity and possible trait correlations. Nevertheless, we found a similar slope of a power law fit in log-log scale than predicted by a large-scale species richness-area model of Gerstner, et al. 2014. Furthermore, we found a deviation from the power law at smaller scales, as was discussed in Nature by Pereira, et al. 2011. We added Suppl. Fig. 11 to illustrate this. Divergence and evenness were scale-invariant in our analysis, which is in agreement with Karadimou, et al. 2016.

Gerstner, K., et al. Accounting for geographical variation in species-area relationships improves the prediction of plant species richness at the global scale. Journal of Biogeography 41, 261273 (2014).

Pereira, et al. Geometry and scale in species-area relationships. Nature 482, E3E4 (2012).

Karadimou, E. K., et al. Functional diversity exhibits a diverse relationship with area, even a decreasing one. Scientific Reports 6, 35420 (2016).

Reviewer #3 (Remarks to the Author):

There remain a few conceptual issues, which require further development.

What is meant by functional diversity and what do we learn from it? Here it seems to be the distribution of several traits that are retrievable from RS indices and can then be mapped. But different traits will give different diversity values, and there should be some context and foundation for the choice linked to larger conceptual questions, presumably about ecosystem function. The functional diversity angle is weak without a clear conceptual framework or link to ecosystem function.

We have rephrased the introduction to better address these issues. We describe the relevance of mapping functional diversity in the context of ecosystem functioning. We also point out the differences and expected similarities between morphological and physiological traits and trait diversity respectively. Although the choice of traits does influence the diversity values, we expect the spatial patterns to converge following broad environmental gradients.

It seems the integration of diversity indices with lidar is the most novel angle rather than advanced trait retrieval and

mapping traits from airborne data. The relationship between trait maps and forest types is described, but many forest types can be mapped from imagery without trait mapping. Clarification of how the insights in the ms are novel is needed. How is it novel to apply indices of functional diversity to airborne imagery, and what is learned by doing so?

By redefining the main goals of the study in the introduction we clarify the main aspects and the novelty of the study. We agree that the comparison of morphological and physiological diversity derived independently from airborne laser scanning and imaging spectroscopy is novel, especially at this scale and resolution. Therefore we specifically lay out why it is important to compare them. Indeed, the functional trait maps reflect differences between forest types, and by comparing them with community data we can show some consistency (as requested by reviewer 1), but they are not limited to it. By mapping functional traits continuously and deriving functional diversity from it, we can provide a much more direct measure of biodiversity, not limited by given vegetation types or units. We strengthen this point in the manuscript on lines 37-40, 90-95. The novelty is in the continuous large-scale diversity mapping, which does include intra-specific trait variability. This is especially important when studying temperate mixed forests, where intra-specific trait diversity can be as large as inter-specific diversity.

The ms reveals low functional diversity of mountain ridges and high functional diversity of disturbed areas. What does this tell us about ecosystem function? That disturbed and early successional areas are more productive and high altitudes are less productive?

The lower functional diversity on the mountain ridge could indeed indicate that ecosystem functioning is reduced (see lines 233-239 of the Discussion). Disturbed areas do add to the diversity at larger scales, but also have low within-community diversity. Therefore it is more difficult to say if more disturbed areas would lead to higher productivity of the whole forest. It is not the scope of this study though to establish a direct link between functional diversity and ecosystem functioning. There are various recent studies showing a positive relationship between taxonomic / functional diversity and productivity, which we now cite in the introduction.

The relationship between lower functional diversity and higher altitude (ridges) with shallower soils that have fewer resources (nutrients, water) is interesting and could be the dominant focus of the ms. The forest traits may correlate with a detailed soil map, if it exists for the area.

In terms of the way functional diversity is calculated, functional richness, evenness and dispersion are all important components of functional diversity. In addition to the number of functionally distinct units (richness), how different they are (dispersion) and in how much they fill trait space (evenness) matters.

Some concepts in the discussion, including competitive exclusion, underdispersion, divergence/convergence are mentioned but not well explained. The interpretation remains speculative.

As requested by the editor and pointed out in the corresponding answer above, we included soil variables in the analysis and we strengthen the discussion on the relationship between environmental variables, following a gradient with altitude, and trait convergence resulting in lower functional diversity at higher altitudes.

The questions of the manuscript need to have context and to be grounded in a foundation for interpretation. What are the expectation for why trait diversity or dispersion patterns should change with scale and what do we learn when the do or do not shift according to expectations? As posed, three questions set the study up to be fairly descriptive.

1) What are the spatial patterns of morphological and physiological trait diversity derived from remotely sensed laser scanning and spectrometer data?

2) How does functional diversity change with scale?

3) Are most of the forest communities structured by trait convergence, trait divergence or randomly distributed traits?

We need to understand why shifts will scale are important and what the expectations are for the functional diversity to vary with scale and how this relates to the ability of remote sensing to detect functional diversity shifts with scale.

Thank you for raising these important questions. First of all, we agree that the initial questions were descriptive and did not reveal all the relevance and novelty of our study. Therefore, we decided to slightly change the format and clearly define three main goals of the study in the introduction. By doing so, we also provide the relevant context and formulate our expectations e.g. for the change of diversity with scale.

Line 45-46: Some imprecision in language: different species can be redundant with regard to their functional diversity - does this really mean species can be redundant in terms of their functional traits?

Exactly, we rephrased the sentence on line 44.

Lines 50-55: Canopy height, density, layering ... influence light availability, resource consumption and species diversity species diversity: Some clarification required here - in the understory? of forest birds? small mammals? what is being referred to?

We rephrased this paragraph, including the referred sentence on lines 63-67.

Line 64: Quantifying functional diversity from morphological and physiological traits reveals the distribution of species or individuals in the functional trait space. This is not actually true. The authors intend meaning here that is not being

conveyed.

We rephrased the beginning of the paragraph to correct this issue starting on line 77.

Line 66: Functional richness is calculated as the convex hull volume of the community niche: This does not account for the filling of the convex hull. Richness would be the number of functional units, and the number of units is independent of the niche volume. Many different units can occupy a small space, but three extreme units can delineate a large space. This is why dispersion and evenness are important in FD. Then one could ask whether all three factors (richness, evenness, dispersion) are needed to explain a certain ecosystem function. This would be interesting avenue for the ms.

It is important to clarify that in our approach the functional units are pixels, and not individuals, species, or functional types of trees or vegetation. Therefore the number of units used to calculate the functional diversity measures does not vary for a given scale. We use the definition of functional richness of Mouillot, et al. 2013 and Villger, et al. 2008. Nevertheless, it is true that this functional richness measure does not account for the filling of the convex hull, this is why we also use functional divergence and evenness in addition. This is explained in detail in the paragraph on lines 77-95.

Lines 84-86: Why do similar pattern in traits indicate that they are mapped correctly? Is this because all of the traits are correlated with each other? and are representative for functional traits in general I am not sure what this is supposed to mean. Certainly not all functional traits are correlated with each other.

We rephrase the importance of comparing the morphological and physiological diversity maps and testing the consistency of our method on lines 96-106. The agreement between our completely independently acquired morphological and physiological metrices is however a strong indicator for the robustness of the derived traits.

Lines 86-86 Nevertheless, we also expect to see differences due to different responses to abiotic factors and expressions of plant health and development Here is where a conceptual framework laying out expectations is important. What kinds of patterns and deviations are expected and how should they change with scale associated with the processes and functions that predominate at different scales? This would provide a means to interpret otherwise descriptive patterns.

We reformulate this statement in the introduction to be more precise and present a context of what we expect based on literature (lines 97-100). Then we specifically discuss the differences on lines 240-257 of the discussion.

Lines 126-128: Patterns of morphological and physiological richness exhibit strongest correlation at medium scale between 60 and 240 m radius. Why is the correlation important to test and what would the expectation be?

We build a stronger argumentation in the introduction, why the comparison and related correlations are important. See lines 95-101.

Lines 280-283: Functional divergence and evenness are generally high, mainly scale invariant and vary only in a small range, scale-dependency of functional diversity in this forest ecosystem is best represented by functional richness. Without using a functional diversity metric that incorporates all three components and allows examination of the influence of each component separately, this conclusion may not be supported. Or one could investigate the influence of each component of functional diversity and its association with a specific abiotic factor or ecosystem function.

We agree that this conclusion is weak. We decided that it should not be drawn based on the proposed analysis. Instead, we now demonstrate the association of each component with abiotic factors such as soil, topography and radiation.

Mouillot, D., et al. A functional approach reveals community responses to disturbances. Trends in Ecology & Evolution 28, 167177 (2013).

Villéger, S., et al. New multidimensional functional diversity indices for a multifaceted frame work in functional ecology. Ecology 89, 22902301 (2008).

3.3.3 NComms-16-23291C

Reviewer #1 (Remarks to the Author):

Overall I am happy with this manuscript and how it has improved with revisions. My one remaining question is with the new statistical analyses and Supplementary Figure 9 - the rebuttal explains this figure as variance partitioning but the description in the methods (lines 541-550) is very cursory. Hopefully a few sentences or references to this type of analysis will clear up confusion, but my impression is that no model selection was done to rule out insignificant predictors or to address multicollinearity, but depending on how the models were constructed (top 2 panels vs bottom 2) the strength of the predictors varied? That seems problematic, along with the lack of testing for spatial autocorrelation... given that this is a relatively small component of the overall paper, and I don't think it would change the points made in the discussion, I would just scale this back to look at individual correlations between the predictors and the traits (using a modified t-test approach to test for significance while considering spatial autocorrelation like that described by Dutilleul et al. (1993)).

Dutilleul, P. et al. 1993. Modifying the t test for assessing the correlation between two spatial processes. Biometrics 49:305314.

We would like to thank the reviewer for detailed comments. We agree that spatial autocorrelation needs to be considered in the statistical analysis. Therefore, we now fit a spatial model and use the estimated covariance matrix to fit a generalized linear model in order to account for spatial dependencies based on first order neighbors. We use the R package spdep and the function errorsarlm to compute relevant statistical figures (cf Bivand and Piras, 2015). Then we perform an ANOVA type I. Supplementary Figure 4 shows now the variance explained based on type-I sum of squares by soil (top panels) and topography (bottom panels), as well as what is additionally explained by adding topography or soil, respectively, and radiation to the model. Within the groups, the order of the explanatory variables was kept constant. For Supplementary Tab. 1, the order of the explanatory topographic variables was determined by the significance when tested individually, with the most significant used first in the combined model. We added this description and the details about the spatial model to the Methods (Statistical analysis, lines 517-534). We performed model selection and found a linear model to be best suited for the analysis. However, we did not aim to exclude any explanatory variable, since we only used variables of interest in the model without including any nuisance variables.

Bivand, R. & Piras, G. Comparing Implementations of Estimation Methods for Spatial Econometrics. Journal of Statistical Software 63 (2015).

Reviewer #3 (Remarks to the Author):

I find the manuscript quite strong. The authors are to be lauded for a tremendous amount of work, a novel, integrative approach, and much additional effort in the course of this lengthy review process.

We appreciate the valuation of our work and value much those comprehensive comments.

Here are a series of small wording edits for clarity/readability:

line 10: change ”could help predicting” to ”can help predict”

Change applied on line 10.

line 18: change ”mixtures of tree functional groups” to ”composition of tree functional groups”

We removed the whole sentence based on an editorial comment.

line 37: You might want to add Williams et al 2017 Nature EE in reference to complementarity effects

Thank you for this suggestion, we added the reference to the manuscript (line 37).

line 46-48: suggest changing: ”Incorporating individual-level functional traits, functional diversity may better predict ecosystem functioning than only using species level means can do” to ”By incorporating individual-level functional traits, functional diversity may better predict ecosystem functioning than species level means.”

Change applied on lines 46-48.

line 230: I suggest replacing the word ”convergence”. The meaning is not clear.

We replaced the word by reduced trait variability (line 225).

line 246: ”ecosystem functioning might be increased” is too vague. You would have to identify the function in order to explain that it increased.

We rephrased the sentence on lines 240-243.

lines 277 & 278; the sentence need some adjustment in construction: Given the continuous nature of the remotely sensed functional trait maps, we were able to study functional diversity at multiple scales and to develop a highly resolved scaling relationship.

Thank you for this comment. We applied these changes on lines 272-273.

Conclusions:

line 320. Delete ”uniquely”. Meaning is unclear and term is not necessary.

Change applied on line 307.

line 330. Using the term ”convergence” is not appropriate because that is an evolutionary term meaning that traits evolved to be similar due to similar environmental selection pressures. ”low variance”, ”homogeneity” or ”similarity” would be ecological terms.

We removed this sentence when merging Conclusions with Discussion, based on an editorial comment.

line 335. Can you avoid using ”should” in the sentence? Also, ecosystem functioning appears twice. Simplify.

How about: Future studies can advance the integration of remotely sensed functional data with databases of plant functional traits, environmental and ecosystem data, and dynamic vegetation models to increase our understanding of the mechanistic linkages between functional diversity and ecosystem function.

Thank you for the suggestion. We applied the changes on lines 310-313.

Chapter

4

Forest diversity and productivity under climate change

This chapter consists of a journal article in preparation and the corresponding supplementary information.

4.1 Predicting diversity and productivity under climate change by combining remote sensing and forest modelling

Schneider, F.D., Moorcroft, P., Paul-Limoges, E., Morsdorf, F.,
Guillén Escribà, C., Schmid, B., Schaepman, M.E.

This section is based on the article:
"Predicting plant diversity and productivity under climate change by combining remote sensing and forest modelling", in preparation.

F.D.S., P.M., F.M., and M.E.S. designed research; F.D.S., P.M., E.P.-L., F.M., C.G.E., and M.E.S. performed research; and all authors wrote the paper, with main contributions of F.D.S.
Article in preparation

To be submitted to Global Change Biology

Predicting plant diversity and productivity under climate change by combining remote sensing and forest modelling

FABIAN D. SCHNEIDER[1,2*], PAUL R. MOORCROFT[3], EUGÉNIE PAUL-LIMOGES[1,4], FELIX MORSDORF[1,2], CARLA GUILLÉN ESCRIBÀ[1,2], BERNHARD SCHMID[1,2,5], MICHAEL E. SCHAEPMAN[1,2]

[1] *Remote Sensing Laboratories, Department of Geography, University of Zurich, CH-8057 Zurich, Switzerland*
[2] *URPP Global Change and Biodiversity and Environmental Studies, University of Zurich, CH-8057 Zurich, Switzerland*
[3] *Department of Organismic and Evolutionary Biology, Harvard University, Cambridge, MA 02138, United States*
[4] *Department of Surface Waters Research and Management, Eawag, Swiss Federal Institute of Aquatic Science and Technology, CH-8600 Dübendorf, Switzerland*
[5] *Department of Evolutionary Biology and Environmental Studies, University of Zurich, CH-8057 Zurich, Switzerland*
*corresponding author: fabian-daniel.schneider@geo.uzh.ch

Abstract

Forest ecosystems play a key role in the global carbon budget and climate system through complex interactions and feedbacks at the biosphere-atmosphere interface. One of the main challenges in ecology and climate science is therefore to predict how forest ecosystems react to climate change, and what role plant functional diversity might play in regulating potential positive or negative impacts. In this article, we present a new approach integrating remote sensing measurements with Earth system models to predict plant diversity and productivity in forest ecosystems with changing meteorological drivers. We used high resolution laser scanning and imaging spectroscopy data to derive forest structure and composition of a temperate mixed forest site as input to the Ecosystem Demography model ED2. We predicted monthly gross primary productivity using diurnal meteorological drivers and forest phenology from passive-optical satellite data driving a predictive phenology model. A comparison with ground-based measurements showed accurate forest structure and composition derived from remote sensing data and the ability to predict monthly carbon fluxes. Preliminary results presented here are based on initial simulations without vegetation dynamics. When simulating dynamic competitive interactions and feedbacks, we encountered several challenges that still need to be resolved. A shortcoming of our current model parametrization is based on the incorporation of intra-specific structural diversity, since pre-defined species-specific allometric relationships are limiting the representation of the overall trait variation. This is inherent to most Earth system models and reduces the amount of realism representable in the model and provided by remote sensing data. In addition, we identified competition for water and plant moisture limitations as a key aspect needing further investigation and model development.

Keywords: functional biogeography, diversity-productivity, ecosystem stability, climate change, remote sensing
January 29, 2018

Introduction

Forests are key ecosystems in the terrestrial biosphere providing a range of important ecosystem services including provisioning services such as timber supply, water purification, cultural services being of recreational and spiritual value, as well as regulating services such as carbon sequestration (Millar & Stephenson, 2015; Braun *et al.*, 2017). In addition to the ecosystem services they provide, forest ecosystems play a important role in the carbon cycle and influence vegetation-atmosphere interactions through complex feedbacks (Schimel *et al.*, 2015). However, there is still considerable uncertainty in how climate change is altering the functioning of forest ecosystems and feedbacks, and even whether forests will remain a carbon sink (Brienen *et al.*, 2015). Furthermore, these effects and feedbacks will also depend on the structure and composition of the forests themselves, that is on the plant diversity contained within them (Barrufol *et al.*, 2013; Liang *et al.*, 2016).

The impact of climate change on forest ecosystems is manifold. Increased levels of atmospheric CO_2 and higher temperatures might lead to increased CO_2 uptake due to a longer growing season as well as faster growth and increased photosynthesis rates, leading to an important potential negative feedback (Schimel *et al.*, 2015; Oehri *et al.*, 2017). However, positive effects of such negative feedbacks on carbon sequestration might be hampered by an increased climatic variability, higher frequency and severity of droughts

and the occurrence of extreme events (e.g. mega-disturbances, Millar & Stephenson, 2015). Droughts have a severe impact on temperate forests, being one of the strongest stressors for trees (Anderegg *et al.*, 2015; Allen *et al.*, 2015). Severe droughts do not only lead to reduced photosynthetic rates and higher rates of tree mortality, but might also increase the susceptibility to insect attacks and large forest fires (Schlesinger *et al.*, 2016). How this will change the functioning and carbon budget of forest ecosystems on longer time scales is still unknown.

To better understand and predict these potential impacts of climate change, it is necessary to understand how forests adapt to changing climatic conditions and how this is influenced by the plant diversity of those forests. Biodiversity plays a key role in ecosystem functioning and stability (Balvanera *et al.*, 2006), and might also be a crucial factor regulating the response of forest ecosystems to climate change (Isbell *et al.*, 2017; Oehri *et al.*, 2017). Functional diversity has been reported as a main driver of forest productivity and stability on global scales (Liang *et al.*, 2016; Duffy *et al.*, 2017). The mechanisms behind, however, are still not well understood. For example, it is unclear whether the relationships established between sites will hold within a site, which is crucial to understand the mechanistic links and develop forest management and climate change mitigation strategies. Studies so far have focused on comparing forest monitoring sites across large scales (Liang *et al.*, 2015, 2016) or developing experimental studies (Cardinale *et al.*, 2007; Scherber *et al.*, 2010; Bruelheide *et al.*, 2014), but few are based on a detailed description of a whole forest ecosystem and how such a system might evolve under climate change (Fyllas *et al.*, 2017). Many studies also quantify productivity by an increase in stem diameter, stem volume or biomass, and do not show how this translates to CO_2 uptake and the whole carbon budget of the forest. We therefore emphasize the need for studying the relationship between diversity and productivity in terms of CO_2 uptake over time, and within a site ideally comprising an environmental or ecological gradient.

Biodiversity plays a crucial role in regulating the response to climate change induced positive and negative impacts and feedbacks (Isbell *et al.*, 2015). We hypothesize that a functionally more diverse system can be more productive and stable over longer time scales, thus supporting positive as well as dampening the negative effects of climate change. The theoretical reasoning for this hypothesis lies in the effect of niche complementarity (complementary traits lead to better resource usage, Williams *et al.*, 2017), selection (higher likelihood to have highly productive individuals under new climatic conditions, Hooper *et al.*, 2005), and ecological insurance (higher likelihood to have highly plastic and resilient individuals adapting to and recovering from disturbance, Silva Pedro *et al.*, 2017).

In this study, we use three remote sensing methods in combination with a process-based dynamic vegetation model (ecosystem demography ED2, Medvigy *et al.*, 2009) to predict current and future carbon fluxes as a function of local plant diversity in a temperate mixed forest. We aim to improve our understanding of what is driving forest productivity in terms of gross primary productivity under current and future climatic conditions. A very detailed description of the current state of the forest, i.e. its functional diversity (Schneider *et al.*, 2017), and high temporal resolution meteorological drivers are therefore crucial and help to improve the predictive capability of the model (Antonarakis *et al.*, 2014; Medvigy *et al.*, 2010). Dynamic interactions, niche complementarity and competition for resources (especially for water, nutrients and light) can be simulated based on the three-dimensional reconstruction of the forest using airborne laser scanning and imaging spectroscopy data (Schneider *et al.*, 2014, 2017). In the temporal domain, the model is driven by diurnal meteorological input variables and phenology predicted using passive optical satellite data (Justice *et al.*, 1998) in combination with a prognostic phenology model (Stöckli *et al.*, 2008, 2011; Garonna *et al.*, 2017).

Our main goals are: (1) to demonstrate the ability to integrate remote sensing measurements of forest canopy composition and structure into terrestrial biosphere models to improve predictions of ecosystem productivity and carbon uptake, (2) to investigate the relationship between plant functional diversity and productivity, and (3) to predict how productivity is going to change under climate change depending on plant functional diversity. For the first goal, we model nine years of GPP on a single plot within the temperate mixed forest site and compare it to the measurements of a flux tower located on the same plot. For the second goal, we extend the model to five plots within the site, covering a range of forest diversity, a change in forest composition and soils. Finally, we extend the simulations to predict forest diversity and productivity until the year 2100 based on four different climate scenarios. The three research goals build on each other and rely on necessary model improvements, which are still part of ongoing research. At the current stage of the manuscript, we will therefore mainly address the first goal in the results and discussion.

Material and methods

Study area

The study area is a temperate mixed forest at the Laegern mountain in Switzerland (47°28'43.0 N, 8°21'53.2 E). It is a diverse beech forest with a total of 13 tree species, with about 70% deciduous broadleaf trees and about 30% evergreen coniferous trees (forest inventory data). The dominating deciduous species are common beech (*Fagus sylvatica*), European ash (*Fraxinus excelsior*), and sycamore maple (*Acer pseudoplatanus*). The dominant coniferous species are Norway spruce (*Picea abies*) and silver fir (*Abies alba*). Trees of the main canopy are about 50 to 185 years old. The forested mountain is characterized by a steep ridge spanning in east-west direction, with slopes up to 60°. There is an elevational gradient from 450 to 860 m above sea level with a decrease of soil depth (100 cm to 10 cm), an increase of the amount of rocky material in the soil (0% to >30%) and a change from mainly *Cambisols* to *Regosols* and *Leptosols* on top of the ridge.

The core study site is a 5.5 ha flux-tower plot, located at 47°28'42.1" N, 8°21'51.7" E on 688 m above sea level (Fig. 1). The flux tower (CH-LAE) is equipped with eddy-covariance measurement instruments and a meteorological station and is centered in the southern part of the plot. The plot contains non-managed forest with 1307 canopy trees (diameter at breast height > 20 cm), of which 88% belong to deciduous broadleaf species and 12% to evergreen coniferous species. The plot is described in detail in Guillén Escribà *et al.* (in preparation). Besides the flux tower plot, we selected five additional plots of 100 x 300 m along the elevational gradient (Fig. 1). The characteristics of the five areas are summarised in Tab. 1.

The ED2 model

The ED2 model is a process-based is a process-based terrestrial biosphere model that represents individual plant-level dynamics (growth, mortality and recruitment), and associated ecosystem-level carbon, water and energy fluxes over timescales ranging from hours to centuries. In contrast to conventional ecosystem as big leaf models that represent the canopy in an highly aggregated manner, vegetation dynamics model utilize the the ecosystem demography (ED) concept introduced by Moorcroft *et al.* (2001), in which vegetation is represented as cohorts of similar height and plant functional type, grouped in patches of similar age within a site of homogeneous environmental conditions with regard to soil, topography and meteorology (Medvigy *et al.*, 2009). Plant growth, mortality and recruitment are simulated as part of vegetation dynamics. The size- and age-structured representation also allows to model disturbance and competition for light, although simplified due to the assumption of flat crown layers without a spatially explicit location within a patch. To improve vegetation dynamics regarding canopy structure and light availability compared to previous ED modelling schemes, heterogeneity in horizontal and vertical light and micro-climate environments has been introduced in ED2 by implementing partial shading based on cohort crown area and the dynamic merging and splitting of cohorts based on their leaf area index (Fisher *et al.*, 2017). The ability of ED2 to represent vertically-stratified and horizontally heterogeneous plant canopies enables the model to incorporate the detailed three-dimensional initialisation based on remote sensing data.

To represent forest composition in the model, we group the species present at our site into corresponding ED2 plant functional types used by Medvigy *et al.* (2009) and Antonarakis *et al.* (2014), namely: late-successional conifers (LCf), and early (EHw), mid (MHw), and late-successional hardwoods (LHw). At the Laegern forest, the two late-successional coniferous needle species are Norway spruce (*Picea abies*) and silver fir (*Abies alba*). Furthermore, we grouped European ash (*Fraxinus excelsior*) and common whitebeam (*Sorbus aria*) as early-successional hardwoods, sycamore maple (*Acer pseudoplatanus*), field maple (*Acer campestre*), sessile oak (*Quercus petraea*), largeleaf linden (*Tilia platyphyllos*) and wych elm (*Ulmus glabra*) as mid-successional hardwoods, and European beach (*Fagus sylvatica*), Norway maple (*Acer platanoides*) and European hornbeam (*Carpinus betulus*) as late-successional hardwoods. There were no early- and mid-successional species present at our site.

Meteorology

Medvigy *et al.* (2010) have shown how short-term (hourly-weekly) meteorological variability has an important effect on ecosystem functioning such as carbon sequestration, and, over decadal timescales, can drive shifts in forest structure and composition. Therefore, it is important to use high temporal resolution meteorological inputs.

Here, we use nine meteorological input variables measured at 10-minute intervals for the years 2006 to 2014. Atmospheric pressure at field elevation (hPa), air temperature (°C), relative humidity (%), wind direction (degree), average wind speed (m/s), maximum wind speed (m/s), global radiation (W/m^2), net radiation (W/m^2), and precipitation (mm) were measured on the flux tower in the Laegern forest as part of the national air pollution monitoring network (NABEL) (Suppl. Figs. 13 to 15). Figure 2 shows the monthly values of temperature, global radiation and precipitation from 2006 to 2014 and average diurnal cycles per month. For gap filling of missing values (<2%), meteorological data were used from the nearby meteorological stations Laegern and Kloten. The same variables as for the Laegern flux tower station were used in 10-minute intervals, except for relative humidity only available as hourly averages. Incoming shortwave and longwave radiation was measured at 30-minutes intervals on the flux tower. Gap filling was done using data from neighbouring meteorological stations at Guetsch and Magadino. More details about the gap filling are provided in Supplementary Note 1.

To predict the development of forest structure, composition and productivity under a changing climate, we use meteorological inputs to ED2 based on four climate models, driven by the IPCC SRES A1B greenhouse gas emission scenario as part of the EU-ENSEMBLES project (van der Linden & Mitchell, 2009). To adapt the large-scale climate

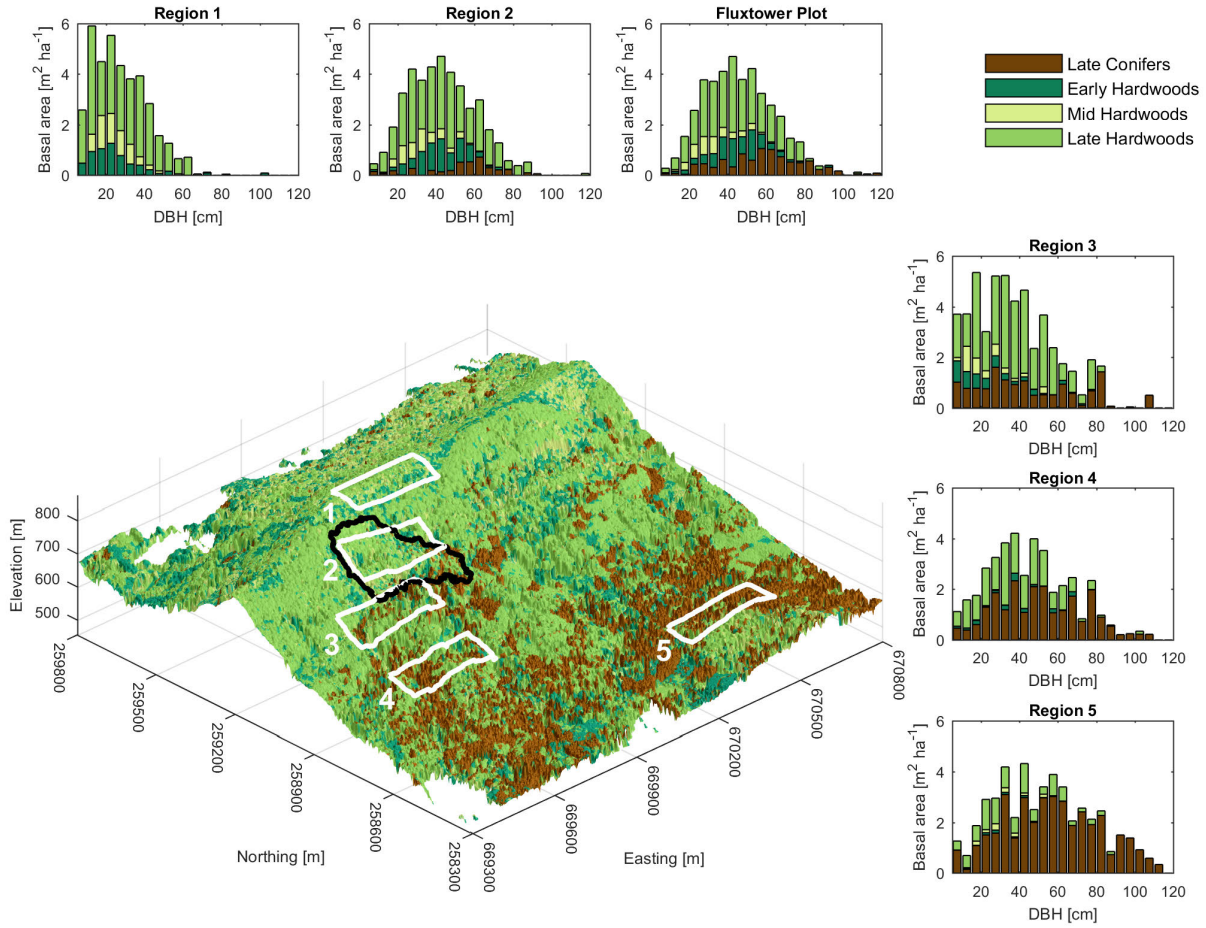

Fig. 1: The core study site is the 5.5 ha flux tower plot, marked with a solid black outline. Five regions of 3 ha are marked with a white outline and numbered from one to five with decreasing elevation, increasing soil depth and a shift from forests dominated by deciduous hardwoods to evergreen conifers.

models to the local conditions at Laegern, a bias correction was applied following the two-step approach of Rajczak *et al.* (2016). This incorporates a first bias correction to a station with long-term measurements following a spatial transfer to a local target station, both using a quantile mapping approach. The variables were corrected for the local meteorological station in Zurich Affoltern that is located close to the Laegern forest (Suppl. Figs. 17-18). To cover a range of possible climatic conditions until the year 2100, we selected the four climate models C4I-HadCM3Q16, ETH-HadCM3Q0, KNMI-ECHAM5 and SMHI-HadCM3Q3 being run by the Irish C4I, the Swiss ETH, the Dutch KNMI and the Swedish SMHI institutes based on the regional climate models RCA3, CLM, RACMO and RCA, respectively (Suppl. Fig. 19). Since the ED2 model incorporates diurnal variability, we modelled hourly values based on the daily climate model mean values, minimum and maximum temperature and hourly measurements from the flux tower from 2005 to 2016. The modelling of hourly values is explained in more detail in Supplementary Note 2. Example time series are shown in Supplementary Fig. 16 and a detailed comparison of seasonal distributions of hourly values is provided in Supplementary Figs. 20 to 26.

Phenology

The phenological timing of growing seasons is another important aspect allowing to model temporal changes in ED2. Since ED2 is based on a simplified phenology scheme, we used the constrained prognostic phenology model Pheno-Analysis introduced by Stöckli *et al.* (2008). This model incorporates a data assimilation scheme and was previously used and validated at local sites up to globally distributed regions (Stöckli *et al.*, 2011) and global scale (Garonna *et al.*, 2017). We ran the model in the data assimilation mode with 12 years of Moderate Resolution Imaging Spectroradiometer (MODIS) fraction of photosynthetically active radiation (FPAR) (see, D'Odorico *et al.*, 2014, for a comparison) and leaf area index (LAI) data from 2005 to 2016, together with gap-filled meteorological measurements from the flux tower, to calculate a set of constraining parameters. These parameters mainly control the range of temperature, vapour pressure deficit and photoperiod.

We then ran the model in prediction mode to simulate daily LAI time series based on meteorological drivers and constraining parameters. To derive the phenological timing of the growing season, we used TIMESAT to fit a logistic

Tab. 1: Five selected regions with varying topography (elevation, slope), soil (soil type, grain type, amount of rocks), composition (fractional cover (FC) of conifers) and diversity. Diversity is specified with regard to plant functional types (Shannon's I) as well as functional richness (FRic) and evenness (FEve) calculated based on six morphological and physiological forest traits (see, Schneider *et al.*, 2017).

Region	Elevation	Slope	Soil Type	Soil Grain	Soil rocks	FC Conifers	Shannon's I	FRic · 10^3	FEve
1	830 m	37.9°	Leptosols	Clayey loam	>30%	0.08%	0.94	0.38	0.85
2	733 m	33.9°	Calcic Cambisols	Clayey loam	>30%	6.37%	1.10	0.25	0.81
3	670 m	24.1°	Cambisols	Loamy silt	<10%	24.4%	1.08	5.71	0.79
4	593 m	26.4°	Cambisols	Sandy loam	<10%	47.3%	0.89	3.14	0.81
5	559 m	13.0°	Dystric Cambisols	Sandy loam	none	64.6%	0.91	1.37	0.83

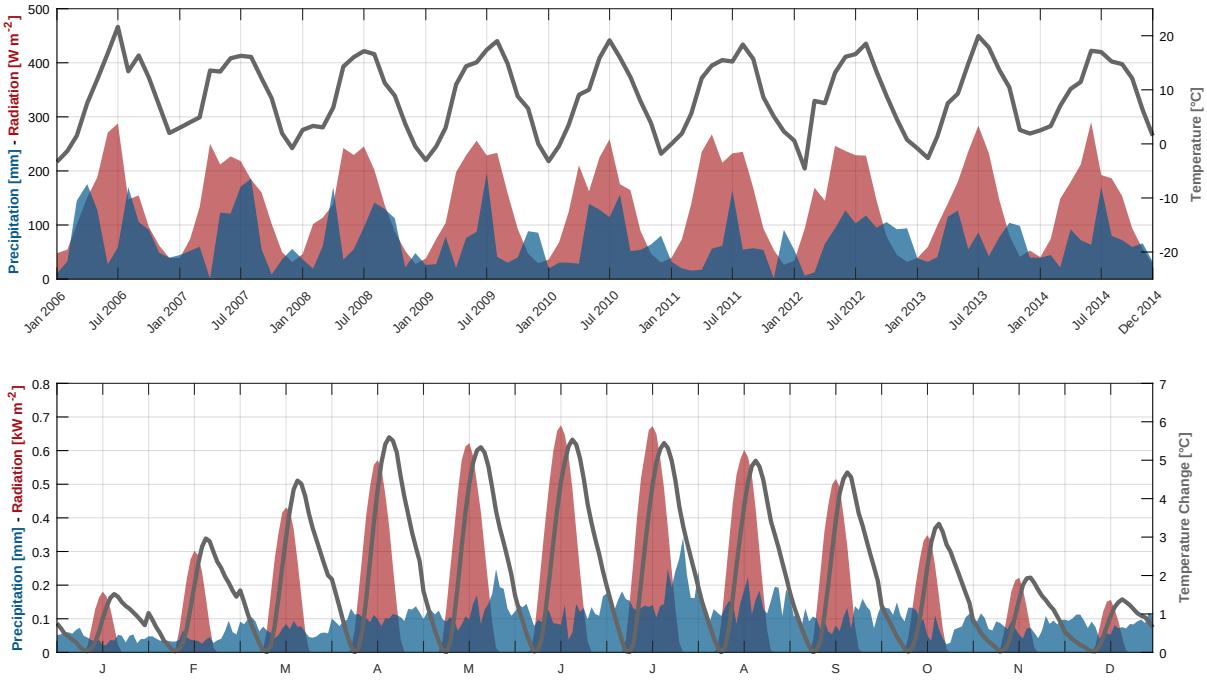

Fig. 2: Monthly mean radiation, sum of precipitation and mean temperature for the years 2006 to 2014 (upper panel) and corresponding mean diurnal cycles per month averaged over the nine years (lower panel). The underlying 10 minutes measurements were part of the meteorological inputs for the dynamic vegetation model ED2.

function to the LAI data (Jönsson & Eklundh, 2004). We then applied a 10% and 90% threshold based on the yearly minimum and maximum LAI to retrieve the day of year (DOY) of start and end of greening as well as start and end of browning for each year (Fig. 3). By applying the same procedure using the climate model data, we were able to predict the phenology until the year 2100 (Suppl. Fig. 27).

Forest structure

The individual-based nature of the ED2 model offers the advantage that it can be initialised with ground- or remote sensing-based data describing the current state of the ecosystem with a high level of detail, thus incorporating the whole history including disturbance or forest management. A recent study by Antonarakis *et al.* (2014) indicates that information of this kind can improve model predictions of carbon fluxes and vegetation dynamics compared to conventional equilibrium vegetation simulations. Here, we use a plant area index (PAI) voxel grid, canopy height and airborne laser scanning data in combination with a detailed field survey and high spatial resolution drone images to derive forest structure information used to initialize the current state in the model. More details about the data are provided in Schneider *et al.* (2014); Kükenbrink *et al.* (2017); Guillén Escribà *et al.* (in preparation) and Supplementary Note 3 and 4. The main structural model inputs are the vertical distribution of plant material (leaves, needles, twigs, etc.) and estimates of diameter at breast height (DBH), tree density and basal area. The PAI and canopy height data used to derive these inputs were available at 2 m spatial resolution. By aggregating to 10 x 10 m areas, we were able to keep the estimates apportioned by plant functional type and optimize the computation time of the model.

Three-dimensional forest canopy structure is described in ED2 by a vertical distribution of PAI. We define the PAI

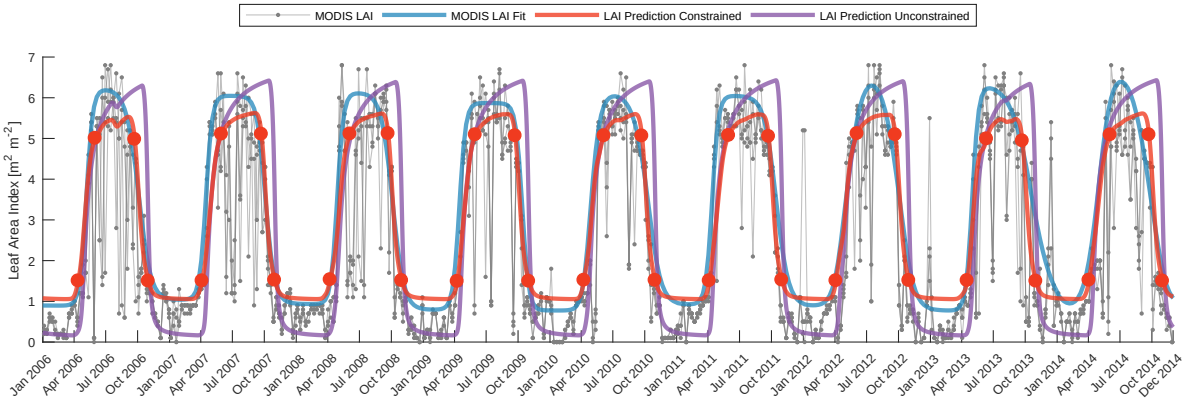

Fig. 3: The red line shows the prediction of leaf area index (LAI) using the constrained prognostic phenology model PhenoAnalysis, with red dots indicating start and end of greening and browning as used in the ED2 model. For comparison, we show the unfiltered MODIS LAI data points (gray), a logistic fit to filtered MODIS LAI data (blue) and predicted LAI without constraining the model (purple). The constraining parameters have been calculated by running PhenoAnalysis in the data assimilation mode using both MODIS data and meteorological drivers at half hourly resolution.

of a 10 x 10 m area (PAI_{10m}) as the sum of all PAI values per plant functional type pft and height z for n height layers:

$$PAI_{10m} = \sum_{pft=1}^{4} \sum_{z=1}^{n} PAI(z, pft) \quad (1)$$

To calculate PAI as a function of height and plant functional type $PAI(z, pft)$, we first used the 2 x 2 m data to calculate the average PAI_{10m} and $PAI(pft)$ based on the fractional cover fc of each plant functional type pft within the 10 x 10 m areas:

$$PAI(pft) = fc_{pft} \cdot PAI_{10m} \quad (2)$$

We then averaged the fractional amount of LiDAR points fp per 4 m height layer z for each plant functional type pft to calculate $PAI(z, pft)$ as:

$$PAI(z, pft) = fp_{z,pft} \cdot PAI(pft) \quad (3)$$

DBH values were modelled based on canopy height. To build the allometry between canopy height and DBH, we fitted an exponential model using the field inventory data of 159 late conifers, 253 early hardwoods, 328 mid hardwoods and 566 late hardwoods:

$$dbh = a \cdot ch^b + \epsilon(std, skew, kurt), \quad (4)$$

where ch is canopy height, a and b are coefficients and ϵ is the residual distribution around the mean. To predict not only the mean but a realistic DBH distribution, we derived the standard deviation std, skewness $skew$ and kurtosis $kurt$ of the distribution to model ϵ (Matlab R2017a, pearsrnd). The resulting values for a, b, std, $skew$ and $kurt$ are summarised in Table 2.

Single-tree delineation was used to provide the number of stems per site. The method is an adapted version of the approach used in Morsdorf *et al.* (2004); Kaartinen *et al.* (2012) and later updated in Wang *et al.* (2016). The algorithm detects local maxima in a smoothed version of the vegetation height model (VHM) and uses those positions as starting points for either a clustering of the point cloud (Morsdorf *et al.*, 2004) or a watershed segmentation of the VHM, which is what we used for this study. The amount of smoothing was varied between deciduous and coniferous trees using an ALS-based forest class differentiation exploiting differences between echo types and other related metrics. Furthermore, a tree height-crown size heuristic (i.e. larger trees have larger crowns) was used to apply differently sized smoothing kernels for trees of different size. The method had a detection rate of 79% overall, 83% for trees $>$ 35 m and 76% for trees $<$ 35 m. The canopy height maps and the segmented stems with assigned DBH values are shown in Fig. 4.

Tab. 2: Coefficients a and b of the exponential function and standard deviation std, skewness $skew$ and kurtosis $kurt$ describing the canopy height to dbh allometry for the plant functional types late conifers (LCf), early hardwoods (EHw), mid hardwoods (MHw) and late hardwoods (LCf).

	LCf	EHw	MHw	LHw
a	11.41	17.31	16.63	11.32
b	0.466	0.280	0.225	0.398
std	18.26	10.70	9.752	16.13
$skew$	-0.475	1.226	1.106	0.443
$kurt$	3.705	6.973	4.332	2.959

To account for possible systematic over- or under-segmentation of stems, we calibrated the stem counts on the flux tower site for different height classes using the field inventory data linked to a crown map derived from high spatial resolution drone images (Suppl. Fig. 29). We then related pixel counts to stem counts per site based on 1 m height classes from 4 to 55 m canopy height. This allowed us to estimate the fractional stem count for each pixel. Finally, we calculated basal area ba (m^2 ha^{-1}) as

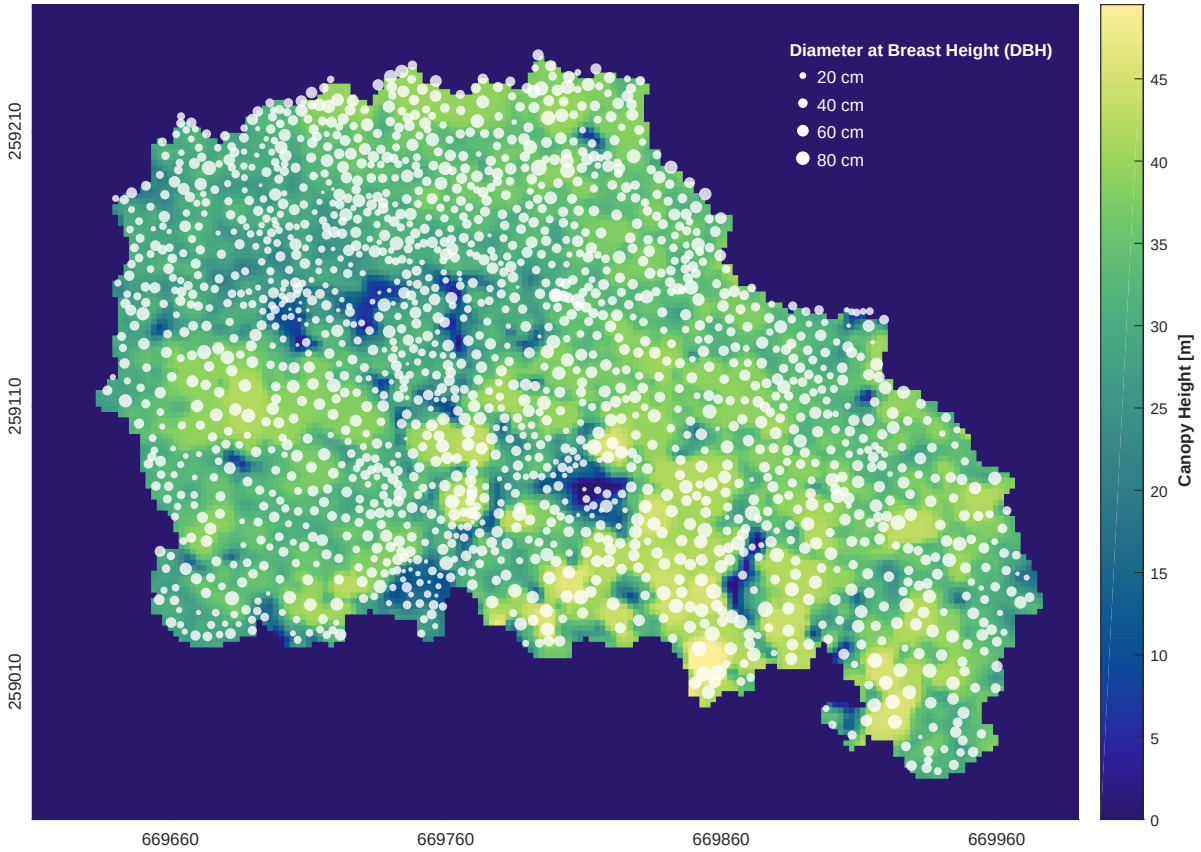

Fig. 4: Canopy height and stem distribution as derived from airborne laser scanning data for the 5.5 ha flux tower plot. Canopy height is a continuous raster at 2 m spatial resolution. The white dots represent segmented tree stems with changing size according to the assigned diameter at breast height (DBH), estimated using allometries based on canopy height. The location and distribution of DBH values is not spatially explicit, but should rather represent the correct size distributions of the plot.

follows:

$$ba = fs \cdot pi \cdot \left(\frac{dbh}{2}\right)^2 \cdot \frac{1}{a}, \tag{5}$$

where fs is the fractional stem count, dbh is the diameter at breast height (cm), and a is the total area of the plot (m^2). Basal area ba was calculated for each 2 x 2 m pixel and then aggregated to 10 x 10 m by summing the pixel values of each plant functional type.

Forest composition

To initialize the forest composition and assign species-specific characteristics to the model cohorts, we classified the forest into corresponding ED2 plant functional types, namely: late conifers and early, mid, and late hardwoods (LCf, EHw, MHw, LHw, respectively). The classification of the four plant functional types was performed using a random forest classifier with remotely sensed input features. Therefore, the classification could be applied to the entire Laegern forest.

We calculated a set of 81 possible input features based on six functional traits, corresponding spatially filtered traits, airborne imaging spectroscopy and laser scanning data to perform a feature selection. The data are described in Schneider *et al.* (2017) and Supplementary Note 3. Based on feature importance, we discarded features with low importance that reduced the overall accuracy of the random forest model. We received the best results with 27 relevant features. We used the six morphological and physiological forest traits at 2 x 2 m spatial resolution as well as the corresponding filtered traits using a spatial median filter with a window size of 7 x 7 pixel. We performed a principal component analysis (PCA) for forested pixels on the 284 surface reflectance bands and selected the PCA bands 1 to 9, 13 and 18. Additionally, we applied a continuum removal (CR) on the 284 surface reflectance bands followed by a PCA and selected the CR PCA bands 1, 2, 4 and 10. This proved to be the best set of input features for the random forest classification of plant functional types.

We used the field inventory data of 1307 dominant and co-dominant trees and the corresponding crown map to derive a raster-based training dataset at 2 x 2 m spatial resolution. In the original dataset, there were 1449 pixels for late conifers, 1960 pixels for early hardwoods, 1916

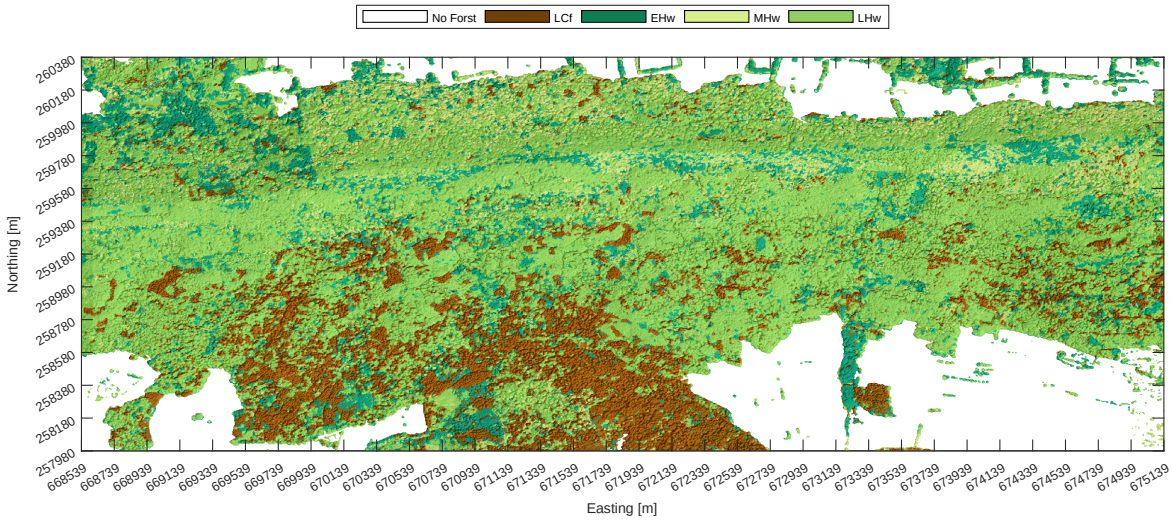

Fig. 5: Map of plant functional types classified using airborne remote sensing data. The plant functional types are late-successional conifers (LCf), early hardwoods (EHw), mid hardwoods (MHw) and late hardwoods (LHw).

pixels for mid hardwoods and 5262 pixels for late hardwoods. We then used prior information from 73 forest stand polygons covering the Laegern forest to build specific training datasets for each polygon. We changed the composition of the four plant functional types in the training datasets based on the percentage coverage of the most dominant species according to the stand polygon data. We trained, tested and ran a random forest classification for each stand polygon of the forest with its specific training dataset. We used 70% of the data for training and 30% for testing and validation. We built 1000 trees with a minimum leaf size of 5. We used the composition of groups in the training dataset as prior information for the random forest classification. We then used all of the data to train the model for predicting the plant functional type for each pixel. We reached an overall accuracy of 74% and a kappa of 61% for the classification of plant functional types over the whole forest. For spatially resolved results for each polygon and a comparison between the predicted plant functional types per polygon and the prior information, we refer to Supplementary Fig. 30.

Carbon fluxes

For validation of the modelling approach, we used carbon flux measurements of the years 2006 to 2014. Eddy-covariance (EC) fluxes (Baldocchi, 2003) were measured continuously at the Laegern flux tower. The EC instrumentation consisted of an open-path infrared gas analyzer (IRGA) (model LI-7500, LI-COR Inc., Lincoln, NE, USA) and a three-dimensional sonic anemometer-thermometer (model HS, Gill Instruments, Lymington, UK). Eddy-covariance (EC) measurements were made at a frequency of 20 Hz and processed to half-hourly averages using the EddyPro software (v6.1.0, LI-COR Inc., USA). Flux quality post-processing was done following Vickers & Mahrt (1997). Standardized gap filling and partitioning of the net ecosystem CO_2 exchange (NEE) into gross primary production (GPP) and ecosystem respiration (R) was performed using the method from Barr *et al.* (2004).

Results

Due to the complexity of the model and its initialisation with an unprecedented level of detail, model improvement and optimisation are still ongoing. An iterative procedure is necessary to understand how the model reacts in a new ecosystem and how it has to be initialised to find a trade off between level of detail (number of cohorts and patches) and technical and computational feasibility. Therefore, we present preliminary results here of the forest structure initialisation and different simulations with and without vegetation dynamics. The current results presented here address the first research goal to demonstrate the ability of a remote sensing initialised model to predict gross primary productivity.

Forest structure initialisation

Figure 6 shows the results of the compositional basal area and tree count distributions as derived from remote sensing data and translated to the ED2 modelling scheme, compared to the reference dataset measured in the field. The remote sensing derived distributions of basal area and tree count over the DBH size classes conform to the distributions measured in the field. There is a slight underestimation of the number of mid-successional hardwoods at small DBH classes, but with little influence on the distribution of basal area. Overall, basal area of late conifers and early, mid and late-successional hardwoods devi-

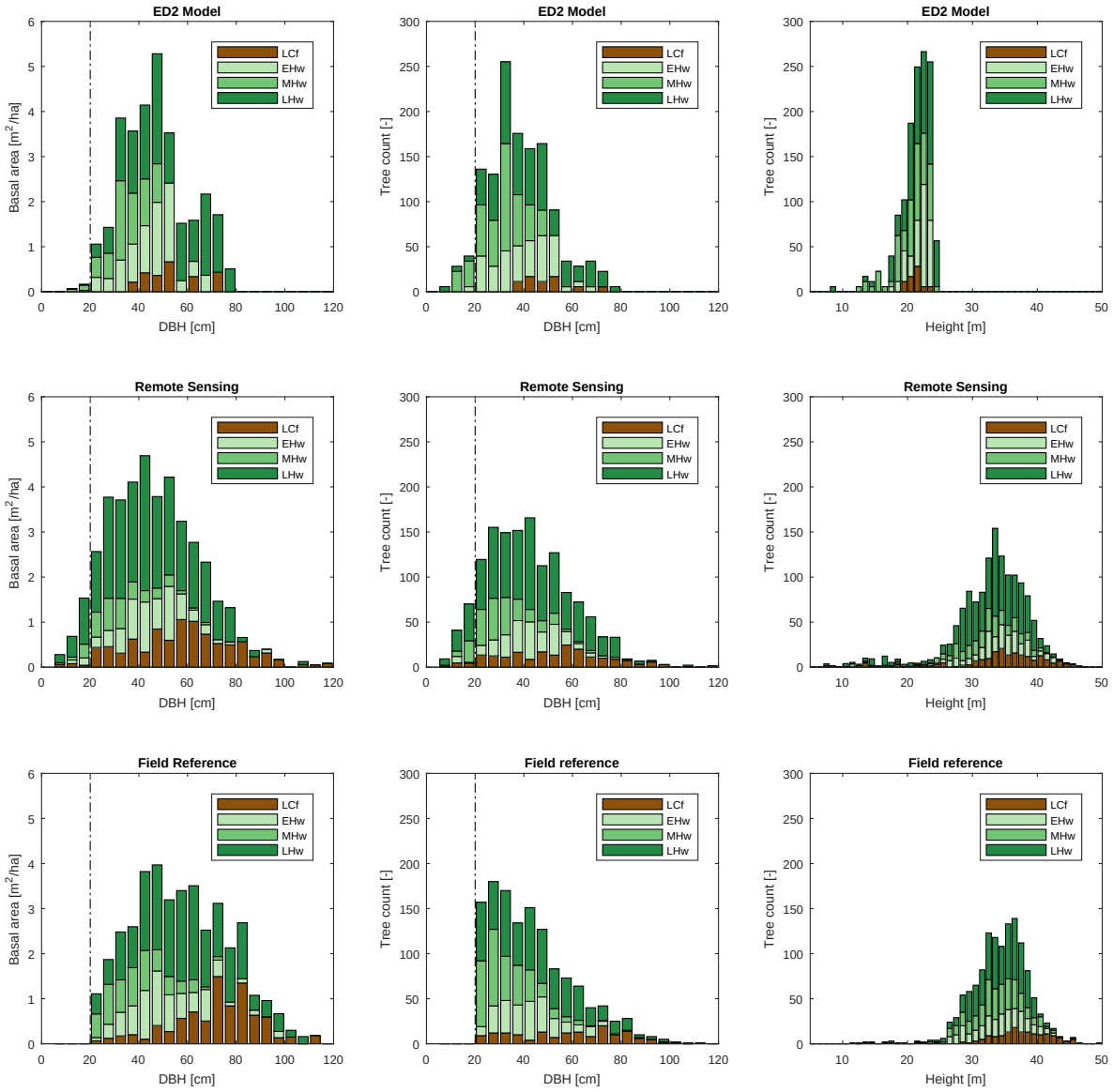

Fig. 6: Forest structure and composition of the flux tower plot as initialised in the ED2 model, derived from remote sensing data and measured in the field (trees $>$ 20 cm DBH). Structure and composition are shown as basal area and tree count per DBH size class and tree count per canopy height class for late-successional conifers (LCf) and early, mid and late-successional hardwoods (EHw, MHw, LHw).

ate 0.3, -0.6, -1.8 and 4.4% from the reference with an RMSE of 0.3, 0.2, 0.2 and 0.6 m^2 ha^{-1}, respectively. Tree count estimates deviate 2.3, -2.6, -9.8 and 9.1% from the reference with an RMSE of 4.3, 5.4, 11.3 and 11.7, respectively. Similarly, the remote sensing based distribution of the number of trees per height class follows the one from the field reference.

When translating the pixel-based remote sensing inputs to model cohorts and patches, a subsetting and splitting of the site was needed to optimise model performance. Therefore, the total basal area and tree count are lower (30.5 m^2 ha^{-1} and 1276) than in the reference (40.0 m^2 ha^{-1} and 1302). Considering this, the distributions of basal area and tree count over the DBH size classes are still comparable to the reference. The major deviation of the model representation lies in canopy height, since it is modelled based on diameter at breast height and the diameter-height allometry functions defined in the model (Suppl. Fig. 28). Therefore, modelled trees are on average 33% smaller than in reality, leading to a more condensed distribution of plant area index

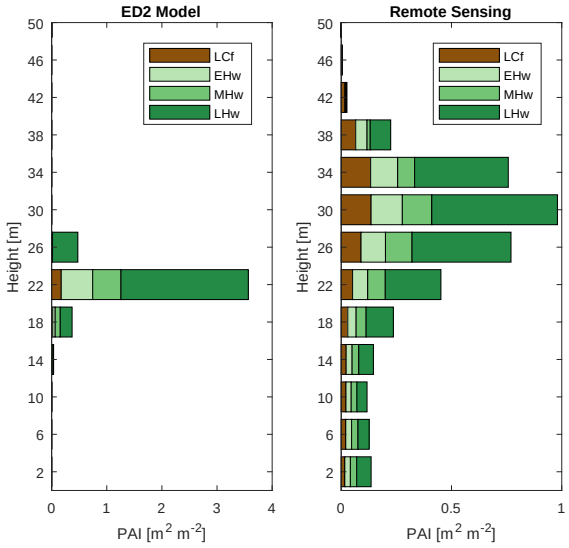

Fig. 7: Vertical distribution of plant area index (PAI) within the canopy as initialised in the ED2 model and derived from airborne laser scanning data on the flux tower plot.

at a lower canopy height (Fig. 7).

GPP driven by meteorology only

Figure 8 shows the modelled and measured monthly GPP values over the period of 2006 to 2014 in comparison to a potential vegetation simulation, started 250 years before from bare soil. It shows that the potential vegetation simulation strongly underestimates GPP in all the years by 13 to 42%, especially during the most productive months in summer. For June to August, the differences peak at up to 188 g C per m^2 and month or 61% of the measured flux. The potential vegetation simulation does not reflect the current composition, since it is dominated by late conifers (57% basal area) and early conifers (31% basal area) with only 12% of the basal area accounted to late hardwoods (Fig. 11). This results in an RMSE of 73 g C m^{-2} mon^{-1}, whereas the remote sensing initialised simulation results in an RMSE of 43 g C m^{-2} mon^{-1}. The GPP deviation from the potential vegetation simulation shows that forest composition and structure explain much of the differences to the measured flux.

The remote sensing initialised flux is run without vegetation dynamics, resulting in an initially fixed canopy structure which does not change over time. Slight differences in timing with an earlier onset and slightly later decline of GPP might thus be explained by a missing phenology of leaves. Without having to invest in the development of leaves, the trees with fixed canopy structure can increase photosynthesis more directly with increasing radiation and temperature. This generally leads to an overestimation of yearly GPP (4% on average). However, in some years there is an underestimation of GPP in the summer and winter months. Fig. 9 shows that a stronger peak of measured monthly GPP in summer might be linked to a generally higher maximum hourly GPP, whereas the higher values in winter seem to come from an unexpected night-time signal. This might be due to the influence of cold temperatures on the measuring device.

GPP simulations with vegetation dynamics

The simulation of GPP without vegetation dynamics shows mainly the influence of forest structure and composition in combination with the meteorological drivers on the simulation of GPP. It is therefore an ideal way to test the quality of the input parameters and whether they are initialised correctly. However, it does not show if the model is able to realistically simulate vegetation interactions and dynamics, including phenology, competition, growth and mortality. This is crucial though to accurately predict plant diversity and productivity under climate change. During the first model runs with vegetation dynamics, we identified several problems in the model implementation that we iteratively resolve.

The first simulation showed a decline in PAI, biomass and basal area, resulting in a reduced GPP over the years (Fig. 10). The model runs stopped after six years with a numerical error. Therefore, we moved to a newer version of the code, running for the years 1997 to 2014. In this version, however, two major die-offs of deciduous hardwood trees happened leading to a complete renewal of the forest with a regrowth of early successional species within only a few years (Suppl. Fig. 31). Figure 10 shows the second mortality event at the end of 2006 and the recovery of the forest until 2014. The mortality was triggered by the a warm winter 2007 followed by a dry spring. This led to an early leaf out in winter and the subsequent death of many trees. However, both events could only happen due to a fundamental limitation in the simulation of deciduous hardwoods. We found that NPP was negative since no carbon could be properly allocated to the modelled trees. Thus there was not enough carbon available to invest in leaves, which led to their death after some years.

Therefore, we went back to the previous model version, where we could identify an excessive moisture limitation in coniferous cohorts of the understory as the main cause of the numerical error in the model. Due to a lack of water, the leaves started to overheat and reach an upper threshold of leaf temperature. By turning off plant moisture limitation, we could simulate the period of 2006 to 2014. However, this lead to a very high GPP and an increase in PAI, biomass

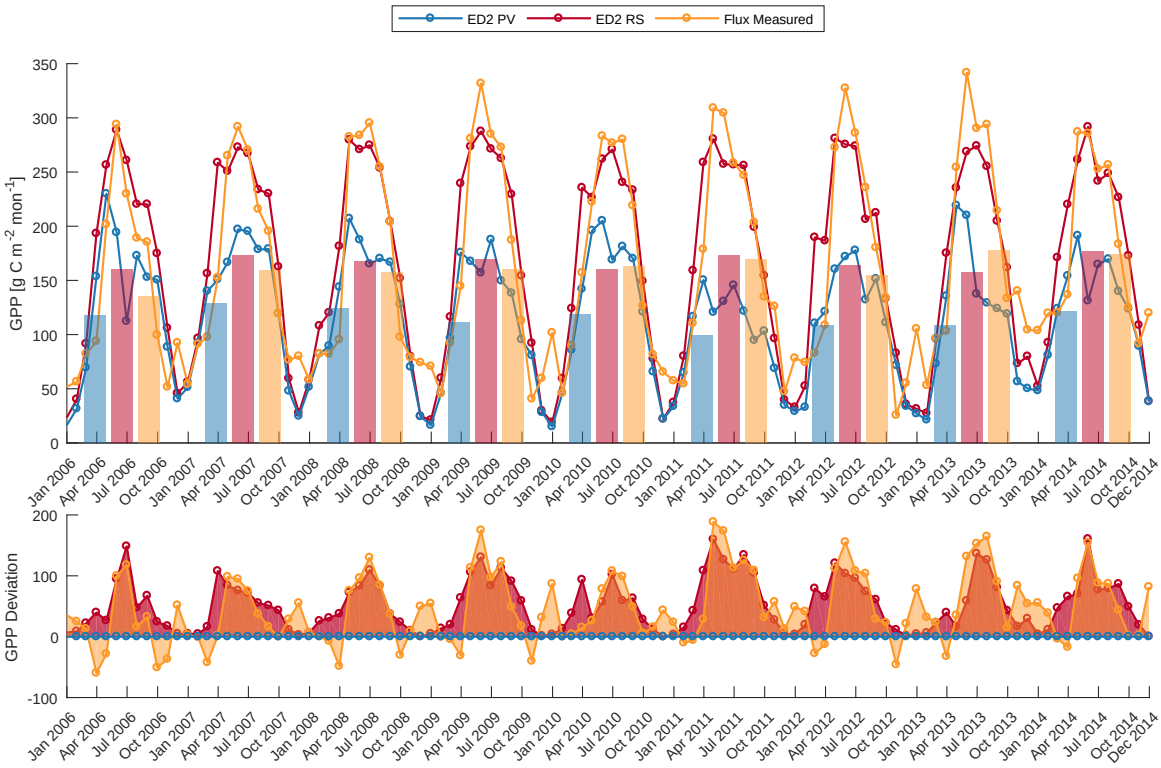

Fig. 8: Monthly GPP (lines) and yearly averages (bars) as predicted by a potential vegetation simulation ('ED2 PV'), predicted by a remote sensing initialised simulation without vegetation dynamics ('ED2 RS'), and measured on the flux tower ('Flux Measured'). GPP deviation shows the difference of 'ED2 RS' and 'Flux Measured' with respect to 'ED2 PV'.

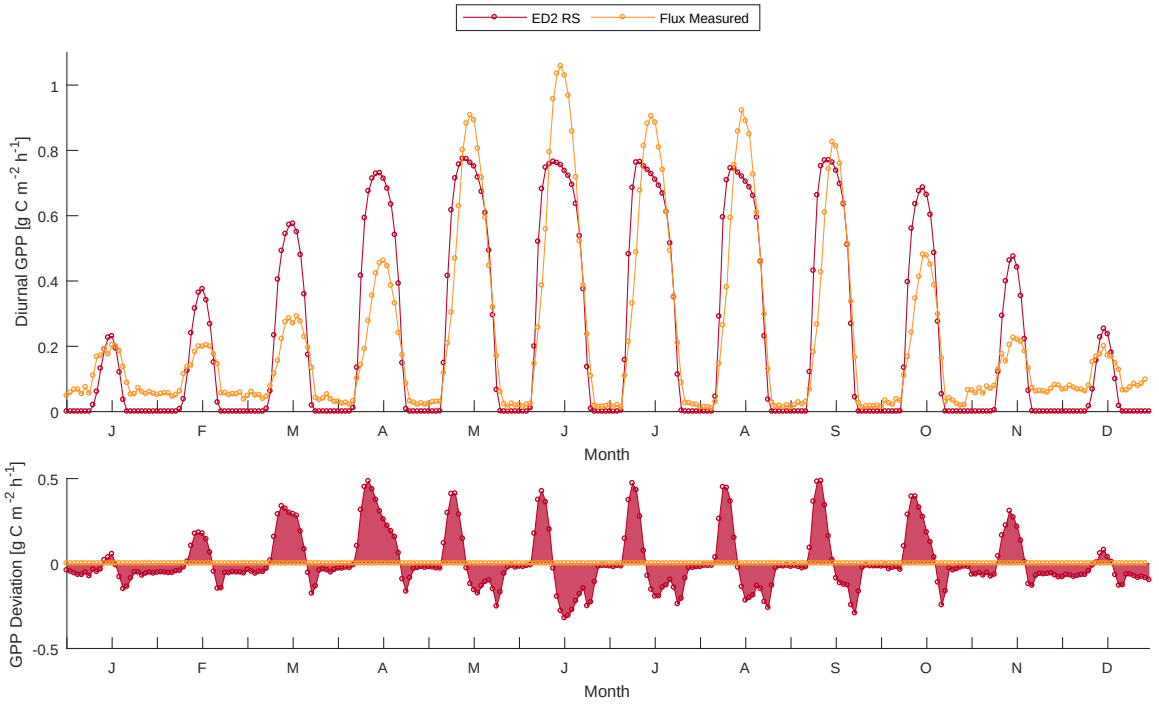

Fig. 9: Hourly diurnal GPP averaged per month over the years 2006 to 2014 as predicted by a remote sensing initialised simulation without vegetation dynamics ('ED2 RS') and measured on the flux tower ('Flux Measured'). GPP deviation shows the difference of 'ED2 RS' with respect to 'Flux Measured'.

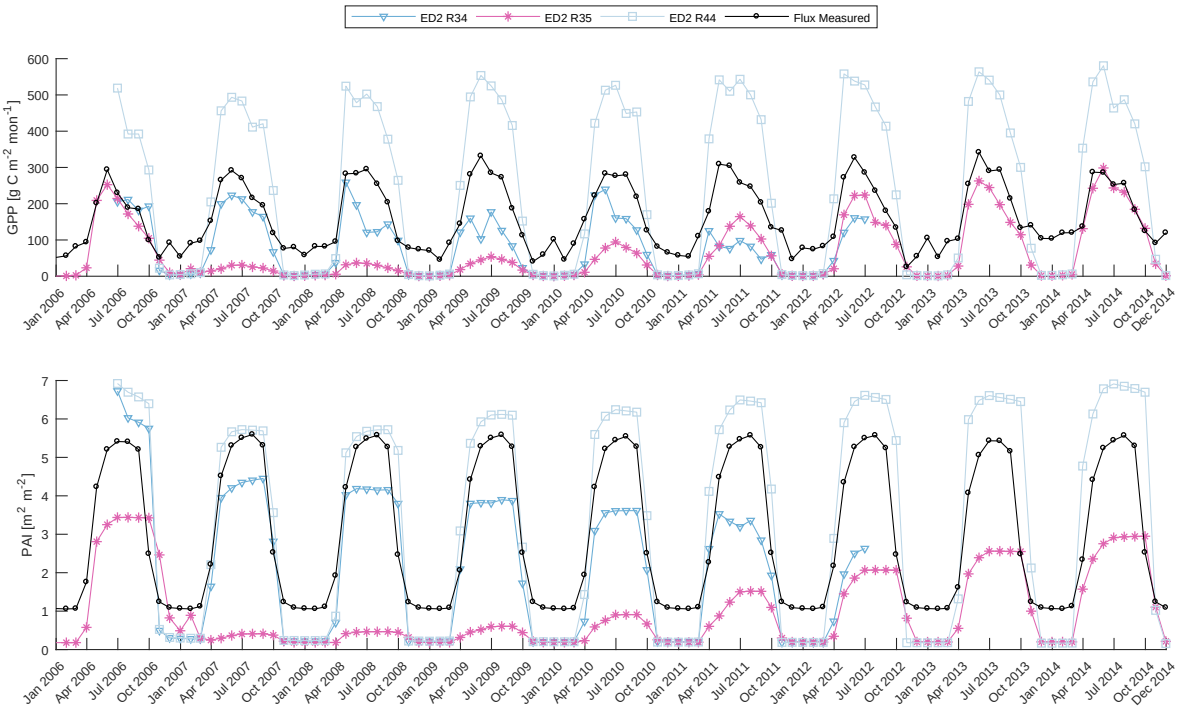

Fig. 10: Monthly GPP simulated with vegetation dynamics in ED2 compared to measured GPP at the flux tower ('Flux Measured'). The first model run showed a decrease in GPP and PAI over the years due to an excessive moisture limitation in the understory ('ED2 R34'). A newer code of the model ('ED2 R35') proved to be unsuitable to simulate deciduous hardwoods, leading to tree mortality due to an early leaf out in February 2007 and regrowth of early-successional hardwoods. Finally, turning off plant moisture limitation in 'ED2 R34' lead to tree growth and an unrealistically high GPP in summer months ('ED2 R44').

and basal area (Fig. 10 and Suppl. Fig. 31). Without moisture limitation and competition for water, yearly modelled GPP was 137 to 159% of the measured flux. When simulating potential vegetation, it also had a strong effect on the structure and composition of the forest. Without moisture limitation, the forest would be dominated by early-succesional hardwoods (66% basal area) and late-successional hardwoods (34% basal area). Moreover, basal area was more than twice and aboveground biomass about five times as high as with strong moisture limitation in the previous potential vegetation simulation (Fig. 11 and 12).

Discussion

The preliminary results presented here show that the initialisation of forest structure and composition can greatly improve the prediction of GPP on a temperate mixed forest site. The density as well as size distributions of trees and their plant functional type have an important influence on the predicted carbon fluxes over time, especially when simulating inter- and intra-annual change. We could demonstrate that we were able to accurately derive detailed information on forest structure and composition purely based on remote sensing data, thus allowing to extend the studied area beyond the field plot. However, the main caveat lies in the translation of the remotely sensed input parameters to the representation of the forest in the model.

First, the site had to be subset and the original remote sensing data aggregated to meet computational and representational constrains of the model, since the total number of patches and cohorts in the model had to be limited. Translating every voxel in the remotely sensed 3D representation of the forest into a cohort without aggregation would have lead to a vast number of very small cohorts. This can have multiple consequences. On one hand, computational power would be limiting the simulations, either leading to the abortion of the model runs or a strongly reduced computation speed. On the other hand, the small cohorts might not comply with thresholds of energy balance anymore, which were designed for larger cohorts representing a collection of trees with similar characteristics. Therefore, a trade-off has to be found between aggregating and preserving functional diversity.

Second, the input parameters had to be adapted

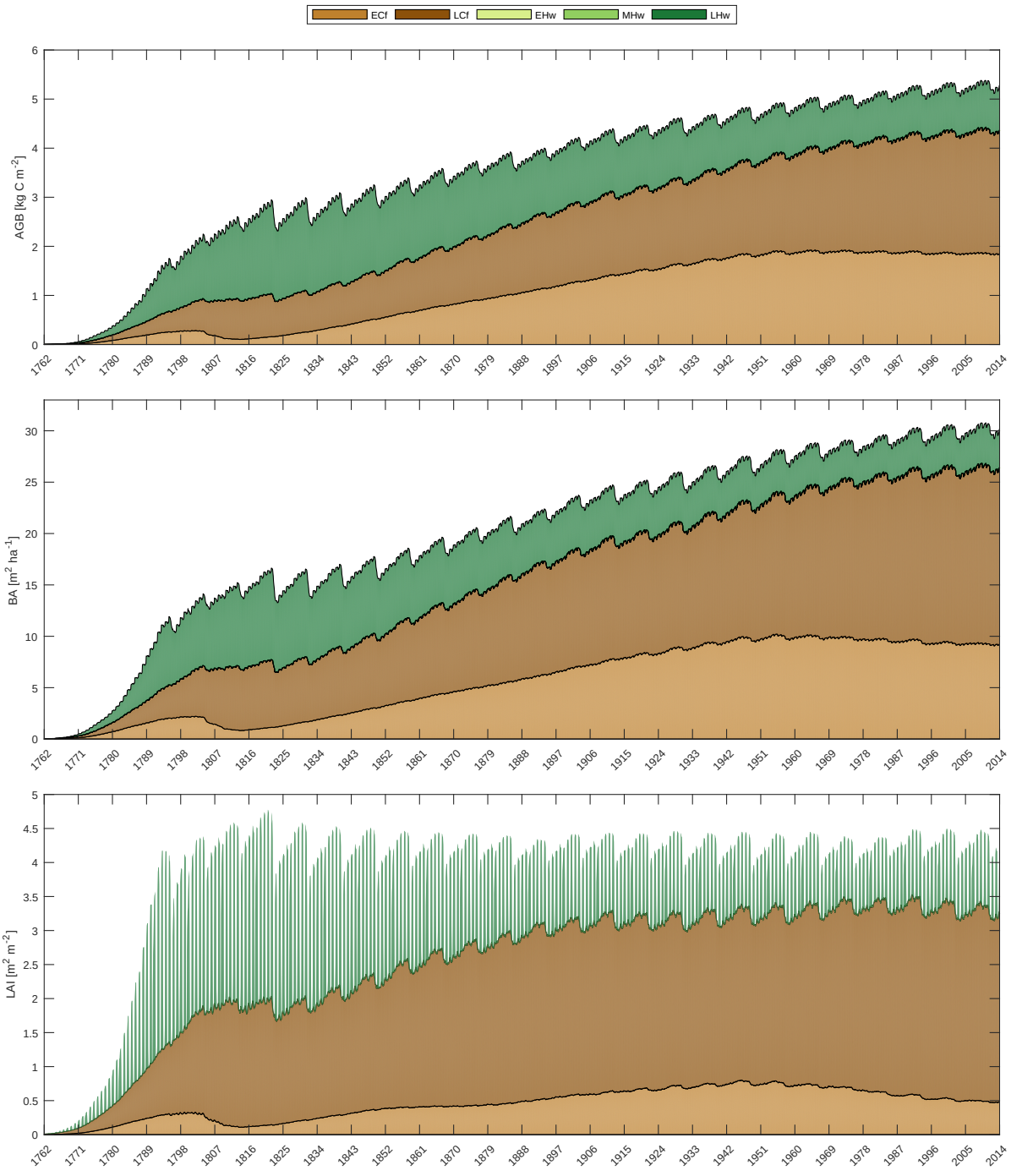

Fig. 11: Above ground biomass (AGB), basal area (BA) and leaf area index (LAI) of a potential vegetation simulation with moisture limitation and competition for water, starting around 250 years before the current state. Early and late-successional conifers (ECf and LCf) mainly outcompete early hardwoods (EHw), mid hardwoods (MHw) and late hardwoods (LHw).

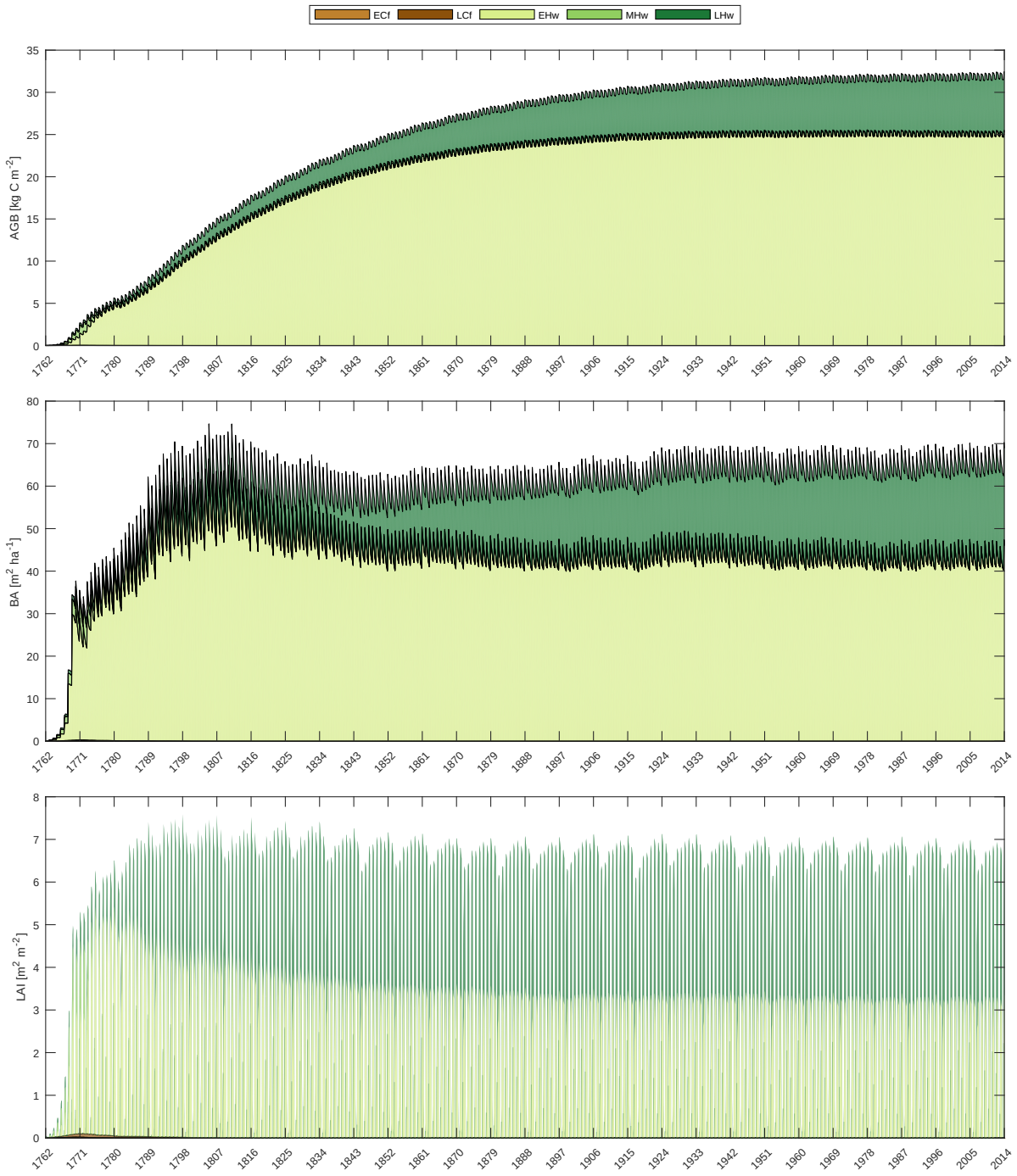

Fig. 12: Above ground biomass (AGB), basal area (BA) and leaf area index (LAI) of a potential vegetation simulation without moisture limitation and competition for water, starting around 250 years before the current state. Early and late-successional hardwoods (EHw and LHw) outcompete mid hardwoods (MHw), early conifers (ECf) and late conifers (LCf).

to fit the allometries defined in the model. Plant allometries describe the relationship between two plant dimensions, and how a change in one dimension relates to the change in another dimension. A fundamental relationship is the allometry between stem diameter and plant height, since it does not only define the most basic structure of a tree but also part of its resource allocation strategy. Allometric relationships can indicate how trees are competing or complementing each other, e.g. whether they invest in height to compete for light or in diameter to tolerate stress (Grime, 1988). Current Earth system models use constant allometries, only allowing one pre-defined combination of traits for an individual tree of a plant functional type. Empirical work has shown, however, that the relationship between diameter and height can be highly variable between and within species (Lines *et al.*, 2012; Pretzsch *et al.*, 2013; Forrester *et al.*, 2017). Similarly, our results show considerable variation in the allometric relationships of the four plant functional types (Suppl. Fig. 28). This might be due to the high intra-specific diversity at our site (Guillén Escribà *et al.*, in preparation), reflecting differences in local environmental conditions and resource availability, competitiveness, phenotypic plasticity and local adaptation (Forrester *et al.*, 2017; Pretzsch *et al.*, 2013).

To estimate realistic size distributions of diameter and basal area of the forest, we thus had to incorporate the variance in the allometric equations. This had the advantage to be able to model realistic size distributions at the plot level, but lead to unrealistic relationships at the individual level. Thus, when initialising the model, canopy height had to be adapted to fit the model allometries to diameter and basal area. And since multiple allometries are interlinked in the model, it is not trivial to adapt these relationships to allow individual traits to vary. This resulted in a smaller range of values and a strong underestimation of canopy height in the model. This is a major drawback of the current model parametrisation, leading to a condensed distribution of leaf area in one height layer.

The reduced variability in canopy height and condensed leaf area resulted in an underestimation of the morphological diversity of the canopy, with increased shading and competition for light among tree crowns. The vertical distribution of leaf area index alone seems not to have a strong influence on the overall carbon budget (Fig. 8), but impacts the simulation of vegetation dynamics and competitive interactions in the model. It has a direct effect on the radiative transfer of the canopy and, with most radiation absorbed or reflected in the top layer of the canopy, on light availability and microclimate in the understory (Jucker *et al.*, 2015). Increased mortality and regrowth might be the response in the model in order to increase crown partitioning (Fig. 10), reducing shading and competition to improve ecosystem functioning through better resource usage. Reactions can be more complex in natural systems though, as recent findings suggest that a strong competitive hierarchy could also have positive effects on productivity due to positive selection effects (Williams *et al.*, 2017).

To address these issues in dynamic vegetation models would require a change of concept from cohort-based models towards individual-based models. It has been recognized already in the 1980's that some of the model generalisations violate basic principles of biology, namely that each individual is different due to unique genetic and environmental influences and that interactions are local, and thus should be modelled based on individuals in a spatially explicit context (Huston *et al.*, 1988). Therefore, Huston *et al.* (1988) supported the notion of individual organisms as the basic units for ecological modelling. Nevertheless, cohort-based models have been widely established and generally proven suitable to simulate dynamic interactions as well as energy and carbon fluxes from local to global scales, but mainly in ecosystems with little within species variation (Restrepo-Coupe *et al.*, 2017; Fisher *et al.*, 2017). With recent advances in remote sensing and the ability for larger scale trait mapping at individual tree resolution (Schneider *et al.*, 2017), the development of trait- and individual-based models is promising to better integrate intra-specific diversity in dynamic vegetation models as crucial aspect for understanding global change responses (Moran *et al.*, 2016; Grimm *et al.*, 2017).

Besides competitive interactions related to light availability and vegetation structure, an essential component driving productivity is related to water availability and competition for water. We found that increased moisture limitation resulted in reduced productivity during summer months, for example during a dry and warm summer 2011 (see Figs. 2, 10). This is expected to occur more frequently in the future (Suppl. Fig. 19), leading to reduced CO_2 uptake and potentially a much shorter growing season. Predictions of forest phenology by 2100 showed an early browning already in July or August for two of the four climate scenarios towards the end of the century (Suppl. Fig. 27). This could hamper the generally positive effects of a longer growing season related to an earlier start of season due to warming. Trends of a longer growing season can already be observed under recent climate change in Europe (Garonna *et al.*, 2014), with an enhanced positive

effect in more diverse ecosystems (Oehri *et al.*, 2017). An earlier browning was only observed in the steppic zone, where plants are already more constrained by moisture availability than in central Europe (Garonna *et al.*, 2014, 2017).

In the long term, we could even expect a change of forest composition. In the potential vegetation simulation with stronger moisture limitation, forest composition shifts from a forest dominated by late-successional *Fagus sylvatica* after about 60 years to a forest dominated by early and late-successional conifers when reaching an equilibrium after about 200 years (Fig. 11). Lindner *et al.* (2014) also predict large possible range shifts of tree species habitat suitability in Europe by 2100. *Fagus sylvatica* dominate natural temperate forests in Europe, but might by outcompeted by other species when the environmental conditions get drier (Geßler *et al.*, 2006). However, it is still largely unknown at which rate a change in forest composition might happen, how well trees can adapt to recurring extreme events plastically and by short-term evolution, and how the performance of individual species depends on co-existing species, or the functional diversity of a forest in general.

Without any competition for water and no moisture limitation of photosynthesis in the leaves, a potential forest would be mainly dominated by highly productive and densely growing early-successional hardwoods according to ED2 simulations (Fig. 12). The high productivity compared to a simulation with moisture limitation shows the strong influence on photosynthesis and light-use efficiency, regulating the productivity of the forest. Therefore, it is essential to correctly parametrise the model for a realistic water availability and plant water competition. Although two of four climate models predict a slight increase in yearly precipitation by 2100 (Suppl. Fig. 19), the increased rainfall would be mainly expected in winter and spring. More frequent and severe heat waves and drought in summer are more likely to occur. A favouring of early-successional hardwoods with an increase in total forest productivity is therefore not to be expected.

The preliminary results presented here have shown that a realistic representation of forest structure and composition is crucial to predict forest productivity, and that remote sensing is able to provide these necessary inputs to initialise the current state of the forest. Current cohort-based models, however, need to meet the pre-defined allometric relationships and can therefore not incorporate the same level of realism than the detailed measurements can provide. Therefore, an individual-based modelling scheme might be needed for a full integration of intra-specific trait diversity. Besides, we identified competition for water and moisture limitation in the leaves as a key factor driving photosynthetic rates and long-term forest composition in the model. To be able to predict productivity at different sites with varying diversity and soil conditions, as well as the long-term effects of climate change, we thus need to further optimise that part of the model parametrisation. Furthermore, it is necessary to better integrate the phenology scheme derived from data assimilation and constrained predictions into the model. Finally, we expect to improve the accuracy of predicting productivity with the fully dynamic model compared to the initial simulations without vegetation dynamics, once the correct parametrisation is found. This will ultimately allow to address the research aims (2) to investigate the relationship between plant functional diversity and productivity, and (3) to predict how productivity is going to change under climate change depending on plant functional diversity.

Acknowledgements

This study has been supported by the University of Zurich Research Priority Program on Global Change and Biodiversity (URPP GCB). Support was also provided by the NASA HyspIRI Preparatory Activity NNH11ZDA001N-HYSPIRI grant Linking Terrestrial Biosphere Models with Remote Sensing Measurements of Ecosystem Composition, Structure, and Function to PRM. We thank Victoria Scholl for developing the original version of the single-tree delineation method, Reik Leiterer for measuring and processing field inventory data (tree stem positions, diameter at breast height, taxonomy), and Jan Rajczak for providing climate model data. Meteorological data was provided by the Federal Office for the Environment (FOEN), the Swiss Federal Laboratories for Materials Science and Technology (EMPA) and MeteoSchweiz (Climap). Stand polygon data was provided by Aargauisches Geografisches Informationssystem (AGIS), Departement Bau, Verkehr und Umwelt, Abteilung Wald (last updated on 27 February 2015) and by Geographisches Informationssystem (GIS-ZH), Amt für Landschaft und Natur, Abteilung Wald (last updated on 16 September 2015). Soil data corresponds to Bodenkarte Baden (Landeskarte der Schweiz 1:25'000, Blatt 1070), provided by Eidgenössische Forschungsanstalt für Agrarökologie und Landbau (FAL).

References

Allen CD, Breshears DD, McDowell NG (2015) On underestimation of global vulnerability to tree mortality and forest die-off from hotter drought in the Anthropocene. *Ecosphere*, **6**, art129.

Anderegg WRL, Schwalm C, Biondi F, *et al.* (2015) Pervasive drought legacies in forest ecosystems and their implications for carbon cycle models. *Science*, **349**, 528–532.

Antonarakis AS, Munger JW, Moorcroft PR (2014) Imaging spectroscopy- and lidar-derived estimates of canopy composition and structure to improve predictions of forest carbon fluxes and ecosystem dynamics. *Geophysical Research Letters*, **41**, 2535–2542.

Baldocchi DD (2003) Assessing the eddy covariance technique for evaluating carbon dioxide exchange rates of ecosystems: past, present and future. *Global Change Biology*, **9**, 479–492.

Balvanera P, Pfisterer AB, Buchmann N, He JS, Nakashizuka T, Raffaelli D, Schmid B (2006) Quantifying the evidence for biodiversity effects on ecosystem functioning and services. *Ecology Letters*, **9**, 1146–1156.

Barr AG, Black T, Hogg E, Kljun N, Morgenstern K, Nesic Z (2004) Interannual variability in the leaf area index of a boreal aspen-hazelnut forest in relation to net ecosystem production. *Agricultural and Forest Meteorology*, **126**, 237 – 255.

Barrufol M, Schmid B, Bruelheide H, *et al.* (2013) Biodiversity promotes tree growth during succession in subtropical forest. *PLoS ONE*, **8**, e81246.

Braun D, Damm A, Paul-Limoges E, *et al.* (2017) From instantaneous to continuous: Using imaging spectroscopy and in situ data to map two productivity-related ecosystem services. *Ecological Indicators*, **82**, 409–419.

Brienen RJW, Phillips OL, Feldpausch TR, *et al.* (2015) Long-term decline of the Amazon carbon sink. *Nature*, **519**, 344–348.

Bruelheide H, Nadrowski K, Assmann T, *et al.* (2014) Designing forest biodiversity experiments: general considerations illustrated by a new large experiment in subtropical China. *Methods in Ecology and Evolution*, **5**, 74–89.

Cardinale BJ, Wright JP, Cadotte MW, *et al.* (2007) Impacts of plant diversity on biomass production increase through time because of species complementarity. *Proceedings of the National Academy of Sciences*, **104**, 18123–18128.

D'Odorico P, Gonsamo A, Pinty B, Gobron N, Coops N, Mendez E, Schaepman ME (2014) Intercomparison of fraction of absorbed photosynthetically active radiation products derived from satellite data over Europe. *Remote Sensing of Environment*, **142**, 141–154.

Duffy JE, Godwin CM, Cardinale BJ (2017) Biodiversity effects in the wild are common and as strong as key drivers of productivity. *Nature*, **549**, 261–264.

Fisher RA, Koven CD, Anderegg WRL, *et al.* (2017) Vegetation demographics in Earth System Models: A review of progress and priorities. *Global Change Biology*, pp. 1–20.

Forrester DI, Benneter A, Bouriaud O, Bauhus J (2017) Diversity and competition influence tree allometric relationships - developing functions for mixed-species forests. *Journal of Ecology*, **105**, 761–774.

Fyllas NM, Bentley LP, Shenkin A, *et al.* (2017) Solar radiation and functional traits explain the decline of forest primary productivity along a tropical elevation gradient. *Ecology Letters*, **20**, 730–740.

Garonna I, de Jong R, de Wit AJ, Mücher CA, Schmid B, Schaepman ME (2014) Strong contribution of autumn phenology to changes in satellite-derived growing season length estimates across europe (1982 - 2011). *Global Change Biology*, **20**, 3457–3470.

Garonna I, de Jong R, Stoeckli R, Schmid B, Schenkel D, Schimel DS, Schaepman ME (2017) Shifting relative importance of climatic constraints on land surface phenology. *Environmental Research Letters*.

Geßler A, Keitel C, Kreuzwieser J, Matyssek R, Seiler W, Rennenberg H (2006) Potential risks for European beech (Fagus sylvatica L.) in a changing climate. *Trees*, **21**, 1–11.

Grime JP (1988) *The C-S-R model of primary plant strategies — origins, implications and tests*, pp. 371–393. Springer Netherlands, Dordrecht.

Grimm V, Ayllón D, Railsback SF (2017) Next-Generation Individual-Based Models Integrate Biodiversity and Ecosystems: Yes We Can, and Yes We Must. *Ecosystems*, **20**, 229–236.

Guillén Escribà C, Schneider FD, Tedder A, *et al.* (in preparation) Remotely sensed within-species functional trait variation of temperate forests. *Methods in Ecology and Evolution*.

Hooper DU, Chapin FS, Ewel JJ, *et al.* (2005) Effects of biodiversity on ecosystem functioning: A consensus of current knowledge. *Ecological Monographs*, **75**, 3–35.

Hueni A, Biesemans J, Meuleman K, *et al.* (2009) Structure, components, and interfaces of the airborne prism experiment (apex) processing and archiving facility. *IEEE Transactions on Geoscience and Remote Sensing*, **47**, 29–43.

Hueni A, Lenhard K, Baumgartner A, Schaepman ME (2013) Airborne prism experiment calibration information system. *IEEE Transactions on Geoscience and Remote Sensing*, **51**, 5169–5180.

Huston M, DeAngelis D, Post W (1988) New computer models unify ecological theory. *BioScience*, **38**, 682–691.

Isbell F, Craven D, Connolly J, *et al.* (2015) Biodiversity increases the resistance of ecosystem productivity to climate extremes. *Nature*, **526**, 574–577.

Isbell F, Gonzalez A, Loreau M, *et al.* (2017) Linking the influence and dependence of people on biodiversity across scales. *Nature*, **546**, 65–72.

Jönsson P, Eklundh L (2004) Timesat - a program for analyzing time-series of satellite sensor data. *Computers & Geosciences*, **30**, 833 – 845.

Jucker T, Bouriaud O, Coomes DA (2015) Crown plasticity enables trees to optimize canopy packing in mixed-species forests. *Functional Ecology*, **29**, 1078–1086.

Justice C, Vermote E, Townshend J, *et al.* (1998) The Moderate Resolution Imaging Spectroradiometer (MODIS): land remote sensing for global change research. *IEEE Transactions on Geoscience and Remote Sensing*, **36**, 1228–1249.

Kaartinen H, Hyyppä J, Yu X, *et al.* (2012) An international comparison of individual tree detection and extraction using airborne laser scanning. *Remote Sensing*, **4**, 950–974.

Kükenbrink D, Schneider FD, Leiterer R, Schaepman ME, Morsdorf F (2017) Quantification of hidden canopy volume of airborne laser scanning data using a voxel traversal algorithm. *Remote Sensing of Environment*, **194**, 424 – 436.

Liang J, Crowther TW, Picard N, *et al.* (2016) Positive biodiversity-productivity relationship predominant in global forests. *Science*, **354**, aaf8957–aaf8957.

Liang J, Zhou M, Tobin PC, McGuire AD, Reich PB (2015) Biodiversity influences plant productivity through nicheefficiency. *Proceedings of the National Academy of Sciences*, **112**, 5738–5743.

Lindner M, Fitzgerald JB, Zimmermann NE, *et al.* (2014) Climate change and European forests: What do we know, what are the uncertainties, and what are the implications for forest management? *Journal of Environmental Management*, **146**, 69–83.

Lines ER, Zavala MA, Purves DW, Coomes DA (2012) Predictable changes in aboveground allometry of trees along gradients of temperature, aridity and competition. *Global Ecology and Biogeography*, **21**, 1017–1028.

Medvigy D, Wofsy SC, Munger JW, Hollinger DY, Moorcroft PR (2009) Mechanistic scaling of ecosystem function and dynamics in space and time: Ecosystem Demography model version 2. *Journal of Geophysical Research*, **114**, G01002.

Medvigy D, Wofsy SC, Munger JW, Moorcroft PR (2010) Responses of terrestrial ecosystems and carbon budgets to current and future environmental variability. *Proceedings of the National Academy of Sciences*, **107**, 8275–8280.

Millar CI, Stephenson NL (2015) Temperate forest health in an era of emerging megadisturbance. *Science*, **349**, 823–826.

Moorcroft PR, Hurtt GC, Pacala SW (2001) A method for scaling vegetation dynamics: The ecosystem demography model (ED). *Ecological Monographs*, **71**, 557–586.

Moran EV, Hartig F, Bell DM (2016) Intraspecific trait variation across scales: Implications for understanding global change responses. *Global Change Biology*, **22**, 137–150.

Morsdorf F, Meier E, Kötz B, Itten KI, Dobbertin M, Allgöwer B (2004) Lidar-based geometric reconstruction of boreal type forest stands at single tree level for forest and wildland fire management. *Remote Sensing of Environment*, **92**, 353–362.

Oehri J, Schmid B, Schaepman-Strub G, Niklaus PA (2017) Biodiversity promotes primary productivity and growing season lengthening at the landscape scale. *Proceedings of the National Academy of Sciences*, **114**, 201703928.

Pretzsch H, Dauber E, Biber P (2013) Species-Specific and Ontogeny-Related Stem Allometry of European Forest Trees: Evidence from Extensive Stem Analyses. *Forest Science*, **59**, 290–302.

Rajczak J, Kotlarski S, Salzmann N, Schär C (2016) Robust climate scenarios for sites with sparse observations: a two-step bias correction approach. *International Journal of Climatology*, **36**, 1226–1243.

Restrepo-Coupe N, Levine NM, Christoffersen BO, *et al.* (2017) Do dynamic global vegetation models capture the seasonality of carbon fluxes in the Amazon basin? A data-model intercomparison. *Global Change Biology*, **23**, 191–208.

Schaepman ME, Jehle M, Hueni A, *et al.* (2015) Advanced radiometry measurements and earth science applications with the airborne prism experiment (apex). *Remote Sensing of Environment*, **158**, 207–219.

Scherber C, Eisenhauer N, Weisser WW, *et al.* (2010) Bottom-up effects of plant diversity on multitrophic interactions in a biodiversity experiment. *Nature*, **468**, 553–556.

Schimel D, Stephens BB, Fisher JB (2015) Effect of increasing co_2 on the terrestrial carbon cycle. *Proceedings of the National Academy of Sciences*, **112**, 436–441.

Schläpfer D, Richter R (2002) Geo-atmospheric processing of airborne imaging spectrometry data. part 1: Parametric orthorectification. *International Journal of Remote Sensing*, **23**, 2609–2630.

Schlesinger WH, Dietze MC, Jackson RB, Phillips RP, Rhoades CC, Rustad LE, Vose JM (2016) Forest biogeochemistry in response to drought. *Global Change Biology*, **22**, 2318–2328.

Schneider FD, Leiterer R, Morsdorf F, Gastellu-Etchegorry JP, Lauret N, Pfeifer N, Schaepman ME (2014) Simulating imaging spectrometer data: 3d forest modeling based on lidar and in situ data. *Remote Sensing of Environment*, **152**, 235–250.

Schneider FD, Morsdorf F, Schmid B, Petchey OL, Hueni A, Schimel DS, Schaepman ME (2017) Mapping functional diversity from remotely sensed morphological and physiological forest traits. *Nature Communications*, **8**.

Silva Pedro M, Rammer W, Seidl R (2017) Disentangling the effects of compositional and structural diversity on forest productivity. *Journal of Vegetation Science*, pp. 1–10.

Stöckli R, Rutishauser T, Baker I, Liniger MA, Denning AS (2011) A global reanalysis of vegetation phenology. *Journal of Geophysical Research*, **116**, G03020.

Stöckli R, Rutishauser T, Dragoni D, *et al.* (2008) Remote sensing data assimilation for a prognostic phenology model. *Journal of Geophysical Research*, **113**, G04021.

van der Linden P, Mitchell J (2009) Ensembles: climate change and its impact: summary of research and results from the ensembles project. Eu fp6 contract number 505539, Met Office Hadley Centre, Exeter, UK.

Vickers D, Mahrt L (1997) Quality control and flux sampling problems for tower and aircraft data. *Journal of Atmospheric and Oceanic Technology*, **14**, 512–526.

Wang Y, Hyyppa J, Liang X, *et al.* (2016) International benchmarking of the individual tree detection methods for modeling 3-d canopy structure for silviculture and forest ecology using airborne laser scanning. *IEEE Transactions on Geoscience and Remote Sensing*, **54**, 5011–5027.

Williams LJ, Paquette A, Cavender-Bares J, Messier C, Reich PB (2017) Spatial complementarity in tree crowns explains overyielding in species mixtures. **1**.

Author Contributions

F.D.S., P.M., F.M., and M.E.S. designed research; F.D.S., P.M., E.P.-L., F.M., C.G.E., and M.E.S. performed research; and all authors wrote the paper.

The authors declare no conflict of interest.

4.2 Supplementary Information

4.2.1 Supplementary Note 1: Gap filling of meteorological variables

For temperature, wind direction, average wind speed, maximum wind speed and humidity, we used the measurements from the meteorological station at the ridge of the Laegern to fill the gaps in the time series of the flux tower. We built a linear model based on monthly mean values to fit the values measured on the ridge to the ones measured at the flux tower. Then we replaced the gaps in the time series by the fitted values from the meteorological station at the ridge. The same procedure was applied for precipitation with data from Kloten, being the closest meteorological station with precipitation measurements. Global radiation did not show a consistent difference between the two measurement stations. Therefore, we used a 5 days window before and after the gap to build the linear model instead of monthly averages. For net radiation, there were no measurements available from nearby stations. We filled the gaps by copying the corresponding period from either before or after the gap. We used global radiation data to build a linear model between the gap and the periods before and after to find out which one was more similar, and to establish a correction factor. We then copied the period from the net radiation data accordingly and applied the correction factor. Atmospheric pressure is a more continuous variable than the other meteorological drivers. Applying the same procedure might thus lead to unrealistic, abrupt changes at the beginning and end of the gap. Therefore, we filled the gaps by copying the values from the station at the Laegern ridge and applying a linear scaling to connect to the values before and after the gap. An example of the gap-filled meteorological data at 10 minutes temporal resolution is shown in Figure 11.

4.2.2 Supplementary Note 2: Estimating hourly values based on climate model data

For relative humidity, mean and maximum wind speed, global radiation and precipitation, we drew the diurnal hourly values from the measurements at the flux tower based on the closest daily mean value. To ensure a realistic seasonality but still allow to find extreme daily means in the measurement series, we used a 91-day window to draw the values following Rajczak *et al.* (2016). When the daily mean of the climate model was higher or lower than the highest or lowest value in the 91-day window, we chose the day with the highest or lowest value respectively and applied a scaling factor to match the daily mean from the climate model. We chose a different approach for atmospheric pressure, since it was more continuous than the other variables and did not show a diurnal cycle. We used a partial least squares regression based on the hourly and daily mean values of the measurement series at the flux tower to predict continuous hourly values of atmospheric pressure. This resulted in relatively similar values than interpolating the daily mean values with a cubic spline, but better predicted high or low pressure peaks. Since daily minimum and maximum temperature were available from the climate models and hourly temperature did show a continuous transition between the days, we used the measurement series to calculate an average temperature series for a year on an hourly basis. We then duplicated the average year of hourly values, determined the daily minimum and maximum and scaled it to the minimum and maximum temperature predicted by the climate model. To ensure a realistic diurnal cycle, we used a sinusoidal function to scale to the minimum and maximum daily values.

4.2.3 Supplementary Note 3: Remote sensing data

Full-waveform airborne laser scanning data based on light detection and ranging (LiDAR) was acquired in the period of June 19 to July 25 as part of a larger flight campaign covering the whole Kanton Aargau. The scanner system with a rotating mirror (RIEGL LMS-Q680i, scan angle $\pm 22°$) was flown under leaf-on conditions at a

nominal height of 700 m above ground, resulting in a footprint size of approximately 35 cm and an average point density of 30 pts/m^2. The LiDAR data was registered to the Swiss national grid CH1903+ with a positional accuracy of < 0.07 m in vertical and < 0.15 m in horizontal direction. For more details about the acquisition and the quality of the data, see Kükenbrink *et al.* (2017).

Imaging spectroscopy acquisitions were flown on 7 July and 17 July 2016 under clear sky conditions using the APEX imaging spectrometer (Schaepman *et al.*, 2015). The study area was covered with one flight line on each of the acquisition dates. The average flight altitude was 4500 m a.s.l. resulting in an average ground pixel size of 2 m. APEX measured at-sensor radiances in 284 spectral bands ranging from 399 nm to 2425 nm. APEX data were processed to hemispherical-conical reflectance factors (HCRF) in the APEX Processing and Archiving Facility (Hueni *et al.*, 2009). Processing started with the raw instrument data, which was split into image, dark current and housekeeping data, thus forming level 0. Level 1 (L1) calibrated radiances were obtained by inverting the instrument model, applying coefficients established during calibration and characterization at the APEX Calibration Home Base (Hueni *et al.*, 2013). The position and orientation of each pixel in 3-D space was based on automatic geocoding in PARGE v3.3 (Schläpfer & Richter, 2002), using the swissALTI3D digital terrain model and automatic image co-registration to swissimage ortho-photos. L1 data were converted to HCRF by employing ATCOR4 v7.1 in the smile aware mode (Schaepman *et al.*, 2015). Finally, HCRF surface reflectance values were corrected by a vicarious calibration based on 27 ground reflectance targets with various brightness levels located within the flight stripes to minimize remaining radiometric differences between overflights. Ground targets were measured using a field spectroradiometer (ASD Fieldspec Pro 4).

Remotely sensed physiological and morphological trait data was used from Schneider *et al.* (2017). Specifically, we used functional trait maps of the Laegern forest with relative content of chlorophyll, carotenoids, and leaf water, as well as plant area index, canopy height, and foliage height diversity with a resolution of 2 x 2 m pixel size. We also used the 3D plant area index voxel grid with 2 x 2 x 2 m resolution. For detailed information about the retrieval of the functional traits and the 3D voxel grid we refer to Schneider *et al.* (2014, 2017).

4.2.4 Supplementary Note 4: Field inventory data

We performed an individual tree inventory on a 5.5 ha plot around the flux tower. We measured the ground position, diameter at breast height and determined the taxonomy in the field for the 1307 dominant and co-dominant trees in that area (all trees $>=$ 20 cm dbh). Exact crown polygon outlines were retrieved for each tree from high-resolution drone ortho-images and linked to the ground positions. For more details and a comprehensive description and analysis of the field inventory data, see Guillén Escribà *et al.* (in preparation). Stand polygons of Kanton Aargau and Zurich include forest stand information on development stage, the percentage coverage of the 6 most dominant species, and the percentage coverage of deciduous broadleaf and coniferous needle trees. The data from Kanton Aargau was provided by Aargauisches Geografisches Informationssystem (AGIS), Departement Bau, Verkehr und Umwelt, Abteilung Wald (last updated on 27 February 2015). The data from Kanton Zurich was provided by Geographisches Informationssystem (GIS-ZH), Amt für Landschaft und Natur, Abteilung Wald (last updated on 16 September 2015). Soil data corresponds to Bodenkarte Baden (Landeskarte der Schweiz 1:25'000, Blatt 1070), provided by Eidgenössische Forschungsanstalt für Agrarökologie und Landbau (FAL).

References

Guillén Escribà C, Schneider FD, Tedder A, *et al.* (in preparation) Remotely sensed within-species functional trait variation of temperate forests. *Methods in Ecology and Evolution*.

Hueni A, Biesemans J, Meuleman K, *et al.* (2009) Structure, components, and interfaces of the airborne prism experiment (apex) processing and archiving facility. *IEEE Transactions on Geoscience and Remote Sensing*, **47**, 29–43.

Hueni A, Lenhard K, Baumgartner A, Schaepman ME (2013) Airborne prism experiment calibration information system. *IEEE Transactions on Geoscience and Remote Sensing*, **51**, 5169–5180.

Kükenbrink D, Schneider FD, Leiterer R, Schaepman ME, Morsdorf F (2017) Quantification of hidden canopy volume of airborne laser scanning data using a voxel traversal algorithm. *Remote Sensing of Environment*, **194**, 424 – 436.

Rajczak J, Kotlarski S, Salzmann N, Schär C (2016) Robust climate scenarios for sites with sparse observations: a two-step bias correction approach. *International Journal of Climatology*, **36**, 1226–1243.

Schaepman ME, Jehle M, Hueni A, *et al.* (2015) Advanced radiometry measurements and earth science applications with the airborne prism experiment (apex). *Remote Sensing of Environment*, **158**, 207–219.

Schläpfer D, Richter R (2002) Geo-atmospheric processing of airborne imaging spectrometry data. part 1: Parametric orthorectification. *International Journal of Remote Sensing*, **23**, 2609–2630.

Schneider FD, Leiterer R, Morsdorf F, Gastellu-Etchegorry JP, Lauret N, Pfeifer N, Schaepman ME (2014) Simulating imaging spectrometer data: 3d forest modeling based on lidar and in situ data. *Remote Sensing of Environment*, **152**, 235–250.

Schneider FD, Morsdorf F, Schmid B, Petchey OL, Hueni A, Schimel DS, Schaepman ME (2017) Mapping functional diversity from remotely sensed morphological and physiological forest traits. *Nature Communications*, **8**.

4.2.5 Supplementary Figures

Supplementary figures are provided on the following pages, with Figs. 13 to 26 related to the meteorological drivers, Figs. 27 to 30 related to the phenological, structural and compositional inputs, and Fig. 31 showing additional modelling results of simulated forest above ground biomass and basal area.

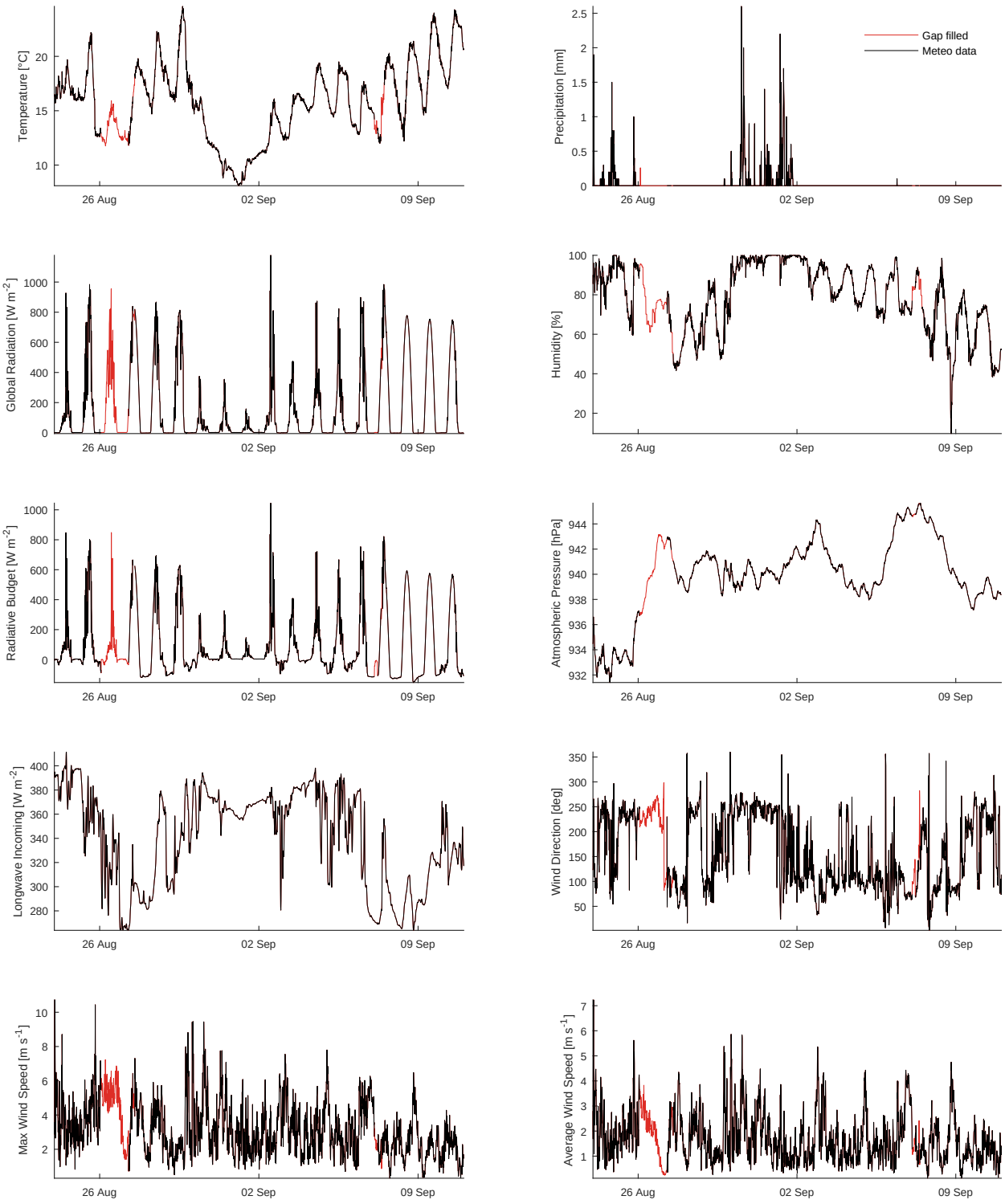

Fig. 13: Example of gap-filled meteorological drivers at 10 minutes temporal resolution in the period of 24 August to 10 September 2012. The gap-filled parts of the time series are displayed in red.

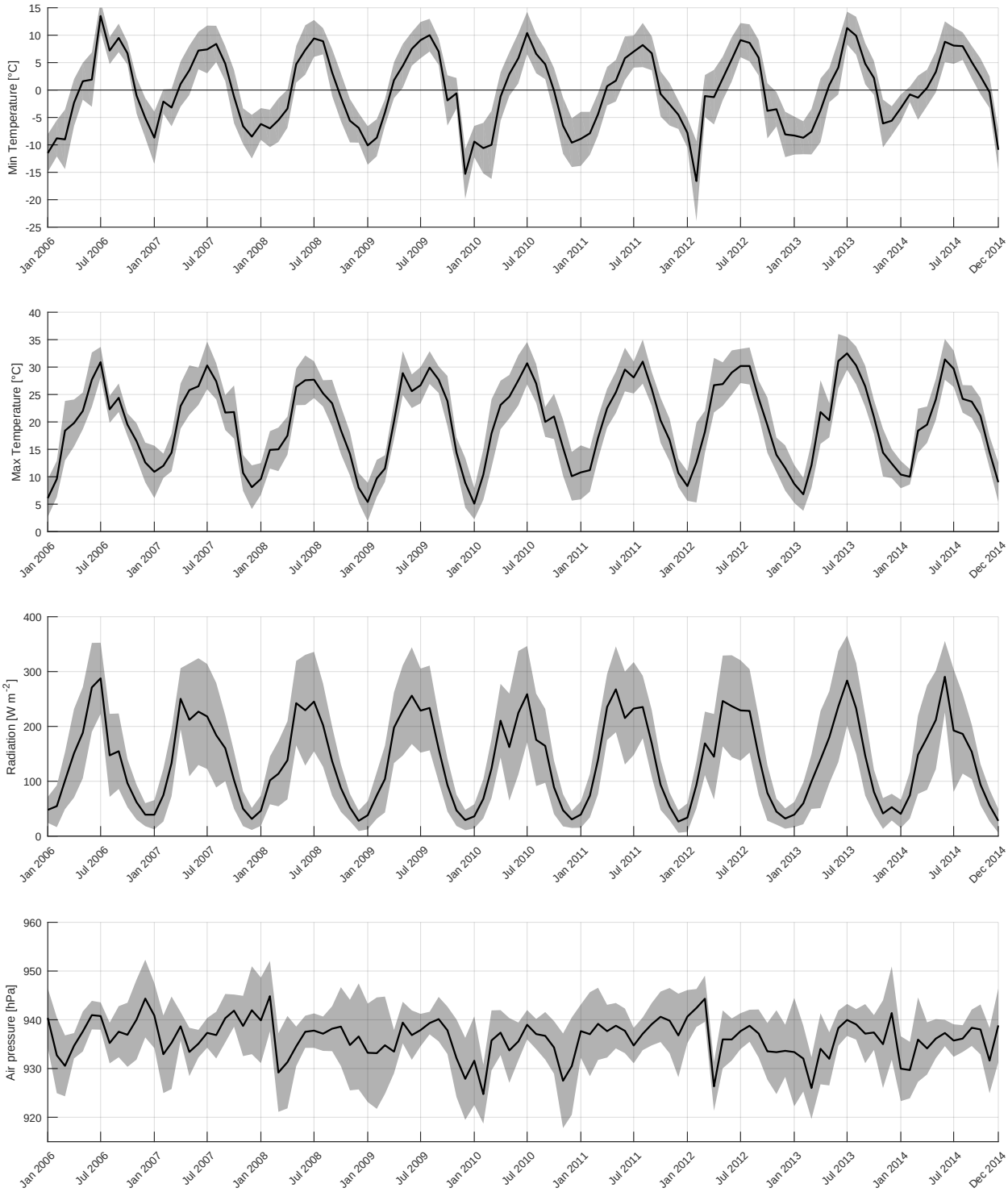

Fig. 14: Monthly mean and standard deviation of hourly minimum and maximum temperature, global radiation, and atmospheric pressure at field elevation measured on the Laegern flux tower for the years 2006 to 2014.

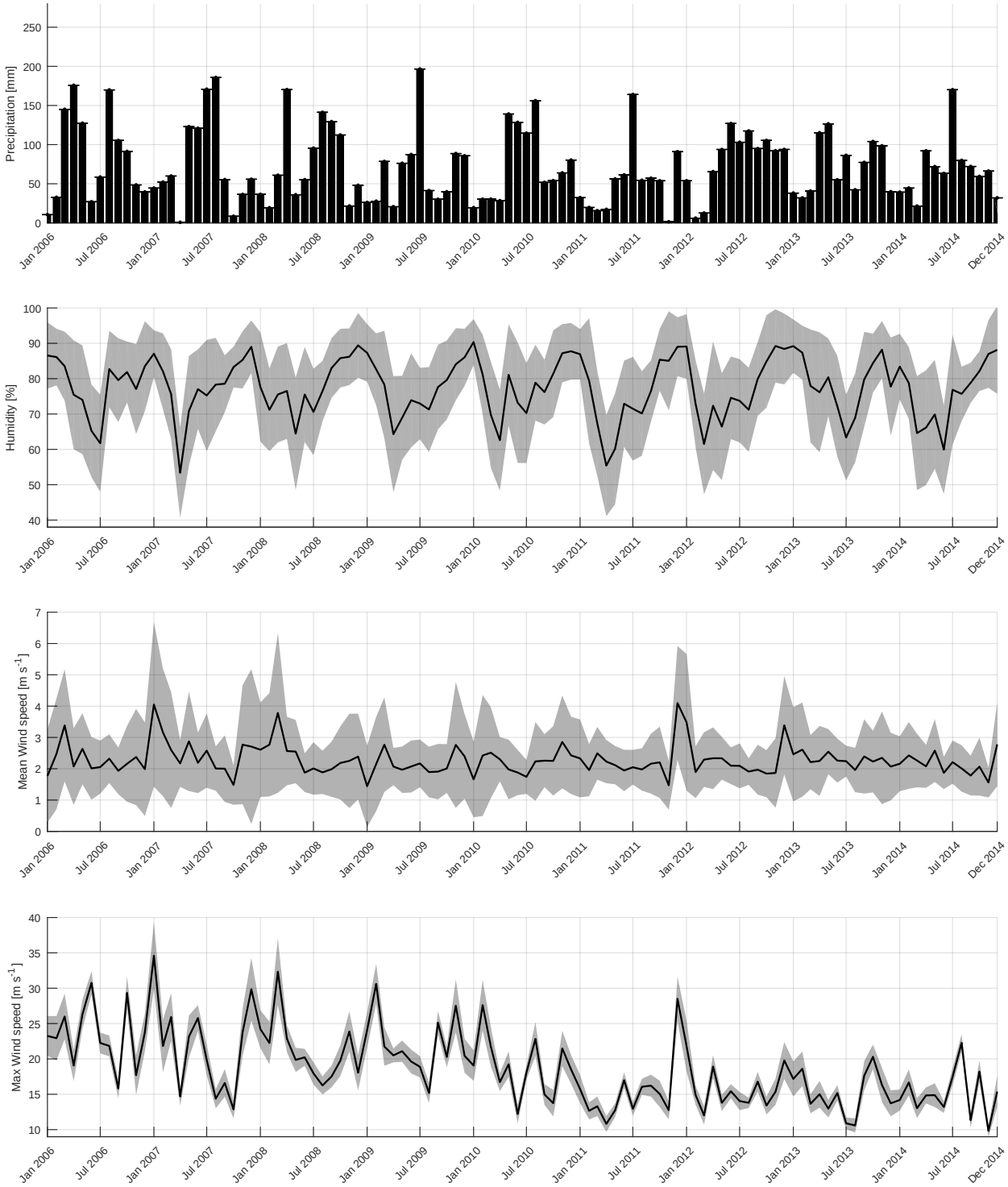

Fig. 15: Monthly sum and standard deviation of precipitation and monthly mean and standard deviation of hourly relative humidity, average and maximum wind speed measured on the Laegern flux tower for the years 2006 to 2014.

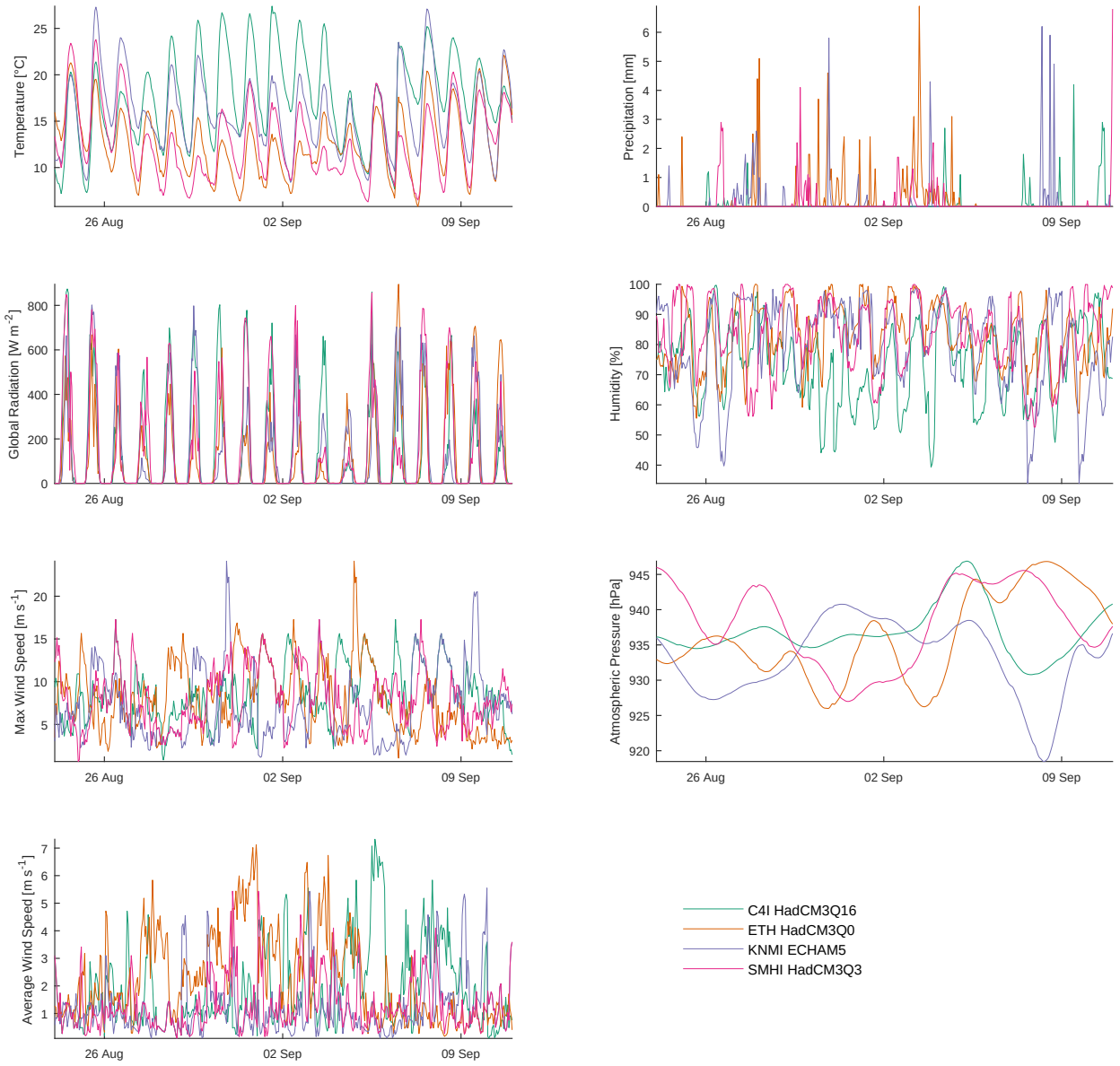

Fig. 16: Example of meteorological drivers at hourly temporal resolution based on four bias corrected climate models in the period of 24 August to 10 September 2012.

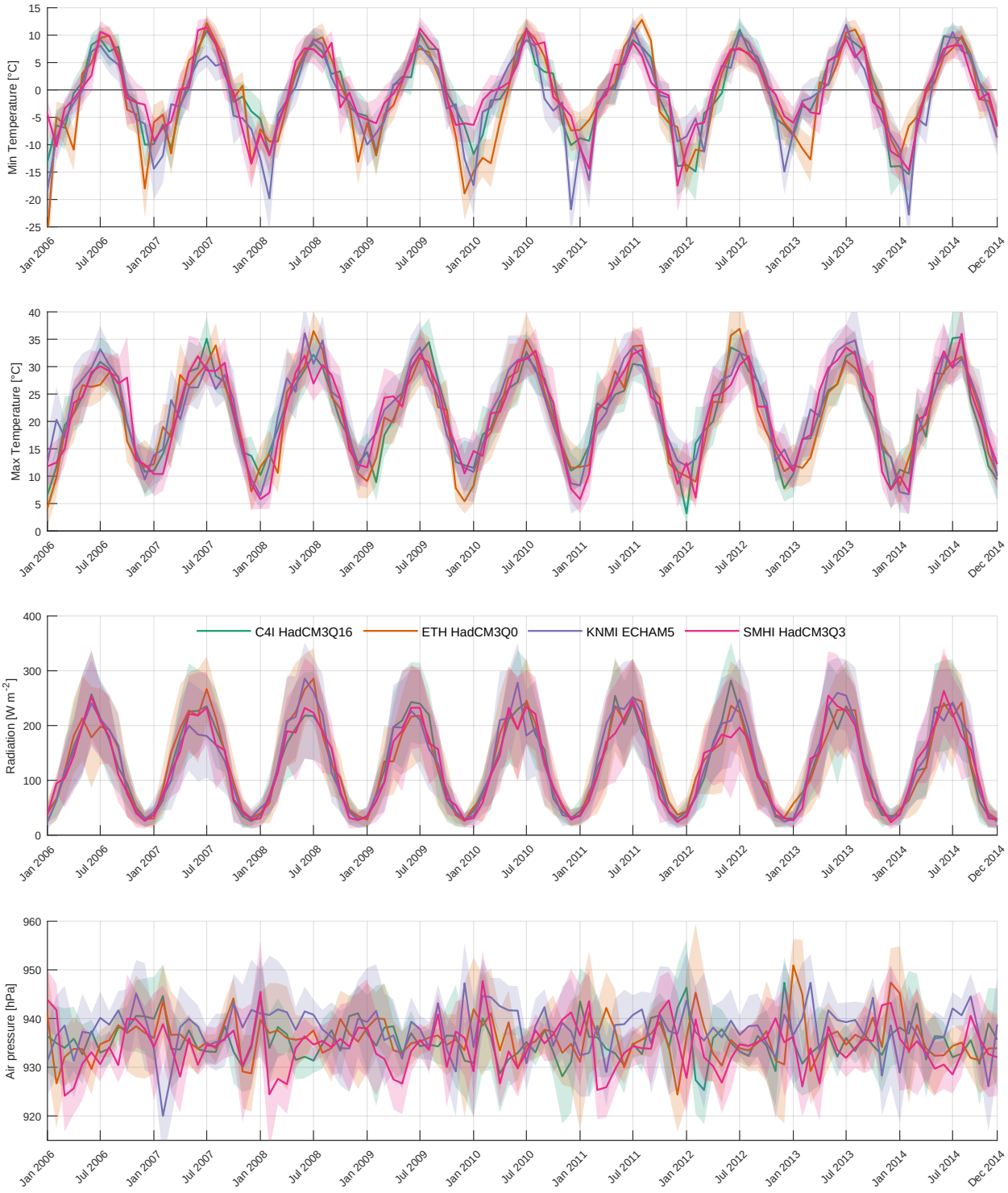

Fig. 17: Monthly mean and standard deviation of hourly minimum and maximum temperature, global radiation, and atmospheric pressure at field elevation of four bias corrected climate models for the years 2006 to 2014.

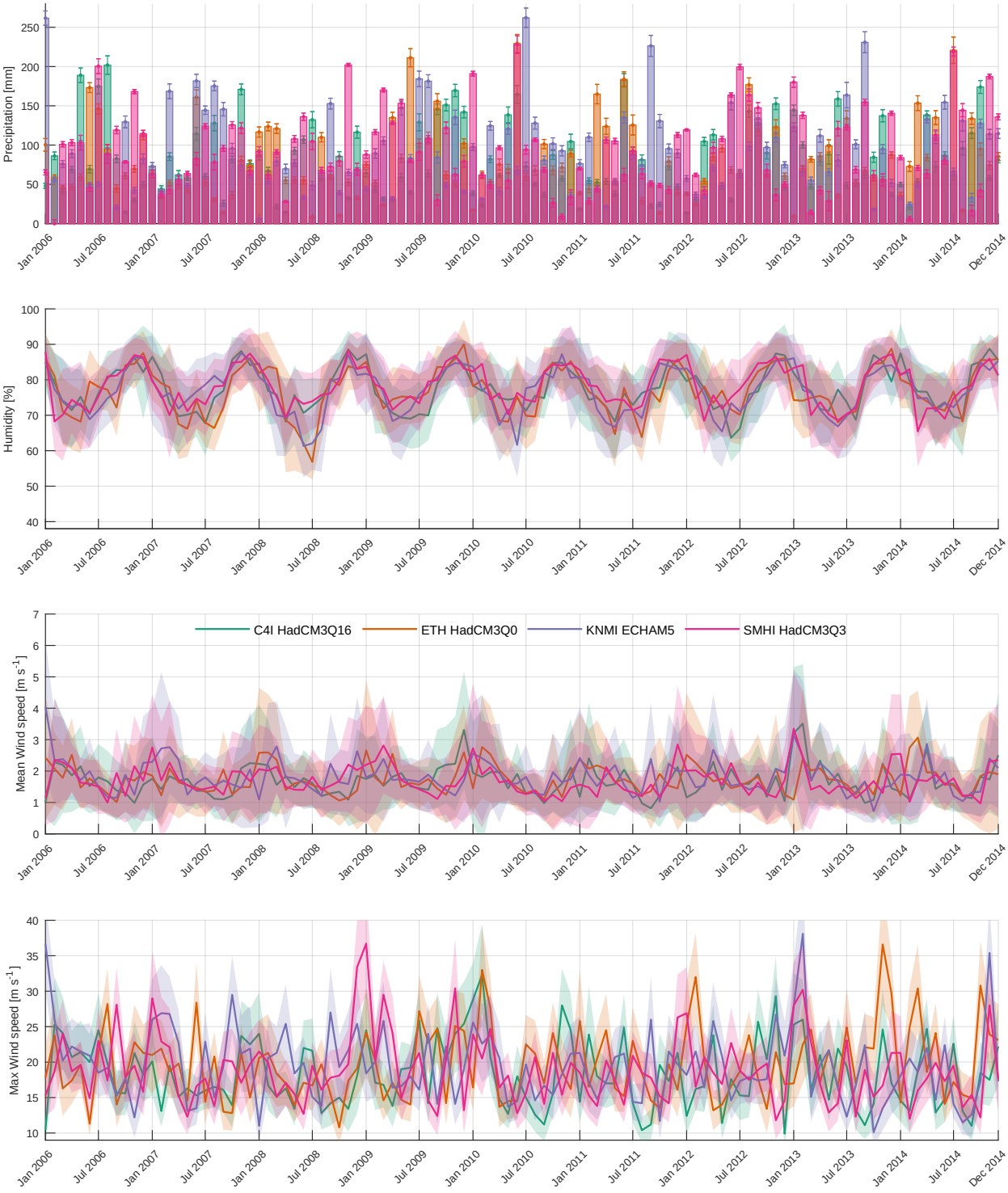

Fig. 18: Monthly sum and standard deviation of precipitation and monthly mean and standard deviation of hourly relative humidity, average and maximum wind speed of four bias corrected models for the years 2006 to 2014.

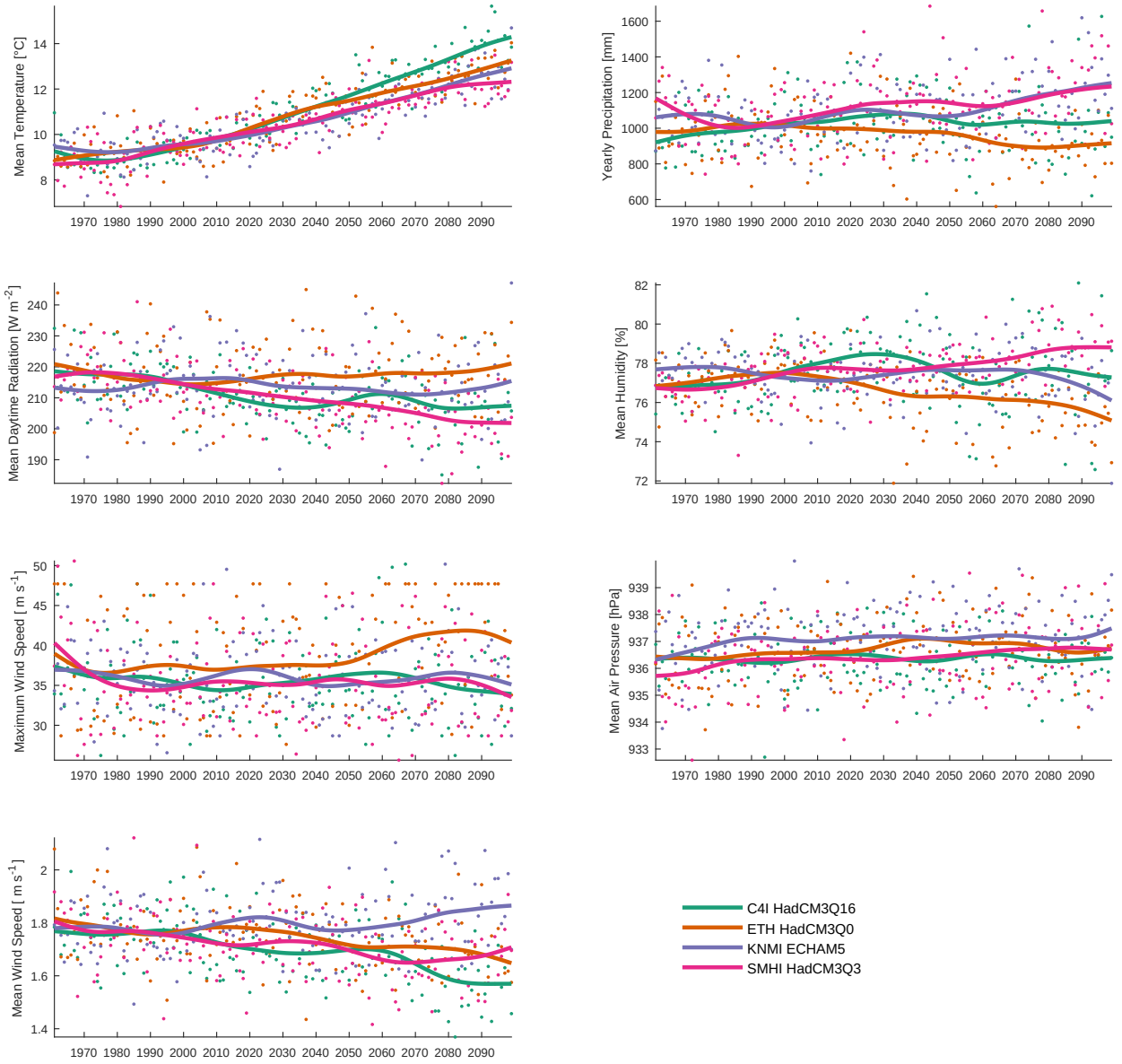

Fig. 19: Yearly meteorological drivers as dots and a smoothing spline displayed as line for indicating trends based on four bias corrected climate models in the period of 1960 to 2100.

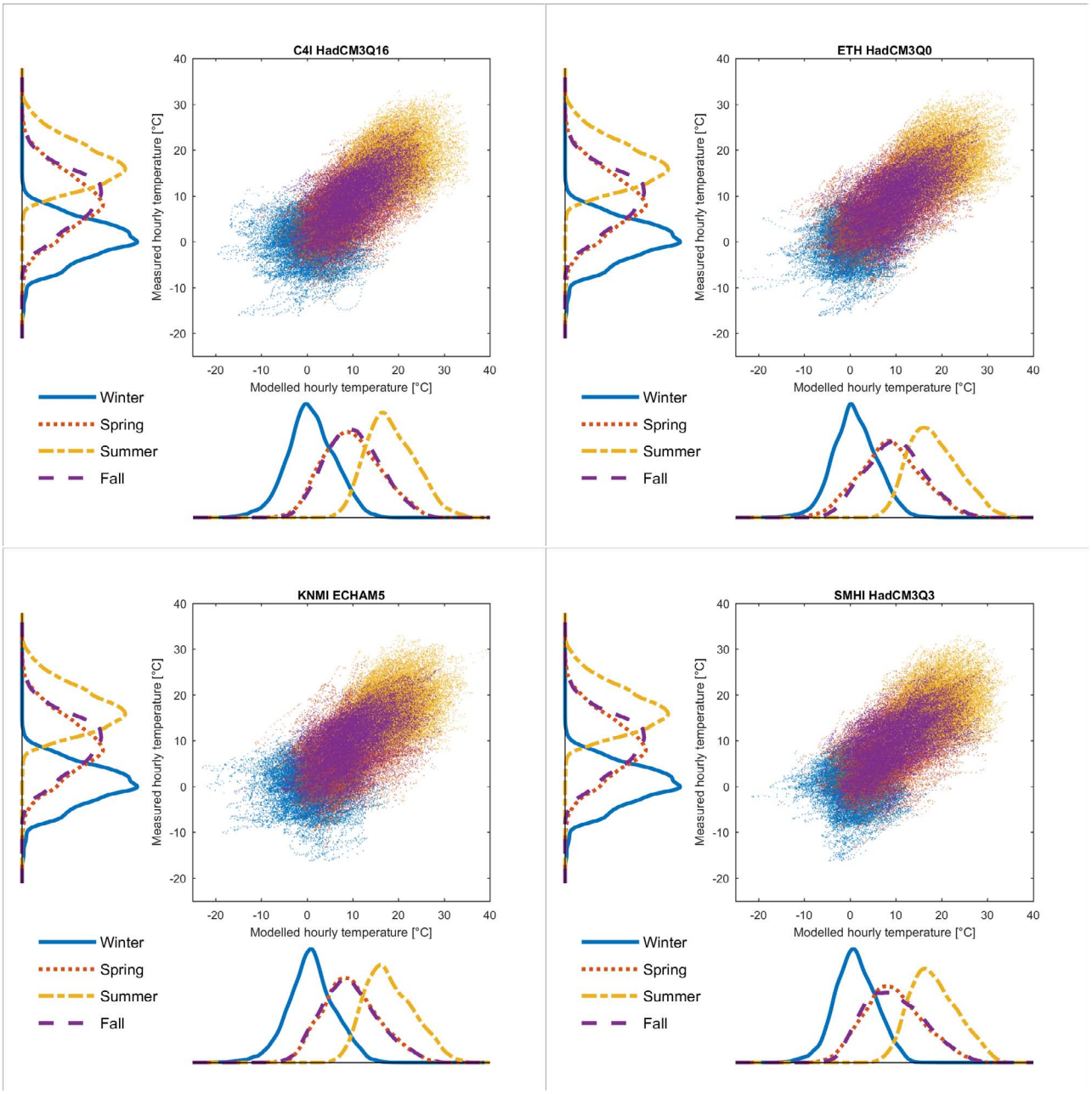

Fig. 20: Comparisons of distributions of hourly mean temperature per season between measured and modelled values based on fluxtower measurements and four bias corrected climate models respectively. Distributions are very similar for the measurements and the four models with most winter temperatures around 0°C, spring and fall temperatures around 10°C and summer temperatures around 18°C.

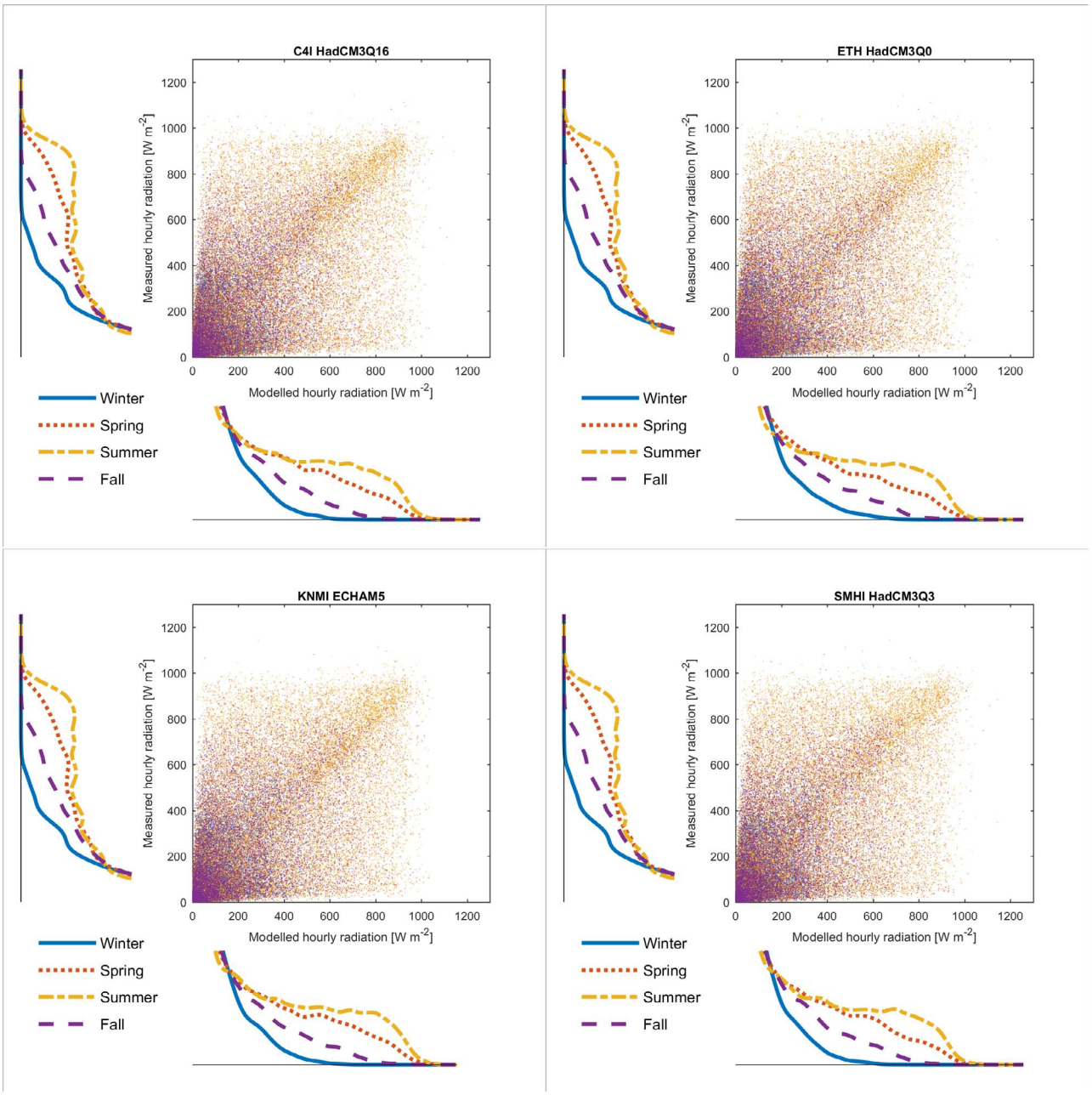

Fig. 21: Comparisons of distributions of hourly mean global radiation per season between measured and modelled values based on fluxtower measurements and four bias corrected climate models respectively. Since radiation is influenced by cloud cover, which is not occurring at the same time in the measured and the modelled climate, the scatter plot does not show a clear trend. More importantly, however, seasonal distributions show an agreement between measured and modelled hourly radiation.

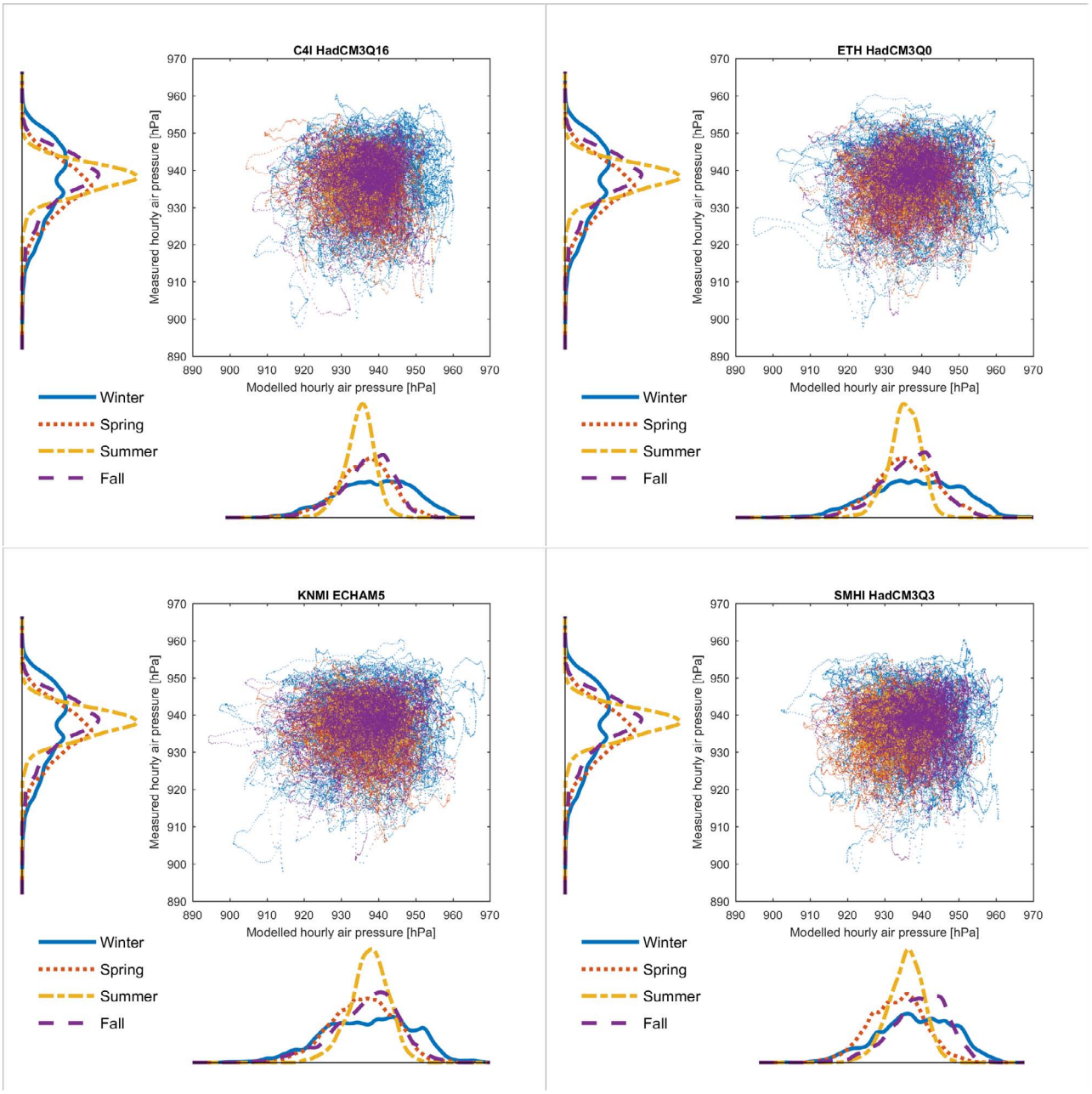

Fig. 22: Comparisons of distributions of hourly mean atmospheric pressure per season between measured and modelled values based on fluxtower measurements and four bias corrected climate models respectively. A stronger peak in summer and a flatter distribution in winter is present in both measured and modelled values.

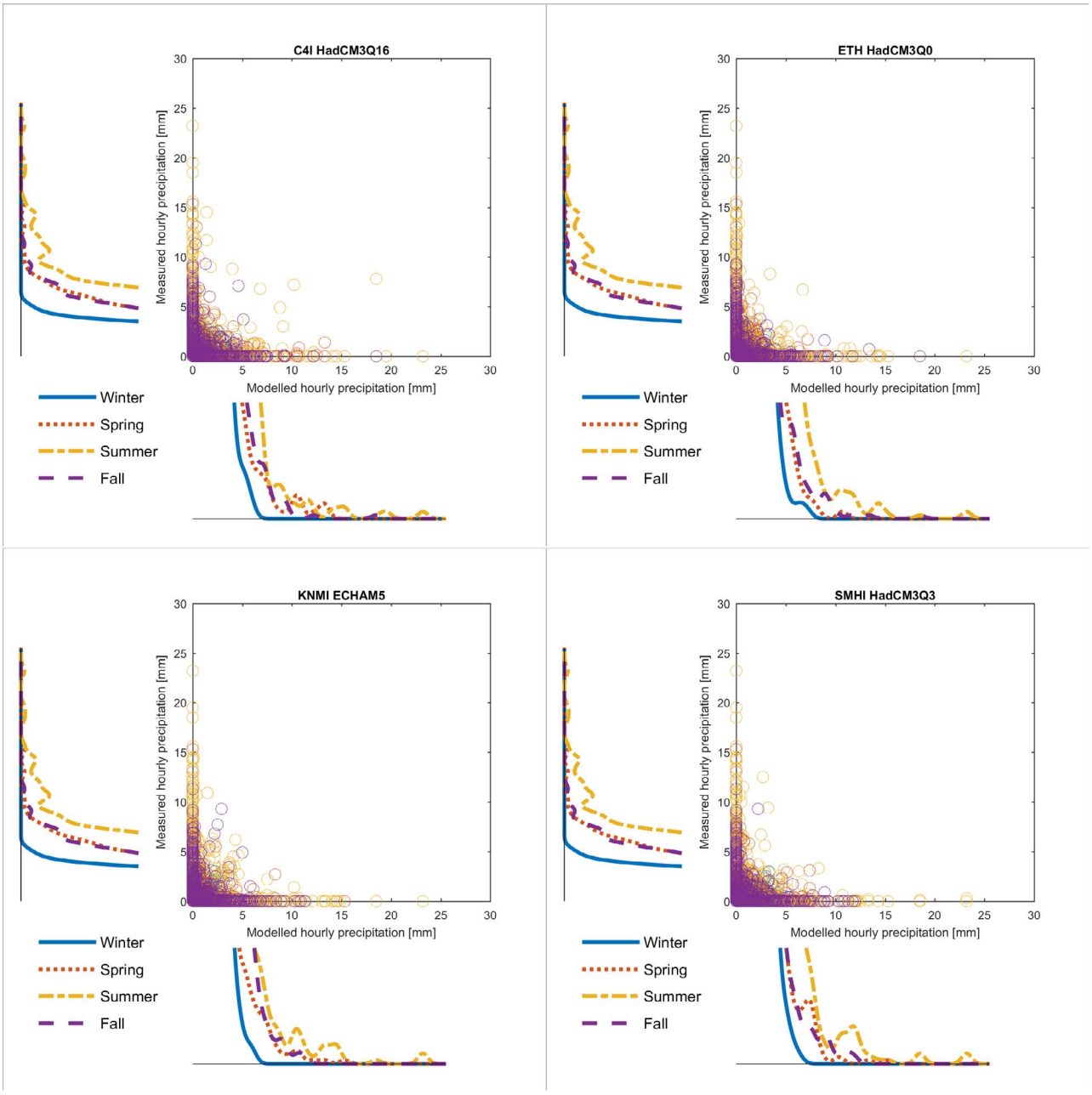

Fig. 23: Comparisons of distributions of hourly precipitation per season between measured and modelled values based on fluxtower measurements and four bias corrected climate models respectively. Since there are many days with little or without any rain, it is more difficult to compare the distributions. Heavy rain of more than 10 mm per hour occurs mainly in summer, with a maximum of about 23 mm per hour in both measured and modelled values.

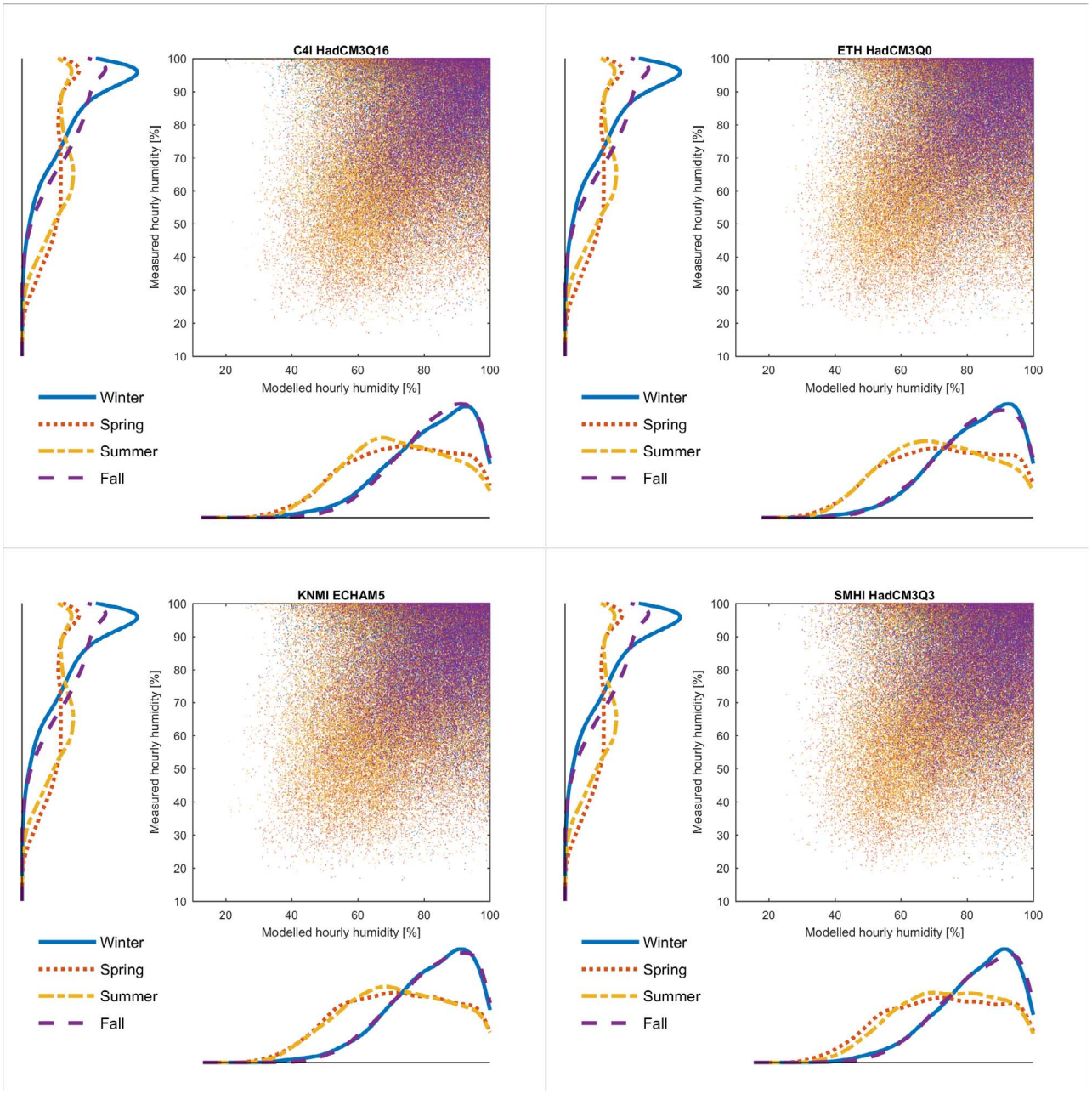

Fig. 24: Comparisons of distributions of hourly mean relative humidity per season between measured and modelled values based on fluxtower measurements and four bias corrected climate models respectively. Widespread fog in fall and winter leads to a concentration of values around 80 to 100% humidity. The winter peak in measured values is more pronounced with more days closer to 100% than in the modelled dataset. Fall and spring distributions are similar, but also with a slight peak close to 100% in the measured values.

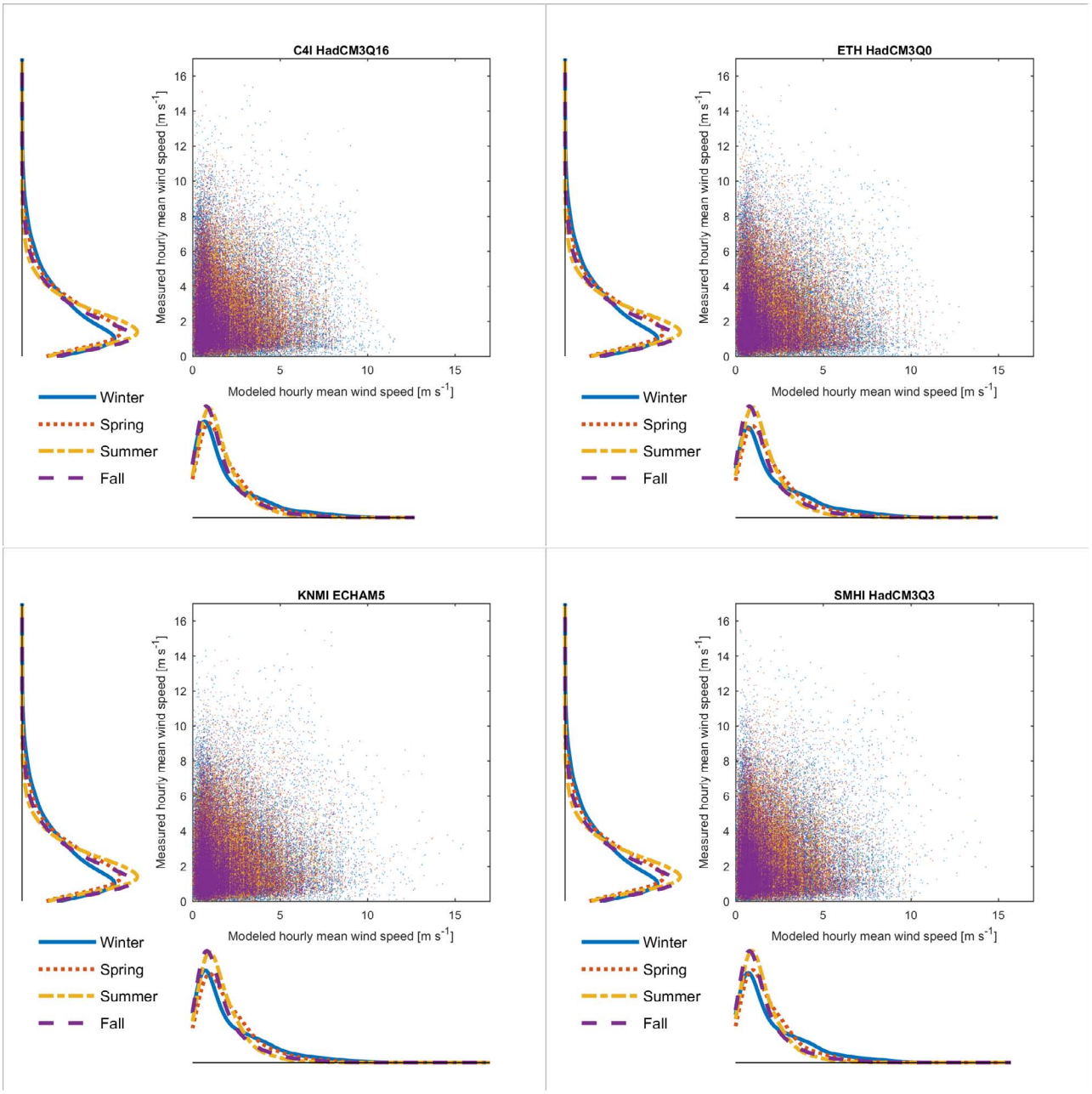

Fig. 25: Comparisons of distributions of hourly mean wind speed per season between measured and modelled values based on fluxtower measurements and four bias corrected climate models respectively. Distributions are very similar between measured and modelled hourly values, with a slight tendency to higher mean wind speed in the measurement.

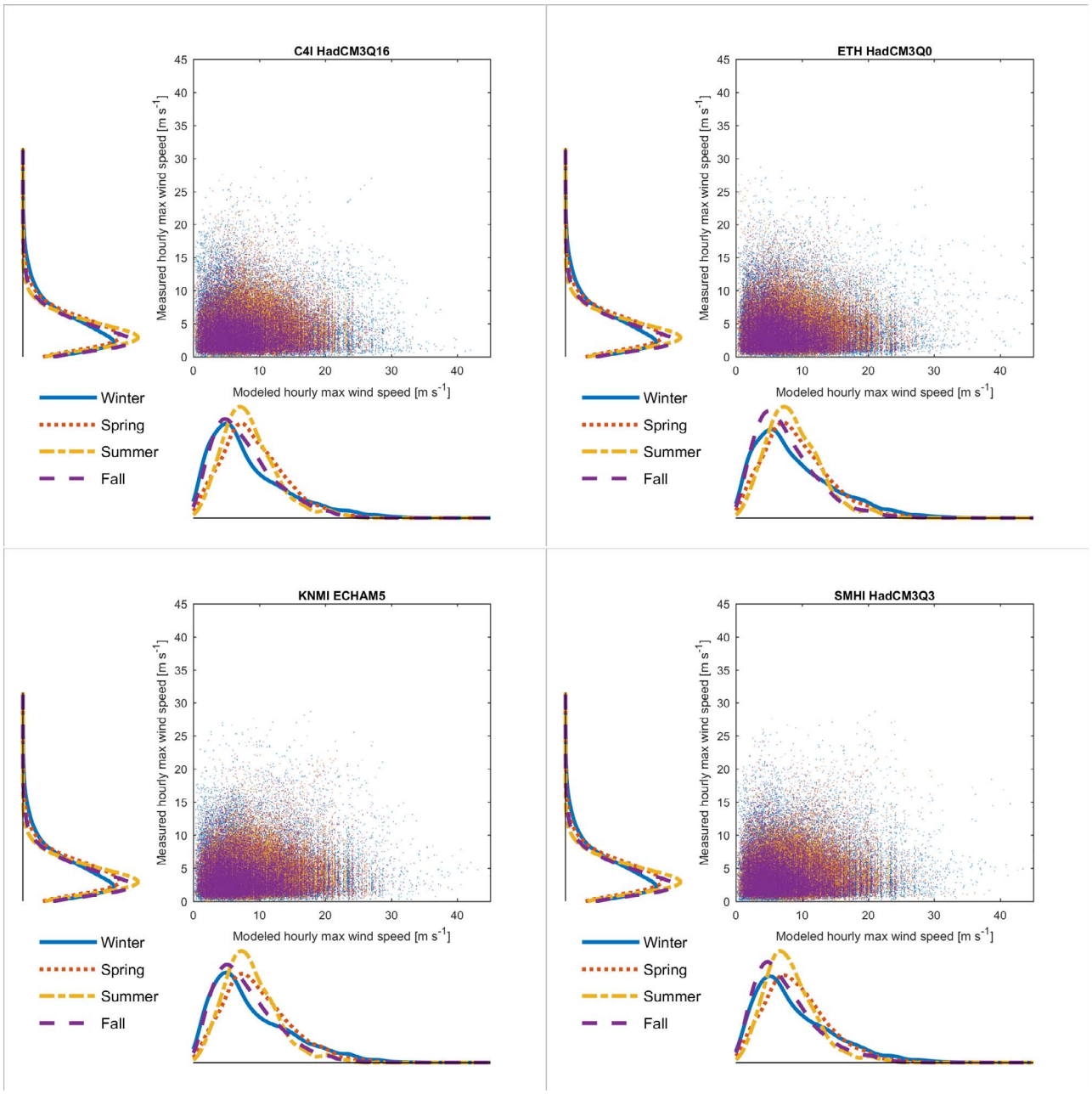

Fig. 26: Comparisons of distributions of hourly maximum wind speed per season between measured and modelled values based on fluxtower measurements and four bias corrected climate models respectively. In contrast to mean wind speed (Suppl. Fig. 25), maximum wind speed is slightly overestimated in the model.

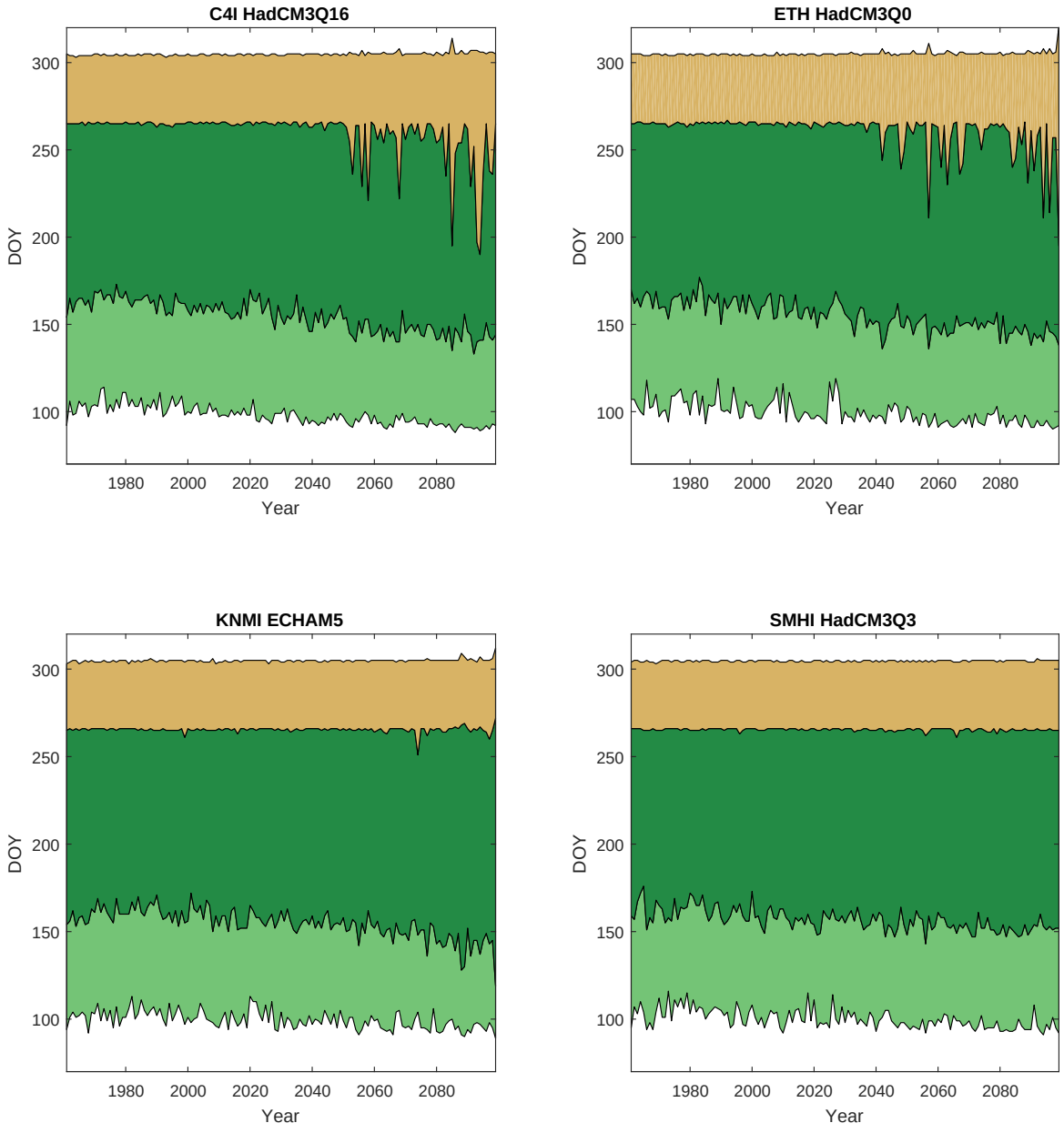

Fig. 27: Timing of the growing season for the years 1960 to 2100 predicted with the phenoanalysis model and meteorological drivers at hourly time scales based on four bias corrected climate models. The greening phase (bright green) is defined by start and end of greening at a 10% and 90% threshold of LAI. Similarly the browning phase (beige) is defined by start and end of browning at a 90% and 10% threshold of LAI.

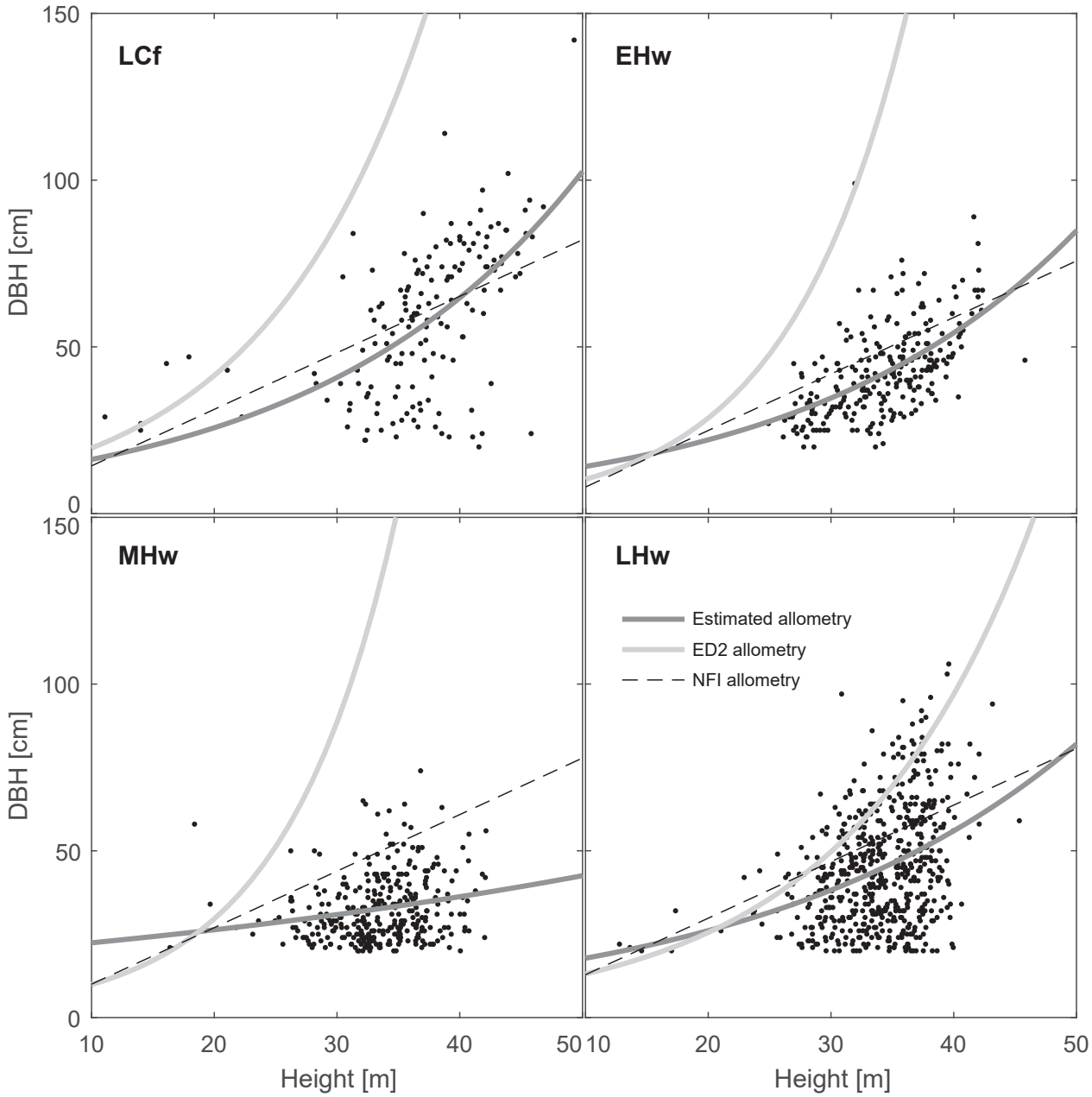

Fig. 28: Tree height to diameter at breast height (DBH) allometries for late conifers (LCf), early hardwoods (EHw), mid hardwoods (MHw) and late hardwoods (LHw). The grey solid line corresponds to the allometry estimated from the plot inventory data (black dots), compared to the allometry implemented in the ecosystem demography model ED2 (light grey line) and a general allometry from the Swiss national forest inventory (NFI, dashed black line).

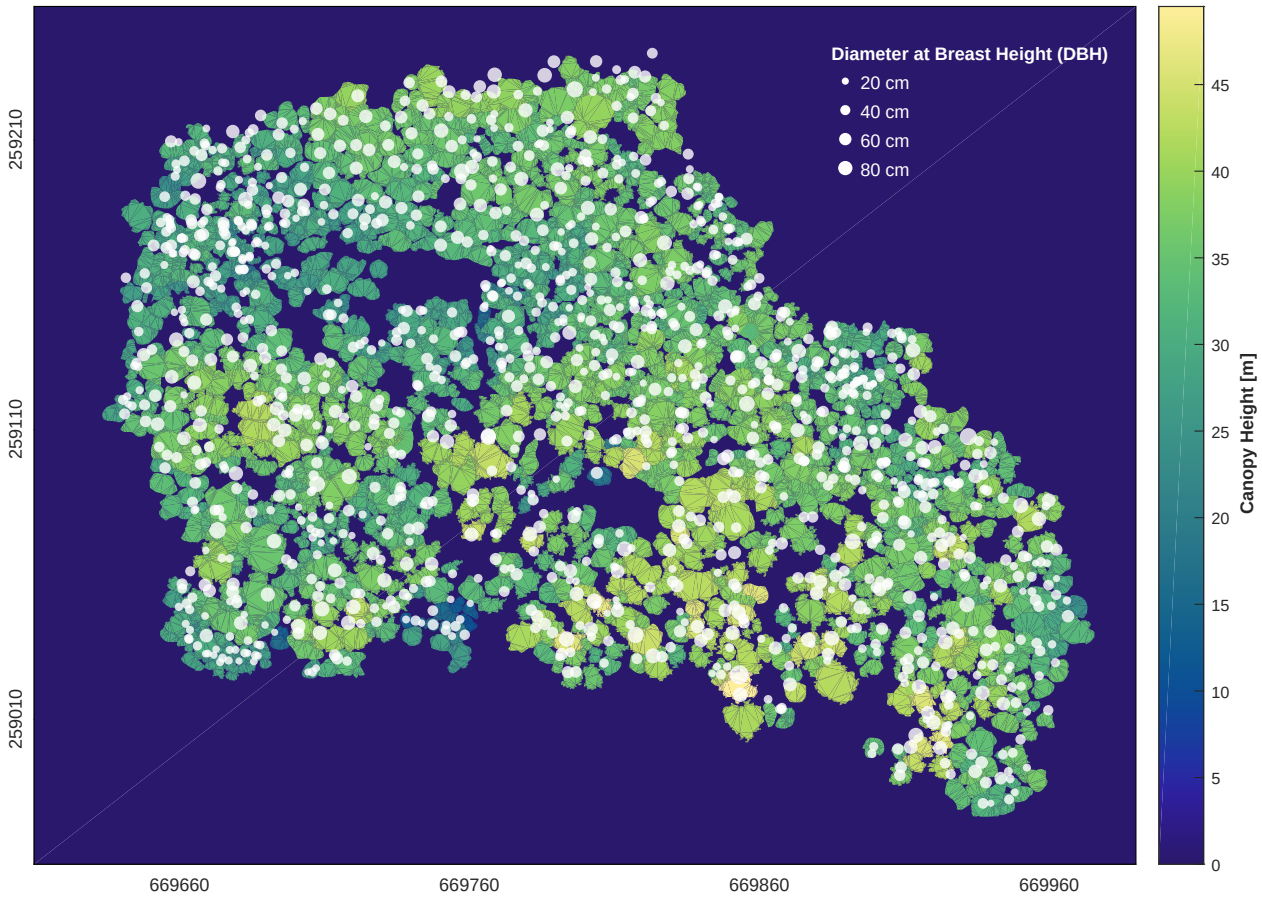

Fig. 29: Crown polygons coloured by canopy height for all dominant and co-dominant trees with a diameter at breast height (DBH) above 20 cm as derived from high-resolution drone images, airborne laser scanning data and field inventory. White dots represent the corresponding tree stem positions with changing size according to the DBH measured in the field.

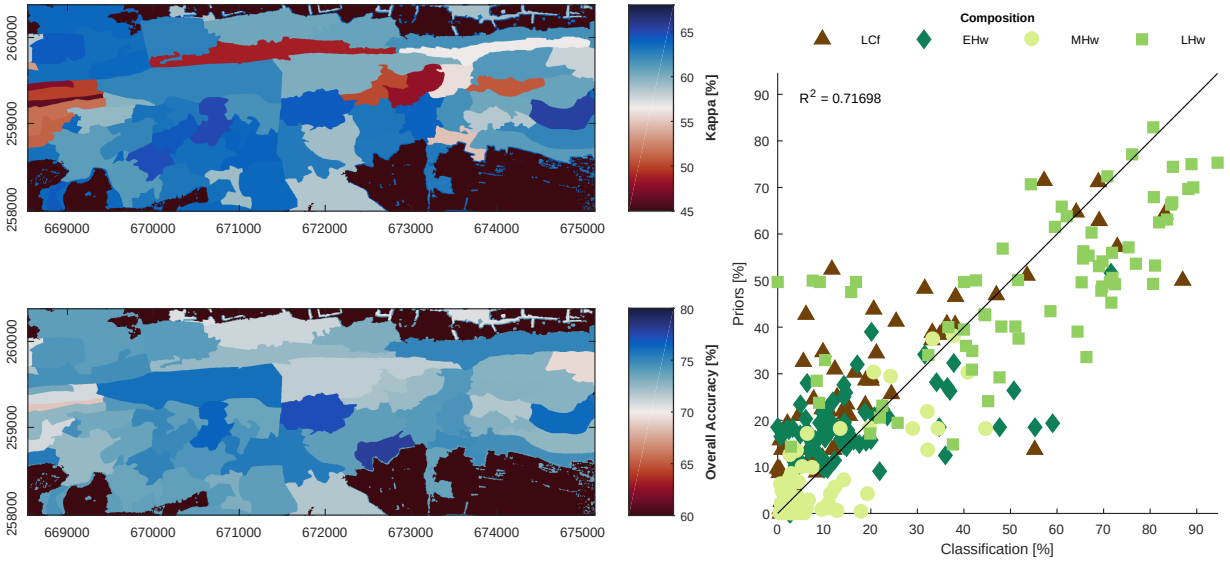

Fig. 30: Results of random forest classification of the plant functional types late-successional conifers (LCf), early hardwoods (EHw), mid hardwoods (MHw) and late hardwoods (LHw). The maps show kappa and overall accuracy for each polygon that was separately trained, tested and predicted. The right panel shows how the prior information of composition of plant functional types compares to the actual classification for each polygon.

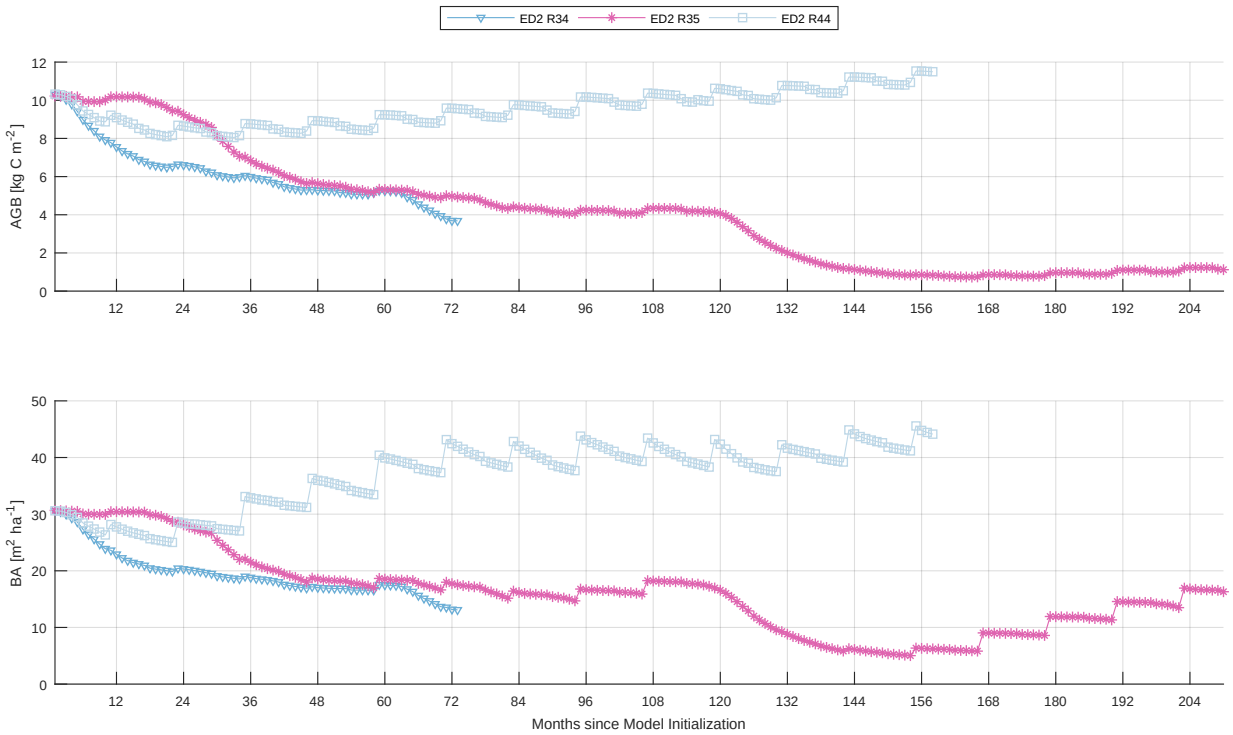

Fig. 31: Above ground biomass (AGB) and basal area (BA) simulated with vegetation dynamics in ED2, initialised in July. The first model run showed a decrease in AGB and BA over the years due to an excessive moisture limitation in the understory ('ED2 R34'). A newer code of the model ('ED2 R35') proved to be unsuitable to simulate deciduous hardwoods, leading to two tree mortality events after 24 and 120 months and a regrowth of early-successional hardwoods. Finally, turning off plant moisture limitation in 'ED2 R34' lead to tree growth in spring and an increase in AGB and BA ('ED2 R44').

Chapter

5

Synthesis

Biodiversity is a key driver of productivity in a wide range of taxa and ecosystems, as affirmed in recent research by Duffy *et al.* (2017) for a range of natural systems and Liang *et al.* (2016) for forest ecosystems in particular. Humans are vastly profiting from natural ecosystem services related to biodiversity, but are at the same time driving biodiversity loss in an unprecedented manner (Isbell *et al.*, 2017). This might pose a severe threat to human well-being with irreversible consequences for ecosystem functioning and related goods and services. With the recent recognition of the importance of trait based biodiversity assessments (Cernansky, 2017), a way to map, monitor, and predict changes in plant functional diversity is urgently needed and demanded by the international community (Jetz *et al.*, 2016; Schmeller *et al.*, 2017; Kulmala, 2018). In this thesis, we aimed to develop and apply a method to study spatial patterns of forest functional diversity with remote sensing, and its implication on ecosystem functioning in a temperate mixed forest. In this Chapter, we provide a comprehensive overview and discussion of our findings, general contributions to the research field and suggestions for future research promoting a pathway to global biodiversity monitoring.

5.1 Main findings

The thesis is structured by three main research questions (RQ) formulated in Chapter 1 and addressed in Chapters 2 to 4, with five related hypotheses:

> I. Airborne laser scanning and imaging spectroscopy can be integrated and compared using a 3D radiative transfer modeling approach (RQ1)
>
> II. Morphological and physiological diversity show consistent spatial patterns following an environmental gradient (RQ2)
>
> III. Relationships between functional richness and area follow a species richness-area relationship (RQ2)

whereas two are more conceptual and part of ongoing research:

> IV. There is a positive relationship between functional diversity and productivity (RQ3)
>
> V. Functional diversity mitigates some of the potentially negative effects of climate change (RQ3)

In the following three subsections, the main findings of the three research questions are presented and discussed with regard to their hypotheses.

5.1.1 Integrating airborne laser scanning and imaging spectroscopy data helps to derive functional traits and their optimal 3D representation in a forest canopy

The parametrization and application of the coupled 3D canopy-atmosphere radiative transfer model DART (Discrete Anisotropic Radiative Transfer) allowed a comparison of airborne laser scanning based forest reconstruction approaches with imaging spectrometer data at the sensor radiance level. Chapter 2 shows that by upscaling the radiative transfer from leaf to canopy and sensor level, we could integrate structural and spectral properties of the forest in order to make the two independent remote sensing approaches comparable. Thus we can support the hypothesis that airborne laser scanning and imaging spectroscopy can be integrated and compared using a 3D radiative transfer modeling approach (hypothesis I).

The results presented in Section 2.1 show that spatial patterns simulated based on airborne laser scanning data are comparable to the measurements by an imaging spectrometer at 2 m spatial resolution. We developed and compared two turbid-medium based forest reconstruction approaches and found that a continuous voxel grid approach was better suited (R^2 = 0.48, λ = 780 nm) to represent the forest canopy than an individual tree approach (R^2 = 0.34, λ = 780 nm) in the context of continuous voxel or raster based trait mapping and modeling. This was an essential finding to further develop the spatially continuous diversity mapping approach (Chapter 3) and the remote sensing based initialization of vegetation demographics in the Earth system model ED2 (Chapter 4).

To enable the spatially explicit comparison at the pixel level, the model needed to be parametrized by 3D information of the terrain, background (incl. understory), forest canopy, solar and observational geometry as well as the atmospheric composition. On one hand, the enormous level of detail, number of parameters and complexity of the model made it challenging to parametrize and run it. On the other hand, comparing to actual spectrometer measurements allowed identifying and addressing several shortcomings of the initial approach. This did not only concern the forest reconstruction approach but also the ability of the model itself to simulate airborne imaging spectrometer data.

First, we found the representation of the observation geometry in the model to be inaccurate for simulating airborne data. The simulation of parallel outgoing rays with a single observation angle for all pixels is a valid simplification for most satellite data, but not suitable for simulating airborne or close-range observations with a wide field of view. In Section 2.2, we therefore present the first results of a new module implemented in DART to simulate the viewing geometry of airborne imaging spectrometer data, improving the accuracy of

simulated at-sensor radiance images. This lead then to the development published in Yin *et al.* (2015) and was a substantial part of the new DART version 5 (Gastellu-Etchegorry *et al.*, 2015).

Second, we detected plant area index patterns related to the scan geometry and flight strip overlap of the airborne laser scanning data when applying a voxel based forest reconstruction on larger areas. To address the overestimation of plant area index in some areas, we normalized the LiDAR point cloud to a maximum of 100 pulses per 2 x 2 m pixel and implemented a new ray tracing scheme for the retrieval of plant area index (Section 2.3). This improved the method substantially, helping to harmonize the voxel grid and resulting in consistent spatial patterns of canopy density across the whole forest.

Third, the comparison of simulated and measured spectra in Section 2.1 (Fig. 6) showed an overestimation of simulated at-sensor radiance especially in the blue part of the electromagnetic spectrum. This was an indication that there was an issue in the atmosphere simulation, which could be resolved by introducing new phase functions and vertical distributions of aerosols and gases in DART (Section 2.2; Gastellu-Etchegorry *et al.*, 2015). In Section 2.4, we used the improved atmospheric modeling scheme to simulate direct and diffuse irradiance at the top of canopy. We demonstrated that the integration of such information is important to derive surface reflectance and can improve the retrieval of vegetation indexes, especially in shadowed areas. However, there is still considerable uncertainty in shadow correction and the retrieval of functional traits in shadowed areas. Further research is needed towards more advanced image-based correction algorithms or modeling with a vast number of directions to correctly simulate diffuse radiation in the shade (Yin *et al.*, 2013). A final comparison of a measured and simulated forest canopy at-sensor radiance spectrum in Section 2.5 Fig. 5 shows the improvements of the modeling approach compared to the initial results shown in Section 2.1 Fig. 6. Deviations of 20 mW m^{-2} nm^{-1} sr^{-1} have been reduced to 10 mW m^{-2} nm^{-1} sr^{-1} and mostly below, with main improvements in the visible part of the spectrum along with a reduction of spectral shifts in the imaging spectrometer data.

Finally, we identified small-scale clumping and gap distribution to be an important aspect in the representation of the canopy in 3D, in particular when simulating multiple scattering and leaf absorption within the canopy. Further research is needed to address the effects, for example of needle clumping within a shoot, in radiative transfer models and the influence of voxel size on forest reconstruction. New developments in laser scanning provide the necessary tools to address such small-scale effects, offering the opportunity to derive plant information down to single leaves (Junttila *et al.*, 2016; Hancock *et al.*, 2017). In Section 2.6, we provide an overview of the current state-of-the-art

of close-range laser scanning, introducing relevant concepts, methods and possible applications for vegetation information retrieval, methodology testing and validation. This paves the way for the further development of a voxel based forest reconstruction and radiative transfer modeling approach. Figure 5.1 illustrates the potential of close-range laser scanning (as combination of TLS and UAVLS) for small-scale forest reconstruction in a tropical and temperate forest ecosystem, forming the basis for future studies on light availability, canopy-atmosphere radiation interactions, influence of voxel size on total plant area density and the estimation of morphological trait diversity.

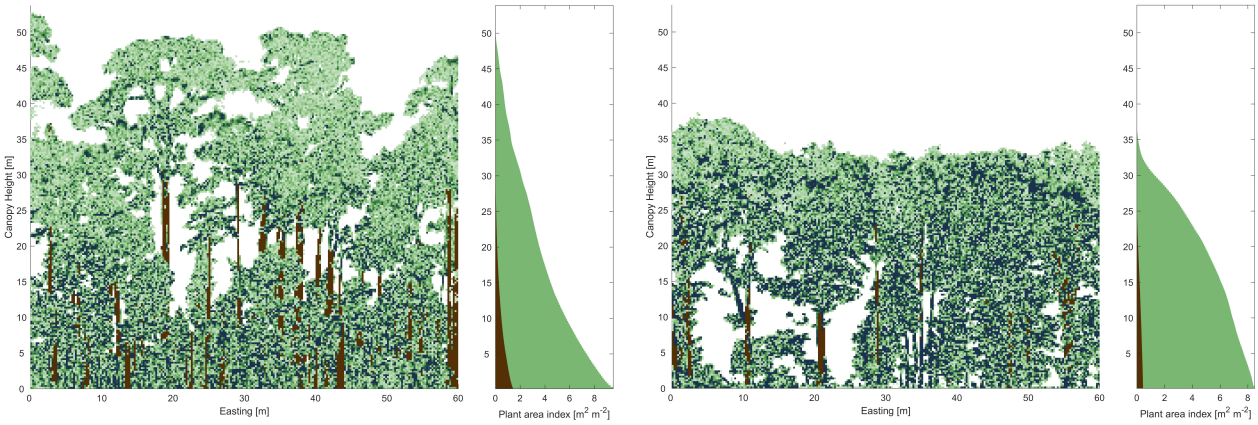

Fig. 5.1: Cross section of a plant area index (PAI) voxel grid at 25 cm spatial resolution and corresponding vertical cumulative PAI derived from below and above canopy close-range laser scanning, with brown voxels classified as stems. The figure illustrates the differences in canopy architecture and PAI distribution between a tropical (left) and a temperate (right) forest ecosystem.

5.1.2 Mapping functional diversity from remotely sensed morphological and physiological forest traits reveals spatial patterns of plant adaptability to the environment

The remotely sensed functional trait maps form the basis for mapping functional diversity in a spatially continuous fashion (Chapter 3). We base the retrieval of morphological forest traits on the voxel-based 3D forest reconstruction presented in Chapter 2, allowing to derive information on canopy height, layering (foliage height diversity) and density (plant area index). Physiological traits were derived from airborne imaging spectroscopy data at comparable spatial resolution (Chapter 2). As discussed above, the retrieval of functional traits in shadowed areas can be highly uncertain (Section 2.4). Therefore, we combined two airborne acquisitions under varying sun angles and aggregated three by three pixels to retrieve information of sunlit pixels only. This allowed the spatially continuous mapping of chlorophyll, carotenoids and leaf water. Figure 5.2 shows a detailed view of the forest functional traits, as a subset of the trait maps shown in Section 3.1 Fig. 3.

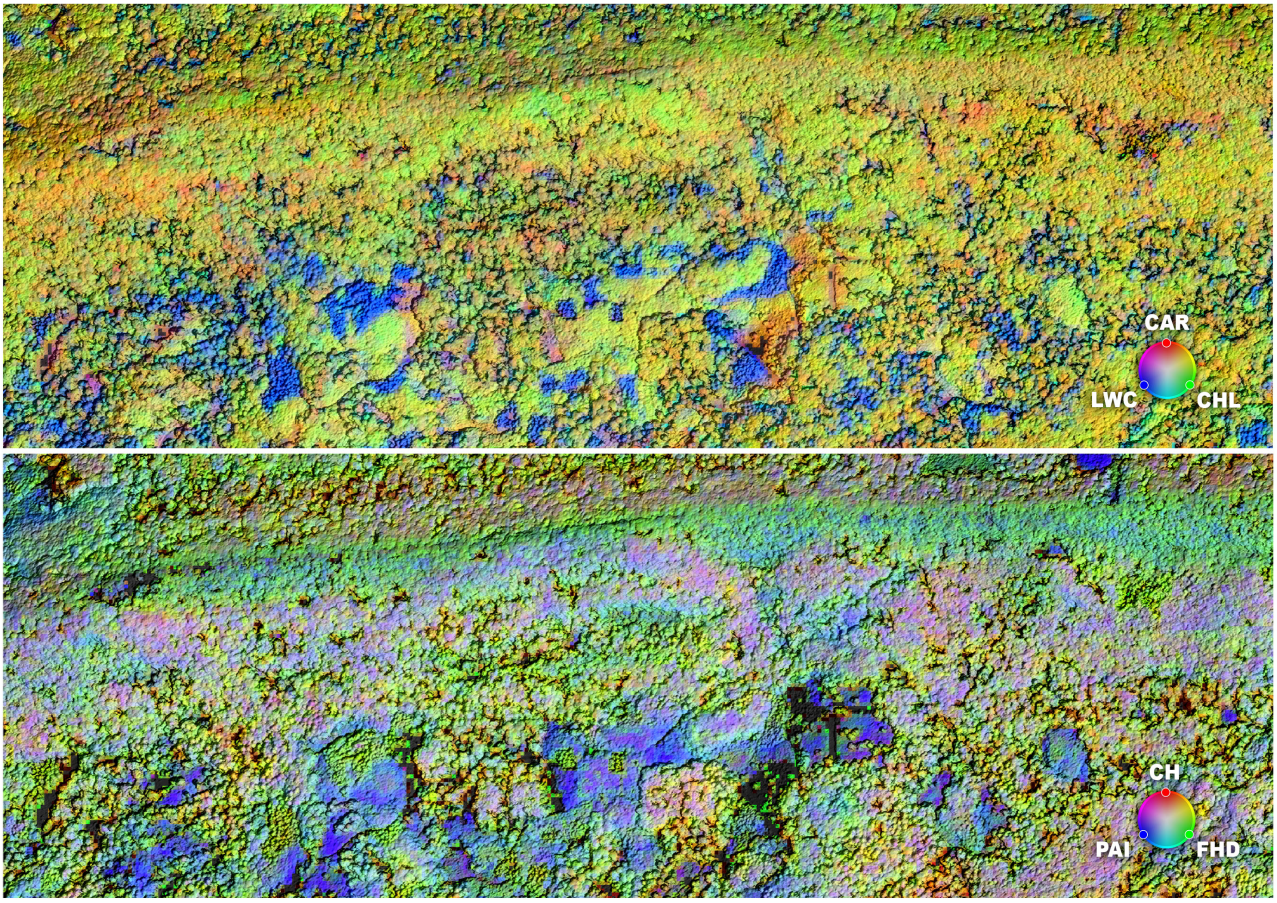

Fig. 5.2: Spatial composition of functional traits shown as RGB color composite based on the relative abundance of traits. The upper panel shows physiological traits of leaf chlorophyll (CHL), carotenoids (CAR) and leaf water content (LWC), derived from airborne imaging spectroscopy data. The lower panel shows morphological traits of canopy height (CH), canopy layering as foliage height diversity (FHD), and canopy density as plant area index (PAI), derived from airborne laser scanning data (Schneider *et al.*, 2017).

Figure 5.2 already provides a first visual impression of the diversity of the forest, with more homogeneous areas in the upper parts (higher elevation) and more diverse and spatially heterogeneous areas in the lower parts (lower elevation) of the subset displayed. To quantitatively map functional diversity at a continuous range of spatial extents, we developed a moving-window based scaling approach to map pixels within a given radial neighborhood in the functional trait space and subsequently derive quantitative functional diversity measures (Chapter 3). The three measures functional richness, divergence and evenness have been developed by Mason *et al.* (2005); Villéger *et al.* (2008) and already been widely used, e.g. in Mendes *et al.* (2015); van der Plas *et al.* (2015); Park & Carpenter (2016). However, the approach has not been applied to spatially continuous remotely sensed trait data, independent of predefined vegetation units, species or plant functional types. Our approach has the advantage to include intra-specific diversity, making up a large percentage of total functional diversity in temperate forests (Siefert *et al.*, 2015; Guillén Escribà *et al.*, in preparation), and to be only dependent on the resolution of

the trait data. This uniquely offers to study spatial patterns of morphological and physiological diversity at any desired scale, and in particular how tree assemblages in a specific neighborhood are filling the functional trait space. The latter is essential to forest communities, since it is indicating the potential range of resource availability, resource use efficiency, and thus ecosystem functioning and stability (Violle *et al.*, 2007, 2014).

We found clear spatial patterns of functional diversity following an environmental gradient from lower altitude, flat and deep soils to higher altitude, steep and rocky soils. We observed reduced trait variability towards the top of the forested mountain ridge coinciding with the harsher environment to grow, with possibly reduced water and nutrient availability due to the shallow and steep slopes, as well as enhanced exposition to wind and radiation. This might only allow trees with specific traits adapted to the environment to exist, leading to a constrained community niche and potentially lower ecosystem functioning and stability. This pattern is consistent between morphological and physiological diversity, whereas more pronounced for functional richness than divergence and evenness, being generally high and low in variance. About 24% of morphological and even 40% of variance in phyiosological richness could be explained by topography and soil. Figure 5.3 shows the consistent patterns along the elevational gradient, supporting hypothesis II. The main differences can be observed in a flat area in the lower left of the images in Figure 5.3, resulting from physiological richness being more strongly driven by forest composition whereas morphological richness was more strongly influenced by the development stages of the forest, and thus indirectly forest management.

Besides the analysis of spatial patterns at a specific spatial extent, the approach presented in Chapter 3 also allowed to study the scale dependency and functional richness-area relationships at our test area. The species richness-area relationship is a well studied concept in ecology gathering increasing attention due to its simplicity and broad application in nature conservation for predicting species richness and biodiversity loss (Thomas *et al.*, 2004; Gerstner *et al.*, 2014; Keil *et al.*, 2015). However, despite the popularity of the species richness-area relationship, little was known yet on how functional richness is changing with area. This could not only be relevant for scaling functional diversity measures but also reveal insights on α- and β-diversity of forest ecosystems. The concept of α-, β- and γ-diversity introduced by Whittaker (1960) relates to the spatial organization of biodiversity as within-community, between-community and between-landscape diversity, often quantified by species richness. In species-poor ecosystems such as temperate forests, much of the total plant diversity might be underestimated when ignoring intra-specific diversity though. In Chapter 3, we showed that functional richness is increasing with area, however not following a power law function as expected from species richness-area

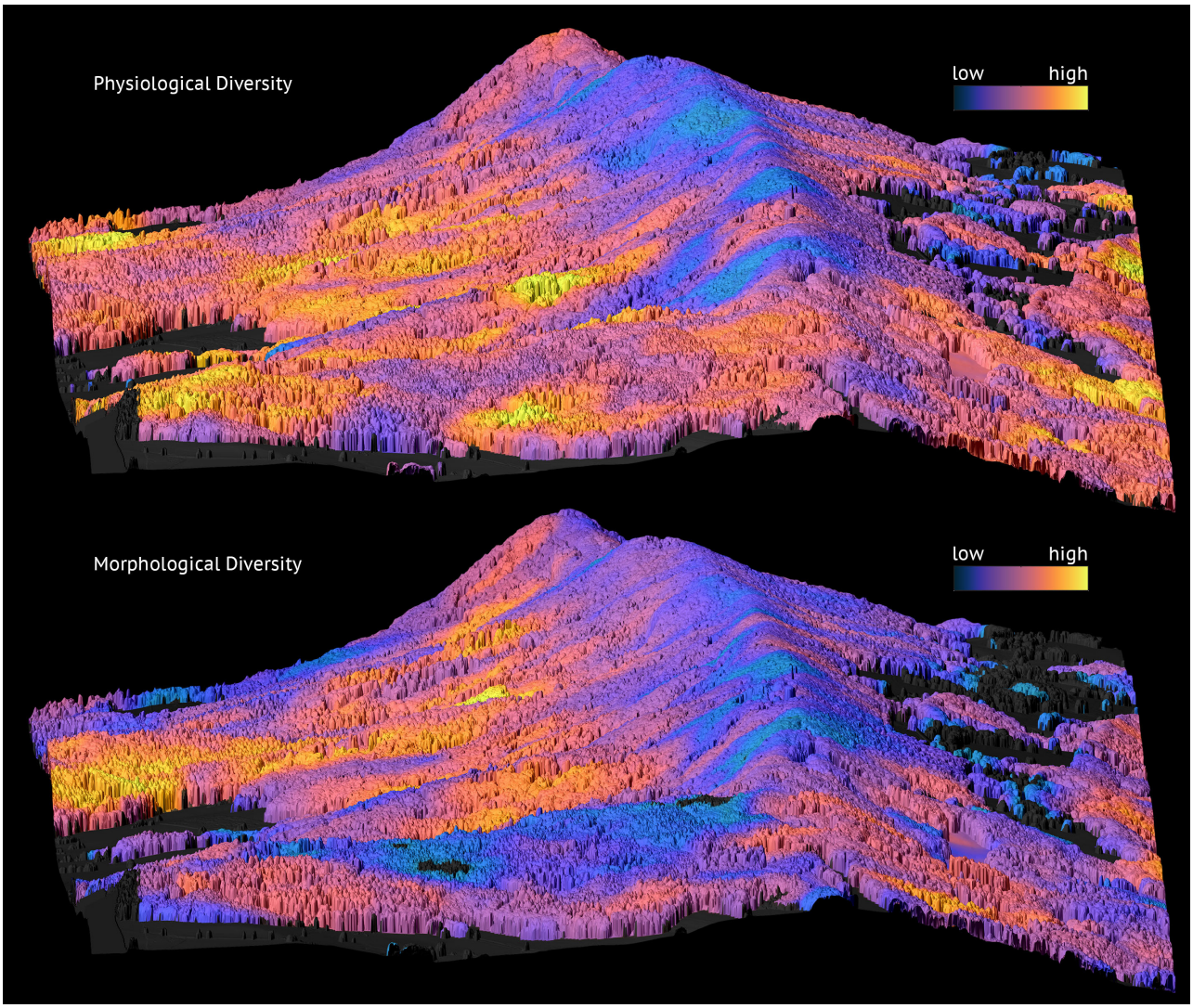

Fig. 5.3: Diversity of physiological traits (leaf chlorophyll, carotenoids and water content; upper panel) and morphological traits (canopy height, density and layering; lower panel) as functional richness at a radial neighborhood of 90 m. Functional richness is generally lower on top of the mountain ridge, since trees have adapted to harsher environmental conditions on the steep and rocky slopes (Schneider *et al.*, 2017).

relationships but rather a logarithmic function. Therefore, we can not fully support hypothesis III. The higher α-diversity of functional traits indicates considerable diversity within species and communities, not reflected in species related measures of diversity nor in large-scale studies (Pereira *et al.*, 2012). On larger scales, the functional richness-area curve is flatter as the predicted increase of species with area, meaning that β-diversity and thus the diversity between communities is lower than expected. This might indicate functional trait redundancy among a large number of species, with some species or individuals having similar functional traits and thus not adding to the overall increase of functional diversity.

5.1.3 Predicting the relationship between functional diversity and productivity at a temperate mixed forest site and its change under climate change scenarios

Mapping functional diversity is important since it can reveal information about ecosystem functioning and the susceptibility of a forest to climate change. Thus it has implications on forest conservation and management. However, in Chapter 3 we could only discuss the potential influence on ecosystem functioning and stability, without having more evidence on how the system would react to different environments with regard to topography and soil but also changing climatic conditions. To be able to predict such changes, we were therefore integrating a remote sensing based forest characterization in an Earth system model (Ecosystem Demography, ED2, Medvigy *et al.*, 2009).

The results presented in Chapter 4 show that remotely sensed input parameters of forest structure and composition are comparable to the reference measurements performed in the field. This demonstrates the ability of airborne laser scanning and imaging spectroscopy for larger scale forest reconstruction and the potential to inform Earth system models with the most relevant model inputs. We could also show that predictions of gross primary productivity could be improved by initializing the model with remote sensing data compared to uninformed potential vegetation simulations.

Further optimization and potentially a re-parametrization of the model is needed to be able to correctly simulate vegetation dynamics on longer time scales. We could identify two major limitations of the current approach, having a considerable influence on the simulation of the forest carbon budget. First, predefined allometric relationships in the model limit the realism of the initialization of forest structure, not allowing intra-specific deviation from the predefined growing functions. Second, moisture limitation and the competition for water proved to be an essential factor driving forest productivity as well as the susceptibility to droughts and resulting tree mortality. Current simulations were either strongly limited or not limited by water availability at all, leading to unrealistic results. To find a feasible parametrization of plant-water relations in the model will be a major but crucial next step for future research.

Therefore, we were not able to answer the third research question in full and remain with the hypothesis that diversity is driving productivity and stability under current and future climates (see hypotheses IV and V). The theoretical reasoning for these hypotheses lie in the effect of niche complementarity (complementary traits lead to better resource usage, Williams *et al.*, 2017), selection (higher likelihood to have highly productive individuals under new climatic conditions, Hooper *et al.*, 2005), and ecological insurance (higher likelihood to have highly plastic and resilient individuals adapting to and recovering from disturbance, Silva Pedro *et al.*, 2017).

5.2 General contributions

Jetz *et al.* (2016) motivate the need and introduce the concept for a global biodiversity observatory (Section 1.1), supported by international initiatives to harmonize global plant and ecosystem trait measurements (Pereira *et al.*, 2013; Skidmore *et al.*, 2015; Pettorelli *et al.*, 2016) and Earth observation efforts related to biodiversity (Walters & Scholes, 2017). The development and implementation of a new satellite mission as a biodiversity observatory requires case studies and a proof of concept in order to be widely supported and funded. This thesis contributes such a case study and a new development of a diversity mapping approach with the potential to be more broadly applied and scaled to global observations. This is the first study addressing the mapping of functional diversity with remote sensing without the need of ground calibration, which is a significant step forward as compared to the only other existing approach developed by Asner *et al.* (2017).

While Asner *et al.* (2017) use laser-guided imaging spectroscopy to derive forest functional traits and group them to functional classes, we promote an approach to map different aspects of functional diversity continuously in space independent of plant functional types, species, or any other prior knowledge of vegetation units. This is beneficial in species-poor ecosystems with high intra-specific trait variation or generally in very heterogeneous landscapes with high α-diversity, where forest functional classes would be highly disaggregated and spatially scattered. For smaller-scale conservation needs and more sustainable local forest management strategies, plant functional diversity within a forest functional class should not be neglected and can be better mapped using our continuous approach. Neglecting functional diversity within forest classes precludes to monitor the effects of selective logging or local disturbance and to assess whether these effects have a positive or negative influence on overall diversity and productivity. On the other hand, the large-scale mapping of forest functional classes can make it easier to track changes related to systematic illegal logging or assign conservation strategies to specific areas or forest types.

Asner *et al.* (2017) derive twenty leaf biochemical compounds by calibrating field and laboratory measurements of leaves with the spectral signatures of the canopies measured by airborne imaging spectroscopy. This set of leaf level traits can only be derived when an extensive library of in-situ measurements is available, though. One main advantage of our approach is its simplicity and independence from field calibration. We mapped functional traits directly, independently, and purely from remote sensing data without the use of any informative priors. Field and laboratory measurements are still needed to validate our method. Validation of forest functional traits in Chapter 3 was achieved with the radiative transfer modeling framework introduced in Chapter

2, with the necessary optimization and testing of the feasibility of the approach. This new way to validate remotely sensed traits was essential for the successful mapping of functional diversity. It allowed a more versatile testing and the integration of a broader range of field data for the validation of the imaging spectroscopy derived traits. We could validate our method not only with the leaf optical properties measured at our site, but also with additional data from spectral libraries and trait databases.

The successful demonstration and application of the 3D radiative transfer model opens up new possibilities for developing, testing and validating more complex and detailed remote sensing products. With the advancement of remote sensing technologies and methods, new products can go beyond what is measurable - or feasible to measure - with traditional field work or ground truth data. In that case, a model environment can offer new possibilities, i.e. validating complex processes such as scaling between leaf and canopy spectra (Mõttus *et al.*, 2012) or even testing new measurement strategies (Abegg *et al.*, 2017).

This thesis promotes the integration of remote sensing data and derived products with physically-based process models, not just for validation but also for the estimation and prediction of energy and carbon fluxes (Fisher *et al.*, 2017). The challenge is that airborne remote sensing data reached a quality and level of detail that cannot yet be resolved by Earth system models and that translating input parameters to the model representation is not trivial. With this thesis, we contribute to the development and testing of the Earth system model ED2 and its implementation of dynamic interactions (Chapter 4). Typical big leaf models are strongly simplifying and averaging the energy balance over the whole forest canopy, leading to an unrealistic resistance to climate change extremes such as droughts. With the detailed initialization of the ED2 model based on remote sensing data, the opposite might happen. The large number of very small cohorts might be oversensitive to drought or moisture limitation. Therefore, a re-parametrization of the model and potentially even a change of concept from cohort-based to individual-based modeling might be necessary to resolve this issue.

5.3 Final considerations and future directions

”Thriving on Our Changing Planet: A Decadal Strategy for Earth Observation from Space,” is the name of the strategic report on the outcome of the decadal survey released by the US National Academies of Sciences, Engineering, and Medicine on Januray 5, 2018. From initially 290 ideas, an interdisciplinary committee selected 35 key Earth science and applications questions that will largely shape future Earth observation missions of NASA (National Aeronautics and Space Administration), NOAA (National Oceanic and Atmospheric Administration) and the USGS (US Geological Survey). The observation of biodiversity and the characterization of ecosystem structure are among the highest-priority questions:

> *”(E-1) What are the structure, function, and biodiversity of Earth’s ecosystems, and how and why are they changing in time and space?”*

together with questions related to the fluxes between and within ecosystems:

> *”(E-2) What are the fluxes (of carbon, water, nutrients, and energy) between ecosystems and the atmosphere, the ocean and the solid Earth, and how and why are they changing?”*

> *”(E-3) What are the fluxes (of carbon, water, nutrients, and energy) within ecosystems, and how and why are they changing?”*

This thesis was key to preparing the statements of the decadal strategy as part of an international effort to stress the importance of biodiversity and functioning in the report. At the same time, it provides a pathway towards answering important parts of these questions and future challenges, with the example of a temperate mixed forest site. In the following sections, potential future directions are discussed to address the most important related research goals.

5.3.1 Quantify the global distribution of the functional traits, functional types, and composition of vegetation, spatially and over time

Airborne imaging spectroscopy is suited for mapping plant functional traits, functional diversity and plant functional types in forest ecosystems, as has been demonstrated in this thesis. The observation of forest ecosystems is already an essential contribution to the global picture of plant functional trait composition

and distribution, since forests are accounting for about 75% of terrestrial gross primary production (Beer *et al.*, 2010) and 80% of terrestrial plant biomass (Kindermann *et al.*, 2008). Together with the potential to map traits, diversity and functional types in other biomes and aquatic systems (see Schaepman *et al.*, 2009, for a comprehensive review), an imaging spectrometer satellite mission specifically tailored towards the global observation of vegetation would be a promising way forward and should have high priority for future mission support.

One of the most important next steps would then be to investigate the scaling between airborne and satellite observations of functional vegetation information. Functional trait maps and diversity mapping approaches as presented in this thesis form a basis for an extensive scale analysis. One important question would be how much information on biodiversity is lost when increasing the grain from individual level airborne observations (≈2 m pixel size) to community level satellite observations (≈30 m pixel size), and what is the detectability threshold of functional diversity and the variation in plant traits for different ecosystems. Furthermore, a question we did not specifically discuss in this thesis is how to select functional traits to characterize an ecosystem, in terms of number of traits, trait redundancy and ecological relevance. As discussed in Petchey & Gaston (2006), this should not be a fixed number but rather a selection of functionally important traits, depending on the processes one wants to investigate. Additionally to the six traits we have selected, there is a range of other ecologically relevant traits that can be measured by remote sensing (e.g. specific leaf area, leaf nitrogen, phosphorus or lignin, see Homolová *et al.*, 2013; Singh *et al.*, 2015). With chlorophyll and carotenoids being related in terms of spectral absorption features and partially in their functional role (Ustin *et al.*, 2009), one might replace carotenoids with other funtionally important traits, for example related to leaf longevity. Moreover, future measurements of sun-induced fluorescence might replace chlorophyll estimates being more closely linked to photosynthesis and physiological activity. Although there is a discussion on which traits are relevant to describe global plant trait variation (Díaz *et al.*, 2016) and how to select traits to calculate functional diversity indexes (Petchey & Gaston, 2006; Maire *et al.*, 2015), there is not yet a consensus within the broader community (including remote sensing) on a prioritized set of traits for diversity assessments. Further efforts to define essential biodiversity variables (Pereira *et al.*, 2013) are therefore needed and will help to clarify and provide guidelines for future research (Skidmore *et al.*, 2015; Pettorelli *et al.*, 2016).

5.3.2 Quantify the global three-dimensional (3-D) structure of terrestrial vegetation, spatially and over time

The quantification of the 3D canopy structure is an important part of this thesis. The laser scanning based forest reconstruction and the radiative transfer modeling approach presented in Chapter 2 could be used to simulate and test future satellite missions. Gastellu-Etchegorry *et al.* (2016) and Yin *et al.* (2016) show the potential of the DART model to simulate satellite lidar waveforms and laser scanning data based on 3D forest scenes. A similar approach has already been used to prepare for the spaceborne lidar mission Global Ecosystem Dynamics Investigation (GEDI Stavros *et al.*, 2017), which is planned to be launched and operated on the international space station (ISS) in 2018 and 2019. Besides the main goal of providing a wall-to-wall biomass map (between latitudes $\approx 50^{\circ}$ North and South), GEDI will reveal important information on the vertical structure of forests. A high-resolution 3D model of the forest as shown in Fig. 5.1 could help to improve the understanding of the measured waveform of a large-footprint spaceborne system. With a footprint of 25 m, GEDI will sample an integrated signal of a tree assemblage with yet unknown coverage of the vertical profile. With simulations of lidar pulses and waveforms the influence of canopy density and structure on occlusion could be tested and potentially addressed in derived products (Kükenbrink *et al.*, 2017), together with possible effects of topography. This will hopefully allow to map the three-dimensional vegetation structure with a near global coverage that could be used to derive morphological diversity and to help interpret passive-optical remote sensing data.

5.3.3 Quantify the physiological dynamics of terrestrial primary producers

Physiological dynamics of an ecosystem are closely linked to their functional diversity and related physiological and morphological traits. Therefore, a combination of imaging spectroscopy and laser scanning observations would be well suited to address this research goal. The most promising satellite mission for the quantification of physiological plant dynamics is ESA's eighth Earth Explorer called FLuorescence EXplorer (FLEX, Rascher *et al.*, 2008; Drusch *et al.*, 2017). The possibility to measure sun-induced fluorescence from space and thus establish a direct link to plant photosynthesis and physiological activity will open new research perspectives, also for linking and understanding diversity-productivity relationships based on spatially resolved measurements. The interpretation of canopy-scale fluorescence signals is challenging though, and requires an advancement of process-based models and retrieval methods. The radiative transfer of fluorescence through plant canopies has already

been implemented in 1D radiative transfer models (Verrelst *et al.*, 2015) and recently added to more complex 3D models (Gastellu-Etchegorry *et al.*, 2017; Hernández-Clemente *et al.*, 2017). Once properly validated, this will offer new possibilities for studying plant photosynthesis and scaling between leaf and canopy signals. A very promising way forward to increase efficiency and enable inversion of complex, computationally expensive process-based models is to emulate them based on invertible machine learning regression algorithms such as Gaussian processes regression or neural networks (Gómez-Dans *et al.*, 2016; Verrelst *et al.*, 2017). A fast and efficient inversion of 3D radiative transfer models cannot only improve the estimation and interpretation of sun-induced fluorescence at leaf and canopy level, but will greatly improve the retrieval of plant functional traits from remote sensing data in general.

5.3.4 Integrating remote sensing and Earth system modeling to quantify the fluxes of CO2 and CH4 globally and the flows of energy, carbon, water, nutrients, etc. within an ecosystem

This thesis highly supports the integration of remote sensing and process-based modeling, and highlights some of the related benefits and challenges. We addressed the integration of remote sensing data with the Earth system model ED2 in Chapter 4 and concluded that future research is needed to correctly initialize and parametrize the model with regard to the forest representation and the simulation of plant-water interactions. Once these issues were resolved, the ED2 model would allow to simulate the energy, carbon and water budget of the forest canopy, or any defined vegetation type (Medvigy *et al.*, 2009, 2010). However, to make a significant step forward in the integration of remote sensing data, field data, global trait databases and Earth system models, data assimilation and model intercomparison exercises with different input types and models would be extremely helpful. Lahoz & Schneider (2014) discuss the benefits of data assimilation for studies of the Earth system, and point out the successful integration of Earth observation and models for weather forecasting. Applications of data assimilation are not limited to meteorological predictions and can be combined with model intercomparison exercises. A good example is the radiative transfer model intercomparison (RAMI) exercise for simulating terrestrial surface reflectance, providing an important basis for the research community to develop and compare models, as well as to provide an overview and consensus on best practices for scene reconstruction and model parametrization (Widlowski *et al.*, 2015). Similar efforts for integrating Earth system models and Earth observation could benefit the research community and help to address the research goals related to the quantification of energy, carbon and water fluxes.

5.4 References

Abegg M, Kükenbrink D, Zell J, Schaepman ME, Morsdorf F (2017) Terrestrial laser scanning for forest inventories-tree diameter distribution and scanner location impact on occlusion. *Forests*, **8**, 1–29.

Asner GP, Martin RE, Knapp DE, *et al.* (2017) Airborne laser-guided imaging spectroscopy to map forest trait diversity and guide conservation. *Science*, **355**, 385–389.

Beer C, Reichstein M, Tomelleri E, *et al.* (2010) Terrestrial gross carbon dioxide uptake: Global distribution and covariation with climate. *Science*, **329**, 834–838.

Cernansky R (2017) Biodiversity moves beyond counting species. *Nature*, **546**, 22–24.

Díaz S, Kattge J, Cornelissen JHC, *et al.* (2016) The global spectrum of plant form and function. *Nature*, **529**, 1–17.

Drusch M, Moreno J, Del Bello U, *et al.* (2017) The FLuorescence EXplorer Mission Concept - ESA's Earth Explorer 8. *IEEE Transactions on Geoscience and Remote Sensing*, **55**, 1273–1284.

Duffy JE, Godwin CM, Cardinale BJ (2017) Biodiversity effects in the wild are common and as strong as key drivers of productivity. *Nature*, **549**, 261–264.

Fisher RA, Koven CD, Anderegg WRL, *et al.* (2017) Vegetation demographics in Earth System Models: A review of progress and priorities. *Global Change Biology*, pp. 1–20.

Gastellu-Etchegorry JP, Lauret N, Yin T, *et al.* (2017) DART: Recent Advances in Remote Sensing Data Modeling With Atmosphere, Polarization, and Chlorophyll Fluorescence. *IEEE Journal of Selected Topics in Applied Earth Observations and Remote Sensing*, **10**, 2640–2649.

Gastellu-Etchegorry JP, Yin T, Lauret N, *et al.* (2015) Discrete Anisotropic Radiative Transfer (DART 5) for Modeling Airborne and Satellite Spectroradiometer and LIDAR Acquisitions of Natural and Urban Landscapes. *Remote Sensing*, **7**, 1667–1701.

Gastellu-Etchegorry JP, Yin T, Lauret N, *et al.* (2016) Simulation of satellite, airborne and terrestrial LiDAR with DART (I): Waveform simulation with quasi-Monte Carlo ray tracing. *Remote Sensing of Environment*, **184**, 418–435.

Gerstner K, Dormann CF, Václavík T, Kreft H, Seppelt R (2014) Accounting for geographical variation in species-area relationships improves the prediction of plant species richness at the global scale. *Journal of Biogeography*, **41**, 261–273.

Gómez-Dans J, Lewis P, Disney M (2016) Efficient Emulation of Radiative Transfer Codes Using Gaussian Processes and Application to Land Surface Parameter Inferences. *Remote Sensing*, **8**, 119.

Guillén Escribà C, Schneider FD, Tedder A, *et al.* (in preparation) Remotely sensed within-species functional trait variation of temperate forests. *Methods in Ecology and Evolution*.

Hancock S, Gaulton R, Danson FM (2017) Angular Reflectance of Leaves With a Dual-Wavelength Terrestrial Lidar and Its Implications for Leaf-Bark Separation and Leaf Moisture Estimation. *IEEE Transactions on Geoscience and Remote Sensing*, **55**, 3084–3090.

Hernández-Clemente R, North P, Hornero A, Zarco-Tejada P (2017) Assessing the effects of forest health on sun-induced chlorophyll fluorescence using the FluorFLIGHT 3-D radiative transfer model to account for forest structure. *Remote Sensing of Environment*, **193**, 165–179.

Homolová L, Malenovský Z, Clevers JG, García-Santos G, Schaepman ME (2013) Review of optical-based remote sensing for plant trait mapping. *Ecological Complexity*, **15**, 1–16.

Hooper DU, Chapin FS, Ewel JJ, *et al.* (2005) Effects of biodiversity on ecosystem functioning: A consensus of current knowledge. *Ecological Monographs*, **75**, 3–35.

Isbell F, Gonzalez A, Loreau M, *et al.* (2017) Linking the influence and dependence of people on biodiversity across scales. *Nature*, **546**, 65–72.

Jetz W, Cavender-Bares J, Pavlick R, *et al.* (2016) Monitoring plant functional diversity from space. *Nature Plants*, **2**, 1–5.

Junttila S, Vastaranta M, Liang X, *et al.* (2016) Measuring Leaf Water Content with Dual-Wavelength Intensity Data from Terrestrial Laser Scanners. *Remote Sensing*, **9**, 8.

Keil P, Storch D, Jetz W (2015) On the decline of biodiversity due to area loss. *Nature Communications*, **6**, 8837.

Kindermann G, McCallum I, Fritz S, Obersteiner M (2008) A global forest growing stock, biomass and carbon map based on fao statistics. *Silva Fennica*, **42**, 387–396.

Kükenbrink D, Schneider FD, Leiterer R, Schaepman ME, Morsdorf F (2017) Quantification of hidden canopy volume of airborne laser scanning data using a voxel traversal algorithm. *Remote Sensing of Environment*, **194**, 424 – 436.

Kulmala M (2018) Build a global Earth observatory. *Nature*, **553**, 21–23.

Lahoz WA, Schneider P (2014) Data assimilation: making sense of Earth Observation. *Frontiers in Environmental Science*, **2**, 1–28.

Liang J, Crowther TW, Picard N, *et al.* (2016) Positive biodiversity-productivity relationship predominant in global forests. *Science*, **354**, aaf8957–aaf8957.

Maire E, Grenouillet G, Brosse S, Villéger S (2015) How many dimensions are needed to accurately assess functional diversity? A pragmatic approach for assessing the quality of functional spaces. *Global Ecology and Biogeography*, **24**, 728–740.

Mason NWH, Mouillot D, Lee WG, Wilson JB (2005) Functional richness, functional evenness and functional divergence: the primary components of functional diversity. *Oikos*, **111**, 112–118.

Medvigy D, Wofsy SC, Munger JW, Hollinger DY, Moorcroft PR (2009) Mechanistic scaling of ecosystem function and dynamics in space and time: Ecosystem Demography model version 2. *Journal of Geophysical Research*, **114**, G01002.

Medvigy D, Wofsy SC, Munger JW, Moorcroft PR (2010) Responses of terrestrial ecosystems and carbon budgets to current and future environmental variability. *Proceedings of the National Academy of Sciences*, **107**, 8275–8280.

Mendes G, Arroyo-Rodríguez V, Almeida WR, Pinto SRR, Pillar VD, Tabarelli M (2015) Plant trait distribution and the spatial reorganization of tree assemblages in a fragmented tropical forest landscape. *Plant Ecology*, **217**, 31–42.

Mõttus M, Rautiainen M, Schaepman ME (2012) Shoot scattering phase function for Scots pine and its effect on canopy reflectance. *Agricultural and Forest Meteorology*, **154-155**, 67–74.

Park A, Carpenter C (2016) Understory species and functional diversity in a chronosequence of jack pine and red pine stands in the south-central boreal forest. *Botany*, **94**, 185–200.

Pereira HM, Borda-de Água L, Martins IS (2012) Geometry and scale in species-area relationships. *Nature*, **482**, E3–E4.

Pereira HM, Ferrier S, Walters M, *et al.* (2013) Essential Biodiversity Variables. *Science*, **339**, 277–278.

Petchey OL, Gaston KJ (2006) Functional diversity: back to basics and looking forward. *Ecology Letters*, **9**, 741–758.

Pettorelli N, Wegmann M, Skidmore A, *et al.* (2016) Framing the concept of satellite remote sensing essential biodiversity variables: challenges and future directions. *Remote Sensing in Ecology and Conservation*, **2**, 122–131.

Rascher U, Gioli B, Miglietta F (2008) FLEX - Fluorescence Explorer: A Remote Sensing Approach to Quantify Spatio-Temporal Variations of Photosynthetic Efficiency from Space. In: *Photosynthesis. Energy from the Sun*, pp. 1387–1390. Springer Netherlands, Dordrecht.

Schaepman ME, Ustin SL, Plaza AJ, Painter TH, Verrelst J, Liang S (2009) Earth system science related imaging spectroscopy - an assessment. *Remote Sensing of Environment*, **113, Supplement 1**, S123–S137.

Schmeller DS, Böhm M, Arvanitidis C, *et al.* (2017) Building capacity in biodiversity monitoring at the global scale. *Biodiversity and Conservation*, **26**, 2765–2790.

Schneider FD, Morsdorf F, Schmid B, Petchey OL, Hueni A, Schimel DS, Schaepman ME (2017) Mapping functional diversity from remotely sensed morphological and physiological forest traits. *Nature Communications*, **8**.

Siefert A, Violle C, Chalmandrier L, *et al.* (2015) A global meta-analysis of the relative extent of intraspecific trait variation in plant communities. *Ecology Letters*, **18**, 1406–1419.

Silva Pedro M, Rammer W, Seidl R (2017) Disentangling the effects of compositional and structural diversity on forest productivity. *Journal of Vegetation Science*, pp. 1–10.

Singh A, Serbin SP, McNeil BE, Kingdon CC, Townsend Pa (2015) Imaging spectroscopy algorithms for mapping canopy foliar chemical and morphological traits and their uncertainties. *Ecological Applications*, **25**, 2180–2197.

Skidmore AK, Pettorelli N, Coops NC, *et al.* (2015) Environmental science: Agree on biodiversity metrics to track from space. *Nature*, **523**, 403–405.

Stavros N, Schimel D, Pavlick R, *et al.* (2017) Iss observations offer insights into plant function. *Nature Ecology & Evolution*, **1**, 1–4.

Thomas CD, Cameron A, Green RE, *et al.* (2004) Extinction risk from climate change. *Nature*, **427**, 145–148.

Ustin SL, Gitelson A, Jacquemoud S, Schaepman ME, Asner GP, Gamon JA, Zarco-Tejada P (2009) Retrieval of foliar information about plant pigment systems from high resolution spectroscopy. *Remote Sensing of Environment*, **113, Supplement 1**, S67–S77.

van der Plas F, Janzen T, Ordonez A, Fokkema W, Reinders J, Etienne RS, Olff H (2015) A new modeling approach estimates the relative importance of different community assembly processes. *Ecology*, **96**, 1502–1515.

Verrelst J, Rivera JP, van der Tol C, Magnani F, Mohammed G, Moreno J (2015) Global sensitivity analysis of the SCOPE model: What drives simulated canopy-leaving sun-induced fluorescence? *Remote Sensing of Environment*, **166**, 8–21.

Verrelst J, Rivera Caicedo J, Muñoz-Marí J, Camps-Valls G, Moreno J (2017) SCOPE-Based Emulators for Fast Generation of Synthetic Canopy Reflectance and Sun-Induced Fluorescence Spectra. *Remote Sensing*, **9**, 927.

Villéger S, Mason NWH, Mouillot D (2008) New multidimensional functional diversity indices for a multifaceted framework in functional ecology. *Ecology*, **89**, 2290–2301.

Violle C, Navas ML, Vile D, Kazakou E, Fortunel C, Hummel I, Garnier E (2007) Let the concept of trait be functional! *Oikos*, **116**, 882–892.

Violle C, Reich PB, Pacala SW, Enquist BJ, Kattge J (2014) The emergence and promise of functional biogeography. *Proceedings of the National Academy of Sciences of the United States of America*, **111**, 13690–13696.

Walters M, Scholes RJ, eds. (2017) *The GEO Handbook on Biodiversity Observation Networks*. Springer International Publishing.

Whittaker RH (1960) Vegetation of the siskiyou mountains, oregon and california. *Ecological Monographs*, **30**, 279–338.

Widlowski JL, Mio C, Disney M, *et al.* (2015) The fourth phase of the radiative transfer model intercomparison (RAMI) exercise: Actual canopy scenarios and conformity testing. *Remote Sensing of Environment*, **169**, 418–437.

Williams LJ, Paquette A, Cavender-Bares J, Messier C, Reich PB (2017) Spatial complementarity in tree crowns explains overyielding in species mixtures. **1**.

Yin T, Gastellu-Etchegorry JP, Lauret N, Grau E, Rubio J (2013) A new approach of direction discretization and oversampling for 3D anisotropic radiative transfer modeling. *Remote Sensing of Environment*, **135**, 213–223.

Yin T, Lauret N, Gastellu-Etchegorry JP (2015) Simulating images of passive sensors with finite field of view by coupling 3-D radiative transfer model and sensor perspective projection. *Remote Sensing of Environment*, **162**, 169–185.

Yin T, Lauret N, Gastellu-Etchegorry JP (2016) Simulation of satellite, airborne and terrestrial LiDAR with DART (II): ALS and TLS multi-pulse acquisitions, photon counting, and solar noise. *Remote Sensing of Environment*, **184**, 454–468.

Curriculum vitae

Fabian Daniel Schneider

Education

2014–2018 **University of Zurich, PhD candidate at the Remote Sensing Laboratories**
· University Research Priority Program on Global Change and Biodiversity URPP GCB
· Project 3: Integration of Cross-Scale Effects Minimizing Feedback Omission: A Latitudinal Gradient Approach
· PhD thesis: *Remotely sensing functional diversity of temperate forest ecosystems*

2011–2013 **University of Zurich, Master of Science**
· Major: Geography
· Specialization: Remote Sensing
· Master Thesis: *Simulating Imaging Spectrometer Data - 3D Forest Modeling Based on LiDAR and In Situ Data*

2007–2011 **University of Zurich, Bachelor of Science**
· Major: Geography
· Bachelor Thesis: *Evaluation aktueller Fernerkundungsansätze zur Schätzung der Bruttoprimärproduktion auf kontinentaler und globaler Ebene*
· Minor: Informatics
· Term Paper: *Automatic Generalization and Simplification of massive Vector and Network Maps*

2000–2006 **Kantonsschule Rychenberg, Matura**
· Profile: Classical Languages (English & Latin)
· Matura Thesis: *Der Lawinenniedergang am Dorfberg*

Teaching and supervision

2014–2017 Teaching assistant for various courses within the Department of Geography, University of Zurich. Namely: GEO113 Fernerkundung und Geographische Informationswissenschaft I - Earth Perspectives, GEO123 Fernerkundung und Geographische Informationswissenschaft II - Introduction to Cartography and Geovisualisation, GEO229 Small Group Teaching in Geography, GEO233 Fernerkundung und Geographische Informationswissenschaft III - Grundlagen Fernerkundung, GEO441 Colloquium in Remote Sensing

2014–2017 Teaching and organization of workshops within URPP GCB and RSL, University of Zurich. Namely: URPP GCB Journal Club, Scientifica 2015 & 2017, Workshops on field spectroradiometer and terrestrial laser scanning measurements

2017–2018 MSc co-supervision, Isabelle Helfenstein. Title: *Mapping functional diversity from physiological forest traits at different spatial scales - upscaling from airborne imagery to satellite remote sensing*

Graduate courses and training

- PhD Seminars I & II
- Graduate School Retreat Seminar (I & II)
- Principles and Theory in Geography
- Scientific Writing
- Project Management
- Voice Training and Presentation Skills
- R4All (ECO322)
- Preparing To Postdoc
- Wirtschafts-Know-How
- URPP GCB Seminar
- Various Conference Visits (see Publications and conference contributions)

Media and public outreach

Swiss TV	SRF Einstein: Mit 3D-Scannern den Regenwald schützen, 07.05.2015 SRF Einstein: Mit 3D-Scannern den Schweizer Wald besser nutzen, 07.05.2015 SRF Einstein: Urwälder werden ”geröntgt”, 29.06.2017 SRF Tagesschau: Abbild von Schweizer Wald, 13.11.2017
Radio	SRF DRS Wissenschaftsmagazin: Laserscanning im Regenwald, 02.05.2015
Newspaper	20Minuten: Forscher bereiten sich im Zoo auf Expeditionen vor, 08.05.2015 Tagesanzeiger: Wissen im Bild - Wald auf der Lägern in anderem Licht, 17.11.2017 Schaffhauser Nachrichten: Pflanzen aus dem All überwachen, 15.11.2017
Magazines	SNSF Horizonte Nr. 110: Vielfalt wird aus der Ferne sichtbar PlantScience News No 28: Cover picture - 3D-Optical and chemical diversity of 48000 reconstructed trees (Laegern, temperate forest)
Art	SNSF Scientific Image Award: Distinction Category ”Scientists” - Measuring leaf spectral signatures at the top of tropical trees

Reviewer / referee for scientific journals

- Remote Sensing of Environment
- Methods in Ecology and Evolution
- Remote Sensing
- Applied Sciences

Publications and conference contributions

Publications

Fawcett, D., Verhoef, W., Schlaepfer, D, **Schneider, F.D.**, Schaepman, M.E., & Damm, A. (2018). Combining imaging spectroscopy, digital object models, and 3D canopy modelling to advance retrievals of vegetation information over forest ecosystems. *Remote Sensing of Environment 204, 583-595.*

Schneider, F.D., Morsdorf, F., Schmid, B., Petchey, O.L., Hueni, A., Schimel, D., & Schaepman, M. E. (2017). Mapping functional diversity from remotely sensed morphological and physiological forest traits. *Nature Communications 8 (1), 1441.*

Morsdorf, F., Eck, C., Zgraggen, C., Imbach, B., **Schneider, F.D.**, & Kükenbrink, D. (2017). UAV-based LiDAR acquisition for the derivation of high-resolution forest and ground information, *The Leading Edge 36 (7), 566-570.*

Kuekenbrink, D., **Schneider, F.D.**, Leiterer, R., Schaepman, M.E., & Morsdorf, F. (2016). Quantification of hidden canopy volume of airborne laser scanning data using a voxel traversal algorithm. *Remote Sensing of Environment, 194, 424-436.*

Jetz, W., Cavender-Bares, J., Pavlick, R., Schimel, D., Davis, F.W., Asner, G.P., Guralnick, R., Kattge, J., Latimer, A.M., Moorcroft, P., Schaepman, M.E., Schildhauer, M.P., **Schneider, F.D.**, Schrodt, F., Stahl, U., & Ustin, S.L. (2016). Monitoring plant functional diversity from space. *Nature plants, 2, 16024.*

Schaepman, M.E., Jehle, M., Hueni, A., D'Odorico, P., Damm, A., Weyermann, J., **Schneider, F.D.**, Laurent, V., Popp, C., Seidel, F.C., Lenhard, K., Gege, P., Küchler, C., Brazile, J., Kohler, P., De Vos, L., Meuleman, K., Meynart, R., & Itten, K.I. (2015). Advanced radiometry measurements and Earth science applications with the Airborne Prism Experiment (APEX). *Remote Sensing of Environment, 158, 207-219.*

Schneider, F.D., Leiterer, R., Schaepman, M.E., & Morsdorf, F. (2015). Canopy height and plant area index changes in a temperate forest between 20102014 using airborne laser scanning. *Proceedings of SilviLaser 2015-September 28-30, 156-158.*

Schneider, F.D., Yin, T., Gastellu-Etchegorry, J.-P., Morsdorf, F., & Schaepman M.E. (2014). At-sensor radiance simulation for airborne imaging spectroscopy. *6th Workshop on Hyperspectral Image and Signal Proecessing: Evolution in Remote Sensing (WHISPERS), 1-4.*

Schneider, F.D., Leiterer, R., Morsdorf, F., Gastellu-Etchegorry, J.-P., Lauret, N., Pfeifer, N., & Schaepman, M. E. (2014). Simulating imaging spectrometer data: 3D forest modeling based on LiDAR and in situ data. *Remote Sensing of Environment, 152, 235-250.*

Articles to be published

Schneider, F.D., Moorcroft, P., Paul-Limoges, E., Morsdorf, F., Guillén Escribà, C., Schmid, B., & Schaepman, M.E. (in preparation). Predicting diversity and productivity under climate change by combining remote sensing and forest modelling. *To be submitted to: Global Change Biology.*

Guillén Escribà, C., **Schneider, F.D.**, Tedder, A., Schmid, B., Furrer, R., Hueni, A., Morsdorf, F., & Schaepman, M.E. (in preparation). Remotely sensed within-species functional trait variation of temperate forests. *To be submitted to: Methods in Ecology and Evolution.*

Morsdorf, F., Kükenbrink, D., **Schneider, F.D.**, Abegg, M., & Schaepman, M.E. (in press). Close-range laser scanning in forests - towards physical-based semantics across scales. *Royal Society Open Science.*

Damm, A., Paul-Limoges, E., Haghighi, E., Simmer, C., Morsdorf, F., **Schneider, F.D.**, van der Tol, C., Migliavacca, M., & Rascher, U. (in review). Remote Sensing of Plant-Water Relations: An overview and future perspectives. *Journal of Plant Physiology.*

Yamasaki, E., Altermatt, F., Cavender-Bares, J., Schuman, M.C., Zuppinger-Dingley, D., Garonna, I., **Schneider, F.D.**, Guillén Escribà, C., van Moorsel, S., Hahl, T., Schmid, B., Schaepman-Strub, G., Schaepman, M.E., & Shimizu, K.K. (in review). Integrating genomics for monitoring and predicting biological responses to global change: phenology, evolution, and biodiversity. *Current Opinion in Environmental Sustainability.*

Conference Talks

SCHNEIDER, F.D., MORSDORF, F., SCHMID, B., PETCHEY, O.L., HUENI, A., SCHIMEL, D.S., & SCHAEPMAN, M.E. (2017). Remote sensing of functional diversity using morphological and physiological forest traits. *British Ecological Society - Ecology Across Borders. 11-14 December. Ghent, Belgium. (invited)*

SCHNEIDER, F.D., MORSDORF, F., & SCHAEPMAN, M.E. (2017). Characterization of forest structure from individuals to the landscape level. *OPTIMISE Workshop - Ecosystem specific metadata definition. 25-26 September. Luxembourg, Luxembourg. (invited)*

SCHNEIDER, F.D., SCHMID, B., PETCHEY, O.L., MORSDORF, F., & SCHAEPMAN, M.E. (2017). Remotely sensing forest functional traits to assess scale-dependent functional diversity. *Ecological Society of America Annual Meeting. 6-11 August. Portland, USA.*

SCHNEIDER, F.D., MORSDORF, F., SCHMID, B., PETCHEY, O.L., HUENI, A., SCHIMEL, D., & SCHAEPMAN, M.E. (2017). Airborne imaging spectroscopy of a temperate forest reveals scale-dependent functional diversity patterns. *10th EARSeL SIG Imaging Spectroscopy Workshop. 18-21 April. Zurich, Switzerland.*

SCHNEIDER, F.D., MORSDORF, F., KUEKENBRINK, D., ABEGG, M., GUILLEN-ESCRIBA, C., & SCHAEPMAN, M.E. (2017). Laser scanning and vegetation structure - towards physically-based semantics across scales. *Royal Society Meeting: The terrestrial laser scanning revolution in forest ecology. 27-28 February. Chicheley Hall, United Kingdom. (invited)*

SCHNEIDER, F.D., LEITERER, R., KUEKENBRINK, D., SCHAEPMAN, M.E., & MORSDORF, F. (2015). Canopy height and plant area index changes in a temperate forest between 2010 - 2014 using airborne laser scanning. *Silvilaser. 28-30 September. La Grande Motte, France.*

SCHNEIDER, F.D. (2015). Remote Sensing of Forest Ecosystems Using Airborne Laser Scanning and Imaging Spectroscopy. *Forest Research Institute Malaysia (FRIM) Symposium. 14 April. Zurich, Switzerland.*

SCHNEIDER, F.D., YIN, T., GASTELLU-ETCHEGORRY, J.-P., MORSDORF, F., & SCHAEPMAN, M.E. (2014). At-sensor radiance simulation for airborne imaging spectroscopy. *WHISPERS. 24-27 June. Lausanne, Switzerland.*

SCHNEIDER, F.D., LEITERER, R., MORSDORF, F., GASTELLU-ETCHEGORRY, J.-P., LAURET, N., PFEIFER, N., & SCHAEPMAN, M.E. (2014). Discrete anisotropic radiative transfer simulation of high-dimensional imaging spectrometer data based on LiDAR and in situ data. *4th International Symposium: Recent Advances in Quantitative Remote Sensing. 22-26 September. Torrent, Spain.*

SCHNEIDER, F.D., LEITERER, R., MORSDORF, F., GASTELLU-ETCHEGORRY, J.-P., LAURET, N., PFEIFER, N., & SCHAEPMAN, M.E. (2013). Simulating imaging spectrometer data of a mixed old-growth forest: A parameterization of a 3D radiative transfer model based on airborne and terrestrial laser scanning. *AGU Fall Meeting. 9-13 Dec 2013. San Francisco, USA.*

Conference Posters

SCHNEIDER, F.D., MORSDORF, F., SCHMID, B., PETCHEY, O.L., HUENI, A., SCHIMEL, D.S., & SCHAEPMAN, M.E. (2016). Scale dependency of forest functional diversity assessed using imaging spectroscopy and airborne laser scanning. *AGU Fall Meeting. 12-16 December. San Francisco, USA.*

SCHNEIDER, F.D., KÜKENBRINK, D., SCHAEPMAN, M.E., & MORSDORF, F. (2016). Mapping the 3D structure of a tropical rainforest using terrestrial laser scanning - a quality assessment. *ForestSAT. 14-18 November. Santiago de Chile, Chile.*

SCHNEIDER, F.D., MORSDORF, F., SCHMID, B., PETCHEY, O.L., HUENI, A., SCHIMEL, D.S., & SCHAEPMAN, M.E. (2016). Remotely sensing functional richness of a temperate forest using airborne laser scanning and imaging spectroscopy. *Global Change and Biodiversity: Integrating Mechanisms of Interactions, Feedbacks and Scale. 28 August - 1 September. Monte Verita, Switzerland.*

SCHNEIDER, F.D., MORSDORF, F., FURRER, R., SCHMID, B., & SCHAEPMAN, M.E. (2015). Linking Remotely Sensed Functional Diversity of Structural Traits to the Radiative Regime of a Temperate Forest. *AGU Fall Meeting. 14-18 December. San Francisco, USA. (invited)*

SCHNEIDER, F.D., LEITERER, R., MORSDORF, F., & SCHAEPMAN, M.E. (2014). Remote sensing of forest ecosystems using airborne laser scanning and imaging spectroscopy. *Swiss Geoscience Meeting. 21-22 November. Fribourg, Switzerland.*

SCHNEIDER, F.D., LEITERER, R., MORSDORF, F., GASTELLU-ETCHEGORRY, J.-P., LAURET, N., PFEIFER, N., & SCHAEPMAN, M.E. (2014). Simulation von Bildspektrometer Daten: 3D Waldmodellierung basierend auf LiDAR and in situ Daten. *Gemeinsame Jahrestagung der DGfK, DGPF, GfGI und GiN. 25-28 March. Hamburg, Germany.*

Acknowledgements

First of all, I would like to thank my advisors Michael Schaepman and Felix Morsdorf for their valuable support, the interesting discussions, as well as their enthusiasm and guidance throughout the four years of my PhD. It has been a great pleasure to work together and profit from your experience, knowledge and ongoing trust in my work. I would also like to thank Bernhard Schmid and Reinhard Furrer for the helpful feedback, explanations and enthusiastic discussions not only during committee meetings but also in many more meetings whenever I was stuck, needed help or another perspective on my ideas.

A great thank you goes to all my fellow colleagues at the Remote Sensing Laboratories, the URPP Global Change and Biodiversity and the J-floor. I would like to specifically thank my office mates Carla, Daniel, Jonas, Marta, Meinrad and Dominic for all the great moments, lots of fun at the office and a comfy, cozy and just the nicest working environment I could imagine. I am happy to not only have shared the office but also experiences traveling to Borneo, Chile, Patagonia and the US for field work and conferences. During the journey of my PhD, including all the ups and downs, I enjoyed talking about work and life issues with Carla, Irene and Rogier, doing sports with Xiu, Victoria, Peter and Gillian, as well as playing kicker with Felix, Hendrik, Rogier, my office mates and many others. Furthermore, Thursday beers and BBQs have always been a great occasion to get to know and talk to everyone, and enjoy life after work.

I am sincerely grateful for having been able to pursue my PhD at the Remote Sensing Laboratories and for all the opportunities I have been provided here. I very much appreciate the collaboration with Paul Moorcroft and Jean-Philippe Gastellu-Etchegorry and the great effort, enthusiasm and work they have invested in common projects. I also profited a lot from being part of the URPP Global Change and Biodiversity, and especially from the interactions with Owen Petchey, Eri Yamasaki, Kentaro Shimizu and Florian Altermatt. I have been provided the opportunity to perform field work at the Laegern in Switzerland and in the Lambir Hills National Park in Borneo, which has only been successful and a great experience thanks to the help of Daniel, Eri, Basil, Carla, Felix and Reik. I am also thankful to David Schimel, Walter Jetz, Reik Leiterer, Dominic Fawcett, Andreas Hueni, Nicolas Lauret, Tiangang Yin, Norbert Pfeifer, Eugénie Paul-Limoges and Carla Guillén Escribà for their contributions to the manuscript at various stages.

Finally, my sincerest gratitude goes to my family and friends, in particular Liselotte, Kurt, Ivo and Philippe, who always supported me and to whom this work is dedicated. Vielen lieben Dank, dass ihr mich immer unterstützt, an mich glaubt und mir auch die nötige Ablenkung vom Doktorat geben konntet. Ich danke Euch von ganzem Herzen und widme Euch diese Arbeit!